Graduate Schools Yearbook 2011

Dam-Johansen, Kim; Xue, Rui; Gernaey, Krist

Publication date:
2011

Document Version
Publisher's PDF, also known as Version of record

Graduate Schools Yearbook **2011**

Editors:
Kim Dam-Johansen
Rui Xue
Krist V. Gernaey

DTU Chemical Engineering
Department of Chemical and Biochemical Engineering

Graduate Schools Yearbook **2011**

Editors:
Kim Dam-Johansen
Rui Xue
Krist V. Gernaey

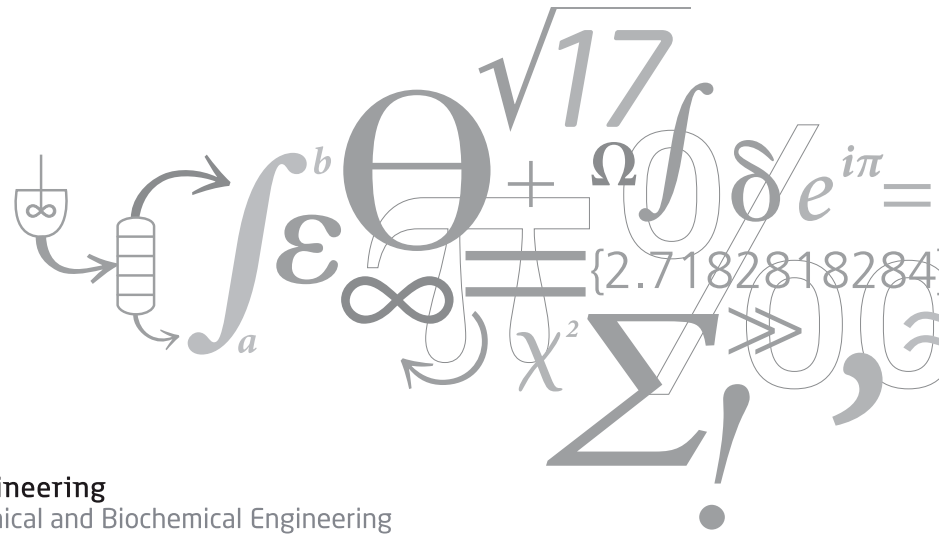

DTU Chemical Engineering
Department of Chemical and Biochemical Engineering

Address: Department of Chemical and Biochemical Engineering
Søltofts Plads, Building 229
Technical University of Denmark
DK-2800 Kgs. Lyngby
Denmark

Telephone: +45 4525 2800
Fax: +45 4588 2258
E-mail: kt@kt.dtu.dk
Internet: www.kt.dtu.dk

Print: J&R Frydenberg A/S
København
Januar 2012

Cover: Suzanne Fog

Cover photo: Klaus Holsting

ISBN-13: 978-87-92481-60-3

Contents

Preface

In this Graduate Schools Yearbook 2011 the PhD students of the Department of Chemical and Biochemical Engineering present their research projects. Some of the students have just initiated their research and therefore provide a short description of their research project in the Yearbook, whereas others are close to concluding their work and present the most significant project results. We hope that the readers will find the Yearbook interesting and we invite you to contact us in case you would like to receive additional details.

The PhD projects cover all areas of the Department, which now includes research, laboratories and pilot plant facilities both at Campus Lyngby and Campus Risø. Indeed, on January 1st 2012 the former section Risø Biosystems as well as other parts of the Risø National Laboratories for Renewable Energy were integrated with the Department of Chemical and Biochemical Engineering. This means a total number of PhD students at the Department that now exceeds 100, and a significant expansion of our research activities in the field of sustainability and bio-based production systems.

Collaboration with industry forms the basis of many of our research projects. We plan to consolidate already existing industrial collaborations, and to start a number of new initiatives involving also our new colleagues at Campus Risø.

We wish you a pleasant reading.

Yours Sincerely

Kim Dam-Johansen
Professor, Head of Department

Krist V. Gernaey
Associate Professor, Editor

Dayang Norulfairuz Abang Zaidel
Phone: +45 4525 2861
E-mail: daz@kt.dtu.dk
Discipline: Enzyme Technology

Supervisors: Anne S. Meyer

PhD Study
Started: August 2008
To be completed: January 2012

Kinetics of Enzyme-catalyzed Cross-linking of Feruloylated Arabinan Oligosaccharides from Sugar Beet

Abstract
Ferulic acid (FA) esterified to arabinose side chains of pectic polysaccharides has the ability to be oxidatively cross-linked by oxidoreductases *i.e.* peroxidase and laccase to form ferulic acid dehydrodimers (diFAs). This present work investigated the kinetics of the enzyme-catalyzed cross-linking of FA and the effect of the size or length of the arabinose chain on the rate of ferulic acid cross linking. Kinetics of arabinan samples from sugar beet with different degree of polymerization (DP) were monitored by the disappearance of FA absorbance at 316 nm. Enzyme concentrations affected the kinetics of the cross linking by increasing the rate as the amount of enzyme increased. At approximately similar FA to arabinan ratio, the cross-linking of longer chain arabinan showed a slower rate of cross-linking than the short chain arabinan. This is due to longer time taken for two ferulates on the longer chain arabinan to link to each other to form dehydrodimers. HPLC analysis signified that the amounts of diFAs increased when FA decreased as a result of the catalytic oxidation treatment with horseradish peroxidase and hydrogen peroxide.

Introduction
The FA bound to the side chains of pectic polysaccharides have long been known to have the ability to be oxidatively cross-linked via enzyme catalysis by oxidoreductases *i.e.* peroxidase or laccase activities [1,2]. Previous work has shown that addition of e.g. peroxidase, together with H_2O_2 or laccase, results in a reduction of the amount of FA esterified to the arabinan chains while the levels of diFAs increase simultaneously [2,3]. The enzyme catalyzed cross-linking of two feruloylated arabinan oligosaccharides takes place via radical coupling of the FA resulting in the formation of different diFAs: 5,5', 8-O-4', 8,5' and 8,8' [2-4]. The formation of diFAs cross-linking between feruloylated arabinans or feruloylated arabino-oligosaccharides may result in gel formation [2,5]. Although studies on the oxidative cross-linking of feruloyl substitutions in polysaccharides have been amply reported [1-3] there are no reports on the effect of the length of the backbone of the arabinans on the rate of the cross-linking of feruloylated arabinan. Currently the arabinan fraction from sugar beet pulp is a by-product, but the utilization of the arabinan as a food additive could help maintain the competitiveness of the sugar beet based industry. Thus the provision of knowledge regarding the cross-linking of feruloylated arabinan would for example be important for the rational design and control of enzymatic processes for upgrading of sugar beet pulp arabinans for use as viscosity-regulating or gelling agents in foods and beverages.

We hypothesized that the rate of cross-linking of feruloylated arabinans obtained from sugar beet pulp might be affected by the backbone length of the arabinan to which the FA moieties are attached. Hypothetically, the rate of cross-linking between FA on longer arabinan chains is expected to be slower than the rate of cross-linking between FA on shorter arabinan chains mainly because of the relatively slower movement (diffusion) of larger molecules. However, once some initial diFAs formation has taken place with the longer chains, hence cross-linking two arabinan chains, the rates of diFAs formation of long and short arabinan chains may approach each other since the diFAs on the longer chains will be in closer proximity, resulting in a sort of "zipping" of the FA esterified to the arabinan chains. The purpose of this study was to test the hypothesis that the kinetics of the cross-linking of feruloylated arabinans is affected by the chain length of the arabinan.

Results and Discussion

The monosaccharide profiles of the starting materials, Ara1 and Ara2 confirmed that the substrates could be classified as arabinans. They were composed of in mmol g^{-1} dry matter; Ara1: arabinose 3.4 (equivalent to 88 mol %); glucose 0.27 (equivalent to 7 mol %), with traces of less than 1 mol % of rhamnose, galactose and galacturonic acid; Ara2: arabinose 2.9 (equivalent to 95 mol %), and traces of less than 1 mol % of rhamnose, glucose, galactose and galacturonic acid. The total FA content in the four different arabinan samples ranged from 1.1 - 7.0 mg g^{-1} dry matter arabinan (Table 1). Ara1 contained the highest amount of FA esterified to the arabinan (7.0 ± 0.5 mg g^{-1}) followed by Ara2 (2.5 ± 0.6 mg g^{-1}), Ara1b (2.4 ± 0.5 mg g^{-1}), and Ara2b (1.1 ± 0.2 mg g^{-1}) (Table 1).

Table 1: Total ferulic acid and diferulates content in arabinan samples before and after the cross-linking using HRP and H_2O_2 analyzed using RP-HPLC.

Sample	FA (mg g^{-1} dry matter)		*Total diFAs (mg g^{-1} dry matter)	
	Before cross linking	After cross linking	Before cross linking	After cross linking
Ara1	7.0 ± 0.5	2.4 ± 0.2	2.4 ± 0.6	5.1 ± 1.3
Ara2	2.5 ± 0.6	1.4 ± 0.3	2.32 ± 0.03	2.82 ± 0.04
Ara1b	2.4 ± 0.5	0.29 ± 0.06	0.44 ± 0.04	1.01 ± 0.08
Ara2b	1.1 ± 0.2	0.1 ± 0.01	0.6 ± 0.2	0.30 ± 0.02

* Total diFAs = 5,5'-diFA + 8,5-diFA benzofuran + 8-O-4'-diFA. Results are shown as average data ± SD of duplicates.

The enzyme catalyzed oxidative cross-linking experiments were done at 25 °C and pH 6 with 14 μM of H_2O_2 and 0.2 mg L^{-1} HRP (equivalent to 0.2 U ml^{-1}). When assessing the reaction rates as amount of FA consumed per minute (μM min^{-1}) it became evident that the initial reaction rates increased with increased FA substrate concentration and moreover that the reaction rates of Ara1 and Ara2 in general were several fold higher, than the reaction rates of samples Ara1b and Ara2b (Figure 1). Hence, at similar FA concentrations of e.g. 20 μM, the rates of cross-linking for Ara1 and Ara2 were 5.6 and 4.1 μM min^{-1}, respectively, and thus statistically significantly higher ($P < 0.05$), than the rates of cross-linking for the longer chain arabinans that were approximately 5 times slower at 0.94 and 0.78 μM min^{-1} for Ara1b and Ara2b, respectively (Figure 1).

Conclusion

It was proven that the rate of FA cross-linking depends on the arabinan oligosaccharides backbone chain length *i.e.* longer arabinans exhibit a slower cross-linking rate than shorter, all other things being equal. It is not only the substrate concentration, but also the molecular size *i.e.* the arabinan backbone chain length, that affects the rate of cross-linking.

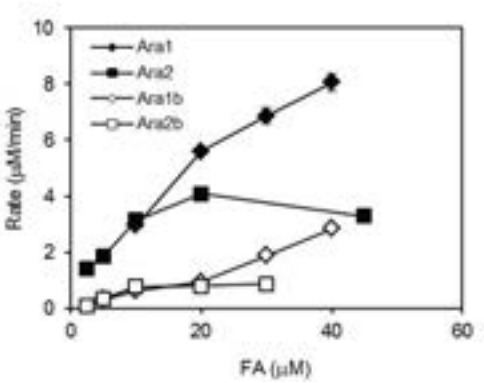

Figure 1: Initial rate of enzyme-catalyzed oxidative cross-linking of FA in feruloylated arabinans; rate was calculated during the first 10 s of the reaction for the original arabinan samples, Ara1 and Ara2, and during the first minute of enzyme catalyzed reaction for the longer chain arabinans, Ara1b and Ara2b.

Acknowledgement

The author would like to acknowledge Universiti Teknologi Malaysia, Skudai and the Ministry of Higher Education, Malaysia for their financial support.

References

1. V. Micard, J.F. Thibault, Carbohydr. Polym. 39 (1999) 265-273.
2. A. Oosterveld, G. Beldman, A.G.J. Voragen, Carbohydr. Res. 328 (2000) 199-207.
3. A. Oosterveld, J.H. Grabber, G. Beldman, J. Ralph, A.G.J. Voragen, Carbohydr. Res. 300 (1997) 179-181.
4. K.W. Waldron, A. Ng, M.L. Parker, A.J. Parr, J. Sci. Food Agric. 74 (1997) 221-228.
5. T. Kuuva, R. Lantto, T. Reinikainen, J. Buchert, K. Autio, Food Hydrocolloid. 17 (2003) 679-684.

For more detail, please refer to the full article published in J. Agric. Food Chem. 59 (2011) 11598 – 11607.

Noor Asma Fazli Bin Abdul Samad
Phone: +45 4525 2912
E-mail: nas@kt.dtu.dk
Discipline: Systems Engineering

Supervisors: Rafiqul Gani
Krist V. Gernaey
Gürkan Sin

PhD Study
Started: January 2009
To be completed: June 2012

A Generic Framework for Systematic Design of Process Monitoring and Control System for Crystallization Processes

Abstract
A generic framework for systematic design of a process monitoring and control system for crystallization processes has been developed in order to obtain the desired end-product properties notably the crystal size distribution (CSD). The design framework contains a generic crystallizer modelling tool-box, a tool for design of operational policies as well as a tool for design of process monitoring and control systems. Through this framework, it is possible for a wide range of crystallization processes to generate the necessary problem-system specific model, the necessary operational policy and a Process Analytical Technology (PAT) system design including implementation of monitoring tools and control strategies in order to produce a desired product with its corresponding target properties. Application of the framework is highlighted through a case study involving the system potassium dihydrogen phosphate (KDP), for which the targeted CSD is defined and achieved in one- and two-dimensional schemes.

Introduction
Crystallization processes have a wide range of applications as solid-liquid separation technique in the chemical, the pharmaceutical and the food industries, due to the fact that high quality crystalline products can be obtained. The specifications of the crystal product are usually given in terms of crystal size, size distribution, shape and purity. A problem, however, in many crystallization processes is how to obtain a uniform and reproducible crystal size distribution (CSD) [1,2]. To this end, supersaturation control is often applied to drive the process within the metastable zone in order to enhance the control of the CSD. Although this approach has been shown to produce high quality crystals, the set point operating policies for the controller are usually chosen arbitrarily or by trial-and-error [2]. Therefore a systematic procedure to generate operational policies that guarantee the matching of a targeted CSD would be very useful. For such a procedure to be generic, *i.e.*, applicable to many chemical systems, it needs to be model-based, preferably linked to a modelling framework that can generate the needed models for a wide range of systems. Furthermore, for monitoring and control purposes, an appropriate Process Analytical Technology (PAT) system ensuring that the critical process variables are identified, monitored and/or controlled within the design limits needs to be integrated as well.

In this work, a generic and systematic framework for the design and use of a process monitoring and control system to achieve the desired CSD and crystal shape for a wide range of crystallization processes is presented. This framework contains a generic multi-dimensional modelling framework [2,3] and tools for design of operational policies and for design of PAT systems [4,5]. Furthermore, for designing the operational policies, the analytical CSD estimator proposed by Aamir et al. [1] has been extended to also cover two-dimensional problems. This estimator and a response surface method are employed to generate the operational policies needed to match the desired target CSD. The application of the systematic design framework is highlighted through a potassium dihydrogen phosphate (KDP) crystallization process case study where the objective is to obtain a desired one- and two-dimensional CSD as well as crystal shape.

Systematic Design Framework for Process Monitoring and Control System
The architecture of the generic framework for systematic design of monitoring and control systems is illustrated in Fig. 1. There are 4 main steps through which the design (operational policy together with the monitoring/control system) proposal is created to achieve the target product properties. The first step is the problem definition for the crystallization process

under study where the overall objective is defined. Step 2, crystallization model development, involves the generation of a problem-system specific model using the generic multi-dimensional modelling framework [2,3]. The third step is concerned with the design of operational policies for the crystallizer. The objective here is to generate operational policies that guarantee that a targeted CSD is achieved. Two methods have been implemented: an analytical CSD estimator based method and a response surface method (RSM). The generated operational policies provide the supersaturation set points that need to be maintained so that the targeted CSD can be achieved. The resulting problem-system specific models and the operational policies are then ready for use in model-based design of a process monitoring and control system (PAT system) [4,5]. If the proposed PAT system design is satisfactory with respect to the desired performance then it is selected as part of the final design proposal. The final design proposal thus contains the proposed design flowsheet with the necessary monitoring tools/techniques, the model equipment data obtained from the monitoring tools for process variables (such as temperature, concentration *etc*.) and the graphs in 3-D to illustrate the evolution of the CSD.

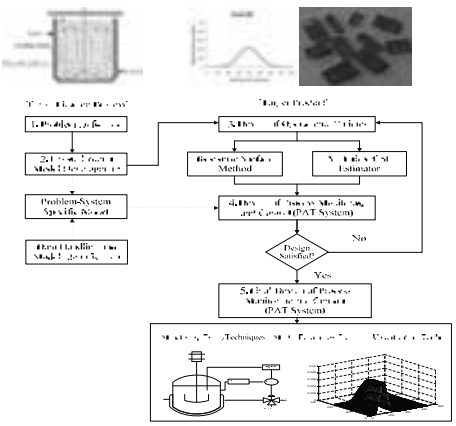

Fig. 1: Systematic design framework for process monitoring and control for crystallization processes.

Application of the Design Framework: Potassium Dihydrogen Phosphate (KDP) Crystallization

Application of the framework is demonstrated for KDP crystallization (adopted from [6,7]) where the objective is to design a PAT system in order to achieve the one- and two-dimensional target CSD as well as the desired crystal shape.

Problem Definition (Step 1)

The desired target for the one- and two-dimensional CSD (Fig. 2) is assumed as a univariate quadratic (mean characteristic length of 60 µm and standard deviation of 2.8 µm) and a bivariate quadratic distribution [6] (mean characteristic length of 60 µm with standard deviation of 2.8 µm and mean characteristic width of 27 µm with standard deviation of 1.34 µm), respectively. The crystal shapes used for the one- and two-dimensional case are cube-shaped and tetragonal prism-shaped, respectively.

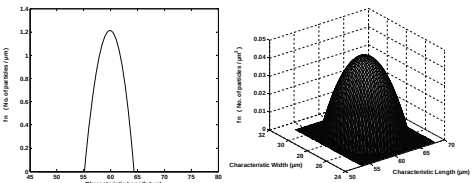

Fig. 2: Target for the one-(left) and two-dimensional (right) CSD.

Crystallization Model Development (Step 2)

The problem-system specific models for the one- and two-dimensional cases are then generated using the generic multi-dimensional modelling framework [2,3] by using similar conditions and assumptions as reported in the literature [6].

Design of Operational Policies (Step 3)

In this section, the operational policies for the one- and two-dimensional CSD are generated using the analytical CSD estimator method and the application of the RSM.

- Analytical CSD Estimator

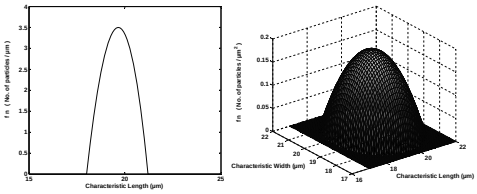

Fig. 3: Initial seed for the one-(left) and two-dimensional (right) CSD

The initial seed distributions for the one- and two-dimensional cases (Fig. 3) are assumed as univariate and bivariate quadratic distributions [6], respectively. A common mean characteristic length (19.5 µm) and standard deviation (0.97 µm) are used for the seeded operations. The total number of crystal particles used for both initial seeds is 736 crystal particles. The analytical CSD estimator (Table 1) for size dependent growth ($\gamma_x=\gamma_y\neq 0$; $p_x=p_y=1$) is used for both the one and two-dimensional case.

Table 1: Generic analytical CSD estimator expressions.

Characteristics	Analytical Expressions
Final CSD	$f_n = f_{n0}\exp^{-(\gamma_x k_{gx} S^{gx} t + \gamma_y k_{gy} S^{gy} t)}$
Final Characteristic Length	$L_x = \frac{(1+\gamma_x L_{x0})\exp^{(\gamma_x k_{gx} S^{gx} t)} - 1}{\gamma_x}$
Final Characteristic Width	$L_y = \frac{(1+\gamma_y L_{y0})\exp^{(\gamma_y k_{gy} S^{gy} t)} - 1}{\gamma_y}$

A model-based approach is then used to optimize the supersaturation set point and the total crystallization time for one- and two dimensional cases in order to achieve the desired target CSD, respectively. The objective is to minimize the sum of squares of the relative errors between the desired target CSD and a predicted CSD obtained through the analytical CSD estimator. The following optimal operational policy for the one-dimensional case was obtained: the supersaturation set point is 0.03 g/g and total crystallization time is 80 seconds. The optimal operation policy was found the same for the two-dimensional case.

- Response Surface Method (RSM)

The RSM using a central composite design (CCD) as sampling method was used for the one-dimensional case first. A total of 9 different operating conditions were evaluated, and the response surface for the one-dimensional case was then obtained (see Fig. 4). It shows that the relative error is the lowest for a supersaturation set point of 0.03 g/g and a total crystallization time of 80 seconds. Therefore the resulting optimal operational policy to achieve the desired one-dimensional CSD with the associated target properties, is as follows: supersaturation set point = 0.03 g/g and total crystallization time = 80 seconds. A similar procedure is repeated for the two-dimensional case and the operational policy obtained is identical to the one-dimensional case.

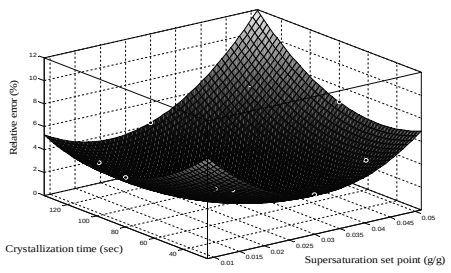

Fig. 4: Response surface for one-dimensional case.

Design of Process Monitoring and Control System (Step 4)

The design of a PAT system has been implemented in the ICAS-PAT software [5] and was applied to the one- and two-dimensional KDP crystallization. As a result of the PAT design, the concentration (see Fig. 5 and 6) is well maintained at the generated operational policy (set point trajectory) until the end of operation for both the one- and two-dimensional cases in the closed-loop simulation.

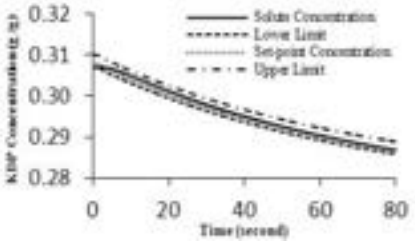

Fig. 5: KDP concentration profiles for one-dimensional case.

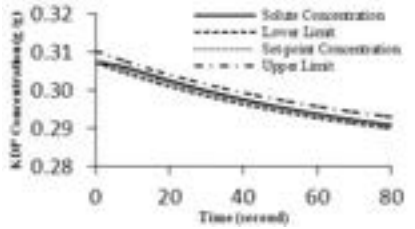

Fig. 6: KDP concentration profiles for two-dimensional case.

The narrow seed distribution (see Fig. 7(a)) for the one-dimensional case has developed into a wider CSD at the end of the crystallization due to the size dependent growth effects (see Fig. 7(b)). The cube-shape seeds have grown to a mean characteristic length of 58.9 µm with a standard deviation of 2.79 µm. Similarly, the final CSD becomes wider for the two-dimensional case (Fig. 8). The final CSD obtained shows that the tetragonal prism-shape of the seeds has been growing to reach approximately 58.54 µm mean characteristic length and 26.55 µm mean characteristic width. Meanwhile the standard deviations obtained from the two-dimensional model are 2.79 µm (length) and 1.33 µm (width), respectively. Both the one- and the two-dimensional CSD obtained are in good agreement with the predefined target CSD. The total number of crystal particles of 736 remains at the end of the operation indicating no generation of new seeds due to secondary nucleation.

Final Process Monitoring and Control System (Step 5)

The final design of the PAT system for one- and two-dimensional KDP crystallization processes is then obtained as shown in Fig. 9. According to this design, the concentration is monitored by attenuated total reflection fourier transform infrared (ATR-FTIR) and the temperature is monitored by a thermocouple. The inlet water temperature is manipulated by blending hot and cold water. Meanwhile the one- and two-dimensional CSD is also monitored by using focused beam reflectance measurement (FBRM).

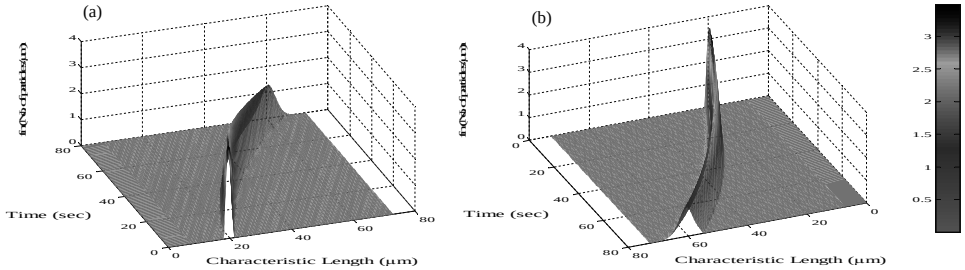

Fig. 7: Evolution of one-dimensional CSD (a) initial seed view (b) final seed view

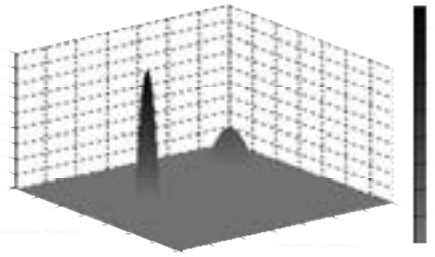

Fig. 8: Evolution of two-dimensional CSD (initial seed (left) to the final seed (right)).

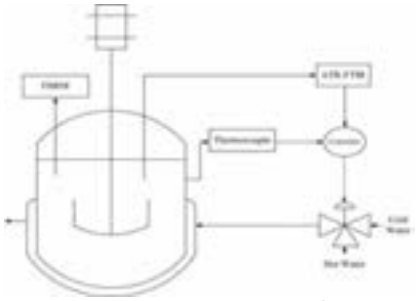

Fig. 9: KDP crystallization process flowsheet with designed PAT system

Conclusions

The potential of the systematic framework to produce the desired one- and two-dimensional CSD as well as crystal shape has been illustrated for a KDP crystallization process. The generation of operational policies using optimization involving an analytical CSD estimator and the response surface method has been highlighted. Applying the model-based optimization using the analytical CSD estimator provides an efficient and computationally effective way to produce the optimal operational policies compared to other approaches. The results of the CSD generated with the systematic design framework have shown good agreement with the published crystallization data, indicating thereby, the power and unique features of this systematic framework.

Acknowledgement

The PhD project of Noor Asma Fazli Abdul Samad is financed by a PhD scholarship from the Ministry of Higher Education of Malaysia and Universiti Malaysia Pahang.

References

1. E. Aamir, Z.K. Nagy, C.D. Rielly, Chem. Eng. Sci., 65 (2010), 3602-3614.
2. N.A.F.A. Samad, R. Singh, G. Sin, K.V. Gernaey, R. Gani, Comput.-Aided Chem. Eng., 29 (2011), 86-90.
3. N.A.F.A. Samad, R. Singh, G. Sin, K.V. Gernaey, R. Gani, Comput. Chem. Eng., 35 (2011), 828-843.
4. R. Singh, K.V. Gernaey, R. Gani, Comput. Chem. Eng., 33 (2009), 22-42.
5. R. Singh, K.V. Gernaey, R. Gani, Comput. Chem. Eng., 34 (2010), 1108-1136.
6. R. Gunawan, I. Fusman, R.D. Braatz, AIChE J., 50 (11) (2004), 2738-2749.
7. D.L. Ma, D.K. Tafti, R.D. Braatz, Ind. Eng. Chem. Res., 41 (2002), 6217-6223.

List of Publications

1. N.A.F.A. Samad, R. Singh, G. Sin, K.V. Gernaey, R. Gani, Comput.-Aided Chem. Eng., 28 (2010), 613-618.
2. N.A.F.A. Samad, R. Singh, G. Sin, K.V. Gernaey, R. Gani, Comput.-Aided Chem. Eng., 29 (2011), 86-90.
3. N.A.F.A. Samad, R. Singh, G. Sin, K.V. Gernaey, R. Gani, Comput. Chem. Eng., 35 (2011), 828-843.
4. N.A.F.A. Samad, R. Singh, G. Sin, K.V. Gernaey, R. Gani, IEEE J., (2011), 783-788.
5. N.A.F.A. Samad, in I. Cameron, R. Gani, Product and Process Modelling: A Case Study Approach, Elsevier Science, (2011), 305-336.
6. N.A.F.A. Samad, R. Singh, G. Sin, K.V. Gernaey, R. Gani, ESCAPE-22 (2011) (Submitted).
7. N.A.F.A. Samad, R. Singh, G. Sin, K.V. Gernaey, R. Gani, Comput. Chem. Eng. (2011), (in preparation).

Hassan Ahmadi Gavlighi
Phone: +45 4525 2947
E-mail: hag@kt.dtu.dk
Discipline: Enzyme Technology

Supervisors: Jørn Dalgaard Mikkelsen
Anne S. Meyer

PhD Study
Started: June 2009
To be completed: May 2012

Extraction and Production of Prebiotic and Hydrocolloids Oligosaccharides from Waste Streams from the Agricultural and Ingredient Industries

Abstract
A prebiotic oligosaccharide is a functional food component that confers a health benefit on the host which is associated with growth modulation of the gut microbiota. The interest in the use of nondigestible oligosaccharides (NDO) as functional food components targeted at gut health has increased during recent years. NDO are selectively fermented in the human colon and can be described as prebiotics. The waste streams from agricultural industry are a large source of oligosaccharides with potential prebiotic effects. The possibilities to manufacture new prebiotic oligosaccharides from large agricultural side-streams are therefore an attractive avenue and especially when it can be carried out using mono-component enzymes.

Introduction
It is now well established that the colonic microflora has a profound influence on health .Consequently, there is currently a great deal of interest in the use of prebiotic as functional food ingredients to manipulate the omposition of colonic microflora in order to improve health. Prebiotics show both important technological characteristics and interesting nutritional properties. Several are found in vegetables and fruits and can be industrially processed from renewable materials. In food formulations, they can significantly improve organoleptic characteristics, upgrading both taste and mouthfeel. For prebiotics to serve as functional food ingredients, they must be chemically stable to food processing treatments, such as heat, low pH, and Maillard reaction conditions. That is, a prebiotic would no longer provide selective stimulation of beneficial microorganisms if the prebiotic was degraded to its component mono- and disaccharides or chemically altered so that it was unavailable for bacterial metabolism determined the effect of processing conditions on the prebiotic activity of commercial prebiotics using a prebiotic activity assay. The results showed that only heating at low pH caused a significant reduction in prebiotic activity, with one of the fructooligosaccharides (FOS) products being the least stable. The other conditions caused little change in activity. Stability of prebiotics to processing conditions has been considered. These results provide the basis for selecting prebiotics for use as functional food ingredients and for predicting the extent to which processing affects prebiotic activity. Most prebiotics and prebiotic candidates identified today are nondigestible oligosaccharides. They are obtained either by extraction from plants (e.g., chicory inulin), possibly followed by an enzymatic hydrolysis (e.g., oligofructose from inulin) or by synthesis (by trans-glycosylation reactions) from mono- or disaccharides such as sucrose (fructooligosaccharides) or lactose (trans-galactosylated oligosaccharides or galactooligosaccharides) .Among these prebiotics, inulin and oligosaccharides are the most studied prebiotics and have been recognized as dietary fibers in most countries .

Specific objectives
The main idea of the proposed project is to employ selective enzymatic catalysis to extract and design beneficial hydrocolloids and prebiotic oligosaccharides from agricultural industry.

Pectin is an abundant ubiquitous and multifunctional component of the cell wall of all land plants [1]. Pectic polysaccharides consist mostly of polymers rich in galacturonic acid (GalA), containing significant amounts of rhamnose (Rha), arabinose (Ara) and galactose (Gal) as well as other 13 different monosaccharides [2,3,4]. The three major pectic polysaccharides currently defined are homogalacturonan (HG), rhamnogalacturonan I (RG-I) and rhamnogalacturonan II (RG-II) [5]. The industrial process for extraction of pectin is generally based on a

chemical treatment at low pH. It generates large amounts of effluents (such as chemical waste) that need further treatment. It may also give rise to undesired degradation of pectin during extraction. There are a growing demand for sustainable processes with mild extraction and modification conditions to produce hydrocolloids and prebiotic oligosaccharides without the use and generation of hazardous substances. The present idea in this PhD study is to evaluate the use of new mono-component enzymes as an environmentally friendly method for pectin extraction and modification.

Current Work

Structural analysis of oligosaccharides is very important to evaluate oligomers functionality. Different technique such as linkage analysis and NMR could be possibility to get more information.

As I mentioned we are analysis oligosaccharides and then test for prebiotics effect with different bacteria.

Conclusion and Future work

In this project, we will extract hydrocolloids with mono or multi enzyme and then evaluate the prebiotic effect. Also, we will produce some oligosaccharides from hydrocolloids that may contain health benefit.

In this case based on structural of the cell wall, we will use enzyme directly to get oligosaccharides or use different enzyme to extract intact hydrocolloids and the use enzyme for production oligosaccharide.

References

1. W.G.T. Willats, P. Knox, J.D. Mikkelsen, Trends Food Sci. Technol. 17 (3) (2006) 97-104.
2. D. Mohnen, Curr. Opin. Plant Biol. 11 (3) (2008) 266-277.
3. J.P.Vincken, H.A. Schols, R. Oomen, M.C. McCann, P. Ulvskov, A.G.J. Voragen, R.G.F. Visser, Plant Physiol. 132 (4) (2003) 1781-1789.
4. J. Vincken, H. SCHOLS, R. JFJ, A. Voragen, Adv. Pectin Pectinase Res. 47 (2003).
5. K. Waldron, M. Parker, A. Smith, Compr. Rev. Food Sci. Food Saf. 2 (4) (2003) 128-146.

Mads Orla Albæk
Phone: +45 6126 4748
E-mail: maoa@novozymes.com
Discipline Process Technology and Unit Operations
Fermentation Technology

Supervisors: Krist V. Gernaey
Morten S. Hansen, Novozymes A/S
Stuart M. Stocks, Novozymes A/S

Industrial PhD Study
Started: April 2009
To be completed: March 2012

Investigation of the Efficiency of Alternative Enzyme Production Technologies

Abstract
The aim of this industrial Ph.D project is to investigate the efficiency of alternative technologies for enzyme production and evaluate these objectively in a comparison with the existing production platform. The stirred tank reactor is the standard technology for industrial enzyme production; however this may not always be the most economical production technology. In this project the reference process is a submerged fed batch fermentation of the filamentous fungus *Trichoderma reesei*. A model of the reference process is used to compare literature data from promising alternative technologies, which have typically been tested in laboratory scale. Based on the literature screening, the airlift reactor has been selected as a promising alternative. The first experiments have been carried out in a pilot scale reactor.

Introduction
Industrial enzymes are currently mainly produced in fed-batch stirred tank reactors using what might be termed traditional technology. This technology platform is well known since it has been the most popular technology for about 50 years. There have been many attempts to improve the current technology by changing dosing strategy, optimizing impeller design, implementing more advanced control strategies etc. A number of alternative technologies which might replace the current one exist and have been reported in the open literature.

The focus of the project is model based reactor comparison. A detailed process model has been constructed based on experimental data from nine fed-batch fermentations in 550 L pilot plant stirred tank reactors. The process model is used to identify promising alternatives to the stirred tank reactor in combination with a literature screening with focus on mass transfer characteristics of a number of technologies described in the open literature.

The key parameters of the enzyme production were identified as:

- Final protein concentration (g/kg)
- Energy yield (g protein/kWh consumed)
- Productivity (g protein/m^3/h)

Preliminary (and scaled) data for two different industrial scales (80 m^3 and 160 m^3 fermentors) were presented in earlier editions of the Yearbook.

The energy consumption for the enzyme production in the stirred tank reactor is comprised of energy for agitation, aeration, and cooling. In laboratory and pilot scale, the energy consumption for agitation typically constitutes 70%, while aeration and cooling each represent 15% of the total energy consumption. In the literature, largely, the energy for aeration and cooling has been ignored. At larger scale, the situation is however different. In a 300 m^3 vessel, agitation accounts for 44%, aeration for 26%, and cooling for 30% of the total energy consumption [1].

Materials and Methods
Modeling enzyme production
A relatively simple, unstructured model for enzyme production by filamentous fungi has been constructed. The model includes the estimation of the available oxygen mass transfer in the fermenter. The mass transfer coefficient, k_La, is modeled with high accuracy using an empirical equation based on power input unit volume, superficial gas velocity, and apparent viscosity [2]

$$k_L a = 32\left(\frac{P_{broth}}{V}\right)^{0.52} v_g^{0.15}\mu_{app}^{-0.50} \quad (1)$$

The transport model is coupled with a biological model of the growth coupled product formation. The biomass concentration is used to model the increasing viscosity of the fermentation broth.

An uncertainty and sensitivity analysis of the model has shown that the largest uncertainty of the model surrounds the eight biological parameters of the model. The fermentation is carried out as a fed-batch with very low growth rates, which makes estimation of growth parameters difficult.

Reactor comparison

The process model has been applied to alternative technologies using the following approach. For each technology, correlations for oxygen mass transfer preferably performed using non-Newtonian viscous media were inserted in the model. The model was then applied to each technology to up-scale to industrial scale. The up-scaling criteria were equal total oxygen transfer, equal fermentation time, and geometrical similarity. For example, a bubble column described in the literature with an aspect ratio of 4.7 and a liquid height of 2.5 m was up-scaled to a new liquid height of 24.5 m, still with an aspect ratio of 4.7. The process model is then applied to the new vessel size and the energy and substrate consumption are calculated. In addition to the evaluation of the efficiency of each alternative technology, an expert evaluation of the likelihood of technical feasibility in relevant industrial scale was performed.

Pilot scale technology evaluation

Initial experiments have been performed using a modified airlift reactor technology. A 550 L pilot plant stirred tank reactor has been retrofitted to simulate the performance of the airlift reactor. The vessel was a split cylinder airlift reactor with equal area of the riser and the downcomer. The split baffle was perforated which allowed for penetration of fluids to allow for liquid circulation at different liquid heights.

Mixing time was measured using the conductivity method. This method has the advantage of a very low response time of the conductivity probe. Various concentrations of xanthan gum (0, 0.125%, and 0.25%) were used to simulate the non-Newtonian properties of the fermentation medium. The salt pulse used was 400 mL of 0.25% (w/w) NaCl. The pulse was injected within 10 s. Mixing time was determined as the time to achieve 90% mixing. Average numbers of 3 mixing time determinations are used.

Fermentations were performed with the same strain, feed medium, temperature, and pH as the stirred tank reactor fermentations. The fed-batch fermentations were also carried out with the same set point for DOT. The mixing in the airlift reactors was more impaired than anticipated, and the design of experiments thus became non-symmetrical. The varied process variables were head space pressure (0.1 barg, 0.6 barg, or 1.1 barg) and superficial gas velocity (0.03 m/s, 0.04 m/s, or 0.05 m/s).

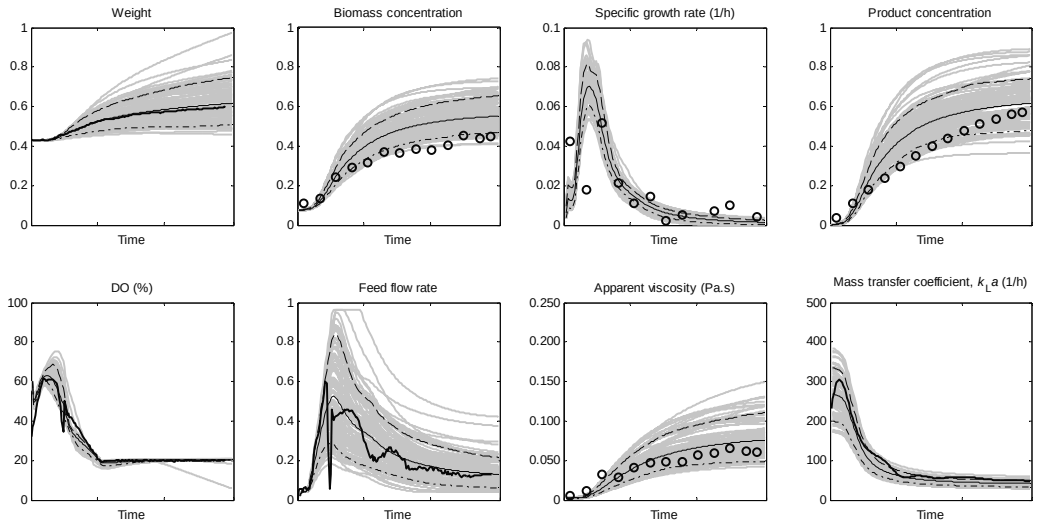

Figure 1. Representation of the model prediction and model uncertainty for weight, biomass concentration, specific growth rate, product concentration, dissolved oxygen, feed flow rate, apparent viscosity, and k_La: Monte Carlo simulations (gray), mean (-), 10^{th} (· -) and 90^{th} (- -) percentile of the predictions as well as the experimental measurements (bold) as shown. The fermentation conditions were: 0.1 kW/m^3, 320 NL/min, and 1.3 barg respectively.

Results and discussion

Modeling of the enzyme production

In Figure 1 a representation is provided of the model prediction and model uncertainty for weight, biomass concentration, specific growth rate, product concentration, dissolved oxygen, feed flow rate, apparent viscosity, and k_La: Monte Carlo simulations (gray), mean (-), 10th (• -) and 90th (- -) percentile of the predictions as well as the experimental measurements (bold) are shown. The fermentation conditions were: 0.1 kW/m^3, 320 NL/min, and 1.3 barg respectively. It is clear, that uncertainty exists in the model outputs. The degree of uncertainty on different outputs is different; e.g. the uncertainties on biomass and product concentration are relatively larger compared with the uncertainty of the prediction of k_La. The mean values of the simulations in Figure 1 overall describe the fermentation process in quite a satisfactory manner. The mean simulated trajectories of weight, specific growth rate, protein concentration, feed flow rate, apparent viscosity and k_La are in fact all very similar to the experimental measurements. The DO is the controlled output and therefore the uncertainty for this parameter is expected to be small. The example shown in Figure 1 is typical for the fermentations performed in this study. On average, the total oxygen transfer of the entire fermentation time is under-predicted by only 13%. A deviation in this order of magnitude is acceptable and within the uncertainty of the model.

Reactor comparison

Selected results of the reactor comparison are presented in Figure 2. If mass transfer is only delivered by static mixers, the efficiency is slightly higher than the reference technology.

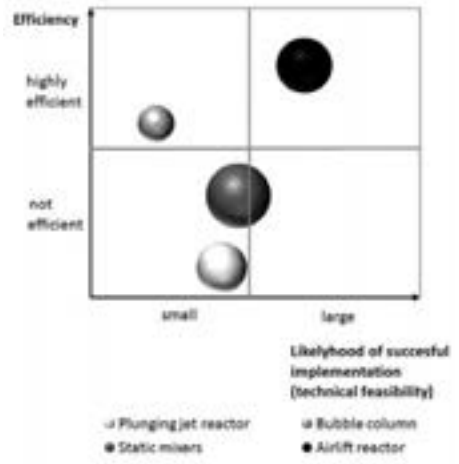

Figure 2. Efficiency (compared to the reference technology) and likelihood of successful. implementation in industrial scale for a number of selected alternative fermentation technologies.

However, the technical feasibility is not yet known, as very little is published in this area. The plunging jet reactor would not be suitable for enzyme production. The efficiency is too low and very high shear rates in the jet nozzle impose a threat to the filamentous fungal growth. Bubble columns are already operated in industrial scale for a range of biological processes. However, mass transfer in bubble columns is relatively low and very large vessel volumes are required. This increases the energy consumption of the air compressor to quite high levels. The airlift reactor seems to have higher energy efficiency and it is also already used industrially in large scale.

Pilot scale airlift evaluation

The airlift reactor had an inner diameter of 0.69 m. This is a larger diameter than most laboratory or pilot scale studies previously published. Figure 3 gives an idea about how large the reactor is.

Figure 3. Top view of the perforated split baffle airlift reactor. The diameter of the reactor is 0.68 m.

The results of the investigations of the mixing time are shown in Figure 4. The xanthan solution of 0.125% is very similar to the typical rheology experiences with fermentation medium (data not shown). The mixing time at 0.03 m/s is 63±8 s. This is a little later than expected, but acceptable at this scale. Mixing time is correlated with liquid velocity, but it was not possible to determine the liquid velocity directly in this study. However, it is seen that mixing time is decreased as superficial gas velocity is increased, which is also expected. At 0.05 m/s the mixing time of the 0.125% xanthan solution is 52±24 s. The large uncertainty is

caused by the fluctuating conductivity measurement. The gas bubbles are non-conductive which gives a high noice to signal ratio, but this is an inherent disadvantage of the method.

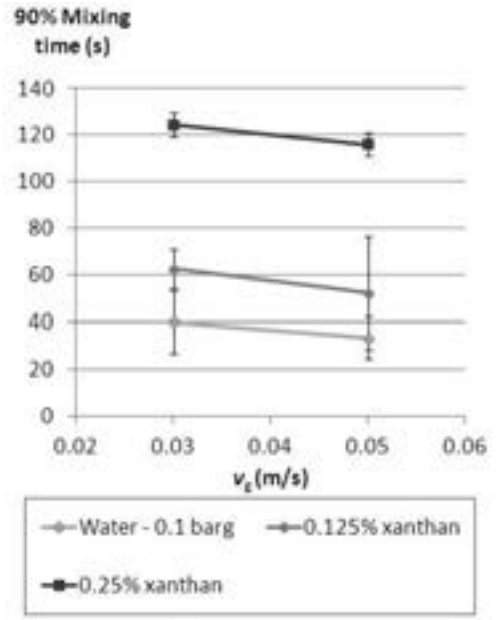

Figure 4. Mixing time measurements using three different media. Each data point is the average of three measurements. The uncertainty of the data is caused by the passage of non-conductive gas bubbles.

Fermentation performance

The initial fermentations of the airlift technology were affected by various technical difficulties. The minimum aeration rate required for sufficient mixing was higher than anticipated. This meant that the design of experiments had to be changed. A related problem meant that the feed rate had to be controlled manually. This meant that comparison with similar fermentations in the stirred tank reactor is not possible.

Conclusions and outlook

A process model has been built that simulates the fed batch process well. The model has furthermore been applied to screen for alternative technologies. Low energy input systems promise a high energy efficiency even at the desired productivity, but require a larger broth volume. The airlift reactor has been identified as a candidate alternative enzyme production technology. The first experimental data suggest that mixing times are less than 60s, which is acceptable at this scale. The reactor will be improved in order to enhance oxygen transfer and mixing, and the final experimental data is to be collected in January 2012. Based on this data, accurate up-scaling of the airlift technology is possible and an objective comparison with the stirred tank reactor is possible.

Acknowledgements

This project is supported by Novozymes A/S and the Danish Industrial PhD Fellowship Programme administered by the Danish Agency for Science, Technology and Innovation.

References

1. NREL, Process Design and Economics for Biochemical Conversion of Lignocellulosic Biomass to Ethanol, Technical Report 5100-47767, 2011.
2. M.O. Albaek, K.V. Gernaey, M.S. Hansen, S.M. Stocks, Biotechnol. Bioeng. 2012 (in press)

Naweed Al-Haque
Phone: +45 4525 2990
E-mail: nalh@kt.dtu.dk
Discipline: Process Technology and Unit Operations

Supervisors: John M Woodley
Rafiqul Gani
Pär Tufvesson

PhD Study
Started: November 2009
To be completed: November 2012

Mathematical Modelling of Two-phase partitioning Biocatalysis Using Solid Resins

Abstract
Biocatalysts (as isolated, immobilized or whole-cell systems) are increasingly being used to assist in synthetic routes to complex molecules of industrial interest. In many cases, the attractive features of higher selectivity and benign reactive operations make it an interesting option. Nevertheless, there are some limitations (inhibition) to biocatalysis which can in some cases be overcome with methods such as controlled release of substrates (*in-situ* substrate supply) combined with *in-situ* product removal (ISPR) using solid resins. In this project, controlled biocatalysis will be studied using a mechanistic model to predict the reactor performance as a basis for process implementation.

Introduction
Biocatalysis is becoming a key tool for organic chemists to synthesize complex reactions. Biocatalytic reactions benefit from benign operating condition, high stereo-, regio- and chemo-selectivity, and more importantly have the potential to enable difficult syntheses to be circumvented [1]. However, when considering the scale-up of bioprocesses, much of the challenge lies associated with substrate/product inhibition at industrially relevant concentrations. An innovative approach can be applied where insoluble (porous) resins are used as a reservoir to supply substrates and remove products simultaneously. This substrate release product removal technology will aid in increasing the productivity and yield of the product. In a parallel project (see page 95), it is being investigated the possibilities of implementing this technology in different reactor configurations at different scale. In this project, a mechanistic models will be developed for guiding the selection of the necessary resin and provide predictions of the performance of this process technology in terms of yield and productivity.

Fundamentals of controlled biocatalysis
This technology will behave such that the resin will act as a 'reservoir' for the substrate and the product. The substrate will slowly diffuse into the solution maintaining an aqueous concentration beneath the inhibitory concentration [2]. The biocatalyst converts the substrate(s) into the required product(s) which can subsequently be recovered by means of *in-situ* product removal (ISPR). At the end of the reaction, the product is eluted from the resin to give a high concentration solution. This therefore represents an innovative way of intensifying bioprocesses, via the combination of controlled substrate supply, reaction and product removal in an integrated unit operation. Figure 1 displays a schematic of the methodology.

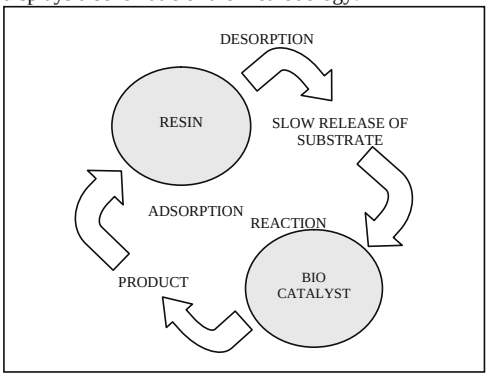

Figure 1: Principle of a resin based ISPR using the slow release mechanism.

Case Study: ω-transamination of acetophenone
To illustrate the methodology, the reaction kinetics of the transamination (TAm) of acetophenone (APH) and

co-substrate 2-propylamine (IPA) to produce (S)-1-phenylethyl amine (PEA) and co-product acetone (ACE) is used. Figure 2 below illustrates the reaction scheme.

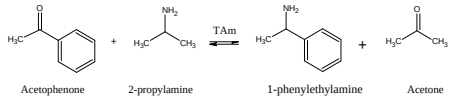

Figure 2: Transamination catalysed by ω-transaminase.

Kinetic Model

The reaction mechanism follows the ping-pong bi-bi mechanism where there is an exchange of amines. However, in this reaction, both substrate and product inhibit the catalytic activity. The kinetic model with the aid of the King and Altman methodology has been expressed in Equation 1 as follows:

$$\frac{d}{dt}[PEA] = \frac{[E_i]\cdot Kcat_f Kcat_r\left([IPA]\cdot[APH] - \frac{[ACE]\cdot[PEA]}{K_{EQ}}\right)}{Kcat_r\cdot K_{APH}\cdot[IPA]\cdot\left(1+\frac{[PEA]}{K_{SPEA}}\right)+ Kcat_r\cdot K_{IPA}\cdot[APH]\cdot\left(1+\frac{[APH]}{K_{SAPH}}\right)+ Kcat_f\cdot\frac{K_{PEA}\cdot[ACE]}{K_{EQ}}\cdot\left(1+\frac{[APH]}{K_{SAPH}}\right)+ Kcat_f\cdot\frac{K_{ACE}\cdot[PEA]}{K_{EQ}}\cdot\left(1+\frac{[PEA]}{K_{SPEA}}\right)+ Kcat_r\cdot[IPA]\cdot[APH]+Kcat_f\cdot\frac{K_{PEA}\cdot[IPA]\cdot[ACE]}{K_{EQ}\cdot K_{PIPA}}+ Kcat_f\cdot\frac{[ACE]\cdot[PEA]}{K_{EQ}}+Kcat_r\cdot\frac{K_{IPA}\cdot[APH]\cdot[PEA]}{K_{PPEA}}}$$

List of abbreviations

$Kcat$	Catalytic turnover [min^{-1}]
$K_{m,i}$	Michaelis constants [mM]
$K_{S,i}$	Substrate inhibition constant [mM]
$K_{P,i}$	Product inhibition constant [mM]
i	Reactants APH, IPA, PEA and ACE

Systematic Methodology for Parameter Estimation

To identify the kinetic parameters of the model, a systematic methodology has been developed as illustrated in Figure 3.

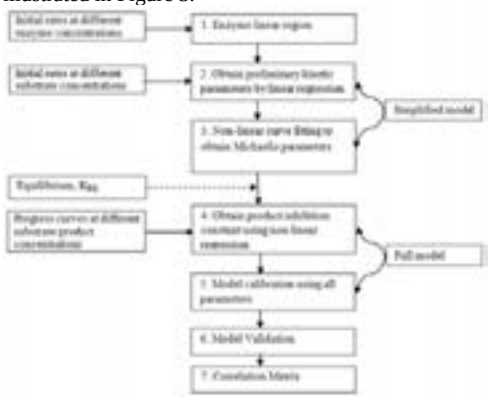

Figure 3: Methodology for kinetic parameter estimation

Results of Parameter Estimation

In the current approach, the linear plotting method along with non-linear regression on both initial rate data and progress curves has been incorporated in the methodology. Although linear plotting includes errors, it is nevertheless quite rational in its use of graphical methods to obtain initial estimates to be used for model calibration. Non-linear regression on the other hand is a quicker method which utilizes all the information from the experiments. However, the existence of the strong correlation between the parameters results in local optima and results in erroneous estimates. Thus a step-wise estimation is used in the current approach which assists in alleviating the risks of obtaining a local minimum such that the parameters are reconciled at every step in order to minimize the estimation errors. The optimized parameter values are shown in Table 1:

Table 1: Estimated parameters

Parameters	Estimated Values	95% CI
Rate Constants [min^{-1}]		
$Kcat_f$	0.05	±0.0001
$Kcat_r$	0.89	±0.002
Michaelis Constants [mM]		
K_{APH}	0.29	±0.007
K_{IPA}	241.15	±2.36
K_{PEA}	3.03	±0.04
K_{ACE}	263.47	±2.21
Substrate Inhibition Constants [mM]		
K_{SAPH}	2.23	±0.03
K_{SPEA}	6.27	±0.02
Product Inhibition Constants [mM]		
K_{PIPA}	0.08	± 0.0006
K_{PPEA}	115.54	± 0.62
K_{PAPH}	208.04	-
K_{PACE}	0.004	-
Equilibrium Constant		
K_{EQ}	0.033	-

The extremely small confidence intervals denote that the estimation of the parameters is quite satisfactory. The data lies within the confidence interval and thus it can be predicted that the uncertainties of the parameter are quite small.

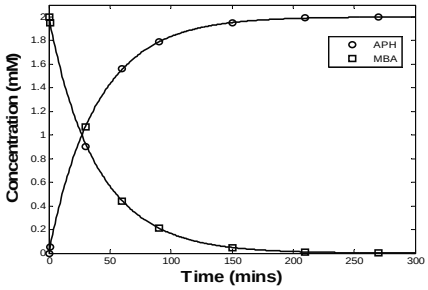

Figure 4: Model verification using the estimated parameters of the model (solid line) and experimental data (symbols). Reaction conditions, E_i = 3.6 g/L, C_{APH} = 0 mM [square], C_{PEA} = 5 mM [triangle], C_{ACE}=1000 mM

Figure 4 shows a comparison of model predictions and experimental data for a second set of reaction conditions. As can be seen, the agreement between the simulated data (solid line) and experimental data (symbols) is very good.

Resin Selection

For the success of this process technology, careful consideration has to be made when screening for a resin. The resin should have a high capacity for both target substrate and product while at the same time is highly selective towards the target product. For the purpose of the economics of the process technology, the resin must be recyclable. The mass transfer rate should be compatible with the rate of reaction in order to optimally use the resin. A systematic methodology to select the resin is illustrated in Figure 4:

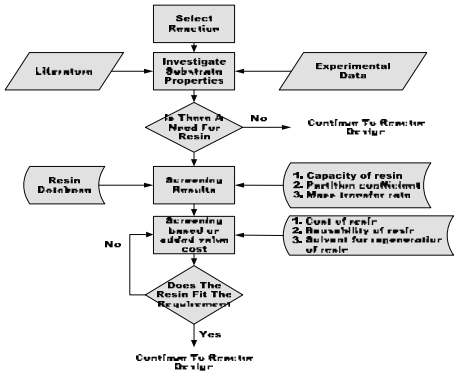

Figure 4: Systematic methodology for screening resin

Resins (Table 2) were tested for their potential to fulfil the selection criteria. All the resins are commercially available and are non-toxic towards the catalyst and stable in the required pH, electrolyte concentration and in the presence of the reactants. The resins differed in surface area, pore diameter and matrix of the resin.

Table 2: Resin properties

Adsorbent	Type	Cost[a] [€/g]	Matrix	Surface Area [m^2/g]	Pore [Å]
MCI gel	CHP20P	1.73	SDB	500	500
Diaion	HP-20SS	1.19	SDB	500	260
Amberchrom	CG300C	1.34	SDB	700	300
Lewatit	VPOC1064	0.23	SDB	800	50
Sepabeads	SP850	0.38	SDB	1000	38
Optipore	L493	0.48	SDB	1100	46
Amberlite	XAD7HP	0.30	A	450	90
Lewatit	VPOC1600	N/A	M	130	150
Combigel	XE305	3.66	SDB	650	--
Polymer	Poly ESDB	0.79	ESDB	650	100
Lewatit	AF5	0.99	C	1200	80

Note: SDB – styrene di-vinyl benzene; A – acrylate; M – methacrylate; ESDB – ethylstyrene di-vinyl benzene; C - carbon

[a]Prices as of December 2011 in Euro listed in sigma-aaldrich assuming purchasing 100 gram of adsorbent

Screening based on 1-phenylethyl amine capacity

The capacity of the resins (mol/kg_{resin}) was measured experimentally. For the resin to be effective, it has to have a high affinity towards the target compound (PEA). The capacity is tabulated in Table 3. As can be the resins with the larger surface area displayed a higher capacity for PEA. However, in the presence of the other reactants, selectivity of PEA over the other compounds is a key point. The selectivity, S is measured using the following equation:

$$S = \frac{\%\text{PEA adsorbed}}{\%\text{C}_i \text{ adsorbed}} \quad (1)$$

where C_i are the other components

The selectivity of PEA over all the other reactants is presented in Table 3. Careful consideration must be taken when screening the resin based on the selectivity.

Table 3: Selectivity of target molecule

Adsorbent	Capacity	Selectivity of PEA		
	[mol_{PEA}/kg_{resin}]	APH	IPA	ACE
CHP20P	1.7	0.18	0.41	1.67
HP-20SS	1.8	0.23	0.88	3.64
CG300C	1.9	0.37	9.55	1.29
VPOC1064	1.8	0.21	0.16	13.10
SP850	2.2	0.20	0.35	Inf.
L493	4.3	0.39	0.94	2.70
XAD7HP	1.7	0.25	0.58	3.34
VPOC1600	1.2	0.24	4.28	0.95
XE305	0.6	0.12	0.34	1.35
Poly ESDB	2.2	0.22	0.44	4.81
AF5	3.4	0.28	2.88	1.97

Screening Based on Partitioning between reactants and resin

The distribution of the different reactants between the resin phase and the aqueous phase was tested for the four candidates selected from previous screening. The isotherms for the different resins either follow L shaped or S shaped curve which is in accordance with adsorption studies done previously for ketones [3] and amino acids [4]. The distributions between the resin and the reactant in the aqueous concentration are very high as shown in Table 4. The partitioning of acetophenone in various aqueous-organic phase systems was measured in a study done previously [5]. The highest partitioning that was achieved was using a 20% v/v mixture of toluene in which it resulted in 191.9. In the same study, the partitioning of PEA in 20% v/v of cyclohexanone in phosphate buffer at pH 7 was measured to be 14.45. Thus comparatively, the solid resin, namely AF5, displayed superior properties than an aqueous-organic phase system (Table 4).

Table 4: Distribution coefficient of the different components in resin-water mixture

Resin	APH	IPA	ACE	MBA
VP OC 1600	12±1	22±9	3±1	39 ± 2
AF5	5405±175	16±1	15±3	85± 3
L493	457±11	29±1	5±1	48± 4
CG300C	49±2	8±2	3±1	43± 3

Based on the superior attributes of the resin AF5, highest capacity for PEA, relatively high selectivity of target compound, PEA over amine donors, IPA and ALA and possibility of high loading of substrate, it was selected to be investigated further. However, the trade-off with using this resin is the affinity of ACE towards the resin was also significant.

Future work

Mass transfer to/from resin

For the optimal rate of supply of substrate acetophenone coupled with the rate of removal of product 1-phenylethylamine, it has to correspond to the rate of reaction at optimal condition (e.g. substrate concentrations, temperature, pH). An optimal rate of supply will result in an aqueous concentration experienced by the catalyst to be within critical toxicity concentration (e.g. the concentration above which 50% or more of the activity is lost). The rate of removal of inhibitory product, 1-phenylethylamine, should equal either the rate of reaction or even higher to ensure that there is no build up of the toxic product in the reaction media. Figure 5 illustrates the operating window for the supply of substrate and removal of product in the presence of the adsorbing resin AF5.

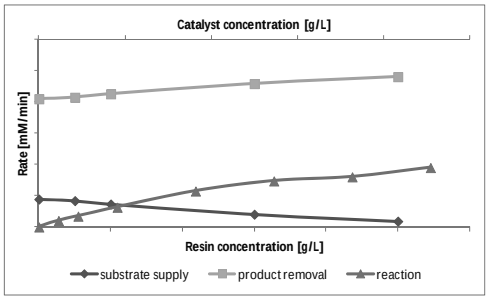

Figure 5: Operating window using resin

From Figure 5, it can be calculated that when using a certain catalyst concentration, the optimal amount of resin that can be used would be at the intersection. At this intersection, the rate of reaction corresponds to the rate of supply of acetophenone and at the same time the rate of removal of 1-phenylethyl amine is high enough.

Re-usability and solvent screening for resins

The economic feasibility of using a resin depends significantly on the number of times the resin can be re-used. Moreover, when the resin is saturated with product, it also needs to be considered what solvent can be applied for eluting the product. It is envisaged that micro packed bed reactors will be designed for this project in order to perform rapid screening of the reusability of the resin (mol_{PEA}/kg_{resin}) and also form the basis for solvent selection. The solvent will be selected on the basis of the partitioning between the product and solvent. The appropriate solvent will assist in optimizing the volume of solvent required for extraction.

Experiments with different scenarios

For the purpose of comparison, it would be very interesting to make a study by testing the reaction in different type of systems – such as single phase system, two phases with fed batch mode and just two phase system. The evaluation of the different systems will assist in the justification of using a two phase reactor design with resins.

Mathematical modelling

The final goal of the project would be to build mathematical models to form a decision making tool. The model would be able to provide predictions of the reactor performance in terms of yield and conversion of the reaction. It is also envisaged that the model can be used for the selection of different *in-situ* product removal techniques and be able to describe different scenarios without the need to invest resources for doing experiments.

Conclusions

With the current research, a mechanistic model will be developed which will incorporate the novel technique of controlled biocatalysis. With the creation of this robust model, the optimal recovery method can be selected. Using this as a basis, a resin selection guide can be created to assist in predicting the appropriate sorbent for the desired system.

Acknowledgement

The author kindly acknowledges Technical University of Denmark and the project AMBIOCAS financed through the European Union Seventh Framework Programme (Grant Agreement no. 245144) for the financial support.

References

1. J.M. Woodley, Trends. Biotechnol. 26 (6) (2008) 321 – 327.
2. P-Y Kim, D.J. Pollard, J.M. Woodley, Biotechnol. Prog. 23 (1) (2007) 74 – 82.
3. I. Hilker, V. Alphand, R. Wohlgemuth, R. Furstoss, Adv. Synth. Catal. 346 (2-3) (2004) 203 – 214.
4. D.S. Grzegorczyk and G. Carta, Chem. Eng. Sci. 51 (5) (1996) 807 – 817.
5. J-K Shin and B-G Kim, Biotechnol. Bioeng. 55 (2) (1997) 348 – 358

Muhammad Waseem Arshad
Phone: +45 4525 2996
E-mail: mwa@kt.dtu.dk
Discipline: Engineering Thermodynamics

Supervisors: Kaj Thomsen
Nicolas von Solms

PhD Study
Started: September 2010
To be completed: September 2013

Thermodynamic Modeling for CO_2 Capture Systems

Abstract
Process simulation of carbon capture processes requires the availability of thermodynamic models for CO_2 capture systems which requires accurate experimental data. The solvent systems used for CO_2 capture are usually aqueous solutions of amines, alkanolamines or their blends, ammonia, amino acids and carbonates. These are electrolyte systems so the thermodynamic modeling of these systems can only be done with electrolyte models. One of the focus in this Ph.D. project is the thermodynamic modeling of CO_2 capture solvent system containing an amines blend of 2-(Diethylamino) ethanol (DEEA) and 3-(Methylamino)propylamine (MAPA). Extended UNIQUAC thermodynamic model for electrolyte systems is planned to be used in this study. Since, this amines blend is a relatively new system and experimental data is very scarce, different types of experimental measurements are also planned to carry out in this work.

Introduction
Carbon dioxide capture by absorption is one of the most common industrial technologies available today and monoethanolamine (MEA), a primary alkanolamine, is a common solvent investigated for CO_2 capture from power plant flue gases. Both primary and secondary alkanolamines are very reactive towards CO_2, form carbamates on reacting with CO_2 and have high heat of reaction. Consequently, the energy consumption is very high during desorption of CO_2 to regenerate the solvent.

Tertiary alkanolamines do not form carbamate with CO_2 and have low heat of reaction. This is due to the sterical hindrance in the reaction between amine and CO_2. Thus as an advantage, low amount of energy is required for desorption of CO_2 in the solvent regeneration process. They generally have high CO_2 loading capacity. The major disadvantage related to these amines is the low reaction rates for CO_2 absorption compared to primary and secondary amines.

A mixture of MEA and methyldiethanolamine (MDEA), a tertiary alkanolamine, has shown a potential to reduce the energy requirements during the solvent regeneration step [1]. 2-(Diethylamino) ethanol (DEEA) is a tertiary alkanolamine and does not form carbamate, and 3-(Methylamino) propylamine (MAPA) has two amine functional groups (both primary and secondary). The motivation of this work is to blend DEEA with MAPA to get optimized solvent with desired properties of fast reaction rate (MAPA), high CO_2 loading capacity and no carbamate formation (DEEA), together with better energy efficiency.

Specific Objectives
The main objectives of this work are as follows:
1. Experimental measurements of freezing point depression (FPD) with and without CO_2 loading, vapour-liquid equilibrium (VLE) and heat of absorption of CO_2 in aqueous binary and ternary solutions of DEEA and MAPA.
2. Thermodynamic modeling of above systems using extended UNIQUAC thermodynamic model.

Experimental Work
Water activity is a key parameter for the amount of water evaporated in the desorber during the solvent regeneration step in CO_2 capture processes. If the water activity is low, less water will evaporate and less energy will be consumed during CO_2 desorption. Freezing point depression data provide accurate water activities and are therefore useful to include in the thermodynamic modeling of the CO_2 capture systems.

Freezing point depression of binary and ternary aqueous solutions of DEEA and MAPA are measured by using modified Beckmann apparatus described by Fosbøl *et al.* [2]. A schematic diagram of the setup is shown in Figure 1. Approximately 5 to 10 gram of sample was taken in the sample glass (C), see Figure 1. The sample glass was then taken into the controlled

temperature ethanol bath (F). Constant temperature was maintained by the cooling jacket (B) which is connected to thermostatic ethanol bath (A). Temperature was lowered down in the sample glass by lowering the temperature in the thermostatic bath to about 5-15 K below the freezing point of the solution in the sample glass. This depends on the concentration of the solution *i.e.* high temperature gradient for high concentration solutions and vice versa. Temperature of solution in the glass sample was recorded by a Pt100 thermometer (G) which is attached to data acquisition unit (H). Once the solution in the glass sample froze, it was taken out and heated up by placing the glass in an ethanol bath at room temperature. When micro ice crystals were left in the solution, the glass was again taken back into the controlled temperature ethanol bath (F) and the procedure was repeated for at least five times. Measurements of freezing point are shown in Figure 2, where vertical lines on the graph represent the freezing points of the solution.

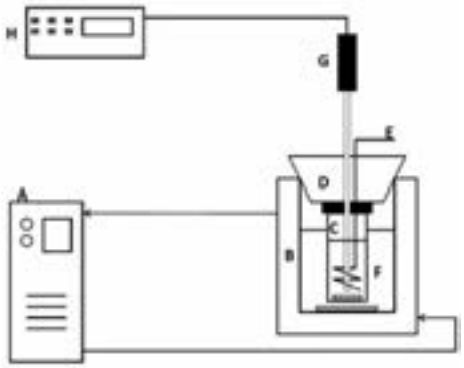

Figure 1: Experimental setup for measuring freezing point. A, Thermostatic bath with ethanol; B, Cooling jacket; C, Sample glass with magnetic stirrer; D, Rubber stopper with sample glass lid; E, Device for manual stirring; F, Controlled temperature ethanol bath with magnetic stirrer; G, Pt100 Thermometer; H, Data acquisition unit.

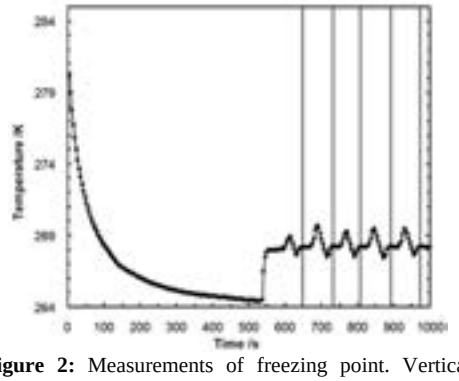

Figure 2: Measurements of freezing point. Vertical lines represent the points at which the freezing points were registered.

Results and Discussion

Experimental results of binary and ternary aqueous solutions of DEEA and MAPA are presented in Figure 2. It can be seen that the measured freezing points on mass percent basis for binary aqueous MAPA are lower than binary aqueous DEEA. Ternary aqueous DEEA-MAPA solutions of different molar ratios also show expected trend of lower freezing points for increasing concentration of MAPA in the mixture and vice versa.

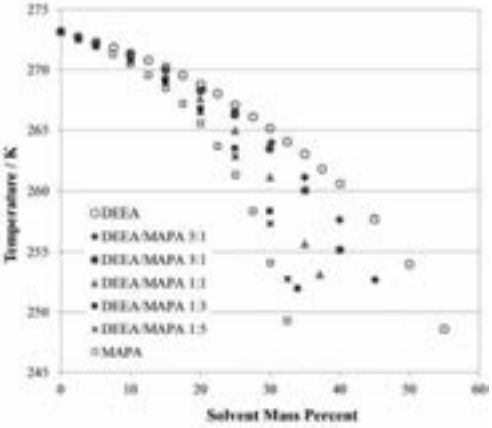

Figure 3: Freezing points of binary and ternary aqueous solutions of DEEA and MAPA. Binary systems; H_2O-DEEA and H_2O-MAPA, and Ternary system; H_2O-DEEA-MAPA with different molar ratios of 5:1, 3:1, 1:1, 1:3 and 1:5 for DEEA/MAPA.

Conclusions

Freezing points are measured for aqueous DEEA and MAPA solutions in a concentration range from 0 to 55 mass percent of solvents. For aqueous solutions of DEEA-MAPA, freezing points are measured for molar ratios of 5:1, 3:1, 1:1, 1:3 and 1:5 for DEEA/MAPA. The measured data can be used for thermodynamic modeling of CO_2 absorption/ desorption system with aqueous blend of DEEA/MAPA.

Acknowledgements

This Ph.D. is a part of iCap project and supported by the European Commission under the 7th Framework Program.

References

1. R. Idem, M. Wilson, P. Tontiwachwuthikul, A. Chakma, A. Veawab, A. Aroonwilas, D. Gelowitz, Ind. Eng. Chem. Res. 45 (2006) 2414-2420.
2. P.L. Fosbøl, M.G. Pedersen, K. Thomsen, J. Chem. Eng. Data 56 (2011) 995-1000.

List of Publications

1. P.L. Fosbøl, R. Neerup, M.W. Arshad, Z. Tecle, K. Thomsen, J. Chem. Eng. Data 2011 (DOI: 10.1021/je200959m)

Deenesh Kave Babi
Phone: +45 4525 2959
E-mail: dkbabi@kt.dtu.dk
Discipline: Systems Engineering

Supervisors: Rafiqul Gani
John M. Woodley

PhD Study
Started: September 2011
To be completed: August 2014

Process Intensification: A Phenomena-based Approach

Abstract
Within the last decade, process intensification (PI) has become a major potential method in the bulk and fine chemicals and pharmaceutical industries by which the overall improvement of a process can be achieved sustainably while improving its overall efficiency (*e.g.* energy efficiency, waste reduction *etc.*). Primarily, PI existed at the unit operations (Unit-Ops) level and currently industry is limited to those intensified Unit-Ops which have been implemented and deemed successful from an industrial perspective *e.g.* reactive distillation, dividing wall columns etc. A systematic synthesis and design methodology for the selection of intensified Unit-Ops for a given process has been developed [1]. However the drawback with this methodology is that it is limited to existing intensified equipment. Therefore the need arises for the further development of a systematic phenomenon-based synthesis and design methodology which not only goes beyond the existing methodology from the Unit-Ops level but also provides the opportunity for the generation of novel intensified equipments. This methodology has been developed by proceeding one fundamental step lower than the Unit-Ops level, this being the phenomena level. The objective of this work is to further expand and enhance the generic nature of the methodology and the creation of a computer-aided tool in order to automatize some of the steps involved when applying the methodology for the intensification of a given process.

Introduction
Process intensification (PI) has been defined as the improvement of an entire process through the enhancement of the involved phenomena in terms of four governing principles [2]: 1) the integration of unit operations (Unit-Ops), 2) the integration of functions, 3) the integration of phenomena and 4) the targeted enhancements of phenomena for a given operation. PI aims to improve processes without sacrificing product quality, by increasing efficiency, reducing energy consumption, costs, volume and waste as well as the overall improvement of plant safety. Recently [1], Lutze et al reported the development of a general systematic synthesis and design methodology incorporating PI at the Unit-Ops level. From this methodology, while process improvements were achieved, the methodology however is limited to pre-defined existing PI Unit-Ops that were retrieved from a developed knowledge base of existing PI equipment. In order to be novel by design that is going beyond the existing PI Unit-Ops one must proceed at a lower level of aggregation, namely the phenomenological level and investigate the underlying driving forces associated with the Unit-Ops level. Starting from the analysis of the underlying phenomena of the flowsheet, the synthesis and design methodology generates a set of process options and reduces that number systematically through several screening steps until the final candidates are optimized in order to find the optimal flowsheet solution.

Objective
The research conducted in this field is primarily within the field of process systems engineering (PSE). The work seeks to further develop a generic synthesis and design methodology and computer-aided software tool for the intensification of processes via a systematic approach. Within the framework all possible flowsheet options are generated and reduced systematically via logical and structural constraints and performance metrics in order to find the optimal intensified flowsheet option.

Methodology
The phenomena-based synthesis and design methodology is presented in Figure 1. The needed information for applying the methodology is either the base case flowsheet design of an existing or conceptual process (recommended) or the input/output

specifications of the existing/conceptual process. In step 1, the synthesis/design problem with respect to PI is defined. In other words the objective function is defined and the constraints together with the constraints that must be fulfilled along with the process scenario (batch or continuous), process and product specifications (raw materials, reactions *etc.*) the performance metrics (operating and capital cost, energy consumption *etc.*) for the evaluation of generated options must be selected. These are then translated into operational and performance metrics.

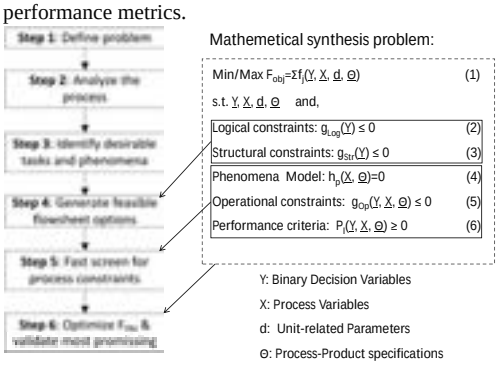

Figure 1 Phenomenon-based Process Intensification (PhenPI) Methodology [3]

In step 2, all process data, e.g. mass and energy balances necessary for the complete understanding of the process is collected. This data can be generated from various tools (steady state simulators: PROII, ASPEN *etc.*). This data is then used for the identification of limitations/bottlenecks together with their accompanying phenomena within the process using different tools (knowledge based search (KBS), analysis of pure component properties [4] *etc.*). This provides insight on which phenomena can be intensified within the process. In step 3, the identified limitations/bottlenecks are used for the identification of desirable phenomena for overcoming the identified limitations/bottlenecks in step 2. In step 4, all phenomena, including those identified for overcoming the undesirable phenomena in step 3, are interconnected to form simultaneous phenomena building blocks (SPB's). Using the SPB's the number of stages and their interconnections (co-current, counter current *etc.*) are determined using an extended Kremser method. This allows the identification of generic superstructures retrieved from a model library which are then subsequently screened by operational and performance metrics (Eq.2-3) for example if only counter-current flow is considered for a given design. In step 5, all remaining PI options are further fast screened using operational and performance metrics for example product yield, energy consumption/kg of product *etc.* The remaining options are then transformed to units using rules, algorithms and knowledge of the construction of existing Unit-Ops. These are then screened by operational constraints as well as performance metrics for example volume *etc.*, at the Unit-Ops level. In step 6 the Unit-Ops that are obtained from step 5 are then optimized by solving a NLP optimization problem to find the optimal intensified flowsheet option and can be further validated via rigorous simulation.

The current methodology has been applied to the production of iso-propyl acetate (IPA) and hydrogen peroxide (H_2O_2).

Conclusion

In conclusion an overview of the phenomena based synthesis and design methodology has been presented. The methodology provides a systematic approach, via a decompositional method, for the intensification of processes. The improvement of the process can be classified into key areas: process efficiency, energy consumption, plant costs, overall plant volume, waste generated, and plant safety. The methodology seeks to systematically use existing plant data for the representation of the flowsheet at the phenomena level. At this level of aggregation limitations/bottlenecks can be identified and the phenomena that overcome these limitations/bottlenecks can then be identified. Phenomena can then be combined to form stages which can be combined to form floswheets. These flowsheets can then be screened to find those flowsheets which provide the highest benefit with respect to operational constraints and performance metrics and these are then further optimized to find the optimal intensified flowsheet.

Current and Future Work

The future work of this PhD project will be the enhancement of the methodology's generic nature by its application to further case studies coupled with the development of a computer-aided tool for the automation of some of the steps involved in the methodology. Currently the methodology is being applied to the production of methyl-acetate. This case study will also be compared to the task based process intensification methodology originally proposed by Sirrola *et al* [5] in order to provide a comparison between the two methodologies.

References

1. P. Lutze, R. Gani, J.M. Woodley, Comp. Chem. Eng. 36 (1) (2012), 189-207
2. P. Lutze, R. Gani, J.M. Woodley, Chem. Eng. Proc. 49 (6) (2010) 547-558
3. P. Lutze, D.K. Babi. J.M. Woodley R. Gani, Phenomena-based Process Synthesis and Design to achieve Process Intensification, International Symposium on Process Systems Engineering, (2012) to be published
4. L. D'Anterroches, R. Gani, Fluid Phase Equilib. 228-229, 141-146.
5. J.J. Siirola, Adv. Chem. Eng., 23 (1) (1996), 1-62

Frederikke Bahrt
Phone: +45 4525 6809
E-mail: frbah@kt.dtu.dk
Discipline: Polymer Technology

Supervisors: Anne Ladegaard Skov
Søren Hvilsted
Anders E. Daugaard

PhD Study
Started: August 2011
To be completed: August 2014

Development of New Materials for Dielectric Electro Active Polymers as Actuators and Generators

Abstract
Dielectric electro active polymers (DEAPs) can be used as actuators, generators and sensors. Polydimethylsiloxane (PDMS) networks are one of the most utilized polymer materials for DEAP applications due to its naturally high capacitance, high efficiency and fast response. This works aims at developing new PDMS networks through the design of novel cross-linkers which could lead to improved material properties through the incorporation of chemical functionality into the cross-linking points. Such novel cross-linkers could also be exploited in a one-step creation of bimodal PDMS networks and in surface functionalization of PDMS films.

Introduction
Dielectric electro active polymers (DEAPs) are polymeric network systems that can be used to convert an electrical input to mechanical deformation of a polymer. DEAPs can be applied as actuators, sensors and generators due to their ability to exhibit a change in size and shape when an external voltage is applied as well as generate electrical energy when the material is exposed to mechanically induced deformations. DEAPs are normally constructed from thin filled elastomer films with compliant electrodes on each side. Polydimethylsiloxane (PDMS) is one of the most used materials due to its natural high capacitance and good thermal stability, long lifetime, high efficiency and fast response [1]. PDMS is usually cross-linked with a platinum catalyst via the hydrosilylation addition reaction as illustrated in Figure 1.

Specific Objectives
The aim of this work is to design new PDMS networks applicable as DEAPs. One of the most important factors for DEAPs is the capacitance and the development of novel materials is focused on increasing this while still maintaining good mechanical properties.

As PDMS has been used for DEAP applications with good results, it is of interest to do material optimization at the PDMS network cross-linking points as modification of this part of the network could lead to enhanced material properties. This could for example be by stabilization of integrated filler particles that could lead to an increased dielectric permittivity and thereby an increased material capacitance.

Design of novel cross-linkers that could allow for incorporation of selected moieties into the cross-linking points of the PDMS network could also be used as a tool to visualize the cross-linking distribution and density. This could be done by labeling the potential cross-linker with a flourophore that would cause the material to be florescent in *e.g.* a fluorescent microscope.

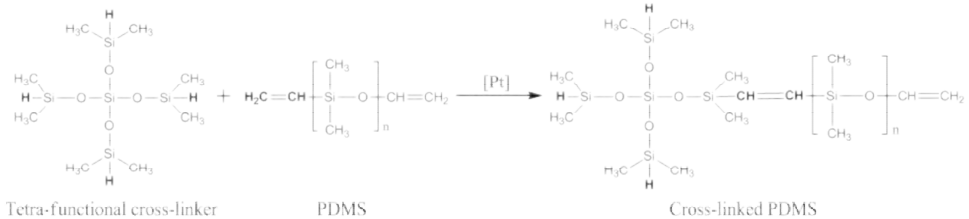

Figure 1: PDMS hydrosilylation addition reaction with a tetra-functional cross-linker to form a PDMS network.

Results and Discussion

The novel cross-linkers should be constructed to allow multiple reactions to occur selectively through orthogonal reactions. The first approach is focused on cross-linkers for PDMS for use in hydrosilylation reactions. In addition to the silanes, a functional group that will allow for chemical modifications and incorporation of an additional functionality through "click" chemistry is envisaged.

An example of a molecule that could be used to prepare such cross-linkers is the readily available glucoside, methyl-α-D-glucopyranoside shown in Figure 2.

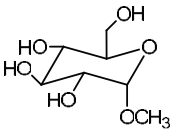

Figure 1: Methyl-α-D-glucopyranoside, a possible cross-linker for PDMS network optimization.

This molecule contains four hydroxyl groups, three secondary and one primary which provides the necessary chemoselectivity. For the cross-linking, more than 2 reactive groups is necessary, therefore the silanes would in this case be introduced via the secondary alcohols. This will permit the primary hydroxyl group to be converted into an azide which provides a possibility to do so called "click" reactions i.e. reactions between an azide group and an alkyne group, that forms 1,4-disubsituted-1,2,3-triazoles [2,3] as seen in Figure 3.

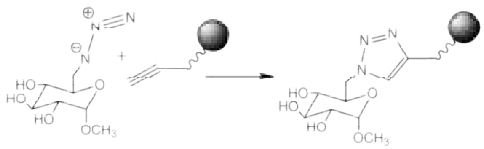

Figure 2: "Click" reaction between an azide group on the glucoside cross-linker and an alkyne group with the desired functionality to be incorporated in the PDMS network.

If the functionalized cross-linker seen in Figure 2 is subsequently used to create a PDMS network, the functionality seen as a sphere in Figure 2 is now incorporated into the material as seen in Figure 4, with a consequent possible improvement of material properties.

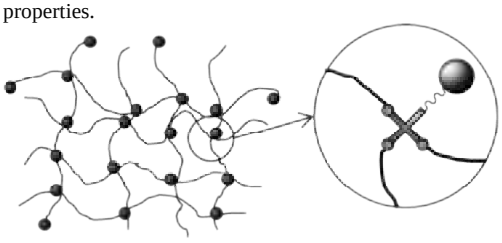

Figure 3: PDMS network with cross-linker and incorporated functionality.

Many types of potential cross-linkers for PDMS networks could be designed as long as the concept of the orthogonal chemistry is preserved. However, when designing new cross-linkers, one needs to consider factors such as ease of chemical modification, number of cross-linking sites (>2) and miscibility with PDMS.

The design of novel cross-linkers for PDMS network formation could also allow for a number of other possible applications than the ones previously mentioned. This could for example include a cross-linker that could selectively add short or long PDMS chains, and in this way bimodal networks of PDMS could be created in a one step reaction. Another possibility is to design a highly activated cross-linker *i.e.* a cross-linker with a low surface energy group attached. When mixed with PDMS, this cross-linker will migrate to the surface of a formed film and hereby create a higher concentration of cross-linker on the surface. This allows for surface functionalization of PDMS films which could change the surface properties drastically without changing the bulk properties. This could for example be relevant for processing issues.

Conclusions

When developing novel materials for dielectric electro active polymers, material optimization can be done by designing new cross-linkers for the PDMS network formation. This could lead to improved material properties by incorporation of selected moieties into the cross-linking points. This could for example be filler particles that would increase the capacitance of the material. Design of new cross-linkers could also lead to a one step creation of bimodal networks and a surface functionalization of PDMS films.

Acknowledgements

The author wishes to acknowledge the Danish National Advanced Technology Foundation for financial support.

References

1. R. Pelrine, R. Kornbluh, Q. Pei, J. Joseph, Science 287 (2000) 836-839.
2. M. Meldal, C.W. Tornøe, Chem. Rev. 108 (8) (2008) 2952-3015.
3. W.H. Binder, R. Sachsenhofer, Macromol. Rapid Commun. 29 (2008) 952-981.

Muhammad Shafique Bashir
Phone: +45 4525 2853
E-mail: msb@kt.dtu.dk
Discipline: Reaction and Transport Engineering

Supervisors: Kim Dam-Johansen
Peter Arendt Jensen
Flemming Frandsen
Stig Wedel

PhD Study
Started: September 2008
To be completed: March 2012

Characterization and Quantification of Deposit Build-up and Removal in Straw Suspension-Fired Boilers

Abstract
Biomass (straw and wood) has been used in Denmark with an increasing trend in the last two decades, and by the end of 2009, there were 8 biomass and 5 biomass co-fired power plants. However, the use of biomass, especially straw, constitutes a serious technical challenge of ash deposit build-up due to the presence of large amounts of alkali metals and chlorine (Cl) in straw ash. The aim of this project is to investigate ash deposition and deposit removal (shedding) in straw suspension-fired boilers and to provide recommendations for the optimal operation strategy of boilers with respect to minimization of deposit related problems. In this regard, a series of full-scale measurements were conducted in different straw and/or wood suspension-fired boilers. It was found that ash deposition rate increases with increased straw share when co-firing with wood and with increasing flue gas temperature, but probe surface temperatures have no significant influence on the measured ash deposition rates. It was also observed that deposit shedding primarily take place by debonding, when a complete layer of deposits detached from the probe surface. The results of artificial deposit removal tests showed that the deposits of less than 91 h exposure time formed at 500 ^{o}C were easy to remove and the PIP (Peak Impact Pressure) needed was less than 55 kPa. However, at 600 ^{o}C probe surface temperature, the PIP needed to remove the deposits increased significantly.

Introduction
Utilization of biomass in power plants is an attractive option to lower CO_2 emissions and to make the energy supply independent of fossil fuels. However, the use of biomass, especially straw, constitutes a serious technical challenge due to the presence of large amounts of alkali metals and chlorine (Cl) [1, 2] that may induce large operational problems due to boiler ash deposition [3]. Strategies to handle ash deposit related problems include leaching of potassium (K) from fuel, inhibition of sintering, use of additives to chemically capture potassium (K) and use of effective deposit shedding techniques [1-3].

Some full-scale experimental studies on deposit build-up and removal have been reported on measurements in grate-boilers. However, most suspension-fired boilers have a better electrical efficiency (46-48 %) than traditional grate-fired systems (25-30 %), but only limited ash deposition data is available from biomass suspension-firing [1-3]. Quantification of deposit build-up and removal in biomass suspension-fired boilers is an area where relatively limited accurate knowledge is available, and improved knowledge on the transient ash deposit formation and removal is wanted to optimize design and operation [1, 2]. In addition, the available full-scale measurements were performed with short testing time, while more extensive full-scale measurements are rare to find [1, 2]. Therefore, more detailed and extensive full-scale studies on transient deposit formation and shedding when firing straw and wood will improve our understanding of boiler ash deposit formation and removal processes.

Specific Objectives of the Project
- Characterization and quantification of deposit build-up and removal in both the boiler chamber and the superheater region.
- Investigation of the influence of boiler load, operation conditions and fuel changes (straw, wood) on ash deposition and removal rate in the boiler chamber and superheater region.
- To provide a model based description of the influence of fuel and boiler operation changes on the deposit formation and removal rate.

Full-scale Experimental Studies

A series of full-scale measurements were conducted in a straw and wood suspension-fired boiler. The aim of the measurements was to provide long time, full-scale data on deposit formation in a 350 MW_{th} suspension-fired boiler. Furthermore, an analysis was carried out, giving quantitative information about deposit formation rates as functions of operating conditions. The influence of fuel type (straw share in wood), probe exposure time, probe surface temperature (500-600 ^{o}C) and flue gas temperature (600-1050 ^{o}C) on ash deposit formation rate and deposits removed were investigated.

Ash deposit build-up

The amount of deposit collected on the probe is a function of both the deposit formation process and shedding events, and the true deposit formation rate (g/m^2/h) cannot be accurately determined, but based on the measured deposit mass increase divided by a given time, the integral deposit formation rate (IDF-rate) or the derivate-based deposit formation rate (DDF-rate), calculated by taking the time derivative of the deposit mass uptake in-between two macro shedding events (see [1, 2] for more details). Some results of the ash deposit formation rates shown in Figure 1. A straight line limit below which the majority of data lies is shown, but clearly a large spread is evident. It can be seen that the DDF-rate increases with increased straw share in wood and with increase in flue gas temperature, but probe surface temperatures have no significant influence on measured DDF-rates. IDF-rates also showed increasing trend with increased K content in the fuel, and with increase in flue gas temperature, but probe surface temperatures have no significant influence on IDF-rates.

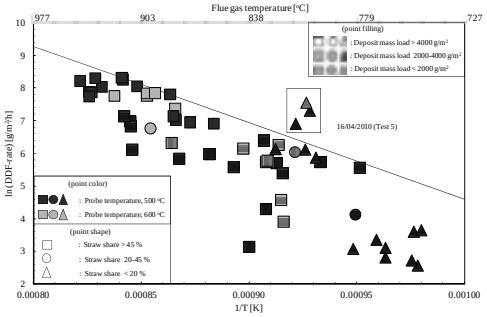

Figure 1: Logarithm of the DDF-rate as a function of reciprocal of absolute flue gas temperature.

Deposit Shedding

The needed Peak Impact Pressure (PIP) of the sootblower jet to remove the probe deposits at different probe conditions was investigated and the results for a probe surface temperature of 500 ^{o}C are summarized in Figure 2. It can be seen that the deposits of less than 91 h probe exposure time formed on a 500 ^{o}C probe could be removed with a PIP of less than 55 kPa. However, it was also found that with an increase in probe surface temperature from 500 ^{o}C to 600 ^{o}C, the PIP needed to remove the deposits significantly increased. The higher probe surface temperature can possibly cause partial melting of the innermost deposit layer (rich in K, Cl and S) and enhance the adhesion strength between the deposit and the superheater tube.

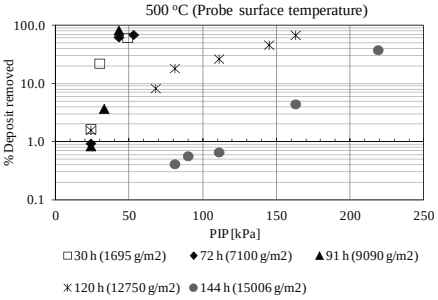

Figure 2: Percentage of deposits removed as a function of applied PIP at probe surface temperature of 500 ^{o}C for different exposure times and deposit mass loads.

Conclusions

- The bulk chemical composition of straw and wood suspension-firing fly ash shows relatively higher contents of Si, Ca, and lower contents of volatile elements (K, Cl and S), compared to grate-firing conditions.
- The DDF-rate increases with increased straw share in wood and with increase in flue gas temperature, but probe surface temperatures have no significant influence on the measured deposition rates.
- PIP needed to remove the deposits increased with increase in probe surface temperature from 500 ^{o}C to 600 ^{o}C. At lower temperatures (< 500 ^{o}C), deposits with exposure time less than 91 hours could be removed with a PIP of less than 55 kPa.

Acknowledgement

The financial support by Energinet.DK under the PSO project 7217 and financial support by Vattenfall A/S is gratefully acknowledged.

References

1. M.S. Bashir, P.A. Jensen, F. Frandsen, S. Wedel, K. Dam-Johansen, J. Wadenbäck, S.T. Pedersen, Fuel Process. Technol. (submitted).
2. M.S. Bashir, P.A. Jensen, F. Frandsen, S. Wedel, K. Dam-Johansen, J. Wadenbäck, S.T. Pedersen, Energ. Fuel. (submitted).
3. F.J. Frandsen, Ash formation, deposition and corrosion when utilizing straw for heat and power production. Doctoral Thesis, Technical University of Denmark. 2011, ISBN 978-87-92481-40-5.

Andreas Baum
Phone: +45 4525 2943
E-mail: aba@kt.dtu.dk
Discipline: Enzyme Technology

Supervisors: Jørn D. Mikkelsen
Max Egebo, FOSS Analytical

Industrial PhD Study
Started: June 2010
To be completed: May 2013

Rapid Near Infrared Spectroscopy for Prediction of Enzymatic Hydrolysis of Corn Bran after Various Pretreatments

Abstract
Efficient generation of a fermentable hydrolysate is a primary requirement in the utilization of fibrous plant biomass as feedstocks in bioethanol processes. In the present study we demonstrate the use of diffuse reflectance near Infrared spectroscopy (NIR) as a rapid and non-destructive analytical tool for evaluation of pretreatment effects on destarched corn bran. NIR was used to achieve classification between 43 differently pretreated corn bran samples using Principal Component Analysis and hierarchal clustering algorithms. Quantification of the enzymatically released monosaccharides by HPLC was used to design multivariate calibration models (biPLS) on the NIR spectra. The models could predict the enzymatic release of different levels of arabinose, xylose and glucose from all the differently pretreteated destarched corn bran samples, thereby potentially replacing the cumbersome HPLC analysis.

Introduction
In the present work, NIR spectroscopy has been applied to evaluate differently pretreated samples originating from corn bran, an agro-industrial residue from corn starch processing [1, 2]. Corn bran represents a complex and recalcitrant biomass stream particularly rich in C-5 carbohydrates mainly present as the structural polysaccharide arabinoxylan, which constitutes approximately 56% of the dry matter [1]. Corn bran also contains significant amounts of cellulose and is therefore an interesting substrate for enzymatic biomass conversion into readily available monosaccharides.

Objectives
The aim of the study was to examine the potential for employing NIR spectroscopy and chemometrics to predict the efficiency of different pretreatments on enzymatic degradation of corn bran.

The spectral data originating from corn bran samples after various pretreatments were compared to results of enzymatic hydrolysis obtained by HPLC analysis of enzymatically released monosaccharides. It was hypothesized that, i) NIR spectroscopy can hierarchically distinguish insoluble corn bran according to pretreatment conditions and ii) that the extent of enzymatic hydrolysis of corn bran after a particular set of pretreatment conditions can be predicted from the insoluble corn bran's NIR spectra.

Methodology
Destarched corn bran after various pretreatments was used as substrate in all enzymatically catalysed conversions and all NIR spectroscopy measurements. The material was milled and enzymatically destarched with α-amylase and amyloglucosidase prior to all pretreatments, measurements and hydrolysis experiments. Pretreatment conditions were categorized into five different set ups (A-E) as described in Table 1.

Table 1: Group assignment of samples according to pretreatment conditions

	pH		Temp (°C)		Time (min)	
	average	interval	average	interval	average	interval
A[1,2]	-	-	-	-	-	-
B[2]	4.2	4.2-4.2	190.0	190-190	10.0	10-10
C	5.8	1.7-9.8	125.0	100-150	65.0	10-120
D	1.5	0.9-2.1	150.0	150-150	32.0	5-65
E	3.8	1.8-9.1	143.8	125-150	187.5	120-240

[1] powders with different particle size due to milling [2] no pretreatment

Results and Discussion
All NIR spectra showed different absorbencies concerning different NIR vibration regions (Figure 1). In addition the figure also shows the spectra of four polysaccharide standards namely, *e.g.*, water-insoluble arabinoxylan (blue), water-soluble arabinoxylan (red), xylan (cyan) and cellulose (green).

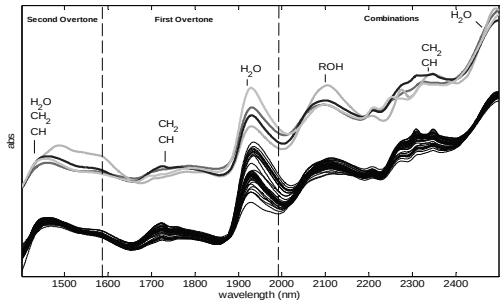

Fig. 1: NIR spectra (incl. colored Polysaccharide Standard spectra)

Strong absorbencies due to moisture appeared at 1950 nm, 2450 nm and less intensely around 1450 nm (Figure 1). Carbohydrate bands could be identified for CH_2 and CH between 2300-2400 nm due to combination bands, at 1700-1800 nm due to first overtone and around 1400-1500 nm due to second overtone bands, respectively

Classification

The spectra were MSC pretreated followed by mean-centering. All 43 samples were considered for PCA Analysis and hierarchal classification based on the PCA scores.

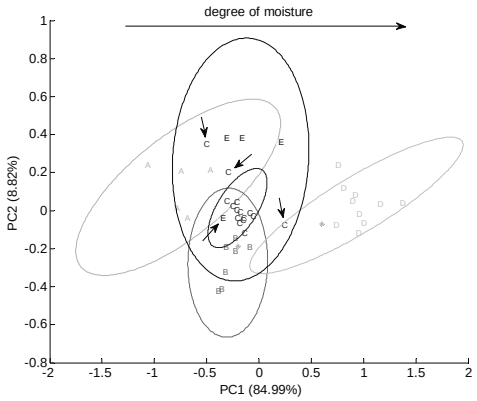

Fig. 2: PCA score plot colored due to pretreatment grouping

The PCA decomposition showed that 11 Principal Components (PC) were necessary to explain the significant variance in the spectra. The number of Components could be reduced to 5 by excluding the spectra of group D (harsh acidic pretreatment) thus indicating that those samples were least comparable to the rest of the groups.

Since water has a high impact on NIR spectra the scores especially along PC1 were highly affected by the water content of the samples as illustrated in Figure 2. The interpretation of the first PCA loading showed that different amounts of moisture in the powder samples imply high leverage on the PC1 scores. Thus the spreading of group A samples, which occurred mainly along PC1, can be explained by large variations of moisture content of the samples.

Two samples from group A (marked with stars in Figure 2) were excluded from the cluster as outliers. Group D samples revealed the highest amount of moisture. In group C there was also one sample which indicated a very high amount of moisture, but this sample has not been identified as an outlier due to the following interpretation using a dendrogram.

Finally it was noted that hierarchal clustering enabled strong classification power along the different sample sets. Especially by interpreting the dendrogram (Figure 3) it was found that four samples were rather clustered to a foreign group. Those samples 6, 9, 10 and 40 have been highlighted with arrows in Figure 3 and recolored according to the groups which they rather belong to. The reassignments could be confirmed by examining the pretreatment parameters of those samples. Sample 40 was pretreated at a pH comparable to that from group C. Thus it can be seen that pH has a strong influence on the NIR spectra and therefore on the carbohydrate composition as described previously in [2].

The findings show that PCA in combination with hierarchal analysis is perfectly suitable for discriminating between the different kinds of pretreatment. Further Discriminant Analysis methods as Linear Discriminant Analysis (LDA) [3] or Partial Least Squares Discriminant Analysis (PLSDA) [4] can be used to establish intelligent instrumentation devices with implemented pattern recognition. At this point such kind of study was beyond the scope of the present work.

Multivariate prediction models for enzymatic hydrolysis using biPLS

PLS models were calibrated for prediction of enzymatic release of glucose, xylose and arabinose using HPLC data from the hydrolyzed samples on the MSC and mean centered NIR spectra of the pretreated material before hydrolysis. Only samples from Groups A, B, C and E were considered for the PLS calibration (Table 1) due to outlying characteristics of groups D as discussed earlier. To highlight the most informative spectral regions iPLS and biPLS regression were applied, respectively. BiPLS generated better model performances and is therefore the only method considered in the following. The associated modeling performance of biPLS in comparison to PLS on the whole NIR spectra is illustrated in Table 2, where also additional important parameters as RMSEC, RMSECV and regression coefficients R^2 are stated.

Table 2: Modeling parameters

	RMSECV (%)		R^2		number of LVs	
	full spectra	biPLS	full spectra	biPLS	full spectra	biPLS
arabinose	3.12	1.39	0.82	0.96	7	6
xylose	1.16	0.77	0.95	0.98	3	3
glucose	8.68	5.69	0.84	0.93	5	5

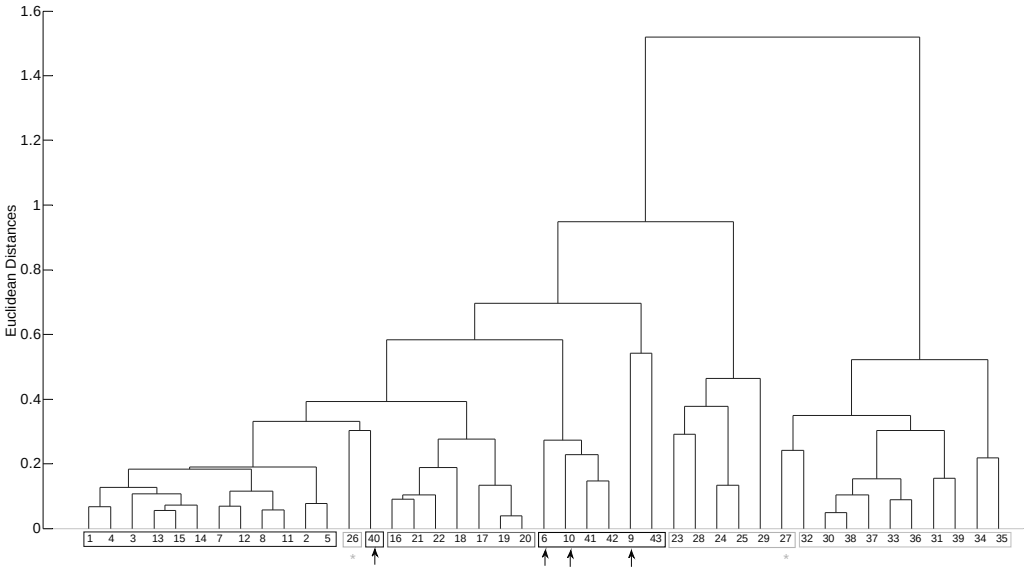

Fig. 3: Hierarchal clustering using a dendrogram

To emphasize the actual underlying chemistry due to the monosaccharide content selected spectral regions have been cut out and pretreated separately.

As an example Figure 4d presents the spectral region from 2172-2272 nm which was highly significant for total arabinose content. Looking at this selected interval it was clearly visible that there were trends in spectra in relation to the total amount of arabinose being present in the pretreated DCB samples.

Additionally it is remarkable that samples with high glucose amounts showed exceptionally strong absorbencies in the second overtone regions around 1600nm, which are highly influenced by cellulose bands, as it can be seen from the cellulose standard spectrum in Figure 1.

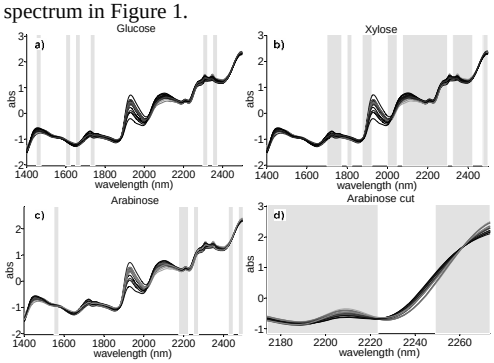

Fig. 4: Selected spectral intervals using biPLS highlighted in grey. xylose (a) glucose (b) and arabinose (c). Spectral range from 2172-2272 nm is cut out to emphasize underlying arabinose bands (d).

The spectral regions have been selected by biPLS. Finally one can state that the spectral regions selected for multivariate calibration can be interpreted in agreement with earlier discussed spectral features of the measured commercial polysaccharide standards. This result emphasizes that interval selection in combination with PLS is suitable for highlighting chemical information about arabinose, glucose and xylose in the NIR spectra. Accordingly strong support for multivariate modeling of monosaccharide content can be ascertained.

All spectral intervals which were selected for the calibration of PLS prediction models are shown in Figure 4. Spectrum color indicated the extent of enzymatic release concerning each monomer (black indicates low releases, light-blue high releases) measured by HPLC. Out of the three monomers in question xylose was modeled with the best performance since it had the highest abundance in DCB as reported in [1]. Meanwhile biPLS also showed that xylose modeling performance could not be improved by leaving rather many segments out as it could for arabinose and glucose. All three models could be improved by leaving out spectral segments with strong water absorbencies due to moisture.

The leave-one-out cross validated result of the biPLS calibration models for arabinose, xylose and glucose are shown in Figure 5.

Results have also been validated by leaving out subgroups while calibrating the models which did not decrease model performance significantly. Poorest performance was reported for the model of glucose release after hydrolysis. This might be influenced by two factors. First, the content of total glucose monomers is lower compared to that of arabinose and xylose [1].

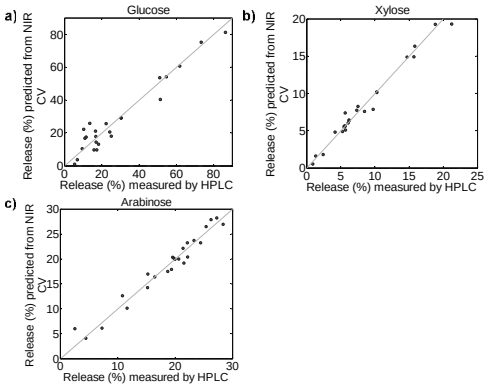

Fig. 5: Cross validated prediction of enzymatic release of xylose (a), glucose (b) and arabinose (c) from NIR vs. measured Monomer Release by HPLC after hydrolysis

As mentioned earlier the spectra were generally best described by the standard spectrum of insoluble arabinoxylan and therefore the crucial information about the glucose monomers in the biomass may be hidden behind the higher content of arabinoxylan constituents. Secondly, differences in glucose origin from either crystalline or amorphous cellulose might also be speculated to interfere with the modeling as crystalline cellulose is more difficult to hydrolyse than amorphous. However previous studies on crystalline lactose [5] have shown that NIR is capable of differentiating between both species.

Conclusion

Two major hypotheses were tested and confirmed in this study. First it was possible to enable classification between the different pretreatments of the DCB samples. It was shown that NIR spectroscopy is a powerful non-destructive tool for rapid evaluation of the pretreatment process. Hence, both of the hypotheses set up for the study were found to be valid, and this offers remarkable potentials for fast screening and evaluation of the effects of biomass pretreatment. Since NIR can also be used to measure suspensions further studies can be carried out measuring NIR spectra even during the pretreatment process and therefore examine the effect of pretreatment time-resolved. This will give valuable information about optimization parameters and thereby enhance monosaccharide release and reduce the process cost. In addition the method is highly suitable for detection of outliers, can be utilized using discriminant analysis and implemented within intelligent instrumentation.

Furthermore, by means of sophisticated chemometric methods it has been demonstrated that the monosaccharide release of the pretreated material can be predicted quantitatively from the solid pretreated DCB samples directly without need for the enzymatic hydrolysis itself. Thus once having a quantitative calibration model established there is no demand for the reducing sugar and HPLC analysis to determine the monosaccharide release or composition of the biomass polymer. The explicit effects of the different pretreatments can be assessed rapidly and reliable.

Industry has not recognized the great potential of NIR spectroscopy yet as a fast and reliable method eminently suitable for high-throughput screening and online monitoring tasks in carbohydrate analytics. The exploitation of this generic method could be extended to a range of biomass feedstocks, using both high throughput and/or On-Line analyses of the pretreatments as well as the enzymatic hydrolysis data. With proper multivariate calibration NIR methodology can be developed further to directly predict enzymatic susceptibility of pretreated biomasses.

Acknowledgement

This work was partially financed by the 7th Framework Programme via the Marie Curie Initial Training Network, LeanGreenFood.

References

1. J. Agger, A. Vikso-Nielsen, A.S. Meyer, J. Agr. Food Chem. 58 (10) (2010) 6141-6148.
2. J. Agger, K.S. Johansen, A.S. Meyer, New Biotechnol. 28 (2) (2011) 125-135.
3. A. Baum, Y. Lu, Z. Muccio, G.P. Jackson, P.B. Harrington, Spectroscopy 25 (2) (2010) 40.
4. Z. Yang, H.Q. Ren, Z.H. Jiang. Spectrosc. Spec. Anal. 28 (4) (2008) 793-796.
5. L. Norgaard, M.T. Hahn, L.B. Knudsen, I.A. Farhatc, S.B. Engelsen. Int. Dairy J. 15 (12) (2005) 1261-1270.

Vijaya Krishna Bodla
Phone: +45 4525 2960
E-mail: vikb@kt.dtu.dk
Discipline: Process Technology and Unit Operations

Supervisors: Krist V. Gernaey
John M. Woodley
Ulrich Krühne

PhD Study
Started: March 2011
To be completed: February 2014

Integrated Microfactories for Enzyme production

Abstract
This project aims to demonstrate for the first time that fermentation and biocatalysis can be integrated. The hypothesis is to construct and operate integrated microscale reactors using a transaminase model system (adapted to the specific microorganism and the biocatalytic reaction) in an intensified and more efficient process. The integrated microfactory can be used to quickly and effectively screen different process conditions. The first part of this study is to evaluate the effect of miniaturization on biochemical reactions and to design and construct a miniaturized reactor.

Introduction
Enzymes for biocatalysis are most often produced in large industrial-scale fermentation processes following a number of expensive – and inefficient – downstream operations. Miniaturization can significantly enhance the productivity of some processes. Miniaturization helps diffusion-limited reactions to occur faster than they would at the larger scale. Of particular interest is the potential for high throughput experimentation for rapid screening of reactions, determining kinetics, exploring hazardous chemistry and developing chemical reactions[1]. The integrated microfactory has a number of features that are advantageous for large-scale production with respect to improved economy of the proposed process: (1) the method for preparing the catalyst is considerably cheaper as no intermediary purification steps are needed; (2) the system process intensity is inherently enhanced through the continuous operation; (3) large hydrophobic substrates would be easily accessible since the cell membranes are to be lysed. The aim of this study is to design a microfluidic system, for rapid screening, that can mimic or improve the performance of the reaction at larger scale using biocatalytic transamination as a model reaction.

Transaminases (TAms) (also known as aminotransferases) catalyze the transfer of an amino group from an amine donor, usually an amino acid or a simple amine such as isopropylamine, to an acceptor molecule yielding a chiral amine as well as a co-product ketone (or alpha-keto acid) and require the cofactor pyridoxal phosphate (PLP) to act as a shuttle to transfer the amine group.

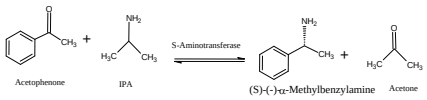

The main challenges are: (1) an unfavourable thermodynamic equilibrium position, necessitating processes to shift the equilibrium; (2) substrate and product inhibition; (3) low substrate solubility, giving low volumetric productivities; (4) high biocatalyst cost[1]. The performance is evaluated by varying the operation conditions, *i.e.* parallel flow, segmented flow, multi-phase system for controlled supply of substrate, varying flow rate, residence time, enzyme concentration *etc*, which influences the performance of the reaction, and to study the reaction rate and mass transfer rate limitations. Computational fluid dynamics (CFD) modelling is used to study the different reactor formats, to maximize the productivity and also to study the influence of the main operational parameters.

Material selection and Design formats
Poly(methyl methacrylate) (PMMA) is widely used and considered biologically compatible material also for medical applications, and is therefore used for our application. A microfluidic meandering channel and microfluidic straight channel (YY) that gives a near laminar flow through the channel have both been designed in PMMA to evaluate the reaction performance with regards to diffusion limited reaction.

Computational Fluid dynamics (CFD) simulations
CFD is used to predict the flow behaviour inside the micro-channels and further helps in decision making.

The simulations showing the velocity contours and pathlines for the two different reaction formats are shown below. Maximum velocities of about 0.004 m/s are observed for a flow rate of 8 µl/min in the meandering channels.

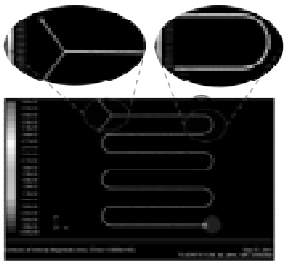

Figure 1: CFD simulations showing the velocity contours inside the meandering channel

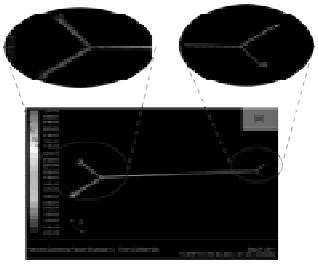

Figure 2: CFD simulations predicting the near laminar flow and flow split at the outlet in the YY reactor

Performance and Analysis

The performance of the biocatalytic transamination reaction is evaluated at different flow speeds or residence times, sampled continuously at regular intervals and analyzed using HPLC.

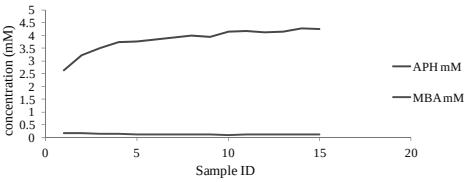

Figure 3: Concentration profile of Acetophenone (APH) and Methylbenzylamine (MBA) at the outlet of the meandering channel (residence time of 13 min).

The analysis shows a low concentration of the product MBA. The concentration profile of APH in Figure 3 illustrates the absorption/adsorption behaviour of APH in PMMA. Further investigation is needed to study the adsorption, flow behaviour and poor reaction performance.

An equilibrium test was performed by immersing the PMMA in APH solutions of various concentrations for several days. The solution was analysed at different times, which shows no adsorption/absorption of APH.

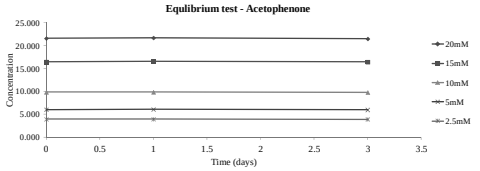

Figure 4: Concentration profiles of different initial concentrations APH solution with immersed PMMA

Figure 5 shows that APH is diffusing much slower compared to the MBA. CFD simulations for different diffusion rates also confirmed the experimentally observed behaviour.

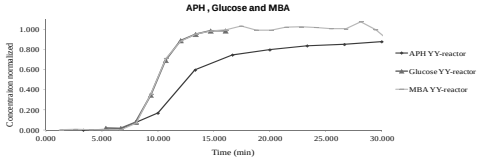

Figure 5: Normalized concentration profiles of APH, D-glucose and MBA in YY reactor

Based on the results, it can be concluded that APH is much slower diffusing than MBA, and a new reactor format is designed to achieve a distributed segmented flow to maximize the mass transfer.

Figure 6: Design format of a distributed segmented flow reactor

Conclusions and Outlook

- CFD simulations can help design the new reactor formats for diffusion/rate limited reactions
- Near laminar flow is achieved in the YY channel
- Poor reaction performance is attributed to slow diffusion rate and mass transfer limited reaction
- A distributed segmented flow reactor is designed to improve the reaction performance and maximize conversion

The performance of the reaction integrated with separation and product recovery into a microsystem is potentially a promising technology for detailed investigation of future biocatalytic reactions.

References

1. S. Matosevic, N. Szita, F. Baganz, J. Chem. Tech. Biotechnol. 86 (2011) 325–471.
2. P. Tufvesson, J. Lima-Ramos, J.S. Jensen, N. Al-Haque, W. Neto, J.M. Woodley, Biotechnol. Bioeng. 108 (2011) 1479-1493.

Kristine Stove Boesgaard
Phone: +45 5180 1559
E-mail: kboe@risoe.dtu.dk

Supervisors: Teis Nørgaard Mikkelsen
Andreas Ibrom
Helge Ro-Poulsen, KU

PhD Study
Started: June 2010
To be completed: May 2013

Physiological Responses of Plants and Ecosystems to Climate Change

Abstract
Response studies in terrestrial ecosystem physiology have so far focused on average climatic changes. However both observations and model projections indicate that climatic variability will be enhanced in the future, which most likely would lead to more serve responses in the ecosystem. In the natural-ecosystem field facility of CLIMAITE the plant physiological responses of 6 years of climate manipulation of CO_2 enrichment, temperature increase and periodical drought are investigated. It is not always possible to investigate certain photosynthetic parameters under field conditions why this PhD project will investigate plant ecophysiological responses to different climate change scenarios based on both field- and laboratory-work.

Introduction
Changes in CO_2 concentration and temperature are expected to have dramatically impact on the precipitation patterns. Higher frequency of extreme event such as summer droughts and heavy precipitation event are pronounced [1].

Photosynthetic uptake of CO_2 is known to be directly influenced by the pronounced increase in atmospheric CO2 concentration, higher temperature or altered water availability [2]. All physiological responses of elevated CO_2 on plants and ecosystem can divided as a result of increased photosynthesis (A) and decreased stomatal conductance (gs) [3]. Plants grown in elevated CO_2 have a significantly higher light saturated photosynthesis (A_{sat}) [4]. However, the maximum carboxylation rate (V_{cmax}) and maximum rate of electron transport (J_{max}) in Photosystem II is significantly decreased to elevated CO_2 [4].

An increased temperature (by few degrees') is known to have a positive effect on the photosynthesis. However, an increased temperature also will lead to an increased transpiration and evaporation from the total ecosystem, leading to lower water availability. Lower soil water will be followed by a stomatal closure and thereby a possible decrease of the photosynthesis [5].

Combination of higher temperature and increased CO_2 might not cause an effect on the photosynthetic CO_2 assimilation, while the stomatal conductance is declining as VPD is increased. This combination is hypnotized to be an additive effect.

Water availability is essentially for all plants and drought periods are known to have a negative impact on the photosynthesis. With increased temperature a higher evapotranspiration of the ecosystem occurs, leading to lower soil moisture in short-term. In longer term continuous lower soil moisture can lead to change soil structure and from that changed the field capacity of the soil. A physiological response to higher soil water might be the same as for increased temperature, while low soil moisture also leads to stomatal closure. In combination with CO_2 an additive effect is expected while the closed stomatal but the higher substrate (CO_2) supply for the photosynthesis will equalize the assimilation rate. However it is also possible that the increased CO_2 will be the main driver resulting in a still higher CO_2 assimilation.

Response studies in terrestrial ecosystem physiology have so far focused on average climatic changes. However both observations and model projections indicate that climatic variability will be enhanced in the future, which most likely would lead to more serve responses in the ecosystem

Specific objective
Two major objectives are addressed to the PhD project; assessing the development of ecophysiological key parameters in the two species after ecosystem stabilization, do to 6 years of climatic manipulation, and assessing the estimation of important parameters for dynamic ecosystem models for simulation of carbon, water and nitrogen fluxes. Combining the CLIMAITE

field experiment with controlled environmental laboratory mesocosm experiments, it will be possible to investigate parameters which are complicated (if not impossible) to investigate in the field.

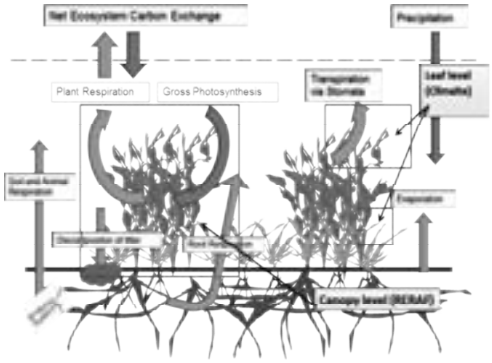

Figure 1: Schematic overview of the responses this project seeks to investigate according to long-term climate manipulations.

Methodology

The field facility of CLIMAITE is a multi-factorial experiment trying to simulate the climate in 2075. The setup includes treatments of un-treated control, elevated CO_2, passive nighttime heating, periodic summer drought and all combination replicated in six blocks in a split-plot design [6] (www.climaite.dk).

The experimental area of CLIMAITE is dominated by two species, heather (*Calluna vulgaris*) and wary-hairgrass (*Deschampsia flexuosa*). Starting in these two species the overall carbon and water-balance of the ecosystem are evaluated. The ecosystem is examined at two levels. In the field leaf level response are examined and in the control growth facility RERAF, at Risø DTU, whole ecosystem responses are investigated (www.risoe.dtu.dk).

To investigate and describe the physiological response of the climate changing over time, gas-exchange CO_2 and H_2O method are used. Concentration on leaf level gas-exchange of CO_2 and H_2O can describe a lot of photosynthetic processes and parameters. During the growing season 2011, data have been collected in the field.

Model theory of leaf gas-exchange:

The most frequent used model to understand C3 photosynthesis is the Farquhar-von Caemmerer-Berry (FvCB) model described in 1980 and later modified [7-9]. Here the FvCB model is briefly examined. The FvCB model considers the biochemical reactions in the photosynthesis to be in one of two, sometime three, steady state phases.

At Figure 2 the three known phases in the A-Ci response is shown [10]. As intercellular mole fraction of CO_2 (C_i) increase from the minimums concentration the photosynthesis (A) is determined the properties of ribulose1,5-bisphosphate carboxylase / oxygenase (Rubisco) assuming the supply of substrate, ribulose-1,5-bisphosphate (RuBP) is saturating**.** This phase is normally referred to as the Rubisco-limited photosynthesis and only occurs at low CO_2 concentration and a high dA/dC_i [10]. With increase of C_i the dA/dC_i is decreasing and the value starts to approach zero, here the photosynthetic rate is limited by the rate of regeneration of RuBP, assumed that the RuBP is used in a constant rate and limited by the electron transport rate (J) [10]. This state is referred to as the RuBP-limited photosynthesis and occurs at higher CO_2 concentrations. The third phase is also related to the regeneration of RuBP, but here the limiting factor becomes the rate of triose-phosphate utilization (TPU-limited) [10]. To simplify the model the third phase is not incorporated in the model.

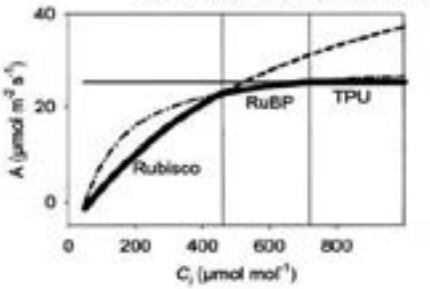

Figure 2: Idealized A-Ci curve [10].

Future work

Data from the growing season 2011 are been processes, chemical analyze of the leaf chemistry is to be obtained and mesocosm experiment will be started up in the start of 2012.

References

1. IPPC: The Physical Science Basis. Intergovernmental Panel on Climate Change, Geneva, 2007.
2. H. Lambers, F. Stuart Chapin, T.L. Pons, Plant physiological ecology, Springer**,** New York, USA, 1998.
3. S.P. Long, E.A. Ainsworth, A. Rogers, D.R. Ort, Ann. Rev. Plant Bio. 55 (2004) 591-628
4. E.A. Ainsworth, A. Rogers. Plant, Cell Env. 30 (2007) 258-270
5. B.E. Medlyn, E. Creyer, D. Ellsworth Plant Cell Env. 25 (2002) 1167-1179
6. T.N. Mikkelsen, C. Beier, S. Jonasson, Func. Eco. 22 (2008) 185-195
7. G.D. Farquhar, S. von Caemmerer, J.A. Berry, Planta 149 (1980) 178-190
8. P.C. Harley, T.D. Sharkey, Photo Res. 27 (1991) 169-178
9. C.J. Bernacchi, E.L. Singsaas, C. Pimentel, J.R. Portis, S.P. Long, Plant Cell Env. 24 (2001) 253-259
10. S.P. Long, C.J.Bernacchi, J. Exp. Botany 392 (2003) 2393-2401

Andrijana Bolić
Phone: +45 4525 2958
E-mail: anb@kt.dtu.dk
Discipline: Process Technology and Unit Operations

Supervisors: Krist V. Gernaey
Anna Eliasson Lantz
Karsten Rottwitt
Nicolas Szita, UCL

PhD Study
Started: March 2010
To be completed: February 2013

Monitoring Continuous Fermentation Processes in Microbioreactor Systems

Abstract
At present, research in bioprocess science and engineering requires fast and accurate analytical data (rapid testing) that can be used for investigation of the interaction between bioprocess operation conditions and the performance of the bioprocess. Miniaturization could provide an attractive tool necessary for obtaining a vast amount of experimental data in a short time. The main objective of this project is to develop a microbioreactor platform for continuous cultivations of *Saccharomyces cerevisiae*, where NIR spectroscopy could be further implemented for rapid on-line measurement of process variables like substrate and biomass.

Introduction
Conventional microbial cell cultivation techniques are no longer sufficient considering the fast development of tools for genetic manipulation of biological systems resulting in a large numbers of strains and conditions that need to be screened. There is a tremendous driving force and interest for development of new techniques, which could provide both high quality data and also a high quantity of experimental data. In recent years, microbioreactors have been researched intensely due to their clear advantages like small volume, little or no need for cleaning, high throughput, high information content and control capabilities [1].

Even though microbioreactors have many advantages, it is important to bear in mind that they also have issues related to their size and handling. Evaporation, proper and reliable stirring, interconnections between micro-scale features and the 'macro world' are just some of the burning problems that need to be solved. In addition, measurements of several process variables in microbioreactors are not straightforward to implement. They rely on analytical methods, which are not sufficiently developed for such a small scale at this point. If the measurements are possible, they are not cheap either.

Another important issue that needs to be addressed is determining the optimal microbioreactor volume while keeping in mind the final objective – application. Does one need a sample or not? Does one talk about cells in suspension or adhered on a substrate? The final microbioreactor design should thus strongly depend on the goal of a specific microbioreactor application.

Microbioreactor Design
To address some of the previously mentioned questions, we are currently developing a microbioreactor platform with 1-2 ml working volume. Considerable effort is placed in developing a system that could provide reproducibility and easy handling at a reasonable cost.

Platform
The microbioreactor surrounding is equally important as the microbioreactor itself. Keeping this in mind, a platform with gas connections, optical fibers for sensing, a specially designed heater and standard temperature sensor was designed and fabricated. It can be seen in Figure 1.

Figure 1: Microbioreactor together with platform

The microbioreactor can be placed on a platform using a 'Lego' approach, which ensures reproducibility in sensing and connections. Furthermore, this configuration lowers the cost per microbioreactor, considering that expensive parts of the system are reusable and placed in the platform, while the

microbioreactor is mostly made from cheap PMMA and has one magnetic ring and two sensor spots.

Microbioreactor and stirrer design

The microbioreactor, made in PMMA, consists of a bottom and top part as shown in Figure 2. The bottom part is made as a negative to the platform and has a thin optically transparent layer to make sure that measurements based on optical properties are possible (pH, DO, OD).

Figure 2: Microbioreactor design

The top part is a cylinder with a shaft in the middle on which a magnetic stirrer is mounted. The microbioreactor also has two tubes for optional aeration. Beside air sparging, there is also the possibility for exploiting surface aeration in which case aeration tubes are removed and connectors are made on the top of the microbioreactor.

The stirrer has two pairs of impeller blades placed at two levels, which can be seen in Figure 3. Each blade can be removed in order to create a different mixing behavior. A permanent magnetic ring, which is magnetized across its diameter, is placed inside the stirrer and is driven by a rotating magnetic field.

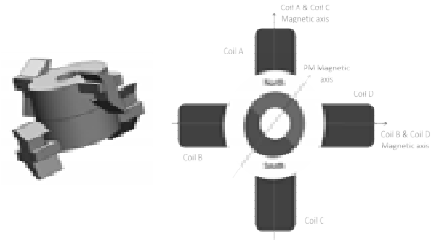

Figure 3: Stirrer design

Electromagnets were incorporated in the mixing device, in order to obtain control over the mixing by changing the speed and direction of the stirrer rotation. In this way, it is possible to prevent formation of a vortex without usage of baffles. The mixing device consists of a base fabricated by micromilling in PMMA (non-magnetic material and part of the platform), illustrated in Figure 1, on which 4 coils (electromagnets) are mounted. The coils are connected to a switch mode power supply, which is controlled by a PC running LabView software. The basic principle of the mixing control is presented in Figure 4.

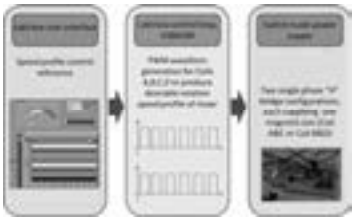

Figure 4: Mixing control

Results

The mixing capability of the microbioreactor was quantified by experiments where mixing time and volumetric mass transfer coefficient (k_La) were evaluated against different stirrer rotational speeds. The mixing time in a 1 ml microbioreactor was 2 s for a rotational speed of 200 rpm and 0.4 s for 1000 rpm.

The correlation between volumetric mass transfer coefficient and rotational speed during surface aeration in a 1 ml microbioreactor is presented in Figure 4. In another case, where air sparging was applied, the maximum k_La value obtained was 450 h^{-1}. Furthermore, when mixing was applied with change of direction every 0.2 s at 1000 rpm, the k_La value was 900 h^{-1}.

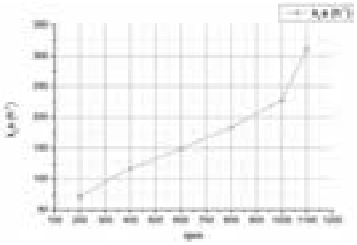

Figure 4: k_La versus rpm

Conclusion

A flexible and cheap microbioreactor with supporting platform was developed. The device can be operated with surface aeration or gas sparging. It shows flexibility in mixing by changing rpm and direction of rotation. Mixing can be considered almost instantaneous. The volumetric mass transfer coefficient obtained by surface aeration is sufficient for a standard fermentation.

Acknowledgements

This project is supported by the Danish Council for Strategic Research in the frame of the project “Towards robust fermentation processes by targeting population heterogeneity at microscale” (project number 09-065160).

References

1. D. Schäpper, M.N.H.Z. Alam, N. Szita, A.E. Lantz, K.V. Gernaey, Anal. Bioanal. Chem. 395 (2009) 679–695

Joussef H. Chaaban
Phone: +45 4525 2846
E-mail: joc@kt.dtu.dk
Discipline: Reaction and Transport Engineering

Supervisors: Kim Dam-Johansen
Søren Kiil
Tommy Skovby, Lundbeck A/S

PhD Study
Started: January 2010
To be completed: December 2012

Novel Reactor Design for Organic-Chemical Crystallization of Active Pharmaceutical Ingredients (APIs)

Abstract
The pharmaceutical industry has been very much attracted by the advantageous continuous operation due to its cost-effectiveness and environment-friendliness compared to batch-wise operation. Additionally, increasing public demand and strict regulatory requirements have sparked the search for reliable continuous crystallization processes to improve chiro-selectivity, control of particle size distribution (PSD) and polymorphism of the APIs. The aim of the present PhD project is to develop a durable, flexible and reliable chiro-selective continuous crystallization process for the separation of chiral APIs and their intermediates focusing on control of chiro-selectivity, PSD and polymorphism.

Introduction
Crystallization is a widely used and the most important separation and purification process in the pharmaceutical industry. However, the use of batch-wise crystallization processes for the separation of active pharmaceutical ingredients (APIs) is disadvantageous due to undesirable properties such as high consumption of energy and chemicals, low separation efficiency, low purity due to batch-to-batch variations etc.

The complexity of the problems using batch crystallization processes increases when considering the fact that more than 50% of known APIs are chiral and 9 out of the top 10 drugs have chiral active ingredients. The chirality here is expressed in terms of enantiomers. The chemical-physical properties of enantiomers are identical, but the difference between them lies within the stereo-chemical configuration, which has an influence on the biological activity of the API [1-4]. The incident of thalidomide dramatically increased the focus on the consequences of chiral APIs and their bioavailability. Therefore, control of chiro-selectivity and polymorphism during API separation by crystallization is of outmost importance to ensure enantiomerically pure APIs.

To ease downstream processing and formulation and to ensure improved drug delivery properties, the particle size distribution (PSD) of the API must essentially be controlled to meet required specifications. One approach to control PSD is by crystallization by entrainment using seed crystals with a certain initial PSD. This additional and important issue again adds complexity to the development and operation of continuous crystallization processes for API separation.

In this PhD project a durable, flexible and reliable chiro-selective continuous crystallization process is developed. The process is investigated for flexibility, chiro-selectivity, control of PSD and polymorphism. Two cases of the solid-liquid phase behavior of conglomerate forming systems of racemic mixtures are investigated: 1) Racemic Threonine (amino acid)-Water system, and 2) API intermediate from H. Lundbeck A/S.

Current Developments: Coupled-Batch System
The development of effective chiro-selective (or preferential) crystallization processes for separation and purification of APIs or their intermediates has attracted great attention due to increasing public demand and strict regulatory requirements for purity and quality of APIs. A variety of developments have been demonstrated for selective crystallization of chiral APIs and their intermediates [3, 5]. For instance, Elsner et al. [3] developed a cooling crystallization process for the simultaneous crystallization by entrainment (seeding) of pure D- and L-Threonine from conglomerate forming DL-Threonine racemate in water by employing two coupled vessels operating batch-wise.

The concept is based on two batch crystallizers coupled by crystal-free liquid exchange streams between the crystallizers. The purpose of coupling by

liquid exchange streams is to improve the separation efficiency of the two enantiomers in the overall process [3]. However, due to thermodynamic restrictions the crystallization process must be stopped before the counter-enantiomer begins to nucleate undesirably to reach the common equilibrium (eutectic composition) thereby decreasing the separation efficiency of the overall process. It is thus desired to develop a chiro-selective continuous crystallization process to overcome the problem of the undesirable nucleation of the counter-enantiomer providing an improved control of the progress of crystallization.

Results and Discussion

Two identical experiments were performed on the newly developed continuous crystallization process having the conglomerate forming system racemic Threonine in water. The objective of these experiments was to verify whether a constant enantiomeric composition in the liquid phase can be achieved without the occurrence of nucleation of the counter-enantiomer and to investigate the ability of growth of seed crystals in the continuous crystallization system. The results are shown in Figure 1 (a) and (b) and Figure 2.

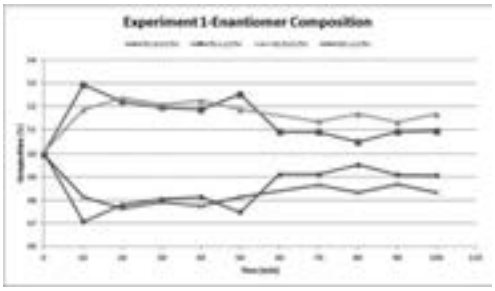

(a)

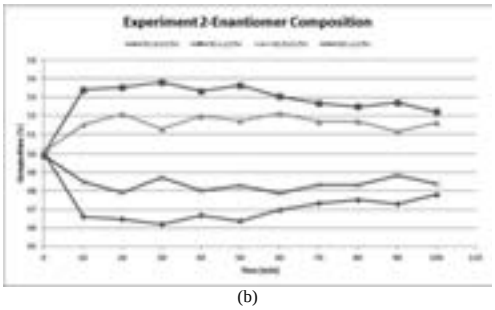

(b)

Figure 1: Liquid phase enantiomer composition.

It is observed in Figure 1 (a) and (b) that the enantiomeric composition in the liquid phase increases during the first 50 minutes of operation. This is due to a transient state at which the seed crystals grow with the desired enantiomer. After 60 minutes of operation steady-state in enantiomeric composition is achieved due to the fact that seed crystals grow with a relatively constant growth rate. It is thus possible to obtain constant steady-state enantiomeric composition.

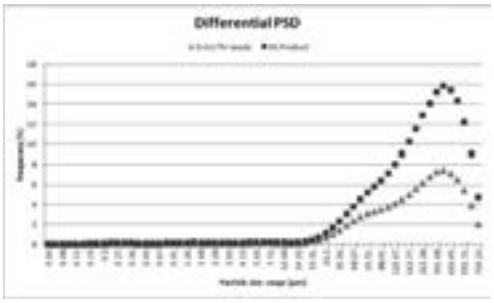

Figure 2: Differential particle size distribution (PSD) of D-Threonine seeds and product.

At the end of each experiment the solid product was filtered off and dried. PSD measurements were then performed and results for D-Threonine are shown in Figure 2. It is observed that the initial PSD of D-Threonine seed is broader than the product achieved. Additionally, the distribution of large crystals is higher for product than for seeds. This indicates the fact that growth of seed crystals occurred during crystallization resulting in bigger crystals with a slightly narrower PSD as expected.

Conclusions

Continuous chiro-selective crystallization enables improved control of the enantiomeric composition in the liquid phase and solid phase growth to ensure separation of enantiopure APIs and their intermediates. However, the main concern is the cost of these processes. Therefore, future work should focus on cost-effective options and alternative designs of durable and flexible continuous crystallizer systems capable of performing chiro-selective crystallization with control of chiro-selectivity, PSD and polymorphism.

Acknowledgments

The author acknowledges the financial and professional support of H. Lundbeck A/S and CHEC Research Center at the Department of Chemical and Biochemical Engineering at DTU.

References

1. A.S. Myerson, Handbook of Industrial Crystallization, Butterworth-Heinemann, USA, 2002.
2. Y. Wang, A.M. Chen, Org. Process Res. Dev. 12 (2008) 282-290.
3. M.P. Elsner, G. Ziomek, A. Seidel-Morgenstern, AIChE. J. 55 (2009) 640-649.
4. H. Lorenz, A. Perlberg, D. Sapoundjiev, M.P. Elsner, A. Seidel-Morgenstern, Chem. Eng. Process. 45 (2006) 863-873.
5. D. Polenske, H. Lorenz, A. Seidel-Morgenstern, Chirality, 21 (2009) 728-737.

Signe Sandbech Clausen
Phone: +45 4677 4151
E-mail: sicl@risoe.dtu.dk

Supervisors: Iver Jakobsen
Mette Grønlund
Ingo Lenk, DLF Trifolium

PhD Study
Started: April 2011
To be completed: March 2014

Symbiotic Growth Depressions in Bioenergy and Forage Crops

Abstract
Phosphorus (P) is an essential nutrient for plant growth. Since P is also one of the least plant-available nutrients in the soil, it is often growth limiting. To solve this problem most plants have engaged in a symbiotic relationship with arbuscular mycorrhizal (AM) fungi. The symbiosis is usually mutualistic and increases plant uptake of mineral nutrients, especially P. This is however not always the case as some grasses exhibit symbiotic growth depressions when colonized by certain AM fungi, which leads to hidden yield losses in the field. To obtain plants with higher P efficiency it is necessary to gain more understanding of how P uptake is regulated in plants. This is highly relevant when you take into account the finite P reserves, increasingly expensive P fertilizers and increasing bioenergy and forage crop production. This project will test the novel hypothesis that AM-colonized plants become P limited and hence growth depressed due to impaired function of direct phosphate (Pi) uptake at the root surface. Furthermore, the potential for increasing plant Pi uptake efficiency will be analyzed.

Introduction
Phosphorus (P) is one of the major macro-nutrients for plant growth and development. Plant roots acquire P from the soil as inorganic phosphate (Pi) which is actively taken up via transporter proteins. Even though P may be present in relatively large amount in the soil, it can still be limiting for plant growth. This is mainly because of a very low solubility and hence a low mobility in the soil [1]. To overcome this, plants have evolved a range of strategies which increase either Pi uptake capacity or Pi availability in the soil. One strategy is to establish a symbiosis with arbuscular mycorrhizal (AM) fungi. The advantage to the plant of this symbiosis is that AM fungi offer an alternative effective pathway from which P can be acquired from the soil. This provides the plant with two alternative Pi uptake routes in AM colonized plants: the mycorrhizal mediated pathway and the direct pathway. The symbiotic association occurs in roots of most soil grown plants, and approximately 80% of all terrestrial plants are colonized by AM fungi [2]. AM colonization often leads to dramatically increased plant growth, primarily because the fungal mycelium assists the plant in scavenging P and other nutrients from larger soil volumes than possible by the root system alone. Nevertheless, there is a considerable functional diversity in the outcome of the symbiosis, ranging from positive to negative effects [3, 4]. In grasses it has been observed that the colonization, in some cases, results in symbiotic growth depression (fig.1A) rather than a positive growth response. This probably result in hidden yield losses in the field as most crop plants are AM colonized by default, depending on the P level, and thereby lead to decreased production of crops. The observed symbiotic growth depressions were conventionally assigned to carbon drain by the fungi. However, a new hypothesis is that the direct Pi uptake in plants is repressed during AM colonization. If the AM-mediated Pi uptake cannot fully compensate for the reduced direct Pi uptake, this results in a P limited plant. Since crop plants grown today are supplied with plenty of P fertilizer and have been bred under plenty of nutrient supply, they may not be the most efficient plants in relation to uptake of P or other nutrients. This provides a global challenge as the mineral phosphate rock resources used for fertilizers are non-renewable. There are considerable debates about the resources left. Nonetheless, on the long term, and so in terms of sustainability, the depletion of phosphate reserves is an inescapable issue. To maintain optimal crop yields using a reduced amount of P fertilizer, it is necessary to work towards new crop varieties with superior P utilization capacity. This could potentially be obtained by breeding plants, in which direct and AM mediated Pi uptake become additive rather than alternative. For this reason, one important issue to clarify is how Pi uptake is regulated in plants.

Specific objective

The objective of the PhD project is to test the novel hypothesis that AM plants can become P limited when they shift to mycorrhiza mediated Pi uptake, if the decrease of the direct uptake is not fully compensated by the mycorrhiza mediated Pi uptake, see figure 1B. The aim is to identify key components in the interplay between the mycorrhiza mediated - and the direct uptake and investigate the potential of increasing direct Pi uptake in mycorrhizal plants through manipulation of key signaling components.

Plant species

The fully sequenced model grass *Brachypodium distachyon* (fig. 1C) is used to study symbiotic growth depressions caused by selected AM fungi. *B. distachyon* is a new and attractive model system for grass molecular biology, as it is closely related to the major cereals wheat and barley, as well as forage grasses [5].

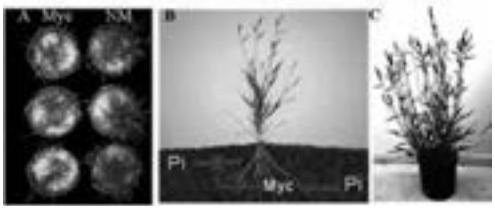

Figure 1: A) Growth depression in 4 weeks old *B. distachyon* plants, colonized with *Funneliformis mosseae Beg*85 (Myc) in comparison to non AM plants (NM). B) A simple illustration of the new hypothesis; during AM colonization unknown regulatory signals lead to a shift in Pi uptake from direct to mycorrhiza mediated Pi uptake. If the decrease of the direct uptake is not fully compensated by the mycorrhiza mediated Pi uptake, plants become P limited, which is observed as growth depressions in AM plants. C) 9 week old model grass *B. distachyon* plant line Bd21-3.

Methods

Key genetic components in the direct Pi uptake pathway *e.g.* Pi transporters and P signalling genes as well as miRNA genes will be identified by quantitative real time PCR (qPCR) and Next Generation Sequencing (NGS). QPCR and NGS are used to describe the expression patterns of the genes of interest under different Pi conditions in AM and non-AM plants. Agrobacterium tumefaciens-mediated transformation of *B. distachyon* with a subset of selected candidate genes will be performed to mitigate the hypothesized P limitation by over-expressing or silencing some of these putative key elements to manipulate direct Pi uptake activity in the model plant. The expression patterns of the transgenic and wild type plants in combination with physiological isotope tracer uptake studies will allow discrimination between Pi uptake via the mycorrhizal and direct pathways. The results will be integrated into a model of the proposed regulatory mechanisms and involved genetic components underlying the observed growth depressions in the model grass *B. distachyon*. The experiments will mainly be performed under controlled conditions in climate chambers. The RERAF (Risø Environmental Risk Assessment Facility) phytotron will be used to study the influence of elevated CO_2 and thereby a changed carbon-balance, on the Pi uptake mechanisms. Results will be sought validated in the field where more variable growth conditions are likely to influence Pi uptake. In a longer perspective, homologues of the identified key candidate genes in *B. distachyon* could be analyzed in the target crop; perennial ryegrass (*Lolium perenne*) in the search of relevant genetic markers of the desired trait; improved Pi uptake. Those candidate markers showing the biggest effect on P uptake could then be direct targets for the development of routine marker assays for future plant breeding and crop improvement.

Results

Thirteen phosphate transporter genes have been identified in *B. distachyon* and their expression pattern analyzed by QPCR in non-mycorrhizal and mycorrhizal plants grown at different phosphate levels. Of the 13 phosphate transporters four are potentially involved in the direct Pi uptake, as they were shown to be down-regulated at high soil phosphate levels and in AM plants.

Conclusion

Growth depressions in mycorrhiza colonized *B. distachyon* plants are potentially caused by down-regulation of phosphate transporter genes in the direct Pi uptake pathway. Currently, molecular and physiological studies are performed to investigate the interplay between the direct Pi uptakes and mycorrhizal mediated Pi uptake pathways.

Acknowledgements

The PhD project is part of the Research Project *Can we prevent symbiotic repression of crop performance?* Funded by The Danish Council of Independent Research | Technology and Production Sciences. It involves close collaboration with plant breeders at DLF TRIFOLIUM A/S and plant scientists at Cornell University and The University of Adelaide.

References

1. D.P. Schachtman, R.J. Reid, S.M. Ayling, Plant Physiol. 116 (1998) 447-453
2. S.E Smith, D.J. Read, Mycorrhizal Symbiosis. Ed 3. Academic Press-Elsevier, 2008
3. S. Ravnskov, I. Jakobsen, New Phytol. 129 (1995) 611-618
4. S.E Smith, F.A. Smith, I. Jakobsen, New Phytol. 162 (2004) 511-524
5. J. Draper, L.A. Mur, G. Jenkins, G.C. Ghosh-Biswas, P. Bablak, R. Hasterok, A.P. Routledge, Plant Physiol. 127 (2001) 1539–1555

Maria del Mar Cortada Mut
Phone: +45 4525 52920
E-mail: mmarc@kt.dtu.dk
Discipline: Reaction and Transport Engineering

Supervisors: Kim Dam-Johansen
Peter Glarborg
Anders Rooma Nielsen, FLSmidth

PhD study
Started: September 2011
To be completed: August 2014

Interactions between Solid Fuels and Raw Materials in Cement Rotary Kilns

Abstract
The cement industry has an interest in replacing fossil fuels with alternative fuels due to economical considerations and environmental concerns. This PhD project aims at improving the understanding of the behavior of solid alternative fuels in the material inlet of the rotary kiln and investigates how it affects the process conditions, stability and the clinker quality. Dynamic combustion models will be developed and verified by experimental data.

Introduction
The cement industry is an energy intensive industry and the energy costs account for 30-40 % of the total costs of the cement production [1]. Cement production has mainly depended on the use of fossil fuel such as coal and coke. However, the cement industry has a great interest in replacing fossil fuels with alternative fuels (waste from other industries) in order to minimize production cost due to environmental concerns and the increase of the fuel prices.

The advantages of the substitution of fossil fuels by alternative fuels are:

- Reduction of fuel and production costs.
- The alternative fuels may be partly or fully CO_2-neutral.
- Waste is effectively utilized as energy.
- The ash residue is incorporated into the cement clinker.

Alternative fuels cover a large range of fuels, typically relatively large particles, with different chemical and physical properties. The most important fuel characteristics to consider when selecting alternative fuels are the heating value, the ash and the moisture content. The heterogeneity amongst the physical and chemical properties affects both the thermal energy input and the process stability. Some of the most common alternative fuels are industrial and municipal waste, tire derived fuels, meat and bone meal, and wood waste.

The process flow sheet of a modern cement kiln system is illustrated in Figure 1. The traditional firing points in a cement plant are the calciner and the kiln burner. The introduction of alternative fuels has lead to modifications of these units in order to optimize the combustion.

Figure 1: Scheme of a modern In-Line Calciner (ILC) cement kiln system [2].

Additional combustion equipments for combustion of coarse alternative fuels have been developed, i.e: a HOTDISC [3]. However, several cement plants are firing the alternative fuels directly into the material inlet end of the rotary kiln, because it requires a minimum of investments. Subsequently, the solid fuels and the cement raw materials are in physical contact with each other. This leads to a modification of the composition and quality of the clinker.

The combustion of alternative fuel may cause local reducing conditions in the material inlet end of rotary

kilns. The sulfates of the raw materials are sensitive to reducing conditions and high temperature, and can decompose. This can potentially increase the sulfur release and internal circulation of sulfur, chlorine and alkali metal species. The modification of process conditions due to the combustion of alternative fuels and the accumulation of sulfur may affect the process operation by build-up deposits because the sulfur species may condense again on cold surfaces, as illustrated in Figure 2. These deposits accumulate typically in the material inlet end of the rotary kiln, or in the riser duct between the calciner and rotary kiln, where they cause blockages. The plant must sometimes be temporarily shut-down in order to remove the deposits [3].

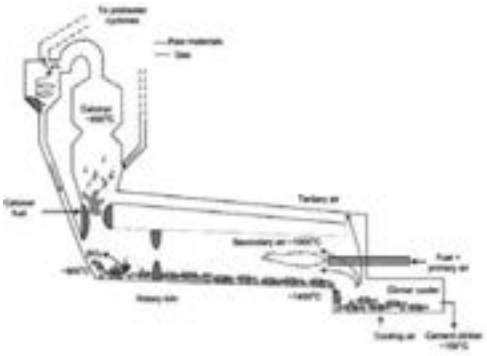

Figure 2: Sulfur species may condense and form deposit buildups [5].

The solid material flow in the kiln can be hindered by the build-ups, so-called kiln rings. This may lead to early melt formation due to high temperatures from the alternative fuels combustion, and nodules may start to form early in the rotary kiln instead in the burning zone. These phenomena may affect the clinker quality, because the heat from the flame may not be able to penetrate into the center of the nodule. Thereby, the formation of alite ($3CaO \cdot SiO_2$), the main strength-giving mineral in cement, may not have been completed.

Specific Objectives

The objective of this project is to improve the understanding of the behaviour of alternative fuels in the material inlet of the rotary kiln and investigate how it affects the process conditions, stability and the clinker quality.

The interaction of the solid fuel with the different raw materials will be studied experimentally by combustion of the solid fuels in a high temperature rotary drum in a pilot scale facility.

A dynamic combustion model combining gas and solid fluid dynamics, mixing and chemical interaction with raw materials and a model for sulfur release in relation to fuel type and accumulation of the combusted particles in the kiln will be developed. These models will be validated against experimental data from lab and full-scale measurements.

Methodology

The experiments for studies of fuel/raw material interactions during fuel combustion will be performed in a high temperature rotary drum, which is able to simulate the process conditions in the material inlet end of an industrial rotary kiln. Figure 3 shows the side view of the high temperature rotary drum setup.

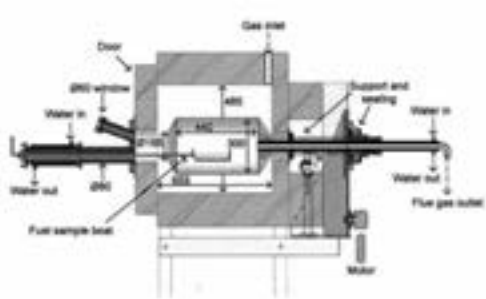

Figure 3: Side view of the high temperature rotary drum [4].

Acknowledgements

This project is part of a research platform on future cement technology financed by The Danish National Advanced Technology Foundation, DTU and FLSmidth A/S.

References

1. Cembureau, Activity Report 2008, http://www.cembureau.be/.
2. FLSmidth In-line calciner preheater system.
3. http://www.flsmidth.com (Accessed on 2/12/2011)
4. FLSmidth HOTDISC^{TM} combustion device.
5. http://www.flsmidth.com (Accessed on 2/12/2011)
6. A.R. Nielsen, Combustion of large solid fuels in cement rotary kilns, DTU, Lyngby, Denmark, 2011.
7. Alternative fuels course in FLSmith, Oct.2011

Sean Grunnet Cuthbert

Phone: +45 4525 2978
E-mail: scu@kt.dtu.dk
Discipline: Engineering Thermodynamics

Supervisors: Kaj Thomsen
Graeme Keith, Lloyd's Register ODS

Industrial PhD
Started: June 2010
To be completed: May 2013

Thermodynamics-Based Electrolyte Screening Tool for Redox Flow Batteries

Abstract
The widespread integration of intermittent energy supplies from wind and solar farms, for example, introduces a level of instability to the electrical transmission/distribution grid that can reduce the reliability of the energy supply to the end users. Large-scale electrochemical energy storage is viewed as a technology that can enable the integration of significant amounts of intermittent energy supplies. However, this technology is not proven for large-scale applications primarily due to the thermodynamic limitations inherent with the system electrochemistry. A theoretically rigorous method of quickly screening for optimal battery electrolytes is needed.

Introduction
The Earth's climate is changing. The Earth's biosphere is a complex and non-linearly dynamic system, but it is also closed. This means that even as the biosphere continues to absorb the negative consequences of ever more energy-hungry human societies, the ability of the biosphere to respond to local perturbations becomes more delayed and smaller in scope. Coupling the phenomena of the slowing response of the nonlinear system (i.e. our biosphere) to an increasing consumption of conventional, easily accessible (i.e. cheap) and highly polluting energy resources accelerates the overall system towards its "tipping point". Once the biosphere reaches the tipping point [1], a slight perturbation – either nature or human induced – causes the system to move rapidly (and, very likely, violently) to the next equilibrium point. However, the new equilibrium point for the system may be very far from that in which human societies have prospered for many millennia.

Conventional energy sources are being exhausted at a rate faster than replacement sources can be found, and societies globally are searching for new energy sources to satisfy demand. Those new, or 'alternative', sources of energy are typically categorised as: wind, solar, wave, tidal, geothermal, nuclear, and biomass. Unfortunately one of the major disadvantages of such alternative energy sources, with the exception of nuclear and geothermal (to a lesser extent, biomass), is that the supply is intermittent. The inherent intermittency of the electrical energy supply thus can cause frequency and voltage instabilities in the electrical distribution grid, which ultimately results in energy supply curtailments (i.e. brownouts) or emergency trips (i.e. blackouts). A typical example of wind and solar energy intermittency is illustrated in Figure 1.

However, as alternative energy projects become more prevalent and the societal demand for low carbon energy increases, the intermittency of wind, wave and solar power technologies limits its effectiveness and widespread implementation. Large-scale electrical energy storage solutions will be the only way of increasing the overall low carbon energy growth and permanence [3]. There are only a few viable means of storing electrical energy on a very large scale (i.e. multi-MWh energy levels): a) Pumped Hydro (PH); b) Compressed Air Energy Storage (CAES); c) Thermal Storage (TS); and d) Electrochemical Energy Storage (ESS). As PH and CAES are limited by geography and TS is inherently inefficient due to exergy losses on energy conversion, the most promising energy storage technology is ESS – specifically Redox Flow Batteries (RFBs).

The RFB, or Regenerative Fuel Cell (RFC), is a chemically-based method of storing energy on a 'utility scale', albeit different in nature from the well-known lead-acid battery systems [2] (see Figure 2). However, these systems are difficult to model thermodynamically due to the complexity of the transition metal electrochemical reactions within the supporting concentrated liquid electrolyte and the hydrodynamics within the porous electrode assemblies [2]. Originally developed by NASA in the 1960s and 1970s, the aqueous and non-aqueous electrolyte-based RFB did not show much promise due to the low energy density and

high parasitic losses due to metal ion migration through the membrane separator.

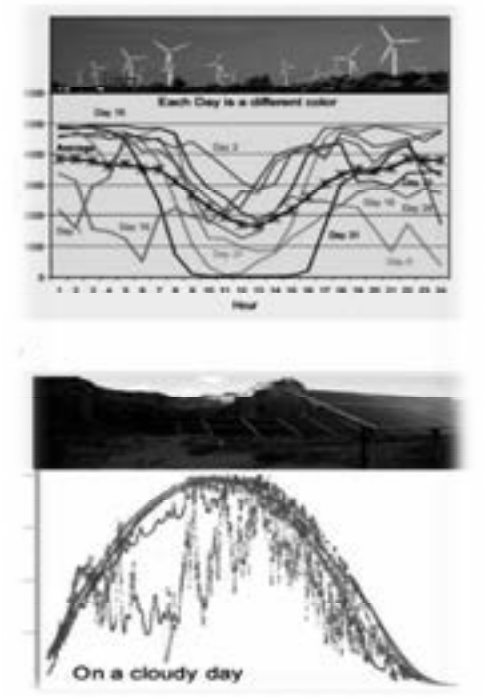

Figure 1: Intermittency of energy from wind and solar sources [5]

Utility-Scale Electrical Energy Storage

Interest in very large – or 'utility scale' – energy storage systems grew significantly through the turn of the 21st century, as energy suppliers sought more optimally efficient ways of operating their transmission and distribution systems with intermittent energy sources such as wind and solar. Recently, RFB systems have become a commercial reality, although the most promising pilot-scale commercial venture built to provide utility scale storage was prematurely shut down for economic reasons [2]. The most common electrolytic chemical combinations currently at the commercial stage or in development are: a) vanadium chloride / polyhalide; b) vanadium / bromine; c) iron / chromium; d) zinc / bromine; e) bromine / polysulphide; and f) zinc / cerium. From these combinations, the three systems most studied have been (a), (d), and (e) [2].

Although much research in the early period of RFB development focused on the screening of transition metal combinations within an aqueous or non-aqueous supporting electrolyte (see Figure 3), there has been little published in the past two decades that has provided a theoretical methodology for determining the most promising redox couples for a RFB. The main focus of the theory-based research on battery electrolyte optimisation has been on the lithium-based solid-state (or polymeric) systems (for examples of methodologies see [4], and for a review of the relativistic effects in battery systems, see [5]).

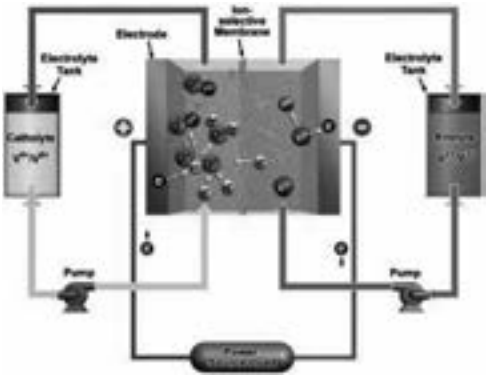

Figure 2: Typical flowsheet for a RFB (vanadium-based chemistry shown) [5]

Thermodynamics of Redox Flow Batteries

To increase the energy density and capacity of a RFB, it is necessary to investigate different chemistries that provide higher potentials. For cost reasons, it is also desirable that the redox chemistry occur in an aqueous environment and that the electro-active materials are plentiful – i.e. low cost to extract from the natural world and refine. Unfortunately, as illustrated in Figure 3, the more energetic redox couples lie within the water dissociation zones, where either H_2 or O_2 can be produced as a byproduct of the redox chemistry. Obviously for safety reasons the evolution of highly combustible gases should be avoided. In the Zn-Br RFB, for example, the evolution of gas (H_2 at the anode, Br_2 at the cathode) is reduced via the complexing of the bromide ion in a non-aqueous phase using polybromide-based ligands [2]. In addition, the reduction of Zn^{2+} to $Zn_{(s)}$ at the zinc anode slows the formation of H_2 gas.

Zinc-based chemistry for RFBs shows the greatest promise to achieving high energy densities and capacities for low unit cost. Compared to the well-known Pb-acid battery, the Zn-Br RFB described above has a theoretical energy density of 430 Wh/kg compared with a Pb-acid cell of 170 Wh/kg. A more promising Zn-based chemistry is the Zn-S cell. With a theoretical

energy density of 572 Wh/kg, the Zn-S chemistry utilises the high charge capacity of sulphur (>1000 Ah/kg) in the form of multiple states of polysulphide, S_x^{2-} [8]. Within the cell, a highly concentrated aqueous alkaline electrolyte (usually KOH) dissolves solid sulphur to form a complex equilibrium of ions of sulphide salts:

$$M_xS_y \rightleftharpoons M^{2y/x} + S_y^{2+}$$

polysulfide ions (S^{2-}, S_2^{2-}, S_3^{2-}, S_4^{2-}, S_5^{2-}), hydrosulphide ions (HS^-), H_2S, H_2O, and, of course, H^+ (as H_3O^+) and OH^-. Based on the work described in [6], there are 29 reactions that can occur in this aqueous system.

The authors of [6] concluded that, although the thermodynamics of aqueous polysulphide solutions favour the formation of thiosulphate (i.e. oxo-anion) species, at sufficiently high concentrations of polysulphide species, the polysulphide solution was stable. However, a recent study has shown that this is not the case. Using Raman spectroscopy, the study concluded that there appears to be "[a] strong argument" for the existence of significant quantities of oxidised species in an aqueous polysulphide solution [8]. It is therefore necessary to investigate the thermodynamics of the Zn-S chemistry at the atomistic level.

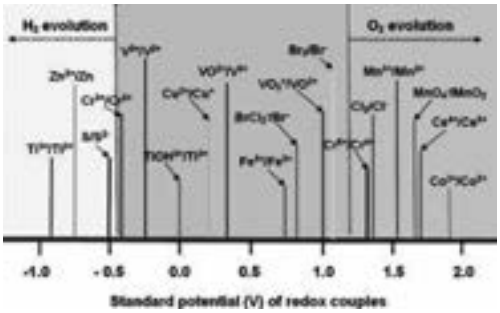

Figure 3: Overview of redox couples of various transition metals [3]

The thermodynamics of an electrochemical energy storage (i.e. battery) system is defined by the Nernst equation:

$$\Delta E^0 = \frac{-\Delta G^0}{nF}$$

where, ΔE^o = standard redox potential

ΔG^o = standard Gibbs free energy of reaction

n = no. of electrons in the redox reaction

F = Faraday's constant

For systems that are not well-defined from an experimental data viewpoint, the determination of the ΔG^o term can be difficult. Given the importance of redox chemistry in, for example, biology, much research has focused on the development of theoretical methodologies for determining the redox potential of a given system. Many research groups have applied DFT or ab initio QM/MM methods [7] to the study of redox potentials in solutions with metal ions and complexes, and have shown a strong correlation between the calculated and experimental Standard Redox Potentials (SRPs).

However, in order to accurately determine the redox potential of a given couple in a supporting liquid electrolyte, it is necessary to first understand the structure of the metal complexes within the solution. As illustrated in [7], determining (with a high level of certainty) the coordination number of highly charged ions in an aqueous environment requires very complex with a significant computational overhead. Other, less computationally intensive, approaches using atomistic-level simulation has shown promise in identifying general trends of the ion structure and thermodynamic properties, whereas a combination of quantum-chemical and atomistic-level theories has provided more insight into the structure of aqueous electrolyte solutions [7].

It is clear that understanding the structure of the ion complexes in concentrated aqueous electrolytes is critical to accurately assessing the thermodynamics – hence, the safety and operating window – of redox flow batteries. Thus, from the perspective of "Life Matters", which is the foundational principle of my employer, Lloyd's Register, this Industrial PhD project will focus on the following;

a) Assessment of the robustness and accuracy of quantum chemical methods of calculating the SRP of a given redox reaction, specifically for aqueous chemistries;

b) Development of a framework for assessing the uncertainty of the thermodynamic assessment of an aqueous RFB system; and

c) Relating the thermodynamic uncertainty to the overall risk analysis of the RFB system.

If time permits, the next step in this project would be the extension of the framework to include non-aqueous RFB chemistries.

In essence, the completion of (b) above entails the development of a screening tool for assessing the thermodynamics of a proposed redox reaction without the need to perform laboratory analyses. The final

product of the project is expected to be screening tool that could be integrated into a multi-scale, multi-physics simulation tool for RFB systems.

References

1. T.M. Lenton, Nature Climate Change (19 June 2011) DOI: 10.1038/NCLIMATE1143
2. A.Z. Weber, M.M. Mench, J.P. Meyers, P.N. Ross, J.T. Gostick, Q. Liu, J. Appl. Electrochem. 41(10) (2011) 1137-1164
3. Z. Yang, J. Zhang, M.C.W. Kintner-Meyer, X. Lu, D. Choi, J.P. Lemmon, J. Liu, Chem. Rev. 111 (2011) 3577-3613
4. E. Peled, D. Golodnitsky, C. Menachem, D. Bar-Tow, J. Electrochem. Soc. 145(10) (1998) 3482-3486
5. R. Ahuja, A. Blomqvist, P. Larsson, P. Pyykkö, P. Zaleski-Ejgierd, Phys. Rev. Lett. 106 (2011) 018301
6. T.A. Bendikov, C. Yarnitzky, S.A. Licht, J. Phys. Chem. 106 (2002) 2989-2995
7. T.S. Hofer, A.K.H. Weiss, B.R. Randolf, B.M. Rode, Chem. Phys. Lett. 512 (2011) 139-145
8. S.A. Khan, R.W. Hughes, P.A. Reynolds, Vibrational Spectroscopy 56 (2011) 241-244

Inês Rodrigues da Silva
Phone: +45 4525 2610
E-mail: ins@kt.dtu.dk
Discipline: Enzyme Technology

Supervisors: Jørn Dalgaard Mikkelsen
Anne S. Meyer

PhD Study
Started: February 2009
To be completed: February 2013

Enzymatic Production of Prebiotic Polysaccharides Using a Bacterial Family 11 RGI Lyase Expressed in *Pichia pastoris*

Abstract
Prebiotics are non-digestible carbohydrates that beneficially affect the host by selectively stimulating the growth of a limited number of bacteria in the colon. The waste streams from agricultural industry are a large source of oligosaccharides with potential prebiotic effects. These streams comprise barley bran, sugar beet pulp and potato pulp from the brewing, sugar and starch industries. Modification of oligomers to achieve the desired prebiotic effect requires a number of specific enzymes which can be acquired by cloning and expression in the yeast *Pichia pastoris*. Aiming for an enzyme able to degrade pectinaceous biomass at elevated temperature we selected a gene encoding a putative rhamnogalacturonan I (RGI) Lyase (EC 4.2.2.-) from *Bacillus licheniformis*. The designed gene was transformed into *Pichia pastoris* and the enzyme was produced in the eukaryotic host with a high titer in a bioreactor. The RGI Lyase was purified by Cu^{2+} affinity chromatography. By use of a statistical design approach, with potato rhamnogalacturonan as the substrate, the optimal reaction conditions for the RGI Lyase were established to be: 61˚C, pH 8.1, and 2 mM of both Ca^{2+} and Mn^{2+} (specific activity 18.4 U/mg). The addition of both Ca^{2+} and Mn^{2+} was essential for enzyme activity.

Introduction
Functional food ingredients possessing potential health benefits have recently attracted strong attention. Some of the functional food ingredients are prebiotic oligosaccharides. Dietary fibers and prebiotics are non-digestible carbohydrates that beneficially affect the host by selectively stimulating the growth and/or activity of one or a limited number of bacteria in the colon. Oligosaccharides could be obtained as products of hydrolysis of plant derived polysaccharides, or directly from plant cell walls. Rational enzyme catalysed reactions are going to be develop to modify heterogeneous samples of substrates to create 'designer' oligosaccharides with defined structures and high prebiotic potential.

Specific objectives
The idea of the project is to use selective enzyme catalysts to convert polysaccharides into oligomers and furthermore decorate the oligomers by hydrophobic residues. Only few commercial enzymes are available for this task. Most of the commercial enzymes in addition contain other enzyme activities which degrade the desired oligosaccharides. Mono-component enzymes can, however, be produced by cloning and expression of suitable enzymes in the yeast, *P. pastoris.* This process can be performed in the laboratory at our department. Furthermore, the optimal conditions of enzymatically catalyzed reactions have to be worked out as well. This include up-scaling of the enzymatic reaction in order to deliver sufficient amount of oligosaccharides with potential prebiotic activity.

Results
A gene encoding a putative rhamnogalacturonan I (RGI) Lyase (EC 4.2.2.-) from *Bacillus licheniformis* was the enzyme selected. The designed gene was transformed into *Pichia pastoris* and the enzyme was produced in the eukaryotic host with a high titer in a bioreactor [1]. We have expressed the enzyme of interests with a MW of 68 kDa. The recombinant proteins we want to produce are isolated by diversity screening or identified in genomic databases. The genes are inserted into *P. pastoris* under the control of the AOX1 (Alcohol Oxidase 1) promotor, in order to induce the gene of interest in the presence of methanol [2, 3].

During the fermentation (95 h) the *P. pastoris* growth was monitored by measuring the OD600, which increased from 1.2 to 620. The OD600 increased slowly from 1.2 to 13 during the glycerol phase (21 h). The

glycerol fed-batch phase (5 h) was characterized by a strong biomass growth where the OD600 values increased from 13 to 74. In the last phase (69 h), the methanol fedbatch phase, the OD600 increased to 620, and the RGI Lyase activity increased almost linearly from 0 to 125 U/ml. The overall activity of the fermentation process (4 l working volume after sterile filtration) was 493 kU. At the Cu^{2+} affinity chromatography step the RGI Lyase was successfully attached by the His6-tag and was selectively eluted by the imidazole gradient (at 50 mM). The total yield of pure recombinant RGI Lyase was 4.29 g protein. The recovery of pure protein in the Cu^{2+} affinity purification process was 81%, with a total activity of RGI Lyase of 79 kU.

The characterization of RGI Lyase was carried out to evaluate the effect of temperature, pH and ions such as Mn^{2+} and Ca^{2+}. The observed activities varied between 0 and 18 U/mg using potato rhamnogalacturonan as the substrate. The response-surface showed the effect of temperature and pH on the activity of RGI Lyase at high concentrations of Ca^{2+} and Mn^{2+} (2 mM). The set of experiments gave rise to a surface with a bell shaped structure that allowed the determination of optimum pH and temperature of the reaction (Fig. 1).

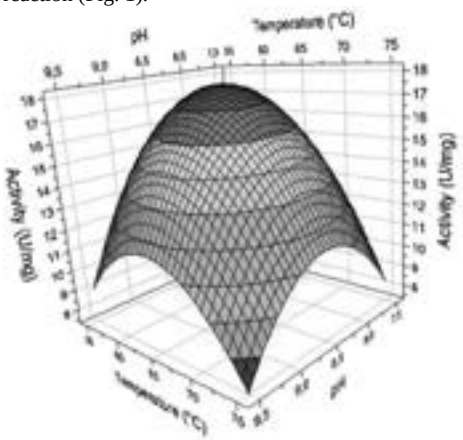

Figure 1: 1st Surface response as a function of Temperature and pH on the RGI Lyase activity. The incubation mixture contained 2 mM Ca^{2+} and Mn^{2+} RGI Lyase activity was measured at pH 8.1 and at a temperature of 61°C. The colours vary from blue (low RGI Lyase activity) to red (high RGI Lyase activity).

Mn^{2+} strongly increased the enzyme activity: from 11 to 18 U/mg, when Mn^{2+} was increased from 0 to 2 mM. Multivariate regression analysis showed that the reaction temperature, Mn^{2+} concentration, and pH significantly influenced the RGI Lyase activity with a statistical significance of $p < 0.001$. The data modeling allowed a definition of the optimum reaction temperature and pH for the enzymatic reaction and also exhibited the positive influence of Ca^{2+} and Mn^{2+} on the RGI Lyase activity. Based on the model, the best factor combination was: temperature 61 ◦C, pH 8.1 and 2 mM concentration of both Ca^{2+} and Mn^{2+} with a RGI Lyase activity of 17.8 U/mg.

In order to assess the thermal stability of the enzyme, enzyme activity assays were performed at the optimum conditions established above, using 2.5, 5, 15 and 30 min of reaction time, at different temperatures (20, 40, 61, 65, 75 and 80 ◦C). When plotting Ln (activity) vs. incubation time a linear relationship was observed showing that the thermal inactivation of RGI Lyase followed first order reaction kinetics (Fig. 2). At 55 ◦C the RGI Lyase had a half-life of 25 min and at 61 ◦C of 15 min. With temperatures higher than 61 ◦C the RGI Lyase activity decreased significantly with incubation time. The enzyme completely lost catalytic activity after half an hour at 80 ◦C.

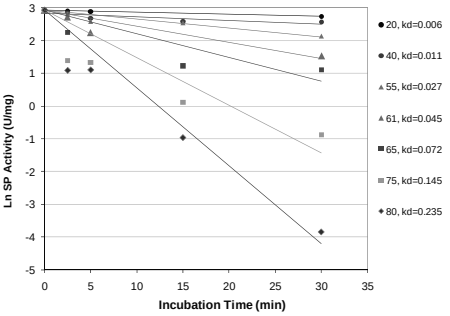

Figure 2: The temperature stability of RGI Lyase was evaluated using temperatures of 20, 40, 55, 61, 65, 75, 80°C and incubation times for 2.5, 5, 15 and 30 minutes. A semilogarithmic linear plot was obtained for time vs. the Ln of the Activity.

Conclusions

This is the first production of a prokaryotic thermostable RGI Lyase in the eukaryotic host *P. pastoris*. The RGI Lyase was active at relatively high temperature (61 ◦C) and high pH (8.1) and showed dependency of manganese. The enzyme is a good target for genetic engineering modifications to increase temperature optimum and thermal stability, and thus serve the need for improved processes to produce healthy prebiotic oligosaccharides from side-streams in the agricultural industries.

References

1. J.L. Cereghino, J.M. Cregg, FEMS Microbiol. Rev. 24 (1) (2000) 45-66.
2. G.P.L. Cereghino, J.L. Cereghino, C. Ilgen, J.M. Cregg, Curr. Opin. Biotechnol. 13 (4) (2002) 329-332.
3. J. Stratton, V. Chiruvolu, M. Meagher, in: D. Higgins and J. Cregg (Eds.) Pichia Protocols, Humana Press, New Jersey, 1998, p 107-120.

Vadim Evseev
Phone: +45 5261 6134
E-mail: vaev@risoe.dtu.dk

Supervisors: Sønnik Clausen
Alexander Fateev

PhD Study
Started: April 2009
To be completed: March 2012

Optical Tomography in Combustion

Abstract
The project concerns the development of methods and equipment for 2-D tomography of gas temperatures in flames and hot gas flows using line-of-sight optical infrared spectroscopy measurements. The equipment developed in the project is aimed for simultaneous time-resolved optical infrared measurements from several lines of sight. The application of the experimental system for simultaneous temperature measurements in the three optical ports of the exhaust duct of the two-stroke Diesel engine is reported. The tomography methods of flame temperature reconstruction from line-of-sight optical infrared spectroscopy measurements are considered.

Introduction
Mixing of cold and hot turbulent reacting gas flows, flame propagation and development are all fast transient phenomena appearing in the three dimensional space. Their temporal development can be described, for example, by a stack of two dimensional slices of tomography images of gas temperature and species concentrations in the direction of the net mass propagation.

Two dimensional temperature and species concentration distributions are necessary for better understanding the combustion phenomena in various environments and force further development of computational fluid dynamics (CFD) codes, burner/engine design, optimization and operation.

Application of optical tomography techniques to internal combustion engines is of particular interest. However practical issues such as limited optical access, vibrations, fouling and soot, high pressures and temperatures make the application of optical techniques difficult.

In the past years, tracer based laser induced fluorescence methods have been widely applied to optically accessible single-cylinder internal combustion engines. These methods offer high spatial and temporal resolution for point measurements as well as provide the possibility to take the 2-D images of equivalence ratio, exhaust gas residuals, fuel concentration, temperature and other quantities [1, 2]. Unfortunately, application of laser-based techniques to industrial engines is difficult and expensive because they need extensive optical access, the alignment of the optical components must be highly accurate and the price of lasers is very high. In addition, tracer laser induced fluorescence requires a tracer to be added to the fuel or intake air, is critical to the types of fuel and purity of the fuel and tracer.

However, some applications of optical methods to close-to-production engines are reported. Barrag et al. [3] imaged temperatures and soot concentrations on a one-cylinder internal combustion engine by designing an optical plate having 16 quartz windows. The plate was mounted between engine cylinder head and engine cylinder block. The plate allows 8 line-of-sight emission/transmission measurements at 0.65 μm. Gas temperature, optical thickness and soot concentration are reconstructed from these line-of-sight measurements by implementing a tomography reconstruction algorithm to obtain 2-D distributions.

Wright et al. [4] developed a technique of chemical species tomography and applied it to a production 4-cylinder internal combustion engine by designing an optical multi-access layer allowing up to 27 line-of-sight measurements in a plane section in the combustion chamber. Each line of sight measurement is a fast dual wavelength ratiometric transmission measurement of hydrocarbon fuel molecules made by two laser sources and a photodiode receiver. The relative fuel distribution is reconstructed from these line-of-sight dual wavelength measurements.

Objectives
A part of this work is focused on developing the equipment for time-resolved optical infrared (IR) measurements made simultaneously on several lines-of-

sight. Simultaneous measurements are essential to provide the data for further tomography reconstruction of gas temperatures and species concentrations in a dynamic system such as a flow of hot gas. The experimental set-up has been successfully applied for time-resolved simultaneous exhaust gas temperature measurements in the three optical ports of the exhaust duct of the two-stroke Diesel engine at MAN Diesel & Turbo, Copenhagen.

Another part of this work is focused on developing the tomography methods of gas temperature reconstruction from several line-of-sight optical IR measurements. The methods are validated using a lab scale methane/air combustion burner producing a stable pre-mixed laminar flame with known temperature profile.

Experimental system

A system has been developed in this work at DTU Chemical Engineering for simultaneous time-resolved IR measurements on several lines of sight.

The system consists of a grating spectrometer and an infrared (IR) camera, Fig. 1. The IR camera is "looking" into the rear focal plane of the grating spectrometer where infrared spectra are formed by the grating. The spectra are then obtained from the infrared images by reading the intensities along the bright strips in the infrared images (see Fig. 1).

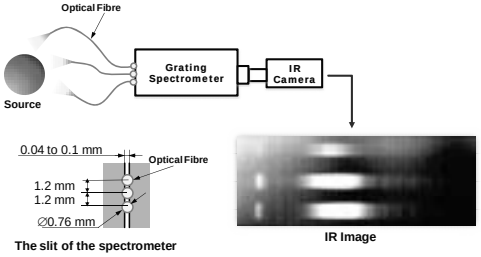

Figure 1: Experimental system.

Major combustion products H_2O and CO_2 have strong absorption bands in the IR spectral range [5] which makes this range useful for combustion diagnostics. Therefore the system is optimized to work in the IR spectral range. The InSb array of the IR camera enables detection in the 1700–10000 cm^{-1} range. The optical set-up of the system also has a long wave pass filter with cut-off at 3300 nm which cuts the wave lengths in higher orders reflected by the grating at the same angles as the wave lengths in the working order. The working spectral range of the system is 2100-2500 cm^{-1} which is sufficient to cover the CO_2 absorption band at 4.3 μm.

The radiation from the source is carried to the entrance slit of the grating spectrometer using three optical fibres which are coupled to the slit with the aid of a dedicated mechanical adaptor. The adaptor is optimized for three fibres which is the requirement of the application (see next Section) but it is possible to couple more fibres. The described experimental system is designed to carry out the IR measurements simultaneously on the three lines of sight.

The temporal resolution of the IR measurements is determined by the frame rate of the camera which is dependent on frame size. The frame size must be sufficient to cover the infrared image obtained from the three optical fibres. Taking account of the present distance between the fibres at the slit, the camera's frame rate can be up to 500 frames per second which is 2 ms of temporal resolution.

Results and discussion

The experimental system was used to carry out fast time-resolved measurements of exhaust gas temperatures in the three optical ports of the exhaust duct of a two-stroke Diesel engine at MAN Diesel & Turbo, Copenhagen.

The simultaneous fast time-resolved IR measurements were carried out in the three optical access ports of the special exhaust duct which was installed in place of a standard exhaust duct on one of the 4 cylinders. Generally, exhaust duct guides the exhaust gases from the exhaust valve of the cylinder to the main exhaust pipe.

The measurement layout is shown schematically in Fig. 2. The blackbody was used to get the reference spectra in the transmission measurements. The emission measurements (without blackbody) were carried out in the three ports simultaneously. The transmission measurements were carried out at different time points in each of the three ports. Nevertheless transmission measurements were necessary to validate the assumption about the emissivity being equal to 0.9. This value was found to be a reasonable approximation based on the analysis of the emission and transmission spectra.

The 2270-2290 cm^{-1} region was chosen for temperature calculation due to this region is free from absorption by cold CO_2 and the absorption by hot CO_2 is sufficient to have a good signal-to-noise ratio. The temperature was calculated directly from the simultaneous emission spectra using Kirchhoff's law [6] and the value of 0.9 for the emissivity. The obtained spectral temperatures in the 2270-2290 cm^{-1} region were averaged over this region at each time point to obtain the temperature points as a function of time. The results of the temperature measurement are shown in Fig. 3.

The temperature obtained in the described above way was compared to the temperature obtained from the UV spectroscopy measurements in the same three optical ports [8]. A good agreement was found (within 50°C).

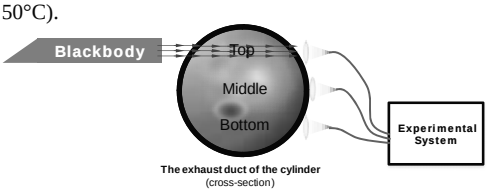

Figure 2: Measurement layout.

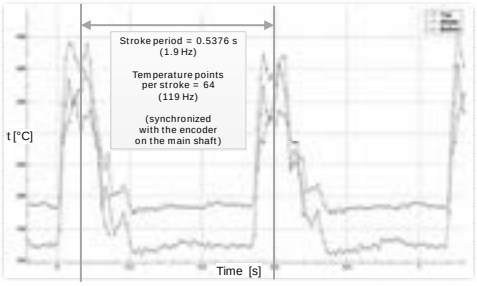

Figure 3: Gas temperature as a function of time in the top (green), middle (blue) and bottom (red) optical access ports in the exhaust duct.

It is important to note that the UV and IR spectroscopy measurements were made at the same engine operation conditions but at different time points. It is also important to mention that the results corresponding to the time points between the valve openings (the sections between the "hills" on the temperature curves, Fig. 3) are strongly affected by noise due to very low signal level and are therefore disregarded.

As one can see from Fig. 3, there are fast variations in the exhaust gas temperature at the time points of the exhaust valve openings ("hills" on the temperature curve). The gas temperature is increasing from the bottom to the top optical port of the exhaust duct due to convection as can be expected from Archimedes' principle. Fig. 3 shows clearly the importance of fast time-resolved and simultaneous measurements that have been achieved using the described experimental system.

Further development

The second part of the PhD project concerns the development of tomography methods of gas temperature reconstruction. This part of the project is under development.

The objective of the experimental work is to perform several line of sight emission/transmission IR measurements on a stable pre-mixed laminar flame having known temperature profile produced by a lab scale methane/air combustion burner [9] (Fig. 4).

The line-of-sight measurements can be arranged as shown in Fig. 5 which is a scheme of parallel scanning or as in Fig. 6 (a) which is a scheme of sweeping scanning.

The parallel scanning scheme is more simple and is used to validate the developed tomography method of temperature reconstruction by comparing the reconstructed temperature profile to the reference one published in [9] (see also below).

The sweeping scanning scheme is more practicable with respect to real conditions of an industrial scale where application of the parallel scanning scheme can be impossible due to limited optical access. The idea is to use several synchronized spectrometers (Fig. 6 (b)] each of which has optically adjustable direction for receiving the incoming beam whereas the walls of a boiler can be regarded as a reference source of radiation.

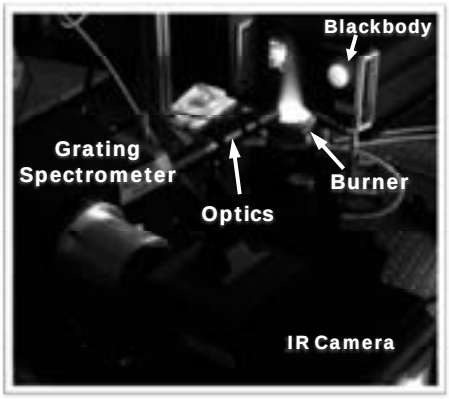

Figure 4: Lab scale methane/air combustion burner producing a stable pre-mixed laminar flame.

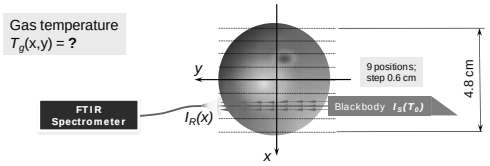

Figure 5: Parallel scanning measurement scheme.

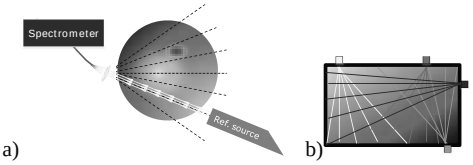

Figure 6: Sweeping scanning measurement scheme.

The theory and methods are based on the the monochromatic radiative transfer equation without scattering [10, 11]

$$\frac{dI(x,y)}{dy} = k(x,y)\left[B(T_g(x,y)) - I(x,y)\right], \qquad (1)$$

where $I(x,y)$ is the irradiance at a wave number ν (omitted in the notation for easier reading), at position x, y (see Fig. 5), $B(T_g(x,y))$ is the Planck blackbody emittance function at wave number ν and temperature $T_g(x,y)$, at x, y, and $k(x,y)$ is the absorption coefficient at ν and x, y. The solution to (1) is

$$I_R(x) = B(T_0)\exp\left(-\int_{y_1(x)}^{y_2(x)} k(x,y)\,dy\right) + \\ + \int_{y_1(x)}^{y_2(x)} k(x,y)\,B(T_g(x,y)) \times \\ \times \exp\left(-\int_{y}^{y_2(x)} k(x,y')\,dy'\right)dy \qquad (2)$$

where $I_R(x)$ is the irradiance on the detector at wave number ν (see Fig. 5), *i.e.* received (measured) total of radiation emitted by the flame plus radiation from the blackbody transmitted through the flame, $B(T_0)$ (denoted as $I_s(x)$ in Fig. 5) is the Planck blackbody emittance function at wave number ν and temperature T_0, and T_0 is the temperature of the blackbody.

Equation (2) can be solved with respect to $T_g(x,y)$ and $k(x,y)$ which is a function of $T_g(x,y)$.

The burner produces an axisymmetric flame with known temperature profile $T_g(r)$ [9] where r is the distance from the centre of the burner to the current point. Axial symmetry simplifies the problem of solving (2) from measured $I_R(x)$ with respect to $T_g(r)$.

Preliminary results for the case of parallel scanning are shown in Fig. 7.

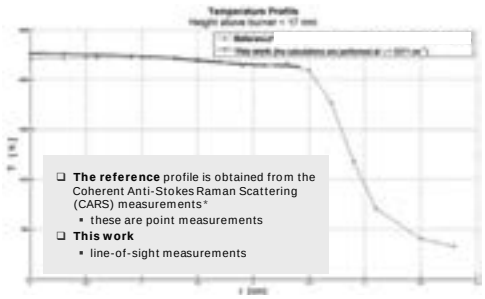

Figure 7: Reconstructed axisymmetric temperature profile from line-of-sight measurements arranged in the parallel scanning scheme in comparison with the reference profile taken from [9].

One can see a good agreement between the reconstructed and reference temperature profiles. Further work has to be done to obtain the reconstructed profile on a more wide range of values of r as well as to implement the algorithm for sweeping scanning.

References

1. C. Schulz, V. Sick, Prog. Energ. Combust. Sci. 31 (1) (2005) 75-121.
2. S. Einecke, C. Schulz, V. Sick, Appl. Phys. B: Lasers Opt. 71 (5) (2000) 717-724.
3. A. Barrag, B. Lawton, Computer optical tomography in the study of internal combustion engine soot concentration, Proceedings of 26th International Symposium Automotive Technology and Automation, Volume The Motor Vehicle and the Environment, Demands of the Nineties and Beyond (ISATA, 1993), 423-430.
4. P. Wright, N. Terzija, J.L. Davidson, S. Garcia-Castillo, C. Garcia-Stewart, S. Pegrum, S. Colbourne, P. Turner, S.D. Crossley, T. Litt, S. Murray, K.B. Ozanyan, H. McCann, Chem. Eng. J. 158 (1) (2010) 2-10.
5. C.N. Banwell, E.M. McCash, Fundamentals of molecular spectroscopy, McGraw-Hill Publishing Company, London, 1994, p. 55-98.
6. R.H. Tourin, Spectroscopic Gas temperature Measurement, Elsevier Publishing Company, Amsterdam, Netherlands, 1966, pp. 14-18, 25-30.
7. R. Oberly, K. Narahari Rao, Y.H. Hahn, T.K. McCubbin Jr., J. Mol. Spectrosc. 25 (1968) 138-165.
8. A. Fateev, S. Clausen, New IR-UV gas sensor to energy and transport sector, Report Risø-R-1758 (EN), Risø National Laboratory for Sustainable Energy, Technical University of Denmark, December 2010.
9. G. Hartung, J. Hult, C.F. Kaminski, Meas. Sci. Technol. 17 (2006) 2485-2493.
10. R.H. Tourin, B. Krakow, Appl. Optics 4 (2) (1965) 237-242.
11. J. Heland, R. Haus, K. Schafer, Sci. Total Environ. 158 (1994) 85-91.

Michael Frost
Phone: +45 4525 2876
E-mail: mifro@kt.dtu.dk
Discipline: Engineering Thermodynamics

Supervisors: Georgios M. Kontogeorgis
Nicolas von Solms

PhD Study
Started: June 2011
To be completed: May 2014

Measurements and Modelling of Phase Equilibrium of Oil-water-polar Chemicals

Abstract
As the exploitable oil resources decrease, more advanced recovery methods are employed in the oil industry. This has led to an increase in used chemicals, in order to ensure a constant and safe production. These chemicals have many applications, and are part of different families like alcohols, glycols, alkanolamines etc. Due to rising demands from environmental agencies and a wish for a more refined product, it is becoming increasingly important for downstream processing to know/predict the solubility of oil and gas with different complex chemicals. The objective of this project is to further develop the CPA equation of state for use in calculation of solubility between oil and polar chemicals.

Introduction
Chemicals are added in almost all stages of oil and gas production. It is generally accepted that efficient and cost effective oil and gas production is not possible without the use of chemicals. Monoethylene glycol (MEG) and methanol are two of the most widely used production chemicals. They are used as gas hydrate inhibitors to ensure safe production and transportation. The prediction of the distribution of chemicals in oil, water and gas streams is important for the oil industry to ensure reliable production and processing. It is also important information to fulfill the demand from environmental authorities, in order to know the amounts of chemicals and hydrocarbons in a processed water stream for ensuring safety of marine life. Furthermore it is important for efficient design/operation of separation equipment. The partitioning of the chemicals can either be measured experimentally or predicted using a suitable thermodynamic model. The experimental method is expensive and challenging, partly due to the difficulties involved in measurements of such low solubilities. The CPA equation of state proposed by Kontogeorgis *et al.* [1] has been successfully applied in the past to well defined systems containing associating compounds (such as water, methanol and MEG). It has also, to a first extend, been successfully applied to reservoir fluids in presence of water and polar chemicals, using a characterization method (Pedersen *et al.* [2]), modified by Yan *et al.* [3]. In order to understand these complex systems and to further develop/validate CPA, more experimental data is desirable. This work focuses on producing new experimental data for both well defined multi-component mixtures, as well as for systems containing oil-water-polar chemicals.

Specific Objectives
As basis for the further development of CPA, the aim of this project is threefold:

- Produce experimental data (LLE/VLLE) for well-defined systems (containing water, hydrocarbons and polar chemicals).
- Carry out oil-water-MEG measurements for oil systems not previously studied – emphasis to heavy oils and those with high aromatic/naphthenic content.
- Develop and validate the CPA equation of state based on data generated and relevant literature data. It is of special importance to develop an oil characterization method which can be used for a wide range of oils and conditions.

Thermodynamic Modeling
Thermodynamic modeling is carried out using the CPA equation of state, with the characterization method described in ref. 3. Both MEG and water have been modeled using four association sites (so-called 4C scheme).

The CPA equation of state uses five pure component parameters, including three for non associating compounds and two for associating compounds. For mixtures containing more than one associating compound, a combining rule is needed for the association parameters. In this work the Elliot Combining Rule (ECR) has been used.

A binary interaction parameter (k_{ij}) is needed for each binary system. For binary interaction parameters between MEG and hydrocarbons, an average value is used. This is done due to lack of relevant experimental data. The binary interaction parameters between water and hydrocarbons are obtained from a generalized expression using a correlation in terms of carbon number as given by the following expression.

$$k_{ij} = -0.026 \cdot N_C + 0.1915$$

where N_C is carbon number of an alkane. The used binary interaction parameter between MEG and water is -0.115 using ECR.

Results and discussions

Experimental data are available for a North-sea condensate with MEG and MEG/water. The composition of the condensate is given in Table 1.

Table 1: Composition of a North-sea condensate

Component	Weight %	MW g/mol	Density kg/m^3
Ethane	0.001	30.07	356.7
Propane	0.351	44.09	506.7
iso-Butane	1.229	58.12	562.1
n-Butane	4.031	58.12	583.1
Neopentane	0.03	72.15	597
iso-Pentane	3.494	72.15	623.3
n-Pentane	4.659	72.15	629.9
C6 total	**7.77**	**85**	**666.2**
C7 total	**13.016**	**91.4**	**736.2**
C8 total	15.293	103.6	768.6
C9 total	**9.363**	**118.5**	**780.6**
C10+	**40.766**	**189.4**	**846.4**

In the MEG - condensate system, MEG is a polar compound which self associates. Condensate consists of several hydrocarbon fractions, which are modeled as non-associating or inert compounds.

Figure 1 presents experimental data and predictions made with CPA for a mixture of condensate – water – MEG. This shows that the solubility of condensate and MEG decreases with increasing water content in the polar phase. The modeling results are satisfactory considering that a single and same temperature independent binary interaction parameter is used for all MEG-hydrocarbon pairs.

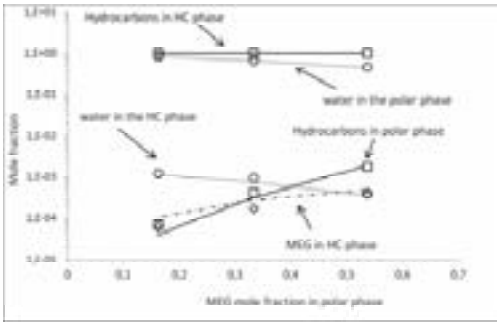

Figure 1: Mutual solubility of MEG - water - condensate. The points are experimental data and the lines are CPA predictions.

Future work

- Modeling of more/new systems of oil-MEG-water
- Further experiments with more aromatic/naphthenic oils
- Further experiments of well-defined systems (VLLE/LLE/VLE)

Acknowledgements

The authors wish to thank the industrial partners in the CHIGP (Chemicals in Gas Processing) consortium for financial support.

References

1. G.M. Kontogeorgis, E.C. Voutsas, I.V. Yakoumis, D.P. Tassios, Ind. Eng. Chem. Res. 35 (1996) 4310.
2. K.S. Pedersen, P. Thomassen, A. Fredenslund, Characterization of gas condensate mixtures, Advances in thermodynamics, Taylor & Francis, New York, 1989
3. W. Yan, G.M. Kontogeorgis, E.H. Stenby, Fluid Phase Equilib. 276 (2009) 75-85.

Kaustav Goswami
Phone: +45 4525 6885
E-mail: kago@kt.dtu.dk
Discipline: Polymer Technology

Supervisors: Anne Ladegaard Skov
Ole Hassager

Started: August 2011
To be completed: July 2014

Surface vs. Bulk Properties and Inhibitors of Poly (Dimethylsiloxane) (PDMS) Films Applied in Dielectric Electro Active Polymer (DEAP) Applications

Abstract
In this study we present the surface and bulk properties of 2mm thick PDMS films by analyzing Fourier transform infrared spectroscopy (FTIR) spectra from three different portions of the film. From the spectra we found that there is a difference in the residual vinyl group concentration from the middle, top and bottom portion of the film also we have tried to find out the reason behind this difference. Apart from the crosslinking reaction of PDMS we have identified potential inhibitors of PDMS hydrosilylation reaction.

Introduction
A Dielectric Electro Active Polymer (DEAP) actuator is basically a compliant capacitor, where a thin elastomer film is sandwiched between two compliant electrodes. When a high DC voltage (kV) is applied to the electrodes, the arising electrostatic pressure squeezes the elastomer film in thickness and thus the film expands in planar directions. When the voltage is switched off, the elastic film returns to its original shape.

Poly(dimethyl siloxane) (PDMS) finds its applications in DEAP material due to its unique properties like flexibility at room temperature (very low glass transition temperature ~-123^{0}C) and fast response time.

For thin films it is required to have a fast and homogeneously curing PDMS, thus vinyl end capped PDMS is considered to be the best choice as it shows very little shrinkage upon curing with reasonably fast curing time.

A three dimensional silicone network is created by the hydrosilylation reaction between the vinyl group of the polymer and the hydride group of the crosslinker [1].

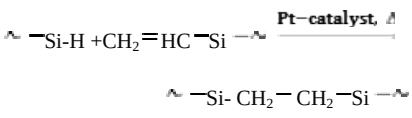

$$\sim\!\!-\text{Si-H} + \text{CH}_2{=}\text{HC}-\text{Si}-\sim \xrightarrow{\text{Pt-catalyst},\ \Delta} \sim\!\!-\text{Si-}\text{CH}_2-\text{CH}_2-\text{Si}-\sim \qquad (1)$$

Apart from the primary reaction (equation 1) between the vinyl group and hydride group, secondary reactions can also occur when there is higher amount of crosslinker or during the 'post-curing' stage. Secondary reactions are shown in the following reactions.

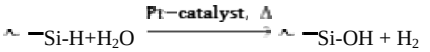

$$\sim\!\!-\text{Si-H} + \text{H}_2\text{O} \xrightarrow{\text{Pt-catalyst},\ \Delta} \sim\!\!-\text{Si-OH} + \text{H}_2 \qquad (2)$$

The first step is the hydrolysis of the crosslinker in the presence of moisture (equation 2). Crosslinking happens in the post curing stage when the newly formed –SiOH reacts with either the crosslinker (equation 3) or with another –SiOH (equation 4) to form Si-O-Si linkages.

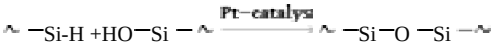

$$\sim\!\!-\text{Si-H} + \text{HO}-\text{Si}-\sim \xrightarrow{\text{Pt-catalyst}} \sim\!\!-\text{Si}-\text{O}-\text{Si}-\sim + \text{H}_2 \qquad (3)$$

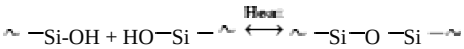

$$\sim\!\!-\text{Si-OH} + \text{HO}-\text{Si}-\sim \xleftrightarrow{\text{Heat}} \sim\!\!-\text{Si}-\text{O}-\text{Si}-\sim + \text{H}_2\text{O} \qquad (4)$$

Reaction 2 and 3 are much slower than the crosslinking reaction (equation 1). Also it has been found that the condensation reaction (equation 4) is even slower than reaction 2 and 3. Equation 2-4 are jointly called the 'post-cure' reacton because it occurs only when the system is forced to completion under favourable condition.

Extensive literature study was done on vinyl terminated PDMS thin films mainly highlighting on the surface and bulk properties and potential inhibitors that can cause a very slow rate of curing or can even stop the curing reaction. In one paper [2] it was mentioned that due to low surface energy of silicone, reactive components such as crosslinker and catalyst can migrate from the bulk to the surface thereby making a concentration gradient of those components along the cross section of the film. Also the paper by Jones [3] it was mentioned that short range mobility of polymer enhances near the free surface. According to Lewis [4] there is a catalytic role of oxygen in the hydrosilylation reaction and as films have a greater surface area to volume ratio, a greater fraction of components can be found in the surface making it much easier for the oxygen to react with the platinum catalyst. It was found that all of these effects coupled together, the reaction kinetics of PDMS thin films differ from that of the bulk. It is also important to keep in mind that the main disadvantage of using vinyl terminated PDMS is that the platinum catalyst is very much prone to inhibition unless proper precautions are taken.

Objective

The objective of the present study is to investigate the surface and bulk properties of PDMS mainly by FTIR and to identify different classes of inhibitors for PDMS hydrosilylation reaction.

Results

FTIR analysis of 2 mm thick PDMS samples was carried out in Perkin-Elmer spectrum one machine from 650 cm^{-1} to 4000 cm^{-1} with 4 cm^{-1} spectral resolution.

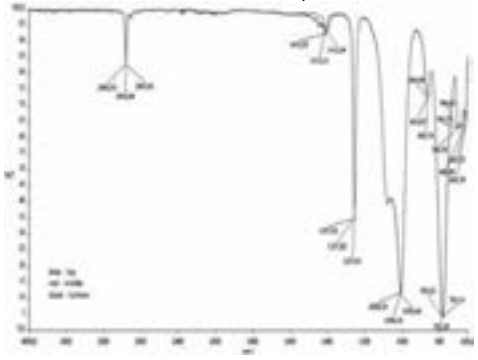

Figure 1: FTIR spectra of 2 mm thick PDMS sample.

The characteristic peaks of PDMS are at 1008 cm^{-1} (-Si- O-Si-), 1260 cm^{-1} (-Si-CH_3), 1413 cm^{-1} (vinyl) and 2962 cm^{-1} (-CH_3 stretching) can be seen clearly in Figure 1. Also a closer look at the vinyl peak reveals that there is a clear difference in the vinyl content at the top, middle and bottom of the PDMS film (Figure 2). The reasons could be because of the previously mentioned factors but the trend was not that found by Keddie and co-workers [2] because we found that the vinyl content at the middle portion of the film is much lower than the top and bottom portion but we can clearly say that due to some effect there is a gradient of crosslinker and catalyst concentration across the thickness of the film (because we found a difference in residual amount of vinyl group across the film).

Table 1 shows different classes of inhibitors of the curing reaction a closer look revealed compounds containing lone pair of electrons which they can share easily with the platinum complex are generally inhibitors.

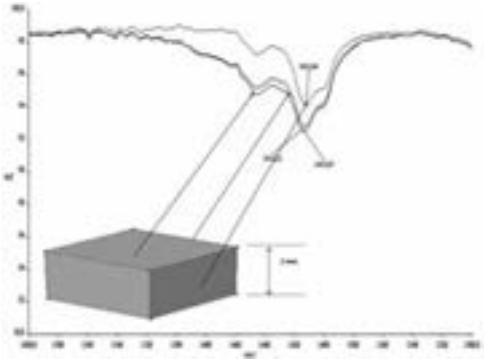

Figure 2: Vinyl peak position of PDMS sample. Blue curve: Top surface, Black curve: Bottom surface, Red curve: Middle portion of the sample.

Table 1: Inhibitors of hydrosilylation reaction.

Nitrogen	Sulfur	Tin	Phosphorus	Solvents/ Monomers
Amine	Sulfides	Tin salts	Phosphine	Esters
Nitroso	Allylthio-urea	-	Phosphite	Alcohols
Chelate	-	-	-	Unsaturated compound

The reaction rate between the inhibitors and platinum complex is much faster than the curing reaction thus in presence of inhibitors the curing reaction is stopped.

Discussion

For thin films we found that there is a differential concentration of the catalyst and crosslinker along the thickness of the film but thicker films (5 mm. and even higher) didn't give any such differences which agrees with the results from Keddie and co-workers.

Reference

1. T.R.E. Simpson, Z. Tabatabaian, C. Jeynes, B. Parbhoo, J.L. Keddie, J. Polym. Sci. Pol. Chem. 42 (2004) 1421–1431.
2. T.R.E. Simpson, B. Parbhoo, K.L. Keddie, Polymer 44 (2003) 4829-4838.
3. R. Jones, Curr. Opin. Coll. Interf. Sci. 4 (1999) 153–158.
4. L.N. Lewis, J Am. Chem. Soc. 112(16) (1990) 5998–6004.

Yao Guo
Phone: +45 4525 2935
E-mail: yg@kt.dtu.dk
Discipline: Enzyme Technology

Supervisors: Jørn Dalgaard Mikkelsen
Carsten Jers

PhD Study
Started: August 2010
To be completed: August 2013

Enzymatic Production of Human Milk Oligosaccharides

Abstract
Human milk oligosaccharides (HMOs) are complex glycans that are present at high amounts in breast milk. The structural complexity of HMOs confers unique benefits on human health [1], e.g. protection of infants against infections and diarrhea. Only trace amounts of these oligosaccharides are present in bovine milk-based infant formula. In order to produce genuine HMOs, this project explores a sustainable way to develop an enzymatic process capable of converting certain kinds of food materials into the desired products.

Introduction
Human milk is usually the sole nutrition source for the first few months of human life. Not only does it contain the essential nutrients for the infants to grow and thrive, but also it provides health benefits beyond traditional nutrients. These distinctive benefits, *e. g.* serving as prebiotics to nourish desirable bacteria in the human intestines [1], protection of infants against infections and diarrhea [2], are attributed to human milk oligosaccharides (HMOs). HMOs are the third largest component in human milk after lactose and lipid. The building blocks of HMOs are D-glucose, D-galactose, N-acetylglucosamine, fucose and sialic acid (Figure 1).

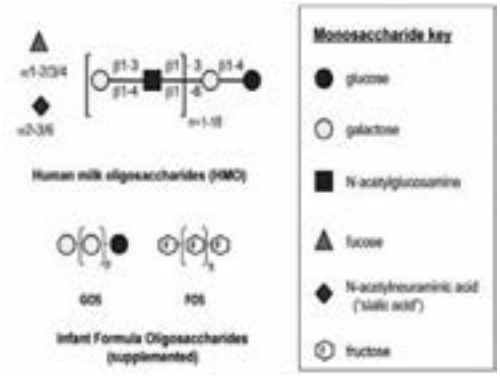

Figure 1: Structural composition of human milk and infant-formula oligosaccharides

Lactose forms the reducing end of HMOs, in which galactose could be sialylated or fucosylated to form sialyllactose or fucosyllactose, respectively. These trisaccharides constitute the short chain HMOs. To form more complex structures of HMOs, lactose is elongated with N-acetyllactosamine repeat units (polylactosamine). Lactose and polylactosamine backbone could be further sialylated or fucosylated in varied linkages. Hence, HMOs differ in molecular weight and structure. Approximately 200 distinct oligosaccharides have been identified in human milk [3]. The beneficial effects of HMOs depend on specific oligosaccharide structures, which include prebiotic, anti-adhesive, glycome modifying and immunomodulatory effects as well as brain development.

Specific Objective
The beneficial effects of HMOs have led to attempts to mimic these using inexpensive alternatives such as galactooligosaccharides (GOS), fructooligosaccharides (FOS), and inulin. While they possibly have prebiotic effects, the fact that many of the traits of HMOs are structure-specific renders them unlikely to effectively mimic HMOs. In this project we aim to develop an enzymatic process for production of some of the key HMOs for supplementation of infant formula. The specific objective of the present PhD study is to develop novel food grade enzymes capable of generating HMOs from side-streams in the agricultural and food industries.

The research focuses on identification of enzymes with desired properties by screening of fungal collections (Figure 2) as well as bioinformatics approaches. Identified enzymes will be further optimized via molecular evolution and then investigated for their applicability in biosynthesis of HMOs. By using several food materials as substrates, desired oligosaccharides will be produced in a reactor.

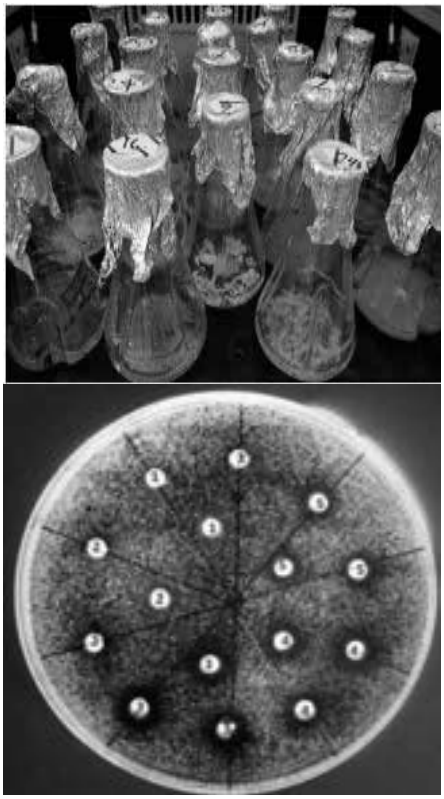

Figure 2: Diversity screening of interesting enzymes from fungal strains

References

1. P. Gyögy, R.F. Norris, C.S. Rose. Arch. Biochem. Biophys. 48 (1954) 193–201.
2. G.M. Ruiz-Palacios, L.E. Cervantes, P. Ramos, J. Biol. Chem. 278 (2003) 14112–14120.
3. L. Bode. Nutr. Rev. 67 (2009) S183–S191.

Stine Hansen
Phone: +45 4525 2846
E-mail: sha@kt.dtu.dk
Discipline: Reaction and Transport Engineering

Supervisors: Peter Glarborg
Peter Arendt Jensen
Flemming Frandsen
Bo Sander, DONG Energy

PhD Study
Started: January 2010
To be completed: January 2014

Model for Deposition Build-Up in Biomass Suspension Boilers

Abstract
In the short term, the most promising way to reduce the CO_2 emission from heat and power production is to replace fossil fuels with renewable fuels such as biomass and waste. However, compared with fossil fuels, biomass and waste are difficult to handle in terms of pre-treatment, boiler operation, and solid residues. In particular, the content of inorganic species such as sulfur, chlorine, potassium, and sodium is a concern due to enhanced propensity for deposition and corrosion. The objective of this project is to develop an engineering model that predicts the rate of deposit build-up and shedding during full-scale suspension firing of wood and/or straw. The model will be validated against full-scale experimental data.

Introduction
In the short term, the most promising way to reduce the CO_2 emission from heat and power production is to replace fossil fuels with renewable fuels such as biomass and waste. However, compared with fossil fuels, biomass and waste are difficult to handle in terms of pre-treatment, boiler operation, and solid residues. In particular, the content of inorganic species such as sulphur, chlorine, potassium, and sodium is a concern due to enhanced propensity for deposition and corrosion. The chlorine is partly or fully released to the gas-phase during combustion, mainly in the form of alkali chlorides. This causes operational risks in effective power plants with high steam temperatures (> 450^{o}C). Alkali chlorides serve to transfer Cl^- to the superheater deposit. The chlorine then decreases the melting point of the deposited fly ash and will at least partly be oxidized to free chlorine, which reacts with the superheater alloy. This reaction acts to corrode the alloy and decreases markedly the lifetime of the superheaters [1-3]. The concern about deposition and corrosion puts severe constraints on the superheater temperatures and thus the electrical efficiency of the biomass-fired units, both the centralized, pulverized-fuel power plants and the decentralized, grate-fired units.

In recent years, significant research efforts have aimed to develop an understanding of the mechanisms responsible for the deposition and corrosion, and their dependence on fuel properties and process parameters. Work has covered combustion conditions in a biomass fuel bed [4, 5], the release of inorganic elements from annual biomass crops [6] and wood [7, 8], gas-phase conversion of K/S/Cl and formation of aerosols [9, 10], and build-up and shedding of deposits [2, 11, 15, 16]. While this work has contributed to a better understanding of issues related to deposition and corrosion, quantitative predictive tools for the deposition build-up as function of fuel composition and combustion conditions have yet to be developed, both for pulverized-fuel fired and grate-fired systems.

Objectives
The objective of this project is to develop an engineering model that predicts the rate of deposit build-up and shedding. The input to the model should be the local flue gas concentration, the flue gas chemistry, the particle size distribution and chemistry of the fly ash particles and local temperatures. The project is limited to deposit build-up during suspension firing of biodust. The model will be validated against experimental data from full-scale measurements of biodust suspension firing [13, 14]

Project
The model needs to address the physical and chemical processes in the deposition build-up and shedding. The modeling study will draw on previous experience at DTU Chemical Engineering and elsewhere, *e.g.* [15,16]. With respect to the modeling of deposit build-up, several mechanisms contribute to the formation and growth of a deposit layer. These mechanisms are illustrated in Figure 1.

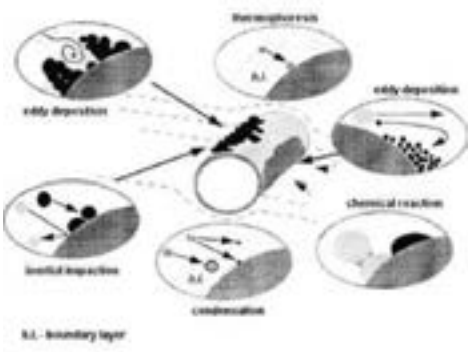

Figure 1: Mechanisms that control deposition and maturation of ash deposits [16].

These mechanisms have been described and modeled for deposition on a probe in a full scale straw-fired grate boiler [15]. Although differences in combustion conditions and ash properties have been observed between grate and suspension firing of biomass [13] the modeling approach used in ref [13] is expected to be applicable to the conditions in a suspension fired boiler.

Once the deposits are formed on a heat transfer or probe surface physical and chemical transformations may occur within the deposit, depending on temperature, chemistry and structure of the deposit [16]. These internal changes are important for the strength and the melting behavior of the deposit and thereby on the mechanism of deposit removal. Figure 2 illustrates the relationship between the deposit characteristics and the shedding mechanism.

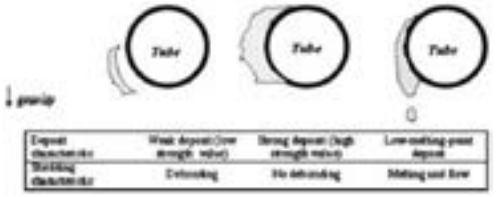

Figure 2: Relationship between the deposit and shedding characteristics. Cases are ordered in the sequence of decreasing viscosity [16].

The strength of the deposit is to some extent determined by the degree of sintering. Sintering is a solidification process serving to consolidate the individual ash particles [16]. Table 1 summarizes various shedding mechanisms and the types of deposit for which they occur. It has been observed in full-scale experiments that the shedding from a probe occurs with different mechanisms in grate and suspension firing of straw [13]. In grate firing of straw, the shedding by melting and flow of a liquid slag is found to be the dominant mechanism with no de-bonding occurring. Contrary, in suspension firing of straw the mechanism of shedding is observed to be de-bonding of 'chunks' of deposit. These differences are most likely related to differences in the deposit chemistry which was also observed at the two full-scale experiments [13].

Table 1: Occurrence of the deposit removal mechanism depending on the type of deposit. Adapted from [16]

Mechanism	**Deposit type**			
	Powdery	Lightly Sintered	Heavily sintered	Liquid Slag
Erosion	++	+	-	-
Gravity Shedding	++	+	-	-
Melting	-	-	-	++
Thermal Shock	-	+	++	-
Mechanical shock	++	++	+	-

With respect to models of sintering and shedding by de-bonding, only scarce data are available [16] and this will be a major challenge in the project.

Acknowledgement
The PhD study is part of the GREEN research center (Power Generation from Renewable Energy) funded by the Danish Strategic Research Center. The PhD study is co-funded by the MP2T Graduate School and by DONG Energy Power.

References

1. B. Sander, N. Hendriksen, O.H. Larsen, A. Skriver, C. Ramsgaard-Nielsen, Proceedings of the First Word conference on biomass for industry. Sevilla, Spain 2002 5-9 June 2002.
2. H.P. Nielsen, F.J. Frandsen, K. Dam-Johansen, Energ. Fuel. 13 (1999) 1114-1121.
3. M. Aho, E. Ferrer, Fuel 84 (2005) 201-212.
4. R. van der Lans, L.T. Pedersen, A. Jensen, P. Glarborg, K. Dam-Johansen, Biomass Bioenerg. 19 (2000) 199-208
5. H. Zhou, A.D. Jensen, P. Glarborg, P.A. Jensen, A. Kavaliauskas, Fuel 84 (2005) 389-403
6. J.N. Knudsen, P.A. Jensen K. Dam-Johansen Energ. Fuel. 18 (2004) 1385-1399
7. S.C. van Lith, V.A. Ramirez, P.A. Jensen, F.J. Frandsen, P. Glarborg, Energ. Fuel. 20 (2006) 964-978
8. S.C. van Lith, P.A. Jensen, F.J. Frandsen, P. Glarborg, Energ. Fuel. 22 (2008) 1598-1609
9. P. Glarborg, P. Marshall, Combust. Flame 141 (2005) 22-39
10. F. Hindiyarti, F.J. Frandsen, H. Livbjerg, P. Glarborg, P. Marshall, Fuel 87 (2008)1591-1600
11. A. Zbogar, F.J. Frandsen, P.A. Jensen, P. Glarborg, Prog. Combust. Energy Sci. 31 (2005) 371-421
12. A. Zbogar, P.A. Jensen, F.J. Frandsen, J. Hansen, P. Glarborg, Energ. Fuel. 85 (2006) 512-519
13. M.S. Bashir *et al*. Fuel Process. Technol. (2011) (Submitted)
14. M.S. Bashir *et al*. Energ. Fuel. (2011) (Submitted)
15. H. Zhou *et al.* Fuel 86 (2009) 1519-1533
16. A. Zbogar *et al.* Prog. Energ. Combust. Sci. 35 (2009) 31-56

Hamid Hashemi
Phone: +45 4525 2809
E-mail: hah@kt.dtu.dk
Discipline: Reaction and Transport Engineering

Supervisors: Peter Glarborg
Jakob Munkholt Christensen

PhD Study
Started: April 2011
To be completed: April 2014

Combustion Characterization of Bio-derived Fuels and Additives

Abstract
Combustion characteristic data of bio-derived alcohols and mixtures of natural gas with different additives at high pressure and intermediate temperature is the major aim of this project. For this purpose, a set of experiments on a high pressure laminar flow reactor is planned. Furthermore, development of a reaction mechanism to address involved processes is desired.

Introduction
In recent years, natural gas has attracted interest as an alternative fuel for use in conventional internal combustion engines. Longer ignition times and slower flame speed resulting in unburned hydrocarbons and performance deficiencies are main challenges in the use of this fuel in such engines. To address these problems, it was suggested to adjust the combustion properties of natural gas via additives for suitable performance in engines. On the other hand, alcohols derived from biofuels have potential as high-quality diesel fuels / additives as they appear to reduce soot formation. One probable scenario to have more "green" engines in mid time is to use alcohols derived from bio-sources in combination with natural gas. Knowledge about combustion characteristics of the mentioned fuels and their combination will facilitate chemical modeling of combustion processes involved in internal combustion engines and other heavy duty applications of natural gas.

Few data are available for combustion characteristics of bio-derived alcohols at high pressures. These limitations influence development of appropriate reaction mechanisms for modeling. Furthermore, effects of additives on natural gas combustion at high pressure and intermediate temperature, attractive for ignition in internal combustion engines, are not investigated thoroughly. In the unique high-pressure flow reactor setup at DTU Chemical Engineering, it is possible to investigate combustion of the natural gas with different compositions and also effects of additives on it. It is possible to achieve up to 100 bar pressure in the reactor while isothermal part is been kept at 900 K temperature.

Objectives
Obtaining characteristic data from combustion of bio-derived alcohols and mixtures of natural gas with different additives at high pressure and intermediate temperature via experiments is the first aim of this project. Furthermore, it is desired to modify current reaction mechanisms [1] developed at our group to address combustion of the mentioned mixtures of fuels. Finally, the implication for use of the selected fuels in diesel engines will be addressed.

Results and Discussion
An extensive work on modeling of previously measured data on ethane/air chemistry at high pressures – intermediate temperatures and in a wide range of stoichiometries has been done. Results suggest minor modifications to the current reaction mechanism developed by Gersen et al [1]. This part of the work is being done in collaboration with the University of Groningen and Gasunie Engineering and Technology, where they are doing experiments on ignition delay time of ethane/air in a rapid compression machine.

Figures 1 and 2 show results for reducing conditions. Ignition was observed at 798 K / 20 bar, 748 K / 50 bar, and 698 K / 100 bar. Results of stoichiometric conditions are shown in Figures 3 and 4. In these conditions, ignition was postponed until higher temperatures; at 848 K / 20 bar, 798 K / 50 bar, and 773 K / 100 bar. Interestingly, as shown in Figure 5, the ignition temperature has not been influenced by further dilution up to oxidizing conditions; ignition was observed at 848 K / 20 bar, 798 K / 50 bar, and 773 K / 100 bar.

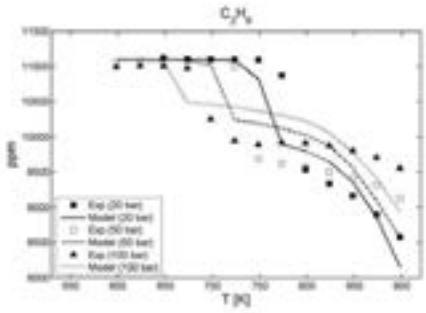

Figure 1: Results of reducing conditions with C_2H_6/O_2. Symbols mark experimental results and lines denote model predictions.

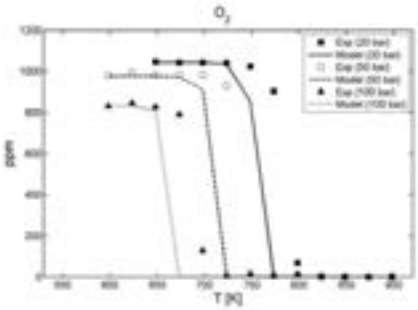

Figure 2: Results of reducing conditions with C_2H_6/O_2. Symbols mark experimental results and lines denote model predictions.

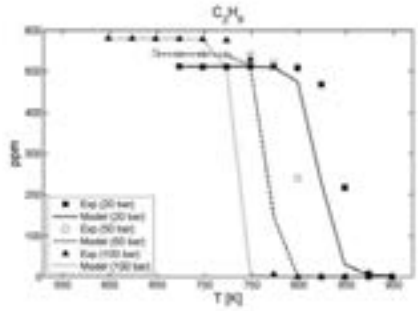

Figure 3: Results of stoichiometric conditions with C_2H_6/O_2. Symbols mark experimental results and lines denote model predictions.

Generally, the model predictions and experimental data are in good agreement. However, there are some differences, *e.g.* for 20 bar pressure, the model predicts that ignition starts at 773 K but experiments show that the mixture is not going to ignite up to 798 K at this pressure. This pre-mature ignition in the model noticeably repeats in other pressures and stoichiometries. While at stoichiometries near unity this premature ignition by the model is insignificant, it becomes more pronounced in oxidizing and reducing conditions.

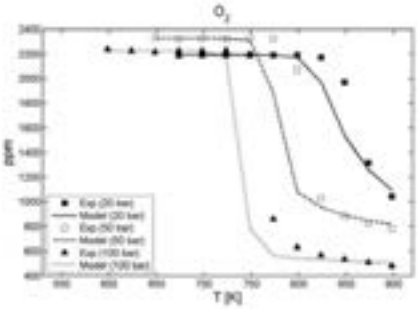

Figure 4: Results of stoichiometric conditions with C_2H_6/O_2. Symbols mark experimental results and lines denote model predictions.

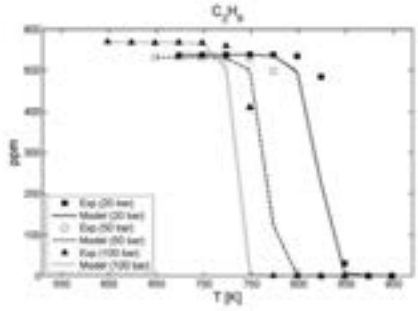

Figure 5: Results of oxidizing conditions with C_2H_6/O_2. Symbols mark experimental results and lines denote model predictions.

Conclusion

Further work on combustion chemistry of ethane is suggested. Meanwhile, valuable data would be obtained via planned experiments on DME, Natural gas, and light alcohols, which are expected to lead to improvement in the current reaction mechanism.

Acknowledgement

Funding from the European Graduate School is gratefully acknowledged.

References

1. S. Gersen, A.V. Mokhov, J.H. Darmeveil, H.B. Levinsky, P. Glarborg, Proceedings of the Combustion Institute, 33 (2011) 433–440.

Stefan Heiske
Phone: +45 2132 5250
E-mail: shei@kt.dtu.dk

Supervisors: Jens Ejbye Schmidt
Ragnhildur Gunnarsdottir

PhD Study
Started: December 2011
To be completed: December 2014

Novel Small Scale Biogas Concepts for Local Waste Handling and Energy Production in Greenland

Abstract
Environmental conditions and available biomasses in arctic regions imply new and complex challenges for biogas technology. The development of a biogas concept for remote areas in Greenland requires detailed analysis of respective conditions, adjustment of operational parameters and adaptation of technology. This project aims on providing an integrated biogas solution suitable for arctic areas which can improve local energy supply and waste handling.

Introduction
Many Greenlandic communities consist of small remote settlements which are in lack of sound waste handling and sanitation. Moreover, their energy supply often depends on costly long-distance oil delivery. Raising energy prices and vulnerability of supply have increased interest in renewable options. Additionally, the disposal of waste and wastewater to the environment and sea raises environmental and hygienic concerns.

The introduction of local biogas plants could potentially be the ideal incentive to approach these problems - the treatment of organic waste in a biogas reactor comes with three major benefits: Reduction of waste, hygienization and renewable energy production. Biogas plants could therefore both improve waste handling and secure energy supply, ensuring the sustainability and endurance of Greenland's peripheral communities.

Implementing biogas plants in Greenland comes with several specific challenges: Low temperature conditions throughout the year require innovative plant design and operational adaptations. Also, the available biomasses in Greenland are largely unexplored as biogas feedstock. Furthermore, irregular seasonal biomass supply to a biogas reactor can cause process failure, implying the need for new measures which can ensure reliable operation. In addition, the remote location and the absence of technical staff require low maintenance and easy-to-handle technology that can be accepted by the local community.

Main strategy
To approach the development of novel small scale biogas concepts suitable for remote settlements in Greenland, the following strategy will be applied: Investigations on local resources and conditions will provide the basis for the concept. In the following, laboratory trials and technical studies will specify plant design and operational approaches. The strategy's milestones are:

1. Mapping, characterization and biogas potentials of waste and biomass resources suitable for biogas production in a selected region in Greenland.
2. Assessment of the biogas process performance and stability with the selected biomasses/wastes in lab-scale digestion experiments.
3. Development of novel and generic biogas concepts suitable for arctic conditions and multiple waste types.
4. Development of (an) innovative small scale biogas plant(s) for a specific case/area and respective biomasses/wastes.

Specific objectives
To identify potential resources, local wastes and residues will be mapped, chemically characterized and the biogas potential of the biomasses will be determined using batch trials. As the involved biomasses are widely unexplored as feedstock for biogas production, the biogas process performance will be tested with regard to specific feedstock and feedstock combinations in newly designed reactor experiments. Further, tests with irregular reactor feed patterns will assess the

vulnerability of the process to unstable biomass supply and identify measures to ensure process stability will be evaluated.

Based on the gained knowledge new biogas concepts will be developed which additionally consider aspects like involvement of residents in daily handling and maintenance.

Finally, a demonstrations plant will be developed, which is designed to handle the respective biomasses and can operate under arctic conditions. The applicability and sustainability of the developed concept will be assessed in a final evaluation.

Acknowledgements
This study is financed by Risø DTU Biosystems Division, Center for Arctic Technology and Innovationsnetværket for Biomasse (INBIOM). I would like to thank Jens Ejbye Schmidt, Ragnhildur Gunnarsdottir, Pernille Erland Jensen and Arne Villumsen for their efforts and input to realize the project.

Peter Jørgensen Herslund
Phone: +45 4525 2863
E-mail: pjh@kt.dtu.dk
Discipline: Engineering Thermodynamics

Supervisors: Nicolas von Solms
Kaj Thomsen
Jens Abildskov

PhD Study
Started: February 2010
To be completed: June 2013

Thermodynamic and Process Modelling of Gas Hydrate Systems in CO_2 Capture Processes

Abstract
Two thermodynamic models capable of describing dissociation pressures of mixed gas clathrate hydrates formed from ternary mixtures of CO_2, N_2 and liquid water, are presented. These models are named Model I and Model II. Both models utilize the Cubic-Plus-Association (CPA) equation of state (EOS) for the thermodynamic description of the non-solid phases (vapour and liquid) combined with the classical van der Waals-Platteeuw model for the solid hydrate phase. With two hydrate formers present (CO_2 and N_2), four parameters in the van der Waals-Platteeuw model are fitted for Model I. Sixteen fitted parameters are required for Model II. The model performances are compared and validated against experimental dissociation pressure- and composition data found in literature.

Introduction
In a new post combustion CO_2 capture concept utilizing precipitated systems, CO_2 is separated from the flue gas by gas clathrate hydrate (gas hydrate) formation. Since gas hydrates are normally formed at high pressure and low temperature conditions, thermodynamic promoters must be applied to the system in order to lower the needed flue gas pressure.

In order to evaluate the efficacy of CO_2 this process, accurate thermodynamic models are required over a wide range of temperatures and pressures.

Specific Objectives
It is the purpose of this work to develop a thermodynamic model for describing the three-phase liquid/vapour/solid behaviour of the ternary H_2O-N_2-CO_2 system. The model should be validated against experimental gas hydrate dissociation pressure and composition data found in the literature.

Gas Hydrates
Gas hydrates are ice-like, solid inclusion bodies of water and guest molecules. Hydrogen bonded water clusters form cavities, where small guest molecules may be encapsulated.

The three most common occurring hydrate structures are; Structure I (sI), Structure II (sII) and Structure H (sH), all with different crystal structures. These three structures are formed by five different water cavities, the 5^{12}, $5^{12}6^2$, $5^{12}6^4$, $5^{12}6^8$ and the $4^3 5^6 6^3$ [1]. These cavities are illustrated in Figure 1.

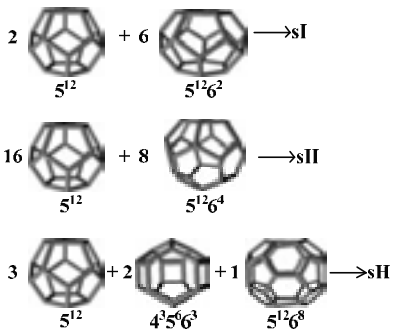

Figure 1. Schematic of the hydrogen bonded water cavities forming the three classical gas hydrate structures, sI, sII and sH. Three-leg intersections represent one oxygen atom with two chemically bonded hydrogen atoms and one hydrogen bond to a neighbouring water molecule [modified from 2].

The unit cell of the sI hydrate contains two 5^{12} and six $5^{12}6^2$ cavities while a unit cell of the sII hydrate contains sixteen 5^{12} and eight $5^{12}6^4$ cavities. Both of these unit cell structures belong to the cubic type. The sH hydrate structure is more complex and contains three 5^{12}, two

$4^3 5^6 6^3$ and one $5^{12}6^8$ cavities [1]. This structure forms a hexagonal unit cell.

A given hydrate structure is typically determined by the size, shape and chemical property of the guest molecule. Each water cavity may encapsulate one or in rare cases more guest molecules of proper sizes.

Thermodynamic Model Set-up

The two models, Model I and Model II, presented in the following both utilize the CPA equation of state (EOS) as presented by Kontogeorgis et al. [3,4] for the thermodynamic description of fluid phases. CPA combines the physical term from the cubic Soave-Redlich-Kwong (SRK) EOS with an association term similar to that found in the Statistical Associating Fluid Theory (SAFT) models.

The solid gas hydrate phase is, in both models, treated separately by the classical van der Waals-Platteeuw model [5]. The model equations and solution algorithm are similar to those presented by Parrish and Prausnitz [6]. Model I and Model II utilize identical overall solution algorithms.

A detailed description of the models and the algorithm used in this work may be found in [2].

Model I and Model II

In the van der Waals-Platteeuw model [5], the encapsulation of dissolved gas molecules inside the hydrogen bonded water cavities is described in a way similar to that of mono-layer Langmuir adsorption.

Model I and Model II of this work [2] are different from each other only in their method for describing the Langmuir adsorption coefficient of the hydrate formers.

Van der Waals and Platteeuw [5] showed that the Langmuir adsorption coefficients of each guest molecule may be estimated from statistical mechanics using Lennard-Jones-Devonshire cell theory with e.g. a Lennard-Jones 12-6 cell potential. Parrish and Prausnitz [6] later refined the model and presented an algorithm making it suitable for computer calculations. They proposed the following expression for the Langmuir adsorption coefficient, *C(T)*,

$$C(T)_{m,j} = 4 \cdot \pi \cdot \left(k_B \cdot T\right)^{-1} \cdot \int_0^{\infty} \exp\left[-w(r)_{m,j} \cdot \left(k_B \cdot T\right)^{-1}\right] \cdot r^2 \cdot dr \quad (1)$$

where k_B is the Boltzmann constant and $w(r)_{m,j}$ is the spherical core cell potential of component j in cavity type m. r is the linear distance from the centre of the cavity.

In Model I of this work [2], the Kihara cell potential is utilized in the form presented by Parrish and Prausnitz [6].

$$w(r)_{m,j} = 2 \cdot z_m \cdot \varepsilon_j \cdot \left[\begin{array}{l} \frac{\sigma_j^{12}}{R_m^{11} \cdot r} \cdot \left(\delta(N=10)_{m,j} + \frac{a_j}{R_m} \cdot \delta(N=11)_{m,j}\right) \\ -\frac{\sigma_j^{6}}{R_m^{5} \cdot r} \cdot \left(\delta(N=4)_{m,j} + \frac{a_j}{R_m} \cdot \delta(N=5)_{m,j}\right) \end{array}\right] \quad (2)$$

z_m is the coordination number for the guest in cavity type m, ε_j is the characteristic energy of guest molecule j, a_j is the core radius of molecule j, σ_j+2a_j is the collision diameter of molecule j and R_m is the radius of cavity type m. $\delta(N)_{m,j}$ is defined by

$$\delta(N)_{m,j} = N^{-1} \cdot \left[\begin{array}{l} \left(1 - r \cdot R_m^{-1} - a_j \cdot R_m^{-1}\right)^{-N} \\ -\left(1 + r \cdot R_m^{-1} - a_j \cdot R_m^{-1}\right)^{-N} \end{array}\right] \quad (3)$$

From equation (2) it is seen that the Kihara spherical core cell potential is undefined in the cavity centre. Also at a distance from the cavity centre of $r = R_m - a_j$ a discontinuity with a change of sign occurs. Approaching $r = R_m - a_j$ from r-values greater than this results in the cell potential approaching minus infinity making the behaviour of the Langmuir adsorption coefficient divergent. Thus care should be taken, when integrating the Kihara cell potential.

The Kihara cell potential is evaluated from the cavity centre to the singularity point at $r = R_m - a_j$. Thus equation (1) is rewritten

$$C(T)_{m,j} = 4 \cdot \pi \cdot \left(k_B \cdot T\right)^{-1} \cdot \int_0^{R_m - a_j} \exp\left[-w(r)_{m,j} \cdot \left(k_B \cdot T\right)^{-1}\right] \cdot r^2 \cdot dr \quad (4)$$

Parrish and Prausnitz [6] also proposed a simpler way of calculating the Langmuir adsorption coefficients, where an empirical, explicit expression is given for the coefficients

$$C(T)_{m,j} = A_{m,j} \cdot T^{-1} \cdot \exp\left[B_{m,j} \cdot T^{-1}\right] \quad (5)$$

$A_{m,j}$ and $B_{m,j}$ are fitting parameters related to guest type j in cavity type m only. Hence in the case where a guest molecule may enter both cavities in both sI and sII hydrates, a total of eight fitting parameters must be determined for this one guest. The use of this method should however be restricted to temperatures within 260K-300K [6]. Model II in this work utilizes the simple explicit expression, equation (5), for the Langmuir adsorption coefficients.

In the cell potential approach (Model I) three component specific parameters are needed to perform the same type of calculation that Model II utilizes eight parameters for. Moreover, only two of the component specific parameters in the Kihara cell potential (equations (2) and (3)) are utilized as fitting parameters in this work (ε_j and σ_j).

Thus, while the Model II approach results in a simpler and faster calculation, it does require a greater number of fitted parameters in the hydrate model. The overall difference in computation times however appear to be neglectable.

Results

Binary interaction parameters (BIP's) for the component pairs considered in CPA have been fitted such that the calculated liquid phase solubilities of CO_2 and N_2 match those found in literature. The BIP for the binary pair

CO_2-N_2 is assumed zero, hence two BIP's have been fitted.

Four parameters ($\varepsilon_j(N_2)$, $\sigma_j(N_2)$, $\varepsilon_j(CO_2)$ and $\sigma_j(CO_2)$) have been fitted in the hydrate model for Model I and sixteen parameters (A and B parameters for both CO_2 and N_2 in all cavities in sI and sII hydrates) have been fitted in the hydrate model for Model II. Pure hydrate [7,8,9,10] and mixed hydrate formation pressure data presented by Kang et al. [11] have been utilized as reference data. Pure CO_2 hydrate is assumed sI and pure N_2 hydrate is assumed sII. A structural cut-off mole fraction of CO_2, $y(CO_2)$, at 0.15 has been assumed during the parameter estimation process. At initial gas phase mole fractions of CO_2 below 0.15, sII hydrates were assumed. For initial gas phase mole fractions at or above 0.15, sI hydrates were assumed. All fitted parameters may be found in [2].

Model I and Model II both succeed in calculating pure hydrate formation curves within an accuracy of plus/minus 3%, for temperatures between 273.15K and 283.15K, when compared to the reference data utilized in the fitting procedure. The differences between the model performances are found when looking at the mixed hydrates. These are illustrated in Figure 2 and Figure 3.

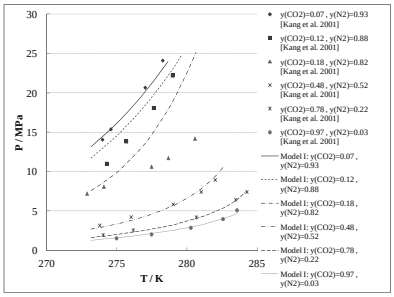

Figure 2. Dissociation pressures of mixed N_2/CO_2 hydrates as a function of temperature for various vapour phase compositions. Comparison of experimental data and fitted modeling results for Model I.

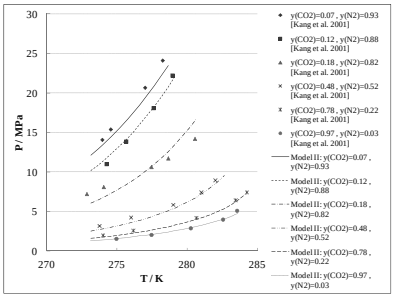

Figure 3. Dissociation pressures of mixed N_2/CO_2 hydrates as a function of temperature for various vapour phase compositions. Comparison of experimental data and fitted modeling results for Model II.

Both models assume a structural cut-off mole fraction of 0.15 for CO_2 between sI and sII hydrates.

It is clear from the results illustrated in Figure 2 and Figure 3 that Model II obtains a higher accuracy than Model I, when compared to the reference data. Especially the mole fraction range from 0.12-0.18 is better described by Model II than Model I. Outside this composition interval the two model responses appear compareable. Hence, the greater number of fitting parameters in Model II appear to improve the description of mixed hydrate formation.

When looking at the composition dependency of hydrate formation isotherms, it becomes clear that the assumption regarding the constant cut-off concentration between sI and sII hydrates renders the two models thermodynamically inconsistent. With the fitted Langmuir constants, Model II predicts sI hydrates to be the most stable structure down to initial mole fractions of CO_2 below 0.02. Model I predicts the cut-off concentration at mole fractions between 0.12-0.14. Both models predict the cut-off concentration to depend on temperature. Hence, the assumption of a structural transition at a mole fraction of 0.15 goes against the true model predictions and should be discarded. Figure 4 and Figure 5 illustrate the predicted cut-off concentrations by the two models at 274K, 277K and 280K. Predictions are compared to experimental data presented by Kang et al. [11]. These data have not been utilized in the parameter optimization procedure.

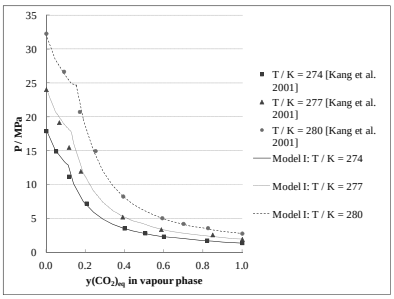

Figure 4. Dissociation pressures of mixed N_2/CO_2 hydrates as a function of equilibrium vapour phase compositions. Comparison of experimental data presented by Kang et al. [11] and predicted results by Model I. $y(CO_2)_{eq}$ denotes equilibrium vapour phase composition of CO_2 after contact with the liquid phase.

Model I gives the most accurate description of the equilibrium data presented by Kang et al. [11]. The structural transitions are clearly identified in Figure 4 as sudden changes in slope at equilibrium mole fractions of CO_2 around 0.11-0.15. The high pressure parts of the curves are sII hydrates while the low pressure parts are sI.

The structure transitions in Figure 5 are difficult to identify since they appear at very low concentrations of CO_2. Almost all mixed hydrate formation is predicted sI by Model II.

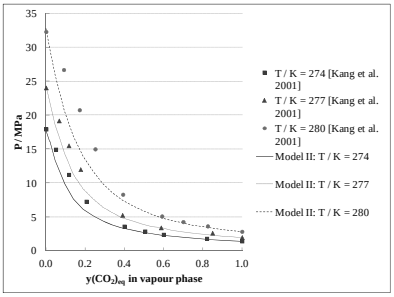

Figure 5. Dissociation pressures of mixed N_2/CO_2 hydrates as a function of equilibrium vapour phase compositions. Comparison of experimental data presented by Kang et al. [11] and predicted results by Model II. $y(CO_2)_{eq}$ denotes equilibrium vapour phase composition of CO_2 after contact with the liquid phase.

Figure 6 illustrates predicted hydrate compositions on a water free basis as a function of the corresponding equilibrium vapour phase composition.

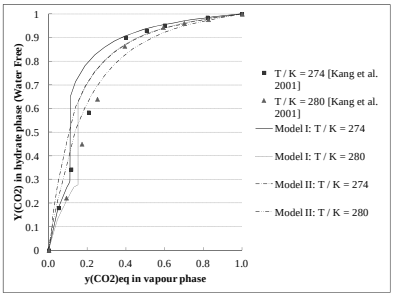

Figure 6. Mole fraction of CO_2 in the mixed N_2/CO_2 hydrates as a function of equilibrium vapour phase composition at constant temperature. Comparison of experimental data by Kang et al. [11] and predicted results by Model I and Model II. $y(CO_2)_{eq}$ denotes equilibrium vapour phase composition of CO_2 after contact with the liquid phase. $Y(CO_2)$ denotes hydrate phase mole fraction of CO_2 on a water free basis. All compositions are balanced with N_2.

Again it is clear that Model I provides the best description of the data measured by Kang et al. [11] in the concentration limits. However hydrates formed from vapour phase mole fractions of CO_2 between 0.15-0.40 are poorly described. Model II is more accurate in the before mentioned interval, but fails at describing the concentration limits.

Furthermore two independent publications of hydrate formation pressure and composition data have been utilized in the model verification work [2]. Due to a disparity of data found in literature, it has however been impossible to rate one model over the other. One model may describe a given data set better than the other model and vice versa when comparing to another data set. More work must be done in the attempt of finding universal sets of fitted parameters. In this attempt, hydrate composition data should be included as additional reference data.

Conclusion

Two models for the thermodynamic description of hydrate formation conditions have been set up for the ternary H_2O-N_2-CO_2 system. Model I has a more physical background than Model II as well as fewer fitting parameters. The accuracies in describing pure hydrate formation pressures are comparable for the two models. Predictions of structural changes in the mixed hydrate formation region are however widely different. Due to a disparity of data between authors in the literature, it has not been possible to determine which of the two model predictions should be trusted.

Future Work

More work on the optimization of component specific fitting parameters in the hydrate model will be done. Alternative assumptions regarding structures of the mixed N_2/CO_2 hydrates will be tested in the optimization work. The presence of low-pressure hydrate formers (promoters) such as tetrahydrofuran and cyclopentane, in the liquid phase, will be implemented in the two models in order to investigate the possibility for lowering the needed flue gas pressure, hence enhancing the capture process feasibility.

Acknowledgements

The financial contributions to this work from the iCap project (EU FP7) and the Department of Chemical and Biochemical Engineering (MP_2T) at The Technical University of Denmark, are greatly acknowledged.

References

1. A.K. Sum, C.A. Koh, E.D. Sloan, Ind. Eng. Chem. Res. 48 (2009) 7457-7465.
2. P.J. Herslund, K. Thomsen, J. Abildskov, N. von Solms, J. Chem. Thermodyn. (2011) (Submitted).
3. G.M. Kontogeorgis, E.C. Voutsas, I.V. Yakoumis, D.P. Tassios, Ind. Eng. Chem. Res. 35 (1996) 4310-4318.
4. G.M. Kontogeorgis, I.V. Yakoumis, H. Meijer, E. Hendriks, T. Moorwood, Fluid Phase Equilibr. 158-160 (1999) 201-209.
5. J.C. Platteeuw, J.H. van der Waals, Mol. Phys. 1 (1) (1958) 91-95.
6. W.R. Parrish, J.M. Prausnitz, Ind. Eng. Chem. Process Des. Develop. 11 (1) (1972) 26-35.
7. J. Jhaveri, D.B. Robinson, Can. J. Chem. Eng. 43 (2) (1965) 75-78.
8. A. Van Cleeff, G.A.M. Diepen, Recueil des travaux chimiques des Pays-Bas. 79 (5) (1960) 582-586.
9. K.M. Sabil, G.-J. Witkamp, C.J. Peters, J. Chem. Thermodyn. 42 (2010) 8-16.
10. L. Ruffine, J.P.M. Trusler, J. Chem. Thermodyn. 42 (2010) 605-611.
11. S.-P. Kang, H. Lee, C.-S. Lee, W.-M. Sung, Fluid Phase Equilibr. 185 (2001) 101-109.

Jeppe Lindegaard Hjorth
Phone: +45 2912 4460
E-mail: jelhj@kt.dtu.dk
Discipline: Engineering Thermodynamics

Supervisors: Søren Kill
John M. Woodley
Rasmus Leth Miller, AAK

Industrial PhD Study
Started: May 2011
To be completed: April 2014

Mathematical Modeling of Vegetable Oil Crystallization

Abstract
The present project concerns improved control and prediction of crystal characteristics in vegetable oils and fats used in the food industry, particularly the confectionary area. The project aims to improve the understanding and predictability of crystal characteristics in terms of polymorphism, nucleation and growth kinetics and particle size distribution using a mathematical model. This model will include mass, energy and population balances together with solid-liquid equilibrium models used to determine the crystallization driving force present in the systems. It is to be developed using experience from literature and experimental work as the fundament, and will function as an iterative tool in the sense that it should be used to prove or disprove constructed hypotheses.

Introduction
To date very little research has been done in the field of predicting crystallization behavior of triacylglycerol (TAG) systems, the main component in vegetable oils and fats. Vegetable oils and fats are added to a wide array of foods to obtain the right structure and behavior, this includes chocolate, margarine, ice cream, bread etc. In this project the main focus will be on fats and oils used in chocolate production.

Often when mixing TAGs in specific ratios, interesting and valuable results are observed such as eutectics, increased texture or molecular compound formation [1]. Obtaining some degree of predictability of the behavior of such systems could serve as a first approach to develop new products tailored to the public demands for example by replacing trans and saturated fats with healthier alternatives without losing the texture and thermal behavior required in the end product.

Triacylglycerol morphology
As triacylglycerols crystallize, complex solid structures are formed resulting in fats having up to six different polymorphic configurations, as in seen in cocoa butter, with distinct physical properties including melting temperature, heat of fusion, solubility, etc [2]. The large number of polymorphs is a consequence of packing patterns of the TAG molecules in the crystalline layers. Three main polymorphs are usually recognized together with a few sub-polymorphs. The main polymorphs are denominated α, β' and β with increasing stability from left to right. The stability of the polymorphs is often correlated to the miscibility between various TAGs. When mixing TAGs in the α-form, exhibiting loose packing patterns, these are often seen to crystallize together forming only one solid α-phase. However, as more stable crystals are formed the packing patterns becomes more specific and different TAGs may be unable to adapt to each other's crystal structures, resulting in more solid phases upon mixing. This is illustrated in Figure 1, showing a binary TAG phase diagram. These considerations greatly complicates solid-liquid equilibrium (SLE) calculation for such systems.

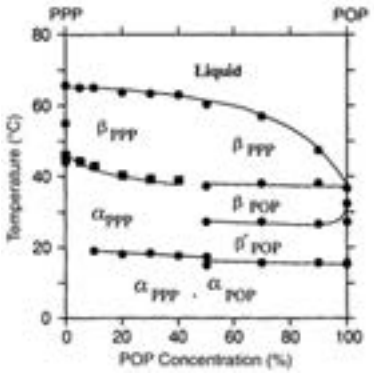

Figure 1: Phase diagram for the binary mixture *sn*-1,3-dipalmitoyl-2-oleoylglycerol (POP) and tripalmitoyl-glycerol (PPP) [3]

Solid-Liquid Equilibrium

Information about the equilibrium existing between different phases in the systems is valuable as it provides a way of quantifying the driving force towards crystallization of the various TAGs and polymorphs. Such SLE calculations are complex due to the various polymorphic states and are further complicated by the nature of the oil systems chosen in the present project. These systems are comprised of an array of TAGs ranging in number from 10 to more than 30 and are thus very different from most model systems used in literature consisting of a limited number of very pure TAGs. Yet, promising results have been published in this field and it is believed that a similar approach in this project will allow one to arrive at SLE data of sufficient accuracy. The SLE model aims to minimize the Gibbs free energy for every solid phase while liquid phase is assumed to be completely miscible and ideal [4]. The required activity coefficients are then to be determined using the two-suffix Margules model which works well for mixtures with similar chemical composition, molar volume and shape

$$RT \ln \gamma_i = -g^E + \sum_{j=1, j\neq i}^{N} A_{ij} x_j \qquad (1)$$

$$g^E = \sum_{i=1}^{N} \sum_{j=i+1}^{N} A_{ij} x_i x_j \qquad (2)$$

This model requires the interaction coefficients A_{ij} of the involved species. These parameters will be determined by conducting a wide array of SLE experiments in which the composition of the liquid and solid phase is analyzed after equilibrium is established. Fitting these experimental data to the model will then allow for approximation of the interaction coefficients.

Crystallization model

A simple model has been developed as a starting point. This model is based exclusively on mass balances and a simple SLE model assuming complete miscibility in the liquid as well as the solid phase. Although the model is greatly simplified is still show the desired predictive nature for some simple TAG systems. Figure 1 shows the solid fat content of a system, consisting of three different TAGs, determined experimentally and theoretically. The experiment shows a kink in the SFC curve after 40 seconds. This can be explained as a consequence of the highest melting TAG crystallizing first followed by crystallization of another TAG.

Comparing this course of crystallization to the curves obtained using the model it is clear that the first simulation fails to predict the correct crystallization behavior while the second simulation gets somewhat closer to the experiment by predicting the kink in the SFC curve. In the first simulation the solid phases were allowed to crystallize together forming only one solid phase, while the second simulation forced the TAGs to crystallize in spate phases. Continuing this line of thought we might guess that the actual system crystallizes in separate solid phases which is indeed in agreement with literature [5]. In this way the model can be used as an iterative tool to prove or disprove theories and hypotheses.

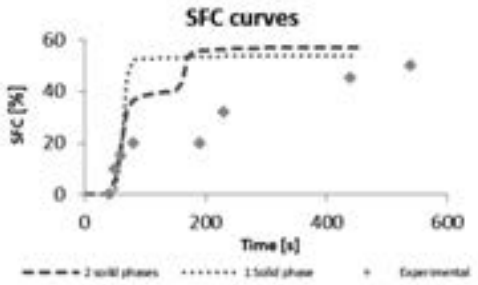

Figure 2: SFC curves obtained experimentally and simulated using the model

Conclusion

Although complex vegetable oil systems are investigated in present project it seems realistic that a model able to predict the overall crystallization behavior such as polymorphism, SFC and particle size distribution, can be developed. As the model deals with complex systems much experimental data is needed to build a versatile foundation able to deal with systems composed of various TAGs. This includes SLE data, stability and polymorphic analyses together with particle size distributions. Such a model may prove a valuable tool when investigating various theories and ultimately as a first approach when designing new vegetable oil products for the industry.

Acknowledgement

The author acknowledges the great financial, professional and collegial support of Aarhus Karlshamn and CHEC Research Center and PROCESS at the Department of Chemical and Biochemical Engineering at DTU.

References

1. K. Sato, Chem. Eng. Sci. 56 (7) (2001) 2255-2265.
2. K.S. Nissim Garti, Crystallization and Polymorphism of Fats and Fatty Acids, 1988, Marcel Dekker.
3. A. Minato et al. J. Am. Oil Chem. Soc. 73 (11) (1996) 1567-1572.
4. M. dos Santos, G. Le Roux, V. Gerbaud, J. Am. Oil Chem. Soc. 88 (2) (2011) 223-233.
5. L.H. Wesdorp, Liquid - Multiple Solid Phase Equilibria in Fats, in Ph.D. Thesis 1990, Delft University of Technology.

Martin Høj
Phone: +45 4525 2842
E-mail: mh@kt.dtu.dk
Discipline: Reaction and Transport Engineering

Supervisors: Anker Degn Jensen
Jan-Dierk Grunwaldt, KIT

PhD Study
Started: September 2009
To be completed: September 2012

Nanoparticle Design using Flame Spray Pyrolysis for Catalysis

Abstract
Flame spray pyrolysis (FSP), a novel method for synthesizing nanoparticle sized metal oxides, is the unifying topic of this project. Nanoparticulate materials have very high surface area, which is advantageous for heterogeneous catalysis. The work mainly focuses on two reactions for applying FSP made catalysts: Selective oxidation of propane to propene and hydrotreating of diesel, two very different areas of heterogeneous catalysis employing oxide and sulfide catalyst, respectively.

Introduction
Liquid fed flame spray pyrolysis (FSP) is a novel one-step synthesis method for preparation of nano-sized particles [1]. Typically, organo metallic compounds are dissolved in an organic solvent and the precursor solution is sprayed as micrometer sized droplets with high velocity oxygen and ignited with a small premixed methane-oxygen flame [2].

The solvent and metal compounds evaporate and combust to form atomically dispersed vapors, which nucleate to form clusters when reaching cooler parts of the flame. The formed clusters grow by surface growth and coalescence, accompanied by sintering [3].

These results in non-porous nanoparticles which coagulate and sinter to form agglomerates and aggregates with high inter particle porosity [1]. The flame process gives high maximum temperature and a short residence time with thermally stable, homogeneous nanoparticles as the product.

Hydrotreating
Hydrotreating is performed at oil refineries in order to remove sulfur and nitrogen from the heterocyclic compounds in which these elements typically occur in crude oil [5]. Industrial hydrotreating catalysts contain cobalt or nickel promoted molybdenum(IV)sulfide as active phase, on an alumina support [5]. The transition metal sulfide phase is obtained after sulfiding an oxide precursor. An oxide precursor containing molybdenum and cobalt on alumina can be prepared by FSP.

Oxidative dehydrogenation of propane
Demands for short chain olefins like ethylene and propylene are expected to increase in the near future [4]. Current production methods include steam cracking, fluid catalytic cracking and catalytic dehydrogenation.

Oxidative dehydrogenation of propane to propylene is another option. This is an exothermic reaction which could be operated autothermally. However, a catalyst with sufficient activity and selectivity for industrial production of propylene by this method has not been discovered yet [4]. The most promising catalyst candidates are supported vanadium and molybdenum oxide [4], which can be prepared by FSP. Supports like Al_2O_3, SiO_2, TiO_2, ZrO_2, MgO and ZrO_2 or mixtures thereof have been used. Mixed oxide phases are easily prepared by FSP in one step.

Specific objectives
The objectives of my project are to prepare catalytically active nanomaterials using the FSP method. The catalysts will be tested for their catalytic activity and the physical and chemical structure will be investigated using spectroscopy, X-ray diffraction and electron microscopy.

Results and discussion
Hydrotreating
Seven $CoMo/Al_2O_3$ samples were synthesized by FSP where all three metallic elements were sprayed in one flame. Four samples contained 8, 16, 24 and 32 wt.% Mo with a Mo:Co atomic ratio of 3:1 (alumina balance), and two samples 16 wt.% Mo with Mo:Co atomic ratio

3:2 and 3:3 and finally one unsupported reference samples with Mo:Co atomic ratio 3:1.

The catalysts had specific surface areas between 221 and 90 m^2/g, with decreasing surface area with increasing transition metal content. This corresponds to average particle sizes of 7 to 13 nm, showing that nanoparticles were the product of the flame synthesis.

The activities of the catalysts for removal of heterocyclic sulfur and nitrogen were measured after sulfidation. The best catalysts contained 16 wt.% Mo with atomic ratio Mo:Co = 3:1, which activity was 75 % of a commercial reference. Increasing the Co content in the FSP material caused a small drop in activity, while increasing or decreasing the Mo content resulted in significantly lower activity.

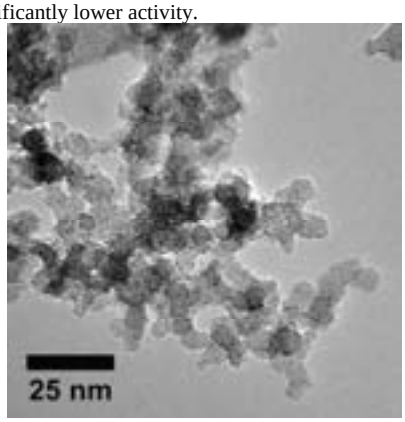

Figure 1: TEM image of 16 wt.% Mo oxide sample.

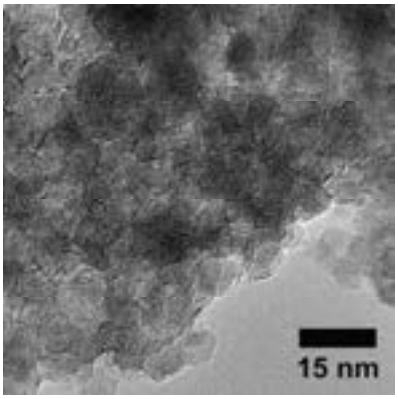

Figure 2: TEM image of 16 wt.% Mo sulfide sample.

TEM images of the flame made oxides shwed nano-sized particles and images of the sulfided catalysts showed a significant increase in MoS_2 particles size with increasing Mo content, explaining the lower activity of the 24 and 32 wt.% Mo catalysts and the unsupported reference catalyst (see Figure 1 and 2).

X-ray diffraction (XRD) and UV-vis reflectance spectroscopy showed that the oxide precursor contained γ-Al_2O_3 with some $CoAl_2O_4$ spinel, while MoO_3 was XRD amorphous. The $CoAl_2O_4$ spinel is unwanted since the cobalt in this form does not promote the MoS_2 active phase. Experiments of suppressing this phase are under way using silica promotion of the support material and by using two-flame FSP where Co and Al will not co-nucleate.

Oxidative dehydrogenation of propane

A new activity test setup with three sequential reactors in series/by-pass configuration has been constructed. The analysis is performed by a dual channel GC-MS, also fitted with FID and TCD detectors.

Several alumina supported vanadia, molybdena and mixed vanadia/molybdena catalysts with varying amounts of transition metal have been synthesized by FSP. The catalysts had surface areas between 140 and 170 m^2/g, showing that the products are nanoparticles. The vanadia and molybdena was XRD amorphous while the support was γ-Al_2O_3. The catalysts were highly active for oxidative dehydrogenation and using either low amounts of vanadia or high amounts of moleybdena propene yields of up to 12 % was achieved at conversion of 30 to 35 % at temperatures around 500 °C. The catalysts were stable to at least 550 °C. The conversion and yield could be interpreted in terms of a kinetic model which allowed the determination of the optimum temperature and contact times for high propene yield.

Conclusion

FSP is a promising new method for preparation of catalytically active nanoparticles. The prepared hydrotreating catalysts show high activity for initial experiments with a new synthesis method and high propene yields were achieved in oxidative dehydrogenation of propane.

Acknowledgements

DSF grant 2106-08-0039. M. Brorson (Haldor Topsøe A/S) for hydrotreating activity tests. J. B. Wagner and T. W. Hansen (DTU CEN) for TEM. L. Mädler and D. Pham (University of Bremen) for two-flame FSP.

References

1. R. Strobel, S.E. Pratsinis, J. Mater. Chem. 17 (2007) 4743-4756.
2. L. Mädler, H.K. Kammler, R. Mueller, S.E. Pratsinis, J. Aerosol. Sci. 33 (2002) 369-389.
3. H.K. Kammler, L. Mädler, S.E. Pratsinis, Chem. Eng. Technol. 24 (2001) 583-596.
4. F. Cavani, N. Ballerini, A. Cericola, Catal. Today 127 (2007) 113-131
5. H. Topsøe, B.S. Clausen, F.E. Massoth, in: J.R. Anderson, M. Boudart (Eds.), Catalysis: Science and Technology, vol. 11, Springer-Verlag, Berlin, 1996.

Publications

1. M. Høj, K. Linde, T.K. Hansen, M. Brorson, J.-D.Grunwaldt, A.D. Jensen, Appl. Catal. A 397 (2011) 201-208.

Qian Huang
Phone: +45 4525 6809
E-mail: qh@kt.dtu.dk
Discipline: Polymer Technology

Supervisors: Ole Hassager
Anne L. Skov
Henrik K. Rasmussen, DTU-Mekanik

PhD Study
Started: February 2010
To be completed: February 2013

Stress Maximum and Steady Extensional Flow of Branched Polymer Melts

Abstract
We report observations of stress in extensional flows using a Filament Stretching Rheometer (FSR) for three polyethylene melts. The observations are compared with the ones in a Cross-Slot Extensional Rheometer (CSER) from the University of Cambridge. The FSR describes the transient stress in start-up of kinematically steady flow, while the CSER describes kinematically steady flow. The steady stress values measured by the FSR after the stress maximum compare favorably with the steady stress values observed in the CSER thereby giving credence to both methods. To cast further light upon the rheological processes involved in the stress maximum, we also report measurements of stress relaxation before and after the stress maximum using the FSR for one of the above polyethylene melts.

Introduction
Accurate and reliable stress-strain measurements of extensional flow play a crucial role in the understanding of nonlinear rheological properties of polymers. A stress maximum during start-up of kinematically steady extensional flow was reported by Meissner in 1985 for low density polyethylene (LDPE) [1]. Subsequently observations of a steady stress following a stress maximum were reported for two LDPE melts (Lupolen3020D and Lupolen1840D) [2]. Steady stress following a stress maximum has also been reported for a model branched (Pom-pom) polystyrene of known architecture [3]. However the rheological significance of the stress maximum as well as the existence of steady flow conditions following the maximum is still a matter of some debate [4].

Here we measure the start-up and steady uniaxial extensional flow for three polyethylene melts using a Filament Stretching Rheometer (FSR). We then compare the measurements of the steady flow with the ones from a planar Cross-Slot Extensional Rheometer (CSER). The FSR describes the transient stress in start-up of kinematically steady flow, while the CSER describes kinematically steady flow. Here we are comparing uniaxial flow to planar flow; but it should be noted that there is no difference between the two in a strain hardening regime [5]. This work is in collaboration between four universities: The modeling and simulation parts are performed in the University of Durham and the University of Leeds; the CSER measurements are performed in the University of Cambridge, and the FSR measurements are performed in DTU. Here we only present the experimental results.

To cast further light upon the rheological processes involved in the stress maximum, we also report measurements of stress relaxation before and after the stress maximum using the FSR for one of the above polyethylene melts.

Materials
One kind of low density polyethylene (LDPE), named Dow 150R, and two kinds of high density polyethylene (HDPE), named HDB4 and HDB6 have been chosen for this study. The materials were previously characterized in shear at the same temperature as the subsequent FSR and CSER measurements. The properties of the three melts are listed in table 1.

Table 1: Properties of polyethylenes investigated

Sample	Code	M_w [kg/mol]	M_w / M_n	T [˚C]
LDPE	Dow150R	242	11	160
HDPE	HDB4	96	2.1	155
HDPE	HDB6	68	2.2	155

All the materials are supplied in pellets and are pressed into cylindrical test specimens by a Carver hydraulic press, with radius R_0=4.5mm and length L_0=2.5mm, giving an aspect ratio $\Lambda_0 = L_0 / R_0$=0.556.

Filament Stretching Rheometry

Our extensional experiments are performed with a FSR equipped with an oven to allow measurements from room temperature to about 200˚C [6]. Nitrogen is used during the elongation to avoid sample degradation. The force $F(t)$ is measured by a load cell and the diameter $2R(t)$ at the mid-filament plane is measured by a laser micrometer. The Hencky strain and the mean value of the stress difference over the mid-filament plane [7] are calculated from observations of $R(t)$ and $F(t)$ as

$$\epsilon(t) = -2\ln\left(R(t)/R_0\right) \tag{1}$$

$$\left\langle \sigma_{zz} - \sigma_{rr} \right\rangle = \frac{F(t) - m_f g/2}{\pi R(t)^2} \tag{2}$$

where R_0 is the radius of the sample at the start of the extension, g the gravitational acceleration and m_f the weight of the polymer filament.

At small strains during the start-up, part of the stress difference comes from the radial variation due to the shear components in the deformation field, especially at small aspect ratios. This effect may be compensated by a correction factor where the corrected mean value of the stress difference is defined as [8]

$$\left\langle \sigma_{zz} - \sigma_{rr} \right\rangle_{corr} = \left\langle \sigma_{zz} - \sigma_{rr} \right\rangle \left(1 + \frac{\exp\left(-5\epsilon/3 - \Lambda_0^3\right)}{3\Lambda_0^2} \right)^{-1} \tag{3}$$

Theoretically it ensures less than 3% deviation from the correct initial stress. For large strains the correction vanishes and the radial variation of the stress in the symmetry plane becomes negligible [9].

The strain rate is defined as

$$\dot{\epsilon} = \mathrm{d}\epsilon / \mathrm{d}t \tag{4}$$

which is often kept as a constant during extension. The corrected extensional stress growth coefficient (also called the transient extensional viscosity), is defined as

$$\bar{\eta}^{+}_{corr} = \left\langle \sigma_{zz} - \sigma_{rr} \right\rangle_{corr} / \dot{\epsilon} \tag{5}$$

Results of Start-up Extensional Flow

In figure 1 we show the experimental results of uniaxial start-up extensional flow for Dow 150R at 160˚C. A significant maximum of the stress growth coefficient is observed at strain rates 0.03 and 0.1s^{-1}. At lower strain rates no maximum is observed. The sample broke during stretching at strain rate 0.3s^{-1} hence we did not see the maximum at this highest strain rate.

In figure 2 we show the same experimental data from figure 1 but plot as the extensional stress vs. Hencky strain. Clear steady stress is reached for all the strain rates (except strain rate 0.3s^{-1} at which the sample breaks) at about Hencky strain 5. The stress maximum and steady state shown here is similar to the observations in Rasmussen et al. [2] for the other two LDPE melts (Lupolen3020D and Lupolen1840D).

In figure 3 we show the measurements of uniaxial start-up extensional flow for HDB4 and HDB6 both at 155˚C. In figure 4 we plot the same data from figure 3 as the extensional stress vs. Hencky strain. Due to shorter branches in HDPE, the strain hardening effect shown in figure 3 is not as significant as LDPE shown in figure 1. Furthermore, it is also observed in figure 3 that HDB6, which is more branching than HDB4, shows more significant strain hardening as well as stress maximum. This indicates the stress maximum in extensional flow is associated with the level of branching. In figure 4 it can be seen the steady stress is reached for all the strain rates at about Hencky strain 4.

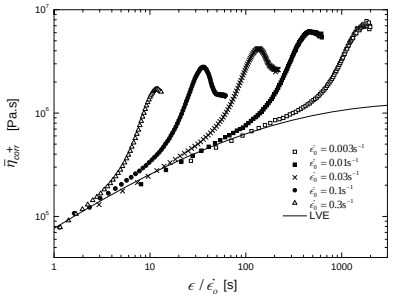

Figure 1: The corrected extensional stress growth coefficient as a function of time for Dow 150R at 160˚C. Strain rates = [0.3, 0.1, 0.03, 0.01, 0.003] s^{-1}

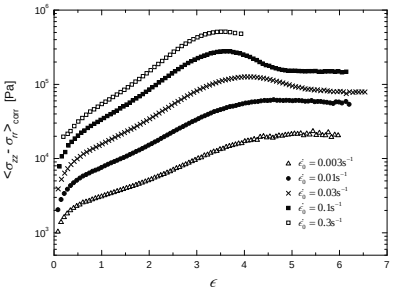

Figure 2: The corrected stress as a function of Hencky strain for Dow 150R at 160˚C.

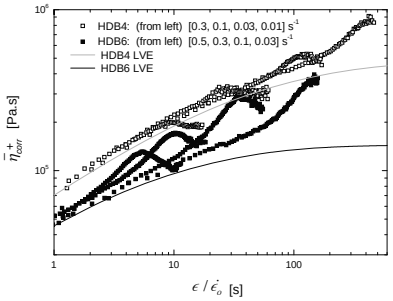

Figure 3: The corrected extensional stress growth coefficient as a function of time for HDB4 (strain rates = [0.3, 0.1, 0.03, 0.01] s^{-1}) and HDB6 (strain rates = [0.5, 0.3, 0.1, 0.03] s^{-1}) both at 155˚C.

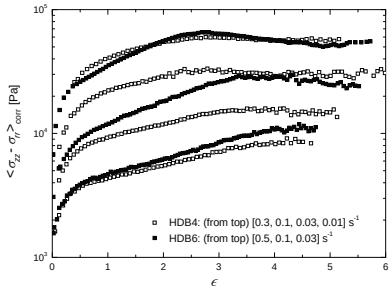

Figure 4: The corrected stress as a function of Hencky strain for HDB4 and HDB6 both at 155˚C.

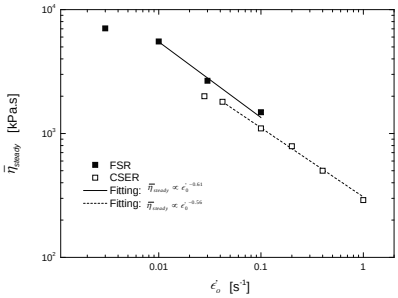

Figure 5: The steady extensional viscosity as a function of strain rate for Dow 150R at 160˚C, measured by FSR and CSER.

Comparison of Steady Flow

In figure 5 we plot the steady extensional viscosity measured by the FSR as a function of strain rate for Dow 150R. The results are compared with the ones measured by the CSER. The CSER uses optical birefringence patterns to determine the steady state extensional viscosity from stagnation point flow [10]. At the stagnation point the measured stress is the result of simple planar elongational flow. Figure 6 compares the steady extensional viscosity measured from the FSR with the ones from the CSER for HDB4 and HDB6 respectively.

In both figures it can be seen that the FSR probes lower strain-rate regime while the CSER probes higher strain-rate regime. And there is excellent agreement between the two methods when the operating regimes overlap. For HDB4 shown in figure 6, although there is no overlapping regime, the steady state values still show a close agreement to the same trend.

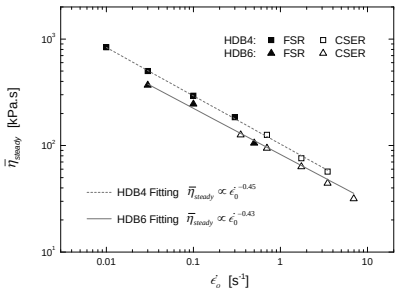

Figure 6: The steady extensional viscosity as a function of strain rate for HDB4 and HDB6 both at 155˚C, measured by FSR and CSER.

Results of Stress Relaxation

Figure 7 shows the measurements of stress relaxation on Dow 150R performed at 160˚C. The flow was started up by a uniaxial elongation with three constant strain rates; for each rate the flow was stopped at two Hencky strains before and after the maximum respectively.

At strain rates 0.03 and $0.1s^{-1}$, a significantly different flow behavior is observed in the stress relaxation performed before ($\epsilon_0 = 3$) and after ($\epsilon_0 = 4.5$) the stress maximum. The measured stress decays much faster in the one performed after the maximum for both strain rates. It can be seen from the figure that the relaxation curve after the maximum goes down across the one before the maximum, which indicates that after the maximum the melt becomes less elastic and relaxes much faster.

In comparison, at strain rate $0.01s^{-1}$ where no stress maximum is observed in the start-up flow, the stress relaxation curve performed at $\epsilon_0 = 4.5$ shows no tend to go across the one performed at $\epsilon_0 = 3$.

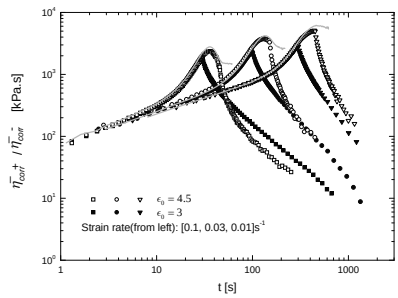

Figure 7: The corrected extensional stress growth coefficient and stress relaxation coefficient of Dow 150R at 160˚C as a function of time. The start-up of the flow was uniaxial elongation with strain rates = [0.1, 0.03, 0.01] s^{-1}; the flow was stopped at an extension of $\epsilon_0 = 3$ and 4.5 respectively for each rate. The solid lines are the data from figure 1 of corresponding strain rates.

Conclusion

The start-up and steady uniaxial extensional flow for three polyethylene melts, Dow 150R, HDB4 and HDB6, have been measured using the FSR. The results of the steady flow from the FSR are compared with the ones from the CSER. The steady stress values measured by the FSR after the stress maximum compare favorably with the ones observed in the CSER thereby giving credence to both methods.

To cast further light upon the rheological processes involved in the stress maximum, stress relaxation before and after the maximum have been also measured by the FSR for Dow 150R at different strain rates. The measured stress performed after the maximum decays much faster than the one performed before the maximum, which indicates after the maximum the melt becomes less elastic.

Acknowledgement

This work is supported by the European Union under the Seventh Framework Programme, ITN DYNACOP (Grant agreement no.: 214627).

References

1. J. Meissner, Chem. Engr. Commun. 33 (1985) 159–180.
2. H.K. Rasmussen, J.K. Nielsen, A. Bach, O. Hassager, J. Rheol. 49(2) (2005) 369–381.
3. J.K. Nielsen, H.K. Rasmussen, M. Denberg, K. Almdal, O. Hassager, Macromolecules 39 (2006) 8844–8853.
4. Y. Wang, S-Q. Wang, J. Rheol. 53 (2009) 1389–1401.
5. H.M. Laun, H. Schuch, J. Rheol. 33(1) (1989) 119–175.
6. A. Bach, H.K. Rasmussen, O. Hassager, J. Rheol. 47 (2003) 429–441.
7. P. Szabo, Rheol. Acta 36 (1997) 277–284.
8. H.K. Rasmussen, A.G. Bejenariu, O. Hassager, D. Auhl, J. Rheol. 54 (2010) 1325–1336.
9. M.I. Kolte, H.K. Rasmussen, O. Hassager, Rheol. Acta, 36 (1997) 285–302.
10. D. Auhl, D.M. Hoyle, D. Hassell, T.D. Lord, O.G. Harlen, M.R. Mackley, T.C.B. McLeish, J. Rheol. 55 (4) (2011) 875–900.

Amol Shivajirao Hukkerikar
Phone: +45 4525 2817
E-mail: amh@kt.dtu.dk
Discipline: Systems Engineering

Supervisors: Gürkan Sin
Jens Abildskov
Rafiqul Gani
Bent Sarup, Alfa Laval, Denmark

PhD Study
Started: July 2010
To be completed: June 2013

Development of Property Models with Uncertainty Estimate for Model Based Product-Process Design

Abstract
The aim of this work is to develop revised and improved model parameters for group-contribution$^+$ (GC^+) models employed for the estimation of pure component properties, together with covariance matrices to quantify uncertainties (eg. the 95% confidence intervals) in the estimated property values. In total 21 properties of pure components, which include normal boiling point (T_b), critical temperature (T_c), critical pressure (P_c), critical volume (V_c), normal melting point (T_m), among others have been modeled and analysed. Important issues related to property modeling such as thermodynamic consistency of the predicted properties (relation of normal boiling point versus critical temperature etc.) have also been analysed. The developed methodology is simple, yet sound and effective and provides not only the estimated property values using the GC^+ approach but also the uncertainties in the estimated property values. This feature allows one to evaluate the effects of these uncertainties on the product-process design calculations thereby contributing to better-informed and reliable engineering solutions.

Introduction
Physical and thermodynamic properties of pure components are needed to carry out tasks such as, product-process design, computer aided molecular/mixture design among others. The experimental values of properties of many important pure components have not been measured due to many reasons and hence they must be estimated. Predictive methods such as GC^+ method (combined group-contribution (GC) method [1] and atom connectivity index (CI) method [2]) are generally suitable to estimate the needed property values. For assessing the quality and reliability of the final design, an engineer needs to know the uncertainties in the estimated property values obtained from the property models. With this information, the engineer can then perform better-informed design calculations by taking into account these uncertainties. Hence given the importance of reliable estimation of properties and uncertainties in the property estimates in the product-process, this work aims to revise and improve GC^+ method based estimation of properties as well as to estimate the confidence intervals of estimated property values.

Specific Tasks
To achieve the aforementioned objective, a systematic methodology for property modeling and uncertainty analysis of GC^+ models was developed and used. The developed methodology includes: (i) a parameter estimation step to develop new and improved property model parameters; and (ii) an uncertainty analysis step to establish statistical information about the quality of parameter estimation, such as the parameter covariance, the standard errors, and the confidence intervals [3]. For parameter estimation, large data-sets of experimentally measured property values of pure components ranging from C3 to C70 were taken from the CAPEC database [4]. The optimization algorithm used for the data fitting was the Levenberg–Marquardt technique.

Results
The model performance statistics for the selected property models is summarized in Table 1 and the model fits to the data for the selected properties are shown in Figure 1. Visual inspection of Figure 1 indicates that the goodness of the models-fits is quite remarkable and most of the data have been fitted to a good accuracy. The residuals (experimental value-predicted value) obtained from most of the models followed a normal distribution curve with mean zero suggesting a good fit of the experimental data used in the regression and there is no bias in the predicted property values as well as the assumptions behind the approach are valid.

Table 1. Performance of selected property models

Property	Datapoints	R^2	SD[a]	AAE[b]	ARE[c]
T_b K	3510	0.99	7.9	6.17	1.44
T_c K	858	0.99	10.77	7.72	1.23
P_c bar	852	0.96	2.38	1.40	3.90
V_c cc/mol	797	0.99	11.65	7.97	2.05
T_m K	5183	0.94	19.16	15.99	5.07

[a] SD = Standard deviation, [b] AAE = Average absolute error
[c] ARE = Average relative error

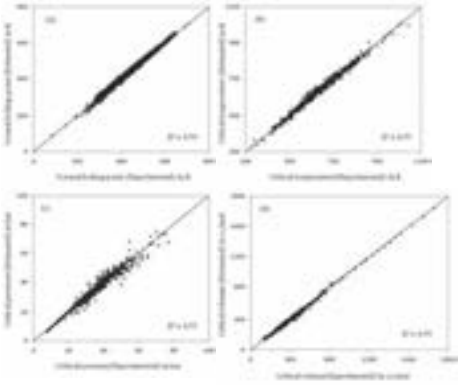

Figure 1. Model fits for (a) T_b, (b) T_c, (c) P_c, and (d) V_c

Reliability of the property models

The reliability of the property models has been tested by comparing model prediction uncertainties with reported range of experimental measurement uncertainties (Table 2) for the properties with related available data from DIPPR 801 database and we can notice that for most of the properties the prediction error is lower than (or at least comparable to) the average measurement error.

Table 2. Comparison of average prediction error with average measurement error

Property	Data-points	Average meas. error	Average pred. error
T_b K	1306	6.32	6.17
T_c K	402	7.95	7.72
P_c bar	293	1.20	1.40
V_c cc/mol	234	22.30	7.97
T_m K	1385	5.10	15.99
G_f kJ/mol	258	4.60	5.24
H_f kJ/mol	704	6.31	5.03

Thermodynamic consistency of the predicted properties

A plot of predicted values of T_b and T_c versus n-alkanes is shown in Figure 2. The experimental data available for T_b and T_c are also shown. In agreement with the basic physical principles, throughout the homologous series, the normal boiling point smoothly approaches the critical temperature as the carbon number increases. Also, the ratio T_c/T_b is positive and greater than unity.

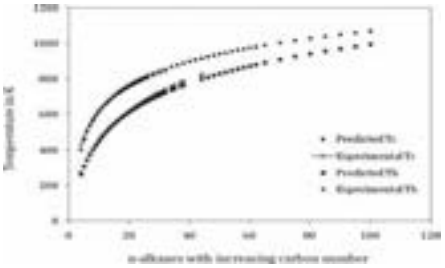

Figure 2. T_b versus T_c for n-alkanes

Conclusions

A systematic methodology for property modeling and uncertainty analysis is developed and used to obtain revised and improved model parameters for GC+ models to provide more reliable and accurate estimations of properties, together with the results of uncertainty analysis such as covariance matrix needed to quantify the uncertainties in the estimated property values. In total 21 properties of pure components have been modeled and analysed. The developed methodology is simple, yet sound and effective and provides not only the estimated property values but also the uncertainties in the estimated property values. Motivated by the results obtained in this work, our current and future work is focused on extension of the developed methodology to other pure component properties, such as transport properties (surface tension, viscosity, and thermal conductivity), and environment-related properties (LogLC50, aqueous solubility etc.).

Acknowledgements

This PhD project is funded by the European Commission under the 7th Framework Programme under the grant agreement no. 238013.

References

1. J. Marrero, R. Gani, Fluid Phase Equilibr. (2001) 183-208.
2. R. Gani, P. Harper, M. Hostrup, Ind. Eng. Chem. Res. 44 (2005) 7262-7269.
3. G. Seber, C. Wild, Nonlinear Regression, Wiley, New York, 1989.
4. Integrated Computer Aided System (ICAS 14.0), Dept. of Chem. Eng., Technical University of Denmark, Lyngby, Denmark, 2010.

Cathrine Heinz Ingvordsen
Phone: +45 23669751
E-mail: cahi@risoe.dtu.dk

Supervisors: Rikke Bagger Jørgensen
Teis Mikkelsen
Michael Lyngkjær, KU-LIFE
Pirjo Peltonen-Sainio, MTT Finland

PhD Study
Started: January 2011
To be completed: December 2013

Climate Change Effects to Plant Ecosystems

Abstract
The climate is changing and it is foreseen that it will continue to change in the future. These changes are affecting the world's natural plant ecosystems as well as our food production. Prognoses for Denmark reveal drastic changes of all seasons such as increased temperature and extreme weather events. In this PhD project 'Climate Change Effect to Plant Ecosystems' the crop species oil seed rape and barley are used as model plants to shed light on the mechanisms functioning in mitigation of and adaptation to the expected future climate changes.

Introduction
Plant ecosystems consist of plant populations wherein the individual plants cannot move and the populations can only move slowly over time. This means that plant ecosystems are highly dependent on the surrounding environment hereof the climate. The agro-ecosystems are also highly affected by the changing climate and by biotic stressors as plant pathogens and herbivores that are also influenced by changes in climate. This raises the question if the production of food in the future climate can feed the rapidly growing population of the world.

In Denmark prognoses show increases in the summer temperatures together with increased emission of the greenhouse gasses carbon dioxide (CO_2) and ozone (O_3). It is also foreseen that Denmark more frequently will experience extreme events such as drought, heat waves and flooding [1]. All events that can be devastating for plant ecosystems. The underlying mechanisms of climate change impact on plant ecosystems have been studied only in recent years, where effects of the changed climate have become measurable. These studies and the ones to come are of great importance in understanding and mitigating the effects from the climate to plant ecosystems.

In this project the crops barley and oilseed rape are used as models for plant ecosystems since molecular tools are available for these species. The use of crop species has caused the interest by plant breeders and in the network 'Sustainable primary production in a changing climate' funded by NordForsk, actions are being taken to identify plant genetic resources of value in plant breeding programs. Here plant genetic resources are identified that are resistant to the fungal plant diseases, net blotch, caused by *Pyrenosphora teres*, spot blotch caused by *Bipolaris sorokiniana*, rust caused by *Puccinia hordei* and *Ramularia* leaf spot caused by *Ramularia coll*o-cygni in spring barley and Verticillium *wilt* caused by *Verticillium longisporum* and *Phoma* caused by *Leptosphaeria maculans* in spring oilseed rape [2].

Specific Objectives
In the phytotron, Risø Environmental Risk Assessment Facility (RERAF) [3], the effects to plant ecosystems from the interactions between increased carbon dioxide, temperature and O_3 will be studied using barley and oilseed rape as model plants. In the next year extreme events like heat waves and severe drought periods will be induced at different times during plant development to study the environmental plasticity in the plant material. Besides studying the basis of environmental plasticity, plant genetic resources will be identified for the use in plant breeding programs for future oilseed rape and barley cultivars in cooperation with Nordic plant breeding companies.

Results and Discussion
One year into the project three experiments have been initiated but not yet completed.
1) Screening in RERAF of 140 barley accessions under single and multifactor climate scenarios envisaged by the Intergovernmental Panel on Climate Change (IPCC, scenarios A1FI) [4]. In collaboration with Nordic plant breeding stations within the network

resistance to diseases mentioned above is screened for in the field.

2) Screening of 12 of the above 140 barley accessions for the net blotch disease under single and multi factor treatments mimicking IPCC scenarios.

3) Amplified fragment length polymorphism analysis has been performed on first and fifth generation of a unique plant material (four cultivars of oilseed rape and barley) that have been selected over five plant generations in single and multi factor climate scenarios [5]. Identification of outlier loci can reveal genes that have been selected for [6], and that might be of interest also to plant breeding.

Add 1) the threshing of the harvested plant material is underway, but already in the cultivation of the barley accessions differences between the climate treatments were noticeable (Fig. 1). As earlier observed a raised CO_2 level induced increased growth and raised temperature caused decreased growth compared to ambient conditions (Fig. 1; b, c, d) [7, 8]. The treatment with a combination of raised CO_2 and temperature showed plant vigour in between the single factor treatments (Fig. 1; a, b, c, d).

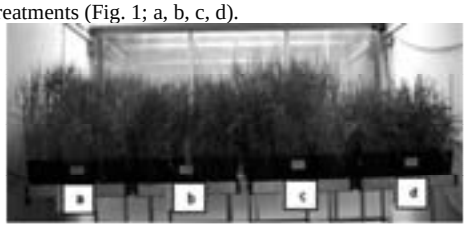

Figure 1: The cultivars Anakin, Columbus and Simba from Sejet Plant breeding Station grown 68 days in different atmospheres. a. 700ppm CO_2, 24°C, b. 385ppm CO_2 (control), 19°C c. 700ppm CO_2, 19°C d. 385ppm CO_2, 24°C.

Increased O_3 is generally found to reduce plant growth, but the result from this study did not show any difference between the ambient treatment and the increased O_3 treatment (increased O_3; 100-150ppb) treatment (results not shown).

Add 2) the screen is running and preliminary results indicate that the symptoms caused by *Pyrenosphora teres* are more severe in the atmospheres that do not stress the plants, e.g. ambient and increased CO_2. This is opposite that work performed with *Bipolaris sorokiniana*, where stressed plants, with defence mechanisms activated showed less disease symptoms in e.g. increased temperature [8]. This will be interesting to follow up on and might expand knowledge about the defence mechanisms against the fungi.

Add 3) the identification of AFLP polymorphisms within the treatments are ongoing. Early analysis revealed a clear difference in marker frequencies between the climate treatments, indicating that adaptation might have taken place from first to fifth generation in the selective conditions [4]. Based on these early results it is suggested that oilseed rape adapt relatively rapidly to climate changes also suggested by Bonin et al. [10]. A rapid adaptation to climate change may suggest that the natural microevolution in the changing environment will help plant breeding in selecting suitable cultivars for tomorrow. Furthermore a raised CO_2 concentration in the atmosphere is functioning as a plant fertiliser and should be a benefit to the primary production. The effects depend to a high degree on the speed of the climate changes; can the plant ecosystems adapt fast enough? And the effect also depends on how the plant ecosystems are influenced by the combination of raised CO_2, O_3 and temperature.

Conclusions

Despite the project is in its first year, interesting preliminary results have been produced. These are in the forthcoming years to be verified and studied further. Much is still to be done before the effects to plant ecosystems from interactions between increased carbon dioxide, temperature and O_3 are unravelled.

Acknowledgements

The author thanks the NordForsk network 'Sustainable primary production in a changing climate' for funding, and her supervisors and Marja Jalli, MTT for scientific discussions and repeatedly encouragement. She also thanks everyone at Risø, Biosystems Division for the positive working environment.

References

1. M. Trnka, J.E. Olesen, K.C. Kersebaum, A.O. Skjelvåg, J. Eitzinger, B. Seguin, P. Peltonen-Sainio, R. Rötter, A. Iglesias, S. Orlandini, M. Dubrovský, P. Hlavinka, J. Balek, H. Eckersten, E. Cloppet, P. Calanca, A. Gobin, V. Vučetic, P. Nejedlik, S. Kumar, B. Lalic, A. Mestre, F. Rossi, J. Kozyra. V. Alexandrov, D. Semerádová, Z. Żalud. Glob. Change Biol. 17 (2011) 2298-2318.
2. http://www.risoe.dtu.dk/nordforsk.aspx
3. http://www.risoe.dtu.dk/business_relations/Products_Services/Risk_Assessment/BIO_RERAF.aspx
4. IPCC, in: R.K. Pachauri, A. Reisinger (Eds.) IPCC, Geneva, 2007, Switzerland, p. 104.
5. Frenck, G. Evolutionary consequences of simulated environmental change. Ph.D. Thesis. (2010) Technical University of Denmark and Aarhus University.
6. A. Pérez-Figueroa, M.J. García-Pereira, M. Saura, E. Rolán-Alvarez, A. Caballero, J. Evol. Biol. 23 (2010) 2267-2276.
7. E.A. Ainsworth, P.A. Davey, C.J. Bernacchi, O.C. Dermody, E.A. Heaton, D.J. Moore, P.B. Morgan, S.L. Naidu, H.Y. Ra, X. Zhu, P.S. Curtis, S.P. Long, Glob. Change Biol. 8 (2002) 695-709.
8. O.K. Atkin, M.G. Tjoelker. Trend. Plant Sci. 8 (2003) 343-351.
9. Pers. comment Michael Lyngkjær, KU-LIFE, Denmark, mlyn@life.ku.dk & Marja Jalli MTT, Finland, marja.jalli@mtt.fi.
10. A. Bonin, P. Taberlet, C. Miaud, F. Pompanon, Mol. Biol. Evol. 23 (2006) 773-783.

Krešimir Janeš
Phone: +45 4525 2926
E-mail: kreja@kt.dtu.dk
Discipline: Process Technology and Unit Operations

Supervisors: Krist V. Gernaey
John M. Woodley
Pär Tufvesson

PhD Study
Started: December 2010
To be completed: November 2013

Scale-Up of Biocatalytic Cascade Reactions: Transaminase Catalysed Synthesis of Chiral Amines

Abstract
Optically pure chiral amines are important building blocks in many pharmaceuticals. Asymmetric synthesis of optically pure chiral amines using transaminases (E.C. 2.6.1.18) is a promising method for obtaining optically pure amines from prochiral ketones. However, it is known that efficient production of chiral amines using transaminases is challenged by both unfavorable thermodynamics and biocatalyst limitations. In order to improve amine production, co-product removal systems have been deployed to pull the reaction towards the product.

Introduction
New small molecule pharmaceuticals are preferably produced as single enantiomers due to safety and regulatory concerns. Biocatalysis is a very good option for such production and is already established in industry owing to its green profile and superior stereoselectivity. An area of research that recently has received a lot of attention is the use of transaminases (ω-TA) for production of optically pure chiral amines. This approach has the advantage over existing biocatalytic and chemical methods that the theoretical yield is 100% compared to 50% for classical resolution technologies. [1]

One challenge that needs to be met in this type of process is to overcome the potentially unfavorable thermodynamic equilibrium for the reaction. This can be done by reacting or recycling one of the reaction co-products *in-situ* using additional enzymatic reactions. [2] These cascade systems have been shown to be feasible in micro-liter scale, however the systems need to be characterized and be shown to be scalable and economically feasible to be able to be industrially implemented.

Four cascade systems that have been chosen (Figure 1.) to be investigated: Lactate Dehydrogenase (LDH)/Glucose Dehydrogenase (GDH), Alanine Dehydrogenase (AlaDH)/Glucose Dehydrogenase (GDH), Pyruvate Decarboxylase (PDC) and Acetolacetate Synthase (ALS).

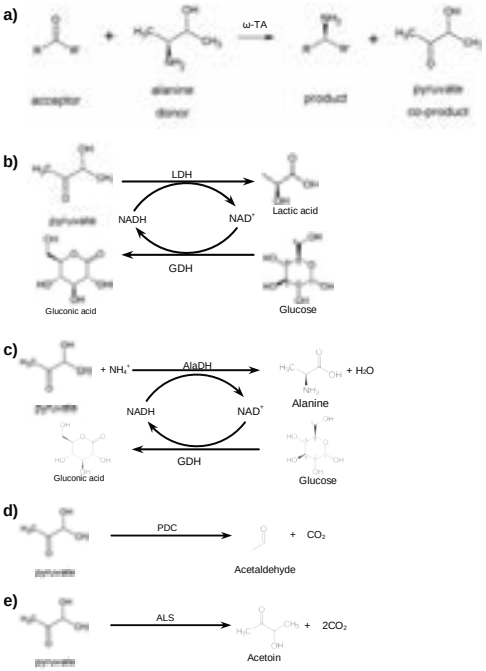

Figure 1. a) Transaminase reaction; b) pyruvate removal by LDH/GDH system; c) pyruvate removal by AlaDH/GDH system; d) pyruvate removal by PCD system; e) pyruvate removal by ALS system.

Specific Objectives

The aim of this project is to determine the effectiveness and constraints of the above mentioned co-product reaction systems under process relevant conditions. An interaction matrix is suggested to describe the effects of the compounds involved in the process on the enzymes present in the reaction mixture.

Results

LDH/GDH System

An ω-TA experiment with an unoptimized LDH/GDH system was carried out to prove the concept. Two different substrates were used, one with lower K_{eq} (1-phenylethanone) and one with higher K_{eq} (4-phenyl-2-butanone). The formation of the products is shown in Figure 2 for both substrates.

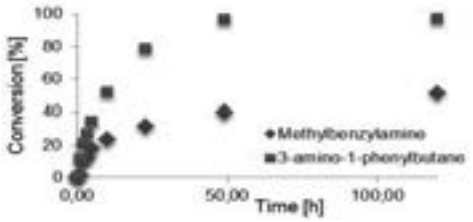

Figure 2. ω-TA Experimental data of ω-TA reaction coupled to LDH/GDH system; Reaction conditions: pH 8, 30°C, c(L-alanine) = 100 mM, c(D-glucose) = 20 mM, ρ(ω-TA ATA-44) = 4.5 g mL^{-1}, c(PLP) = 1 mM, c(1-phenylethanone)[(a)] = 10 mM; c(4-phenyl-2-butanone)[(b)] = 10 mM, E(LDH) = 88.89 U mL^{-1}, E(GDH) = 33.33 U mL^{-1}, c(NAD^+) = 2 mM[(a)]; 3 mM[(b)]

Current research is focused on defining constraints under industrially relevand conditions for both LDH and GDH enzymes. If proven succesful and economically feasibile, a process set-up and scale-up can be considered.

AlaDH/GDH System

The aim of this co-product degradation system is to react pyruvate and transform it back to alanine which is the substrate for transaminase catalyzed reaction. Alanine is added in high excess to overcome unfavorable thermodynamics of the system therefore it was sensible to investigate the AlaDH system in the presence of high product concentrations. As shown in

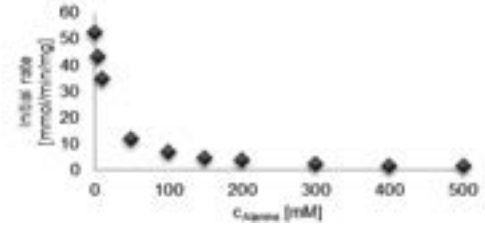

Figure 3. Product inhibition of AlaDH system.

Conclusions

LDH/GDH System

This system so far exhibits no industrially relevant constraints. Its dependence on NADH and two other enzymes makes it a less robust system to be handle under industrial conditions. Additional research is needed to understand and improve the system and to deploy it at industrial scale.

AlaDH/GDH System

This is a potentially interesting system due to its theoretical capability of recycling the co-product pyruvate back to the substrate alanine. It was shown that at this moment and with the current enzymes, it is impossible to achieve the desired effect. Strong product inhibition is currently the bottleneck of this system and without protein engineering and enzyme design which would allow reaching much higher product concentrations; industrial implementation seems very hard at best.

Future Work

- Determination of fundamental kinetic parameters and establishment of a mathematical kinetic model for each of the enzymatic reactions; use of optimal experimental design (OED) as supporting method/tool.
- Validation of the reaction model at process relevant conditions
- Application of reaction model together with economic model of the system (in place) to select the economically most favorable reaction conditions and process set up
- Design and selection of one or more process set ups for scale up of experiments
- Validation and feasibility study of scaled up system

Acknowledgments

The support from the AMBIOCAS project financed through the European Union 7th Framework Programme (Grant agreement no.: 245144) is acknowledged.

References

1. M. Höhne, S. Kühl, K. Robins, U.T. Bornscheuer, ChemBioChem 9 (2008) 363-365.
2. D. Koszelewski, K. Tauber, K. Faber, W. Kroutil, Trend. Biotechnol. 28 (6) (2010) 324-332
3. P. Tufvesson, J. Lima-Ramos, J.S. Jensen, N. Al-Haque, W. Neto, J.M. Woodley, Biotech. Bioeng. 108 (2010) 1479-1493

Morten Jensen
Phone: +45 2132 8032
E-mail: morj@risoe.dtu.dk

Supervisors: Jens Ejbye Schmidt
Katja S. Johansen, Novozymes A/S
Thomas Didion, DLF TRIFOLIUM A/S

PhD Study
Started: November 2010
To be completed: November 2013

Combined Silage Pretreatment and Enzymatic Hydrolysis of Energy Grasses for 2G Bioethanol Production

Abstract
Pretreatment and enzymatic hydrolysis for conversion of lignocellulosic biomass to fermentable sugars is often the most expensive steps in 2nd generation bioethanol production. The aim of this project is to develop a pretreatment method using ensiling combined with enzymatic hydrolysis. Ensiling of biomass has a great potential as storage method for bioenergy feedstock. At the same time the silage process might function as a simple pretreatment method given its moist acidic conditions, and hereby facilitate better enzymatic hydrolysis of the lignocellulosic structure.

Introduction
Ensiling is an anaerobic biological process that conserves biomass. This method of moist forage preservation is widely used for fodder preservation all over the world. The aim of producing silage is to preserve the crop with minimum loss of nutrients and carbohydrates. In a successful silage process, lactic acid bacteria dominate the fermentation process; fermenting free sugars into lactic acid and acetic acid causing the pH to drop which inhibits microbes that decompose polysaccharides, in that way effectively minimizing the degradation of sugars and polycarbohydrates in a crop [1]. The main products from the anaerobic metabolism by lactic acid bacteria can be seen in Figure 1.

Homofermentative		
1 Glucose (or 1 fructose)	→	2 Lactic acid
	→	1 Lactic acid + 1 Acetic acid
Heterofermentative		
1 Glucose	→	1 Lactic acid + 1 Ethanol + CO_2
3 Fructose	→	1 Lactic acid + 2 Mannitol + 1 Acetic acid + 1 CO_2
2 Fructose + 1 Glucose	→	1 Lactic acid + 2 Mannitol + 1 Acetic acid + 1 CO_2
1 Pentose	→	1 Lactic acid + 1 Acetic acid

Figure 1: Main products of anaerobic metabolism by lactic acid bacteria

A study by Oleskowicz-Popiel *et. al.* [2] at DTU Risø has shown that silage treatment of maize whole crop as well as clover grass is a promising pretreatment method for 2G bioethanol production. The results indicate that ensiling may serve as sufficient pretreatment for 2G bioethanol production. For example the conversion of cellulose to glucose in maize silage (whole crop) was more than 77%. The ethanol yield after 120 hours was nearby 90% when inoculated with yeast. The results also indicate that further studies on optimization of this method will help to improve the process efficiency. Thus achieved yields are comparable to yields achieved after pretreatment methods using high temperature, high pressure and/or chemicals.
Based on those initial results, it can be concluded that this innovative method has a great potential to be applied in full scale bioethanol production. However, the influence of silage treatment of energy grasses and better understanding of silage process for bioethanol process is necessary to optimize the process, reduce cost and make it industrially.

Hypothesis
A low cost low energy process by means of ensiling and enzymatic hydrolysis can be developed for combined pretreatment and storage in the production of 2G bioethanol from energy grasses:

- The ensiling process can open the lignocellulosic biomass structure and facilitate a <90% conversion of the cellulosic polymers to monomeric sugars in a following enzymatic hydrolysis.

- Efficiency of silage treatment depends on dry matter (DM) at ensiling and use of inoculums, and optimal condition concerning these factors can be identified.

- Efficiency of enzymatic hydrolysis of silage treated energy grass depends on duration, load and enzyme mixture, and optimal conditions concerning these factors can be identified.

The biomass to be used in the project is high yielding forage grass, developed and produced by DLF TRIFOLIUM A/S. This grass, *Festulolium* Hykor, is a hybrid cross between the species *Festuca* and *Lolium*. It grows well in northern temperate regions due to high resistance against cold conditions and yields around 15-17 ton DM/hectare. A characterisation of a first cut harvest of *Festulolium* Hykor can be seen in Table 1.

Table 1: Composition of *Festulolium* Hykor

Biomass component	g/g DM
Free sugars	14.8
Cellulose	29.5
Hemicellulose	20.1
Klason lignin	11.8
Ash	7.7

Several biomasses could be considered. Compared to the use of traditional high yielding annual crops like maize with a high energy content, more diversified perennial pastures like *e.g.* mix of clover and ryegrass (Lolium perenne L.) require fewer inputs (fertilizer, energy for soil treatment), produce more biomass and larger amount of bioenergy/hectare, reduce greenhouse gas emissions more than annual cropping systems, and have the ability to grow on marginal land [3]. Silage of whole crops and pastures is a traditional practice originally developed to "fuel the animal power" on the farm. Increasingly, farmers must consider managing for multifunctionality and include effects on environmental quality in their management decision-making. Thus, investigating ensiling as pretreatment and combined storage method include in principle considerations about managing for emerging ecosystem services such as enhancement of carbon (C) sequestration, mitigation of GHG emissions, and to capitalise on new opportunities, such as bioenergy production, to diversify the traditional cropping systems to achieve these outcomes for the future.

The Silage treatment is carried out using vacuum packaging according to the method of H.E. Johnson *et. al.* [4], performed on a Variovac EK10, see Figure 1. Freshly harvested *Festulolium* Hykor is chopped into 2-5 cm pieces and packed in plastic bags, see Figure 2.

Figure 1: Vacuum packaging machine, Variovac EK10

Figure 2: Grass silage bag

Current work

Optimization of the silage treatment. A large factorial design experiment is carried out testing different ensiling conditions of dry matter concentrations and silage inoculants (commercial lactic acid bacteria cocktails) and correlates them to changes in chemical composition and enzymatic cellulose convertibility of the silaged biomass. This test is performed on four cuts over the season to determine seasonal changes and compare these to the effect of dry matter and inoculation.

Acknowledgements

The project is financially supported by The Danish Energy Agency under the programme of EUDP (Energiteknologisk Udviklings- og Demonstrationsprogram)

References

1. D.N. Thompson, J.M. Barnes, T.P. Houghton, Appl. Biochem. Biotechol. (2005) 121-124.
2. P Oleskowicz-Popiel, A.B. Thomsen, J.E. Schmidt, Biomass Bioenerg. (2011)
3. B.S. Dien, H.J.G. Jung, K.P. Vogel, M.D. Casler, J.F.S. Lamb, L Iten, R.B. Mitchell, G. Sarath. Biomass Bioenerg. 30 (10) (2006) 880-91
4. H.E. Johnson, R.J. Merry, D.R. Davies, D.B. Kell, M.K. Theodorou, G.W. Griffith, J. Appl. Microbiol. 98 (1) (2005) 106-13.

Joakim M. Johansen
Phone: +45 4525 2830
E-mail: jjoha@kt.dtu.dk
Discipline: Reaction and Transport Engineering

Supervisors: Peter Glarborg
Peter A. Jensen

PhD Study
Started: September 2011
To be completed: August 2014

2nd Generation Suspension Fired Biomass Burners

Abstract
In the strive for at CO2-neutral energy profile the exploitation of biomass in central and decentral heat and power plants has continuously increased in recent decades. This PhD-project aims to establish a scientific basis for the development of a new generation of biodust burners for utility boilers. The project focuses on particle ignition and flame stabilization through parametric studies both in full-scale measurements and from a CFD point of view.

Introduction
In recent decades, central power and heat production through thermal conversion of biomass has gained ground concurrently with the political agenda both on a national and an international level. The development of high efficiency biomass plants are required in order to balance the fluctuating power production from wind mills and other alternative energy sources, while still striving towards a CO_2-neutral energy profile. In addition, thermal plants are a necessary need in the provision of district heating.

Development and implementation of high efficiency biomass combustion technology is arguably the best near-term solution to provide stable and CO_2-neutral centralized power and district heating to larger cities and industrial areas.

Biomass differs from conventional solid fossil fuels (traditionally coal) in a number of essential area; including both chemical composition (cf. Figure 1) and physical structure and appearance. Thus, direct utilization of existing high efficiency pulverized power or combined heat and power facilities is not an option when considering biodust as the energy source.

The fibrous nature of the biomass complicates particle pretreatment implying larger and oddly shaped fuel particles; changing the aerodynamics and particle size distributions. In addition, the larger fraction of volatile matter changes the conditions at which a stable flame is achieved. A turbulent development of the technology aiming to convert existing high efficiency burner installations has been conducted in Denmark throughout the past couple of decades. However, technical difficulties lower the efficiency and limit the operation flexibility both with regards to biomass type and quantity.

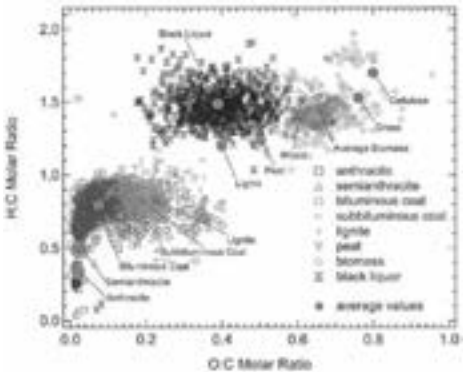

Figure 1: A van Krevelen diagram comparing the molar composition of coals and biomasses [1].

The fibrous nature of the biomass complicates particle pretreatment implying larger and oddly shaped fuel particles; changing the aerodynamics and particle size distributions. In addition, the larger fraction of volatile matter changes the conditions at which a stable flame is achieved. A turbulent development of the technology aiming to convert existing high efficiency burner installations has been conducted in Denmark throughout the past couple of decades. However, technical difficulties lower the efficiency and limit the operation flexibility both with regards to biomass type and quantity.

Objectives
This work aims to establish a scientific basis for the development of a new generation of biomass burners designed to facilitate simultaneous high power efficiency and fuel flexibility combined with good particle burn-out and stable flame capabilities of dedicated biodust fueled plants. The project will link fuel properties to flame properties, considering both fluid dynamic effects due to the differences in particle characters and chemical effects due to changes in the chemical composition and kinetics.

Content
The project will include full scale combustion measurements from relevant plants operated by the industrial partners: Dong Energy Power and Vattenfall. This will include advanced in-situ high speed thermal imaging, optical and extractive probe measurements of the flame, ear burner area, and fuel conveying system. Close coordination with other work-packages will ensure thorough fuel characterization of a range of different biomass fuels. Flame detection by state of the art diagnostic techniques will be evaluated for optimized operational control.

Fundamental research will be conducted in pilot, bench and/or lab-scale facilities both at DTU Chemical Engineering and during an external stay at Stanford University, Department of Mechanical Engineering. This will form the basis for modeling work applicable to computational fluid dynamics calculations taking both chemical kinetics and aerodynamic differences between fossil fuels and biodust into account, for the development of novel burner designs.

Swirling Jets
Swirling jets are the main objective of this work. Multiple independent wall mounted burners introduces both fuel and combustion air to the furnace. A fuel-air mixture is introduced to the furnace through a central tube. Secondary and tertiary air is introduced at high velocities (60–80 ms) through annular inlets surrounding the central tube. By angling the secondary air stream relative to the primary jet, introduces a tangential velocity component, stabilizing the flame. As the angular-to-linear-momentum ratio reaches a critical value, described by the non-dimensional swirl number, *S*, vortex breakdown will occur and a toroidal recirculation will be established in the central region of the jet. Controlling this toroidal recirculation pattern is a key element in the concept of swirling jet combustion of pulverized solid fuels; the effect is illustrated in Figure 2. By introduction of a proper recirculation, intense mixing and combustion may be achieved along with good flame stability. The backward motion ensures a convective heat flux through burning matter from the hot jet back to the nozzle exit at reverse velocities close to the forward motion of the primary jet. This significantly raises the temperature in the near burner field facilitating early ignition and close flame attachment. However, the high degree of mixing in the high temperature zone significantly increases the formation of thermal NO_x.

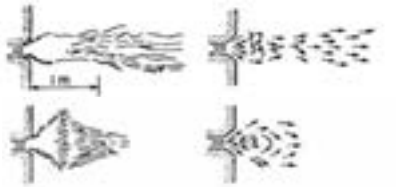

Figure 2: (Top) Low swirl flame, long flame and high degree of main jet penetration. (Bottom) High swirl flame, short flame and large recirculation zone.

Full-Scale Campaigns
The interpretation of full-scale measurements can be difficult and the exact influence of each parameter almost impossible to assign. The idea behind the upcoming full-scale campaigns is to investigate the influence on biodust ignition and flame stabilization of large variations in central parameters, e.g. fuel load, particle sizes, swirl, etc. The process parameter influence will be evaluated by in-flame measurements on key values: temperature, velocity fields, imaging techniques in both in the ultra-violet, visible, and infra-red spectra, extractive gas probe and particle sampling, etc.

The experiments are to be carried out in two different full-scale wall fired utility boilers capable of burning 100 % biodust: Amager Unit 1 and Herningværket operated by Dong Engery Power and Vattenfall, respectively. The equipment are of zeroth and first generation biodust burners, i.e. coal burners fueled with biodust and coal burners with physical modification aiming to optimize the process for biodust combustion.

CFD as an Engineering Modeling Tool
Numerical modeling tools in the form of CFD simulations will be employed on simplified burner geometries for qualitative analysis of a parametric study. This will provide valuable information on the understanding of the mechanisms taking place when disturbances are introduced to such a system. Correlation to the full-scale results will hopefully open up new ways of utilizing a tool where precision and high degrees of details have conventionally been considered as alpha and omega.

Acknowledgements
This PhD project is part of the GREEN Research Center (Center for Power Generation from Renewable Energy) financed by the Danish Strategic Research Council.

References
1. L.L. Baxter, H. Lu, Mechanisms and rates of aspherical, large particle conversion in suspension, in press 2011.
2. J.M. Beér, J. Chomiak, L.D. Smoot, Combust. Sci. Technol. 175 (11) (2003) 1979-2014

Jan Hein Jørgensen

E-mail: jajr@kt.dtu.dk
Discipline: Reaction and Transport Engineering

Supervisors: Anker Degn Jensen
Peter Arendt Jensen
Henrik Hassing, FORCE Technology

Industrial PhD Study
Started: December 2010
To be completed: December 2013

Grate Combustion of Municipal Waste

Abstract
The project is entering its second year and many activities are progressing. The present paper focuses on the project background, with an overview of the role of grate combustion of waste in society, motivations for the project and the project plan. A short introduction to the current experimental activities is also presented.

Introduction
The PhD project, 'Grate combustion of municipal waste.' is a collaboration between FORCE Technology, Department of Industrial Processes and DTU, Department of Chemical Engineering. It is funded by the Danish Agency for Science, Technology and Innovation and FORCE Technology.

Utilizing energy from MSW (municipal Solid Waste) can contribute to a society less dependent on fossil fuels. Combustion of MSW is recognized as partly non-fossil, as much of the content is biomass or products derived from renewable resources. In Denmark MSW is legally recognized as having 60% non-fossil content [1], where the fossil based content is mostly plastics and other oil based products. As the use of more environmentally friendly packaging materials, like bio-plastics, becomes more prevalent it can be expected that the non-fossil content in MSW recognized by regulators will rise, eventually making MSW combustion almost CO_2 neutral.

Globally the utilization of energy from MSW mainly occurs in incineration plants utilizing grate combustion, with a smaller number of plants using fluidized bed combustion. Denmark has made great strides in utilization of MSW combustion compared to other countries and Danish producers of grate fired incineration plants are important players on the world market.

With the current state of incineration technology the thermal conversion of MSW has a high efficiency, with the best efficiencies above 90% for combined heat and power plants. There is however a desire to increase the combustion rate on the grate to either increase throughput or decrease the size of the incineration plants and thereby increase the surplus of operating the plant. It is speculated that an increased combustion rate will also improve the residual bottom ash, giving a lower content of unburned fuel, and less harmful substances emitted to the environment.

Project goal
In the Ph.D. project there will be developed an improved description of the solid waste grate combustion process, along with evaluation of different technologies to improve burnout and the quality of slag and ash. The PhD project has three main objectives:

- To develop a basic model description of the combustion process for MSW on a grate.
- Identification of methods to evaluate suggestions for new technologies to improve the waste combustion grate process.
- To test identified technologies influence on the grate combustion process and burnout and to evaluate the economical, environmental and the energy efficiency potential of such technologies implemented on an incineration plant.

The first goals will be approached by a literature review of the current state-of-the-art in combustion modeling of MSW and biomass fuels, development of a model of the combustion process on a grate and experimental work made to support and enhance the model.

The second goal will be approached by reviewing available testing methods, assemble a robust objective testing method for evaluating combustion properties, such as combustion intensity, pollutant formation and burnout.

The third goal will be approached by applying the developed testing method on different technologies that can improve waste fuel burnout. The currently selected technologies are oxygen enhanced combustion, mechanical excitation (shaking grate) and ultra sound assisted combustion.

Project progress

Currently the literature study of modeling of grate combustion is being finished.

Work on modeling of the combustion process on the grate in a MSW incinerator awaits the completion of the literature study, as it will incorporate some of the sub models and the experience from previous work in the field.

An experimental study has been defined and prepared. The study is a test of the combustion enhancing technologies. The applied experimental facility is a further development of a test method developed by FORCE Technology. It is possible to test the influence of different combustion enhancing technologies on fixed bed solid fuel combustion.

Previous experiments showed some improvement with ultra sound assisted combustion, but a mechanism to explain the improvement was not established.

This new experimental study will look closer on the mechanisms of the enhancing technologies, to evaluate if the technologies have potential to be efficient and effective at an industrial scale.

Experimental work

The experimental study that has been prepared is a continuation of a previous experiment at FORCE Technology, which was set up to test a technology, which FORCE Technology has now patented.

The experiment showed a significant improvement of the combustion rate, but could not conclusively determine the mechanism with which the improvement was obtained. One of the motivations for the PhD project is to investigate the mechanism of this technology to evaluate its business potential.

A PI diagram of the experimental setup is shown on Figure 1. The central element in the setup is the combustion chamber with the coal bed. Below the bed is the air inlet along with elements to test various technologies, like ultra sound and mechanical excitation.

In the combustion chamber there are ports for measuring the temperature in the bed as well as in the freeboard.

After the combustion chamber is mounted a counter flow air cooling jacket to lower the temperature rapidly after the chamber, to stop further combustion and also to make it easier to use standard plastic tubing for subsequent flue gas measurements.

After the cooling section flue gas is sampled for analysis. The measurements focus on the species CO, CO_2 and O_2 as these are indicators of the combustion rate in the bed.

Finally the volume flow is measured to give sufficient information to analyze the combustion.

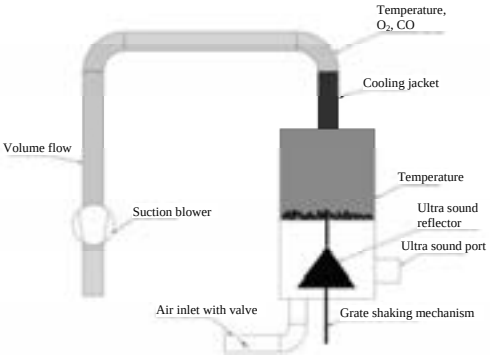

Figure 1: PI diagram of experimental setup with coal bed and different ways to influence the combustion on the bed. Measurement positions are indicated.

The experimental plan is set up with a number of similar runs without any outside influence of the combustion, to establish a good baseline. Subsequently the setup will be run with external influence on the combustion process, first one technology at a time, and later combinations of the different technologies.

The results from the different experimental runs will be post processed to determine if theories of the mechanism of combustion influence for the different technology can be falsified or supported.

Based on the results of this experimental setup, new experiments will be devised to further study the mechanisms of combustion enhancement. The work with these studies will also form the basis for the objective evaluation tools that are to be identified during this project.

References

1. **Internet page:** Ministry of climate and energy, Denmark. Bekendtgørelse om oprindelsesgaranti for VE-elektricitet. [Online] 2010. [Cited:] https://www.retsinformation.dk/Forms/R0710.aspx?id=134574.

Petra Lachouani
Phone: +45 2133 1955
E-mail: alac@risoe.dtu.dk

Supervisors: Henrik Hauggaard-Nielsen
Per Ambus

PhD Study
Started: September 2010
To be completed: August 2013

Nitrogen Cycle Assessments and Greenhouse Gas Emissions in Low-Input Legume Management Systems

Abstract
Open nitrogen cycles in agriculture have negative effects like nitrate leaching and connected eutrophication of aquatic ecosystems as well as increased nitrous oxide emissions, a greenhouse gas (GHG) 300 times more potent than CO_2. This project seeks to optimize agricultural nitrogen use and close the agricultural nitrogen cycle while maintaining food production and productivity.

Introduction
Nitrogen (N) is the most important plant nutrient for crop productivity in most agroecosystems. Therefore the introduction of Haber-Bosch derived N fertilizers into agriculture resulted in a sharp increase in yield per ha. This development led to undesired side-effects like decreasing soil organic matter content and nitrate leaching with subsequent eutrophication of natural ecosystems, groundwater contamination, and made agriculture widely dependent on fossil fuel reserves.

Legumes obtain N through biological nitrogen fixation (BNF), rather than through fossil energy-derived fertilizer N. However, legumes are not generally considered as climate change mitigation option.

Specific Objectives
The first step is to quantify N_2-fixation in annual and perennial legume cropping systems. Subsequent residue incorporation and release of N through soil microbial decomposition will be studied with focus on soil N dynamics, potential N_2O emissions and optimization of N transfer efficiency to subsequent cereal crops.

Project Outline
For legumes to be effective N suppliers for future cropping systems several points have to be considered:

a) High SNF fixation rates [1]
b) Microbial decomposition, synchronized N release time and transfer efficiency to subsequent crop
c) Potential risks of nitrous oxide (N_2O) emissions after soil incorporation.

The present study focuses on management options:
Intercropping offers the advantage of covering more niches in a field and therefore compliments resource use. Intercropping is potentially a management option to tighten the nitrogen cycle, reduce greenhouse gas emissions and mitigate climate change [2].
Brassica species can be intercropped with legumes. The breakdown of Brassica-derived glycosinolates has an influence on the soil microbial biomass and the release of carbon and nutrients from the microbial biomass pool is facilitated (biofumigation) [3]. There are indications that nitrification can be inhibited in the short-term. Biofumigation could be used in nutrient management.
Temporal dynamics after incorporation of residues will be evaluated [4].

Figure 1: Annual intercropping experiment at Risø

Annual Field Experiment

To study the effects of interspecific interactions on N_2-fixation and soil N use an annual intercropping experiment is conducted at Risø DTU. Fig. 1 shows the experiment in which grain legumes (faba bean, pea) and Brassica are intercropped (seeding density: legume 100%, cereal 50%) with oat in a completely randomized plot design with 4 replicates. Atmospheric N_2 fixation is measured at significant growth stages using ^{15}N natural abundance methodology (EA-IRMS). Common agronomic parameters are monitored as well as soil N in the topsoil (0-10 cm). The experiment is conducted twice in 2011 and 2012 to cover inter-annual variation.

Perennial Field Experiment

The effects of perennial legume-grass mixtures on atmospheric N_2 fixation, short-term use of soil N sources and N_2O emissions are studied in a 2-year field trial at Flakkebjerg, Denmark. A grass-perennial legume (white clover, red clover and alfalfa) mixture gets undersown to spring barley. Atmospheric N_2 fixation is measured at significant growth stages using ^{15}N natural abundance methodology (EA-IRMS) and N_2O emissions are measured (sampling from field chambers and GC analysis) during campaigns after soil incorporation of the sward. Furthermore soil N is monitored in the topsoil (0-10 cm).

Fig. 2 shows barley yield data from 2010, indicating an increase of the straw yield in case of barley-grass treatments, while undersown legume seems to have no effect on the barley yield. However, we hypothesize that the biomass yield and nitrogen fixation in the subsequent year is positively influenced by legumes.

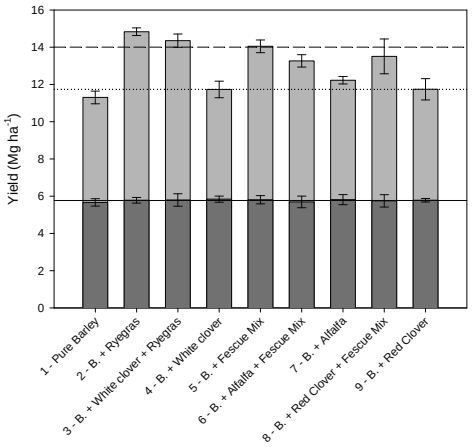

Figure 2: Barley yield 2010 in the perennial field experiment in Flakkebjerg (n=4). Treatments are shown on the x-axis (all treatments contain barley). Dark columns show the grain yield component, while the light columns show the straw yield component. The full line indicates average grain yield, the dotted line indicates average straw yield and the dashed line indicates average straw yield of grass-grass intercrop.

Lab incubation experiment – Brassica

The he potential for Brassica as a management tool for soil nitrogen cycling in agriculture has been tested in a 3-week incubation experiment.

Fig. 3 shows preliminary results and indicates an increase in ammonium (NH^4_+) values after Brassica incorporation. The treatment with either glycosinolates or a nitrification inhibitor shows the highest ammonium values. Further data analysis is necessary to determine the cause. Soil microbial biomass was monitored using Chloroform-Fumigation extraction and nitrification rates were analysed using the ^{15}N pool dilution method. The potential to conduct further in-depth genetic analysis of soil microorganisms and their activity on frozen soil (-80 degrees) in cooperation with GEUS is currently being reviewed.

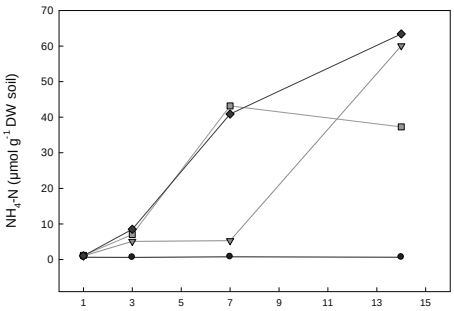

Figure 3: Ammonium concentrations in the Brassica incubation experiment (n=2). Circles (o) represent the control treatment (soil only), triangles(▽) soil with Brassica addition containing glycosinolates, squares (□) soil with Brassica addition not containing glycosinolates and diamonds (◊) soil with Brassica addition not containing glycosinolates but amended with a nitrification inhibitor. x-axis gives experiment days.

Acknowledgements

This PhD study is part of the SOLIBAM project (Strategies for Organic and Low-Input Integrated Breeding and Management) which is funded by the European Commission under the SEVENTH FRAMEWORK PROGRAMME with the grant number FP7 KBBE – 245058.

References

1. M.B. Peoples, D.F. Herridge, J.K. Ladha, Plant Soil. 174 (1995) 3-28
2. H. Hauggaard-Nielsen, S. Mundus, E.S. Jensen, Nutr. Cycling. Agroecosyst. 84 (2009) 281-291
3. A.L. Gimsing, J.A. Kirkegaard, Phytochem. Rev. 8 (2009) 299-310
4. P. Ambus, E.S. Jensen, Commun. Soil. Sci. Plant Anal. 32 (2001) 981-996

Rita Lencastre Fernandes
Phone: +45 4525 2993
E-mail: rlf@kt.dtu.dk
Discipline: Process Technology and Unit Operations

Supervisors: Krist V. Gernaey
Anker D. Jensen
Ingmar Nopens, Ghent University

PhD Study
Started: November 2009
To be completed: December 2012

Population Balance Models and Computational Fluid Dynamics: an Integrated Model Framework to Describe Heterogeneity in Fermentors

Abstract
Traditionally, cells in a microbial population are considered identical and characterized by averaged properties in studies of fermentation processes. However, research has shown that a typical microbial population in a fermentor is heterogeneous. The aim of this Ph.D. project is to establish a model framework where Population Balance Models (PBM) and Computational Fluid Dynamics (CFD) are integrated in order to describe heterogeneous microbial populations in stirred-tank reactors. This contribution focuses on the formulation of a PBM with protein content as the model variable. Besides describing the development of the microbial population structure under varying substrate availability, the model additionally accounts for cell-to-cell variability due to cell cycle.

Introduction
A heterogeneous microbial population consists of cells in different states, and it implies a heterogeneous distribution of activities (e.g. respiration, product efficiency). Furthermore, cell-to-cell variability implies different responses to extracellular stimuli. This will result in the development of a heterogeneous population with a possibly different structure when the microbial population is subjected to changes in the surrounding environment, relatively to when growing under a constant extracellular environment. In fact, this difference in the population structure may explain the lower productivities and higher viability obtained for cultivations in large-scale reactors where substrate and oxygen gradients are observed, relatively to cultivations in well-mixed bench scale reactors [1].

This PhD project aims at understanding and modeling the development of heterogeneous microbial populations subjected to varying environmental conditions. Given the short time frame of a typical cultivation (i.e. days, weeks), the contribution of genetic drift to the development of heterogeneity within a population was assumed negligible, and the focus of this project is set on understanding and modeling phenotypic heterogeneity.

Specific Objectives
The first part of this PhD project consists of developing a PBM, which is able to simulate a dynamic microbial population under varying substrate availability conditions. In order to achieve this goal, it was defined that the model would predict the development of a heterogeneous population of *Saccharomyces cerevisiae*. The following specific objectives were defined:

- Identify the main factors responsible for cell-to-cell variability within microbial populations (with special focus on *S. cerevisiae*).
- Identify a population model structure, (i.e. model variable(s), nr. of stages) which can account for the heterogeneity drivers.
- Establish correlations between substrate availability and the PBM kernel functions, based on experimental observations.
- Formulate and solve the PBM; compare the model predictions with experimental observations.

Results and Discussion
Phenotypic heterogeneity arises as a result of the variability inherent to the metabolic mechanisms of single cells. Cell size is a key feature affecting cellular design, fitness and function [2]. In fact, cell growth and division are tightly coupled, and this is reflected on the cellular capability of adjusting the growth rate to nutritional availability [1, 2]. The regulation of growth ensures that cells attain a critical size before initiating the division process [5, 6]. In the particular case of *S. cerevisiae*, two critical sizes corresponding to the regulation points START (committing to budding, or budding transition) and division have been identified. A schematic representation of the cells transition through

the cell cycle and the associated cell growth (i.e. size increase) is presented in Fig. 1. Experimentally, cell size of individual cells is relatively easy to measure by using flow cytometry [7]. In particular, the total protein content has been used as reliable measure for cell size [7–9]. Using cell size as population descriptor allows, thus, for describing the distribution of cellular states. Moreover, a better description of the cellular state is obtained by determining the distribution of cells in cell cycle phases (i.e. measuring DNA distributions).

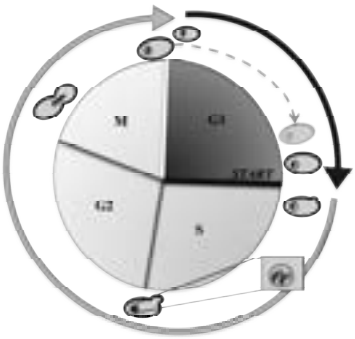

Figure 1: Schematic representation of the *S. cerevisiae* cell cycle. The dark arrow corresponds to the duration of the non-budding stage (G1 and eventually G0 phases). The *START* point represents the regulation point defining the initiation of the DNA replication and budding process, i.e. transition to the S phase. Upon entry to the G2 phase, two copies of the cell DNA are present. Due to their bigger size, the G1 phase is shorter for mother cells than for daughter cells.

It was thus found desirable to use a PBM based on protein content as model variable, which is applied to different stages (i.e. subpopulations) corresponding to non-budding and budding (cell cycle) phases, as depicted in Fig. 2. Upon transition to the S-phase (initiation of the budding process), cells in the non-budding stage are transferred to the following budding stage. Upon division, both mother cells and newborn daughter cells transition to the non-budding stage. The budding and division transitions are governed by probability density functions, which have maxima at the critical budding and division sizes (i.e. total protein contents), μ_B and μ_D.

Generally, the link to the extracellular environment is accounted for by including substrate dependency in the growth function (increase of cell protein content) as well as transition functions (budding and division) for each of the stages: (1) growth: a linear kinetic expression describing the increase of the cell protein content is multiplied with a specific growth rate that is calculated based on the substrate availability; (2) budding and division transitions: the critical cell protein contents are function of the substrate consumption rate.

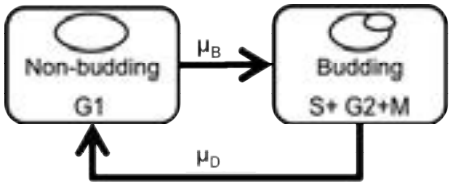

Figure 2: Schematic representation of the two stage representation of a microbial population consisting of a non-budding stage (NB) and a budding (B) stage. The critical size (protein content) that determines the budding transition is designated μ_B, while the critical cell size necessary for division is defined as μ_D.

Transition functions for changing substrate availability

The formulation of the budding and division transition functions, for a dynamic model, relies on understanding the effect of the changing substrate availability on the critical transition sizes. In order to establish realistic transition functions, the experimental data was collected in triplicate for a batch cultivation of a haploid *S. cerevisiae* strain on glucose (in 2 L bioreactors with controlled pH). Samples were taken along the cultivation, with a higher frequency during non-balanced growth periods (i.e. diauxic shift, and entrance to stationary state). Besides the traditional monitoring of optical density, glucose and ethanol concentrations, samples were analyzed by flow cytometry. Distributions of forward scattering (typically proportional to cell size), side scattering (a measure of intracellular granularity) DNA and protein content distributions were obtained by fluorescence staining for each sample.

Flow cytometry: data analysis

Flow cytometry (FCM) is a robust technique that relies on the properties of light scattering, excitation and emission to measure a variety of properties at single cell level. The ability of FCM to measure the properties of single cells allows the study of phenotypic diversity of individual microorganisms [10]. Measurements are collected for each analyzed cell (i.e. event) and the resulting data are typically present in the form of histograms (measured property vs. cell count) or 2D density plots (Fig. 3).

The DNA distribution is commonly used for classifying cells according to cell cycle phase. The histogram contains two peaks separated by an intermediate flatter area. The first peak corresponds to cells in G_1 cell cycle phases (i.e. cells possessing one DNA copy, Fig. 1). The second peak corresponds to cells in phases G_2/M that have two copies of the DNA (Fig. 1). Cells in the S-phase can be found in the inter-peak region.

Based on a manual gating strategy [6], a standardized procedure was developed in order to isolate a subpopulation with a high fraction of cells undertaking the budding transition (Fig. 3). The critical budding size is estimated as the mean size of the cells in this subpopulation. The critical division size is similarly

estimated based on isolating a subpopulation that is part of the 2C peak (Fig. 3).

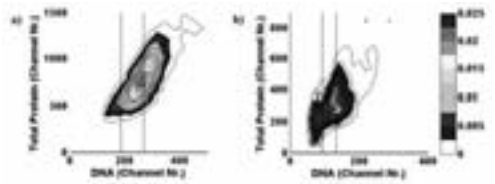

Figure 3: Experimental bivariate distribution of total protein content and DNA during a batch cultivation of *S. cerevisiae*: exponential growth on glucose (a) and on ethanol (b). The color code corresponds to the number density of the cells. The vertical lines corresponds to the critical budding (to the left) and division (to the right) threshold identified estimated on the DNA distribution.

During the cultivation, a subtle adjustment of the budding and division sizes was observed during the late growth phases on glucose or ethanol leading to a smooth shift of the total protein distributions towards smaller fluorescence intensities (i.e. smaller sizes), and a rather slight decrease in fraction of budding cells in the population (budding index, BI).

An abrupt change on the cell cycle position (steep decrease of the BI) was observed upon glucose depletion and beginning of the diauxic shift. These observations reflect the two different mechanisms proposed by Brauer et al. [11] when explaining the changes in the gene expression patterns observed during the late growth phase - metabolic adjustment - and diauxic shift - metabolic rearrangement. In light of the experimental results, and considering the gene expression patterns reported in the literature, it is likely that the adjustment of cell size is triggered by a steep increase in the glucose consumption rate, and the ethanol consumption rate when considering the second growth phase in the cultivation.

Model formulation

The PBM developed for this study is based on a multi-stage model proposed in the literature [12]. It consists of two population balance equations (PBE) that describe cell growth, initiation of the budding process, division and cell birth (Eq. 1 and 2), and corresponding initial and boundary conditions.

$$\frac{\partial N^{NB}(m,t)}{\partial t}+\frac{\partial}{\partial m}\left[r_m(m|Y)N^{NB}(m,t)\right]= \\ =-\Gamma_{NB}(m|Y)N^{NB}(m,t)+2\int_m^{\infty}\Gamma_B(m'|Y)P(m,m'|Y)N^{B}(m',t)dm' \quad \text{(Eq. 1)}$$

$$\frac{\partial N^{B}(m,t)}{\partial t}+\frac{\partial}{\partial m}\left[r_m(m|Y)N^{B}(m,t)\right]= \\ =-\Gamma_{NB}(m|Y)N^{B}(m,t)+\Gamma_B(m|Y)N^{NB}(m,t) \quad \text{(Eq. 2)}$$

The budding and division transitions, Γ_{NB} and Γ_B, are mathematically described as the product of the growth rate and hazard functions (Eq. 3-5) where the probability that a cell of mass *m* initiates the budding process, i.e. transitions to the budding stage, or divides into two new cells is described by a Gaussian probability density function with mean μ_B and μ_D, respectively. As discussed, these two parameters are functions of the substrate availability. For notation purposes, the variable Y generally designates the extracellular environment. The standard deviation is assumed to be the same for the two transition functions and is constant along the cultivation.

$$\Gamma_{NB}(m|Y)=r_m(m,Y)\frac{h_{NB}(m|Y)}{1-\int_{m_0}^{m}h_{NB}(m')dm'} \quad \text{(Eq. 3)}$$

$$h_{NB}(m|Y)=N(\mu_B(Y),\sigma_B) \quad \text{(Eq. 4)}$$

$$r_m(m,Y)=k_m m\cdot\lambda(Y) \quad \text{(Eq. 5)}$$

A mother and a daughter cell are generated upon division, where the ratio of the mother cell size to the daughter cell is defined by the partitioning function, $P(m|Y)$. This function consists of a beta probability density function: during exponential growth on glucose, the distribution is taken symmetrical ($\alpha=\beta=50$), while during exponential growth on ethanol it is left-skewed ($\alpha=40$; $\beta=60$). The change in the shape parameters reflects the decrease in the ratio of daughter to mother cell size that has been observed experimentally after the diauxic shift.

The growth rate of individual cells (r_m) depends on the mass of each cell (first-order kinetics) and on the available concentration of glucose, ethanol and oxygen, as described by Eq. 4. The substrate factor in the growth kernel, $\lambda(Y)$, can be regarded as a specific growth rate and it is derived from an unstructured model describing the consumption of glucose by oxidation and reduction, formation and consumption of ethanol, and supply and consumption of oxygen [13]. For each time instant, the PBM yields the distribution of the number of cells per cell size, which can then be summed in order to determine the current biomass concentration. This concentration is then used to determine the updated concentrations of glucose, ethanol and oxygen in the extracellular environment, based on the unstructured model.

The partial differential equations forming the PBM were discretized according to the fixed-pivot method [14, 15], and the resulting systems of ordinary differential equations (ODE), as well as the ODEs of the unstructured model, were solved using a MatLab ® solver for stiff ODE systems.

Model Predictions vs. Experimental Results

The multi-scale model consisting of the PBM coupled to the unstructured model for the extracellular environment, allows for both estimation of the macroscopic variables: glucose, ethanol, oxygen and overall biomass; as well as for prediction of the distribution of cell sizes for each of the non-budding and budding stages.

As illustrated in Fig. 4-a), the predictions for the macroscopic variables are in good agreement with the experimental data. Also the model predictions for the distributions of cell size for the overall population follow the same dynamics as the experimental data (Fig. 4-b) and c)).

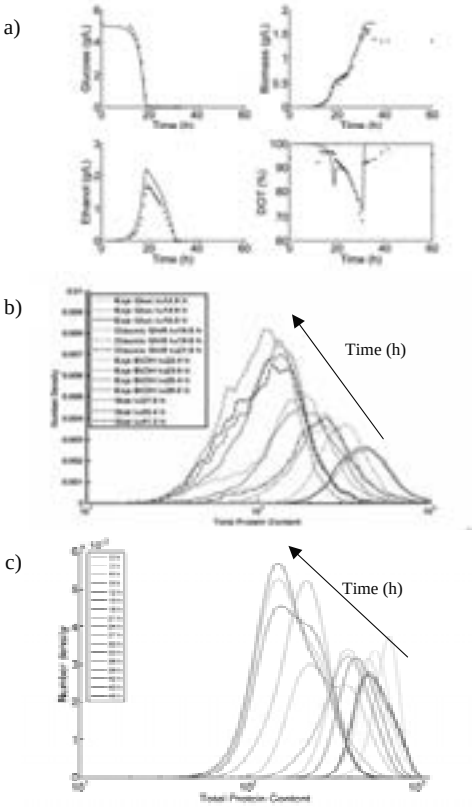

Figure 4: Comparison of model predictions and experimental observations: a) variation of glucose, ethanol, biomass and oxygen during the cultivation (blue full lines correspond to model predictions, green dots to experimental data points); b) Distribution of total protein content along the cultivation, measured experimentally by flow cytometry; c) Model predictions for the distributions of cell total protein content (cell size, in arbitrary units) along the cultivation.

Conclusions

Individual microorganisms, even if part of an isogenic population, may differ greatly in terms of physiology, biochemistry, or behavior [10]. This heterogeneity results from differences in the microenvironment surrounding each individual cell, as well as the physiological stage of an individual cell when subjected to a given change in the extracellular medium.

Based on the analysis of flow cytometric data correlations of the critical transition protein content for both budding and division to substrate availability were determined. These correlations allowed for the formulation of a PBM describing the protein content distribution of the microbial population for each of the non-budding and budding stages. The PBM was coupled to an unstructured model describing the extracellular environment. The resulting multi-scale model predictions are in good agreement with the experimental data.

Acknowledgements

The Danish Council for Strategic Research is gratefully acknowledged for financial support in the frame of the project "Towards robust fermentation processes by targeting population heterogeneity at microscale" (project number 09-065160).

References

1. S.-O. Enfors, M. Jahic, A. Rozkov, B. Xu, M. Hecker, B. Jürgen, J. Biotechnol. 85 (2) (2001) 175-185.
2. P. Jorgensen, M. Tyers. Curr. Biol. 14 (23) (2004) 1014-1027.
3. A.J. Saldanha, M.J. Brauer, D. Botstein, Mol. Biol. Cell 15 (9) (2004) 4089-4104.
4. P. Jorgensen, J.L. Nishikawa, B.-J. Breitkreutz, M. Tyers. Science 297 (5580) (2002) 395-400.
5. I. Rupeš, Trends Genet. 18 (9) (2002) 479-485.
6. D. Porro, L. Brambilla, L. Alberghina. FEMS Microbiol. Lett. 229 (2) (2003) 165-171.
7. D. Porro, F. Srienc, Biotechnol. Prog. 11(3) (1995) 342-347.
8. L. Alberghina, C. Smeraldi, B. M. Ranzi, D. Porro, J. Bacteriol. 180 (15) (1998) 3864-3872.
9. C. Cipollina, L. Alberghina, D. Porro, M. Vai, Yeast 22 (5) (2005) 385-399.
10. B.F. Brehm-Stecher, E.A. Johnson, Microbiol. Mol. Biol. Rev. 68 (3) (2004) 538 -559.
11. M.J. Brauer, A.J. Saldanha, K. Dolinski, D. Botstein, Mol. Biol. Cell 16 (5) (2005) 2503-2517.
12. C. Hatzis, D. Porro, J. Biotechnol. 124 (2) (2006) 420-438.
13. B. Sonnleitner, O. Käppeli. Biotechnol. Bioeng. 28 (6) (1986) 927-937.
14. I. Nopens, D. Beheydt, P.A. Vanrolleghem, Comput. Chem. Eng. 29 (2) (2005) 367-377.
15. S. Kumar, D. Ramkrishna, Chem. Eng. Sci. 51 (8) (1996) 1311-1332.

List of Publications

1. D. Schäpper, R.L. Fernandes, A.E. Lantz, F. Okkels, H. Bruus, K.V. Gernaey, Biotechnol. Bioeng. 108 (4) (2011) 786-796
2. R. Lencastre Fernandes, M. Nierychlo, L. Lundin et al. Biotechnol. Adv. 29 (6) (2011) 575-599

Xiaodong Liang
Phone: +45 4525 2891
E-mail: xlia@kt.dtu.dk
Discipline: Engineering Thermodynamics

Supervisors: Georgios Kontogeorgis
Kaj Thomsen
Wei Yan, DTU-Kemi

PhD Study
Started: August 2011
To be completed: July 2014

Thermodynamic Modelling of Oil-Sea Water Mixtures

Abstract
The oil accident in the Gulf of Mexico was a wake-up call. It emphasizes how little we know about how oil behaves in water and how it interacts with water, especially in Deepwater Horizon. How to detect oil and gas leaks around the sub-sea well head to enable a faster response, and how to map the oil in the water column are very crucial during oil accident and clean process, which could be resolved by sonar technology. The properties that sonar technology concerned mostly about are the speed of sound, density (compressibility) and the solubilities. The purpose of our project is to develop a sophisticated thermodynamic model for the oil-sea water system that could describe the phase behavior and those physical properties with high accuracy.

Introduction
Thermodynamic models can provide solid basis for state-of-the-art sonar products, which can be used to reduce the environmental effect of offshore oil exploration, such as (1) detection of oil and gas leaks around the sub-sea well head enabling a faster response especially in deep water and/or ice covered areas; (2) detection and mapping of oil in the water column after an oil spill to be used during cleanup process. Sophisticated mathematic models connect the sonar products and thermodynamic models, as illustrated in Figure 1.

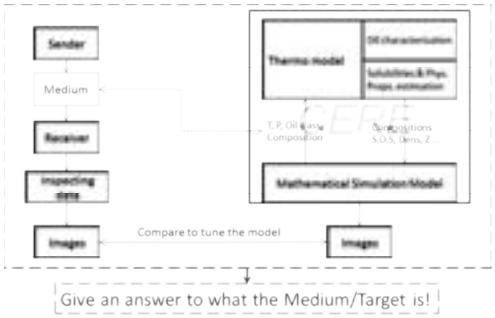

Figure 1: Overview of the broader project

Models
Classical thermodynamic models used by oil industry are semi-empirical and not suitable for mixtures containing water and other polar chemicals. The Cubic-Plus-Association (CPA) [1] and Statistical Associating Fluid Theory (SAFT) [2, 3, 4, 5, 6] equations of state, contain an association term. These advanced equations of state have been proven to be useful tools for describing complex mixtures, and they have been already used in the petroleum and chemical industries.

Specific Objectives
The purpose of this PhD project is to further develop SAFT models capable of predicting various properties (phase behavior/solubilities, densities, speed of sound, etc.) in oil-sea water mixtures over a wide range of conditions with respect to pressure, temperature, salinity of water and for a wide range of oil mixtures of different types and origins. Specifically, the project contains the following four major directions in SAFT developments:

- Acoustical and other properties of relevance to Sonar products
- Oil systems with appropriate characterization methods
- Electrolyte solutions
- Oil-sea water systems

If time permits it, extension of the model to a wider range of mixtures and improvements on the model computing speed will also be investigated.

Results and Discussion
Speed of Sound is a very important property in sonar technology. We have conducted an evaluation of the

performances of the classical cubic equation of state SRK [7], and the advanced CPA and SAFT models for the speed of sound of some normal hydrocarbons, associating and polar compounds. The results at one specific temperature are showed in Figure 2 for Methane, Propane, n-Hexane, n-Decane, Water and Methanol respectively.

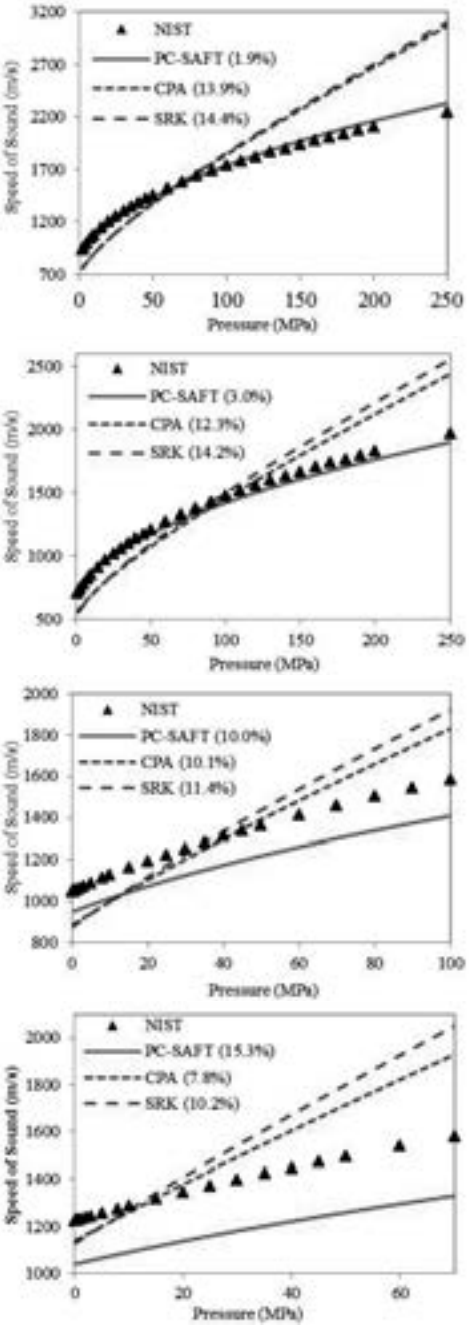

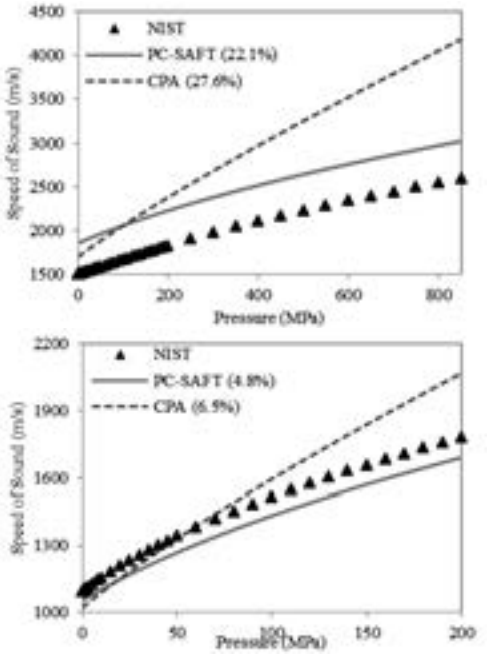

Figure 2: Speed of Sound from top to bottom of Methane at 150K, Propane at 300K, n-Hexane at 300K, n-Decane at 300K, Water at 300K, and Methanol at 300K sequentially.

It can be seen that PC-SAFT [5, 6] performs better than other two models, especially at high pressures. So PC-SAFT will be used as the basis model for further developments.

Acknowledgements
This PhD project is founded by the Danish National Advanced Technology Foundation (DNATF) and the Department of Chemical and Biochemical Engineering, Technical University of Denmark.
We also thank PhD student Bjørn Maribo-Mogensen for useful discussion and assistance in calculations.

References

1. G.M. Kontogeorgis, E.C. Voutsas, I.V. Yakoumis, D.P. Tassios, Ind. Eng. Chem. Res. 35 (1996) 4310-4318.
2. W.G. Chapman, K.E. Gubbins, G.Jackson, M. Radosz, Ind. Eng. Chem. Res. 29 (1990) 1709-1721
3. S.H. Huang, M. Radosz, Ind. Eng. Chem. Res. 29 (1990) 2884-2294
4. S.H. Huang, M. Radosz, Ind. Eng. Chem. Res. 30 (1991) 1994-2005
5. J. Gross, G. Sadowski, Ind. Eng. Chem. Res. 40 (2001) 1244-1260.
6. N.Von Solms, M.L.Michelsen, G.M. Kontogeorgis, Ind. Eng. Chem. Res. 42 (2003) 1098-1105.
7. G. Soave, Chem. Eng. Sci. 27 (1972) 1197-1203.

Watson Neto
Phone: +45 4525 52958
E-mail: wan@kt.dtu.dk
Discipline: Process Technology and Unit Operations

Supervisors: John M. Woodley
Pär Tufvesson

PhD Study
Started: June 2010
To be completed: May 2013

Development of An Integrated Downstream Processing for Biocatalytic Reactions

Abstract
Chiral amines are important building blocks for the chemical and pharmaceutical industries and they can be produced enzymatically with high enatioselectivity using ω-transaminase (EC 2.6.1.18). However, the use of this enzyme has some drawbacks such as substrate and product inhibition and a potentially unfavorable equilibrium, which together limit the process productivity. In order to make its industrial utilization more attractive and efficient, these drawbacks need to be addressed. The aim of this project is to develop process technology for an efficient integrated downstream process for chiral amines, alleviating these drawbacks, hence increasing the process attractiveness.

Introduction
In the past decade the amount of research and publications related to the use of ω-transaminase (ω-TAm) has greatly increased. The potential of this enzyme to synthesize a broad range of products such as amino acids, chiral amines, chiral alcohols, sugars and others with high enatioselectivity and reasonably high reaction rate and stability [1-2], gives it an advantage over the traditional chemical synthesis to produce chemical and pharmaceutical intermediates containing chiral amines and makes this enzyme very attractive for synthetic chemistry.

However, despite all the advantages, limiting factors have been reported in reactions using ω-TAm, making its application only possible if such issues are solved. The list includes high product and substrate inhibition, potentially unfavorable equilibrium and low water solubility of substrates [3].

For instance, in the asymmetric synthesis of (*S*)-(-)-α- methylbenzylamine (MBA) using isopropylamine (IPA) as amine donor and the acetophenone (APH) as amine acceptor (Fig. 2), both APH and MBA cause severe inhibition to the enzyme, negatively affecting the reaction rate. Furthermore, this reaction is also more favorable in the reverse direction which limits the production of MBA. A common strategy normally used to alleviate this issue is to use an excess of one of the substrates [4], for instance, using 200-1000 fold excess of IPA.

A second strategy to improve the productivity of this process is to solve the substrate and product inhibition and this can be achieved applying controlled supply of the inhibitory substrate (fed batch or *in situ* substrate supply - ISSS), ensuring that it is present at non toxic concentrations and also removing the inhibitory product as soon as it is formed in the reactor (*in situ* product removal – ISPR).

ISPR has the advantage of both alleviating product inhibition and at the same time shifting the equilibrium towards product formation. Together with controlled supply of substrate, this technology can play an important role in increasing the productivity in transaminase catalyzed reactions or any other equally limited process [5].

Specific objectives
The aim of this project is to research and develop process technology that allows the production of high concentrations (50 g/L) of chiral amines, both at small scale (≤100 ml) and liter scale (1-6 L). This will be achieved by exploring different chemical and physical properties of the compounds involved in the reaction (Fig. 2). A methodological approach to develop and apply these technologies in processes will be developed, models will be created and different reactor configuration will be studied.

The project is divided in three main topics:

Integrated downstream processing (ISSS and ISPR):
In a first approach, tools to supply substrates and recover products while the reaction takes place will be developed. Some research regarding the screening and selection of polymeric porous resins as well as modeling of substrate supplying and product removal has been started in a parallel project (see page 13). Similar work regarding organic solvents will be developed and the application of both technology as strategy to alleviate: substrate and product inhibition; the equilibrium constrains; and consequently increase the productivity in biocatalytic processes will be addressed in this PhD project.

Design of the reactor set up:
Applying ISSS and ISPR will imply design of the reactor set up. Conditions have to be made to make possible the application of these technologies. Decisions concerning the location of the recovery method (internal or external), the formulation of the biocatalyst (free or immobilized cells) among others need to be made. Figures 1A and B compare two examples of reactor configurations using polymeric resins that will be tested in this project. In A, free biocatalyst is used in a fed batch reactor (in order to control the substrate inhibition) from where the reaction mixture is continuously pumped (through a membrane) to a packed bed column containing polymeric resin which should have selective affinity for the product. In this case immobilized biocatalyst can also be used and the membrane could easily be replaced to a filter mesh with a lager cut off. In B, a fed batch reaction is again applied, this time with both biocatalyst and polymeric resins located within the tank.

Relative the use of organic solvents, the reactor design needs to be more elaborate, especially if one desires a continuous removal of the solvent and continuous supply of fresh entrainer.

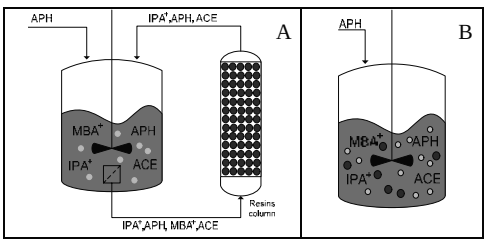

● Free biocatalyst, ◍Immobilized biocatalyst, ●Polymeric resins
IPA: Isopropylamine (at pH 7 it is charged); APH: Acetophenone
MBA: Methyl benzylamine (at pH 7 it is charged); ACE: Acetone

Figure 1: Examples of reactor configuration for ISPR using resins.

Process scale up:
The most promising setup obtained in the laboratory will be scaled up to 1-6 L in order to test the operability of the developed method at a larger scale and estimate cost.

Results and Discussion
In order to successfully carry out ISPR, key properties of the target product that allow its separation from the substrate and co-product need to be found. Recently we have been focusing in collecting data on the substrates and products of different transamination reactions. In Figure 2, an example for production of MBA can be see, where it becomes clear that the properties of the compounds involved in this reaction are very similar (similar pKa for both amine donor and chiral amine product, which makes the use of the charge difference difficult, as well as similarity between octanol-water partition coefficients between the pro-chiral ketone and the chiral amine product, which make difficult the use of organic solvents to selectively remove the product).
Deeper investigation on this topic is required to fully address this issue and establish windows of operation for each method (*i.e.* to identify to which extent each method can be applied, whether it improves the process or not and quantify/estimate the product and or substrates loss). A compromise between product removal and substrate loss need to be found for the selected methods.

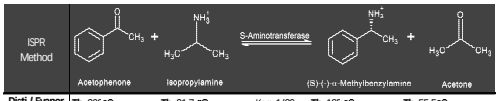

Disti / Evapor	Tb: 202 °C	Tb: 31.7 °C	Keq=1/30	Tb: 185 °C	Tb: 55.5°C
Preci / Crysta	Tm: 20 °C	Tm: -95.3°C		Tm: -65 °C	Tm: -98.3 °C
Ion exchange	Pka: N/A	Pka: 10.63 = Pi		Pka: 9.75 = Pi	Pka: N/A
Adsob/Extract	LogP: 1.58	LogP: 0.26		LogP: 1.49	LogP: -0.24
Disti / Evapor	pvap: 3.97E-1 mmHG	pvap: 5.80E+2 mmHG		pvap: 5.00E-1 mmHG	pvap: 2.32E+2 mmHG
Preci / Extract	Wsol: 6.13 g/L	Wsol: 1.00E+3 g/L		Wsol: 42.00 g/L	Wsol: 1.00E+3 g/L

Figure 2: Example of transaminase catalyzed reaction and physical-chemical properties of compounds involved.

Conclusions
The current research shows the important role ISPR can play in the transaminase catalyzed processes. The process productivity can substantially be improved by removing the inhibitory product, which will also be reflected in process economics, since fewer steps will be required in the downstream processing. Different alternatives will be tested to achieve the desired goal.

Acknowledgements
The student acknowledges the support from BIOTRAINS Marie Curie ITN, financed by the European Union through the Seventh Framework People Programme (Grant Agreement no. 238531).

References
1. J.S. Shin, B.G. Kim, A. Liese, C. Wandrey, Biotechnol. Bioeng. 73 (3) (2001) 179-87.
2. B.Y Hwang, B.K. Cho, H. Yun, K Koteshwar, B.G Kim, J. Mol. Catal. (37) (2005) 47-55
3. J.S Shin, B.G. Kim, Biotechnol. Bioeng. 60 (5) (1998) 534-540.
4. D. Koszelewski, D. Clay, K. Faber, W. Kroutil, J. Mol. Catal. B-Enzym. 60 (2009) 191–194.
5. P. Tufvesson, J.L. Ramos, J.J. Skibsted, N. Al-Haque, W. Neto, J.M. Woodley, Biotechnol. Bioeng. 108 (2011) 1479-1493

Joana de Lima Ramos
Phone: +45 4525 2990
E-mail: jlr@kt.dtu.dk
Discipline: Process Technology and Unit Operations

Supervisors: John M. Woodley
Pär Tufvesson

PhD Study
Started: March 2010
To be completed: February 2013

Guiding Biocatalytic Processes Improvements Using Engineering Evaluation Tools

Abstract
While biocatalysis is a useful tools to assist with organic synthesis to date few reports have documented the economics or environmental profile of such processes. As a relatively new technology many processes do not immediately fulfill the economic and environmental requirements for commercial operation (e.g. low biocatalyst productivity and process intensity, among others). Hence early stage economic and environmental assessment could be powerful tools to guide research and development activities in order to achieve commercial potential.

Introduction
During the development of a biocatalytic process and in particular during its scale-up, there are some required considerations. Two of the most important are the economic and environmental profile. The present project will be focused on the development of engineering tools in order to assist a fast and accurate economic and environmental analysis. When applied to a given process these have a decisive role in helping to identify bottlenecks in process development, and to justify where to put effort and resources.

In processes at an early stage of development, process feasibility can be achieved in two ways: process methods (as *in-situ* product removal, ISPR, reactor configuration, among others) and enzyme engineering (e.g. improve catalyst activity and tolerance to high product and substrate concentrations via protein engineering). However, there is no systematic method focused on process selection and development, where the process bottlenecks are analyzed and resolved. The outcome of the proposed research will establish new tools and methodologies to guide biocatalyst and (bio)process development.

The foremost step to assess the operating cost and environmental profile is to define the life cycle inventory (LCI), based on mass and energy balances. For a correct assessment it is necessary to define the process operating conditions. The operating conditions can be defined using operating windows.

The process evaluation (including tool development and validation) will be performed on the ω-transaminase (TAm) catalysed synthesis of optically pure chiral amines, as a case study.

Biocatalytic production of optically pure compounds has emerged as an attractive complement to chemical synthesis, due to high enantioselectivity[1] and mild conditions avoiding protecting and de-protecting steps leading to a more efficient process[2], the possibility to tailor the biocatalyst properties using molecular biology tools and a potential green profile[3,4].

In spite of the many attractive features of transaminase catalyzed reactions, there are still a number of challenges that need to be dealt with in order make transaminase processes competitive for a wider range of amines. Guidelines for a successful biocatalytic production of chiral amines will be identified through process economic and environmental assessment.

Specific objectives
The project objectives are:

- Development a fast and accurate tool that allows selection (distinguish between different synthetic routes) and evaluation (economic and environmental analysis) of alternative processes. This includes bottleneck identification of the model process, followed by solution suggestions.
- Application of the proposed tool using a specific model process: synthesis of phenyl amines using the biocatalyst TAm.
- Revision and application of the developed tool using case studies provided by industrial and/or academic partners.

Evaluation tools, which are built on top of the developed model, have as an output an economic and environmental evaluation of a given process. The economic and environmental analysis obtained will allow the identification of process bottlenecks leading to several solution suggestions (Figure 1).

Figure 1: Methodology for the engineering tool use for process evaluation.

Methodology for operating window

Operating windows are a convenient method to quantify process performance and feasibility where interactions between unit operations are significant and provide the ability to visualize process operability. This methodology proved to be useful to guide biocatalytic process development, identifying the constraints with greater influence on the process feasibility. The operating window methodology includes 9 steps:

1) Define main reaction system
2) Investigate solubility and other physical limitations: Physical properties of the substrates, products and reaction can be found in literature or determined by CAPE software
3) Determine thermodynamic reaction equilibrium: Reaction thermodynamics is perhaps one of the key issues that need to be addressed in chiral amines production by transaminase catalyzed reactions, as it will determine the adopted strategy and the process feasibility[5].
4) Define minimum required economic metrics

Table 1: Required economic metrics for a successful biocatalytic process

	Whole-cell	Free-Enzyme	Immobilized Enzyme
Required conversion (%)	90	90	90
Required product concentration (g/L)	50	50	50
Biocatalyst productivity ($g_{product}/g_{biocatalyst}$)	10	75	100
Required space time yield ($g_{product}/L/h$)	1	1	1
Required catalyst concentration ($g_{biocatalyst}/L$)	5	0.67	0.5
Number of catalyst recycles	5	1	100
Required catalyst activity ($g_{product}/g_{biocatalyst}/h$)	0.04	1.5	0.02

5) Define effort for equilibrium shifting
6) Define kinetic model
7) Define *in-situ* product/co-product removal limitations (process limitations)
8) Define operating space by combining kinetic model and equilibrium. Check whether any operating window has been found or not.
9) Perform a sensitivity analysis repeating the previous steps.

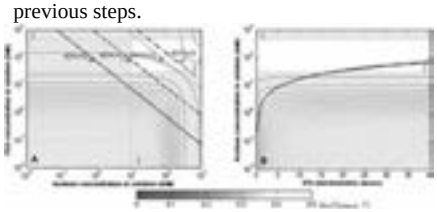

Figure 2: Window of operation for the synthesis of (S)-1-phenyl-ethylamine (PEA) using soluble ω-transaminase A) with simultaneous removal of product and co-product using resins and acetone stripping, respectively, and different amine donor excess (0, 1, 10 and 20 times excess); B) removal of product using resins at different amine donor excess and assuming that acetophenone concentration is kept constant at 50 mM applying a substrate feeding strategy. 1) Physical limitations: PEA solubility limit. 2) ISPR limitations: PEA removal by resin adsorption. 3) IScPR limitations: acetone stripping limitation.

As with any new technology, an evaluation of the cost of the biocatalyst improvement against the added value to the process needs to be performed with a cost-benefit[6]. In a biocatalytic process, direct development of the catalyst specifically for the reaction of interest is frequently required. However, some industries (such as the pharmaceutical industry) cannot always afford time-consuming research on protein development, and the possibility for process development is limited. This PhD-project aims at the development a fast method to assess costs, environmental constrains, set guidelines for biocatalytic process, and in a later stage to quantify the development efforts needed.

Acknowledgements

The author would like to acknowledge the support from BIOTRAINS Marie Curie ITN, financed by the European Union through the 7th Framework people Programme (Grant agreement no.: 238531).

References

1. P. Tufvesson, W. Fu, J.S. Jensen, J.M. Woodley, Food Bioprod Process 88 (2010) 3-11.
2. A. Schmid, J.S. Dordick, B. Hauer, A. Kiener, M. Wubbolts, B. Witholt, Nature 409 (2001) 258–268.
3. N.J. Turner, Nature Chemical Biology, 5 (2009) 567–573.
4. P. Tufvesson, J. Lima-Ramos, J.S. Jensen, N. Al-Haque, W. Neto, J.W. Woodley, Biotech Bioeng 108 (2011) 1479 – 1493.
5. P. Tufvesson, J.S. Jensen, W. Kroutil, J.M. Woodley, Biotech Bioeng, submitted
6. P. Tufvesson, J. Lima-Ramos, M. Nordblad and J.M. Woodley, Org Process Res Dev 15 (2001) 266-274.

Baoguang Ma
Phone: +45 4525 6813
E-mail: baom@kt.dtu.dk
Discipline: Polymer Technology

Supervisors: Anne Ladegaard Skov
Søren Hvilsted

PhD Study
Started: August 2011
To be completed: August 2014

Self-Healing Materials

Abstract
Polymers and rubbers have been widely used in the past decades in a variety of products. However, the long-term stability of polymer is largely related to the small cracks and defects which were formed during usage. Therefore, more and more attention has been paid on self-healing material to reduce or eliminate the small cracks or deformation in the recent years. Self-healing materials are a class of smart materials that have the ability to repair damage which is inflicted upon themselves. With designed structures or healing agents buried inherently, self-healing materials can elongate the life time of polymers and rubbers.

Introduction
Self-healing materials have attracted more and more attention in the recent years because of their ability to elongate the life time of polymers and rubbers. Due to the progress in development of self-healing materials, there now exist self-healing materials from zero to second generation.

For the zero generation, the main target for designing such materials is to retard the damage by using surface modification or mixing reinforcing components to prevent the damage rather than repair it. Because dispersed materials can increase the toughness and the impact strength by loading some specified composite, lots of biomaterials have been improved by applying such a method. For example, poly-L-lactide (PLLA) is kind of biodegradable material used in surgery [1]. However, the mechanical properties are not good enough to sustain the weight of bone. Therefore, self-reinforcing PLLA has been employed to increase the strength as well as toughness. Due to self-reinforcing PLLA gets a 2-fold higher strength than common PLLA, hence the usage for PLLA has largely increased in surgery.

When it comes to first generation, the main focus of self-healing materials is the repair of the crack by releasing the healing agent after the damage. Take PDMS based self-healing materials as an example, the healing agent hydroxyl end functionalized PDMS (HOPDMS) and polydiethoxysiloxane (PDES) [2] have been encapsulated and dispersed in the matrix. Not only can these materials reinforce the strength and toughness of PDMS by 200%, but also HOPDMS and PDES can serve as healing agent when damage occurs. When a micro crack forms on the surface, HOPDMS and PDES will be released into the matrix and react with the residual catalyst in the matrix. The fracture toughness recovers up to 88% after the self-healing process in comparison to original material. However, the materials in this generation have to face a critical problem, namely phase separation, which is inevitable when dispersing microencapsulated microspheres in homogeneous materials. The healing process is shown in Fig.1[2].

In order to avoid phase separation, self-healing materials has been upgraded to second generation. The main characteristics of this generation is the absence of encapsulation which is then replaced by the usage of thermal or ultraviolet light or even just bringing the fracture surfaces together to trigger the healing process. For example, a very interesting material synthesized by fatty acid and diethylenetriamine[3] can recover itself by just bringing two parts into contact without any stimulation. The strain of this self-healing elastic rubber exceeds 500% in origin, while the elastic rubber after healing process can still possess the ability to sustain a strain of 400%. After the self-healing procedure, the material can to a large extent recover its original properties. The supermolecular structure is shown in Fig.2[3]

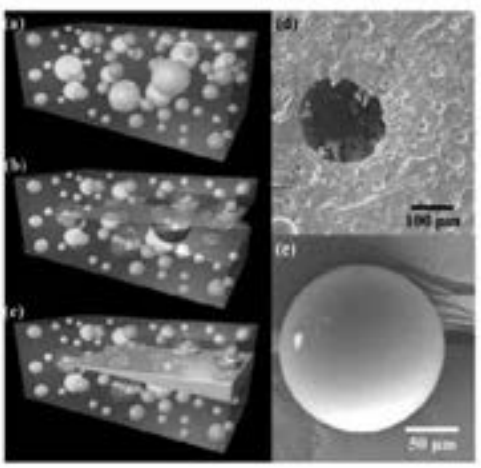

Fig. 1 Schematic of self-healing process: a) self-healing composite containing microecapsulated catalyst and phase seperated healing agent droplets b) crack on the surface c) repolymerization was triggered to heal the matrix d) the fracture surface in SEM before healing e) the fracture surface in SEM after healing

Fig.2 Schematic view of a reversible network formed by supermolecular interactions. Blue represents the mixtures of two-functional ended amide and red represents the mixtures of three functional ended amide. Dots represent the H-bonds.

Specific Objectives

The aim of the project is to design self-healing materials that can be used in blocking the fracture in oil reservoir. Since vinyl-terminated PDMS possess the ability to crosslink by adding crosslinker and catalyst, we may design a system to use such a system to block the fracture in the oil reservoir.

By using IR, SEM, TEM, NMR, rheometer, we may be able to understand how the self-healing materials serve in the oil reservoir.

Conclusion

Self-healing materials are a new promising area that may benefit materials science in many application fields. While there are several approaches in the development, the aim of these approaches is to get them realistic, feasible and reasonable effective. With certain innovations, self-healing materials should be able to be widely used in the future.

Acknowledgements

This work is funded by Mærsk Oil and Gas and Department of Chemical and Biochemical Engineering and Danish Polymer Centre.

References

1. P.Tormala, Clin. Mater. 10 (1992) 29-34.
2. S.H. Cho, H.M. Andersson, Adv. Mater. 18 (2006) 997-1000.
3. P. Cordier, F. Tournilhac, Nature 451 (2008) 977-980.

Christine Malmos
Phone: +45 4525 2892
E-mail: mmos@kt.dtu.dk
Discipline: Engineering Thermodynamics

Supervisors: Nicolas von Solms
John M. Woodley

PhD Study
Started: August 2011
To be completed: July 2014

Inhibition of Gas Hydrate Formation by Ice-structuring Proteins

Abstract
Ice-structuring proteins (ISPs) have been shown to be very effective at preventing hydrate formation and at the same time being environmentally benign. A particularly potent ISP is found in the Danish bark beetle. The aim of this PhD project is to evaluate the potential of ISPs as low-dosage hydrate inhibitors for the oil and gas industry. This will be achieved by setting up laboratory scale experiments to simulate realistic hydrate formation scenarios. Experimental methods for various setups are being developed based on the Second Germination (SG) method and a new Crystal Growth Inhibition (CGI) method.

Introduction
A combination of low temperature, high pressure and presence of water and natural gas is known to provide conditions for formation of gas hydrates, which may precipitate in pipes and production gear during oil recovery. Especially subsea pipelines are exposed to this phenomenon which is also why gas hydrates are listed as the major technical problem in offshore energy development.

In some cases the formation of gas hydrates leads to pipeline blockage which may enforce production shutdown, resulting in major economical losses. Assuring a continuous flow of oil and gas through the pipeline can be achieved using different tactics. One of them is based on heat conservation i.e. if the temperature in the pipeline is held high enough hydrates will not form. Such an approach often requires a multimillion dollar investment for insulation of subsea pipelines. Another preferred method is to use chemicals to prevent hydrate formation. Traditionally methanol or ethylene glycol has been injected in the relevant places during production of oil and gas to lower the hydrate formation temperature. Massive amounts of chemicals are needed; in particular if the water production is high, and worldwide methanol costs for hydrate inhibition are estimated at US$220 million annually [1]. Besides the costs these types of chemicals represent a threat to health, safety and environment given their toxicity and flammability. Alternatively other types of chemicals can be used which are effective at concentrations 10-1000 times less compared to methanol and glycol. These compounds are known as low-dosage hydrate inhibitors and are often polymeric type of molecules which prevent hydrate formation by obstructing the crystal formation and growth. Unfortunately most of these molecules have low biodegradability meaning that they cannot be used in the North Sea energy development sector.

Recently studies have shown that so-called ice-structuring proteins (ISPs) may hold a promising potential to work as a low-dosage hydrate inhibitor while at the same time being environmentally benign [2]. ISPs are molecules that enable certain plants and animals living in cold climates to survive though their internal temperature is far below the freezing point of their cell fluids and blood. In particular the ISP identified in the Danish bark beetle has been shown to be effective at preventing hydrate formation; to a greater extent than even the best commercially available low-dosage hydrate inhibitors.

Specific Objectives
The objective of the PhD project is to investigate if ISPs can be applied in field applications to control the formation of gas hydrates i.e. can ISPs substitute conventional types of chemicals like methanol as hydrate inhibitors.

This objective will be achieved by setting up laboratory scale experiments to simulate realistic hydrate formation scenarios using three different experimental methods: high pressure micro-Differential Scanning Calorimeter (HP-DSC), Rocking Cells, and a pressurized stirred cell. Different types of commercial low-dosage hydrate inhibitors will be evaluated and the

performance will be compared to ISPs. Synergy effects between inhibitors and other production chemicals will be studied and an evaluation of health, safety and environmental matters related to ISPs will be carried out. Finally a feasibility study will be carried out to investigate if ISPs can be implemented in field applications.

Results and Discussion

The HP-DSC was validated as a method of determination of thermodynamic conditions for gas hydrates by measuring the methane hydrate dissociation temperatures and ice melting temperatures versus pressure. Figure 1 shows the recorded thermogram at a pressure of 103 bar.

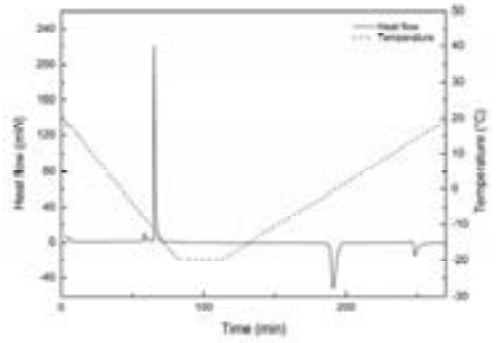

Figure 1: Thermogram recorded of a methane-water system by HP-DSC at 103 bar.

In the figure, ice melting at -0.9 °C and hydrate dissociating at 13.6 °C can be seen. The melting points at different pressures were recorded and the results are shown in Figure 2.

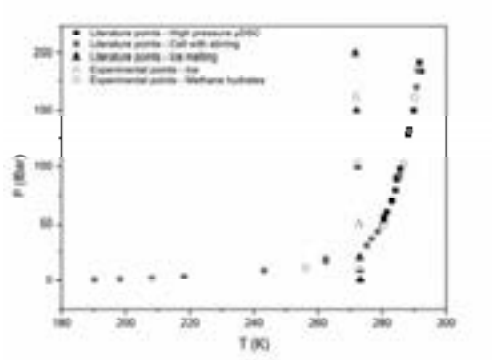

Figure 2: Methane dissociation and ice melting measured by HP-DSC at a pressure of 12, 50, 103 and 161 bar and compared to literature points.

A good correlation is found between the experimental points measured in this work and the points from literature for both the dissociation of methane hydrates and ice melting.

Nucleation of hydrates has been investigated for a number of years. Induction time (the time taken for hydrates to form) measurements are stochastic in nature leading to large variations and poor reproducibility.

Duchateau et al. developed the Second Germination (SG) method to overcome this problem. The principle of the method is formation of hydrates followed by melting the hydrates close to the temperature of dissociation of the hydrates in order to preserve some hydrate nuclei (hydrate history). During the second formation of hydrates these nuclei contribute to a more consistent nucleation pattern [3].

Based on the SG method Anderson et al. developed a new Crystal Growth Inhibition (CGI) method. The principle of the method is that if a kinetic hydrate inhibitor (KHI) is able to prevent nuclei becoming crystals or delay this process significantly rather than inhibiting nucleation alone, then KHIs may be able to do the same for viable crystals. After the first formation of hydrates a small fraction of hydrates remains. In this way the subsequent cycles represent the ability of the KHIs to inhibit further growth of hydrates and primary nucleation processes can be avoided [4].

Based on the SG method initial experiments have been performed in the HP-DSC and for the CGI method in the pressurized stirred cell. Further experiments will develop methods for the experimental setups to be able to simulate realistic hydrate formation.

Conclusion

The new HP-DSC has been validated on methane hydrate and water and it has been shown that the equipment produces reliable results compared to other published HP-DSC points and with points from stirred cells. Method developments for the experimental setups are ongoing.

Acknowledgements

The project is a part of the advanced technology project ‘Biotechnology in Oil Recovery’, funded by the Danish National Advanced Technology Foundation, the Technical University of Denmark, Maersk Oil A/S, Dong Energy A/S, Novozymes A/S, Danish Technological Institute and Roskilde University.

References

1. E.D. Sloan, Nature. 426 (2003) 353-363.
2. L. Jensen, K. Thomsen, N. Von Solms, Energ. Fuel 25 (2011) 17-23.
3. C. Duchateau, J. Peytavy, P. Glénat, T. Pou, M. Hidalgo, C. Dicharry, Energ. Fuel 23 (2009) 962-966.
4. R. Anderson, H. Mozaffar, B. Tohidi, Development of a Crystal Growth Inhibition based method for Evaluation of Kinetic Hydrate Inhibitors, ICGH, UK, 2011

Bjørn Maribo-Mogensen
Phone: +45 4525 2869
E-mail: bmm@kt.dtu.dk
Discipline: Engineering Thermodynamics

Supervisors: Georgios M. Kontogeorgis
Kaj Thomsen

PhD Study
Started: August 2010
To be completed: March 2014

Development of an Electrolyte CPA Equation of State for Applications in the Petroleum and Chemical Industries

Abstract
Complex mixtures of associating/polar components and electrolytes are often encountered in the oil- and gas and chemical industry. It is important to be able to adequately describe the phase behaviour of these mixtures e.g. in order to reduce the environmental impact of natural gas processing, to optimize the performance of CO_2 capture and sequestration, and to improve purification of complex chemicals in the pharmaceutical and biochemical industries. This PhD project works on developing a new equation of state for modelling phase behaviour of complex mixtures containing electrolytes.

Introduction
Complex mixtures of associating/polar components and electrolytes are often encountered in the oil- and gas and chemical industry. It is well-known in the oil- and gas industry that electrolytes have a substantial effect (typically decreasing) on e.g. solubilities of gases in water-hydrocarbon mixtures (salting-out effect), and furthermore, the presence of electrolytes may enhance the inhibitory effect of methanol and glycol on the formation of gas hydrates in natural gas pipelines, thus allowing for problem-free flow. In the pharmaceutical and biochemical industry, electrolytes, associating and polar compounds are present during downstream processing. Electrolytes are also very important to the energy industry *e.g.* with regards to wet flue gas desulphurization or CO_2 capture from power plants using aqueous solutions of alkanolamines.

Despite their great importance, thermodynamic models have been *separately* developed over the last years for hydrogen bonding mixtures e.g. water-alcohol-hydrocarbons and for salt-solutions e.g. NaCl-water, but *few* systematic approaches have been proposed for mixtures which contain both polar compounds and salts or other electrolytes. Many of the proposed models have an overwhelming number of parameters and they have not been tested with practical multi-phase mixed solvent systems that are of interest to the oil- and gas industry.

Theoretical Background
The most widely used thermodynamic models are the cubic equations of state (EoS) such as Soave-Redlich-Kwong (SRK), where the liquid-vapor equilibrium is modeled using Eq. (1) [1, p. 42]:

$$P = \frac{RT}{V_m - b} - \frac{a(T)}{V_m(V_m + b)} \quad (1)$$

where P is the pressure, T is the temperature, V_m is the molar volume, and the parameters a and b are calculated from pure component parameters using e.g. the van der Waals one-fluid mixing rules shown in Eqs. (2 & 3) :

$$a = \sum_i \sum_j x_i x_j \left[a_i(T) a_j(T) \right]^{0.5} \left(1 - k_{ij}\right) \quad (2)$$

$$b = \sum_i \sum_j x_i x_j \left(\frac{b_i + b_j}{2} \right) \quad (3)$$

While the cubic EoS performs well for predicting vapor-liquid equilibrium at both high and low pressures for simple compounds such as hydrocarbons, it is usually not applicable to mixtures containing polar or associating compounds, especially for multicomponent mixtures. Despite the shortcomings, cubic EoS is the most widely used models due to e.g. their relatively simple implementation and large parameter databases. Additionally, advanced mixing rules for the equation parameters can yield much better agreement with experimental data.

The cubic EoS gives a macroscopic description of repulsive and attractive intermolecular forces. Through the Helmholtz energy it is possible to extent the EoS to incorporate new terms that describe other intermolecular

forces, such as association (hydrogen bonding) and electrostatic interactions as illustrated by Eq. (4)

$$A^r = A^r_{SRK} + A^r_{Association} + A^r_{Electrostatic} \quad (4)$$

Other physical properties can be determined from derivatives of the Helmholtz energy – e.g. is it possible to calculate the pressure using Eq. (5):

$$P = \frac{RT}{V_m} - \left(\frac{\partial A^r}{\partial V} \right)_{T,\mathbf{n}} \quad (5)$$

The association term is calculated using a model for the hydrogen bonding. A popular chemical model originates from the perturbation theory of SAFT (Statistical Associating Fluid Theory) where the association energy is expressed as Eq. (6) [1, p. 202]:

$$A^r_{Association} = \sum_i^{Comp-onents} n_i \sum_{A_i}^{Association\ Sites} \left(\ln X_{A_i} - \frac{X_{A_i}}{2} + \frac{1}{2} \right) \quad (6)$$

In which n_i is the amount of molecule i and X_{Ai} is the fraction of the sites A on molecule i not bonded to other molecules, which can be calculated from Eq. (7):

$$X_{A_i} = \left(1 + \frac{1}{V_m} \sum_j x_j \sum_{B_j} X_{B_j} \Delta^{A_i B_j} \right)^{-1} \quad (7)$$

Where Δ^{AiBj} is the association strength between site A on molecule i and site B on molecule j.

Electrostatic Forces

A salt such as NaCl will fully dissociate into its ionic constituents Na^+ and Cl^- when placed in a good solvent. This introduces new energetic interactions between molecules; namely the energy of charging the spheres in the medium and the long-range electrostatic forces between the ions using Coulombs law:

$$F(r) = \frac{1}{4\pi} \frac{1}{\varepsilon_r \varepsilon_0} \frac{q_i q_j}{r^2} \quad (8)$$

where ε_0 is the vacuum permittivity, ε_r is the relative static permittivity of the medium, q_i is the elementary charge of molecule i, and r is the separation distance between the two charges.

The electrical potential of a charged sphere with q_i charge in a medium with relative static permittivity ε_r can be calculated from Eq. (9):

$$V = \frac{1}{4\pi\varepsilon_r\varepsilon_0} \int_{\sigma_i}^{\infty} \frac{q_i}{r^2} dr = \frac{1}{4\pi\varepsilon_r\varepsilon_0} \frac{q_i}{\sigma_i} \quad (9)$$

The work of charging the ions gives a contribution ot the Helmholtz energy as shown in Eq. (10):

$$A^E = \frac{N_A e^2}{8\pi\varepsilon_r\varepsilon_0} \sum_i \frac{n_i z_i^2}{\sigma_i} \quad (10)$$

Once ions are charged, the forces between ions must be accounted for using Eq. (8). There are two widely used models for that account for electrostatic interactions; the Debye-Hückel theory developed by Debye and Hückel in 1923 [2] from linearization of the Poisson equation, and the MSA (Mean Spherical Approximation) derived by Blum in 1975 [3] from statistical mechanics. The Debye-Hückel theory assumes that ions are point charges but cannot approach eachother closer than the distance d_{ij}=½(d_i+d_j), whereas MSA treats ions as hard spheres with diameters σ_i from a statistical mechanical approach where the molecules cannot approach eachother closer than the distance σ_{ij}=½(σ_i+σ_j). The differences are visualized in Figure 1:

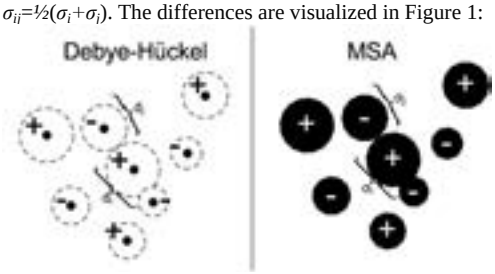

Figure 1: Visualization of the differences in the derivation of the Debye-Hückel and the MSA theories. Debye-Hückel treats ions as point charges whereas MSA treats ions as hard spheres.

The two theories arrive at different expressions for the Helmholtz energy. The Debye-Hückel theory may be written as Eq. (11) [1, p. 470]:

$$A^r_{Debye-Hückel} = -\frac{1}{4\pi} \frac{k_B T}{N_A \sum_i n_i q_i^2} \sum_i n_i q_i^2 \chi_i \quad (11)$$

where k_B is the Boltzmann constant, N_A is Avogadros constant, and χ_i is given by:

$$\chi_i = \frac{1}{d_i^3} \left[\ln(1 + \kappa d_i) - \kappa d_i + \tfrac{1}{2} (\kappa d_i)^2 \right]$$

where d_i is the distance of closest approach of molecule i, and the inverse Debye length κ is calculated from Eq. (12):

$$\kappa^2 = \frac{1}{k_B T} \frac{1}{\varepsilon_r \varepsilon_0} \frac{1}{V} \sum_i^N n_i q_i^2 \quad (12)$$

The MSA theory is presented in Eq. (13) [1, p. 470]:

$$A^r_{MSA} = k_B T V \frac{\Gamma^3}{3\pi} - \frac{V e^2}{4\pi\varepsilon_r\varepsilon_0} \sum_i^N \rho_i z_i \left[\frac{\Gamma z_i + \eta\sigma_i}{1 + \sigma_i \Gamma} \right] \quad (13)$$

where σ_i is the hard sphere diameter of ion i, and the κ - equivalent of the MSA theory may be calculated from Eq. (14):

$$(2\Gamma)^2 = \frac{1}{k_B T} \frac{e^2}{\varepsilon_0 \varepsilon_r} \sum_k \rho_k (z_k + N_k \sigma_k)^2 \quad (14)$$

As N_k depends on Γ, the MSA theory is implicit and must be solved for the shielding length.

Both models have been used in equations of state [1, Chap. 15] but the MSA theory is frequently cited as being more physically sound, especially at higher concentrations since it has been derived from statistical mechanics. A comparison of the two models has been carried out to determine whether the more complex MSA model is indeed better than Debye-Hückel. A characteristic result is presented in Figure 2 where the

Pauling ionic radii are adopted as values for the characteristic sizes in the two models, *i.e.* $\sigma_{Na^+} = d_{Na^+} = 2.04$ and $\sigma_{Cl^-} = d_{Cl^-} = 3.62$.

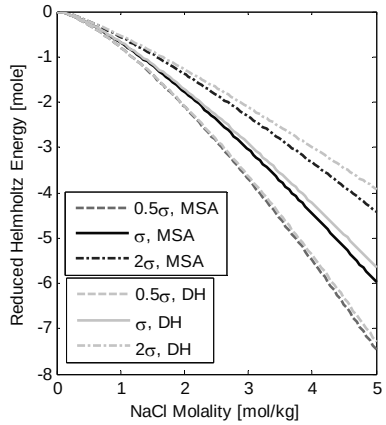

Figure 2: Comparison of the results obtained using Debye-Hückel and the MSA theory at the constant relative static permittivity of water at 25°C.

Figure 2 shows that the results obtained with the two models are similar. By fine-tuning the ionic diameter in Debye-Hückel we can obtain the same results for the Helmholtz energy and its derivatives as for MSA, showing that the difference between the two models is small. However, the calculations in Figure 2 were carried out disregarding the fact that the relative static permittivity decreases with increasing ion concentration, as presented in Figure 2. The decrease may partially be attributed to the non-polar ion hydration shells causing an effective decrease of the relative static permittivity.

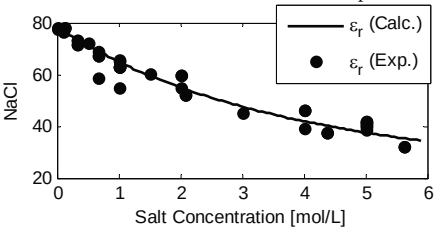

Figure 3: Effect of increasing salt concentration on the relative static permittivity for NaCl at 25°C. Exp. data is taken from the collections [4] and [5]. Line made using empirical correlation from [6].

By correlating the experimental data in Figure 2, we may assess the effect of the relative static permittivity on the two models. We are primarily interested in the effect on the compositional derivative of the Helmholtz energy as this is related to the activity of ions, and this is shown in Figure 4:

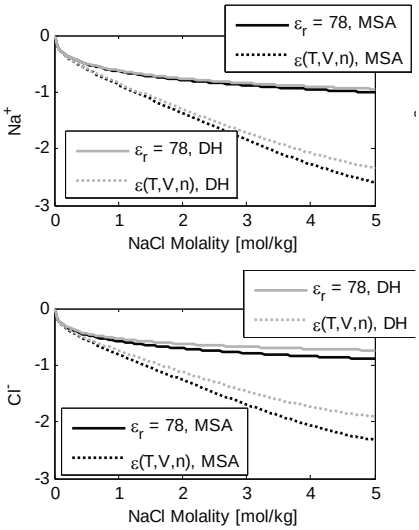

Figure 4: Effect of including the compositional dependence of the relative static permittivity on compositional derivative of Helmholtz energy.

From Figure 4 It is evident that at higher concentrations the difference between using MSA or Debye-Hückel is negligible compared to the effect of using a compositional dependent relative static permittivity.

Modeling Static Permittivity of Mixed Solvents

The static permittivity has been identified as the most important physical property for calculating the electrostatic interactions. While the use of correlations of the static permittivity is acceptable for single-solvent single-salt solutions, they must be used with care when applied to prediction of solubility in complex mixtures containing water, alcohols and even multiple salts. There is a need for the development of a new model that can predict the static permittivity in mixed solvents, and that has been one of the main topics of this PhD study over the past year.

Origin of the Static Permittivity

The static relative permittivity (dielectric constant) is a measure of the propagation of an electrical field in a non-conductive medium. The Clausius-Mossotti or Lorentz-Lorentz theories given by Eq. (15) relates the macroscopic static permittivity and microscopic polarizability for non-polar molecules [6].

$$\frac{\varepsilon_r - 1}{\varepsilon_r + 2} = \frac{1}{3\varepsilon_0}\frac{N\alpha}{V} \qquad (15)$$

The Debye and Langevin equation defines the molecular polarizability from the electronic and atomic polarizability α_0 and the permanent dipole moment μ:

$$\alpha = \alpha_0 + \frac{\mu^2}{3k_B T} \qquad (16)$$

Debye (1912) inserted Eq. (16) into Eq. (15) and obtained an equation for the dielectric constant as a function of temperature. While the underlying assumptions of this approach are valid for gases at low pressures it is not acceptable for dense systems. In 1936 Onsager developed a consistent theory for the static permittivity that accounted for the effect of permanent dipoles on the static permittivity. In the formulation by Fröhlich, the Onsager theory may be written as Eq. (17) [6]:

$$\frac{(2\varepsilon_r + 1)(\varepsilon_r - \varepsilon_\infty)}{\varepsilon_r (\varepsilon_\infty + 2)^2} = \frac{N}{9V} \frac{g?_0^2}{k_B T} \qquad (17)$$

Where ε_∞ is the infinite frequency permittivity that may be approximated by the squared refractive index n^2 at optical frequencies. μ_0 denotes the dipole moment in vacuum whereas g is a function that accounts for the orientation of dipoles leading to either a net increase or net decrease in the vacuum dipole moment.

Towards a New Model for the Static Permittivity

The new model relates the net dipole moment $g?_0^2$ to the mixture of different molecules in the mixture and the number of hydrogen bonds in the system. The number of hydrogen bonds can be assessed by the association theory from SAFT through the knowledge of the fraction of sites *A* on molecule *i* not bonded to other molecules (X_{Ai}). Using the new theory, we can correlate the static permittivity of pure components from the freezing point up to the critical point as shown in Figure 5. Similarly we can calculate the static permittivity of mixtures as shown in Figure 6.

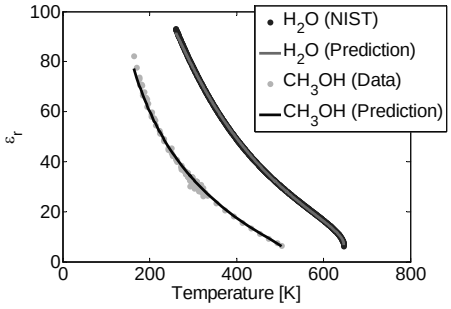

Figure 5: Correlation of static permittivity from the freezing point to the critical point using the new model with two pure component parameters.

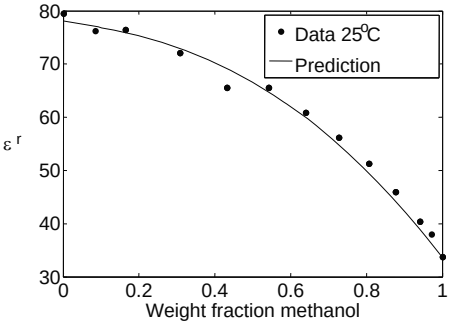

Figure 6: Calculation of the static permittivity of a mixture of methanol and water using the new model with a single binary parameter. Data from [4,5].

Conclusions

The thermodynamic framework for an equation of state for electrolytes and associating molecules has been developed. The simpler Debye-Hückel model for electrostatic interactions yields comparable results to the more complex MSA model. The key physical property for both models is the static permittivity and a new predictive model has been developed as an alternative to the commonly used empirical correlations. Work continues in order to develop the theory to account for the effect of salts on the static permittivity, and furthermore apply the equation of state to calculation of salting out of gases and gas hydrate inhibition due to the presence of salts.

Acknowledgement

This work is funded by the Department of Chemical and Biochemical Engineering and the CHIGP consortium (Mærsk Oil, DONG Energy, Statoil, GASSCO, BP)

References

1. G.M. Kontogeorgis, G.K. Folas, Thermodynamic Models for Industrial Applications-From Classical and Advanced Mixing Rules to Association Theories, Wiley, 2010
2. P. Debye and E. Hückel, Physikalische Zeitschrift 24 (1923) 179-207
3. L. Blum, Mol. Phys. 30 (5) (1975) 1529-1535
4. Y.Y. Akhadov, Dielectric Properties of Binary Solutions: A Data Handbook, Elsevier, 1980, ISBN 978-0080236001
5. J. Barthel, R. Buchner, M.Münsterer, Electrolyte Data Collection, Part 2: Dielectric Properties of Water and Aqueous Electrolyte Solutions, Dechema, Frankfurt, 1995, ISBN 3-926959-62-2
6. M.L. Michelsen, J.M. Mollerup, Thermodynamic Models: Fundamentals & Computational Aspects, Tie-Line Publications, Holte (Denmark), 2007, ISBN 87-989961-3-4
7. B.K.P. Scaife, Principles of Dielectrics, Oxford Press, 1998, ISBN 0-19-8565577

Michele Mattei
Phone: +45 4525 2959
E-mail: micu@kt.dtu.dk
Discipline: Systems Engineering

Supervisors: Rafiqul Gani
Georgios Kontogeorgis

PhD Study
Started: August 2011
To be completed: July 2014

A Systematic Methodology for Design of Emulsion Based Chemical Products

Abstract
The consumer oriented chemical based products are used every day by millions of people. They are structured products constituted of numerous chemicals, and many of them, especially household and personal care products, are emulsions where active ingredients, solvents, additives and surfactants are mixed together to determine the desired emulsified product. They are still mainly designed and analyzed through trial-and-error based experimental techniques, therefore a systematic approach for design of these products could significantly reduce both time and cost connected to the product development by doing only the necessary experiments.

Emulsion Based Chemical Product Design
The chemical industry is changing, going beyond commodity chemicals to higher value added products [1]. These structured products are still mainly designed on an experimental base, with a consequent large amount of time and money needed, so that a systematic approach for design of these products could act as a big improvement. Such a procedure has been successfully developed recently with regards to liquid formulation products [2]. Many of these products, however, especially in household and health-care, are emulsions, needing a different methodology for their design. Moreover, data for many properties of single ingredients of the emulsion as well as the emulsion itself are not available in open literature while available models are lacking in accuracy. They need therefore to be improved, and/or new models need to be developed.

A Systematic Methodology
The methodology to be developed in this project consists of seven steps, as shown in Figure 1. The first step is in charge of defining consumer assessments and then translating them into main needs, to be satisfied by active ingredients; secondary needs, to be satisfied by additives; and constraints on some physio-chemical properties, that is, target properties. This first stage is then followed by five steps where one adds one-by-one all the necessary ingredients, selected into structured databases through optimization methods as selection criteria.

Figure 1: Hierarchical steps of Systematic Methodology for Design of Emulsion Based Chemical Products

The first ingredient to be identified is the active ingredient(s), followed by its solvent, commonly constituting the dispersed phase of the emulsion, then the continuous phase, emulsifiers and finally the additives. Each of these five steps involves several sub-tasks, different in terms of specific ingredients, but

having all a similar structure: first one creates a large list of chemicals that can satisfy the need they have to (this can be the main need for active ingredients as well as solubilize one ingredient for a solvent, etc.); then, as a second sub-task, one performs a choice in order to find the most advantageous chemical between those listed before (the selection can be based on effectiveness, safety, toxicity, environment, legislation, cost or on a combination of the aforementioned criteria); and finally the last sub-task is in charge of searching or calculating all the physio-chemical properties that one needed for the selected ingredients. Once all the ingredients have been chosen, the seventh step considers the overall composition of the emulsion in order to satisfy the constraints on target properties decided at the first step of the procedure.

Pure Property Prediction

One of the main issues to be faced in this methodology is the calculation of the needed properties. As a matter of fact, selection sub-tasks are often considering effectiveness as one of the main criteria for the selection. Effectiveness depends on the ingredient considered; for example, effectiveness of an active ingredient as a UV sunscreen is its ability to absorb UV radiations, while for a solvent it is the capability to dissolve some selected solid ingredients. It is clear, then, that many properties need to be calculated or retrieved as measured data in order to make a proper selection. Unfortunately, data for these properties are not available as measured data and at the same time models to calculate them are needed. One of the biggest tasks of this project, then, is to improve pure component property models, when existing, or to develop new ones when they are not available. Surfactants, key-ingredients of emulsified products, are the ingredients needing the largest modeling effort here since even their most relevant properties, such as hydrophilicity and lipophilicity, temperature boundaries, critical micelle concentration and surface tension have very few data available and only a few models to calculate them [3]. The property models to be here developed will need to be group-contribution models, based on M&G methods [4]. Probably the introduction of some new groups characterizing the most common surfactants will be needed.

Emulsion Property Models

Once all the ingredients needed by the product have been selected, it is necessary to set the overall composition of it by considering constraints on the target properties. This step needs the availability of dedicated models able to calculate bulk properties such as density, viscosity and others like surface tension of evaporation time regarding emulsions. A few models are already available for viscosity [5], while density can be estimated through an equation of state (PVT). On the other hand, models regarding “secondary” properties such as surface tension and evaporation time for emulsions need to be developed using pure compound properties. In this case, the reliability of these models developed needs to be carefully checked.

Conclusions

A systematic methodology to design formulated emulsified products is being developed. This model based methodology, that can save time and money by reducing the number of necessary experiments, provides a short list of candidate ingredients of the desired product and its overall composition based on consumer assessments related to that product itself. It is important to underline that this procedure is not replacing experiments, but just to address the attention on a small number of candidate formulation to be experimentally validated.

Further works

Besides the aforementioned need to develop dedicated models for pure and for emulsion properties, other works are necessary to make the whole methodology complete and reliable. First of all, it will be necessary to add a step regarding stability of designed products as emulsions. This task will probably need some experimental efforts, since available models related to stability of emulsions do not consider destabilization mechanisms all together and the most reliable theory about stability of colloids (DLVO) does not take into account any kind of steric stabilization, a key-function of surfactants in emulsions. Besides, a process-product integrated design step will be needed, at a basic level, in order to estimate costs connected to the manufacture of the desired product and also to evaluate whether the desired droplet average size, crucial for some calculation steps, is actually possible to realize from the process point of view. The whole methodology will be highlighted as implemented in the software “The Virtual Process-Product Design Laboratory” (Virtual PPD Lab) as a new feature, allowing users to be able to perform virtual formulation design and verification for emulsified products.

References

1. E.L. Cussler, G.D. Moggridge, Chemical Product Design, Cambridge University Press, New York, 2011.
2. E. Conte, R. Gani, K.M. Ng, AIChE J. 57 (9) (2011) 2431-2449.
3. J. Hu, X. Zhang, Z. Wang, Int. J. Mol. Sci. 11 (2010) 1020-1047.
4. J. Marrero, R. Gani, Fluid Phase Equilibr. 183-384 (2001) 183-208.
5. C. Wibowo, K.M. Ng, AIChE J. 47 (12) (2001) 2746-2767.

Kresten Troelstrup Meisler
Phone: +45 4525 2912
E-mail: kretm@kt.dtu.dk
Discipline: Systems Engineering

Supervisors: Rafiqul Gani
Krist V. Gernaey
Nicolas von Solms

PhD Study
Started: March 2011
To be completed: February 2014

Multi-Dimensional Population Balance Models of Crystallization Processes

Abstract
The kinetics in crystallization operations are modeled and used in population balance models. This modeling allows obtaining a better insight into the mechanisms in crystallization and allows process analysis, operation policy design and optimization of crystallization operations. A systematic approach for the use of collected data is suggested in order to analyze the processes.

Introduction
Crystallization is an efficient separation process for separation of compounds, which are solid in their pure form at the given separation conditions [1]. These operations involve multiple phenomena and understanding of these phenomena and interactions have gained interest as it is recognized that this affects several properties of the final product. The polymorph, the size distribution and derivative properties of these (such as filterability) are strongly influenced or even governed by the kinetics of the chemical system.

Modeling these phenomena and their interaction through a population balance approach could help the understanding and hence the optimization and design of crystallization operations. In order to accommodate the wide range of crystallization systems being in operation a generic procedure is established for the systematic development of models for use in design, analysis and simulation of crystallization operations.

Specific Objectives
The project aims at developing models for the description of crystallization operations including the necessary phenomena in order to describe a process completely. A multi-dimensional population balance approach is used: The crystals are described with variations in the growth rate for different directions, and by also including nucleation, breakage and agglomeration the description of the kinetic phenomena is concluded. The kinetics are used for the constitutive equations in the population balance model and, in combination with mass and energy balances, the crystal size distribution from the operation can be calculated. With this result the simulation and practical operations can be compared and the models and experiments can be evaluated. In case of a mismatch between the experimental result and the model result it is possible to re-evaluate the parameters for the model.

Results and Discussion
A framework has been established for handling multiple crystallization-oriented scenarios [2]. The framework combines the advantages of data-based and model-based analysis in a general approach. The approach is illustrated for a data-based problem in Figure 1. The approach allows multiple crystallization based scenarios to be handled such as parameter estimation and model generation for crystallizers, operational policy analysis and data translation of data types in order to extract information of crystal size distribution.

In order to establish the kinetics of the crystallization operations kinetic data are necessary. For industrial operations different technologies are used in order to monitor crystallizations and exploiting the data from these sources a better understanding of the process is possible. These data must be translated in order to give the necessary information. Such data-translation can be non-trivial. This is the case for the translation of Focused Beam Reflectance Measurements (FBRM) from which a chord length distribution is obtained. This chord length distribution is not directly transferrable to a particle size distribution and several challenges have been identified for the translation of data from FBRM measurements. Guidelines for experiments from which the necessary data can be obtained will be developed in the project. One such experiment is the growth cell where a single crystal is grown in order to study the

growth kinetics. The growth cell allows the growth of each facet of a crystal to be observed during growth.

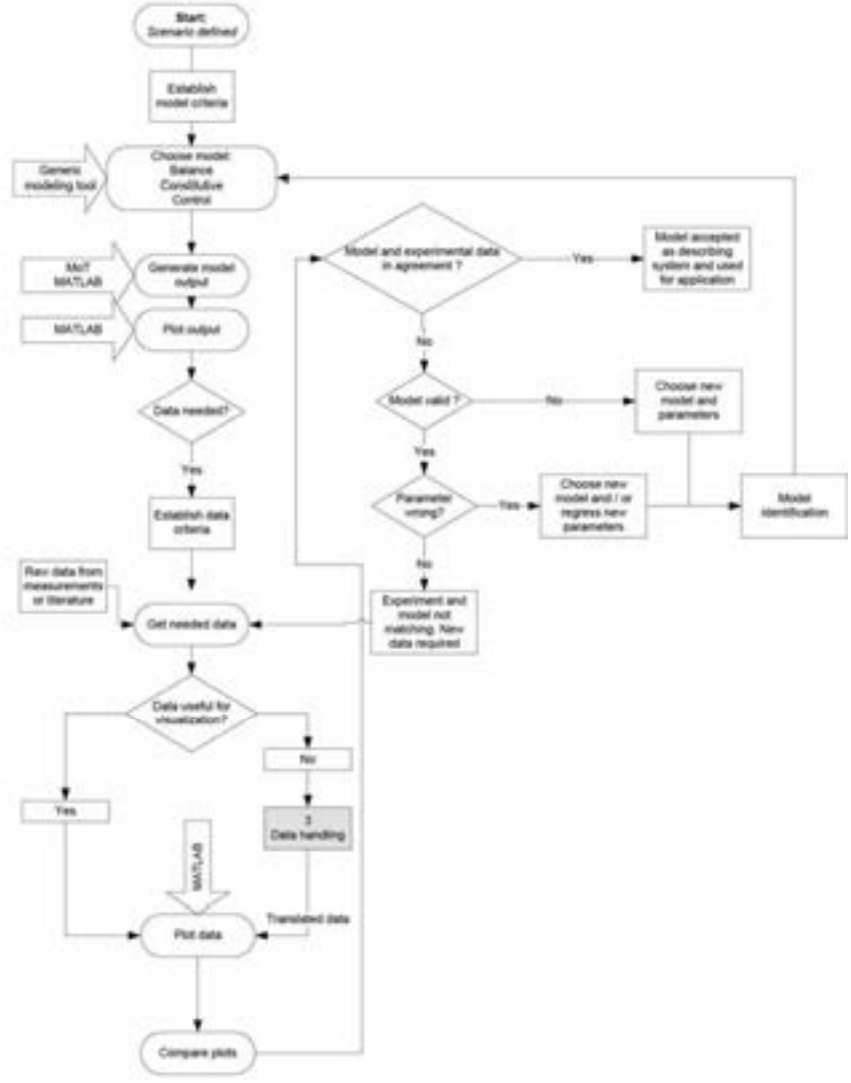

Figure 1: The proposed framework for crystallizer modeling

Conclusion

A framework for crystallization operations is being developed which, when complete, will handle all operations related to crystallization. So far the overall framework has been developed and case studies with simulation of sucrose crystallization have been investigated.

Acknowledgements

DTU Chemical Engineering for funding this research.

References

1. N.A.F.A. Samad, R. Singh, G. Sin, K.V. Gernaey, R. Gani, Comput. Chem. Eng. 35 (2011) 828-843
2. K.T. Meisler, N.A.F.A Samad, K.V. Gernaey， N. von Solms， R. Gani， Generic Model and Data Based Framework for Analysis and Development of Crystallization Processes, Conference contribution, AIChE Annual Meeting, 2011

Malwina Michalak
Phone: +45 4525 2979
E-mail: mmi@kt.dtu.dk
Discipline: Enzyme Technology

Supervisors: Jørn Dalgaard Mikkelsen
Gunnar Jonson
Manuel Pinelo

PhD Study
Started: November 2008
To be completed: September 2012

Production and Purification of Prebiotic Oligosaccharides by Chromatography and Membrane Systems

Abstract
Prebiotics are non-digestable food ingredients that have beneficial effect on the host microbiota. Known examples of prebiotic food ingredients are oligosaccharides, e.g. maltooligosaccharides from starch or dietary fibers, like pectins. Dietary fibers and oligosaccharides with potential prebiotic effects can be obtained by degradation of side streams from the agricultural industry. E.g. potato pulp, which is a side stream from potato starch manufacturing can be enzymatically processed to β-1,4-galactan-rich soluble potato pulp polysaccharides (SPPP) of molecular weights >100 kDa. These polysaccharides are highly bifidogenic in human fecal sample fermentations *in vitro.* The objective of the present study was to use potato β-1,4-galactan and the SPPP as substrates for enzymatic production of potentially prebiotic compounds of lower and narrower molecular weight. A novel endo-1,4-β-galactanase from *Emericella nidulans*, was produced in a recombinant *Pichia pastoris* strain. The *E. nidulans* enzyme expressed in *P. pastoris* generated a spectrum of poly- and oligo-saccharides which were fractionated by membrane filtration. The potential growth promoting properties of each fraction were evaluated by growth of beneficial gut microbes and pathogenic bacteria. All the galactan- and SPPP-derived products promoted the growth of probiotic strains of *Bifidobacterium longum* and *Lactobacillus acidophilus* and generally did not support the propagation of *Clostridium perfringens* in single culture fermentations.

Introduction
Functional food ingredients possessing potential health benefits have become popular nowadays. Some of compounds displaying capability to improve the food are prebiotics. Use of potato pulp, which is a side-stream from the starch industry as a substrate for prebiotics production together with monocomponent enzymes as catalysts would make this process sustainable and selective. Moreover, it would improve the competitiveness of the potato starch industry.

Enzymatically solubilized polysaccharides from potato pulp have been demonstrated previously to exert potentially beneficial properties as dietary fibers and prebiotics in both *in vitro* (human fecal fermentations) and *in vivo* (rat and human) studies [1-3]. Recently, the enzyme catalyzed polysaccharide solubilization process of potato pulp has been optimized further resulting in release of pectinaceous polysaccharides with molecular weights up to 400 kDa. These soluble potato pulp polysaccharides (SPPP), which are presumably made up of mainly RGI β-1,4-galactan chains, appeared to be particularly promising as prebiotics as this substrate selectively and significantly increased the densities of *Bifidobacterium* spp. and *Lactobacillus* spp. when fermented *in vitro* by microbial communities in human fecal samples [3].

Different types of galacto-oligosaccharides are already well recognized in the literature for their bifidogenic and prebiotic effects. We hypothesized that further enzymatic digestion of the SPPP to form β-1,4-galactan derived poly- and oligo-saccharides of lower, and more narrow, molecular weights might unravel the ultimate health benefits of β-1,4-galactans from potato pulp. In order to targetly produce such galactosaccharides we produced and explored a new cloned endo-1,4-β-galactanase from *Emericella nidulans* and examined the optimal reaction conditions. Our aim was therefore to use the high molecular weight potato pulp polysaccharides, SPPP, as a substrate for further targeted enzyme catalysis to provide new opportunities for designing functional food ingredients with significant health benefits and at the same time provide a valorization route for potato pulp.

Fermentation of endo-1,4-β-galactanase from *E. nidulans* in *P. pastoris* and enzyme purification

The level of extra-cellular protein in the high cell density fermentation of *P. pastoris* containing the recombinant endo-1,4-β-galactanase reached 2.11 g/L after 95 hours. The protein expression was followed by SDS-PAGE and the endo-1,4-β-galactanase protein band at 39 kDa was observed shortly after methanol induction of the AOX1 promotor controlling the expression of the gene. The endo-1,4-β-galactanase activity at the end of the fermentation was 109 kU (equivalent to at total of 393 kU in the 3.6 L fermentation volume).

The endo-1,4-β-galactanase produced in *P. pastoris* contained several other protein bands. A purification of the enzyme was therefore necessary. The endo-1,4-β-galactanase was purified on a CIM-Cu^{2+} affinity column using the His-Tag binding module and an Äkta system [4]. The bound proteins were desorbed with imidazole buffer and the combined fractions were analyzed by SDS-PAGE and Western blot analysis.

Optimal temperature and pH of endo-1,4-β-galactanase from *E. nidulans* produced in *P. pastoris*

To determine the pH and temperature optimum of the endo-1,4-β-galactanase from *E. nidulans* expressed in *P. pastoris* a statistically designed, quadratic central composite experiment was applied to evaluate the individual and interactive effects of 4 factors (pH, temperature, enzyme to substrate ratio, E/S (v/w), and reaction time) in 24 experimental combinations. The optimal pH and temperature combination was determined to be pH 5 and 49°C with the regression model forming an almost symmetric bell-shaped response surface optimum (Fig. 1).

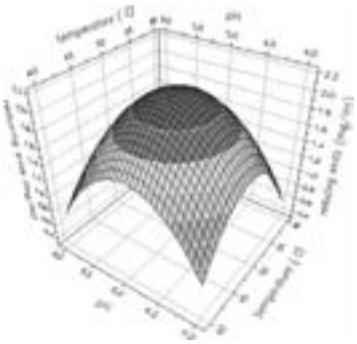

Figure 1: Surface response as a function of temperature and pH of the endo-1,4-β-galactanase activity. The colors vary from blue (low endo-1,4-β-galactanase activity) to red (high endo-1,4-β-galactanase activity).

The optimal pH of 5 was in agreement with the findings of Bauer et al. [5], but the relatively high optimal temperature has not been determined previously. As expected, increasing the ratio of E/S (v/w) increased the yield of reducing ends. The same was observed with increased reaction time up to 8 hours, despite that the enzyme lost half of the activity in 27 minutes at 49 °C; the half life, $t_{½}$ of the endo-1,4-β-galactanase from *E. nidulans* expressed in *P. pastoris* was 57 minutes at 40°C, 27 minutes at 49°C and ~10 minutes at 60°C as assessed in phosphate buffer. Since the temperature optimum of the investigated enzyme was 49°C (in the presence of substrate) and a relatively low thermal stability was observed for the enzyme when incubated without the substrate at elevated temperatures, the results strongly indicate that the endo-1,4-β-galactanase is very stable in the presence of the substrate.

Kinetic parameters and metal ions interactions

The kinetic parameters K_M and V_{max} for endo-1,4-β-galactanase from *E. nidulans* expressed in *P. pastoris* were determined to 0.51 g/L and 73.3 U/mg protein, respectively using a Hanes plot.

The influence of metal ions on the *E. nidulans* enzyme activity was also tested. The enzyme was pretreated with EDTA prior to incubation with the specific metal ions (and the EDTA pre-incubation was compared to the results obtained without EDTA added). Except for the significantly lower activity in the presence of $AlCl_3$, the endo-1,4-β-galactanase activity was not affected by the metal ions. The influence of metal ions on fungal endo-β-1,4-galactanases performance described in the literature is usually observed as weak or inhibitory. Pb^{2+} and to a lesser extent Zn^{2+} and Ag^{+} have previously been found to decrease the activity of endo-β-1,4-galactanases from *A. niger* and *A. aculeatus* [6], and the activity of an endo-β-1,4-galactanase from *A. sojae* has also been reported to be significantly inhibited by Mn^{2+}, Hg^{2+}, Ag^{+}, and Fe^{3+} [7]. The fact that the majority of metal ions had no effect on the activity of endo-1,4-β-galactanase from *E. nidulans* produced in *P. pastoris* could make this enzyme better suited for the industrial applications than the other endo-galactanases discussed above.

Release of poly- and oligosaccharides from potato galactan

The optimized conditions established above for endo-1,4-β-galactanase from *E. nidulans* expressed in *P. pastoris* were used to create potentially prebiotic poly- and oligosaccharides by enabling enzyme catalyzed hydrolysis of the potato galactan polymer and the SPPP. The galactan polymer had a molecular mass of about 150 kDa, and the composition of monosaccharides (in mole%) was 86% galactose, 4% rhamnose, 7% arabinose, 3% galacturonic acid. The galactan polymer was progressively enzymatically degraded to lower molecular weight products in time course experiments (2 – 270 min) using E/S ratios of 0.03% and 0.3% (Fig. 2 and 3). The molecular weights (MW) of the products were examined by HPSEC, and the experimental conditions yielding the optimal level of the products were selected for further studies at 100-ml scale reactions. Galactan derived poly- and oligosaccharides

were separated according to molecular weight using 3 kDa, 10 kDa or 100 kDa membranes. A 3 kDa permeate referred to as PG1 (Potato Galactan, 60 min; E/S 0.03%) was obtained with a yield of 28.7% (172 mg). PG2 was the retentate corresponding to PG1; the hydrolyzate had been filtered through a 10 kDa membrane prior to the 3 kDa membrane filtration, and PG2 thus contained saccharides of 3 – 10 kDa (Fig. 3).

PG3 was a 10kDa permeate produced by 15 min hydrolysis using an E/S ratio of 0.3%. The yield was 67% (402 mg). PG4 was the retentate of PG3, and contained oligo- and polysaccharides of ~10-100 kDa (obtained at a yield of 29% by weight).

PG5 was the 3kDa permeate produced by an extended, intensive endo-β-1,4-galactanase treatment of galactan for 270 min at an E/S ratio of 0.3%. The yield was 43% (257 mg). The content of free galactose was relatively high in both of the 3 kDa fractions, i.e. in PG1 and PG5. The high amounts of low molecular weight galactose oligosaccharides were further analyzed by HPAEC, where accumulation of galactose and galactobiose coincided with extended incubation time and high E/S ratio of 0.3 % E/S. One possibility for the high galactose released could be that the endo-β-1,4-galactanase from *E.nidulans* expressed in *P. pastoris* acted according to a multiple attack mechanism and that the monosaccharide release therefore was an "accidental" result of multiple attacks on the substrate as detailed by van de Vis [6].

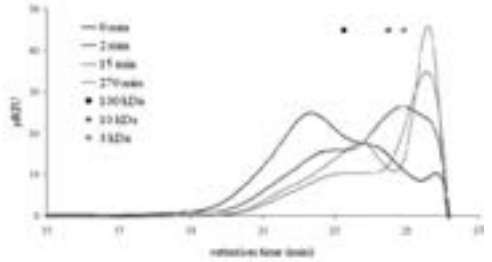

Figure 2: HPSEC analysis after enzymatic hydrolysis of potato galactan (Megazyme), E/S (v/w) = 0.3%

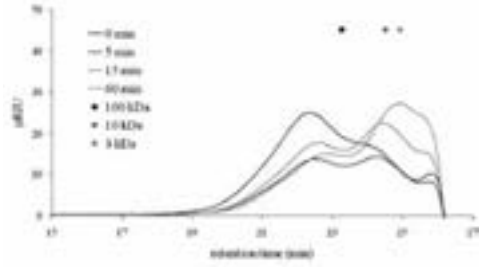

Figure 3: HPSEC analysis after enzymatic hydrolysis of potato galactan (Megazyme), E/S (v/w) = 0.03%

Release of poly- and oligosaccharides from high molecular weight solubilized potato pulp polysaccharides (SPPP)

The high MW solubilized potato pulp polysaccharides (SPPP) were prepared from crude potato pulp via a short, minimal enzyme treatment with pectin lyase and polygalacturonase, as described by Thomassen et al. [3, 8]. The molecular mass of the SPPP was higher than 400 kDa and the molar monosaccharide composition (mole%) was 66% galactose, 2 % rhamnose, 9% arabinose, 14% galacturonic acid, 7% glucose, and 2% mannose. Different samples of oligosaccharides derived from the SPPP were obtained by treatment of this substrate with an E/S ratio of 0.03% in combination with incubation for 60 minutes or by using an E/S 0.3% and 15 minutes of incubation. The HPSEC chromatograms of the reaction products are detailed in Fig. 4. After incubation for 15 minutes the reaction mixture was separated by a 10 kDa membrane and two fractions were obtained, the permeate fraction SPPP1 and the 10kDa retentate (fraction SPPP2). The yield of SPPP1 was 21% by weight (124 mg). The majority of the galacturonic acid was present in the SPPP2 fraction which constituted 65% by weight (390 mg) of the originally enzyme treated material.

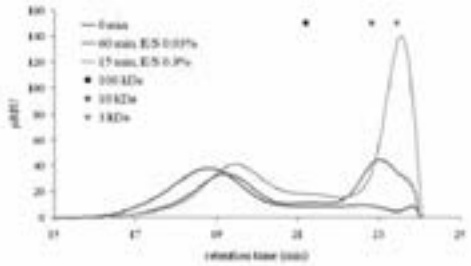

Figure 4: HPSEC analysis of *E. nidulans* endo-1,4-β-galactanase catalyzed hydrolysis of SPPP.

Bacterial growth on prebiotic candidates

The potential prebiotic properties of the fractionated oligosaccharides generated by enzymatic catalysis of galactan and SPPP were evaluated by measuring their growth promoting activity on selected pure cultures using a Bioscreen microtiter system. The growth performance expressed as area under the growth curve [9] was assessed for five different bacteria comprising three probiotic strains, *L. acidophilus, B. longum*, and *B. lactis*, one pathogenic strain of *Cl. perfringens*, and one commensal *E. coli* strain. Fructooligosaccharides (FOS) were used as a control due to their prebiotic properties on bifidobacteria and lactobacilli.

The growth of each individual test bacterium was affected differently by the different compounds. In addition, the different bacteria also responded differently to the same substrate.

The PG5 fraction stimulated the growth of *L. acidophilus* and *B. longum* significantly better than any of the other hydrolysates; the stimulation of the *L.*

acidophilus growth was at the same level as that achieved with FOS but significantly better ($p < 0.05$) than that obtained with pure galactose and unhydrolysed galactan. The stimulation of *B. longum* was more than 6-fold better than that of FOS and significantly better ($p < 0.05$) than that achieved with galactose or the unhydrolysed galactan. The PG1 fraction and the SPPP1 also stimulated the growth of both *L. acidophilus* and *B. longum* to a significant extent – for *B. longum* the growth stimulation by PG1 and SPPP1 as well as by PG4 was significantly better than that obtained with either FOS, galactose or the original galactan ($p<0.05$). The samples PG1, PG3, PG5, and SPPP1 all contained low molecular weight oligomers and some galactose, which might explain some of the growth stimulation of *L. acidophilus* and *B. longum* promoted by these substrates. It is important to note, however, that the growth of *B. longum* was better on all these fractions (PG1, PG4, PG5, SPPP1) than on neat; this result might indicate that each of these hydrolysates contained particular galactan or arabino-galactan structures, of relatively low molecular weight, which were particularly effective to stimulate the growth of *B. longum*. An additional point is that the presence of galactose would most likely not be important *in vivo* since the human organism would absorb the galactose before it reaches the colon. The data also showed that the growth of both *E. coli* and *Cl. perfringens* was not supported by these particular low molecular weight hydrolysates ($p < 0.05$) (and significantly more decreased than the corresponding growth on galactose and FOS) as it was low on galactan – the only exception being the growth on PG5 which for the *E. coli* was the same as that obtained on galactose, but which for *Cl. perfringens* was lower than that on galactose, but higher than on FOS. Whether PG5 is as promising prebiotic agent as some of the other produced fractions requires further investigation. Galactan, as well as, samples PG2 and PG3 did not appear to support the growth of *Cl. perfringens*. Neither of these substrates supported the growth of very high levels of any of the three "probiotic" strains, and the growth of *E. coli* was also much lower than that achieved with galactose.

In summary, contemplation of the bioscreen data showed that among the tested samples the lower molecular weight fractions exhibited more and various potentially prebiotic features.

Whether the observed low or no growth supporting effects on *Cl. perfringens* have any significance in the genuine competition among the bacteria in the mixed microbiota in the gut deserve further investigation.

The present work was conducted using single cultures, but the results obtained are in good accord with reported prebiotic effects of galacto-oligosaccharides [10]. The data also agree with recent data from a human study, which have shown that certain enzymatically synthesized β-galacto-oligosaccharides, consumed at levels of 7 g/day, significantly increase the bifidobacteria ratio compared with a commercial galacto-oligosaccharide ($P <0.05$) [11]. The data clearly suggest that β-galacto-oligosaccharides possess promising beneficial properties in relation to gut health. The available data also suggest that different sub-structures of these β-galactosides, e.g. certain molecular sizes and/or branching patterns, exhibit differential prebiotic effects. It can be speculated that the different human gut bacteria respond differently to compounds and metabolites produced by other bacteria and thus interact highly differently to cross-feeding phenomena.

Conclusions

A very active endo-1,4-β-galactanase from *E. nidulans* expressed in *P. pastoris* has successfully been produced in a 5 l scale fermentation. The enzyme was used to design oligosaccharides from high molecular weight β-1,4- galactan-rich potato fibers (SPPP) as well as from potato galactan in membrane reactors. A range of these products were demonstrated significant prebiotic potential on single cell cultures of gut microbes. The results of this present work have provided an additional positive foundation for biocatalytic design of β-galacto-oligosaccharides with putative health effects. The work has also shown a direction for potential valorization of the potato pulp byproduct stream.

Acknowledgements

The project is carried out within the Center for Biological Production of Dietary Fibers and Prebiotics at DTU ("Prebiotics Center").

References

1. H.N. Lærke, A.S. Meyer, K.V. Kaack, T. Larsen, Nutr. Res. 27 (2007) 152-60.
2. M. Olesen, E. Gudmand-Hoyer, M. Norsker, L. Kofod, J. Adler-Nissen, Eur. J. Clin. Nutr. 52 (1998) 110-4.
3. L.V. Thomassen, L.K. Vigsnæs, T.R. Licht, J.D. Mikkelsen, A.S. Meyer, Appl. Microbiol. Biotechnol. 90 (2011) 873-84.
4. I.R. Silva, D.M. Larsen, A.S. Meyer, J.D. Mikkelsen, Enzym. Microbiol. Technol. 49 (2011) 160-6.
5. S. Bauer, P. Vasu, S. Persson, A.J. Mort, C.R. Somerville, PNAS 103 (2006) 11417-22.
6. J.W. van de Vis, M.J.F. Searle-van Leeuwen, H.A. Siliha, F.J.M. Kormelink, A.G.J.Voragen, Carbohydr. Polym. 16 (1991) 167-87.
7. I. Kimura, N. Yoshioka, S. Tajima, J. Ferm. Bioeng. 85 (1998) 48-52.
8. L.V. Thomassen, D.M. Larsen, J.D. Mikkelsen, A.S. Meyer, Enzym. Microbiol. Technol. 2011 *online: 13-JUN-2011 DOI:10.1016/j.enzmictec.2011.06.006*
9. H. Mäkeläinen, M. Saarinen, J. Stowell, N. Rautonen, A.C. Ouwehand, Benefic. Microbiol. 1 (2010) 139-48
10. A.R. Martins, C.A. Veiga Burkert, Braz. J. Food Technol. 12 (2009) 230-40
11. F. Depeint, G. Tzortzis, J. Vulevic, K. l'Anson, G.R. Gibson, Am. J. Clin. Nutr. 87 (2008) 785-91

Aleksandar Mitic
Phone: +45 4525 2949
E-mail: asmi@kt.dtu.dk
Discipline: Process Technology and Unit Operations

Supervisors: Krist V. Gernaey
Kim Dam-Johansen

PhD Study
Started: November 2010
To be completed: November 2013

Operational Aspects of Continuous Pharmaceutical Production

Abstract
Establishment of continuous production is a great challenge for the modern pharmaceutical industry. Traditional batch and semi-batch processes have plenty of disadvantages which can be avoided by applying eco-friendly and economical continuous manufacturing. Furthermore, process analytical technology (PAT) can reach its full benefits in this type of production system. The main aim of this PhD thesis is to accelerate slow chemical reactions in the production of zuclopenthixol, a product of H. Lundbeck A/S, as well as to complete continuous manufacturing and establish in- line process monitoring and control. Production of zuclopenthixol involves several steps: Grignard alkylation, hydrolysis, liquid-liquid separation, dehydration and hydroamination. Applications of mini- and micro-sized devices, as well as microwave assisted organic synthesis (MAOS) have been tested.

Introduction
Organic synthesis is essential for the production of an important class of pharmaceuticals. Implementation of organic chemistry on an industrial scale is a great challenge. To date, pharmaceutical manufacturing is mainly based on batch and semi-batch processes. However, besides their flexibility and versatility there are many disadvantages compared to continuous production, such as the risk of occurrence of hot-spots, non-ideal mixing, undesirable temperature gradients, difficulties in implementing PAT applications, and so on.

The main aim of this PhD project is to complete continuous manufacturing of zuclopenthixol, with the main focus on acceleration of slow chemical reactions. Figure 1 depicts the current process flowsheet for production of this API.

Figure 1: Zuclopenthixol production flowsheet

Different process solutions are tested with the main focus on mico- and mini- sized devices. For instance, Grignard alkylation is a very fast reaction which occurs almost in the mixing zone [1]. Application of a mini-sized tubular reactor by forcing laminar flow has proven to be a great choice. This reaction is followed by immediate hydrolysis of the obtained intermediate product. After hydrolysis, water and water soluble by-products should be separated before performing the dehydration reaction. To this purpose, a membrane PTFE micro-separator is used which shows a very high efficiency in practice [2, 3]. Furthermore, N714 Allylcarbinol is dehydrated in N714 Butadiene which is a starting reactant for a very slow hydroamination reaction. The dehydration reaction is carried out in a tubular reactor under increased pressure (5 bars) which allows higher temperature of the reaction media and a higher reaction rate at the same time. The last step of the process, the hydroamination of N714 Butadiene, shows quite a good efficiency under microwave irradiation.

Specific Objectives
In order to complete continuous production of zuclopenthixol, it is necessary to increase the reaction rate of the last hydroamination step. Selectivity of the last step should be improved, as well, because the cis-isomer is the most desirable stereoisomer.

In general, acceleration of slow reactions in organic synthesis can be performed by applying different methods. Pressure increase has already been demonstrated to be a good choice in the dehydration reaction. Sometimes, applications of homogeneous catalysis are defined as good manufacturing practices,

but difficulties in finding suitable purification methods of final products put this approach as the last potential solution. Furthermore, combination of chemical catalysts and pressure increase is a good approach for very slow reactions, but possible deactivation of chemical catalysts due to a long-time exposure to very high temperatures actually forms a limitation to this approach.

In the last decade of the 20th century a new approach has been introduced, the so-called microwave assisted organic synthesis (MAOS). This is a modern and a very efficient way for speeding up slow chemical reactions. The main advantages of this approach are faster heating caused by electromagnetic radiation and the specific temperature profile inside reactors. For example, a comparison of the temperature profiles inside a microwave irradiated reactor and a reactor heated in an oil bath is shown in Figure 2.

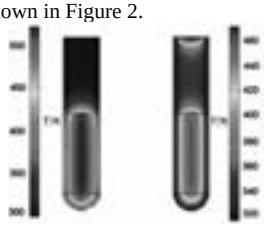

Figure 2: Inverted temperature gradients in microwave (left) versus oil bath heating (right) [4]

As expected, applications of oil baths cause the highest temperature at the reactor walls. Moving to the center of the reactor means a significant decrease of the temperature. This problem may be avoided by using a reactor with smaller diameters, as well. Therefore, experiments in micro- or mini- sized reactors should be done. However, if reaction times are quite long, those reactor types are not the most desirable choices because of the need for very long residence times.

Comparison of MAOS and microreactor technology would recommend micro-sized reactors for faster reactions, especially because of lower prices and easier integration of tubular micro-reactors in an overall process unit. On the other hand, if the reaction times are longer, MAOS and so called "stop and flow" continuous mode is the most desirable choice.

Results and Discussions

Acceleration of a slow hydroamination reaction might be performed in several ways. The first experimental runs were done in batch mode by using toluene as a solvent. The results showed a very high conversion of N714 Butadiene at 90^0C in 24 hours (90%). Further temperature increase caused degradation of the chlopenthixol isomers whereas longer reaction times at lower temperatures caused polymerization of N714 Butadiene. Hence, the main idea was to find a sufficiently low reaction time with optimal high reaction temperature.

Small scale trials in microwave ovens have been done. For this purpose a Biotage Initiator was used. All the samples were up to 1 ml and with excess of 1-2(hydroxythyl)piperazine (HEP), a compound which shows a good absorption of microwave irradiation. Different temperatures were tested, from 80^0C to 250^0C, as well as different reaction times: from 20 min to 5 hours. All the experiments were carried out in 2 different solvents, THF and toluene. The first one is a more desirable choice because all the previous steps are run in THF, and by also performing this reaction in THF a solvent swap can be avoided. The main aim of the experimental runs were to find the best conditions for performing the reaction, and thereby just qualitative analyses were done. The obtained results showed almost total conversion of N714 Butadiene at 120^0C during 4 hours. The API degradation increases rapidly with further temperature increase whereas applications of longer reaction times and lower temperatures are unjustified from the economical point of view. More precise analyses will be done in the future.

Conclusions and future work

Applications of microreactor technology, as well as, microwave assisted organic synthesis, have shown great advantages in the zuclopenthixol production. The Grignard alkylation and the dehydration reaction are carried out in mini-scale tubular reactors with increased yields and lower reaction times. Furthermore, a micro-scale liquid-liquid separator with PTFE membrane showed great results in practice, as well. Microwave assisted organic synthesis (MAOS) and its "stop and flow" continuous regime implied great advantages in the hydroamination reaction. Nevertheless, further investigations should be done.

After establishing completely continuous production of zuclopenthixol, on- and in- line monitoring and control will be applied. For this purpose spectroscopic method (NIR) and MATLAB® Simulink will be used. In addition, further options for process simplification might be tested. Indications that a Wittig reaction could be used in order to avoid the Grignard alkylation, hydrolysis and dehydration [5], sounds very promising and experiments for this reaction will be done in the near future as well.

Acknowledgment

DTU is acknowledged for financial support of the project. H. Lundbeck A/S is acknowledged for financial and technical support of the project.

References

1. H. Wakami, J. Yoshida, Org. Process Res. Dev. 9 (2005) 787-791
2. J.G. Kralj, H.R. Sahoo, K.F. Jensen, Lab Chip 7 (2007) 256-263
3. R.L. Hartman, K.F. Jensen, Lab Chip 9 (2009). 2495-2507
4. C.O. Kappe, Angew. Chem. Int. Ed. 43 (2004) 6250-6284.
5. E. Sinkovec, M. Krajnz, Org. Process Rec. Dev. 15 (2011) 817-823

Igor Mitrofanov
Phone: +45 4525 2817
E-mail: igm@kt.dtu.dk
Discipline: Systems Engineering

Supervisors: Rafiqul Gani
Gürkan Sin
Jens Abildskov

PhD Study
Started: November 2010
To be completed: October 2013

Computer-Aided Solvent Selection and Design Framework: Solvents for Organic Synthesis, Separation Processes, Phase Transfer Catalysis and Ionic-liquids Solvents

Abstract
This paper is presenting a systematic framework for solvent selection and solvent design. Such a framework is divided into several modules, which can tackle specific problems in various solvent-based applications. In particular, four modules are highlighted. The modules presented are for 1) solvent selection and design for organic synthesis, 2) model-based solvent screening and design of solvent mixtures for pharmaceutical applications, 3) ionic liquids selection and design as solvents and 4) solvents in phase transfer catalysis process.

Introduction
Solvents are used in many industrial sectors such as chemical, pharmaceutical, food, and agrochemical industries within a wide range of applications including extraction and cleaning, separation processes, organic synthesis, and product delivery. Therefore, solvent selection is a complex problem since solvents must satisfy cost, processing, environmental, safety and health related specifications. Currently, most of the solvents-related industry is based on trial-and-error procedures and solvent selection is mainly empirical. Such a procedure implies getting results that may be far from the optimal. From a mathematical point of view, the possibilities are in thousands and, by considering solvent mixtures, the combinatorial problem grows even more. A systematic approach is then highly desirable. Such an approach should possibly be independent from the need for experiments. The solvent selection framework that is presented here is based on the combination of knowledge from industrial practice, computer-aided tools, and molecular design (CAMD) principles and it is intended for solvent selection and design in product design as well as process design

Framework
The proposed systematic approach is depicted in the framework in fig. 1, where it can be noted that there are 7 modules to cover all possible solvent screening/design problems. In this paper, modules I, II, III and IV are being presented.

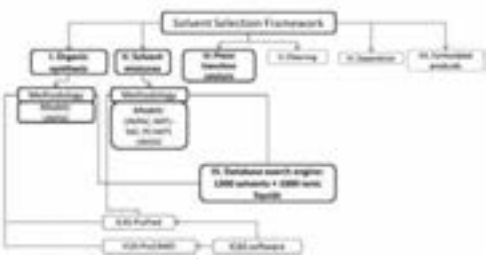

Figure 1: Framework for solvent screening and Design.

Module I
This module is dedicated to solvent selection and design for organic synthesis. It uses the solvent selection methodology developed by Gani et al. [1, 2]. The methodology involves five steps for each reaction:
1. Problem identification: an objective for the given system is chosen by identifying the actual functions of the solvent.
2. Search criteria definition: the solvent functions that satisfy the operational needs of the process are defined in terms of a set of search criteria (R-indices), which, in turn, are defined in terms of physical and chemical properties.
3. Performing the search: the search step consists of the generation and property identification of solvent candidates and the assignment of the RS-indices following the reaction–solvent properties.

4. Score table assignment: the scores are assigned to each solvent based on the calculated values of RS indices that is, giving a weight to each of the calculated RS indices.
5. Matrix of solvents: after the scores table has been generated, a short list of feasible solvents is obtained for each reaction step and presented as a matrix with rows of solvents and columns of reactions. The best solvent should appear in more than one column.

Module II
This module is dedicated to solvent selection for separation processes in the pharmaceutical industry. One of the important tasks is often the identification of a pure solvent or anti-solvent for a specific Active Ingredient (API). Solvents, lipids and other compounds are commonly employed in product formulation as well as in API processing. In addition, it might be needed to design solvent mixtures to improve the solubility performance. This module consists of the following steps:
1. Preliminary solvent screening by CAMD approach: here the design constraints are imposed on important properties, such as, the solubility parameter, melting and boiling temperatures.
2. Secondary screening: this is achieved by ranking the candidates in decreasing order of solvent power, which is calculated through an appropriate model for activity coefficient.
3. Solubility verification: here the solubility of the API is calculated with different rigorous models (UNIFAC, NRTL-SAC, PC-SAFT).
4. Solvent mixture design: this step is needed to improve the solubility performance of the system. Two non-ideal mixing effects can occur, 1) a decrease or 2) an increase of solubility. In both cases a model-based procedure is used to identify the best mixture for the assigned purpose.
5. Final selection/verification: a proper experimental design can be set-up to identify the best from the remaining few candidates.

Module III
Ionic liquids (ILs) are potential solvents for liquid extraction processes. ILs are characterized as designer solvents [3] since it is possible to fine-tune their intrinsic thermo-physical properties by simply replacing the cation and/or the anion for a specific application such as extractive distillation and liquid–liquid extraction. This module includes a database of organic solvents (ca. 1300 compounds) and ionic liquids (ca. 1000 compounds) and a search engine based on chemical properties of the compounds, including their characterization in terms of UNIFAC and other group-contribution method parameters so that solubility and other needed calculations with ICAS can be performed.

Module IV
The fourth module is solvent selection in phase-transfer-catalysis. As pointed out by Piccolo et al [4], a typical biphasic system can be decomposed into four sub-systems: a) water-organic solvent equilibrium, b) inorganic salt (source of reactive anion)-water, c) phase transfer catalyst-organic solvent, d) phase transfer catalyst-water. For each sub-system, data have been collected and representative models to calculate the liquid phase activity coefficients and from it, the solubilities and phase equilibrium, have been developed and tested for the systems of interest. The sub-system models are integrated in a continuous reactor model so that a quick evaluation of the process behaviour at different operational conditions is possible.

This module makes use of a model-based strategy for selection of the best organic solvent in PTC-based reacting systems where the organic solvent plays an important role since solubility of different forms of the PTC in the organic solvents affects ultimately the catalyst partition coefficients. Through this module, it is possible to find opportunities for improving reacting system performance and replacement of solvents.

Conclusions
An integrated computational tool for solvent selection and design has been developed and showed good performances for different common solvent-based processes. Further features will be added to the tool in order to extend the domain of application of such a tool.

References

1. R. Gani, C. Jimenez-Gonzalez, D.J.C. Constable, Comput. Chem. Eng. 29 (2005) 1661-1676.
2. M. Folic, R. Gani, C. Jiménez-González, D.J.C. Constable, Chinese J. Chem. Eng. 16 (3) (2008) 376-383.
3. H. Rodríguez, G. Gurau, R.D. Rogers, in: W.H. Flank, M.A. Abraham, M.A. Matthews (Eds), Innovations in Industrial and Engineering Chemistry, American Chemical Society, 2009, p 389–400.
4. C. Piccolo, G. Hodges, P.M. Piccione, R. Gani, Comput. Aided Chem. Eng. 29 (2011) 266-270

Ane Høyer Mollerup
Phone: +45 4525 2812
E-mail: molle@kt.dtu.dk
Discipline: Systems engineering

Supervisors: Gürkan Sin
Peter Steen Mikkelsen
Dines Thornberg, Udviklingssamarbejdet
Niels Bent Johansen, Københavns Energi

Industrial PhD Study
Started: August 2011
To be completed: August 2014

Optimizing Control of the Integrated Urban Wastewater System

Abstract
Design and assessment of control in wastewater collection and treatment systems has to be tackled at all levels, including supervisory and regulatory level. This project aims at developing a methodology for determining the best control structure and technique for an integrated system of both sewer system and wastewater plants, when optimizing towards defined objectives.

Introduction
Since the EU Water Framework directive came into force in 2000, wastewater systems (sewer system and wastewater treatment plants) in Europe have been put under pressure to reduce the number of combined sewer overflows[1] (CSOs) from the system to protect the aquatic environment. And as the future climate changes are predicted to induce an increase in precipitation in the northern part of Europe [1] the strain on the performance of the wastewater systems will only become larger in the future.

To cope with the increasing pressure the wastewater system can be expanded by building larger pipes and new storage tanks. But expanding the wastewater system requires a significant capital investment and intensive civil building works and therefore the need for this should be limited as much as possible. Instead of expanding the system, research has shown that the implementation of Real Time Control (RTC) in the sewer system can increase the utilization of the existing storage volume and thereby reduce the need to build new storage capacity [2] The use of RTC allows for the control of pumping stations and diversion or retention gates according to online measurements at critical points, thereby making it possible for the system operation to respond to rain events.

To further increase the utilization of the system, research is now primarily focused on how to do a system wide optimization. In particular, research on how to use real time optimisation (RTO) and model predictive control (MPC) in the control structure.

The problem of finding the optimum control structure that best serves both the sewer system and wastewater treatment plant(s) is a challenging and formidable problem. The main objective of the control system is to minimize the risk of flooding and the volume of overflow and bypass from the system.

One way to address the control problem is to decomposition it according to the time scales of the actions. From this it becomes possible to identify a number of layers, linked by master-slave relations. For the sewer system the decomposition can look as depicted in figure 1.

Based on decomposition one can look at the different levels of control separately, starting from the lowest level and moving upward.

Using the system decomposition it becomes obvious that the research today on control of the wastewater system is focused on higher layers in the system decomposition. However these methods are supervisory layer controllers that require a control structure as given. Therefore it becomes imperative that the regulatory level control functions optimally.

However, in practice the design and implementation of RTCs in wastewater systems have been done incrementally as the utility management companies have identified the potentials. Over time as more and more controls have been implemented in the wastewater system and the number of controlled actuators in the system has increased, important interactions among the different control loops may have appeared, that was not accounted for in the design of the individual controls.

[1] Combined Sewer Overflow: The discharge from a combined sewer system that handles both wastewater and stormwater. During rain the system can discharge from overflow structures into a recipient such as a stream, river, lake or sea, if the capacity of the system is exceeded.

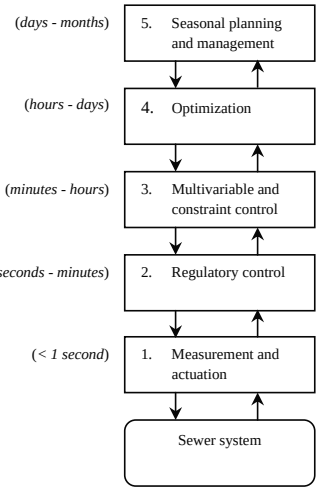

Figure 1: The system decomposition with respect to time scale (based on Seborg et al. [3]).

Depending on the interactions among the control loops this may appear impairing on the performance of the control system. Therefore attention should be paid to aspects related to the regulatory level such as the analysis of controllability properties of the system according to the design of control loops, pairing of variables, among others. This analysis of control problem and designing of control structure needs to be performed in a formal and structured way as required by process control engineering good practice (e.g. see [4]).

Specific objectives

The aim of this project is to formulate the problem of design and analysis of the regulatory level from a process control perspective and to develop a methodological approach to find the optimal solution.
The project aims at developing a methodology for determining the best control structure and technique for an integrated system of both sewer system and wastewater plants, when optimizing towards defined objectives, e.g. minimizing flooding, overflow from the sewer system, bypass from the WWTP, electrical consumption, etc.

Methodology

Integrated sewer and WWTP systems are complex systems involving a high number of catchments, subsections affected by hydrological aspects as well as hydraulic of sewer systems.

The research problem will therefore be broken down into steps as stated in Table 1.

One of the issues to be examined is the robustness of the control structure with respect to actuator failure and uncertainty on measurements.

Also the optimization of the system is addressed. With the introduction of better climate models and radar predictions of the precipitation it might be possible to introduce a supervisory control layer with Real Time Optimization (RTO).

Table 1: Research steps

Step	Possible methods to be used
Understanding the problem	Expert knowledge
Generate alternatives/solutions	Plantwide control methodology
Evaluate the performance	System model
Iterate over different scenarios	Model uncertainty
Implement/test the optimal solution	Verification on full scale system model

Case study

The model used for modelling the sewer system in the utilities is a Mike Urban which is a 1D model based on the St. Venant equations of continuity and momentum. Full scale models of a sewer system in Mike Urban takes a long time to run, due to the complexity and size of the model. Mathematical representation of these systems as performed in Mike Urban type software involves dimensions state variables and parameters making it difficult to solve efficiently. It is therefore not suitable to look at a full system to begin with. Instead a simplified model will be used to begin with.

Using the simplified model different control structures and control techniques can be generated and tested, i.e. test of different types of pairing between actuators and measurements and tests of different control techniques such as for example MPC, PI, manual, etc.

Working with a simple model will help to understand the control structure and validate the systematic methodology.

Acknowledgement

AHM acknowledges the Danish Agency for Science Technology and Innovation, Copenhagen Energy and Copenhagen Wastewater Innovation for financial support.

References

1. R. Watson, M. Zinyowera, R. Moss, IPCC Special Report on the Regional Impacts of Climate Change. An Assessment of Vulnerability, Cambridge University Press, 1997.
2. M. Marinaki, M. Papageorgiou, J. Water Resour. Plan. Manage. 123 (5) (1997) 274-283.
3. D. Seborg, T. Edgar, D. Mellichamp, F. Doyle Process Dynamics and Control, Wiley, 2011, third edition.
4. S. Skogestad, Comput. Aided Chem. Eng. 10C (2002) 57-69.
5. A.H. Mollerup, M. Mauricio-Iglesias, N.B. Johansen, D. Thornberg, P.S. Mikkelsen, G. Sin, Model-Based analysis of control performance in sewer systems, Preceedings of NPCW 17 (in press) (2012).

Peter Mølgaard Mortensen
Phone: +45 4525 2809
E-mail: pmm@kt.dtu.dk
Discipline: Reaction and Transport Engineering

Supervisors: Anker Degn Jensen
Jan-Dierk Grunwaldt
Peter Arendt Jensen

PhD Study
Started: August 2010
To be completed: August 2013

Catalysts for Hydrodeoxygenation of Bio-oil

Abstract
A prospective route for the production of alternative fuels is the conversion of biomass to bio-oil through flash pyrolysis followed by catalytic upgrading through hydrodeoxygenation (HDO), ultimately giving a crude oil like product. One of the major challenges in this concept is to find a catalyst which has a sufficient activity for HDO and at the same time a resistance toward impurities in the bio-oil and potential carbon formed in the process. The scope of this project is to investigate different catalyst for this and further elucidate their durability. So far four different groups of catalysts have been investigated: oxide catalysts, methanol synthesis catalysts, noble metal catalysts, and reduced metal on oxide catalysts. In total 13 different catalysts were tested for HDO of phenol in water at 100 bar and 275 °C. Of these, only Ru/C, Ni-V_2O_5/SiO_2, and Ni/SiO_2 showed sufficient activity. The relative activity was found as: Ru/C≈Ni-V_2O_5/SiO_2>Ni/SiO_2. Evaluation of the carbon balance and carbon build up on the catalysts further showed that Ni-V_2O_5/SiO_2 had a lower affinity for cracking and coking compared to the two others. Overall Ni-V_2O_5/SiO_2 seems as an interesting catalyst for HDO and this type of catalysts will therefore be the scope of the further work.

Introduction
A prospective route for production of bio-fuels in the future is the conversion of biomass into bio-oil through pyrolysis followed by upgrading via hydrodeoxygenation (HDO) [1]. Pyrolysis is advantageous in order to minimize transportation cost of biomass and homogenize it, as the production can be facilitated at small plants with low capital cost [1]. However, the bio-oil is viscous, polar, and acidic and has a low heating value, making it unsuitable as a fuel. These unfavourable characteristics are all associated with high contents of water (10-30 wt%) and oxygen containing organic compounds (30-40 wt% oxygen) in the oil [2].

In HDO the bio-oil is treated with hydrogen at a pressure of up to 200 bar and temperatures in the range from 200-400 °C. This converts the oxy-compounds to a hydrocarbon product which will separate from the water and ultimately give a product equivalent to crude oil. The reaction can be written as (normalized to feed carbon) [1]:

$$CH_{1.4}O_{0.4} + 0.7H_2 \rightarrow 1CH_2 + 0.4H_2O$$

One of the major challenges in this concept is to find a catalyst for HDO which has a high activity for the deoxygenation reaction, but at the same time a sufficient lifetime, as carbon deposition has proven to be a severe problem [1]. Furthermore poisons as sulphur or alkali metals could be present in the bio-oil, which potentially could deactivate a catalyst [1,2].

Specific Objective
The scope of the project is to develop alternative catalysts and processes for HDO. Currently, four different types of catalysts for HDO have been tested: oxide catalysts (1), methanol synthesis catalysts (2), reduced metal on oxide catalysts (3), and noble metal catalysts (4).

Experimental
MnO/C, WO_3/C, MoO_3/C, V_2O_5/C, Cu/SiO_2, Cu/ZnO/Al_2O_3, Ni/SiO_2, Ni-V_2O_5/SiO_2 and NiCu/SiO_2, were all prepared through the incipient wetness method on the relevant supports and then calcined at 400 °C. The active carbon was Daihope 009 which was supplied by Haldor Topsøe A/S. The silica was supplied by Saint-Gobain NorPro, type SS6*138 with a surface area of 241 m^2/g and a purity of ≥ 99.5%. Ni$OMoO_3/Al_2O_3$ and Co$OMoO_3/Al_2O_3$ were obtained from Haldor Topsøe A/S, and Ru/C was obtained from Sigma-Aldrich.

The screening experiments were performed in a 300 ml batch reactor from Parr, type 4566, constructed of

Hastelloy C steel. In an experiment the catalyst was initially loaded in the reactor and hereafter a mixture of phenol in water (as a model system for bio-oil) was added. This was heated to 275 °C in a hydrogen atmosphere, giving a final pressure of 100 bar. The heating rate was in the order of 10-15 °C/min. During the experiments, hydrogen was added continually to maintain the pressure, if needed. To stop the experiment, the reactor was lowered into an ice bath. Some of the catalysts were pretreated with hydrogen to reduce the active metals.

Analysis of the product was done with a Shimadzu GCMS/FID-QP2010UltraEi fitted with a Supelco Equity-5 column. Identification was made on the mass spectrometer (MS) and quantification was done on the flame ionization detector (FID). The activity for HDO was primarily evaluated on the potential for conversion of phenol in to cyclohexane.

Results

Figure 1 summarizes the results from the tested catalysts. A very low activity was found for the oxide (group 1) and methanol synthesis (group 2) catalysts and neither of these achieved a conversion above 10%.

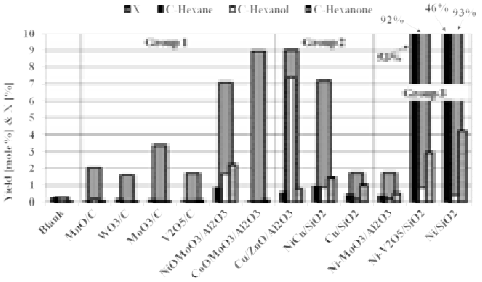

Figure 1: Yield and conversion over oxide (group 1), methanol synthesis (group 2), and reduced metal on oxide catalysts (group 3). The experiments were made with 0.5 g of catalyst in 90 ml water and 10 g phenol. T=275 °C, P=100 bar, reaction time=4 h.

Contrary to the group 1 and 2 catalysts, the group 3 catalysts (reduced metal on oxide) showed a high conversion and further a high production of cyclohexane.

As specifically Ni/SiO_2 and $Ni\text{-}V_2O_5/SiO_2$ seemed promising, these were tested in pure phenol as well, shown in Figure 2. The activity of these was compared to the noble metal catalyst Ru/C. From Figure 2 it can be seen that the Ni/SiO_2 had a significantly lower production of cyclohexane compared to Ru/C, but $Ni\text{-}V_2O_5/SiO_2$ showed a cyclohexane production almost comparable to Ru/C.

Discussion

In the comparison of the different catalysts it should be emphasized that neither of them have been optimized for the reaction. However, the results clearly indicate that only Ru/C, $Ni\text{-}V_2O_5/SiO_2$, and Ni/SiO_2 have a significant activity for HDO.

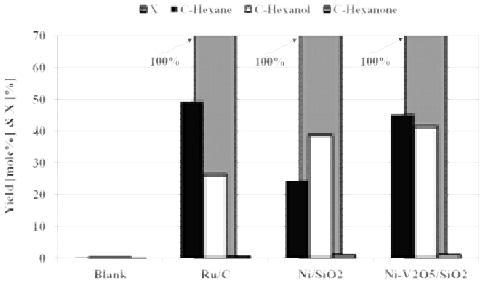

Figure 2: Yield and conversion over most promising catalysts. The experiments were conducted with 1 g of catalyst in 50 g phenol. T=275 °C, P=100 bar, reaction time=5 h.

Evaluation of the carbon balance for the three interesting catalysts indicated that Ru/C and Ni/SiO_2 produced a larger byproduct of carbon or smaller hydrocarbons compared to $Ni\text{-}V_2O_5/SiO_2$.

The results in figure 3 indicate that the phenol initially is hydrogenated to produce cyclohexanol and thereafter deoxygenated to produce cyclohexane. Overall giving the following reaction path:

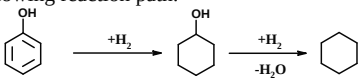

Some traces of cyclohexanone and cyclohexene were observed in the product, indicating that these might act as intermediates in the reaction.

Conclusions

A series of screening experiments have been performed for identification of potential catalysts for HDO of bio-oil being a prospective future liquid fuel. All in all, 13 catalytic systems have been tested.

Ru/C, $Ni\text{-}V_2O_5/SiO_2$, and Ni/SiO_2 were found as the most active catalysts and their relative activity was found as: $Ru/C \approx Ni\text{-}V_2O_5/SiO_2 > Ni/SiO_2$.

Further work will focus on the reduced metal on oxide type catalysts, as the $Ni\text{-}V_2O_5/SiO_2$ has shown an interesting potential for the HDO process.

Acknowledgments

The present work is financed by DTU and The Catalysis for Sustainable Energy initiative (CASE), funded by the Danish Ministry of Science, Technology and Innovation.

References

1. P.M. Mortensen, J.-D. Grunwaldt, P.A. Jensen, A.D. Jensen, Appl. Catal. A 407 (1-2) (2011) 1-19.
2. Q. Zhang, J. Chang, T. Wang, Y. Xu, Energ. Convers. Manage. 48 (1)(2007) 87-92.

List of Publications

1. P.M. Mortensen, J.-D. Grunwaldt, P.A. Jensen, A.D. Jensen, Appl. Catal. A 407 (1-2) (2011) 1-19.

Nikolai E. Musko
Phone: +45 4525 2923
E-mail: nm@kt.dtu.dk
Discipline: Reaction and Transport Engineering

Supervisors: Georgios M. Kontogeorgis
Anker Degn Jensen
Jan-Dierk Grunwaldt, KIT

PhD Study
Started: October 2009
To be completed: October 2012

Heterogeneously Catalysed Chemical Reactions in Dense and Supercritical Carbon Dioxide

Abstract
The aim of this PhD project is to combine heterogeneous catalysis with the use of supercritical carbon dioxide. Due to the unique properties of carbon dioxide near and above its critical point, its use in many cases may significantly improve the catalytic performance of a heterogeneous catalyst. The number and the composition of co-existing phases may drastically change as the reaction proceeds. The following chemical reactions have been investigated in the present study: (i) selective hydrogenation of unsaturated aldehydes in CO_2 media, (ii) direct dimethyl carbonate synthesis from methanol and CO_2, and (iii) propylene carbonate synthesis from propylene oxide and carbon dioxide. The Cubic-plus-Association Equation of State (CPA) has been successfully used in order to predict phase equilibria during the reaction. For the first process it was found that depending on the amount of carbon dioxide added to the reaction system the conversion achieves either minimum (at low concentrations of CO_2) or maximum (near the supercritical point). For the other two the optimal reaction conditions have been found.

Introduction
Heterogeneous catalysis combined together with the use of dense and supercritical carbon dioxide provides a number of opportunities for the improvement of conventional technologies [1]. This is due to the fact that carbon dioxide combines both gas- and liquid-like properties, which are strongly temperature and pressure dependent.

Phase behaviour plays an important role during heterogeneous reactions [2]. Sometimes, reaction rates significantly increase when the reactions run in a single phase region [3], sometimes the two-phase regime is beneficial [4], and in some cases a transient "expanded liquid" region provides the highest conversion and selectivity [5].

The knowledge of the phase behaviour can provide a deeper insight into the understanding of chemical processes. It may give some hints as to how to modify and optimise both catalysis and the following separation. However, the experimental study of the phase composition and phase transition during chemical reactions, especially *in situ*, is very complicated, time consuming, expensive, and, in some cases, even impossible. Thermodynamic models may be a reliable alternative to laboratory measurements [6].

In the present study the advanced Cubic-plus-Association (CPA) model is used [7]. CPA takes into account strong cross-association between components, i.e. hydrogen bonding; and it has been used successfully for predicting various properties of complex multicomponent system at high temperatures and pressures [8-9]. The CPA equation of state consists of two parts – the Soave-Redlich-Kwong (SRK) equation of state and an association term. In the case when no hydrogen-bonding components are present in the mixture, the association term disappears and CPA reduces to SRK.

VLE, VLLE or any other experimental data for binary systems comprising the whole reacting mixture are required in order to estimate binary interaction parameters k_{ij}.

One of the reactions that have been studied in the present study is the selective hydrogenation of 2-butenal into butanal in carbon dioxide media, Fig.1. This reaction is particularly important because it is the first step of the "one-pot" synthesis with the consequent second step of the aldol reaction of the saturated aldehydes [10]. Some further studies have already been performed by us in that direction [11].

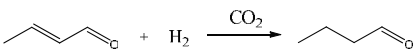

Figure 1: Selective hydrogenation of 2-butenal in carbon dioxide reaction medium.

The purpose of this research was to investigate the influence of the amount of carbon dioxide added into the batch reactor on the catalytic performance. Besides that, the experimental bubble point pressures of the 2-butenal – CO_2 binary were experimentally measured and the obtained data were used for fitting the interaction parameter k_{ij} for CPA.

It is important to note that in this type of reaction carbon dioxide is a solvent and the number of its moles does not change over time, unlike the reactions discussed further below.

Another type of the reactions investigated in this study is the formation of organic carbonates e.g. (i) the direct dimethyl carbonate (DMC) synthesis, (cf. Fig.2) and (ii) propylene carbonate (PC) synthesis from propylene oxide (PO) and CO_2 (cf. Fig.3). These two reactions involve the consumption of carbon dioxide during the reaction. Therefore, this fact may cause even stronger dependency of the catalyst performance from the phase behaviour. Thus, the purpose of this part of the study was to apply CPA in order to predict the phase behaviour during both reaction and suggest further measures for process optimisation.

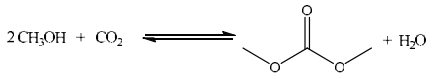

Figure 2: Dimethyl carbonate synthesis.

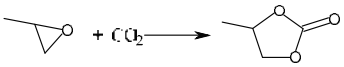

Figure 3: Propylene carbonate synthesis.

Experimental

Catalyst performance was tested in the selective hydrogenation of 2-butenal. A 5%wt.Pd/C catalyst sample was prepared using the incipient wetness impregnation technique with consequent drying and reducing in a 5%vol.H_2/N_2 flow for 2 hours at 110°C.

Homemade stainless steel autoclaves (IKFT) with magnetic stirring bars were used for performing the reaction (T_{max} = 250°C, P_{max} = 200 bar, inner volume ~125 ml). Before use, the reactors were thoroughly washed with organic solvents and dried with compressed air. Required amounts of the prepared catalyst and 2-butenal were loaded into the autoclaves and the latter were tightly closed. After that, the reactors were carefully flushed with hydrogen several times and pressurised up to a required pressure. At a next step, carbon dioxide was added using a CO_2-pump (NWA PM - 101). After the reaction, the autoclaves were quickly cooled down to room temperature in a water bath, slowly and carefully depressurised, and opened. A sample of the reaction mixture was taken out, diluted with toluene and analysed employing a gas chromatograph (Shimadzu, GC 2010+, polar column).

Phase behaviour of the 2-butenal – carbon dioxide binary was visually monitored in a high pressure view cell (SITEC, Switzerland) with a sapphire window and a magnetic stirrer. The pressure was adjusted by changing the volume of the cell by means of a screw-type manual pump. Temperature was controlled by an oil-containing heating jacket connected to a thermo/cryostat. Before every experiment the view cell was thoroughly cleaned with acetone and CO_2, and dried with air jet. The desired amount of 2-butenal (Aldrich, 99.8%+) was loaded into the cell. After that the cell was closed, tightened, and flushed with CO_2 to substitute the air. CO_2 was added using a CO_2-compressor (NWA, Loerrach, Germany). The view cell was further heated up to a desired temperature and pressurised to a pressure higher than the expected bubble point pressure. At this stage the cell was left for equilibrating for a minimum of 2 hours. Small stepwise pressure drop (0.2 – 1 bar) with consequent sufficient equilibrating after each step was applied to find the bubble point pressure of the desired system.

CPA model

The CPA EoS combines the classical Soave-Redlich-Kwong (SRK) equation of state with an advanced association term [7]. The full description of the model and all its parameters may be found in [6].

In general, CPA requires the knowledge of five pure fluid parameters – three for SRK (a_0, b and c_1) and two for the association term (association energy and volume). These parameters are estimated using the experimental liquid density and vapour pressure data. When there are no associating components present in the system, the two association parameters disappear.

As it was mentioned above, the model also requires the knowledge of the interaction parameters k_{ij} for the binaries comprising the reaction mixtures. These parameters are obtained by fitting the model predictions into the experimental VLE, VLLE or other data. In the present study, when the parameters were not available in the literature, they were set to zero.

Results and Discussion

Selective hydrogenation of 2-butenal.

A number of catalytic experiments with a 5%Pd on activated carbon catalyst were performed. The only parameter that was changed is the amount of CO_2 loaded into the autoclave.

In order to obtain the binary interaction parameter for the CO_2 – 2-butenal mixture the bubble point pressures of four mixtures of different composition at three different temperatures were measured and the CPA predictions were fitted into obtained experimental data. The model quite nicely describes the experimental results, which are presented in Fig. 4.

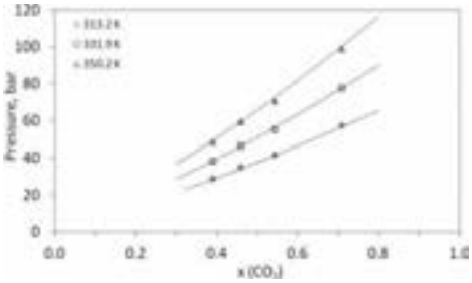

Figure 4: CO_2 – 2-butenal VLE. Experimental data (points) measured in the present study at different temperatures and CPA calculations (lines) with a temperature independent k_{ij} = -0.0180.

In catalytic experiments it was found that depending on how much carbon dioxide was added into the system, the conversion was different. A local minimum was observed when a little CO_2 was used. When higher loads were introduced the conversion was steadily increasing, Fig. 5.

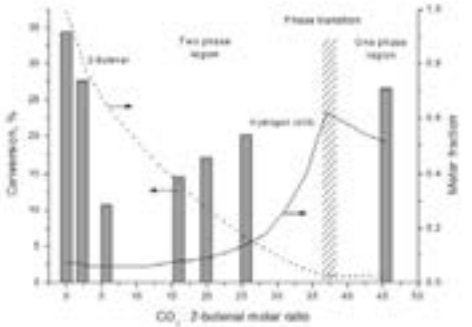

Figure 5: Molar fractions of hydrogen (solid line) and 2-butenal (dash line) in the *liquid (dense) phase* which is in contact with the catalyst and conversion (bars) of the substrate depending on the initial CO_2 : substrate molar ratio. *The reaction conditions*: substrate 0.04 mol, H_2 : substrate molar ratio 2.5 : 1, m_{cat} = 0.01 g, temp. 323.2 K, reaction time 60 min.

The number of the co-existing phases and their composition were calculated and plotted against the CO_2 : substrate molar ratio together with the conversion, Fig.5. It turned out that the concentration of hydrogen in the liquid layer at low concentrations of CO_2 was constant and at some point it started to rise. The concentration of 2-butenal, in contrast, was steadily decreasing when the system was diluted with carbon dioxide.

The initial drop of the substrate concentration at a constant concentration of hydrogen in the liquid layer, where the reaction was proceeding, might explain the significant decrease in the conversion. However, when more hydrogen molecules were in contact with the catalyst the conversion increased. At the CO_2: substrate molar ratio of around 37: 1 the phase transition occurred. According to the calculations the concentration of hydrogen at this point was the highest. Unfortunately, no experimental catalytic data is available around this point; however, the conversion may achieve a maximum. Further experiments will be performed in order to study the catalytic reaction in carbon dioxide media in the near critical region. Furthermore, the results will be used to optimize continuous flow operation.

Dimethyl carbonate synthesis.

The phase behaviour of the direct synthesis of DMC from methanol and carbon dioxide (Fig.2) was modelled in order to know how the number of phases is changing as the reaction proceeds. Previously the phase behaviour of this system has been studied with the SRK model; however, it gave quite high deviations from the experimental data for binary systems [12]. The predictions obtained with the CPA model are presented in Fig.6.

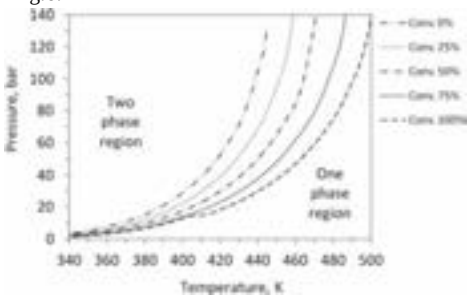

Figure 6: The dew point line CPA predictions of the methanol – CO_2 – DMC – water quaternary system with molar feed composition MeOH : CO_2 = 1 : 2 and different conversion.

It was shown that depending on the conversion of methanol, the number of phases is changing over time. The “two phase” region is “expanding” in the direction of higher temperatures and pressures. This means that at some reaction conditions, it might happen that the reaction starts in one phase region, but at a certain degree of conversion the phase splitting might occur. This might be explained by the fact that water has a very low solubility in dense carbon dioxide and DMC has a high critical temperature. Moreover, the reaction is occurring against the thermodynamic equilibrium. The free Gibbs energy ΔG of the reaction is positive. Hence, water removal, the use of more reactive reactants or related procedures should be applied to shift the equilibrium towards the products. Another option is to facilitate phase separation and recycle the methanol-rich phase.

The CPA model is a very powerful tool for predicting the phase behaviour of hydrogen-bond containing multicomponent systems. For the binaries studied in the present work, the predictions made with CPA come very close to the experimental data with slight discrepancies in VLE at high temperatures.

Especially it is important for the binaries containing methanol and water, since these two components are prone to association.

The model was also successfully used for describing the phase behaviour of the reacting four component system. This information may be very useful in terms of optimisation and further improvement of the process and subsequent products separation.

Propylene carbonate synthesis.

The CPA model with the parameters obtained in this research was used to model the phase behaviour of the three component reaction system of propylene carbonate (PO) synthesis. (Fig.3). It turned out that like in the reacting system of DMC formation the two phase region during the PC synthesis is also "expands" significantly, Fig.7. Interestingly, this phase behaviour has been previously observed experimentally, using IR spectroscopy [5].

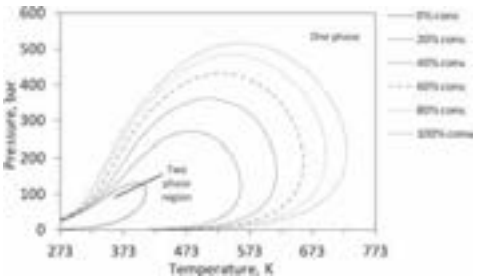

Figure 7: CPA predictions of the bubble and dew point curves for the reaction mixtures during the propylene carbonate synthesis from propylene oxide and CO_2.

Such a behaviour during the reaction helps to understand how to optimise the reaction conditions. It was previously shown that the "expanded liquid" regime is the most beneficial for this reaction [5]. The experimental determination of such a region might be very complicated; however, using the CPA model this task becomes easily achievable.

The further work in this direction will be devoted to performing catalytic experiments under optimised experimental conditions. CPA will be exploited for calculating the number, composition, volumes, etc. of the co-existing phases.

Conclusions

In the present PhD project it has been shown that the combination of catalysis and thermodynamic modelling provides a better understanding of the processes happening in the catalytic reactor. It also gives some hints as to how to modify and improve the reactions in dense and supercritical carbon dioxide. It was shown that the CPA model allows not only investigating the phase behaviour during chemical reactions, but also predicting the optimal conditions.

For example, the knowledge of phase behaviour and phase composition during the selective hydrogenation of 2-butenal helped to explain the catalytic behaviour and predict the maximum and minimum conversion points. Whereas, the phase transition point was skipped during the catalyst screening.

The application of the CPA model to the carbonate syntheses (both DMC and PC) will help to find the optimal reaction conditions, i.e. the conditions where the reaction mixture exists in the "expanded" liquid region, and estimate the volumes of the phases.

Acknowledgements

The authors are grateful for financial support to DTU, The Danish Research Council for Technology and Production Sciences, DanScatt (synchrotron radiation), Institute of Catalysis Research and Technology (IKFT) and Karlsruhe Institute of Technology. Dr. Loubna Gharnati, Dr. Matthias J. Beier are acknowledged for their help with the experiments and complementary studies. Dr. Ioannis Tsivintzelis is acknowledged for his help with the thermodynamic calculations.

List of Publications

1. N.E. Musko, J.-D. Grunwaldt, Topics Catal. 54 (2011) 1115-1123

References

1. A. Baiker, Chem. Rev. 99 (1999) 453-473.
2. J.D. Grunwaldt, R. Wandeler，A. Baiker, Catal. Rev. 45 (2003) 1-96.
3. P.G. Jessop，W. Leitner, Chemical synthesis using supercritical fluids, Wiley-VCH, Weinheim, 1999.
4. M.J. Beier, in Heterogeneously Catalyzed Oxidation Reactions Using Molecular Oxygen, Vol. The Technical University of Denmark, Lyngby, Denmark, 2011, p. 204.
5. M. Ramin, J.D. Grunwaldt, A. Baiker, Appl. Catal. A 305 (2006) 46-53.
6. G.M. Kontogeorgis, G.K. Folas, Thermodynamic Models for Industrial Applications: from classical and advanced mixing rules to association theories, Wiley, 2010.
7. G.M. Kontogeorgis, E.C. Voutsas, I.V. Yakoumis, D.P. Tassios, Ind. Eng. Chem. Res. 35 (1996) 4310-4318.
8. G.M. Kontogeorgis, M.L. Michelsen, G.K. Folas, S. Derawi, N. von Solms, E.H. Stenby, Ind. Eng. Chem. Res. 45 (2006) 4855-4868.
9. G.M. Kontogeorgis, M.L. Michelsen, G.K. Folas, S. Derawi, N. von Solms, E.H. Stenby, Ind. Eng. Chem. Res. 45 (2006) 4869-4878.
10. T. Seki, J.D. Grunwaldt, A. Baiker, Chem. Commun. (2007) 3562-3564.
11. N.E. Musko, J.D. Grunwaldt, Topics Catal. 54 (2011) 1115-1123.
12. S. Camu, J.S. Pic, E. Badens, J.-S. Condoret, J. Supercrit. Fluids, (2003) 19-32.

Azizul Azri Bin Mustaffa
Phone: +45 4525 2811
E-mail: azm@kt.dtu.dk
Discipline: Engineering Thermodynamics
Systems Engineering

Supervisors: Rafiqul Gani
Georgios Kontogeorgis

PhD Study
Started: April 2009
To be completed: September 2012

Development and Analysis of Original UNIFAC-CI and Modified UNIFAC-CI Models for the Predictions of Vapor-Liquid Equilibrium Systems

Abstract
In this work, further development and analysis of the Original UNIFAC-CI and Modified UNIFAC (Dortmund)-CI models, developed through the GC^{Plus} approach are presented. Model parameters for the CI-models have been regressed against VLE data for groups formed by C, H, O, N, Cl and S atoms. Initially all the VLE data are checked using a quality assessment algorithm which combines four widely used consistency tests (Herington, Van Ness, Differential and Infinite Dilution) and also a check on the consistencies of the data with the pure component vapor pressures. The overall quality factors, Q_{VLE} obtained for each dataset are then used as weighting factors, in the objective function for the parameter regression. The performances of the CI-models are compared in terms of the prediction accuracies with their reference Original UNIFAC model.

Introduction
The Group-Contribution^{Plus} (GC^{Plus}) approach was first developed by Gani et al. [1] through the establishment of a methodology for predicting missing group contributions for the Marrero and Gani [2] group contribution method for pure component property estimation with the aid of valence connectivity indices. Following the previous work, a GC^{Plus} approach for predicting mixture properties by combining the UNIFAC [3] group contribution based activity coefficient model with valence connectivity indices (CI) developed by Kier and Hall [4] to be called UNIFAC-CI have been developed [5]. Note that the group interaction parameters (GIPs) for any UNIFAC model are regressed from experimental data separately for vapour–liquid equilibrium (VLE) data or liquid–liquid equilibrium (LLE) data. Other data, such as activity coefficients at infinite dilution data and heat of mixing data, may also be added to the VLE and/or LLE data. There are, however, many gaps in the UNIFAC parameter tables due to lack of the necessary experimental data, some of which may not be possible to measure. The objective therefore is to predict the missing GIPs of the reference UNIFAC model through the GC^{Plus} approach. In this way, the application range of the reference UNIFAC model can be significantly increased by providing a reliable predictive option for obtaining the necessary GIPs in a fast, cheap and efficient manner. In the developed UNIFAC-CI method, an expression was established for relating the GIPs to the number of atoms involved in the UNIFAC groups, the connectivity indices of each group and a set of atom interaction parameters (AIPs). The atom stoichiometry and the values of the CIs can be obtained directly from the group definition while the AIPs were regressed using available experimental data. González et al. [5, 6, 7] published the AIPs and the corresponding GIPs for the Original UNIFAC-CI model for groups formed by C, H, O, N, Cl and S atoms and for the Modified (Dortmund) UNIFAC-CI model for groups formed by C, H, O, and N atoms [7]. In this current work, all the VLE data that are used in the parameter regression step are checked using a quality assessment algorithm [8] which combines four widely used VLE consistency tests which are the Herington, Van Ness, Point (Differential) and Infinite Dilution tests and also a check on the consistencies of the data with the pure component vapor pressures. The overall quality factors, Q_{VLE} obtained for each dataset indicate the quality of each datasets. These quality factors are then used as weighting factors, in the objective function for the parameter regression with VLE data.

Specific Objectives
The specific objective of this current work is to develop, analyze and present the performance of the Original

UNIFAC-CI and Modified (Dortmund) UNIFAC-CI models, for parameters regressed against VLE data using a data quality criterion.

General Methodology

The general methodology for this current work is displayed in Figure 1. Initially, all the VLE data that are going to be used in the parameter regression step will be checked using the quality assessment algorithm which will generate the Q_{VLE} quality factor for each of the dataset. Then, using the generated quality factors as weighting factors in the objective function, the AIPs are regressed for the Original UNIFAC-CI and Modified (Dortmund) UNIFAC-CI models. Moreover, using the regressed parameters, the performances of the CI-models are evaluated by comparing the prediction accuracies with the experimental data and also the prediction using their reference UNIFAC models.

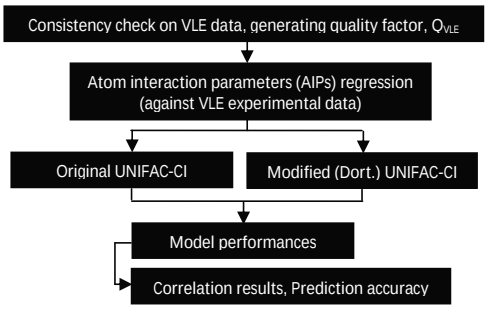

Figure 1: General methodology of the current work

Consistency Check

In this work, all the VLE data were checked using a quality assessment algorithm, developed by Kang et al. [8]. The algorithm combines four widely used VLE consistency tests and they are the Herington, Van Ness, Point or Differential and Infinite Dilution tests which are based on the requirements of the Gibbs-Duhem equation. Besides that, the consistencies of the binary data with the pure component vapor pressures are also checked. The algorithm can be applied to VLE data sets with at least three variables reported which are pressure, temperature and liquid and/or vapor composition (P, T and x/y).

For each test, quality factors $F_{test,\ i}$ can be evaluated (range of values between 0.025 to 0.25), resulting in the sum of factors with values, 0.1 to 1. The sum of the four quality factors is 1 when all tests are passed (see Equation 1). For the check of the consistency between the 'end point' of the VLE curve, a quality factor F_{pure} is generated (maximum value =1). Simultaneous use of all five tests provides the opportunity to establish an overall VLE data quality factor, Q_{VLE} obtained for each dataset which indicate the quality of each datasets (see Equation 2).

These quality factors can then be used as weighting factors in the objective function for parameter regression with VLE data. The idea is that when the datasets fails certain tests (while passing others), they are given a lower quality factor. A dataset is considered anomalous when the value of Q is ≤ 0.05. In this work, the average Q_{VLE} obtained for *P, T, x, y* data is 0.83 while for *P, T, x* data is 0.47.

$$F_{test1,max} + F_{test2,max} + F_{test3,max} + F_{test4,max} = 1 \quad (1)$$

$$Q_{VLE} = F_{pure}(F_{test1} + F_{test2} + F_{test3} + F_{test4}), Q_{VLE} \leq 1 \quad (2)$$

Parameter Regression

In this work, the parameter regression is based on the temperature, liquid composition, activity coefficient and pressure (T, x_i, γ_i, P) VLE data and only isothermal data VLE data are used for the regression. The objective function below (Equation 3) have been chosen to regress the parameters which is expressed as the average relative pressure and activity coefficient quadratic deviation.

The overall objective function (OF) used is as follows:

$$OF = \sum_{set} Q_{VLE} \frac{1}{N} \sum_{i=1}^{N} \left[\left(\frac{P_{i,exp} - P_{i,calc}}{P_{i,exp}} \right)^2 + \left(\frac{\gamma_{i,exp} - \gamma_{i,calc}}{\gamma_{i,exp}} \right)^2 \right] \quad (3)$$

where $\gamma_{i,exp}$ and $\gamma_{i,calc}$ is the experimental and calculated activity coefficients, $P_{i,exp}$ and $P_{i,calc}$ is the experimental and calculated pressures and N is the number of experimental data points used for the estimation,

The equilibrium pressures, $P_{i\text{-}calc}$ were calculated in two different ways depending on whether the systems need an association term (such as systems involving carboxylic acids) or not. For systems without association term, the pressure is calculated as follows:

$$P_{i\text{-}calc} = \sum_{i} x_i \gamma_i P_i^{sat} (POY_i) \quad (4)$$

where i is an index running over all species in the mixture and POY_i is the Poynting factor

However, for the systems with organic acids, the equilibrium pressure is calculated using association constant based on the method of Hayden and O'Connell [9]. On the other hand, the the calculated activity coefficients, $\gamma_{i\text{-}calc}$ were calculated using the UNIFAC model with the regressed parameters.

In this work, the atom interactions parameters (AIPs) are regressed in series. Initially, only systems with C-C atom interactions are used for the parameter regression. For this step, a total of 49 data sets of VLE systems. The parameters involved in the regression of AIPs related to C-C interaction are $b_{C\text{-}C}$, $c_{C\text{-}C}$, $d_{C\text{-}C}$, $e_{C\text{-}C}$, $bh_{C\text{-}C}$, $ch_{C\text{-}C}$, $dh_{C\text{-}C}$, $eh_{C\text{-}C}$. Next, systems related to the C-O and O-C atom interactions are used for parameter regression where the AIPs, $b_{C\text{-}O}$, $c_{C\text{-}O}$, $d_{C\text{-}O}$, $e_{C\text{-}O}$, $b_{O\text{-}C}$, $c_{O\text{-}C}$, $d_{O\text{-}C}$, $e_{O\text{-}C}$, $bh_{C\text{-}O}$, $ch_{C\text{-}O}$, $dh_{C\text{-}O}$, $eh_{C\text{-}O}$, $bh_{O\text{-}C}$, $ch_{O\text{-}C}$, $dh_{O\text{-}C}$, $eh_{O\text{-}C}$ are regressed while fixing the AIPs related to the C-C interactions which were regressed earlier. A total of 130 data sets of VLE systems were used.

Following in the next sequence are the systems related to the O-O interactions, where the AIPs, b_{O-O}, c_{O-O}, d_{O-O}, e_{O-O}, bh_{O-O}, ch_{O-O}, dh_{O-O}, eh_{O-O} are regressed while fixing the AIPs related to the C-C, C-O and O-C interactions which were regressed earlier. A total of 36 data sets of VLE systems were used in this step. The regression continued in the same procedure where the parameters related to interactions C-N, O-N, N-N, C-Cl, O-Cl, C-S, O-S and Cl-S were added sequentially. In each step, the previously fitted parameters were fixed. The overall regression procedure are illustrated in Figure 2.

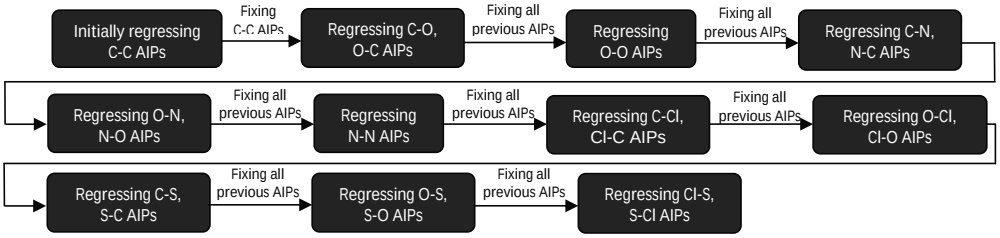

Figure 2: Overall regression procedure for the AIPs regression work

Equilibrium Data

The inputs for the parameter estimation are VLE experimental data (involving C, H, O, N Cl and S atoms) and the statistics of data used in the regression work are summarized in Table 1. For the parameter regression work, a total of 371 VLE datasets with 5707 data points consisting of T, x_i, γ_i, P have been used. Only a moderate amount of experimental data were used because the purpose of the development of the UNIFAC-CI models is to be able to predict phase equilibria with a limited amount of experimental data and without using new experimental data.

Table 1: Statistics and classification of the VLE data used for parameter regression

Types of system	Type of data	No. of data
Hydrocarbons	T, x, γ, P	49
Oxygenated	T, x, γ, P	166
Nitrogenated	T, x, γ, P	28
	T, x, P	30
Chlorinated	T, x, γ, P	41
	T, x, P	35
Sulfurated	T, x, γ, P	14
	T, x, P	3

Correlation Results

The correlation error or deviation between the experimental data and the regressed/predicted values are defined in terms of the average absolute relative deviation (AARD) defined in Equation 5 in the following way:

$$AARD(\%) = \frac{1}{N}\sum_{i=1}^{N}\left|\frac{P_{i\text{-}exp} - P_{i\text{-}calc}}{P_{i\text{-}exp}}\right| ? \ 00 \qquad (5)$$

Using the above expression, the deviation statistics (average AARD %) between Original UNIFAC-CI & Modified (Dortmund) UNIFAC-CI models and their reference models for all the subsystems considered in this work are displayed in Table 2. For the Modified (Dortmund) UNIFAC-CI model, only the parameters with respect to C, O and H atoms related to hydrocarbons and oxygenated systems have been regressed at moment.

Table 2: Correlation results in AARD% for Original UNIFAC-CI and Modified (Dortmund) UNIFAC-CI models and their reference models for all the subsystem considered

	AARD (%)			
System	**Orig. UNIFAC**	**Orig. UNIFAC -CI**	**Mod. (Dort.) UNIFAC**	**Mod. (Dort.) UNIFAC-CI**
COH-systems	6.7	4.7	5.2	6.0
N-systems	8.4	6.1		
Cl-systems	7.1	5.5		
S-systems	9.4	11.3		

From Table 2, we can see that the correlation results obtained for the Original UNIFAC-CI models are acceptable and also lower than that were obtained for the reference Original UNIFAC model except for the sulfurated system where the correlation error for the CI-model is slightly higher with 11.3% compared to 9.4% for the reference model. On the other hand, for the Modified (Dortmund) UNIFAC-CI model, the correlation error obtained for the COH atom related systems is more or less the same as the reference model with 6.0% compared to 5.2 %.

Predictions and Comparisons

In this section, using all the regressed parameters, the performance of the Original UNIFAC-CI and the Modified (Dortmund) UNIFAC-CI models in terms of the prediction accuracies are presented by comparing the phase diagram predicted using the CI-models with the experimental data as well as the predictions made by their respective reference UNIFAC models. Figure 3 shows the VLE phase diagrams using Original UNIFAC

for systems involving Methyl tert-Pentyl Ether-Cyclohexane at 313.15 K and Ethanol-Chloroform at 328.15 K.

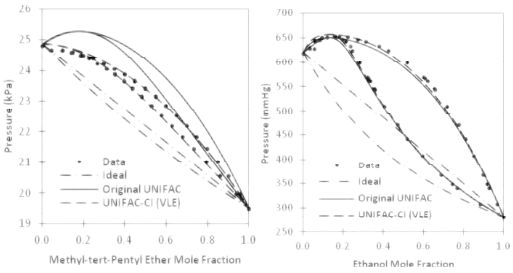

Figure 3: VLE diagrams of systems: (a) Methyl tert-Pentyl Ether-Cyclohexane at 313.15 K (Q_{VLE} =1.00) and (b) Ethanol-Chloroform at 328.15 K (Q_{VLE} =0.86)

From the phase diagrams shown in Figure 3, we can see that in Figure 3 (a), the predictions by the CI-model conforms closely to the experimental data compared to the reference UNIFAC model while in Figure 3 (b), both reference UNIFAC and Original UNIFAC-CI model are in good agreement with the experimental data.

In addition to that, Figure 4 presents the VLE phase diagrams using Modified (Dortmund) UNIFAC for systems involving 2-Methyl-2-Propanol-Ethylbenzene at 313.5 K and Ethanol-Methyl Propionate at 346.30 K.

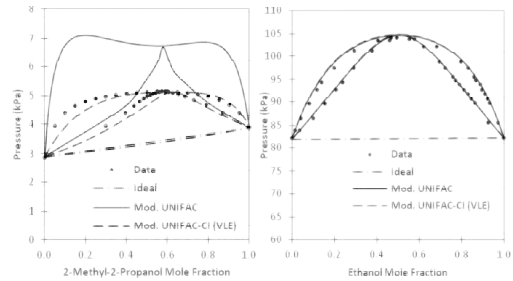

Figure 4: VLE diagrams of systems: (a) 2-Methyl-2-Propanol-Ethylbenzene at 313.5 K (Q_{VLE} =1.00) and (b) Ethanol-Methyl Propionate at 346.30 K (Q_{VLE} =0.59)

In Figure 4 (a), the prediction made by the CI-model is in a very good agreement with the data compared to the reference model. On the other hand, for the Ethanol-Methyl Propionate system, the predictions made by both reference and CI-model are also good and quite close to the experimental data.

Conclusion

The UNIFAC-CI models developed by González et al. [5] are powerful predictive tools which can be used in cases where reference UNIFAC model parameters are missing. In this work, the model parameters are re-estimated using quality factors which are used as weighting factors for each VLE datasets in the objective function to regress the atom interaction parameters (AIPs). The quality factors will determine the quality of each of the VLE data used for the parameter regression. In addition to this work, the parameter regression for the Modified (Dortmund) UNIFAC-CI model will be completed for all five atoms considered and SLE systems will also be added to regress the model parameters in order to improve the UNIFAC-CI model to be able to predict solid-liquid equilibrium (SLE) systems reliably.

Acknowledgement

The author gratefully acknowledges the financial support from the Ministry of Higher Education, Malaysia and Universiti Teknologi Malaysia.

References

1. R. Gani, P. Harper, M. Hostrup, Ind. Eng. Chem. Res. 44 (2005) 7262–7269.
2. J. Marrero, R. Gani, Fluid Phase Equilibr. 183–184 (2001) 183–208.
3. H. Hansen, P. Rasmussen, Aa. Fredenslund, M. Schiller, J. Gmehling, Ind. Eng. Chem. Res. 30 (1991) 2352–2355.
4. L. B. Kier, L. H. Hall, J. Pharm. Sci. 70 (1981) 583– 589.
5. H.E. González, J. Abildskov, R. Gani, P. Rosseaux, B. Le Bert, AIChE J. 53 (6) (2007) 1393–1634.
6. H. E. González, J. Abildskov, R. Gani, Fluid Phase Equilibr. 261 (2007) 199–204.
7. H.E. González, Development of Group Contribution Plus Models for Properties of Organic Chemical Systems, PhD Thesis, Technical University of Denmark, 2009.
8. J.W. Kang, V. Diky, R.D.Chirico, J.W. Magee, C.D. Muzny, I. Abdulgatov, A.F. Kazakov, M. Frenkel, J. Chem. Eng. Data, 55 (2010) 3631-3640.
9. J.G. Hayden, J.P. O'Connell, Ind. Eng. Chem. Process Des. Dev. 14 (1975) 209–216.

List of Publications

1. A.A. Mustaffa, G.M. Kontogeorgis, R. Gani, Fluid Phase Equilibr. 302 (2011) 274–283.
2. C.A. Diaz-Tovar, A.A. Mustaffa, A. Hukkerikar, A. Quaglia, G. Sin, G.M. Kontogeorgis, B. Sarup, R. Gani, ESCAPE 21, Comput. Aided Chem. Eng. 29 (2011) 256-260.
3. C.A. Diaz-Tovar, A.A. Mustaffa, A. Hukkerikar, A. Quaglia, G. Sin, G.M. Kontogeorgis, B. Sarup, R. Gani, ICMSAO 2011, IEEE Xplore, 237-243.

Vikas Narayan
Phone: +45 4525 0361336
E-mail: vina@kt.dtu.dk
Discipline: Reaction and Transport Engineering

Supervisors: Peter Glarborg
Peter Arendt Jensen
Ulrik Birk Henriksen

PhD Study
Started: July 2011
To be completed: May 2014

Ash Chemistry in Circulating Fluidized Bed

Abstract
A Low Temperature Circulating Fluidized Bed System gasifier allows pyrolysis to occur at low temperatures thereby improving the retention of alkali and other elemental species within the system. The aim of the PhD project is to study the behavior of alkali metals and biomass ash in a Low Temperature Circulating Fluidized Bed System. The focus of the study would be ash transformation in the reactor system and bed de-fluidization.

Introduction
Gasification of agro based fuels poses a large potential for power generation in the energy market, with fluidized bed systems being a suitable technology. Agro based fuels however, contain high amounts of alkali metals especially potassium, alkali earth metals like Ca, Cl, and some Si. Alkali metals get volatilized at high temperatures and form salts of low melting points and thus condense on pipelines, reactor surfaces and cause deposition. Fluidized beds using high alkali fuels often de-fluidize and thereby have to be stopped. This brought out a need for an improvement and innovation in the existing fluidized bed technology. The low Temperature Circulating Fluidized Bed Reactor is a solution found in this context. As claimed in previous work [1-3], the gasifier functions without in-situ ash sintering and deposit problems and most potassium and chlorine are simply retained in a separate biomass ash stream. In this way a fuel-gas with low alkali content and a relatively high calorific value is produced that can be used for power production by use of a boiler.

Low Temperature Circulating Fluidized Bed System

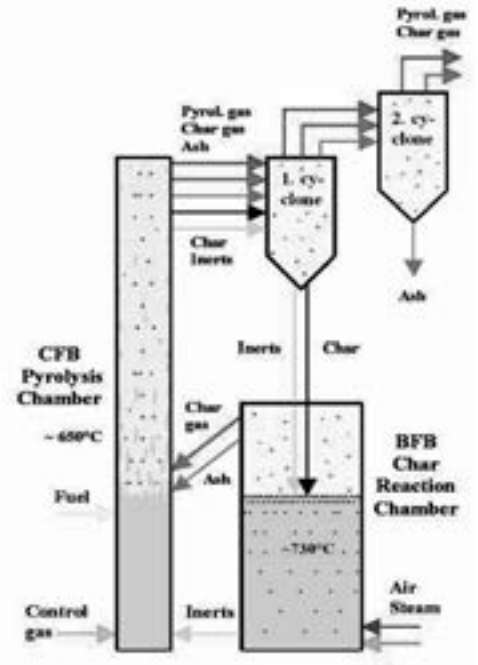

Figure 1: LT-CFB flow diagram [1-3]

As shown in Figure 1, the LT-CFB process consists of two reactors. The biomass fuel enters the first reactor which is the pyrolysis chamber. The fuel is now pyrolysed at around 650^0C due to good thermal contact

with mainly re-circulated sand and ash particles from the other (char) reactor. The heat for the pyrolysis reaction is thus provided by the sand bed particles and hot re-circulated char and ash particles.

The residual char, pyrolysis gases and inert particles are blown upwards to the primary cyclone, which separates char and inert particles to a bubbling bed char reactor. In this reactor, the char is exposed to air to undergo gasification, at typically around 730°C. Some steam or water may also be added in order to improve the conversion of char and limit the reactor temperature. The exit stream out of the pyrolysis chamber has a lower temperature compared to the temperature in the char reactor. Consequently, at most only small amounts of alkali species and similar ash components get carried off with the product gas but are retained in the solid state and can therefore be separated efficiently in the cyclones. Moreover, the relatively low temperatures in the process limit the tendencies of de-fluidization in the system.

Objectives of the PhD Study and present status

The aim of the PhD project is to study the behavior of alkali metals and biomass ash in a Low Temperature Circulating Fluidized Bed System. The focus of the study would be release of alkali from the reactor system, ash transformation and bed defluidization. A literature study was done to understand the probable mechanisms and parameters that affect the release of inorganic elements like alkali. The literature work was also done to understand the mechanisms of agglomeration and defluidization of ash and bed materials. To understand the behavior of alkali and ash in LTCFB reactors, available test data from runs made on a 100 kW plant at Risø and a 6 MW plant at Kalundborg were analysed. A preliminary mass balance was done with the available data to calculate the alkali concentrations in the product gas and the fractions retained in the cyclone ash and bed materials. Test data were available for fuel, cyclone ash and bed materials. The analysis of the product gas was done on an indirect basis based on the mass balance.

Conclusion and Future Work

It was seen from the mass balance analysis that the data was not sufficient enough to provide a good prediction of alkali retention in the system. Based on the above observations, it was therefore suggested to have direct measurements done on the product gas. The main aim of the measurements would be to measure the concentration of K, Na, Cl and S in the exit gas. Based on the results from the above experiments and mass balance, a better analysis and understanding on the state of the alkali and other species in the system could be made. Further work involves the development of a model that describes ash transformation in a LTCFB system. The model would begin with a thermodynamic approach using Fact Sage software.

References

1. P. Stoholm, R.G. Nielsen, The Low Temperature CFB Gasifier-Latest 50 kW Test Results and New 500kW Plant, Proceedings of World Conference and Technology Exhibition on Biomass for Energy and Industry (ISBN), ETA-Florence & WIP-Munich, Rome, 2004.
2. P. Stoholm, R.G. Nielsen, L. Sarbæk, L. Tobiasen, M.W. Fcok, K. Richardt, B. Sander, L. Wolff, U. Henriksen, The Low Temperature CFB Gasifier-Further Test Results and Possible Applications, Proceedings of the European Biomass Conference (ISBN),ETA-Florence & WIP-Munich, pages: 706-709, 2002.
3. P. Stoholm, J. Cramer, J. Krogh, R.G. Nielsen, B. Sander, J. Ahrenfeldt, U. Henriksen, The Low Temperature CFB Gasifier-100 kW_{th} Tests on Straw and new 6 MW_{th} Demonstration Plant, International Biomass Conference, Lyon, 2010.

Tatyana Nesterova
Phone: +45 4525 2848
E-mail: tan@kt.dtu.dk
Discipline: Reaction and Transport Engineering

Supervisors: Søren Kiil
Kim Dam-Johansen

PhD Study
Started: January 2009
To be completed: March 2012

Development of a Self-healing Epoxy-based Anticorrosive Coating

Abstract
Self-healing anticorrosive coatings are the novel and perspective approach to corrosion protection. In this project epoxy-based self-healing coating is being developed. Self-healing is based on incorporation of microcapsules filled with active healing agent which can react when the crack propagates through the coating and ruptures the capsules. Capsules are synthesized, analysed for storage and solvent stability, and stability towards stirring. A model based on Monte-Carlo simulations has been developed for prediction of healing efficiency of microcapsule-based self-healing coatings.

Introduction
Self-healing anticorrosive coatings have become a very intensive field of research in the last decade [1;2]. The potential ability of these coatings to repair microcracks autonomously and thereby restore functionality and prolong coating service life has attracted attention of scientists of many research groups in USA [3;4], China [5;6], India [7] and Europe [8;9]. Various approaches to self-healing of thermoset materials have been proposed in the literature based on different mechanisms triggering the process. Among them is temperature, UV-light, pH, and mechanically induced healing [10;11]. Judging from the number of publications [11] and robustness and versatility of the method, the approach utilizing mechanical stimulus seem to be the most realistic route to truly autonomous self-healing coatings. The method was proposed by S. White [3] and is based on incorporation of microcapsules, filled with reactive chemicals, into a polymer matrix. Microcapsules are spherical, sometimes elongated [8], particles with diameters of 10 – 200 μm depending on the application. They consist of a solid, impermeable polymeric shell and a liquid core, which is a healing material. When a microcrack propagates through the coating, capsules rupture and healing agents are released and react, forming a cross-linked network in the fracture plane. Figure 1 illustrates mechanism of the microcapsule-based approach is illustrated in.

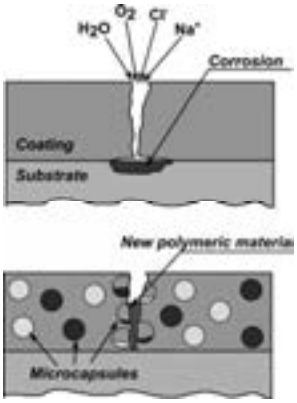

Figure 1. Schematic drawing of a self-healing mechanism in microcapsule-based coatings.

Specific Objectives
This PhD project is dedicated to development of a "smart" anticorrosive coating with a built-in capacity to substantially recover properties - tensile strength and barrier properties after a microcrack has occurred without any manual intervention. The project is divided into 3 parts: preparation of microcapsules, formulation of a coating containing microcapsules, and assessment of the coating's performance.

The first part of the project includes a choice of polymer matrix and materials for encapsulation,

development of experimental procedures, and their optimisation. The objective of this part is to synthesize

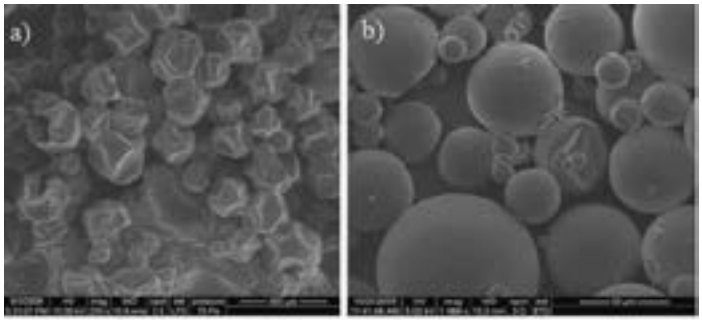

Figure 2. SEM micrographs of microcapsules prepared at the same experimental conditions filled with a) bisphenol A epoxidised resin, b) alkylglycidylether.

microcapsules, which remain intact during coating formulation and application but rupture readily when a coating is damaged, are compatible with the polymer matrix and exhibit good adhesion, are chemically stable, and filled with reagents possessing fast reaction kinetics in an industrially relevant temperature range.

The second part of the project focuses on the coating preparation and has the following objectives: investigation of solvent resistance of the capsules; investigation of microcapsule dispersion (assessment of dispersion quality, microcapsule stability under stirring in viscous medium, need and use of solvents and dispersing agent); estimation of a critical microcapsule volume concentration; formulation and application of a microcapsule-containing anticorrosive coating. At this stage a model for prediction of healing efficiency of microcapsule-based coatings needs to be developed.

The third part of the project deals with investigation of self-healing ability of the formulated coating, as well as with assessment of a coating's performance and its comparison to a coating with pigments or fillers in place of the microcapsules.

Results and Discussion

System chosen

Polyepoxide barrier coating intended for above water heavy duty anticorrosion protection has been chosen as a model system for modification and further investigation. For the maximum materials compatibility with the matrix and cross-linking at the application temperature interval an epoxy-amine pair was considered as a desired self-healing system. The materials of interest were bisphenol A and F epoxidized resins, alkylglycidyl ether (C12-C14) and triglycidyl ether of polyoxypropyleneglycol. Encapsulation of dicyclopentadiene and linseed oil was also performed. Poly(urea-forlmaldehyde) and poly(melamine-urea-formaldehyde), known for cross-linked and insoluble polymer formation, were used as the shell materials to ensure mechanical strength and stability of the capsules.

Preparation of microcapsules

Four out of several microencapsulation methods, proposed in the literature, have been investigated. Each method has been evaluated and compared to the alternatives. The important parameters considered were stability of the microcapsules and ease and time of their preparation. The results of the performed study are described in [12].

Due to difficulties with viscous liquids encapsulation, *poly*(urea-formaldehyde) capsules filled with linseed oil and *poly*(melamine-urea-formaldehyde) microcapsules filled with alkylglycidylether have been prepared and used, as a first approach, in the current investigation as model microcapsules. Figure 2 illustrates the difference in appearance of microcapsules prepared at the same conditions using different core materials: viscous epoxy resin (a) and a very thin diluent (b).

Solvent and storage stability of microcapsules

Xylene has been chosen as a solvent for investigation due to its adequate solvent strength towards shell material and a wide use in heavy duty anticorrosive coatings production. Other solvents such as acetone, tetrahydrofuran, and artificial seawater were used mainly for comparison and for revealing the tendencies.

The study has shown that shells of both kinds of microcapsules did not degrade in xylene during one month exposure. However, degradation was significant after 1 year exposure. Capsules stored in xylene do not show any signs of degradation, capsules stored in tetrahydrofuran are more degraded, and capsules stored in acetone are heavily degraded with very few intact microcapsules seen in the micrograph. Capsules stored in artificial seawater have small dents on their shells probably due to osmotic pressure. Degraded microcapsules show a tendency to agglomeration and have wrinkled shells. If degradation continues, capsules lose their spherical form and only the shells or even their fragments can be observed in the sample. Although no investigation of solvent resistance of linseed oil or tung oil-filled microcapsules was found in the literature [7;13;14], a stability study of *poly*(urea-formaldehyde)

microcapsules performed by Tong et al. [15] revealed similar behavior of microcapsule shells, being introduced to acetone, ethanol and "solutions with strong pH value". Yuan et al. has demonstrated degradation of *poly*(urea-formaldehyde) shell and diffusion of epoxy resin core material from microcapsules exposed to acetone more than 1 day [6].

Observation of microcapsules stored in dry form after syntheses, in closed jars, has revealed that *poly*(urea-formaldehyde) capsules filled with linseed oil get oxidized with time (after approximately 3 month they change color from yellow to reddish) and even form firm lumps of the microcapsules, which are "glued" together perhaps by released and polymerized linseed oil. Figure 3 shows the difference in appearance of freshly made microcapsules and microcapsules stored 1.5 year. *Poly*(urea-melamine-formaldehyde) microcapsules filled with alkylglycidylether did not show any signs of degradation after two years of storage at the same conditions.

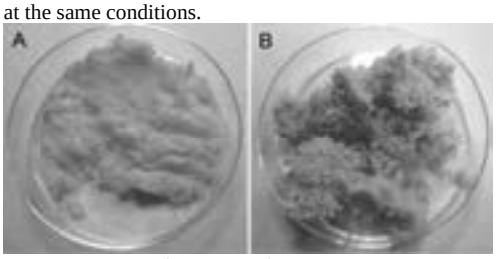

Figure 3. Photos of *poly*(urea-formaldehyde) linseed oil-filled microcapsules A) stored 3 weeks after the synthesis and B) stored 1.5 year.

Dispersion of microcapsules

In the available literature sources, dispersion of microcapsules has been conducted using laboratory mechanical stirrers and applying very low stirring rate – 200 rpm [7;14]. In this study an industrial disperser with a minimal stirring rate of 550 rpm was used. A stirring rate of 1100 rpm was also applied.

During the dispersion stage the most drastic decrease in number of intact linseed oil-filled capsules was observed during the first 5 minutes of stirring in undiluted epoxy resin. Figure 4 gives a visual comparison of the quantity of intact capsules in the sample before and after stirring in undiluted epoxy is given. Addition of 20 wt % solvent to the epoxy resin allowed the majority of microcapsules to stay intact 30 minutes under 550 rpm stirring rate. This confirmed that the lower viscosity (0.2 kg/(m·s) compared to 1.5 kg/(m·s) of undiluted epoxy) and therefore the lower share rate was more favorable for the microcapsule stability. During dispersion of microcapsules under the high stirring rate (1100 rpm) some capsules were damaged even in the diluted (20 wt %), low viscous sample. Eventually, 10 wt % solvent concentration and 550 rpm stirring rate were found to provide optimal conditions for dispersion of the capsules in the binder.

The investigation has shown that dispersion of linseed-oil filled microcapsules, if capsules are produced in a good quality (free flowing powder that does not contain polymer particles) is very straightforward and can actually be done in the lab just by using a spatula and not a high stirring rate disperser. Meanwhile, if the microcapsules form a somewhat denser product, due to polymer nanoparticles formed in the synthesis [12], then stirring time of minimum 20 minutes was found as sufficient for breaking agglomerates without addition of dispersion agents. Moreover, it has to be pointed out that large (dimensions of a few millimeters) polymer particles, which are also formed in the synthesis, or microcapsule lumps formed during storage, could not be dispersed in the binder even after 1 hour of vigorous agitation. This sets additional requirements to synthesis, separation, and storage of microcapsules. It has also been found that capsules with *poly*(melamine-urea-formaldehyde) possess superior strength compared to *poly*(urea-formaldehyde) capsules and can be dispersed in undiluted binder.

Modeling

A model based on Monte-Carlo simulations has been developed for prediction of healing efficiency of a microcapsule-based anticorrosive coating. The model is based on assumption that when crack is formed in the coating, free volume is formed and need to be filled with a healing agent released from the ruptured microcapsules. Thus, the model takes into account volume of the crack formed, its geometry and linear dimensions, as well as diameter, volume concentration and shell wall thickness of the microcapsules, embedded in the coating. All these parameters are variable, and finding of dimensions of the crack which can be healed, optimal concentration and diameter values is possible.

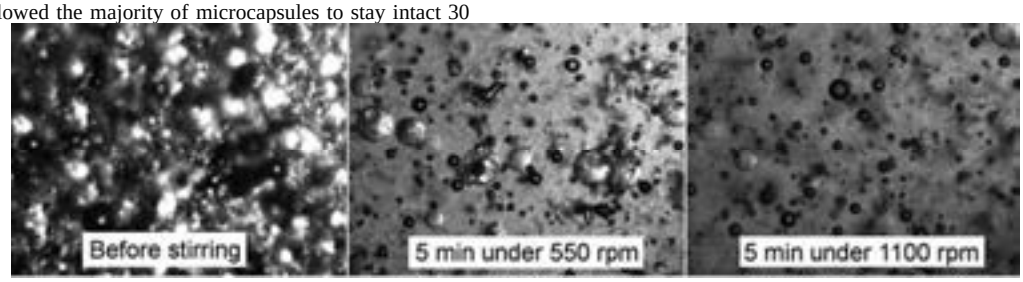

Figure 4. Optical microscopy images of undiluted epoxy resin, containing *poly*(urea-formaldehyde) linseed oil-filled microcapsules before and after stirring. 5x magnification.

It found that there is a clear distinction between healing small and large cracks. Thus, maximum healing of small microcrack can be achieved even at low concentration of microcapsules if they have an optimal diameter. Healing of large cracks progresses with diameter and concentration and is only dependent on the amount of healing agent available in the coating. Figure 5 shows the graphs of dependence of healing efficiency (defined as a ratio of the volume released from the capsules to the volume formed due to the crack) on diameter of microcapsules obtained for the crack dimensions A 100x50x26 mkm and B 1000x200x26 mkm.

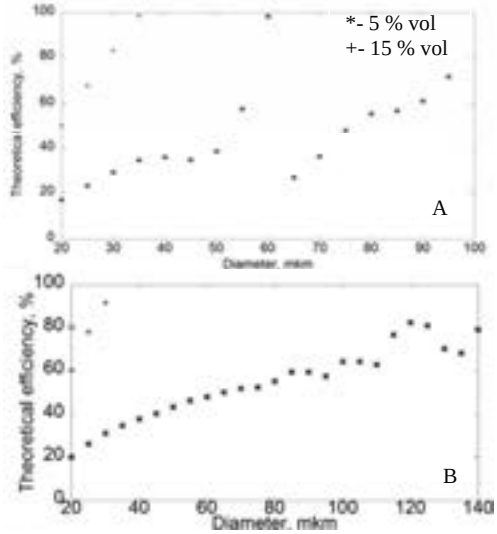

Figure 5. Graphs of dependence of healing efficiency on diameter of microcapsules for small (A) and large (B) cracks.

Conclusions

A prototype of microcapsules filled with reactive healants has been synthesized and studied for storage solvent and dispersion stability. It was shown that both poly(urea-formaldehyde) and poly(melamine–urea-formaldehyde) microcapsules retained integrity of their shells during one month storage in xylene. Meanwhile, stability towards stirring in viscous medium was considerably higher for poly(melamine-urea-formaldehyde) capsules. Furthermore, it was shown that both kinds of microcapsules remain intact when viscosity of the epoxy resin was adjusted to an optimal value. The model for prediction of healing efficiency has been also developed.

Further work

Further investigations will be dedicated to a study of microcapsule performance and assessment of the capsules' influence on coating properties and to attempts to go from the prototype core materials to more relevant healing agents. Critical capsule volume concentration will also be determined. Subsequently, a coating, containing microcapsules, will undergo adhesion and mechanical strength tests, and finally self-healing ability of the coating will be assessed.

References

1. D.Y. Wu, S. Meure, D. Solomon, Prog. Polym. Sci. 33 (2008) 479-522.
2. P.A. Sørensen, S. Kiil, K. Dam-Johansen, C.E. Weinell. J. Coat. Technol. Res. 6 (2) (2009) 135-176.
3. S.S. White, N.R. Sottos, P.H. Geubelle, J.S. Moore, M.R. Kessler, S.R. Sriram, E.N. Brown, S. Viswanathan, Nature 409 (2001) 794-797.
4. A. Kumar, L.D. Stephenson, J.N. Murray, Prog. Org. Coat. 55 (2006) 244-253.
5. T. Yin, M.Z. Rong, M.Q. Zhang, G.C. Yang, Compos. Sci. Technol. 67 (2007) 201-212.
6. L. Yuan, A. Gu, G. Liang, Mater. Chem. Phys. 110 (2008) 417-425.
7. K. Suryanarayana, R. Chowdoji, D. Kumar, Prog. Org. Coat. 63 (2008) 72-78.
8. S.D. Mookhoek, 2010. Novel routes to liquid-based self-healing polymer systems. Ph.D. Thesis. Delft University of Technology, Delft. 165 pp.
9. D.G. Shchukin, H. Moehwald, Small, 3 (6) (2007) 926-943.
10. W. Feng, S.H. Patel, M-Y. Young, J.L. Zunino III, M. Xanthos, Adv. Polym. Tech. 26 (1) (2007)1-13.
11. E.B. Murphy, F. Wudl, Prog. Polym. Sci. 35 (2010) 223-251.
12. T. Nesterova, K. Dam-Johansen, S.Kiil, Prog. Org. Coat. 70 (2011) 342-352.
13. R.S. Jadhav, D.G. Hundiwale, P.P. Mahulikar, J. Appl. Polym. Sci. 119 (2011) 2911-2916.
14. M. Samadzadeh, S.H. Boura, M. Peikari, A. Ashrafi, M. Kasiriha, Prog. Org. Coat. 70 (2011) 383-387.
15. X.M. Tong, T. Zhang, M.Z. Yang, Q. Zhang. Colloid. Surface. A. 371 (2010) 91–97.

Mads Møller Nielsen
Phone: +45 4525 6819
E-mail: mon@kt.dtu.dk
Discipline: Polymer Technology

Supervisors: Søren Hvilsted
Katja Jankova

PhD Study
Started: March 2010
To be completed: February 2013

Tailoring Proton Exchange Membranes for Fuel Cells

Abstract
Two strategies toward improved macromolecular architectures for use as proton conducting membranes in fuel cells are pursued. I) A hydrocarbon system based on a modified polysulfone with various side chains, introduced by copper (I) catalyzed azide-alkyne "click" chemistry. Solvent casting gave flexible, transparent films exhibiting water uptake and IEC values in the same range as Nafion®. With short, linear side chains the proton conductivities were low, however this synthetic procedure looks promising since all sorts of structures can be tailored from the same backbone. II) A partially fluorinated system consisting of fully sulfonated P(VDF-*co*-CTFE)-*g*-sPS/PVDF blends. At water uptakes of 25-40% (IEC=0.60-0.75 mmol/g) the proton conductivity was 48-51 mS/cm.

Introduction
The commercial breakthrough of low temperature Fuel Cells (FC) is closer now than ever. FC powered buses were operated during the 2010 Winter Olympics in Whistler, BC, cars are already available for lease, and commercial launch is planned to start in 2015 [1]. The main challenge at this point is the cost. FC's are highly reliable, efficient and they are environmentally friendly compared to today's electrical power generation from fossil fuels. Besides for transportation there are FC's targeted stationary and portable purposes. The focus of this project is low temperature FC's as a potential substitute for the diesel engine, which is limited by the Carnot cycle (the highest conversion of chemical to electrical energy obtained so far is 54.4%[1]). FC's do not have this restriction, which opens up for an enormous potential. The system described here is the hydrogen fuelled Proton Exchange Membrane (PEM) FC, which typically is operated at 60-80 °C. With hydrogen being the fuel PEMFC has the advantage that water is the sole waste product, as the cell reaction shows:

$$Anode: \quad H_2 \rightarrow 2\,H^+ + 2\,e^-$$
$$Cathode: \quad 1/2\,O_2 + 2\,e^- \rightarrow O^{2-}$$
$$Cell\ reaction: \quad H_2 + 1/2\,O_2 \rightarrow H_2O$$

Figure 1 illustrates how PEMFC works. Hydrogen enters via a bipolar plate toward the anode whilst oxygen enters via a bipolar plate toward the cathode. Electrons run from the anode to the cathode, thereby converting chemical energy to electric power. Simultaneously the protons migrate through virtual (water) channels in the PEM towards the cathode, where they combine with oxygen ions and form water. The half-cell reactions take place in a porous carbon supported platinum electrode and Gas Diffusion Layer (GDL). The electrodes, GDL and PEM are typically pre-assembled into a Membrane Electrode Assembly (MEA) prior to insertion in the FC.

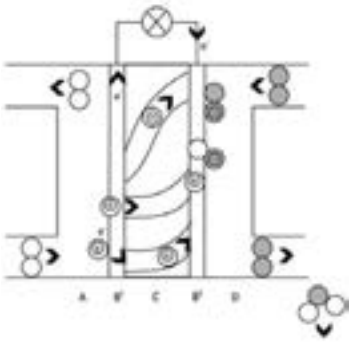

Figure 1: Simplified illustration of a PEMFC. A) H_2 inlet, B) GDL+catalyst, C) PEM, D) O_2 inlet & H_2O outlet. Grey circle=oxygen; White circle=hydrogen.

Each cell typically produces a voltage of 0.5-1.0 V so multiple cells are arranged in stacks to obtain higher voltages. PEMFC was invented in the 1950s and

[1] Obtained by the low-speed diesel engine MAN S80ME-C7.

became known to the general public in the 1960s due to its role in the US space program, where it was developed to supply electricity and drinking water for the astronauts. Since then the individual components have been optimized, but the basic principle remains the same. Also, the chemical structure of the preferred PEM is still a PerFluoroSulfonic Acid (PFSA) polymer, e.g. the current benchmark Nafion® shown in Figure 2. A step in lowering the cost of PEMFC's is to find an economically more feasible alternative to Nafion®[2], preferably with a higher glass transition temperature (T_g(Nafion® 117)=80-130 °C [2]). Nafion® consists of a hydrophobic backbone with flexible side chains with a hydrophilic, proton conducting $-SO_3H$ in the end. The phase separation of hydrophobic and hydrophilic domains is key to proton conductivity.

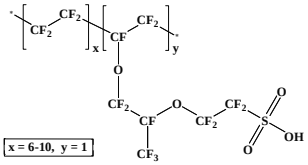

Figure 2: Nafion® is the benchmark PFSA polymer.

The exact mechanisms of proton transport in PEM are not fully understood but the general perception is that there are two contributors: 1) proton hopping, where protons are exchanged between adjacent sulfonic acid groups, and 2) the vehicle mechanism, where protons are moving between water molecules [3]. Different architectures have been investigated over the years, including PFSA's with different side chains and lengths thereof, partially sulfonated polymers and non-fluorous polymers. Examples of structures comprise directly sulfonated backbones [4], block copolymers [5] and graft copolymers [6-8].

Three key parameters in the characterization of the films are described in the following. Membrane swelling is characterized by Water Uptake (WU) (wt%), which is measured as water content in the wet membrane divided by the dry weight of the membrane:

$$WU = \frac{m_{wet\ membrane} - m_{dry\ membrane}}{m_{dry\ membrane}}$$

Ion Exchange Capacity (IEC) is a measure of the content of ion conducting groups in the membrane (mmol $-SO_3H$/g dry membrane). It is determined by titration of the protonated, wet membranes with NaOH:

$$IEC = \frac{c_{NaOH} \cdot V_{NaOH}}{m_{dry\ membrane}}$$

Proton conductivity, σ_i, is measured by AC impedance spectroscopy as thickness of the membrane, l_e, divided by the product of the uncompensated resistance, R_u, and the cross-sectional area of the membrane, A [9]:

$$\sigma_i = \frac{l_e}{R_u A}$$

Two approaches are presented here. The first is a hydrocarbon system based on a commercially available polysulfone (PSU) (T_g=190 °C) backbone with short side chains introduced by copper (I) catalyzed Azide-Alkyne Cycloaddition (CuAAC or "click") reaction [10]. The second approach is based on previous work on a partially sulfonated poly(vinylidene difluoride-*co*-chlorotrifluoroethylene)-*g*-polystyrene (P(VDF-*co*-CTFE)-*g*-sPS) by Holdcroft et al.[3] [6-8]. High IEC values were obtained and still the polymer did not dissolve when immersed in water, which is important for fuel cell membranes. Further, Wide Angle X-ray Scattering (WAXS) studies showed that the presence of unsulfonated PS did not contribute to the crystallinity of the copolymer [8]. Hence the intention, as presented here, was to complete the sulfonation of the same system at three different lengths of side chains. To compensate for the resulting increase in hydrophilicity (and thus water swelling) the grafts are blended with PVDF of high molecular weight to increase the crystallinity and the entanglement [8]. Two different blend ratios of each side chain length are investigated to obtain different ionic contents.

Specific Objectives

The guideline in this project is the application of synthetic strategies that are new in the context of macromolecular PEM architectures. The frames of investigation comprise small-scale lab syntheses, compound characterization and basic membrane testing (water swelling, proton conductivity etc.), aiming at scale-up for test in a single fuel cell.

Results and Discussion

The synthetic pathway of the hydrocarbon system is shown in Figure 3. The starting material, PSU, **I**, is modified with a benzoyl chloride to give **II**. Three different batches with different targeted degrees of substitution (DS=25%, 54% and 67%) were prepared. The samples are named as structure number followed by DS. **II** of each DS had the chlorine exchanged by an azide and became **III**. The syntheses of terminal alkyne/sulfonic acid structures **V** and **VI** are shown in Figure 4. These were "clicked" onto the azide group to give **IV** (Figure 3). All reactions were followed by ^{1}H NMR and FT-IR. A full attribution of the protons of **VI67** is provided in Figure 5. An overlay of IR spectra of **II67** through **IV67** is provided in Figure 6. The most characteristic peaks are $-N_3$ at 2096 cm^{-1} for **III** and the SO_2 of the acid at 1044 cm^{-1} for **IV**. Application of the "click" reaction in PEM's has shown its potential from a

[2] Nafion®, a product developed by DuPont, costs around 500 \$/m^2 in 2011. Nafion 117 (the number refers to the membrane thickness) that is used here is approximately 210-230 μm thick when fully wetted.

[3] Work on the blend project was performed August-December 2011 at Simon Fraser University under the supervision of Professor Steven Holdcroft.

synthetic point of view. The often quantitative yields enable a control of even more complex structures, i.e. well defined architectures and sulfonic acid content, leaving no unreacted functional groups.

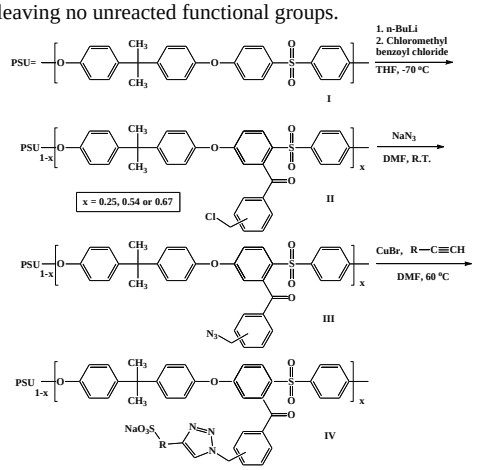

Figure 3: Synthetic pathway for the PSU based system.

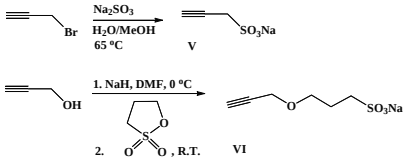

Figure 4: Synthesis of prop-2-yne-1-sulfonic acid and 3-(prop-2-ynyloxy)propane-1-sulfonate.

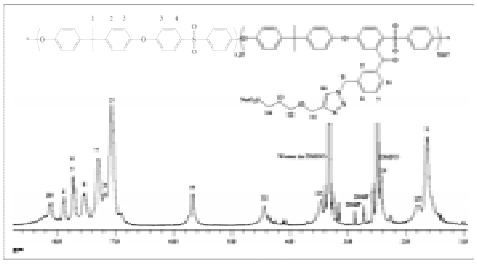

Figure 5: ^{1}H NMR spectrum of **VI67**.

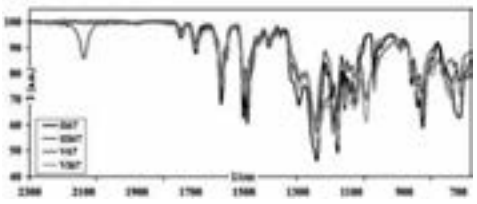

Figure 6: IR spectra of **II67**, **III67**, **V67** and **VI67**.

Flexible, transparent films of **IV** were cast from dimethyl sulfoxide (DMSO) at 50 °C. In some cases the edges were darker and more brittle than the center of the films, hypothesizing an undesired macro phase separation of the hydrophilic and hydrophobic domains. Preliminary IEC values and proton conductivities were lower than expected from ^{1}H NMR and IR, which suggests that there is a need for an optimization of the film casting.

Previously partially sulfonated P(VDF-*co*-CTFE)-*g*-sPS with a graft density (GD) of 2.6% and degrees of polymerization (DP) of 39, 62 and 79 (referred to as Short, Medium and Long or S, M and L) [8] were sulfonated to completion over 24 hours with the reaction conditions shown in Figure 7. ^{1}H NMR confirmed the full substitution of protons in the para position of the aromatic ring with sulfonic acid. The purified material was dissolved in dimethyl acetamide (DMAc) and homogeneous films were cast at room temperature (RT) on a leveled Teflon sheet. WU, IEC and proton conductivity were investigated. When immersed in water the pure graft copolymers with GD=2.6% visibly swelled tremendously. Long and Medium length side chains even partially dissolved. Therefore three blends of the GD=2.6% series were prepared: S blend 1, M blend 1 and L blend 1. The "1" refers to their targeted volumetric sPS contents that are equivalent to a fully sulfonated P(VDF-*co*-CTFE)-*g*-sPS with GD=1.1% and DP=24 (referred to as GD=1.1%). The blends were prepared by mixing with PVDF and film casting under the same conditions as those of the pure graft copolymers. A second blend series with half the graft copolymer content was made: S blend 0.5, M blend 0.5 and L blend 0.5 - hence the suffix "0.5".

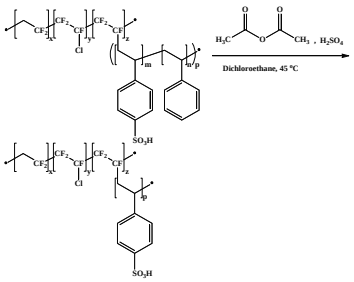

Figure 7: Sulfonation of partially sulfonated P(VDF-*co*-CTFE)-*g*-sPS.

Water uptake is plotted against IEC in Figure 8. IEC values of the first blend series are 1.12-1.31 mmol/g, i.e. in the targeted range of GD=1.1% (IEC=1.10 mmol/g) and WU is lowered relative to this reference pure graft copolymer from 192% to 66-98%. WU is high compared to Nafion (WU=25% at IEC=0.89 mmol/g) but IEC is also higher. WU vs. IEC typically follows a linear trend, for the second blend series at IEC=0.60-0.75 mmol/g, WU was 25-40%, i.e. a level of swelling that is comparable with Nafion®. There was no trend in graft length-dependency of WU in the blends.

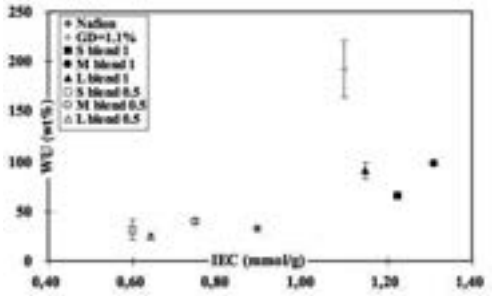

Figure 8: Water uptake vs. IEC.

Proton conductivity (measured under fully humidified conditions at RT) is plotted against IEC in Figure 9. The blend series having IEC values in the same range as GD=1.1% showed higher proton conductivities for all three side chain lengths: 62-63 mS/cm compared to 46 mS/cm. Hence blending both decreases swelling and improves proton conductivity. The pure graft copolymer content in the "0.5" blend series is half that in the "1" blend series but proton conductivities were as high as 48-51 mS/cm, i.e. only slightly lower and still higher than GD=1.1%. This suggests that the proton conducting groups in blend membranes with higher PVDF content are more effective. There seems to be no clear trend in the effect of the DP of the graft copolymer in the blends, but rather trends within each group of blends. WAXS data supported the explanation that the properties are improved due to three factors: increased hydrophobic domains, increased entanglement and increased crystallinity, which is consistent with previous experience [8].

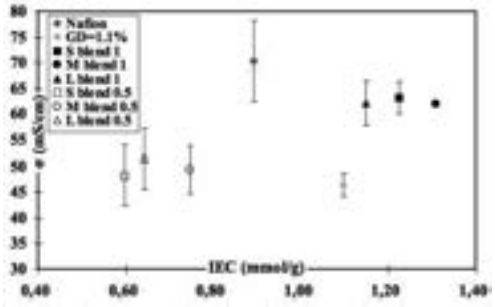

Figure 9: Proton conductivity vs. IEC.

Conclusions

Two strategies toward improved macromolecular architectures for use in PEMFC were pursued. In the first, two different short side chains were attached to a modified polysulfone by "click" chemistry. Overall the products were good film formers, however smaller inhomogeneities might explain why preliminary IEC values and proton conductivities were lower than expected from ^{1}H NMR and IR. This suggests a need for optimized film casting. Yet, the synthetic approach has shown its great potential as a way to obtain a wide variety of polysulfone based structures. The second strategy proved how water swelling of a fully sulfonated P(VDF-*co*-CTFE)-*g*-sPS was reduced by blending with high molecular weight, crystalline PVDF. Further, proton conductivity was improved; Blends with IEC=1.12-1.31 mmol/g reached WU=66-98% and σ=62-63 mS/cm compared to WU=192% and σ=46 mS/cm obtained for a pure graft copolymer with IEC=1.10 mmol/g. Decreasing the IEC value by blending to 0.60-0.75 mmol/g gave in WU=25-40% and conductivities of 48-51 mS/cm, i.e. more effective proton conductivity of the sulfonic acid groups. There was no apparent difference between the three different chain lengths when the volume ratio of sPS to PVDF was kept constant.

Acknowledgements

S. Takamuku, Lund University (LU) and I. Dimitrov, DTU are acknowledged for their cooperation on the hydrocarbon system. A. C. C. Yang, Simon Fraser University (SFU) is acknowledged for her contributions to the blend system. R. Narimani, SFU is acknowledged for performing WAXS. For financial support the Danish Council for Strategic Research is acknowledged, and the partners on contract no. 09-065198 at University of Southern Denmark, LU and IRD A/S are acknowledged for useful discussions.

References

1. Various authors, The Fuel Cell Today Industry Review 2011, www.fuelcelltoday.com, 29.11.11.
2. F. Bauer, M. Willert-Porada, J. Membr. Sci. 233 (2004) 141-149.
3. T. Ueki, M. Watanabe, Macromolecules 41 (2008) 3739-3749.
4. B. Lafitte, P. Jannasch, Macromol. Rapid Commun. 26 (2005) 1464-1468.
5. Y.A. Elabd, M. Hickner, Macromolecules 44 (2011) 1-11.
6. E.M.W. Tsang, Z. Zhang, Z. Shi, T. Soboleva, S. Holdcroft, J. Am. Chem. Soc. 129 (2007) 15106-15107.
7. E.M.W. Tsang, Z. Zhang, A.C.C. Yang, Z. Shi, T.J. Peckham, R. Narimani, B.J. Frisken, S. Holdcroft, Macromolecules 42 (2009) 9467-9480.
8. A.C.C. Yang, R. Narimani, B.J. Frisken, S. Holdcroft, unpublished.
9. A. Parthasarathy, B. Davé, S. Srinivasan, A.J. Appleby, J. Electrochem. Soc. 136 (6) (1992) 1634-1641.
10. W.H. Binder, R. Sachsenhofer, Macromol. Rapid Commun. 28 (2007) 15-54.

Kristian Petersen Nørgaard
Phone: +45 4525 2922
E-mail: kpno@kt.dtu.dk
Discipline: Reaction and Transport Engineering

Supervisors: Søren Kiil
Kim Dam-Johansen
Pere Català, Hempel A/S

PhD Study
Started: January 2011
To be completed: December 2013

Design and Testing of Robust and Efficient Intumescent Coatings

Abstract
An ever present concern when using steel as load bearing elements in buildings is the significant loss of mechanical stability at temperatures above 500 ^{o}C, during a fire. An efficient method to protect the steel structures is the use of fire protective intumescent coatings. Intumescent coatings swell and form a thermally insulating char when exposed to sufficiently high temperatures. In this Ph.D. project the mechanisms of a selected intumescent system are investigated. The main focus is on how outer parameters, such as heating rate or gas composition, affect the performance of the selected coating system. Ultimately, this investigation will give a better basis for fast development of coatings.

Introduction
Exposed to the elevated temperatures of a fire the mechanical strength of steel is reduced significantly; hence collapse of the structure with potential loss of lifes or assets is an imminent danger. Therefore thermal insulation of load bearing steel structures is important. A space saving and efficient fireproofing method is intumescent coatings. Intumescent coatings swell when exposed to elevated temperatures and form a thermally insulating char. The swelling occurs through a complex reaction sequence where the binder polymer melts to a thick viscous liquid, gasses are released and subsequently a solid porous char is formed. At higher temperatures the char will start to degrade [1, 2]. When intumescent coatings are marketed, they need to be approved by various institutions, e.g. Underwriters Laboratories and British Standards. Although these institutions use well defined heating- and heat flux-curves, external factors such as radiation, shielding by other building elements and turbulence may cause significant variations in the severity of the fire environment. Also in practical applications of the coatings, special situations may arise, where the coating is exposed to extremely fast heating may happen. Therefore one focus in this project is to investigate the influence of a very fast heating rate, “shock heating”, where the temperature is increased very rapidly. The use of very fast heating rate is important to simulate so-called hydrocarbon fires which are known from oil and gas industry. But also for slower developing fires, so-called cellulosic fires typically occurring inside buildings, a fast heating rate may occur for instance if the formed char is damaged by a falling object or a door which opens fast. An example of such a situation is illustrated in Figure 1 where the picture to the left shows the situation before the object falls and the picture to the right shows the situation following the object has fallen.

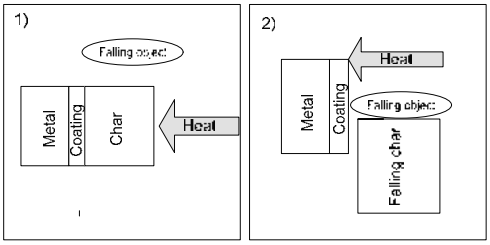

Figure 1. Illustration of the special case where the char is damaged due to a falling object.

Specific Objectives
In this Ph.D. project a selected intumescent coating is used to investigate how variations in external parameters, e.g. heating rate, temperature or gas composition affect the performance of the coating. Based on the results it is intended to setup a model that can help predicting the performance of a coating tested by a third party organization.

Results and discussion
To obtain the fast heating rate, the samples were inserted into a muffle oven (Nabertherm LVT 5/11/180)

under atmospheric air. By insertion of the sample into the oven, the temperature increases from 900 ^{o}C to 1100 ^{o}C in 5 minutes. Circular samples with a diameter of 10 mm and dry film thicknesses of 147 and 598 µm were heated using the in cylindrical alsint crucibles from W. Haldenwagner. The height and inner diameter of the crucible were 40 mm and 26 mm, respectively.

Following the fast heating a TA XT plus – Texture analyzer from Stable Microsystems was used to measure the maximum vertical expansion and the work necessary to compress the samples after heating. A cylindrical piston with a diameter of (2 mm) was set to move at a constant speed of 0.1 mm/s and 500 data points were recorded per second.

An illustration of the Texture Analyzer is seen in Figure 2.

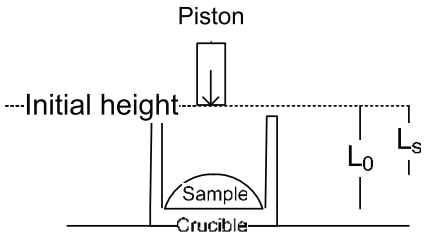

Figure 2. Drawing of Texture Analyzer. L_0 is the distance from the bottom and L_s is the height of the sample. The height of the sample is the difference between L_s and L_0.

Samples with two different dry film thicknesses, 147 and 598 µm, were heated under the conditions previously described. The results are summarized in Table 1. All results shown in Table 1 are measured at the highest vertical point of the char. Two repetitions of were made for each sample. An expansion factor defined as the final height divided with the initial height is shown. From the table it is seen that this expansion factor appear independent of the initial film thickness, whereas the residual mass is somewhat affected by the initial film thickness. Table 1 also shows the work which is necessary to reach 1 mm into the sample. The deviation of the mechanical resistance show large deviations between the samples.

Table 1. Vertical expansion factor, residual mass fraction and work to move the piston 1 mm into the char.

Coating sample	DFT [mm]	Expansion factor [-]	Residual mass fraction [%]	Work for 1 mm [mJ]
C1	0.147	21.8±2.7	31.8±0.1	0.03±0.02
C2	0.598	20.9±0.3	36.1±0.1	0.05±0.04

Discussion and conclusive remarks

From the results it is seen that the initial film thickness of the coating affects the residual mass fraction of the coating, but not the expansion. From other results it has been found that the measured work of destruction is dependent on the horizontal position of the coating. This is interesting to notice because it shows that there is not a direct correlation between expansion factor and the mechanical resistance to compression, as would be expected [3].

Acknowledgments

Financial support by J.C. Hempel's Foundation is gratefully acknowledged. The authors wish to thank Peter Stubbe and Heidi Olander Petersen from DTU FOOD for their help with the compression measurements.

References

1. K.M. Butler, Physical Modeling of intumescent fire retardant polymers. in Polymer Foams: Science Technology, Ch. 15, ASC symp., Ser. 669, ASC Book.
2. B.K. Kandola, A.R. Horrocks, Polym. Degradation Stab. 54 (1996) 289-303.
3. E.D. Weil, J. Fire. Sci, 29 (6) (2011), 259-296

List of Publication

1. Abstract for "European Coatings conference – Fire retardant coatings", Berlin, 13th and 14th of March 2012. Has been accepted for oral presentation. https://www.european-coatings.com/Events/Fire-retardant-coatings.

Linda Nørskov
Phone: +45 4525 2952
E-mail: lin@kt.dtu.dk
Discipline: Reaction and Transport Engineering

Supervisors: Kim Dam-Johansen
Peter Glarborg
Peter Arendt Jensen
Morten Boberg Larsen, FLSmidth A/S

Industrial PhD Study
Started: January 2009
To be completed: July 2012

Fuel Flexible Burners for Cement and Mineral Industry

Abstract
In cement production there is an increasing environmental and financial motivation for substituting fossil fuels with alternative fuels; waste and biomass. The alternative fuels introduce new challenges in the combustion processes. The present Industrial PhD project focuses on combustion of alternative fuels in the cement rotary kiln burner. An experimental setup for simulating combustion of large suspended particles in a flame has been built for studies of combustion characteristics and conversion paths of the new fuels. Initial results of the combustion simulation are presented for dried sewage sludge which is a possible alternative fuel in cement industry. A simplified devolatilisation model for dried sewage sludge based on heat transfer and devolatilisation kinetics is presented.

Introduction
Alternative fuels are combustible waste-derived products or biomass that can replace traditionally fossil fuels for heat and energy generation. Cement production requires a high thermal energy input for raw material calcination and clinker formation. During the last 20-30years an increasingly amount of fossil fuels have been replaced by alternative fuels, motivated by the following reasons:

- Low fuel cost.
- The alternative fuels may be partly or fully CO2-neutral.
- Waste disposal problems can be solved as waste is utilised as energy and the ash residue is incorporated into the product.
- The fossil fuel resources are saved.

In cement production a suspension fired burner positioned in a rotary kiln provides the thermal energy for cement clinker reactions. The limiting parameter for maximising the substitution of fossil fuels with alternative fuels in the rotary kiln burner is not known to a sufficient degree. The limiting parameter may differ from one type of alternative fuel to another and from one cement production plant to another. At present, limited systematic knowledge about the alternative fuels combustion properties and their influence on the flame formation is available, and industrial introduction of new fuels is often based on trial-and-error and practical experiences.

Specific Objectives
The objective of the present PhD project is to develop a novel scientific framework for effective utilisation of alternative fuels in the main burner of cement and mineral rotary kilns.
The success criteria in the project are identified to be;

1. Develop simplified mathematical modelling tools for evaluating alternative fuels based on knowledge of their physical and chemical properties.
2. Verify model predictions from experimental data on pilot and/or full-scale.
3. Evaluate the influence of alternative fuel properties on flame formation, fuel burn-out, and heat transfer in the rotary kiln burner.
4. Evaluate the effect of fuel properties on clinker product quality, and production stability.
5. Provide recommendations for optimised use of alternative fuels in the kiln burner.

In the present yearbook contribution only a part of the work in the PhD project will be presented. A novel experimental combustion reactor and results obtained herein will be described for dried sewage sludge as an alternative fuel in cement industry.

Experimental - Combustion Simulation
A novel combustion reactor has been designed and built at CHEC Research Centre for simulating combustion of larger single fuel particles (>1mm) in suspension in a well-defined environment of gas temperature, gas flow velocity and O_2 concentrations.
The information gained from the setup is

- Time for ignition, devolatilisation, and char oxidation
- Fuel particle conversion pathway and shape changes during the combustion stages

The setup addresses especially alternative fuels which typically have larger particles sizes than traditional fossil fuels due to cost of downsizing. The larger fuel particle may not be suitable for studies in a drop reactor or entrained flow reactor requiring pulverised fuel.

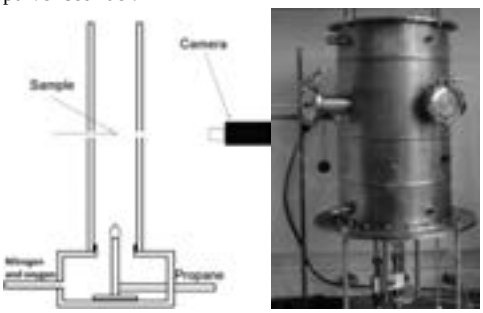

Figure 1 Experimental setup for single particle combustion.

The experimental setup and the schematics are seen in figure 1. The reactor is an insulated ceramic tube with four insertion ports positioned above a gas burner. A fuel particle is held by a platinum wire and inserted into a flow of hot gases provided by a propane flame. The fuel particle will undergo heating, devolatilisation, and char oxidation. The reactions and conversion are recorded by means of a high speed camera. To inhibit premature heating and reaction of the particle during insertion the particle is inserted into a ceramic tube introduced oppositely which shields the particle from the hot environment until positioned in the centre of the reactor in focus of the camera.

Further development of the setup is planned to improve the accuracy of the determination of the duration of the combustion reactions. The setup will be equipped with a gas analysis probe positioned above the combusting fuel particle for analysis of CO and CO_2 as an indication of the progress of the reactions. This has not been implemented in the experiments presented in the present yearbook contribution.

Figure 2 shows an example of conversion of a sewage sludge particle in the experimental setup. From the experiments the time for ignition, devolatilisation and char oxidation may be found as function of oxygen concentration, temperature of the combustion gas, and gas flow velocity.

The composition of the sewage sludge fuel and lower heating value (LHV) are found in table 1.

Table 1: Composition of the sewage sludge fuel (based on 'as received' mass).

Moisture [wt%]	Volatile [wt%]	Char [wt%]	Ash [wt%]	LHV [MJ/kg]
13.9	63.5	6.1	16.5	16.1

Experimental -TGA

Thermogravimetric analysis (TGA) is performed on the sewage sludge to obtain intrinsic pyrolysis kinetics. The initial fuel sample is 5mg. The sample is dried at 105^{o}C for 30min then heated to 1000^{o}C in inert atmosphere. Three heating rates are applied; 5, 50, and 500^{o}C/min.

Results and Discussion –Combustion Simulation

The following section describes experimental results obtained from combustion studies of dried sewage sludge particles.

Figures 3 and 4 show the time for devolatilisation of the sewage sludge as function of gas temperature and O_2 concentration, respectively. The devolatilisation is the process where the combustible volatile components of the fuel are released. The volatiles burn in contact with O_2 from the surrounding gas forming a luminous flame around the particle, as seen in figure 2 b).

The devolatilisation process is mainly controlled by the gas temperature whereas the oxygen concentration is seen to have insignificant influence.

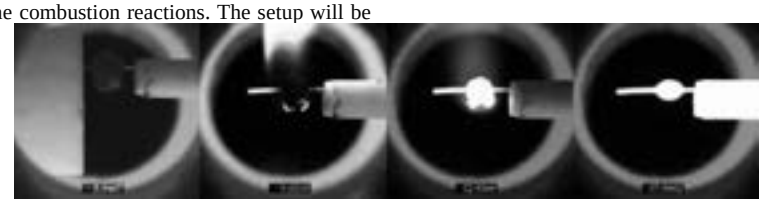

a) b) c) d)

Figure 2: The photos show the conversion of a sewage sludge particle. a) The virgin particle is inserted and the ceramic shield is seen to the left being removed. b) devolatilisation c) char oxidation d) the ash residue.

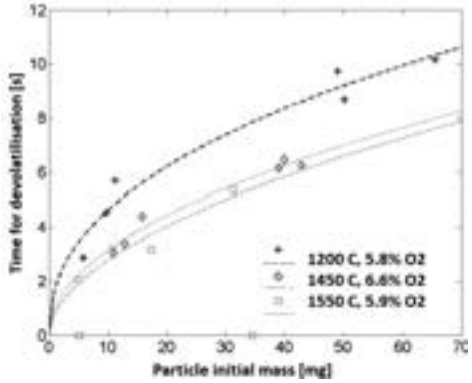

Figure 3: Dried sewage sludge devolatilisation as function of gas temperature. Experimental points and corresponding trend lines.

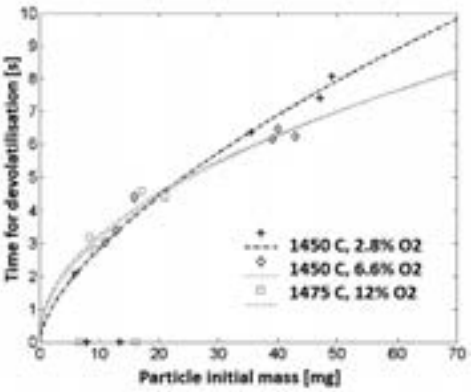

Figure 4: Dried sewage sludge devolatilisation as function of gas O_2 concentration. Experimental points and corresponding trend lines.

Figures 5 and 6 show the time for char oxidation of the sewage sludge as function of gas temperature and O_2 concentration, respectively. The char oxidation is the process where the solid combustible components of the fuel, main being fixed carbon, are oxidised and released as CO or CO_2. The onset of the char oxidation is found when the luminous flame around the particle extinguishes. The end of the char oxidation is found when the particle cease to shrink and only ash remains, see figure 2 c) and d).

The char oxidation process is mainly controlled by the oxygen concentration whereas the gas temperature only has a limited influence.

Results and Discussion –TGA

In the following section results from thermogravimetric analysis (TGA) are presented and kinetics parameters are found. The TGA results for sewage sludge devolatilisation are seen in figure 7.

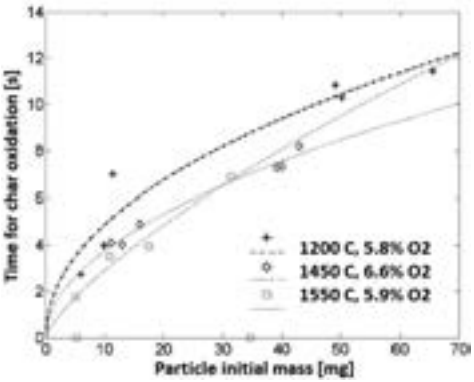

Figure 5: Dried sewage sludge char oxidation as function of gas temperature. Experimental points and corresponding trend lines.

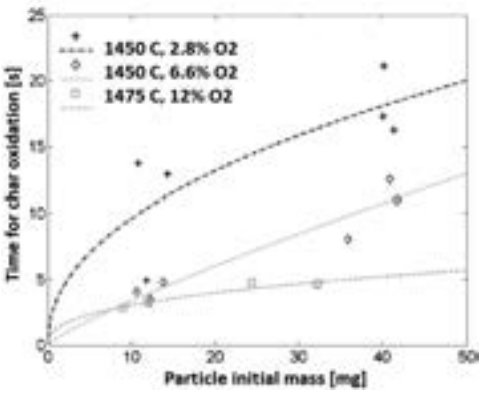

Figure 6: Dried sewage sludge char oxidation as function of gas O_2 concentration. Experimental points and corresponding trend lines.

Increasing the heating rate is seen to shift the release of volatiles to higher temperatures and the temperature interval of devolatilisation is broadened. The char amount formed is constant for changing heating rates.

The devolatilisation is modelled as a single nth order reaction based on an Arrhenius expression

$$\frac{dX}{dt} = A\left(\frac{dT}{dt}\right)^{b} \exp\left(\frac{-E_A}{RT}\right)(1-X)^{n} \qquad (1)$$

where X is the degree of conversion based on mass, E_A is the activation energy, R is the gas constant, T is the temperature, t is the time, n is the reaction order, and the pre-exponential factor , $A\left(\frac{dT}{dt}\right)^{b}$, is described by a power function of the heating rate.

The found kinetic constants for the sewage sludge are given in table 2.

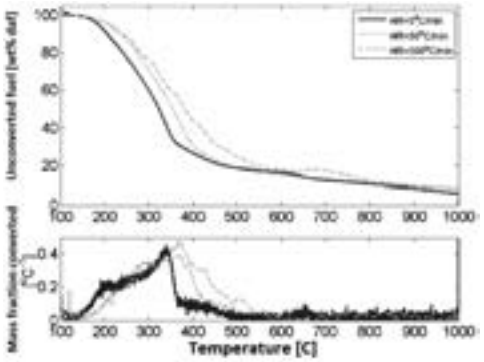

Figure 7: Release of sewage sludge volatiles as function of temperature and heating rate by TGA.

Table 2: Kinetic parameters for sewage sludge devolatilisation.

n	E_A	a	b
[-]	[kJ/mol]	[-]	[-]
0.79	24.7	1.83	0.85

The devolatilisation in the combustion experiments was found mainly to depend on the heat transfer to the particle. Hence, a simplified devolatilisation model is developed by modelling the transient heating of the particle, equation (2), which provides the local particle temperature, T, and heating rate, $\frac{dT}{dt}$, for equation (1) . The coupled equations (1) and (2) are solved simultaneously for the progression of the devolatilisation through the fuel particle.

$$\frac{\partial T(t,r)}{\partial t} = \frac{k_t}{C_p \rho} \frac{1}{r^2} \frac{dt}{dr}\left(r^2 \frac{\partial T(t,r)}{\partial r}\right) \qquad (2)$$

where r is the spherical particle radius, k_t, C_p and ρ are material properties of the fuel, i.e. thermal conductivity, specific heat capacity, and density, assumed to be constant. The boundary condition at the particle surface takes into account the external heat transfer by convection and radiation from the gas flow and reactor walls. The enthalpy of devolatilisation is assumed to be zero.

Figure 8 shows the experimental combustion results for devolatilisation of sewage sludge and the modelled curves of the devolatilisation time. The modelled devolatilisation time of sewage sludge particles is found to be in good agreement with the experimental results.

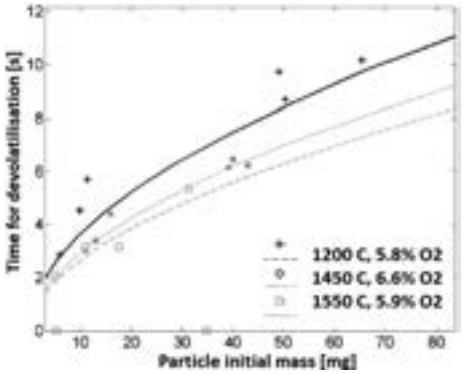

Figure 8: Experimental and modelled time for devolatilisation of sewage sludge as function of gas temperature and initial particle size.

Conclusions

A laboratory setup has been built for combustion studies of large fuel particles in suspension. Time for ignition, devolatilisation, and char oxidation can be obtained together with information of particle conversion pathway. A simplified mathematical model of devolatilisation of dried sewage sludge was found to be in good agreement with experimental results.

Acknowledgements

This project is an Industrial PhD project performed in corporation between FLSmidth A/S and CHEC Research Centre with co-funding from The Danish Agency for Science, Technology and Innovation. The project is a part of the research platform 'New Cement Production Technology', funded by the Danish National Advanced Technology Foundation, the Technical University of Denmark, and FLSmidth A/S.

The results presented in the present yearbook contribution are prepared in a master thesis by Paw Jensen in cooperation with the present PhD project [1].

References

1. P. Jensen, Combustion and modeling of alternative fuels, Master thesis at Department of Chemical and Biochemical Engineering, Technical University of Denmark, Sep. 2011

List of publications

1. L. Nørskov, M.B. Larsen, K. Dam-Johansen, P. Glarborg, P.A. Jensen, Danish Chemistry (Dansk Kemi), Oct. 2010
2. L. Nørskov, M.B. Larsen, K. Dam-Johansen, P. Glarborg, P.A. Jensen, *Alternative fuel combustion in cement rotary kilns*, Poster at Danish Chemical Engineering Conference (DK2), 16-17th July 2010

Sharat Kumar Pathi
Phone: +45 4525 2923
E-mail: skp@kt.dtu.dk
Discipline: Reaction and Transport Engineering

Supervisors: Kim Dam-Johansen
Jytte Boll Illerup
Weigang Lin
Klaus Hjuler, FLSmidth A/S

PhD Study
Started: January 2010
To be completed: December 2012

CO_2 Capture by Carbonate Looping Process from Cement Pyro-process

Abstract
Carbonate looping process is a promising technology for reduction in CO_2 emissions, which is particularly suitable for the cement industry as limestone in the raw meal could be used to capture CO_2. A process model was developed to study the integration of carbonate looping process using raw meal as sorbent. Carbonate looping experiments were carried out in the fluidized bed reactor to study the reactor performance. The results from the experiments at mild conditions showed similar carbon capture capacity for both limestone and mixture of clay in limestone used as sorbent, where mixture of clay and limestone was used to simulate raw meal. However, by thermo gravimetric analysis conducted at realistic conditions revealed large difference in carbon capture capacity of limestone and mixture of clay in limestone. Further in detail investigation was carried out to investigate the influence of major clinker forming compounds in the raw meal i.e. Al_2O_3, Fe_2O_3 and SiO_2 on carbon capture capacity of the limestone by forming binary, tertiary and quadruple mixtures as sorbents. The investigation revealed that Al_2O_3 has the most negative effect on carbon capture capacity of limestone followed by Fe_2O_3, but addition of SiO_2 to the mixture had slightly positive effect on the final capture capacity.

Introduction
According to Intergovernmental Panel on Climate Change, carbon capture from large stationary sources is considered as the mid-term mitigating option for climate change [1]. Cement industry is one of the major sources of CO_2, which emits CO_2 both from combustion of fuel and calcination of limestone. One of the promising technologies for carbon capture is carbonate looping process. The main reaction in this process is calcination and re-carbonation of limestone,

$$CaO + CO_2 \Leftrightarrow CaCO_3 \quad \Delta H_{298^{o}K} = -178 kJ/mol \qquad (1)$$

which is governed by equilibrium expression

$$P_{CO_{2,eq}} = 4.137.10^{12} \exp(-20474/T) \qquad (2)$$

Limestone is the major ingredient in the raw meal for clinker production. Application of raw meal as sorbent for carbon capture is relatively easy to integrate with cement plant. Most of the studies in carbonate looping process were focused on applying natural occurring limestone as sorbent. The carbon capture capacity of different limestone showed similar decay profile [2]. However, there was no study on applying raw meals as sorbent for carbon capture, which might be influenced by interaction between major clinker forming compounds. CO_2 emissions from cement production processes can be minimized by applying raw meal sorbent along with energy recovery from carbonator [3]. A Schematic representation of the carbonate looping process integrated to the cement plant is shown in Figure 1.

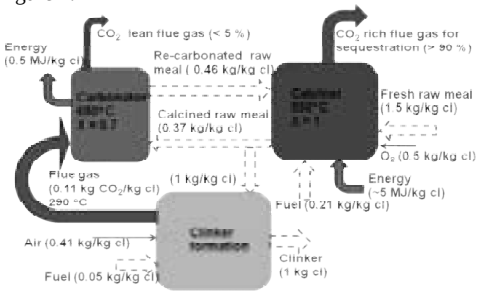

Figure 1: Schematic representation of mass and energy balance for de-carbonization of cement plant using raw meal as sorbent.

Specific objectives
The objective of this project is to investigate the application of raw meal as sorbent for carbon capture from the cement pyro-process. In order to achieve the objective, work is divided into experimental part and modeling part:

Experimental work

1. Investigate the carbon capture capacity and decay mechanism of raw meal used as sorbent.
2. Calcination and re-carbonation behavior in the fluidized bed reactor at different operating conditions.

Modeling work

1. Process modeling of carbonate looping process integrated to cement pyro process. This model could be used for optimization of the carbonate looping process and for investigating the influence of important parameters
2. Reactor modeling to investigate the performance of fluidized bed reactor as carbonator.

Experimental Results

Experiments were performed to simulate looping process in the fluidized bed reactor. The figure 2 below shows the carbon capture capacity of limestone and mixture of 30 [w/w. %] of clay in limestone to simulate raw meal. The carbon capture capacity of limestone and mixture of clay in limestone was similar with respect to looping cycle in the fluidized bed reactor at mild calcination conditions i.e. at low temperature.

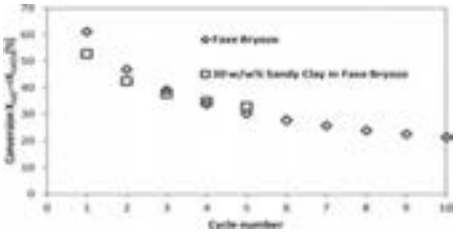

Figure 2: Comparison of degree of re-carbonation for limestone and mixture of clay and limestone in fluidized bed reactor at mild conditions.

However at realistic calcination condition (TGA apparatus) the decay in carbon capture capacity is different as shown in figure 3. The reason for higher loss in capture capacity might be due to sintering of limestone along with enhanced sintering or reaction due to presence of other compounds.

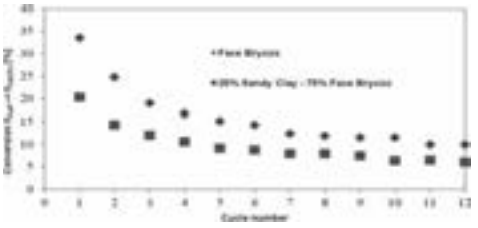

Figure 3: Comparision of CO_2 capture capacity for mixture of clay and limestone with limestone in TGA at realistic conditions.

So the experiments were performed to investigate the influence of major clinker forming compounds on the capture capacity of limestone. Figure 4 summarizes the influence of major clinker forming compounds on the carbon capture capacity of limestone.

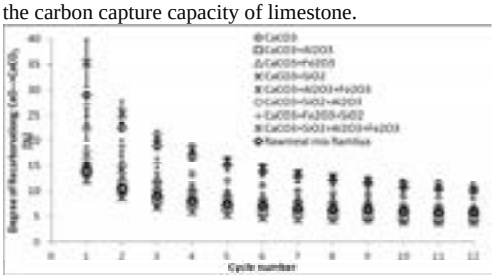

Figure 4: Carbon capture capacity of limestone compared with binary, tertiarya, qudruple mixtures and the industrial raw meal.

Overall from these results addition of Al_2O_3 has negative effect on the carbon capture, which is contrary to literature data, and whereas SiO_2 has slightly positive effect on the capture capacity.

Conclusions

Carbonate looping process has a potential technology for reducing CO_2 emission from Cement industries.

- At realistic calcination conditions there is significant difference in carbon capture capacity of limestone and mixture of clay and limestone.
- Al_2O_3 has the most negative effect followed by Fe_2O_3 on the sorbent capture capacity, but addition of SiO_2 showed slightly positive effect.

Future work

Detailed investigation will be carried to study the decay mechanism of the limestone influenced by major clinker forming compounds by performing BET, XRD and SEM analysis on the sorbent mixtures samples exposed to carbonate looping process conditions. Further experiments will be performed in the fluidized bed reactor under fast regime to study the influence of operating parameters on the carbon capture efficiency.

Acknowledgement

This project is a part of Research Platform on New Cement Production Technology financed by Danish National Advanced Technology Foundation, FLSmidth A/S and DTU.

References

1. B. Metz et al. Special report on Carbon Dioxide Capture and Storage (IPCC), Cambridge University Press, 2005.
2. J. Christensen, CO_2 reduction via carbonate looping, Master's thesis, DTU, 2010
3. S.K. Pathi et al. Carbonate Looping for De-Carbonization of Cement plants, 13th International Congress on the Chemistry of Cement, 2011.

Michael Jønch Pedersen
Phone: +45 3643 7056
E-mail: mjped@kt.dtu.dk
Discipline: Reaction and Transport Engineering

Supervisors: Kim Dam-Johansen
Søren Kiil
Tommy Skovby, H. Lundbeck A/S
Michael J. Mealy, H. Lundbeck A/S

Industrial PhD Study
Started: August 2011
To be completed: July 2014

Design of Continuous Reactor Systems for API Production

Abstract
Continuous manufacturing of active pharmaceutical ingredients is believed to become the new paradigm shift within the pharmaceutical industry. It has received a lot of attention since the Food and Drug Administration legalized it in 2004. H. Lundbeck A/S is one of the world leaders in development, manufacturing and distribution of medicines for treatment of central nervous system disorders. During the last couple of years, two full-scale continuous reactor setups have been designed and implemented as part of the production in Lumsås. Continuous manufacturing is seen as an important strategy for Lundbeck to remain competitive.

Introduction
Over the last decade the pharmaceutical industry has turned its focus towards continuous manufacturing in an attempt to remain competitive in an business area with pressures from legislations, competitors, search for new and better medicines to mention a few. It is believed that optimization and improvement of current and new syntheses can be achieved by converting towards continuous processing methods. Modernization of legislations and regulations concerning pharmaceutical manufacturing has enabled changes towards continuous pharmaceutical production; however, continuous operation necessitates a greater insight in the syntheses than is needed with batch production [1, 2]. H. Lundbeck Lumsås and the Department of Chemical and Biochemical Engineering at DTU have the last five years been working together on continuous manufacturing of active pharmaceutical ingredients (APIs).

The pharmaceutical industry today mostly relies on multipurpose batch equipment for their production [2]. Comparable to batch equipment, a continuous reactor setup is often more specific towards the reaction step it is intended for, but the general design is typically based on common reactor modules in various combinations, for instance continuous stirred tank reactor (CTSR) or plug flow reactor (PFR). If the continuous reactor setup is regarded as combination of standard modules of continuous reactors, each module can be considered as a building block for “plug and play” solutions to select between, when the process parameters of importance for the synthesis have been determined.

Several benefits could be obtained if continuous processes are chosen compared to batch processes. Lonza [3] estimated that 50 % of the pharmaceutical industry would profit financially by changing to continuous production methods. In Table 1, some of the advantages of continuous processing are stated, and where the advantage originates from, i.e. continuous flow and/or microreactor technology [4, 5].

Table 1: The advantages of continuous processing compared to batch processing, and the setup from which the advantages originate from, i.e. continuous flow (CF) and/or microreactor technology (MRT) [4, 5].

Advantages	Origin
Good mixing:	CF
Good heat transfer	MRT>CF
Minimization of reactor	MRT/CF
Tool concept	MRT/CF
Rapid dynamic response	CF
Mechanically robust	CF
Improved process control	CF

Organometallic reactions (for instance Grignard alkylation and Organolithium synthesis) are some of the most common and important methods in the formation of new carbon-carbon bonds in the pharmaceutical synthesis industry [6]. The reaction time for organometallic syntheses is fast (within seconds) and the reaction is typically highly exothermic. Because of these characteristics organometallic syntheses are ideal as case studies for continuous manufacturing. Typically organometallic reactions progress in the liquid phase, making them ideal for flow chemistry.

Specific Objectives

The aim of the project is to develop a methodology for selection of a reactor setup for continuous pharmaceutical production, and to determine standard reactor modules for "plug and play" solutions. Case studies will be performed on organometallic reactions, but the methodology is expected to be applicable for other syntheses as well.

In order to attain the development of a methodology an understanding of how important process parameters affect different reactor types must be established.

In a short time perspective, the aim is to potentially transform old batch and semi batch processes into continuous production. In a longer time perspective it is desired to attain continuous processes for new APIs coming directly from the R&D laboratory.

Results and Discussion

One of the largest obstacles in the development of continuous processes for pharmaceutical production is the limited solubility of many reactants, intermediates and/or products in the reactions [3]. Most of the processes progress in the liquid phase. Potentially the reactions could be processed highly diluted, and in a simple flow system (for instance PFR), but may not necessarily be the solution to the problem from an economic perspective. Alternatively a more complex continuous reactor setup might be necessary capable of handling solid material in excess amount. The setup's capability of handling solid material might be the most important parameter to be able to control.

At present time, one reactor module capable of handling solid material as initial reactant has been developed and is operating in full-scale production at Lundbeck's production facility in Lumsås. However, this module has some limitation in solid handling [7]. At present time research on another synthesis is carried out for a continuous reactor module capable of handling solid loadings up to 50 % [8].

Continuous operating necessitates the need for process control and this is also the reason why better understanding of the syntheses must be obtained in comparison to batch processes. State of the art microreactor technology and online spectroscopic measurement can be used to attain the required process knowledge. Online spectroscopic measurements of the process are also stated by the Food and Drug administration (FDA) as a method to ensure proper quality of the APIs in a continuous process by process analytical technology (PAT) [9].

Conclusions

Continuous pharmaceutical manufacturing is still in its earliest stage of development, and is believed to have a significant influence on the industry in the near future. H. Lundbeck A/S is considered as a front runner in acquisition of continuous pharmaceutical production technology having installed two continuous reactor setups for full-scale manufacturing within the last couple of years.

Several obstacles remain to gain a more general design methodology. In particular, solid handling is a significant challenge. Furthermore, in order to fully benefit from continuous processing, a change in mindset in the earliest development phases of new APIs must be made. By considering flow chemistry as early as possible in the development, scale-up would be less complicated, and potentially pilot scale-up could be completely avoided.

Acknowledgements

I express my gratitude to my supervisors at H. Lundbeck Lumsås (Tommy Skovby and Michael J. Mealy), and at the Department of Chemical and Biochemical Engineering (Kim Dam-Johansen and Søren Kiil). H. Lundbeck A/S is acknowledged for their financial support of the project.

References

1. C. Jimenéz-González et al. Org. Process Res. Dev. 15 (4) (2011) 900-911.
2. K. Plumb, Chem. Eng. Res. Des. 83 (6) (2005) 730-738.
3. D.M. Roberge, L. Durcy, N. Bieler, P. Cretton, B. Zimmermann, Chem. Eng. Technol. 28 (3) (2005) 318-323.
4. D.M. Roberge, N. Bieler, M. Thalmann, PharmaChem 5 (6) (2006) 14-17
5. D.M. Roberge, Industrial Design, Scale-Up, and Use of MicroReactors, FROST3, Budapest, Hungary, 2011.
6. S.D. Roughley, A.M. Jordan, J. Med. Chem. 54 (10) (2011) 3451-3479.
7. M.J. Pedersen, T.L. Holm, J.P. Nielsen, T. Skovby, M.J. Mealy, K. Dam-Johansen, S. Kiil, Grignard Alkylation in a Continuous Heterogeneous Reactor Setup, FROST3, Budapest, Hungary, 2011.
8. X. Ni, Innov. Pharm. Technol. 20 (2006) 90-96.
9. N.G. Anderson, D.C. Burdick, M.M. Reeve, Org. Process Res. Dev. 15 (1) (2011) 162-172.

List of Publication

1. M.J. Pedersen, T.L. Holm, J.P. Nielsen, T. Skovby, M.J. Mealy, K. Dam-Johansen, S. Kiil, Grignard Alkylation in a Continuous Heterogeneous Reactor Setup, FROST3, Budapest, Hungary, 2011.
2. K.M. Christensen, M.J. Pedersen, K. Dam-Johansen, T.L. Holm, T. Skovby, S. Kiil, Chem. Eng. Sci. (2011) (Accepted)
3. A. Cervera-Padrell, J. Nielsen, M.J. Pedersen, K.M. Christensen, A. Mortensen, K. Dam-Johansen, S. Kiil, K. Gernaey, Org. Process Res. Dev. (2011) (Submitted)

Jason Price
Phone: +45 4525 2992
E-mail: japr@kt.dtu.dk
Discipline: Process Technology and Unit Operations

Supervisors: John M Woodley
Jakob Kjøbsted Huusom
Mathias Nordblad

PhD Study
Started: September 2011
To be completed: October 2014

Operation and Control of Enzymatic Biodiesel Production

Abstract
This work explores the control of biodiesel production via an enzymatic catalyst. Biodiesel is formed from the transesterification of oils/fats with an alcohol, using enzymatic catalysts to generate mono-alkyl esters (the basis of biodiesel) and glycerol as by-product. Currently enzymatic catalysts are not used in commercial-scale biodiesel production. This is mainly due to non-optimized process designs. Furthermore is it unclear what process variables need to be monitored and controlled to ensure optimal economics. Critical to the project is to develop a control methodology to optimize the productivity of biodiesel production. Presented is an overview of the PhD project, with the end goal being a dynamic simulation model of the continuous biodiesel process including a strategy for monitoring and process control.

Introduction
Biodiesel (BD) is defined as the fatty acid alkyl monoesters derived from renewable feedstocks, such as vegetable oils, animal fats, etc. Recent incentives to reduce greenhouse gases, particularly carbon dioxide, have led to great interest in vegetable-based fuels because of the inherent ability of plant's to capture solar energy through photosynthsis while efficiently sequestering carbon dioxide from the atmosphere as their primary carbon source.

The EU has also been active in creating policy to increase the use of biofuels. In 2008 the EU adopted the Renewable Energy Directive 2009/28 (RED), which introduced a 10 percent binding target for renewable energy use in transport by 2020[1,2]. According to the European Biodiesel Board, the EU produced approximately 9.57 million metric tons of BD in 2010, a 5.5 % increase compared to the previous year [3].

The major operation in BD production that decides the process route is the transesterification of the vegetable oil or animal fat into fatty acid methyl esters (FAME), the primary product. Transesterification is an ester conversion process that splits up the triglycerides; that is, takes the glycerol of the triglyceride and replaces it with alkyl radical of the alcohol used. Typically methanol is used for the transesterification producing methyl esters and glycerin as byproduct (see Figure 1). This process reduces the viscosity of the vegetable oil to a value closer to that of petroleum diesel fuel while the cetane number and heating value are saved. This makes BD a strong candidate to replace petroleum diesel, as their characteristics are generally to that of petroleum diesel [5,6]. This reaction can be carried out by various forms of catalysts; either acids, bases, both liquid and heterogeneous, as well as free or immobilized enzymes. Compared to the conventional base-catalyzed biodiesel process, the enzymatic process is considered a "green reaction", requires less energy and is also highly selective producing less byproducts and waste. Using immobilized lipases also makes it easy to remove and reuse the catalysts [7].

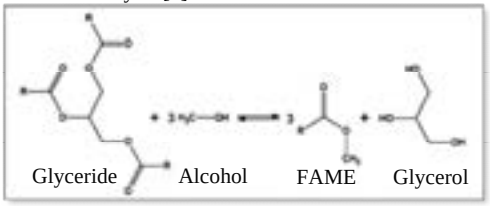

Figure 1 Simplified transesterification reaction [4].

Motivation for control
The production of fuel-grade BD can be simple as in Figure 2, the characteristics of feedstock however are very important and the fuel properties mainly depend on the feedstock properties [8]. Accordingly, the analysis of biodiesel and monitoring of the transesterification reaction is also important to successfully commercialize biodiesel, as a high quality fuel with no operational problems. Also methanol is widely used in the

transesterification reaction, but severe methanol inhibition of the enzyme can occur compared to higher alcohols. This issue however, may be remedied by the stepwise addition of alcohol while the reaction proceeds [9].

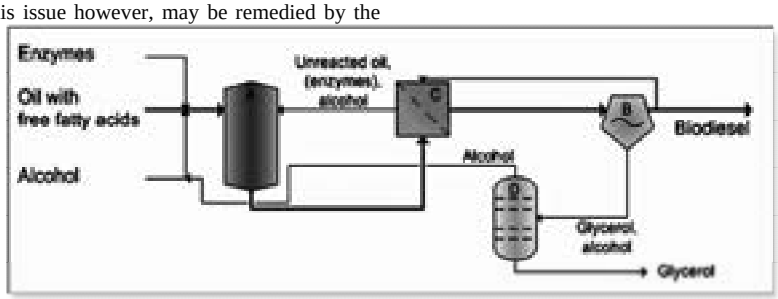

Figure 2 Ideal process design for enzymatic BD. (A) Reactor; (B) Separation (centrifuge or decanter); (C) Filter [9].

The improved operation resulting from implementation of a control system to handle changes in the feed composition and the correct dosing of alcohol can potentially lead to very large energy savings and at the same time provide a more consistent product quality. However given most conversion and quality analyses of biodiesel are commonly done by chromatographic methods [10], suitable measurement techniques will need to be investigated to obtain real-time information on the states of the system.

Specific objectives

For this project, focus is placed on the operational aspects such as process control, and the supply of alcohol. The main deliverable is a steady state and dynamic simulation model of the process including a strategy for monitoring and process control. This model and the proposed strategies will be validated experimentally on the department's pilot facilities. The project goal will be achieved by fulfilling the tasks through three main stages:

Phase 1: Evaluation of current kinetic model

This is essential for the development of the steady-state/ dynamic simulations and proper fitting of the experimental data. The model will need to take into consideration the effect of alcohol and glycerol inhibition as well as loss of enzyme activity over time.

Phase 2 - Identification of critical process parameters for batch and continuous operation

The aim is to identify which process variables the system is sensitive to by identifying the input variables to the system and the responses that are to be measured. Experimental design (ED) will be used to systematically identify critical process parameters. The information gleaned from the ED is then used in developing a monitoring and control strategy and will be validated in a closed loop test in the pilot plant.

Phase 3 - Scale up and economic evaluation

During this phase development of a steady state and dynamic simulation using a commercial software package is undertaken. Scale up and an economic evaluation of the proposed continuous process is developed along with a sensitivity analysis of the economic evaluation.

Acknowledgments

The project is just part of a wider initiative with Novozymes A/S and linked to the existing team of researchers at DTU, Århus University, Emmelev A/S and Novozymes A/S working on next-generation biodiesel processes.

References

1. B.M. Smyth, B.P. Ó Gallachóir, N.E. Korres, J.D. Murphy. J. Clean. Prod. 18 (2010) 1671-1685.
2. M Canakci, H Sanli. J. Ind. Microbiol. Biotechnol. 35 (2008) 431-441.
3. EBB (European Biodisel Board), EBB Official Press Releases, 2011.
4. L.F. Sotoft, B Rong, K.V. Christensen, B Norddahl. Bioresour. Technol. 101 (2010) 5266-5274.
5. S Al-Zuhair. Biotechnol. Prog. 21 (2005) 1442-1448.
6. W Parawira. Crit. Rev. Biotechnol. 29 (2009) 82-93.
7. P.S. Bisen, B.S. Sanodiya, G.S. Thakur, R.K. Baghel, G.B.K.S. Prasad. Biotechnol. Lett. 32 (2010) 1019-1030.
8. S Al-Zuhair, A Almenhali, I Hamad, M Alshehhi, N Alsuwaidi, S Mohamed. Renewable Energy 36 (2011) 2605-2614.
9. L Fjerbaek, K.V. Christensen, B Norddahl. Biotechnol. Bioeng. 102 (2009) 1298-1315.
10. N Ellis, F Guan, T Chen, C Poon. Chem. Eng. J. 138 (2008) 200-206.

Ke Qin
Phone: +45 4525 2890
E-mail: ke@kt.dtu.dk
Discipline: Reaction and Transport Engineering

Supervisors: Anker Degn Jensen
Peter Arendt Jensen
Weigang Lin

PhD Study
Started: January 2009
To be completed: June 2012

Biomass Gasification Behavior in an Entrained Flow Reactor

Abstract
In the present study, a gasification system including a bench-scale atmospheric pressure entrained flow reactor and other auxiliary facilities was utilized. Effects of operating conditions and biomass type on the solid and gas products were investigated. Biomass was completely converted at all investigated operating conditions but the syngas still contained some soot. A reasonable carbon mass balance closure was achieved for all conditions. Higher temperature, steam addition, relatively higher excess air ratio, longer residence time and increasing feeder air flow can significantly decrease the soot yield, while the inlet oxygen level seems not to influence the soot yield significantly. Wood and straw gasification provides similar gas composition. However, the soot yield was much lower in straw gasification than that in wood gasification possibly due to the high potassium content in straw, which may have a catalytic role on straw soot gasification.

Introduction
Gasification is a thermochemical process currently available for biofuel production. It used to convert solid carbonaceous materials, such as coal, waste and biomass, to synthesis gas, a mixture rich in H_2, CO, CO_2, CH_4, by partial oxidation at elevated temperature [1,2]. The produced syngas can be used to synthesize liquid fuels and chemicals or to produce heat and power. Among the renewable sources, biomass has a high potential because the use of biomass for energy and chemicals leads to low net CO_2 emission, which has complied with the target to reduce the CO_2 emission in the world [3,4]. Gasification is one of the key technologies for biomass utilization [5]. Compared with moving bed and fluidized bed gasifiers, entrained flow gasifiers operate at higher temperature with smaller particles, often achieves a high carbon conversion, and produces a high quality syngas with low tar and methane content [6,7]. However, the utilization of biomass in entrained flow gasifiers originally designed for coal remains with some challenges, thus a systematic study of biomass gasification in an entrained flow reactor is still of great interest.

Experimental
A gasification system including a bench-scale atmospheric pressure entrained flow reactor and other auxiliary facilities were developed and used for biomass gasification experiments, see Figure 1. The inner diameter of the reactor tube is 0.08 meter and its length is 2 meters. The reactor is externally heated by seven independent electric heating elements, which can be heated to a maximum temperature of 1500°C. A reasonably uniform temperature in the reactor can be realized. Besides the reactor, the complete system includes fuel feeder, gas supply system, gas preheater, gas sampling and analysis system, solid particle sampling system, tar sampling system and flue gas treatment. Fuel and feeder gas are fed through a central water-cooled tube while the remaining gas (named main gas) is preheated to the reactor temperature and fed in a co-axial tube around the fuel feeder tube. The solid particle sampling system consists of a cyclone and a metal filter, which are heated to 400°C to avoid liquid products (such as tar) condensation. A cyclone with a cut size of 2.5 μm is used to collect the char, and a metal filter is used to capture soot. A Petersen Column is used to collect produced tar samples. The flue gas sampling line is heated to 100°C in order to prevent water condensation. Then water is condensed in a gas cooler and the dry flue gas is analyzed by a NDIR gas analyzer and by a gas chromatography. The analytical error from these two equipments is less than 5%. The flue gas measurements include the concentration of H_2, CO, CO_2 and hydrocarbons (up to C_3 species) and the mass of char and soot particles. The system is especially designed to study heterogeneous reaction at high temperature and in short residence time [8].

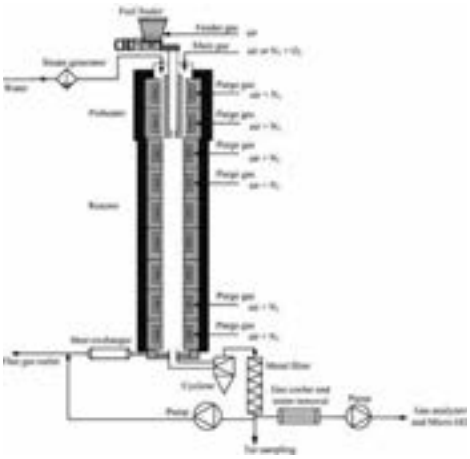

Figure 1: Sketch of entrained flow gasification system

Two types of biomass were used in the experiments: wood (beech saw dust) and straw (pulverized wheat straw pellets). The results of ultimate and proximate analysis are listed in Table 1.The compositions of wood and straw are quite similar except for the ash content. Straw has a high alkali content which may have a catalytic influence on the gasification processes [9]. Comparing with coal, the volatile content is higher in biomass, while the fixed carbon content and the heating value are lower. The wood and straw particles are smaller than 700 µm and 500 µm respectively. The medium diameter of wood particle (310µm) is bigger than that of straw particle (130µm).

Table 1 Analysis of fuel (as delivered basis)

Properties	Wood	Straw
Moisture (wt%, ar)	9.04	5.40
Volatile (wt%, ar)	76.70	72.27
Ash (wt%, ar)	0.61	4.54
Fixed carbon (wt%, ar) (by diff.)	13.65	17.79
Lower Heating Value (MJ/kg, ar)	16.44	16.35
C (wt%, ar)	45.05	43.42
H (wt%, ar)	5.76	5.58
O (wt%, ar) (by diff.)	39.41	40.60
N (wt%, ar)	0.13	0.37
S (wt%, ar)	0.01	0.09

Biomass gasification was investigated concentrating on the effects of biomass type (wood and straw) and operating conditions, such as reactor temperature, steam/carbon ratio, excess air ratio, inlet oxygen level, residence time and feeder air flow on solid and gas product yields. During the experiment, it was not possible to measure the total flow of gas products directly, so the total flow is calculated by using N_2 as a tracer. The yield of gas product from one kilogram fuel (Nm^3/kg fuel, dry and ash-free basis) can be calculated. Also, the yield of solid product can be expressed by the similar unit (g/kg fuel, dry and ash-free basis). The objective of the study is to provide valuable insights into the biomass gasification in an entrained flow reactor and especially to fill in a gap of knowledge on soot formation and yield in this process.

Results and discussion

In all conditions, biomass was completely converted, no char was collected but soot was found. A reasonable carbon mass balance closure was achieved in all experiment, generally being higher than 95%.

Effect of reactor temperature: The reactor temperature range is 1200-1400°C at fixed other parameters (wood and straw, steam/carbon ratio=0.5, excess air ratio=0.3, inlet oxygen level=21% and feeder air flow=10Nl/min). The product distribution is shown in Figure 2. It is widely observed that soot is produced in high temperature processes (1000°C-2500°C), such as pyrolysis and gasification. Thus increasing the reactor temperature favours soot formation, but at higher temperature, soot or its precursors have higher gasification reactivity. As a result, from 1200°C to 1400°C the soot yield decreases. The yields of H_2 and CO increase while CO_2 decreases with increasing temperature due to the endothermic soot and char gasification reaction with CO_2 and H_2O. The increased H_2 and CO_2 formation is also caused by the conversion of tar and larger hydrocarbons into lighter gaseous products. The yield of C_xH_y (hydrocarbons up to C_3 species) decreases because it is converted to soot and light gases at higher temperature.

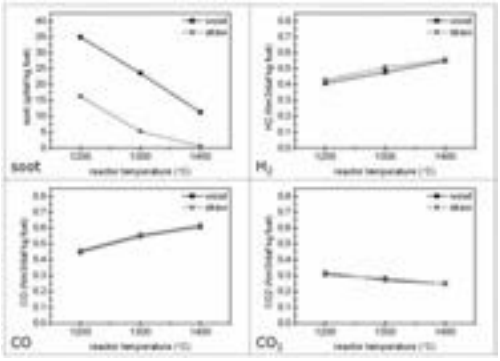

(a)

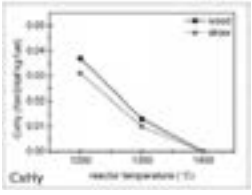

(b)

Figure 2: Effect of reactor temperature on product yield

Effect of steam/carbon ratio: The researched range of steam/carbon ratio is 0-1 at fixed other parameters (wood and straw, reactor temperature=1400°C, excess air ratio=0.3, inlet oxygen level=21%, and feeder air flow=10Nl/min). The product distribution is shown in Figure 3. The yield of soot decreases clearly with increasing steam/carbon molar ratio due to steam gasification of the soot. As the steam/carbon ratio increases, the H_2 and CO_2 yields increase, accompanied with a decrease of the CO yield, because the steam addition tends to promote the water gas shift reaction.

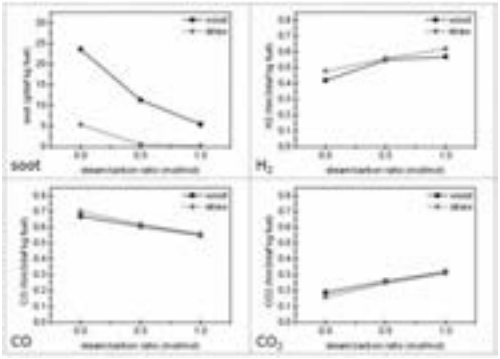

Figure 3: Effect of steam/carbon ratio on product yield

Effect of excess air ratio: The investigated range of excess air ratio is 0.25-0.35 at fixed other parameters (wood and straw, reactor temperature=1400°C, steam/carbon ratio=0.5, inlet oxygen level=21%, and feeder air flow=10Nl/min). The product distribution is shown in Figure 4. The amount of soot decreases with increasing excess air ratio because a larger part of the soot or its precursor is combusted. The H_2 and CO yields decrease with increasing excess air ratio, whereas the CO_2 yield increases due to oxidation reaction.

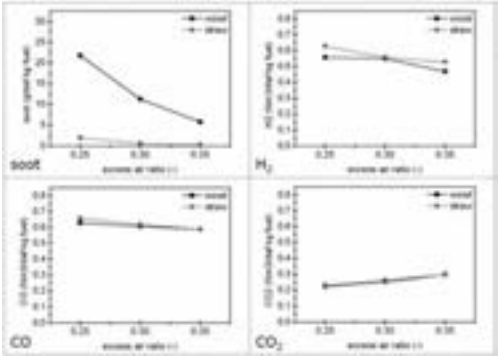

Figure 4: Effect of excess air ratio on product yield

Effect of inlet oxygen level: The range of applied inlet oxygen level is 16-26% at fixed other parameters (wood and straw, reactor temperature=1400°C, steam/carbon ratio=0.5, excess air ratio=0.3, and feeder air flow=10Nl/min). The product distribution is shown in Figure 5. It is observed that there is no big influence on the product yields except the soot yield increase a little with the increasing inlet O_2 level.

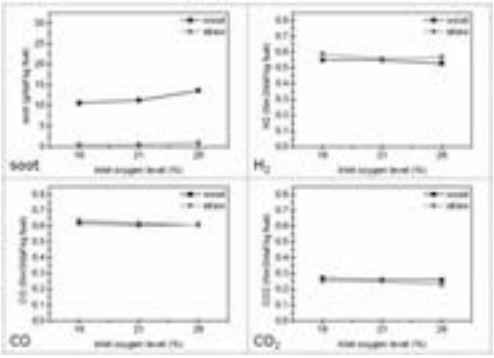

Figure 5: Effect of inlet oxygen level on product yield

Effect of residence time: The researched range of residence time is 2.4-3.6s at fixed other parameters (wood, reactor temperature=1400°C, steam/carbon ratio=0.5, excess air ratio=0.3, and inlet oxygen level=21%). The product distribution is shown in Figure 6. With increasing the residence time, the soot yield decreases since more soot can be gasified in a longer reaction time, while the gas product yields almost keep constant probably because in the reactor condition, high temperate with steam addition, the equilibrium condition is already achieved in a short reaction time.

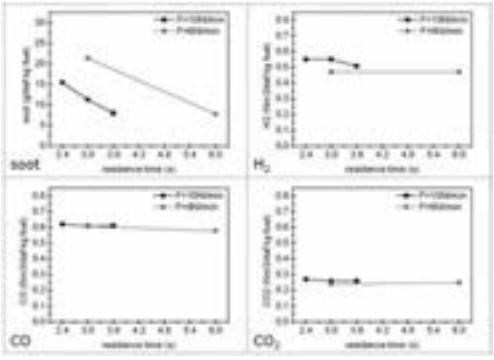

Figure 6: Effect of residence time on product yield

Effect of feeder air flow: The applied feeder air flow range is 6-14Nl/min at fixed other parameters (wood, reactor temperature=1400°C, steam/carbon ratio=0.5, excess air ratio=0.3, and inlet oxygen level=21%).The product distribution is shown in Figure 6. The soot yield decreases while the gas product yields increase because increasing the feeder air flow can improve the mixing condition. Probably improved mixing leads to tar converted to light gases instead of soot.

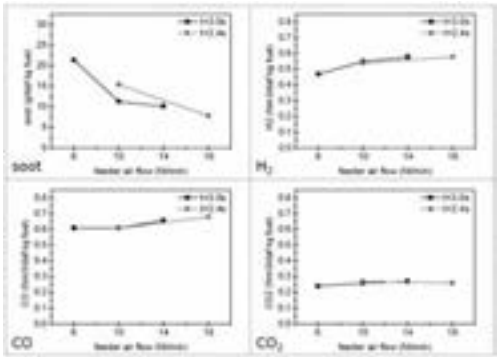

Figure 7: Effect of feeder air flow on product yield

Comparison between gasification and pyrolysis: The wood pyrolysis and gasification are compared in Figure 8. Compared with pyrolysis condition, much less soot is produced since the formed soot to a significant extent can be gasified. The H_2 and CO yields are higher in pyrolysis but CO_2 yield is higher in gasification due to the oxidation reaction in the gasification process. In the pyrolysis condition, a small amount of hydrocarbon is produced, while in the corresponding gasification condition, there is no hydrocarbon produced because the formed hydrocarbons can be oxidized or gasified in the gasification process.

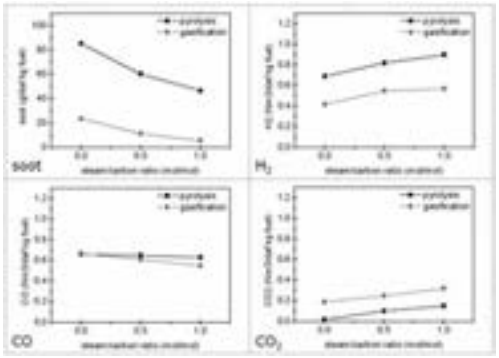

(a)

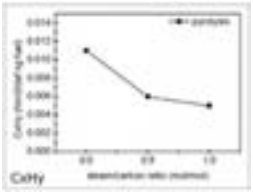

(b)

Figure 8: Comparison of gasification and pyrolysis

Comparison between wood and straw gasification: From Figure 2 to Figure 5, it is observed that the soot yield is much lower in straw gasification than that in wood gasification possibly due to the high potassium content in straw, which may have a catalytic role to speed up the soot gasification reaction. However wood and straw gasification provides similar gas composition.

Conclusions

Biomass was completely converted at all investigated operating conditions but the syngas still contained some soot. A reasonable carbon mass balance closure was achieved for all conditions. Higher temperature, steam addition, relatively higher excess air ratio, longer residence time and increasing feeder air flow can effectively decrease the soot yield, while the inlet oxygen level seems not to influence the soot yield significantly. Compared with pyrolysis condition, much less soot is produced since the produced soot can be gasified a lot in gasification. Wood and straw gasification provides similar gas composition. However, the soot yield is much lower in straw gasification than that in wood gasification possibly due to the high potassium content in straw, which may have a catalytic role on straw soot gasification.

References

1. J. Rezaiyan, N.P. Cheremisinoff, Gasification technologies: a primer for engineers and scientists, America, 2005.
2. P.N. Sheth, B.V. Babu, Bioresour. Technol. 100 (2009) 3127-3133.
3. World Energy Outlook 2004
4. H.L. Chum, R.P. Overend, Fuel. Process. Technol. 71 (2001) 187-195.
5. G.J. Stiegel, R.C. Maxwell, Fuel Process. Technol. 71 (2001) 79-97.
6. C. Higman, M. van der Burgt, Gasification, America, 2003
7. E. Henrich, F. Weirich, Environ. Eng. Sci. 21 (2004) 53-64.
8. W. Hao, P. Glarborg, F. Frandsen, K. Dam-Johansen, P.A. Jensen, Energ. Fuel. 25 (2011) 2862-2873.
9. D.W. McKee, Fuel 62 (1983) 170-175.

List of Publications

1. K. Qin, W. Lin, P.A. Jensen, A.D. Jensen, International Conference on Polygeneration Strategies, 2009.
2. K. Qin, W. Lin, P.A. Jensen, A.D. Jensen, 1st Joint Meeting of the Scandinavian-Nordic and French Section of the Combustion Institute, 2009.
3. K. Qin, W. Lin, P.A. Jensen, A.D. Jensen, Fuel (2011), in press.
4. K. Qin, W. Lin, P.A. Jensen, A.D. Jensen, General Meeting-Scandinavian-Nordic section of the Combustion Institute, 2011.
5. J. Ahrenfeldt, U.B. Henriksen, J. Münster-Swendsen, A. Fink, L.R. Clausen, J.M. Christensen, K. Qin, W. Lin, P.A. Jensen, A.D. Jensen, Production of methanol/DME from biomass, Report No. EFP06, Technical University of Denmark, 2011.

Siqiang Qin
Phone: +45 4525 2835
E-mail: siq@kt.dtu.dk
Discipline: Reaction and Transport Engineering

Supervisors: Søren Kiil
Brian Brun Hansen

PhD Study
Started: June 2010
To be completed: May 2013

Analysis and Quantification of Foaming Phenomena in Wet FGD Plants

Abstract
Spontaneous foaming can cause a range of operational problems in industrial processes such as wet flue gas desulphurisation (FGD) at power plants. This work investigates the performance of selected antifoaming agents on foams generated by adipic acid, egg white albumin (protein), and sodium dedecyl sulfate (SDS) at conditions of relevance for wet FGD. The investigations include long-term (up to 200 hrs) lab-scale Bikerman experiments with variations of salt concentration and pH. The impact of antifoaming agents on SO_2 removal efficiency and gypsum quality will furthermore be studied in a wet FGD pilot plant. SDS and protein are powerful foaming agents that in the absence of antifoaming agents will cause will cause overflow from the Bikerman column. Adipic acid (10mM) forms very weak foam even at high gas velocities (0.018 m/s). Two commercial antifoaming formulations (one silicone-based and one oil-based) and one pure vegetable oil have been tested in this lab-scale investigation.

Introduction
Stricter emission control legislation on acid gases (SO_2, HCl, and HF) has caused coal and oil-fired power plants to install high efficiency flue gas desulphurisation (FGD) systems, especially wet FGD in recent years. In wet FGD plants, the flue gas containing SO_2 and other acidic gases enters the wet FGD absorber and is brought into contact with alkaline limestone slurry to remove SO_2. The overall chemical reaction is described by equation 1:

$$CaCO_3 + SO_2 + \frac{1}{2}O_2 + 2H_2O \rightarrow CaSO_4 \cdot 2H_2O + CO_2 \quad (1)$$

Foaming (dispersion of gas in a liquid matrix) can be an operational problem in wet FGD plants, where it can interfere with the liquid level measurement and the online density measurement. This can result in gypsum scaling, excessive solid concentrations, carryover of slurry into the duct work and the booster fan, and potential cavitation of recycle pumps. When discovered, foaming can be controlled by antifoam addition, but the required dosage and the duration of its effect can vary with time.[1] [2]

Experimental procedure
This investigation of foaming and antifoaming agents at wet FGD conditions has been carried out in Bikerman lab-scale experiments and will later be verified in a wet FGD pilot plant. The Bikerman setup is a bubble column, which can be used for studies of foaming as a function of gas flow rate (see Figure 1). SDS, egg white albumin (protein), and adipic acid were chosen as foaming agents. Several different commercial antifoam formulations have been tested in this work and two were selected, in addition to a pure vegetable oil, for further studies. The influence of pH, salt concentration and temperature will be furthermore be investigated. The obtained lab-scale experiments will be verified by experiments in a wet FGD pilot plant as shown in Figure 2. The wet FGD pilot plant consist of a 7 meter PVC tube absorber (inner diameter of 0.033 m), which simulate a single channel in the packing zone of a packed wet FGD scrubber.

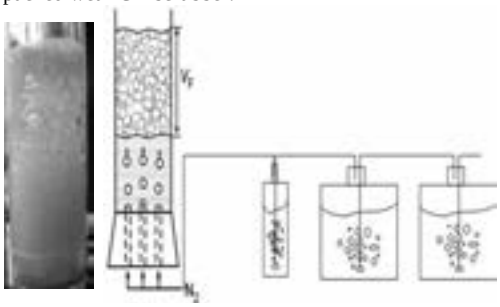

Figure 1: Bikerman column with humidifiers.

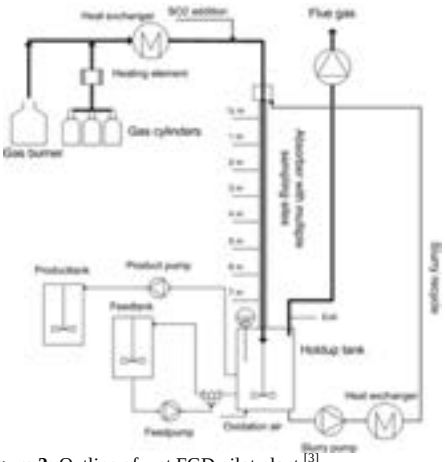

Figure 2: Outline of wet FGD pilot plant.[3]

Results

SDS experiments

SDS is a powerful foaming agent capable of producing considerable foam volumes. Two commercial antifoams have been tested on SDS foam: Foamtrol 2290 (silicone based) and Nalco FM-37 (oil based). Of these only 2 gram/L Foamtrol 2290 was able to control the SDS foaming for up to four hours, before overflow occurred. The oil based Nalco FM-37 antifoam was unable to control the foaming even at a concentration of 30-40 g/L.

Egg white albumin experiments

Egg white albumin is another powerful foaming agent, which in the absence of antifoaming agents will cause overflow. However, it takes some time for the protein to adsorb to the interface, adjust its structure and form a viscoelastic network, which can increase the elasticity of the lamella, increase the viscosity and introduce sterical interactions across the lamella thereby producing foam. Figure 3 shows the foam height of multiple experiments with 0.2 wt% protein and 6.36±.0.03 g/L Nalco FM-37, demonstrating a similar induction time (~ 50 min), but considerable variation regarding the time at which the foam height peaked – additional work will done addressing this issue. The foam height begins to decrease after two hours, possibly due to protein particle coalescence, or deposition of foaming agent on the walls.

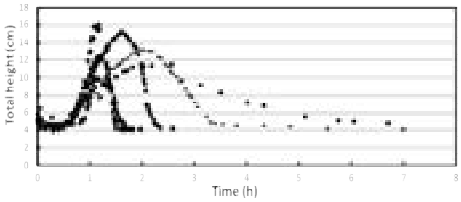

Figure 3: Foam height of 0.2 wt% egg white albumin solution with 6.36±0.03 g/l Nalco FM-37 (v = 1.4 cm/s).

Adipic acid experiments

Adipic acid consists of two acid groups connected by a short hydrocarbon chain, which makes adipic acid a weak surfactant. Figure 4 shows four long term tests using Nalco FM-37 as antifoam (added after 50 hrs). As the antifoam ability decreases with time the foam height gradually returns to the original level after an induction time without foaming. Higher antifoam concentrations cause longer inductions times

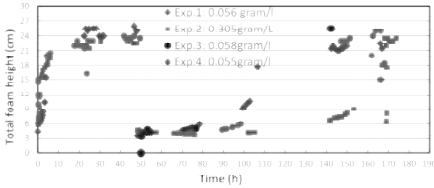

Figure 4: Adipic acid (10mM) and Nalco FM-37 tests (v_{N2} = 0.02 m/s).

Conclusions and further work

A series of long-term lab-scale foaming and antifoam experiments have been conducted with a Bikerman column in order to evaluate the performance of commercial antifoam formulation and the long term performance at FGD relevant operating conditions. The silicone-based antifoam, Foamtrol 2290, can control SDS foam for up to four hours (dosage 2 g/l), while the oil-based antifoam, Nalco FM-37, is unable to control SDS foaming even at 30 g/l. Nalco FM-37 can, however, prevent overflow of protein foam (dosage 6 g/l) and control adipic acid foam for several days (dosage 0.05 g/l). Further optimization of the experimental procedure is to be carried out in addition to test of more commercial antifoam formulations and pilot plant experiments.

Acknowledgments

CHEC is financially supported by the Technical University of Denmark, DONG Energy A/S, Vattenfall A/S, FLSmidth A/S, Hempel A/S, Energinet.dk, the Danish Research Council for Technology Sciences, the Danish Energy Research Program, the Nordic Energy Research Program, and EU. This project is a part of the 'Våd røggasafsvovling 2009-2014' Research Platform financed by DONG Energy A/S and Vattenfall A/S.

References

1. H.N. Soud, Developments in FGD. IEA Coal Research, London, 2000.
2. R. Thiele, I&EC Res. 42 (7) (2003) 1426-1432.
3. B.B. Hansen, I&EC Res. 50 (8) (2011) 4238–4244.

Alberto Quaglia
Phone: +45 4525 2812
E-mail: aq@kt.dtu.dk
Discipline: Systems Engineering

Supervisors: Gürkan Sin
Rafiqul Gani
Bent Sarup, Alfa Laval

PhD Study
Started: June 2010
To be completed: May 2013

Incremental Refinement of Process Design

Abstract
The design, development and reliability of a chemical product and the process to manufacture it, need to be consistent with the end-use characteristics of the desired product. One of the common ways to match the desired product-process characteristics is through trial and error based experiments which can be expensive and time consuming. An alternative approach is the use of a systematic model-based framework in product-process design, replacing some of the time consuming and/or repetitive experimental steps. In this approach, the development of a computer-aided tools for product-process design is very important for analysis, design, and/or identification of feasible chemical product candidates because it allows one to consider processing issues during the development of the product. In general the use of process simulation tools is not common in the food and biofuels industries, much due to the complexity of fundamental modeling of thermodynamics and transport properties of the involved chemical species and their interactions. This project aims at introducing a paradigm shift in product-process design through application of Process Systems Engineering (PSE) tools.

Introduction
For processing companies, the synthesis and design of optimal processing network includes all the strategic and tactical decisions such as the selection of raw materials and products portfolio, as well as the synthesis and design of the processing network and the optimization of the material flows through it. The solution of this problem requires extensive cross-functional co-ordination through the enterprise, as well as business management, operational and engineering expertise, resulting thereby to large multi-dimensional problems.

Recent developments in Process System Engineering have focused on managing the complexity of different company functions by integrating them in an enterprise-wide model.

The goal of the integration is the simultaneous solutions of the different layers of enterprise-wide problems, to i) reduce the effort needed to solve the problem while improving the reliability of the solution and ii) increase the impact of analysis techniques such as uncertainty and sensitivity analysis by extending their scope to the whole problem, including the cross-functional issues.

In this contribution, we propose an integrated Business and Engineering framework for synthesis and design of enterprise-wide processing networks. In our framework, an adopted formulation of the transhipment problem is integrated with a superstructure2, leading to a Stochastic Mixed Integer Non Linear Program (sMINLP), which is solved to determine simultaneously the optimal strategic and tactical decisions with respect to the processing network, the material flows, raw material and product portfolio.

The framework is complemented with all methods and tools necessary for its execution, including i) a data structure for efficient data-flow, ii) a generic structural model for description of each process alternative considered in the superstructure, starting with simple models and customizable in an incremental manner to more complex forms, iii) a library of algorithms to solve the deterministic and the stochastic problem, and iv) results analysis techniques to provide further insights for the decision making with respect to sustainability, management of the uncertainty and R&D prioritization.

A case study illustrating the application of the framework to the synthesis and design of soybean processing, including 43 process alternatives and 20 candidate products (food, feed and intermediate for pharmaceuticals) leading to the formulation of more than 300,000 equations is presented. The problem is solved both in deterministic conditions (for a given and a priori known market conditions) and under market price uncertainty, which results in a stochastic

programming problem. The robustness of the optimal solution and the value of stochastic solution are discussed, and strategies to manage the consequences of the uncertainty for decision making at business and engineering levels are proposed.

The Framework

An integrated Business and Engineering framework for Computer-Aided Synthesis and Design of Processing Network has been developed and applied to the synthesis of soybean processing network.

A graphical representation of the framework is given in Figure 1.

In the workflow the problem is first defined and formulated as a MINLP (step 1, 2, 3), and then solved to determine simultaneously the optimal selection of raw materials, of product portfolio and of processing path, as well as the optimal material flow through the network.

The objective of step 1 is to define the synthesis/design problem. Also, project purpose (new product/process, process improvement, retrofit), performance metrics and objective function structure are defined at this stage.

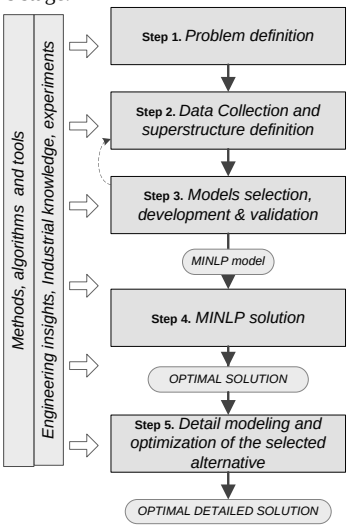

Figure 1: Systematic framework for Synthesis and Design of Processing Network.

In Step 2 all the existing knowledge (industrial know-how, engineering insights, commercial knowledge...) relevant to the problem is collected. Being this knowledge multidisciplinary and multisource, particular emphasis is given to reconciliation and systematization, as well as to the development of an appropriate infrastructure for efficient data management, composed by a superstructure representing different flowsheet alternatives, structural constraints list, compounds and unit operations inventory and databases of reconciled data, structured in such a way to be accessible from all project levels [1]. Furthermore, performances metrics of similar and competing processes/products are collected for benchmark purposes.

All submodels needed for the multiscale model formulation are generated in step 3 (in collaboration with the Integrated Product-Process Design project). These include physical properties, unit operations, operational and investment cost and sustainability models; a systematic model generation framework is used to ensure consistency among the different models and scales. In order to cope with the lack of consolidated models and of public available data typical of this industry segment, an iterative procedure is followed for incremental model refinement and validation, based on uncertainty and sensitivity analysis to identify the model parameters which have the biggest impact on the model output and to estimate the uncertainty on model output due to parameter errors. Design of experiments techniques are then used to plan experiments in order to maximize the information gain with limited number of trials. Experimental results are added to the databases compiled in step 2 and used for model identification in step 3. The procedure is iterated until model output uncertainty is considered acceptable.

Generic input output models can be employed to describe each process interval included in the superstructure, especially to employ the tool for screening purposes at early project stage [2].

All the model equations together with the constraints and the objective function are collected in a MINLP model, which is solved in step 4, employing one of the consolidated MINLP solution techniques.

If relevant, the selected alternative can be further investigated and optimized by detail modeling and optimization, with the use of traditional process modeling and optimization methods and tools. Performances metrics are calculated for the selected optimal options and are compared against the benchmark.

Depending on the project purpose defined at level 1, project financial indicators (such as IRR, NPV etc) can be calculated for the selected option and used as inputs for project management decision.

The framework is applied to the flowsheet synthesis and design problem for soybean oil extraction and refining. According to the above described approach, the problem is formulated and solved to determine the optimal processing network for the vegetable oil extraction and refining (including biodiesel production and various options for byproducts valorization), as well as the optimal material flows to each processing step.

Case Study: Soybean Processing

Soybean (Glycine max) has become one of the most important agricultural commodities with a steadily increasing global production, which reached 248 MMT in 2009 [3].

Soybean can be used as raw material for a wide range of food, feed and pharma products: soybean oil is widely used as cooking or dressing oil, but can also have feed or technical applications, as well as raw

material for biodiesel production. Extracted soy-beans are a cheap source of protein, used to displace animal protein in a wide range of feed and food products.

Several soy by-products have high end applications due to their functionality: soy lecithin is used in food and pharma applications as emulsions stabilizer, and tocopherols are sold as antioxidant both for pharmaceutical applications or as natural preservants for packaged food. Other by-products such as hulls and fatty acids are mostly used as feed ingredients [4]. Average soybean composition is reported in Table 1.

Table 1: Average US Soybean Composition (dry basis) [5].

Component	Weight fraction	Standard Deviation
Protein	40.69%	0.51
Lysine	2.56%	0.11
Methionine	0.57%	0.03
Cysteine	0.72%	0.06
Tryptophane	0.52%	0.05
Threonine	1.54%	0.07
Oil	21.38%	0.64
Ash	4.56%	0.34
Carbohydrate	29.4%	3.29

Being a low margin operation, soybean processing profitability can be achieved only by optimizing the allocation of the different seed components to commercially valuable products and by-products. The wide spectrum of potential products and their mutual influence make the determination of the optimal resource allocation a not trivial task. Moreover, because of agricultural commodities market volatility, this problem needs to be solved frequently in order to have up-to-date solutions.

For these reason, we estimate that the soybean industry sector in particular (and in general all the agro industrial sector) could benefit of the development and the application of the Integrated Business and Engineering framework.

The case study has been developed in collaboration with Alfa Laval.

For sake of simplicity, the production of biodiesel has been considered out of the scope of the case study, and therefore not included in the superstructure. In the following paragraph, a brief description of each step in the methodology will be given.

Step 1: Problem definition.
The problem is defined as a resources allocation problem, assuming the availability of 2 soybean supplies of different quality and no topological constraint given by pre-existing processing plants. The selected optimality condition is Gross Operating Margin.

Step 2: Data collection and superstructure definition
The knowledge and data relevant to the problem are collected by integrating the information available in the open literature with the industrial knowledge of Alfa Laval.

The superstructure, composed by 65 intervals, is reported in Figure 1. More detailed explanation of each of the processes considered in the superstructure can be found in [6].

The list of components includes 24 process components and 11 utilities components.

Step 3: Model selection and validation
The generic model process description model described by Zondervan for the synthesis of optimal biorefinery is employed for to model each of the considered process intervals [2]. Such an approach is based on simple input output models, describing any processes as a succession of 5 tasks: 1) inlet mixing, 2) utilities application, 3) reaction, 4) wastes separation, 5) outlet.

Step 4: MINLP solution
All the equations generated by the above described steps are grouped to generate a large scale MINLP problem. Problem statistics are reported in Table 2.

Table 2: Case study problem statistics

Total number of parameters:	**163,750**
Total number of process constraints equations:	**159,250**
Number of logical constraints	15
Number of binary variables	65
Number of continuous variables	174,378
Number of activation constraints	6,825
Objective function	1
Optimization problem size	**166,091**
Indicators (calculated after the solution)	147,875
Total number of equations	**313,966**

Step 5: Detail modeling and optimization
Even though this step is extremely important for the industrial application of the methodology, it has not been included in the scope of the case study since it does not represent a scientific challenge, being a well-known procedure for which methods and tools are available and consolidated.

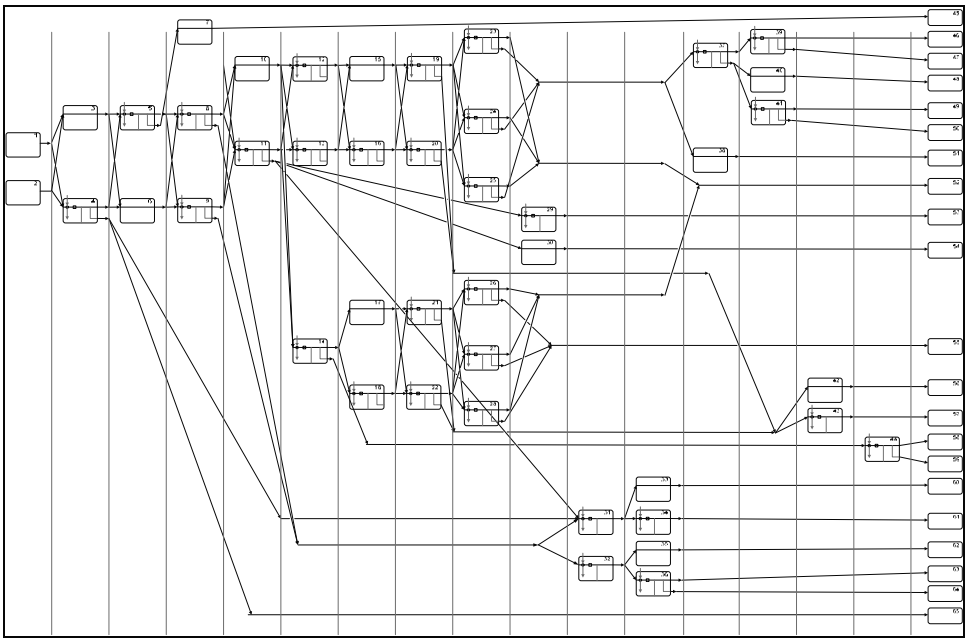

Figure 2: Soybean Processing Superstructure

Current Status and Future Perspective

The MINLP problem formulated with the above mentioned methodology is implemented in GAMS and solved with the use of standard MINLP solver DICOPT [7].

Results analysis and validation is being performed, via comparison of the optimal results with industrial standards.

Future developments include the solution of the problem under different scenarios, as well as the extension of the generic process model to include a wider range of processes.

Moreover, sensitivity analysis to determine the most influent parameters on the final solution, as well as the adaptation of the framework for the solution under uncertainty of parameters will be performed.

References

1. R. Singh, K. Gernaey, R. Gani, Comput. Chem. Eng. 33 (2009) 22–42.
2. E. Zondervan, M. Nawaz, A.B. de Haan, J.M. Woodley, R. Gani, Comput. Chem. Eng. 35 (2011) 1752-1766.
3. P. Thoenes, 2009, "Oilseeds, Oils and Meals" in Food Outlook - June 2009 FAO.
4. M.N. Riaz, Soy Applications in Food, CRC Press, 2005.
5. F. Shahidi (ed), Bailey's Industrial Oil and Fat Products, Volume 2 (6th Edition), John Wiley & Sons, Hoboken, New Jersey, 2006.
6. F. Shahidi (ed), Bailey's Industrial Oil and Fat Products, Volume 5 (6th Edition), John Wiley & Sons, Hoboken, New Jersey, 2006.
7. J. Viswanathan, I.E. Grossmann, Comput. Chem. Eng. 14 (1990) 769-782.

List of Publications

1. A. Quaglia, B. Sarup, G. Sin, R. Gani, Comput. Chem. Eng. (submitted)
2. C.A. Diaz-Tovar, A.A. Mustaffa, A. Hukkerikar, A. Quaglia, G. Sin, G. Kontogeorgis, B. Sarup, R. Gani, Comput. Aided Chem. Eng. 29 (2011) 256-260

Hemalata Ramesh
Phone: +45 4525 2958
E-mail: hemra@kt.dtu.dk
Discipline: Process Technology and Unit Operations

Supervisors: John M. Woodley
Ulrika Törnvall
Pär Tufvesson

PhD Study
Started: October 2011
To be completed: October 2014

Process Development for Oxidase-based Biocatalysis

Abstract
Enzymes have gained key importance as biocatalysts and are being used in many applications today including process to produce pharmaceutical, agrochemical and fine chemicals. Oxidases have been identified as potential biocatalysts to carry out industrial oxidation reactions. In particular, monoamine oxidases (MAO), a class of enzymes from the oxidase family, have been used for resolution of chiral amines. However, for the reactions to be employed in a larger scale, further process development and conceptual advances will be required. The aim of this investigation is therefore to develop process technology including strategies for oxygen supply, for the production of optically pure chiral amines through deracemization using MAO.

Introduction
Optically active compounds such as chiral amines have gained significant importance in recent years since they find widespread application in many pharmaceutical syntheses. FDA regulations from 1992 have lead to the increase in the search for processes which can yield homo-chiral compounds [1]. Although both chemical and biological methods are available for chiral resolution, exploiting biological catalysts is advantageous due to the high selectivity of the enzymes employed. Several enzymes have been exploited for chiral resolution through different processes such as kinetic resolution, stereo-inversion and deracemization [2]. Of these, stereo-inversion and deracemization methods alone are capable of giving a 100% yield. However, industrial production of chiral amines is today often obtained by resolution resulting in a low yield (since 50% of the starting material is the undesired isomer). In fact, resolution of a racemic amine mixture into an optically pure enantiomer can be performed using few enzymes. The families of enzymes employed are serine hydrolases, transaminases and amine oxidases. Serine hydrolases use enantioselective acylation thereby concentrating the chiral amine that is not converted, leading to a loss in yield. Transaminases can be employed for synthesis of chiral amines. Asymmetric synthesis using this class of enzyme can give a 100% yield; however, the reaction suffers from severe product inhibition and reversible interaction between the substrate and product. On the other hand, amine oxidases, such as MAO [E.C. 1.4.3.4], can be employed for chiral resolution by deracemization and give a 100% yield of the desired enantiomer. The aim of this study is to develop process technology to employ biocatalytic methods for deracemization of chiral amines using MAO.

Deracemization
Deracemization can potentially lead to 100% theoretical yield of the product and has therefore gained significant attention. Furthermore, a high enantiomeric excess of the desired product can be obtained making it a potential method of choice for production of chiral amines when a racemic mixture is used as substrate. Monoamine oxidases (MAOs) have been identified as a family of enzymes that can contribute extensively to this purpose. MAOs are flavin containing enzymes which can catalyze the selective deamination to the aldehyde through the formation of an imine. Turner and co-workers have successfully produced improved biocatalysts (mutant MAO producing cells) that have enhanced selectivity and activity [3]. Deracemization of racemic substrate is carried out using a selective MAO and a non-selective reducing agent as shown in Figure 1. This method has been validated for primary [4], secondary [5] and tertiary amines [6]. Table 1 summarizes the chemical research that has been performed in this field and the enantiomeric excess (ee) obtained from these processes.

Table 1 Deracemization employing MAO

Substrate	Product	Reducing agent	ee	Reference
o-Methyly-N hydroxylamine	R enantiomer	H_2/Pd, Tf_2O	99%	[7]
Crispine A	S enantiomer	Ammonia Borane	97%	[8]
Álpha methyl benzylamine	R enantiomer	Ammonia Borane	93%	[9]
N-methyl-2-phenylpyrrodiline	R enantiomer	Ammonia Borane	99%	[6]
Methylteterahydroisoquinoline	R enantiomer	Ammonia Borane	99%	[5]
2-phenylpyrroldine	R enantiomer	Ammonia Borane	98%	[5]

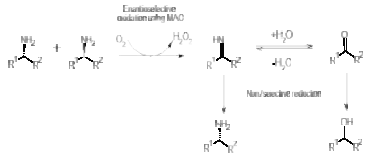

Figure1: Deracemization of chiral amines using MAO

Aims and Objectives

To date, the concept of deracemization by MAO has only been performed at very low substrate concentrations (10 mM). Such low concentrations cannot be applied in a commercial process as it is not scalable. In this project, the objective is to apply suitable process technology to operate MAO successfully at high substrate concentrations for a range of suitable substrates. The increase in substrate concentration in turn leads to process challenges including the need for new substrate feeding strategies and improved product recovery. Additionally, the kinetics of such a reaction is little known. Kinetic constraints have to be identified as the first step of the process design and would hence form the first objective of the project. Reactor design should take these considerations into account and the choice of reactor incorporated would therefore depend on the kinetics of the reaction. For instance, if substrate inhibition is observed, then substrate-feeding strategies must be developed, while for cases with product inhibition, methods such as *in-situ* product removal must be adopted. In addition, in order to obtain high ee of the required isomer in a two-step deracemization process, about 6 to 7 cycles of oxidation and reduction need to be performed [9]. This implies that the system employed should be capable recycle. Secondly, the reaction with MAO requires the supply of oxygen to enable the biocatalytic reaction. The optimum supply of oxygen also has to be evaluated. An attempt will be made to define the operating conditions based on oxygen supply. This will enable an identification of the mass transfer and kinetically limited regions of operation [10]. Furthermore, oxygen supply can cause damage to the enzyme and thereby lower catalytic activity. Alternative methods of oxygen supply, such as bubbleless aeration will be investigated as a potential process technology. As seen from Figure 1, the product of the oxidation stage is hydrogen peroxide. This can then be reduced to hydrogen and molecular oxygen using a co-catalyst such as catalase. The possibility of such a reaction will be investigated and the effect of hydrogen peroxide on the catalyst will also be examined. Initial experiments will be conducted in a stirred tank reactor (STR) with separate oxidation and reduction cycles. The schematic representation of the process would be similar to Figure 2. A one-pot chemo-enzymatic process will later be evaluated. Based on the preliminary evaluations, alternative reactor configurations such as packed bed, membrane and fluidized bed reactors will be considered for the process.

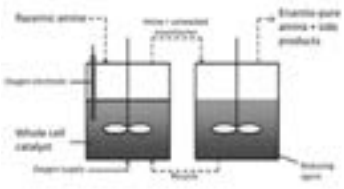

Figure2: Reactor system for MAO

Conclusions and Significance

Use of biocatalysts for transformation of racemic mixtures into enantiopure components capitalizes on the high enzymatic selectivity. Enzymatic oxidation reactions for the production of pharmaceutical products which include chiral amines have been carried out at very low concentrations. However, for this to be applied in industrial scale, process technology to handle high substrate concentration is required.

References

1. C.C. Gruber, I. Lavandera, K. Faber, W. Kroutil, Adv. Synth. Catal. 348 (2006) 1789-1805.
2. H. Ismail, Enzymatic Kinetic resolution of amines, Proefschrift, ISBN: 978-90-9021925-7, 2007.
3. N. Turner, Curr. Opin. Biotechnol. 14 (2003) 401-406.
4. M. Alexeeva, A. Enright, M.J. Dawson, M. Mohmoudian, N. Turner, Angew. Chem. Int. Ed. 41 (2002) 3177-3180.
5. R. Carr, M. Alexeeva, M.J. Dawson, V. Gotor-Fernandez, C.E. Humphrey, N.J. Turner, Chem. Bio. Chem. 6 (2005) 637-639.
6. C.J. Dunsmore, R. Carr, T. Fleming, N.J. Turner, J. Am. Chem. Soc. 128 (2006) 2224-2225.
7. T.S.C. Eve, A. Wells, N.J. Turner, Chem. Commun. 1530-1531.
8. K.R. Bailey, A.J. Ellis, R. Reiss, T.J. Snape, N.J. Turner, Chem. Commun. (2007) 3640-3642.
9. M.V. Alexeeva, A. Enright, M. Mahmoudian, N.J. Turner, US Patent 12/947,164. (2010).
10. S. R. Tindall, PhD. Thesis, Scale up of oxidase catalyzed reaction (2011), University College of London.

Claus Maarup Rasmussen

Phone: +45 4525 2829
E-mail: cma@kt.dtu.dk
Discipline: Reaction and Transport Engineering

Supervisors: Kim Dam-Johansen
Karsten H. Clement
Klaus Hjuler, FLSmidth

PhD Study
Started: January 2010
To be completed: January 2013

Preheater Design for High Energy Efficiency and Low Emissions

Abstract
The preheating facility in the cement industry facilitates the heat exchange between the hot flue gasses and the cold raw materials. The aim of this PhD project is to develop and test new a pre-kiln concept, which is more economic beneficial than the existing in terms of either capital or operational costs. This pre-kiln process can either be a new design for the preheating process or an alternative plant design with an integrated power production system, which obviates the need for a preheating process as we know it today.

Introduction
The chemical active component in cement is produced by burning mainly calcium carbonate and clay at temperatures above 1400 °C followed by a rapid cooling in order to freeze the high temperature crystalline structure of the clinker.

In a modern cement plant, this process is typically facilitated in a dry kiln system containing; a rotary kiln, a cyclone based preheater tower, a calciner and a clinker cooler.

The preheating process is carried out in a series of cyclones arranged in a counter current pattern where the cold raw meal is fed to the top cyclone, and the hot process flue gases is introduced to the bottom cyclone. The counter current pattern ensures high particle temperatures after preheating.

Figure 1 provides a schematic drawing of a typical pyroprocessing unit found in cement plants.

The basic layout for the preheating process is more than fifty years old [1], and parameters such as pressure drop, power consumption, heat loss, maintenance requirements and environmental impact have been optimized within the limitations of the overall design. However, the existing preheating process has some inherent disadvantages properties, such as:

- High capital costs, due to the necessary height of the preheating tower.
- High heat loss from unit surfaces and through hot dust and gases leaving the system.
- Not capable of operating with gas/solid ratios different from 1 (Process not adaptable to different operation conditions).

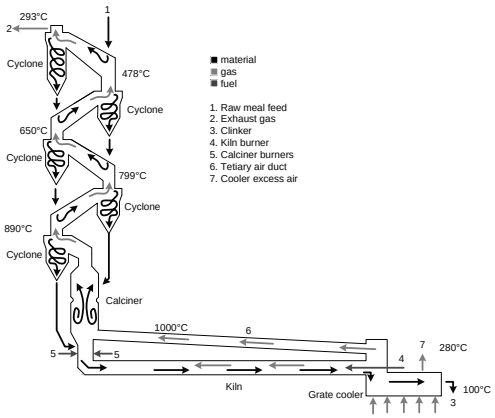

Figure 1: Schematic drawing of a typical pyroprocessing unit in a cement plant.

Other process designs may be more suitable than the existing as cement manufacture face a more and more restrictive legislation with respect to emissions of NO_x, SO_2, Hg and possible also CO_2 in the future, increasing energy prices and the wish for using alternative fuel sources, etc.

This new design must be cheaper to either operate or construct. There are several principal ways to achieve this. Some of these are:

- Compact, modular and scalable unit design (lower design and capital costs)

- Higher energy efficiency than existing design (lower heat losses or better utilization of the thermal energy)
- Acceptable operation over a range of G/S ratios
- Better emission control.

Objective

The main objective of this project is to investigate and develop a new pre-kiln concept for application in the cement industry, which can compete with the existing process design in terms of overall economy and environmental impact.

Alternative Preheater Design

A study of the general heat exchange processes between particles and solids as well as a close cooperation with FLSmidth A/S has lead to several ideas for new pre-kiln concepts.

The most promising of the gas/solid heat exchange concepts has been tested in a cold single stage lab-scale setup and a cold four stage lab-scale setup in order to study the particle and gas flows. The operation principle of this gas/solid heat exchanger is analogous to the existing preheating process, consisting of a series of alternating mixing and separation processes of particles and gas. The overall contacting pattern is counter current. This new design is modular and more compact than the existing design.

The results of the experiments indicate that it is possible to obtain an overall stage efficiency with respect the particle transport of up to 0.8 – 0.9. The gas/solid ratio was varied in the range from 0.2 to 1.2. The experiments were isothermal, why only particle and gas transport can evaluated.

Powder Properties of Raw Meal

During the cold tests of the gas/solid heat exchanger, it became evident that both the fluidization properties and flowability of the raw meal are important for the operation of the process.

Raw meal is calcium carbonate and clay which is milled to sizes below $d_{50} \approx 20$ µm. An example of a cumulative size distribution is provided in Figure 2.

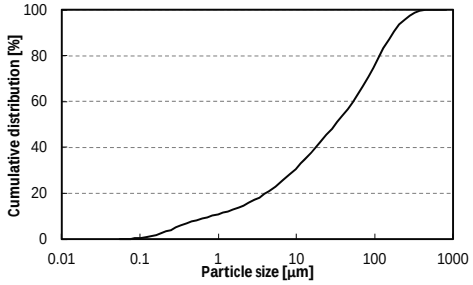

Figure 2: Typical cumulative mass based size distribution of raw meal.

From the data in Figure 2, it is evident that raw meal has a broad size distribution, which for fluidization purposes complicates matters, as the particles fluidize at different gas velocities.

Furthermore, raw meal is cohesive in nature, and will typically not fluidize at all. Particles with this behavior are categorized as group C particles by Geldart [2]. Typical fluidization behavior for this category is plug lift and/or generation of channels upon attempt to fluidize.

This cohesive nature also affects the flowability of the raw meal. Thus a bed of raw meal will tend to form arches and bridges, thus prohibiting a flow of raw meal from the powder bed. This phenomena has been widely studied at ambient temperature, e.g. by Schülze [3], in connection with design of feeders, hoppers and silos. Little knowledge is however available on the flowability of powders at higher temperatures (above 80°C).

Experimental setups

A direct measurement of the flowability of a powder in a given process is very difficult as it depends on both powder and process properties. However tests can be performed to characterize the powders and thereby gain qualitative information on the flowability. For this purpose a hot powder laboratory test setup is under construction. The results from this setup will provide knowledge how temperature, chemical composition and particle size distribution of the powder affects the flowability and inter particle forces.

A pilot test rig which can test the gas / solid heat exchanger under process like conditions is also under construction.

Conclusion

A new gas / solid heat exchanger concept for application in the cement industry is under development. Initial experiments have shown promising results, but the performance at elevated temperature has not been investigated yet. Two experimental facilities which can provide information on the performance of the new concept at temperatures similar to the conditions of the preheating facility of a cement plant are under construction.

Acknowledgements

This project is a part of a Research Platform on Future Cement Technology financed by Danish National Advanced Technology Foundation, FLSmidth A/S and DTU.

References

1. J.I. Bhatty, Innovation in Portland Cement Manufacturing, Portland Cement Association (2004), p. 224
2. D. Geldart, Powder Technol. 7 (1973) 285-292.
3. D. Shülze, Powders and Bulk Solids, Springer (2008)

Sabine Reinsch
Phone: +45 2132 5380
E-mail: sare@risoe.dtu.dk

Supervisors: Per Ambus
Iver Jakobsen

PhD Study
Started: December 2009
To be completed: November 2012

Long-Term Climate Change Effects on Dynamics of Microorganisms and Carbon in the Root-Zone

Abstract
Changing climatic conditions such as elevated temperature and drought in combination with rising CO_2 concentrations affect the terrestrial carbon cycling. Plants re-allocate carbon from the atmosphere belowground, where part of it is utilized by microbes for growth and reproduction. Anticipated changes in microbial activity and community composition in response to climatic changes may alter pathways and process rates in the carbon cycle and, CO_2 may consequently be released from the soil. Within this study, the effects of rhizosphere microbial communities on belowground carbon cycling will be investigated with *in-situ* $^{13}CO_2$-pulse-labeling under climatic conditions as predicted for Denmark in 2075.

Introduction
Microbial communities consist of bacteria and fungi. Saprophytic fungi are highly important for soil organic matter (SOM) mineralization. Symbiotic mycorrhizal fungi receive carbon (C) from their host plants and provide part of its nutrients in return. This symbiosis facilitates plant growth and performance. Gram-negative bacteria appear frequently in the plant rhizosphere consuming preferentially plant derived C. In contrast, gram-positive bacteria are more widespread and feed on plant derived C and subgroups are also able to mineralize the more recalcitrant SOM [1, 2]. Changes in environmental conditions will also affect rhizosphere properties and hence conditions for the microbial community [3].

Natural occurring C isotopes ($^{13}C/^{12}C$, 1.1 % vs. 98.9 %) can be used to determine C sources within an ecosystem. $^{13}CO_2$ pulse-labeling will increase the ^{13}C content compared to natural background levels. This enrichment can be used to trace the C from the atmosphere through plants into rhizosphere, microbes and SOM (Figure 1). Microbes will incorporate the transferred C isotopes e.g. into fatty acids.

Some phospholipid fatty acids (PLFAs) are characteristic for certain microbial functional groups and are therefore used as natural biomarkers. Biomarker detection provides a detailed insight into C fluxes through the rhizosphere microbial community.

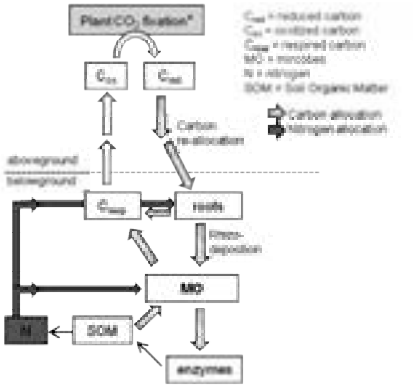

Figure 1: Connection of aboveground and belowground C cycling. *atmospheric CO_2 can be experimentally exchanged by $^{13}CO_2$ to study belowground C transport.

Specific Objectives
We want to follow the short term C turnover under natural conditions with emphasis on the importance of the rhizosphere microbial community by using non-invasive stable isotope labeling.

We hypothesize that future climatic conditions will i) rise the activity of the rhizosphere microbial community, ii) change the microbial community composition and, iii) decrease the microbial diversity.

Methodology

Field scale *in-situ* $^{13}CO_2$-pulse-labeling was performed at the climatically manipulated field site "Climaite" (Denmark) in May 2011 [4]. The experimental setup consists of a full combination of elevated CO_2 (eCO_2), elevated temperature and drought.

Each experimental sub-unit was coupled to one gas-reservoir to maintain constant CO_2 concentrations in the experimental chambers over a period of 5 hours (Figure 2). Soil samples were taken 1, 2 and 8 days after labeling to follow the C translocation over time. PLFAs were extracted from freeze dried root and soil samples following a modified protocol of Bligh and Dyer [5]. PLFA samples were analyzed on a GC-c-IRMS for biomarker fatty acids and their $\delta^{13}C$ content. Furthermore, chamber measurements for soil and ecosystem respiration (R_S and R_E) were conducted the same days. Gas samples were analyzed at a GasBench system for $\delta^{13}C$ and CO_2 concentration.

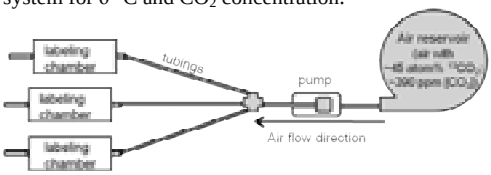

Figure 2: Experimental field labeling setup.

Results and Discussion

We succeeded in treating all plots simultaneously and similarly (Figure 3). The ^{13}C atom% content in the labeling chambers was about half of the gas reservoir due to mixing with background CO_2 from atmosphere and soil.

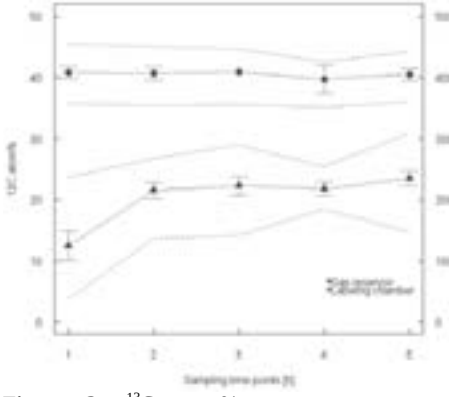

Figure 3: ^{13}C atom% measurements over the experimental time in the gas reservoir (circles) and labeling chambers (triangles).

PLFAs were successfully extracted from root samples and run on the GC-c-IRMS. Evaluation of the data is pending. However, an increase in $\delta^{13}C$ of some fatty acids has been detected.

Soil (p=0.010) and ecosystem (p=0.024) respiration was significantly reduced under drought conditions. Elevated CO_2 showed no effect on respiration. However, the variability in respiratory processes within the eCO_2 treatment was high (mean±sd, R_S: 1.01±0.89 µmol CO_2*m^{-2}*sec^{-1}, R_E: 1.55±1.33 µmol CO_2*m^{-2}*sec^{-1}). Generally, eCO_2 was found to facilitate respiration processes [6] which might be masked by the high variability in our experiment.

Conclusions

Plants are affected by soil water content (e.g. drought periods) which influences photosynthesis rates and thus, the starting point of belowground C allocation. Elevated CO_2 provides favouring conditions for increased belowground biological activity, but changes in respiratory activity could not be observed in this study.

However, root growth was enhanced under eCO_2 conditions [7] and potentially more C was allocated belowground and provided more rhizodeposits. Litter produced under eCO_2 conditions is known to be more recalcitrant [8] and therefore poorly available for some microbes. A shift in the microbial community is assumed towards a more fungal based community that is able to use more recalcitrant SOM for survival.

Acknowledgements

The authors would like to thank the "International Research Education Programme for Soil Technology And inter-disciplinary Research in Soil and Environmental Sciences" (www.stair.agrproject.dk), the project "Climate Change Effects in Terrestrial Ecosystems" (www.climaite.dk) and the Technical University of Denmark (www.dtu.dk) for financial support. Climaite project members and Risø-Eco colleagues are also greatly acknowledged for many fruitful discussions and great practical help.

References

1. C. Kramer, G. Gleixner, Soil. Biol. Biochem. 40 (2008) 425-433.
2. J. Garcia-Pausas, E. Paterson, Soil. Biol. Biochem. 43 (2011) 1705-1713.
3. P. Marschner, S. Timonen, Appl. Soil. Ecol. 28 (2005) 23-36.
4. T.N. Mikkelsen, C. Beier, S. Jonasson et al., Funct. Ecol. 22 (2008) 185-195.
5. E.G. Bligh, WJ Dyer, Canad. J. Biochem. Physiol. 37 (1959) 911-917.
6. K. Carney, B. Hungate, B. Drake, J. Megonigal, PNAS. 104 (2007) 4990-4995.
7. pers. comm. Marie Arndal
8. M.F. Cotrufo, M.J.I. Briones, P. Ineson, Soil. Biol. Biochem. 30 (1998) 1565-1571.

Negar Sadegh
Phone: +45 4525 2821
E-mail: nes@kt.dtu.dk
Discipline: Engineering Thermodynamics

Supervisors: Kaj Thomsen
Erling H.Stenby
Georgios Kontogeorgis

PhD Study
Started: April 2009
To be completed: April 2012

Thermodynamics of Acid Gas Removal from Natural Gas with Alkanolamines as A Solvent

Abstract
This PhD project is about thermodynamics of natural gas cleaning process with alkanolamines (MDEA/MEA) as solvent. The research combines both experimental and thermodynamic modeling studies. High pressure VLE data for CH_4-H_2S-MDEA-H_2O system, atmospheric VLE data for CO_2-MDEA-H_2O system over whole amine concentration range, atmospheric VLE data for CO_2-MDEA–PZ- H_2O system and density data for aqueous MDEA solutions and aqueous mixtures of MDEA and PZ (Piperazine) were measured in the experimental part of the project. For the modeling part the Extended UNIQUAC model was used for representation of the behavior of CO_2-MDEA- H_2O, CO_2-MEA-H_2O, CO_2-MDEA–MEA-H_2O, H_2S-MDEA-H_2O and CH_4-H_2S-MDEA-H_2O. The model parameters are fitted to plenty of different kinds of data covering an extensive pressure, temperature and concentration range.

Introduction
A thermodynamic model is required for designing of acid gas removal plant. It is important to have the model that can well represent the behavior of acid gas-methane-alkanolamine-water systems over whole amine concentration range, extensive pressure and temperature range. Most of the commercial simulators could not show good results at high amine concentration, so there is a need for improving modeling in this area.

Thermodynamic modeling of these systems has been done through 3 different ways: empirical correlations, such as: Kent and Eisenberg (1976) for CO_2+MEA/DEA+H_2O systems and Gabrielsen et al. (2005) for CO_2+MEA/DEA/MDEA+H_2O systems; equations of State, such as: Chunxi and Fürst (2000), Huttenhuis (2008), Vrachnos et al. (2004) , Solbraa (2002) and activity coefficient models, such as: E-NRTL (Austgen et al. (1989)), Extended UNIQUAC (Faramarzi et al. (2009)), UNIQAC-NRF (Haghtalab and Dehghni (2007)), Modified Clegg-Pitzer (Kundu at al. (2003)).

Empirical correlations fail when being extrapolated to conditions other than what they are based on. Equations of state mostly are limited to certain conditions. For instance Solbraa EoS can only show good results at ambient temperature. Currently, the best approach for modeling the behavior of these systems is by activity coefficient models for electrolyte solutions.

In this work extended UNIQUAC model is developed on the basis of original model [1] presented by Thomsen et al. Model is used to estimate various thermodynamic properties of the alkanolamine systems required for the design of natural gas treating units.

The problem with the VLE (vapor-liquid equilibrium) data available in the open literature is that they are not generally very consistent. Moreover, there are a few sources for high pressure VLE data, data with presence of methane. According to our knowledge there is not any source that covers whole amine concentration range. In this work VLE data for CH_4-H_2S-H_2O-MDEA, CO_2-MDEA-H_2O, CO_2-MDEA-PZ-H_2O systems and density data for aqueous MDEA and aqueous mixtures of MDEA and PZ (Piperazine) were measured.

Specific Objectives
The purpose of this study in the modeling part is to get an accurate estimation of both VLE and thermal properties of the acid gas-methane-water-alkanolamine systems over broad range of temperature, pressure and amine concentration.

This was done by gathering experimental VLE data on acid gas-methane-alkanolamine-water systems, and thermodynamic modeling of the system with the Extended UNIQUAC model. For the experimental part the aim is to get data in the areas that there is a gap in the open literature.

Results and Discussion

Modeling

The extended UNIQUAC model as presented by Thomsen and Rasmussen [1] is used for the thermodynamic calculations of this work. Extended UNIQUAC is the original UNIQUAC equation (Abrams and Prausnitz [2] and Maurer and Prausnitz [3]) combined with the Debye–Hückel term. The latter term is added to account for the electrostatic interactions caused by the presence of the ionic species in the solution. Therefore, the excess Gibbs energy is expressed as the combination of three terms: the entropic and enthalpic terms of the original UNIQUAC equation to consider the non-electrostatic interactions and, the electrostatic term (Debye–Hückel):

$$\frac{G^E}{RT} = \left(\frac{G^E}{RT}\right)_{UNIQUACEntropic} + \left(\frac{G^E}{RT}\right)_{UNIQUACEnthalpic} + \left(\frac{G^E}{RT}\right)_{Debye-Huckel}$$

Parameter Regression Database

Parameters are optimized from the available experimental solubility and thermal data, covering high pressure, high temperature and high amine content. Some of the modeling results are shown in the following figures.

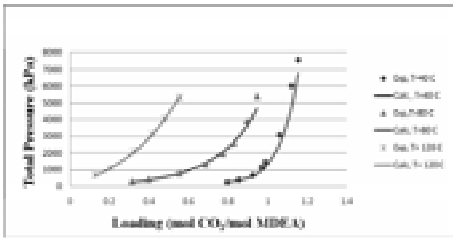

Figure 1: P-x diagram for MDEA-H_2O-CO_2 system for solvent molality of 8, at 40, 80 , 120 °C and 0-80 bar

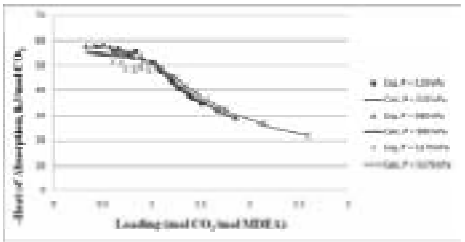

Figure 2: -Heat of absorption diagram for MDEA-H_2O -CO_2 system for solvent molality of 1.48 , at 50 °C and 5, 10, 50 bar

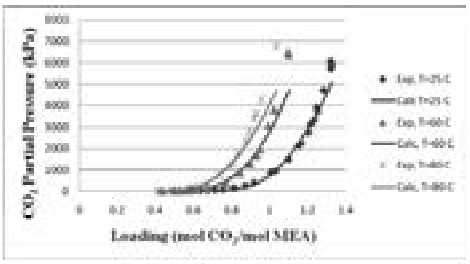

Figure 3: P-x diagram for MEA- H_2O -CO_2 system for solvent molality of 3, at 25, 60, 80 °C and 0-80 bar

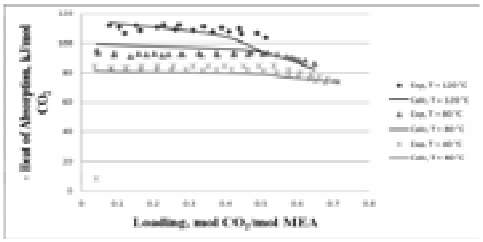

Figure 4: -Heat of absorption diagram for MEA- H_2O -CO_2 system for solvent molality of 7, at 40, 80, 120 °C and 0-1.2 bar

The obtained results revealed that the Extended UNIQUAC model can effectively predict both the gas solubility and heat of absorption over an extensive range of conditions with only a unique set of parameter.

Experimental

CH_4-H_2S-MDEA-H_2O system

VLE measurements were done for mixtures of methane, H_2S, MDEA and water at total pressure of 70 bar, temperatures of 50 and 70 °C, MDEA concentration of 50 weight percent, and H_2S partial pressure of 0.2 to 10 bar. Figure 5 shows the measured points.

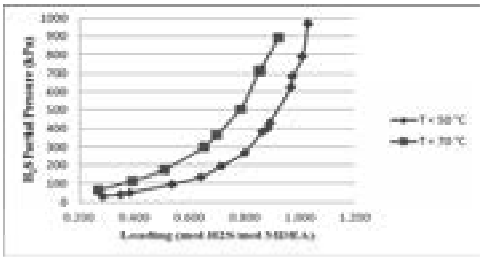

Figure 5: VLE measurements for CH_4-H_2S-MDEA-H_2O system at 70 bar total pressure and MDEA wt% = 50

CO_2-MDEA-H_2O system

VLE measurements for CO_2-MDEA-H_2O system were performed at atmospheric pressure, temperature between 40 and 80 °C, MDEA concentration from 10 wt% to pure MDEA. Figure 6 shows the measured data.

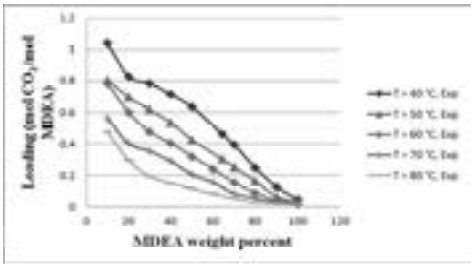

Figure 6: VLE measurements for CO_2-MDEA-H_2O system at 1.1 bar total pressure

According to our knowledge this data, in aspect of covering whole amine concentration range, are unique.

CO_2-MDEA-PZ-H_2O system

VLE measurements for mixtures CO_2, MDEA, Piperazine and water is done at atmospheric pressure, temperature range of 40 to 70 °C, MDEA wt% between 25 to 75 and Piperazine wt% of 5 and 10. Figures 7 to 10 show the experimental data at 40, 50, 60 and 70 °C, respectively.

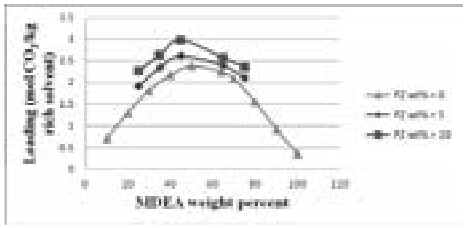

Figure 7: VLE measurements for CO_2-MDEA-PZ-H_2O system at T = 40 °C and 1.1 bar total pressure

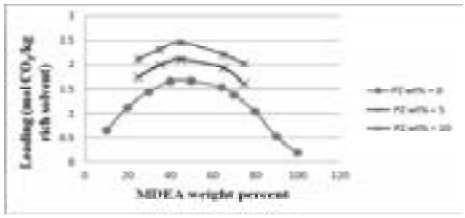

Figure 8: VLE measurements for CO_2-MDEA-PZ-H_2O system at T = 50 °C and 1.1 bar total pressure

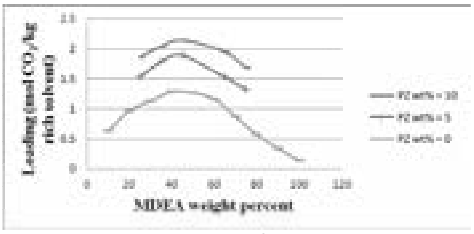

Figure 9: VLE measurements for CO_2-MDEA-PZ-H_2O system at T = 60 °C and 1.1 bar total pressure

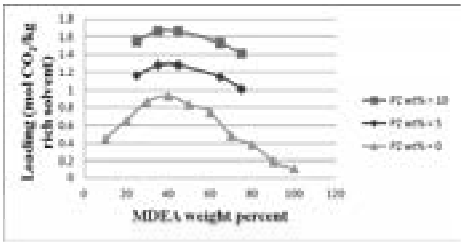

Figure 10: VLE measurements for CO_2-MDEA-PZ-H_2O system at T = 70 °C and 1.1 bar total pressure

As it can be seen from figures 7-10, absorption capacity is at its highest level at around 45 MDEA wt% and it will increase with Piperazine weight percent.

Density of aqueous MDEA and aqueous MDEA+PZ

Figure 11 shows density measurements for aqueous MDEA solutions at 40, 50, 60, 70 and 80 °C.

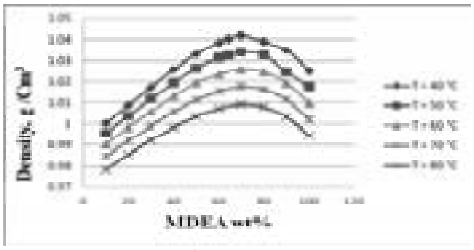

Figure 11: Densities of aqueous MDEA solutions at atmospheric pressure

Figure 12 plots densities of aqueous MDEA and Piperazine solutions at temperature range of 40 to 80 °C against MDEA weight percent.

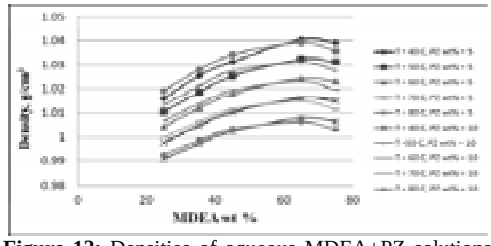

Figure 12: Densities of aqueous MDEA+PZ solutions at atmospheric pressure

Conclusion:

In this work Extended UNIQUAC model is developed for modeling phase behavior and thermal properties of acid gas-methane-alkanolamine-water systems over extensive range of temperature, pressure and amine concentration. It has been shown that Extended-UNIQUAC can accurately represent the behavior of these systems.

Relatively unique vapor-liquid equilibrium data with good accuracy was measured both at high and atmospheric pressures for H_2S-CO_2-CH_4-MDEA-PZ–

H_2O systems. Density of aqueous MDEA and aqueous MDEA and PZ solutions was also measured in this study.

Acknowledgment:
We would like to thank Statoil for funding this PhD project and giving the opportunity to do the experiments in their well-equipped laboratories.

References

1. K. Thomsen, P. Rasmussen, Chem. Eng. Sci. 54 (1999) 1787–1802.
2. D.S. Abrams, J.M. Prausnitz, AIChE J. 21 (1975) 116–128.
3. G. Maurer, J.M. Prausnitz, Fluid Phase Equilibr. 2 (1978) 91–99.

List of Publications

1. N. Sadegh, K. Thomsen, E.H. Stenby, G. Kontogeorgis, Thermodynamic modeling of water-acid gases-alkanolamine systems, full conference paper in proceedings of the 9th AIChE annual meeting , USA, 2009
2. N. Sadegh, K. Thomsen, E.H. Stenby, G. Kontogeorgis, Thermodynamic modeling of water-acid gases-alkanolamine systems, Oral Presentation at the 9th AIChE conference , USA, 2009
3. N. Sadegh, E.H. Stenby, G. Kontogeorgis, K. Thomsen, Thermodynamic modeling of sour gas cleaning process with alkanolamines, Oral Presentation at ICCT-2010 conference, August 2010, Japan
4. N. Sadegh, E.H. Stenby, G. Kontogeorgis, K. Thomsen, Thermodynamic modeling of sour gas cleaning process with alkanolamines, Invited speaker at SPE (STC-2010) conference, October 2010, Germany
5. **N**. Sadegh, E.H. Stenby, G. Kontogeorgis, K. Thomsen, Thermodynamic modeling of sour gas cleaning process with alkanolamines**,** Oral Presentation at 25th European symposium on applied thermodynamics, ESAT-2011, June 2011, Russia

Suriyati Saleh
Phone: +45 4525 2927
E-mail: ss@kt.dtu.dk
Discipline: Reaction and Transport Engineering

Supervisors: Kim Dam-Johansen
Peter Arendt Jensen

PhD Study
Started: January 2010
To be completed: December 2012

Pretreatment of Biomass via Torrefaction Process

Abstract
Torrefaction is a thermal pretreatment techniques for improving the properties of herbaceous and woody biomass in order to deal with such problems as high moisture content, low energy density, poor grindability, and high bulk volume. In this study, wheat straw and wood chips (spruce) were torrefied at different torrefaction temperatures and durations in order to improve the properties of the biomass to be used for pulverized fired boiler. The grindability of torrefied biomass was evaluated by the particle size distribution. The temperature and reactor residence time strongly affected the torrefied biomass and the type of feedstock influenced the conversion rate.

Introduction
The use of renewable energy is a topic of great interest, as it represents a diversification of the energy sources and contributes to preserving the climatic stability. Among the different energy sources, biomass holds a large promise for increasing use in the next few years. Moreover, biomass is considered as a carbon neutral fuel because the carbon dioxide released during its utilization is an integral part of the carbon cycle [1]. Biomass can be processed to produce energy by different technologies such as thermochemical (combustion, pyrolysis and gasification), biological (anaerobic digestion and fermentation), and chemical processes (esterification) [2]. On the other hand, there are several major shortcomings in the direct utilization of biomass owing to the characteristics of the biomass. The lignocellulosic materials with fibrous structure are difficult to grind and fine particles are needed during combustion of biomass in suspension fired boilers [2].

Pretreatment technology can improve the biomass properties and lead to a reduction of the cost of the transport and storage of biomass. Researchers have recently paid more attention to pretreatment technologies, especially those of thermal chemical conversion methods in order to upgrade the biomass properties. A well-known pretreatment technology is flash pyrolysis carried out at high heating rate and relatively higher temperatures with a short residence time of several seconds. However, another technology is a mild pyrolysis process called torrefaction. Torrefaction is a process of thermal degradation of biomass at relatively low temperatures and low heating rate of less than 50 °C min^{-1} under anoxic conditions. During a torrefaction process, the density and the specific heating value of the product increased, the grindability is improved and the moisture content is reduced.

Specific Objectives
An ideal biomass pretreatment method would provide the heating value of the biomass for the boiler, but in a way such that the fuel is easily pulverized. In order to achieve this goal, a simultaneous torrefaction and grinding process will be used as a pretreatment method. The main objective for the current study is to investigate the influence of temperature and residence time on the grindability of biomass. The focus will be on how to produce fine particles that is suitable for suspension firing. Furthermore, the solid yield on torrefied biomass from torrefaction process will be investigated and compared with the result from thermal-gravimetric analysis (TGA).

Experimental work
The experiments were conducted by using a simultaneous torrefaction and grinding reactor. Straw and wood chips (spruce) has been torrified at temperatures from 240 °C – 380 ° C with different residence time (30 minutes and 90 minutes). A continuous flow of nitrogen is used to keep the system inert. The weight of the char was measured in order to determine the mass loss of the samples. In order to study the grindability of the torrified biomass, the samples were sieved into different size fractions to

evaluate the particle size distribution. D_{50} values were obtained from this particle size distribution curves.

Results and Discussion

1. Grindability of torrified product

During torrefaction, the orientation of microfibrils is displaced through decomposition of the hemicelluloses, depolymerization of cellulose and thermal softening of lignin. The cell wall in the biomass sample is greatly weakened after torrefaction. The increased brittleness and friability introduced by torrefaction improves the grindability of biomass.

The decreased in d_{50} value as presented in Figure 1 shows that the grindability properties of torrefied biomass is increased. Figure 1 shows that torrefaction temperature and residence time have a significant influence on grindability of biomass. D_{50} for untreated straw is 1315 µm, and this value is reduced to 220 µm when straw is torrefied at 350 °C for 30 minutes, showing 83% size reduction. When longer residence time is introduced, d_{50} is reduced to 50 µm at 300 °C.

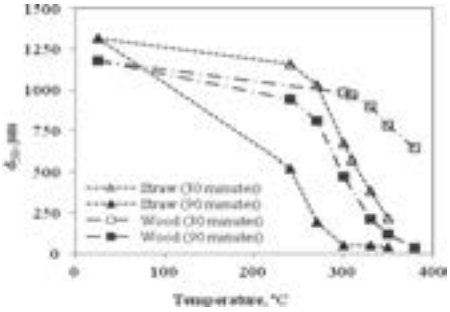

Figure 1: Effect of temperature and residence time on d_{50} value of torrified biomass

Untreated wood chips has a smaller d_{50} of 1180 µm compared to straw, but for 30 minutes torrefaction, wood chips only achieve a 34% reduction of d_{50} value at 350 °C. The grindability of wood chips is significantly increased when torrefaction is performed for 90 minutes. 90% reduction of d_{50} is achieved for torrefaction at 350 °C. For both cases, straw shows a better grindability improvement compared to wood chips. This may be caused by different phenomena. Woody biomass has a higher lignin content, and the single wood particle are heavier compared to straw, so a longer heating time of the wood chips is needed to obtain the same degree of conversion, compared to the herbaceous biomass (straw).

2. Yield of torrified product

The variation in the mass yield of torrefied char product with the final reactor temperature is shown in Figure 2. The results indicate that, for 30 minutes torrefaction, the weight loss of biomass depends significantly on the temperature. However, for 90 minutes torrefaction, when the torrefaction temperature is relatively high, above 330 °C, the weight losses of the two biomass materials tend to become uniform. At temperature lower than 330 °C, straw shows a higher degree conversion than wood chips. Result from TGA pyrolysis experiments as presented in Figure 3 shows an initial higher conversion of straw at low temperature. Straw has higher content of hemicelluloses and cellulose compared to the wood chips (higher lignin content). Straw also have a higher alkali content that may catalyze the pyrolysis process.

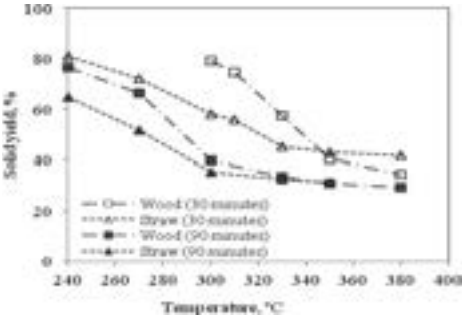

Figure 2: Effect of torrefaction temperature and residence time on the solid yield of torrefied biomass

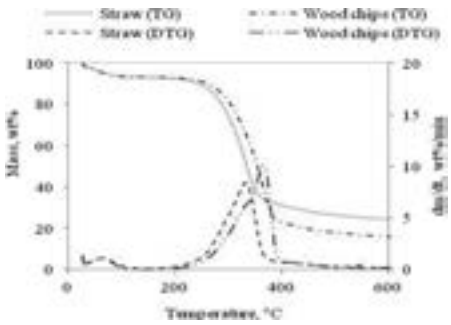

Figure 3: TG and DTG curve for straw and wood chips

Conclusions

Torrefaction of biomass produces a solid fuel with better grindability properties compared to those of fresh biomass. Improved grindability of torrefied biomass is being due to decomposition of lignocellulosic materials during torrefaction.

Acknowledgement

The author acknowledges the financial support by the Ministry of Higher Education (MoHE) of Malaysia, Universiti Malaysia Pahang (UMP) and by the company Energinet.dk.

References

1. B. Arias, C. Pevida, J. Fermoso, M.G. Plaza, F. Rubiera, Fuel Process. Technol. 89 (2008) 169–175.
2. A. Demirbas, Prog. Energ. Combust. Sci. 31 (2005) 171–192.

Sara Bülow Sandersen
Phone: +45 4525 2983
E-mail: sbs@kt.dtu.dk
Discipline: Engineering Thermodynamics

Supervisors: Nicolas von Solms
Erling H. Stenby

PhD Study
Started: May 2008
To be completed: March 2012

Enhanced Oil Recovery with Surfactant Flooding

Abstract
Experimental work is carried out on a high pressure DBR JEFRI PVT cell, to conduct several phase behavior studies at ambient temperatures and pressures. A surfactant model system has been studied, (sodium dodecyl sulfate/1-butanol/heptane/water/sodium chloride). This system was exposed to reservoir temperatures and pressures and the present pressure effect showed a significant change in the phase behavior. Also a crude oil/brine system has been examined at similar reservoir conditions. Different brine solutions were used to provide a better understanding of which effects that may alter the oil recovery. It was found that both pressure, temperature and sulfate concentration influence on the phase behavior.

Introduction
Enhanced Oil Recovery (EOR) is widely applied. However, the exact interactions of oil/brine/surfactant and detailed understanding of the effect from salinity, pressure, temperature, etc. is not to conclude from literature e.g. most experimental work is carried out at room temperature.

Surfactant flooding is an EOR technique to attain higher and more optimal oil recovery. Surfactants are injected into the reservoir to reduce the interfacial tension (IFT) to an ultra low IFT between oil and water, which should mobilize the oil. Along with this EOR method, several complex issues are related, where the design of the added chemicals must be tailored to the specific rock and fluids. The principle of flooding is illustrated in figure 1.

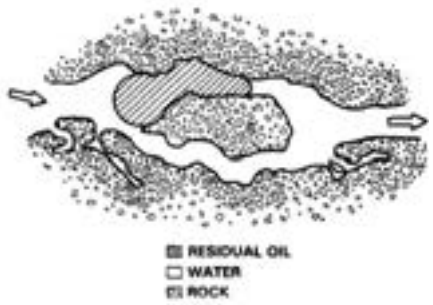

Figure 1: Principles of flooding, where residual oil is trapped in the reservoir, [1]. The residual oil trapped in narrow capillary pores is held back thanks to capillary forces and it is required to reduce the IFT between oil and water to 0.001 dynes/cm to mobilize the oil.

Usually the remaining oil is distributed in the pores in the reservoir, where the oil is trapped due to capillary and viscous forces. The mobilization of the residual oil is achieved through surfactants generating a sufficiently low oil/water IFT. Low IFT further gives capillary numbers large enough to overcome the capillary forces. The recovery efficiency is highly dependent on the capillary number which is defined as equation 1.

$$N_c = \frac{\mu_w v_w}{\varphi \gamma_{wo}} \quad (1)$$

where N_c is capillary number, μ_w is viscosity of the aqueous or displacing phase in [Pa Sec], v_w is flow rate of the displacing fluid in [cm/sec], φ is effective porosity of formation and γ_{wo} is interfacial tension between water and oil in [N/m].

Usually co-surfactants are blended into the liquid aqueous solution to improve the properties of the surfactant solution. It is experienced that due to chromatographic separation during flooding it is very complicated to design a surfactant/co-surfactant solution that can perform optimal throughout the reservoir. There will be losses due to adsorption and trapping to the rock. It is essential to assure stability of the surfactant solution, which must resist physical conditions such as high temperatures, high pressures and high salinities. [2]

Recent experimental results have shown that an increase in oil recovery is observed with sulfate

enriched brine. Could this be understood better from phase behavior studies? An oil/brine study has been carried out concurrently with the phase behavior study of surfactants. IFT measurements at room temperature have shown that sulfate concentration did not induce any significant changes, [3], where effect from pressure, temperature and brine composition may be the explanation.

One surfactant system with sodium dodecyl sulfate (SDS)/heptane/1-butanol/sodium chloride (NaCl)/water is examined for pressure effect on the phase behavior. Additionally two crude oils are examined with different brine solutions with varying sulfate concentration.

Specific Objective

This Ph.D.-project handles the study of the potential of single component surfactant systems in contrast to the more ordinary systems with surfactants and co-surfactants and examines the effect from realistic reservoir pressure. Furthermore an oil/brine study is carried out to achieve better understanding for such systems, which is exposed to different sulfate concentration at reservoir conditions.

Surfactant Flooding and Emulsions

EOR with surfactant flooding has been investigated for many years. Unfortunately, it has not yet been commercial employed, as it has not been tested successfully in full scale yet. [4]

Chemical EOR is the injection of one or more specific liquid chemicals, the so-called surfactants, that controls the phase behavior properties in the reservoir. Surfactants should reduce the IFT between the injected liquid and oil to 0.001dynes/cm, which will then overcome the existing capillary forces and thus mobilize the oil towards the production well.

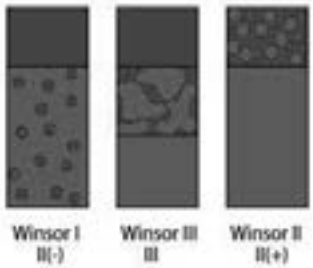

Figure 2: Surfactant systems are typically considered as so-called Winsor type systems. The desired microemulsion phase which creates the ultra low IFT is the Winsor III situation.

Surfactant flooding EOR involves microemulsions, where oil/water and water/oil micelles are formed, see figure 3 for illustration. In the beginning of a surfactant flood the surfactant concentration is low and then the concentration increases. At low surfactant concentrations the surfactant molecules are dispersed as monomers. As surfactant concentration is increased the surfactants molecules starts to aggregate and at some point the concentration will reach the critical micelle concentration (CMC). Any further addition of surfactants will form into micelles.

Surfactants are frequently classified by their ionic nature of the head group as anionic, cationic, nonionic or zwitterionic. Anionic surfactants are the most widely used surfactants for surfactant flooding and according to Austad *et al.* (1996) [5] promising surfactants, for single component surfactant flooding, are branched ethoxylated sulfonates.

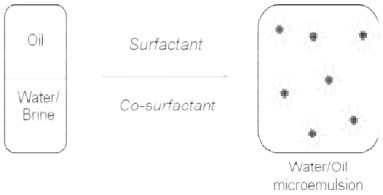

Figure 3: Oil and brine/water mixed with surfactants forming microemulsions.

The formation of microemulsions is very important to attain a successful surfactant flood, as the ultra low IFT is obtained when these are present. Also the formation of emulsions for general oil/brine systems can contribute to alter the oil recovery.

Phase Behavior Experiments

It is reported in literature that an increase in temperature increases the optimal salinity for the surfactant system.

Aside from the influence of temperature the effect of pressure on the phase behavior of the microemulsion is widely discussed as results from different researchers disagree. Reservoir conditions are typically at elevated pressures, why the possible effect from such should be understood well.

Observing surfactant systems there are three types of systems to be considered.

Figure 4: From left to right: multiphase region with lower-phase microemulsion with excess of oil (Winsor II(-), middle-phase microemulsion (Winsor III) and upper-phase microemulsion with excess of water/brine (Winsor II+).

Figure 4 represents the phase environment where surfactant/water/oil systems can equilibrate as either a single phase or as multiple phases.

The experimental activities have been focused on the phase behavior of a model system; SDS/brine/1-butanol/heptanes, at elevated temperatures and pressures. The model system is investigated in a DBR JEFRI PVT cell, a high pressure and high temperature cell which allow visual observation of phase change and measurement of phase volume through its window. The set up is pictured in figure 5. The purpose for the model

system is to study if effects pressure e.g. changes in the phase behavior, such as the number of present phases. Furthermore the same setup was used for an oil/brine study to examine oil/brine interaction at reservoir conditions. Afterwards these systems were analyzed for any effects on the crude oil dependent on the operation or the different sulfate content in the brine solutions.

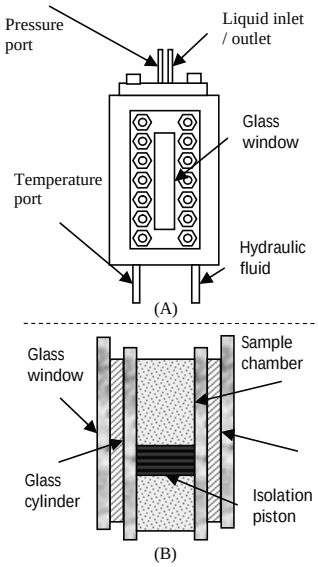

Figure 5: Drawing of the DBR JEFRI PVT cell used for high pressure phase equilibrium experiments. (A) Shows the outside of the cell and (B) shows the inside construction of the cell.

As introduced there are two parts in the experimental work carried out. Part one is a study with a surfactant model system. Table 1 show examples of compositions of this system, which has been studied.

Table 1: Surfactant model system with two different examples of composition in wt%.

Comp.	water	NaCl	SDS	1-butanol	heptane
#1	0.616	0.043	0.025	0.051	0.265
#2	0.532	0.037	0.022	0.044	0.365

The other experimental part of this project is an oil/brine system with different brine solutions. Table 2 shows the properties of the studied crude oil.

Table 2: Properties of Latin America crude oil.

Density [g/cm^3]	Acid No. [mhKOH/g]	Base No. [mgKOH/g]	Asphaltene [%]	Visc. [cp]
0.846	0.163	0.563	3.42	24.4

The oil/brine study is carried out in collaboration with another Ph.D. from this group (CERE).

Results from Work with Surfactant System

The model surfactant system has earlier been studied at room temperature and at atmospheric pressure [6], where the present phase diagram in figure 6 shows the results.

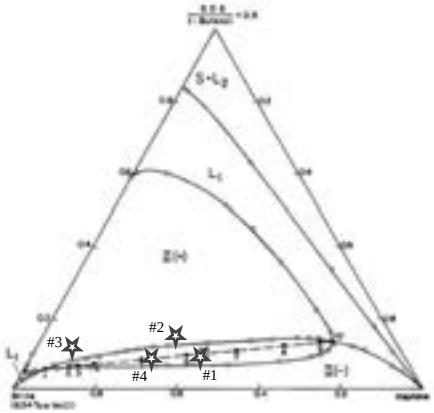

Figure 6: Phase diagram for brine/SDS/1-butanol/heptane at atmospheric pressure and room temperature. Stars indicate at which compositions this system has been studied at elevated pressure and temperature, where phase behavior depends on these parameters.

A number of experiments have been carried out at different compositions for the model surfactant system, where it has been exposed to different pressures and temperatures in the range of 1-400 bars and 35-50˚C, respectively. At several compositions it was observed that e.g. a two phase system could be changed to a three phase system only dependent on an increase in pressure, which is located by the stars in figure 6. The physical conditions, pressure and temperature, are tabulated in table 3.

Table 3: Overview of the physical conditions when phase shifts are observed and the changes in the number of phases.

Experiment No.	Phase shift	Temp. [˚C]	Pressure [Bar]
#1	3 to 2	35	156
#2	2 to 3	35	302
#3	2 to 3	40	100-200
#4	3 to 2	40	160

All observations for the experimental work are reversible. They include shift from a lower-phase microemulsion with excess of oil to the middle-phase microemulsion region and further shift from the middle-phase microemulison region to the upper-phase microemulsion with excess of water/brine all due to an increase in pressure. These observations cannot be described by thermodynamic models, due to the characteristics of the surfactants, co-surfactants and NaCl. The lately progress in the project has been a LLE

study on water/alcohol/alkane systems to decide if the pressure effect for such systems could possibly be in cooperated theoretically.

Results from Work with Oil/Brine System

The oil/brine study is carried out experimentally similar to the surfactant study approach. Two crude oils were studied, Latin American Crude Oil (LACO) and Middle East Crude Oil (MECO). The purpose is to study if different brine solutions, (with varying sulfate concentrations), has an effect on the crude oils. As seen in figure 7 formation of emulsion was observed in the case of MECO. After operation in the DBR JEFRI PVT cell the crude oils are analyzed, where the viscosity and IFT are measured. The viscosity results for the LACO are graphically shown in figure 8.

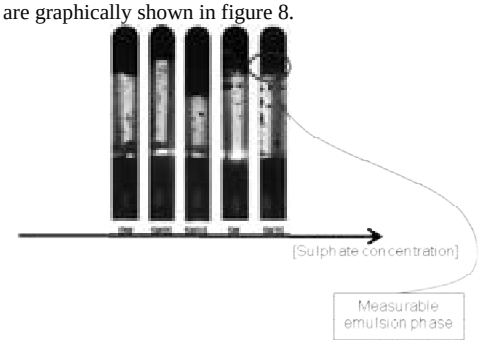

Figure 7: Observation from the inside of the DBR JEFRI PVT cell, showing MECO mixed with brine with increasing sulfate concentration from left to right.

With respect to the viscosity of LACO, it is found that there is a significant decrease in the oil viscosity when the measurements are done before and after operation. The increase in sulfate concentration alters the viscosity after operation. This was not the case for MECO, which formed emulsions with increasing pressure, temperature and sulfate concentration. In contrast the effect on LACO was mainly de-emulsification during operation.

Discussion

As the surfactant system tested is only a model system further studies will be required to establish a more general understanding of the observations. However, the results agree that the phase behavior is dependent on the pressure.

Regarding the oil/brine study the results show that at high temperatures and pressures in the case of LACO sulfate ions may help decrease the crude oil viscosity and for MECO formation of emulsions was observed. This indicates that any trend may be very crude oil specific. In addition it should be noticed that the reservoir rock also will interact as an important agent with respect to both observations.

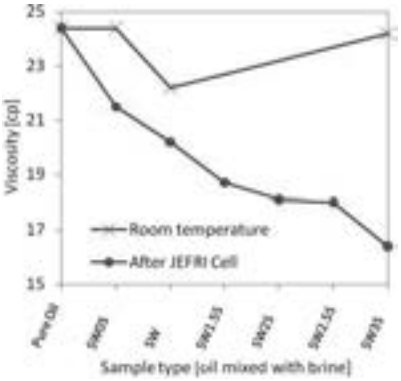

Figure 8: Graphical illustration of the viscosity results of the crude oil before and after the oil/brine system was processed in the DBR JEFRI PVT cell. Measurements are at different brine solutions, where SW0S is with no sulfate and then the sulfate concentration is increased from 1 to 1.5to 2 to etc. thereafter.

Conclusion

Experimental activities regarding phase behavior has been conducted.

Phase behavior of oil/ surfactant/ alcohol/ brine systems at elevated temperatures and pressures has been examined. The model system studied, heptane/ SDS/ 1-butanol/ brine, shows that both temperature and pressure has an effect on the equilibrium system. Change in pressure entails change in number of present phases from 2 to 3 phases and 3 to 2 phases. Furthermore a LLE study on relevant water/alcohol/alkane systems has been started.

The oil/brine study showed that increase in temperature and pressure has an effect on the system. Depending on the crude oil, the pressure, temperature and the sulfate concentration the system starts forming emulsions for MECO and a significant decrease in viscosity is observed for LACO.

References

1. B.M. O'Brian, J. Am. Chem. Soc. 59 (1982) 839a-852s
2. D.W. Green, G.P. Willhite, Enhanced Oil Recovery, SPE Textbook Series, 6 (1998) 7
3. P. Zhang, Austad, SPE 94209, SPE/Europe/EAGE Annual Conference, Spain July 13th-16th, 2005
4. Y. Wu, P. Shuler, Y. Tang, W.A. Goddard, SPE 95404 presented at SPE Annual Technical Conference and Exhibition, Dallas, Texas, 2005
5. T. Austad, H. Hodne, S. Strand, K. Veggeland, Colloid. Surface. 108 (1996) 253-262
6. J. van Nieuwkoop, G. Snoei, J. Colloid Interf. Sci. 103 (1984) 400-416

Lei Shang
Phone: +45 2132 4979
E-mail: lesh@risoe.dtu.dk

Supervisors: Jesper Ahrenfeldt
Ulrik Birk Henriksen
Jens Kai Holm, Dong Energy

PhD Study
Started: January 2010
To be completed: December 2012

Upgrading Fuel Properties of Biomass Fuel and Waste by Torrefaction

Abstract
Torrefaction is a mild temperature (200-300˚C) pretreatment of biomass in an inert atmosphere, which has received increased attention in recent years applying to upgrade fuel properties. During the process, the biomass looses moisture and a proportion of the volatile content, and becomes dry, darker, and brittle. Torrefied biomass is more hydrophobic, has a higher calorific value and is easier to grind.

Introduction
Biomass, as a kind of sustainable energy resource, has recently gained more focus from both politically and scientific view. However, these biomass sources will need special attention and more expensive solutions in terms of storage, handling, milling and feeding compared to existing systems used for coal. Especially in pulverised firing systems [1], size reduction of biomass material is much more demanding than for coal due to its fibrous and more tenacious structure. Other challenges with biomass include low energy density and great inhomogeneity of biomass fuels. Torrefaction is a technique to improve the energy density of biomass, which involves the heating of biomass to moderate temperatures typically between 200 and 300 ˚C in the absence of oxygen and under atmospheric pressure. During the treatment, biomass starts to decompose and release combustible torrefaction gas together with moisture. Thereby, the energy density of the torrefied biomass is increased. Moreover, during the torrefaction the structure of the torrefied biomass is changed to be more brittle, and thus much easier to be ground. [2-4] This effect would lower the energy demand during size reduction of the biomass prior to the combustion or pelletization. Furthermore, if combine torrefaction with pelletization, it will significantly increases the energy density of biomass fuels and thus energy and emission savings could be made in the transport of fuel.

The process of torrefaction has been known for processing of wood since about 1930. However, it is only recently that it has been claimed to be beneficial for modern biomass utilization due to the increasing demand of fuel and arising concerns of global warming problem. Previous research [5-7] shows that the result of the torrefaction process depends on the temperature, heating rate, time and composition of the biomass heated, and the amount of hemicelluloses is a major factor for how the material will react during torrefaction. Because hemicellulose is reactive at lower temperatures than the other main components of biomass, lignin and cellulose. However, the full extent of these reactions is unknown. Meanwhile, the knowledge of torrefaction is not clearly defined yet. For example, different temperature ranges of torrefaction are found in literature, there is lack of detailed understanding about chemistry occurring during torrefaction, and no mathematical model developed, etc. Therefore, the overall goal of this project is to develop and upgrade fuel properties of biomass fuel and waste by torrefaction. The study involves experimental studies in both lab-scale and bench-scale reactors at Risø, establishing chemical reaction mechanisms and kinetics of torrefaction, and optimizing the process of torrefaction.

Specific Objectives
It is the aim of this project to elucidate the complex physio-chemical reactions taking place during such treatment of biomass as well as testing and evaluating the potential effects that such an upgrading will have on the fuel chain from the production site of the fuel to transport, storage and processing at the power plant. Furthermore, the basic conceptual structure of a torrefaction plant is shown in Figure 1. More possible research objectives are also marked.

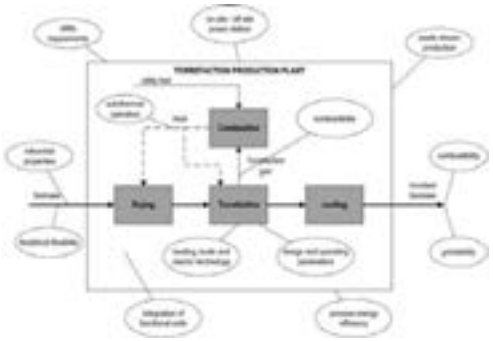

Figure 1: An outline of torrefaction process and possible research objectives. [8]

Experimental

Torrefaction was held by placing oven dried samples in an air tight metal container that could be heated in an oven to the desired temperature. Nitrogen was pumped through the sample container to create an inert atmosphere. The temperature of the oven was measured in the centre of the chamber using thermocouples and this measurement was used for temperature control. The heating rate programmed for the oven was 6 ˚C/min. The residence time of the torrefaction process starts when the material temperature has reached the set temperature until it starts to cool down. Torrefaction was carried out at 200 to 300˚C. Anhydrous weight loss (AWL %) was determined by recording the weight loss during torrefaction. So far, 3 different biomass materials have been torrefied, they are wood chips, wood pellets and wheat straw.

Grindability of biomass fuels were tested on a standard Hardgrove grinder by feeding 50 cm^3 samples with particle size between 0.6-1.18 mm. The equivalent Hardgrove Index was determined by Eq. (1), which was obtained in our earlier work from the reference coal samples:

$$HGI_{equiv} = \frac{(wt.\%+5.2521)}{0.357} \quad (1)$$

where *wt.%* is the weight percent of the ground product passing the 75 μm sieve. The specific energy required for grinding was determined on a bench scale disc mill by integrating the area under the power demand curve for the total time required to grind the sample minus the idling power.

Hygroscopicity of biomass fuels were measured by placing samples in 3 different relative humidity, and recording the weight change once a week.

Gas products evolution during torrefaction was studied on a mass spectrometer coupled TGA, which allows analyzing the evolved gas on-line.

In the end, the heat-induced chemical modification of wheat straw was monitored by both Attenuated Total Reflectance (ATR) – FT-IR spectroscopy and chemical analysis of cell wall composition.

Results and Discussion

The correlation between torrefaction temperature and AWL% is shown in Figure 2. Wood chips and wood pellets have almost the same weight loss during torrefaction, while wheat straw looses more weight than wood pellets and wood chips under same torrefaction condition when above 200℃. Higher heating value (HHV) and anhydrous weight loss (AWL %) for 3 biomass on dry and ash free basis (daf) are shown in Figure 3.

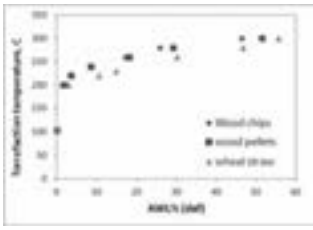

Figure 2: AWL% (daf) vs. Torrefaction temperature (2h). [9]

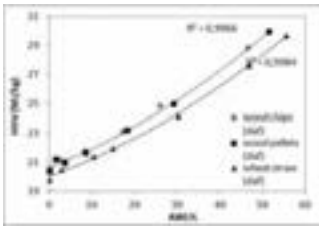

Figure 3: HHV vs. AWL % for wheat straw, wood pellets and wood chips. [9]

The results of equivalent Hardgrove Grindability Index for different biomass samples torrefied at different temperatures are shown in Figure 4. The grindability of torrefied wood pellets was not improved satisfactorily according to HGI results, while the grindability of wheat straw was proved to be enhanced by the torrefaction treatment most. In order to achieve similar grindability as coal, torrefaction tempertature of above 240 ˚C would be needed for wheat straw and wood chips, and 290 ˚C would be required for wood pellets.

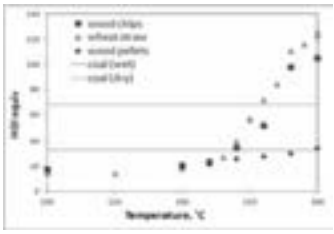

Figure 4: Results of Hardgrove Grindability test for biomass torrefied at different temperatures (2h), coal in wet and dry condition were also tested as reference. [9]

Figure 5 shows the results of specific energy requirement of grinding pellets and wood chips torrefied

at different degrees. Different from the HGI results, wood chips consumed more grinding energy than pellets, except for the highest AWL% (about 50%) where energy use in grinding these two fuels are tend to be close. It means that HGI tests do not have direct correlation with energy consumption during grinding. Moreover, energy use for both wood chips and pellets showed a sharp decrease in the first 25% and 10% AWL respectively, and then followed by decreases with lower rates. Therefore, these two AWL % can be suggested as the optimal torrefaction condition to achieve the maximum energy saving during grinding while maintain as much HHV as possible. Particle size distribution analysis showed that torrefied wood chips ended up with much higher percent of fines (75 μm) than pellets after grinding, and the higher torrefaction temperature the higher percent of fines. This is consistent with the results from HGI.

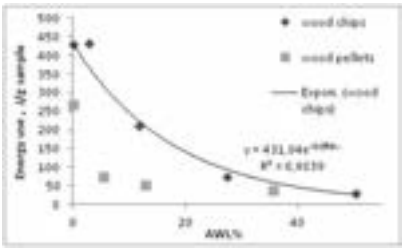

Figure 5: The specific energy required for grinding pellets and wood chips (J/g) vs. anhydrous weight loss (AWL %). [9]

Hygroscopicity study showed that when relative humidity increases, equilibrium moisture content (EMC) of all samples (wood chips, wood pellets and wheat straw) increase correspondingly. Wheat straw samples absorbed moisture most among these 3 kinds of biomass, while pellets uptake least. The higher torrefaction temperature, the less moisture absorbed. EMCs of torrefied samples can be reduced by about 5%, 6% and 10% in 75.5%, 85% and 92.5% relative humidities respectively.

Gas products during torrefaction of wood chips, wood pellets and wheat straw detected by MS are methane (m/z 16), water (18), hydrogen cyanide (27), carbon monoxide (28), formaldehyde (30), methanol (31), acetic acid (43), carbon dioxide (44), lactic acid (45), formic acid (46), traces of acetone (58) and carbonyl sulfide (60) are also found in the torrefaction temperature of 300 ˚C. In order to make a quantitative comparison of gas products released from different biomass during torrefaction, integral subtended by the MS curves for different kinds of biomass during torrefaction have been calculated. The ratio of cumulative release of gas products from 3 biomass and from wood chips are presented in Figure 6. Generally, wood pellets released least gas among these 3 kinds of biomass, except for HCN. Wheat straw released much more acetic acid, formic acid, lactic acid, acetone, carbonyl sulfide, CO_2, and a bit more water than wood chips. On the other hand, during torrefaction wood chips produced more methane, CO, formaldehyde, and methanol than wheat straw and wood pellets.

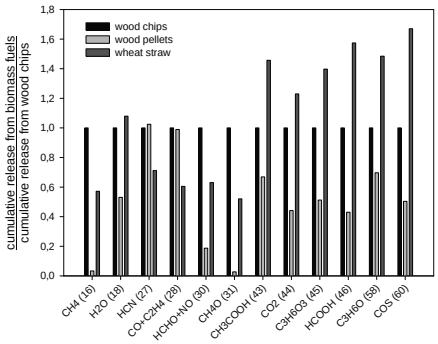

Figure 6: Ratio of cumulative release of different gas products from 3 biomass fuels by using wood chips as the standard. [9]

Infrared spectra taken from wheat straw samples torrefied at different temperatures are shown in Figure 7 with the bands of interest being identified by their wavenumbers. The band placed at 670cm^{-1} at the lower edge of the wavenumber range is characteristic for cellulose and is an OH torsional vibration band. The fact that a significant decrease of this band is seen only for the highest temperatures between 270 and 300˚C shows that the cellulose component is largely stable until these temperatures are reached. The peak observed at 1505cm^{-1} is diagnostic of lignin and is placed in a spectral region devoid of polysaccharide peaks. No clear change of this peak is observed for most of the temperature range. At 300˚C it does appear to have diminished. The band at 1732cm^{-1} is attributed to the carbonyl band stretch of carboxylic acid groups in hemicelluloses. It starts to reduce from 250˚C, when torrefaction temperature reaches 300˚C, 1732cm^{-1} band is totally shifted to 1700cm^{-1} band, which suggests the complete removal of hemicelluloses.

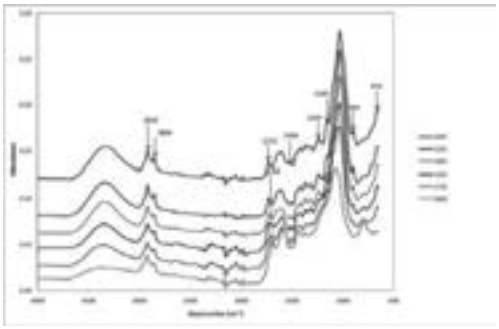

Figure 7: ATR-FTIR spectra of oven dried (104 ˚C) and torrefied wheat straw samples. All spectra are separated to ease the comparison. [10]

By analyzing the FTIR spectra of torrefied wheat straw samples, it can be concluded that there is no major structural change of the wheat straw samples torrefied below 200˚C. Increasing the temperature form 200˚C to 250˚C introduces distinct changes in the spectrum. These appear not to involve lignin or cellulose to any major extent, as the two characteristic bands of these components at 1505 and 670cm^{-1} do not change. Thus degradation and depolymerization of hemicelluloses is proposed to account for the initial low temperature torrefication effects. A higher temperature effect is most notable for the 270˚C to 300˚C transition and consists in the degradation of lignin and cellulose. The cell wall composition of both untorrefied wheat straw and wheat straw torrefied at 300˚C were determined, and the results (Table 1) support the findings from FTIR. At 300˚C torrefaction conditions, hemicelluloses are almost completely removed and cellulose is also reduced substantially.

Table 1: Mass% of hemicelluloses, cellulose and lignin in both raw and torrefied (300 ˚C, 2h) wheat straws (dry and ash free basis). [10]

	lignin (%)	**cellulose (%)**	**hemicellulose (%)**
raw straw	21.28	35.64	27.78
torrefied straw	98.40	1.02	0.34

Conclusions

It is proved that energy density, grindability, and hygroscopicity of biomass fuels were improved by means of torrefaction. Moreover, the correlation between these properties and degree of torrefaction was also estabilished. By analyzing the chemical changes in the wheat straw during the torrefication process**,** it was confirmed that the removal of hemicelluloses, the degradation of which starts at 200-250˚C and finishes at about 300˚C, is the main reason of the improvement of these properties in this temperature region.

By comparing the cumulative release of gas products during the whole torrefaction reaction for 3 biomass fuels, it can be concluded that wood pellets released least gas, except for HCN. Wheat straw released much more acetic acid, formic acid, lactic acid, acetone, carbonyl sulfide, CO_2, and a bit more water than wood chips. While wood chips produced more methane, CO, formaldehyde, and methanol than wheat straw and wood pellets.

Acknowledgements

This work was financially supported by ENERGINET.DK and the ForskEL program (Project 2009-1-10202, Torrefaction of Biomass).

References

1. T. Bridgeman, J. Jones, A. Williams, D. Waldron, Fuel 89 (12) (2010) 3911-3918.
2. T. Bridgeman, J. Jones, I. Shield, P.T. Williams, Fuel 87 (6) (2008) 844-56.
3. B. Arias, C. Pevida, J. Fermoso, M.G. Plaza, F. Rubiera, J.J. Pis, Fuel Process. Technol. 89 (2008) 169-75.
4. P.C.A. Bergman, Combined torrefaction and pelletisation: the TOP process. Report ECN-C--05-073, ECN (2005).
5. J. Deng, G. Wang, J. Kuang, Y. Zhang, Y. Luo, J. Anal. Appl. Pyrol. 86 (2009) 331-7.
6. S. Sadaka, S. Negi, Environ. Prog. Sust. Energ. 28 (2009) 427-34.
7. J.S. Tumuluru, S. Sokhansanj, C.T. Wright, J.R. Hess, R.D. Boardman, A review on biomass torrefaction process and product properties. INL/CON-11-22634.
8. P.C.A. Bergman, A.R. Boersma, R.W.H. Zwart, J.H.A. Kiel. Torrefaction for biomass co-firing in existing coal-fired power stations. Report ECN-C--05-013, ECN, Petten (2005a).
9. L. Shang, W. Stelte, R.Z. Zhang, T. Thomsen, L.S. Bach, J. Ahrenfeldt. Physical and chemical property changes of 3 biomass fuels caused by torrefaction, accepted by WSED Next: 29.Feb – 2.Mar 2012, Wels, Austria.
10. L. Shang, J. Ahrenfeldt, J.K. Holm, A.R. Sanadi, S. Barsberg, T. Thomsen, W. Stelte, U.B. Henriksen, Biomass Bioenerg. (2011) (Submitted)

List of Publications

1. W. Stelte, C. Clemons, J.K. Holm, A.R. Sanadi, J. Ahrenfeldt, L. Shang, U.B. Henriksen, Biomass Bioenerg. 35 (11) (2011) 4690-4698.
2. L. Shang, W. Stelte, R.Z. Zhang, T. Thomsen, L.S. Bach, J. Ahrenfeldt. Physical and chemical property changes of 3 biomass fuels caused by torrefaction, accepted by WSED Next: 29.Feb – 2.Mar 2012, Wels, Austria.
3. L. Shang, J. Ahrenfeldt, J.K. Holm, A.R. Sanadi, S. Barsberg, T. Thomsen, W. Stelte, U.B. Henriksen, Biomass Bioenerg. (2011) (Submitted)

Anna K. Sitarz
Phone: +45 4525 2993
E-mail: aks@kt.dtu.dk
Discipline: Enzyme Technology

Supervisors: Anne S. Meyer

PhD Study
Started: September 2008
To be completed: March 2012

Biofuels from Important Foreign Biomasses

Abstract
Biomass is a renewable source of energy that is more sustainable than fossil fuels and more dependable than wind and solar. Moreover it provides the environmentally friendly and safe alternative for production of biofuels, especially when using the 2nd generation approach. In this project, the overall objective is to develop a method for the most optimal pretreatment of the biomass, leading to the low inhibitory content and the high yields of monosugars and produced ethanol.

Introduction
In the development of economically feasible conversion technologies for production of biofuels from renewable resources, the utilization of low cost biomass residues is of crucial importance. The most important parameters of these biomass residues are that they should contain a high amount of carbohydrates, which can be produced in large quantities [1]. Therefore the utilization of sugarcane bagasse will be the aim of the project.

The bagasse is a by-product from the sugar extraction process and is usually used in low-efficiency boilers at the processing plant. This lignocellulosic residue has a large content of relatively easily-available carbohydrates that could be utilized as substrate for 2nd generation bioethanol production. It is mainly composed of 40-50% cellulose and 25-30% hemicellulose with the remainder that is mostly lignin, minerals, wax and other compounds [2].

2nd generation bioethanol is made from residual lignocellulosic material. This approach of producing biofuels is beneficial in avoiding displacing agriculture for food and preventing from land clearing.

Lignocellulolytic materials are formed by three main polymeric constituents; cellulose, lignin and hemicellulose. Cellulose is linear and highly ordered (often crystalline) polymer of cellobiose (D-glucospyranosyl-β-1,4-D-glucopyranose).

Hemicellulose is made up of different pentoses and hexoses polymers, which are often acetylated and generally form branched chains forming a matrix with cellulose fibrils. The third component, lignin, is a three dimensional network buildup of dimetoxylated (syryngyl, S), monomethoxylated (guaiacyl, G) and non-methoxylated phenylpropanoid (*p*-hydroxyphenyl, H) units derived from the corresponding *p*-hydroxycinnamyl alcohols, which give rise to a variety of subunits including different ether and C-C bonds. Therefore lignin is very resistant toward chemical and microbial degradation.

Figure 1 shows the way of processing sugar cane. It begins with shredding the sugarcane with rotating knives and extraction of the juice to produce bagasse. This residual material is usually burnt to create heat. When the water evaporates from the juice, thy syrup is made. The seed crystals added to it will initiate the syrup to crystallize.

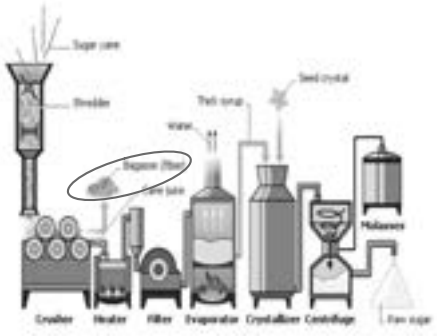

http://images.encarta.msn.com/xrefmedia/aencmed/targets/illus/ilt/T304793A.gif

Figure 1. Schematic processing of sugarcane with bagasse as the side stream.

Pretreatment as a method of improving sugars accessibility

Pretreatment is used to improve the biomass accessibility by destruction of harsh lignocellulosic structure and partially hydrolyzing the substrate. Current pretreatment methods, however, contribute to 30-40% of total costs of bioethanol production from lignocellulosic biomass. Hence, the pretreatment is one of the biggest bottlenecks for low-cost production of bioethanol. Therefore, the improvements in obtaining the most optimal parameters for disrupting the lignocellulose matrix will be investigated. In this project focus will be put on wet explosion, which is a combination of steam explosion and wet oxidation, applying both, the addition of oxygen and pressure release. The treated sample will be further hydrolyzed and fermented [3].

The hydrolysates released from the pretreatment are usually treated with enzymes in order to break down the cellulose and hemicellulose into hexoses and pentoses, which are later fermented to ethanol. The bottleneck of this process is the cost of the enzymes and the fact that enzymes can become inactive, due to the adsorption to lignin or shear stress. Therefore the need for finding ways to overcome those difficulties is needed. Hence, a new minimal cocktail of enzymes degrading lignocellulose material will be designed and evaluated [4].

Main objectives

The aim of the proposed PhD project is to develop the most optimal strategy and conditions for the pretreatment of lignocellulosic biomass, sugarcane bagasse, and obtain low yields of inhibitory compounds, high yields of free sugars, both xylose and glucose, and high yields of ethanol.

Acknowledgements

This PhD study is sponsored by the Strategic Program: Research in Renewable Energy (Det Strategiske Forskningsråd).

References

1. **A.**E. Wheals, L.C. Basso, D.M.G. Alves, H.V. Amorim, Trend. Biotechnol. 17 (1999) 482-487
2. C. Martin, H.B. Klinke, A.B. Thomasen, Enz. Microbiol. Technol. 40 (2007) 426-432
3. P.F. Morjanoff, P.P Gray, Bioethanol. Bioeng. 29 (1987) 733-741
4. H.B. Klinke, B.K. Ahring, A.S. Schmidt, A.B. Thomsen, Bioresour. Technol. 82 (2002) 15-26

Guotao Sun
Phone: +45 4525 4100
E-mail: sngu@risoe.dtu.dk

Supervisors: Jens Ejbye Schmidt
Pablo Kroff

PhD Study
Started: December 2011
To be completed: November 2014

Optimizing the Anaerobic Digestion of Manure

Abstract
Most of the Danish biogas plants co-digest manure and industrial organic waste which give sufficiently high biogas production. The amounts of the industrial waste are, however, limited and future biogas plants may have to be based solely on manure [1] ; at the moment this is not possible. The present PhD project will thus focus on optimizing the anaerobic digestion (biogas production) of swine and cattle manure.

Introduction
One of the goals in the Danish "Grøn vækst" (Green growth) agreement is to increase the amount of manure used for bioenergy production from 5% today to 50% in 2020. With a yearly manure production of 40 mill tons, this goal requires a huge expansion of the Danish biogas industry and the construction of several new biogas plants. Until now, as default manure has been treated together with industrial waste in order to make the biogas plants economical feasible. Optimizing the anaerobic digestion of manure is one option to fulfill the national goals.

The content of the Ph.D. project will be divided in 4 steps:

Pretreatment methods:
Because of the complex lignocellulosic structure [2], combined pre-separation and pre-treatment techniques are expected to increase the biogas potential of manureRisø DTU has a long tradition of developing pretreatments methods and has the necessary equipment available. The methods that will be tested include:

- High thermal treatments of separated biofibers (lignocellulosic material).
- Plasma treatment of separated biofibers.
- Chemical treatment of separated biofibers.

Process optimization:
Conventional Danish biogas plants are operated as one-stage digestors under constant mesophilic (35-37 °C) or moderate thermophilic (52-55 °C) conditions. However, splitting the process in two steps gives the possibility of using more than one temperature and thereby applies a broader range of microorganisms for degradation [3]. Different concepts for two-stage processes - differing in retention time and temperature - will be tested during the study.

Posttreatment methods:
The unexploited methane potential left in manure following anaerobic digestion can easily constitute 15-30% of the total potential and consequently makes up a large energy resource. Traditional Danish biogas plants requires long retention times because the microbial populations is mixed with the substrate and is continuously diluted and lost during plant operation (feeding and removal of effluents). Thus, full utilization of the biogas potential of manure requires excessive high retention times and is too expensive. In biogas reactors with immobilized microorganisms like Upflow Anaerobic Sludge Bed reactors (UASB), a much lower retention times can be used. These reactors are excellent for treatment of low-solid waste such as wastewaters. The reactors have also been successfully – but sporadic - applied on raw filtered/non filtered swine manure [4] and can potentially be used for treatment of reactor effluents from traditional plants in a second treatment step. Digestion of biogas reactor residuals in high rate UASB reactors will be tested for the effect of filtration, hydraulic retention time, temperature conditions, organic loading and other operational conditions, on the methane production efficiency.

Nutrient recovery:
Post-separation of digested manure giving a fertilizer product with higher value will be of high importance for future biogas plants. Low cost N/P removal in conjunction with biogas plants will be studied including

N-removal by stripping in conjunction with anaerobic digestion.

Specific Objectives

The overall goal of this project is to optimize the anaerobic digestion of mature and make it applicable for future biogas plant based solely on manure. Specific objectives are as follows:

1. Develop pretreatments methods to increase the biogas potential of manure.
2. Select sustainable retention time and temperature of digestion to apply a broader range of microorganism for degradation.
3. Integrate UASB reactors to digestion of mature and evaluate its efficiency.
4. Study on low cost N/P removal in conjunction with biogas plant.

References

1. H.B. Nielsen, S. Heiske. Water Sci. Technol. 64 (8) (2011) 1723-1729.
2. M. Madsen, J.B. Holm-Nielsen, K. H. Esbensen, Elsevier 15 (2011) 2141-3155.
3. A. Bouskova, M. Dohanyos, J.E. Schmidt, I. Angelidaki. Water Res. 39 (2005) 1481-1488.
4. D. Karakashev, J.E. Schmidt, I. Angelidaki. Water Res. 42 (2008) 4083-4090.

Eike Marie Thaysen
Phone: +45 5180 1481
E-mail: emth@risoe.dtu.dk

Supervisors: Iver Jakobsen
Per Ambus

PhD Study
Started: August 2010
To be completed: July 2013

Climate Change Mitigation by Plant-mediated Transfer and Transport of Carbon to Aquifers

Abstract
Emission of CO_2 causes climate change [1]. In the present work, the potential for mitigating CO_2-induced climate change through storage of CO_2 in aquifers was investigated. Barley was grown in mesocosms (19x80cm) packed with coarse-sanded soil. $CO_{2(g)}$ and alkalinity samples were collected at different depths in the mesocosms and dissolved inorganic carbon (DIC) was measured in the effluent from the mesocosms. Results show increasing $CO_{2(g)}$ content with plant age reaching a maximum of 5-6 vol% in the soil air. The amount of DIC leached to the aquifer depends on [DIC] in the soil water and on the amount of effluent. After harvest, $CO_{2(g)}$ decreases exponentially.

Introduction
The present atmospheric concentration of CO_2 of 390 ppm (2010 figures) and its increment rate of 2.3 ppm/yr accelerate global warming, soil degradation, desertification and environmental pollution [2] Worldwide concern about climate change and the effects on the future environment requires a better understanding of the global carbon cycle [3] and gives rise to the question of whether and how vegetation and soils can store additional carbon [4]. In this work we tested a new approach for carbon sequestration; increased storage of CO_2 as dissolved inorganic carbon (DIC) in aquifers beneath agricultural fields.

Specific Objectives
The objective was to identify the main factors controlling solubility of CO_2 in the soil water and its transport to the aquifer. It was hypothesized that transport of CO_2 in agricultural systems is controlled by type of crop, irrigation amounts and frequencies as well as pH. Mesocosm experiments in climate chambers are carried out in which these factors are varied and screened for their ability to enhance CO_2 transport down to the aquifer. Selected factors will subsequently be tested in the field (done by the Geological Survey of Denmark and Greenland (GEUS).

Results and Discussion
Partial pressure of CO_2 in the soil air under growth of barley increased with plant age and reached concentrations of 5-6 vol% 51 days after planting (Fig. 1). After harvest when roots were degrading $CO_{2(g)}$ content fell rapidly towards a stable level of ~1 vol% 32 days after harvest. CO_2-levels during degradation never reached levels as high as those measured during growth of barley.

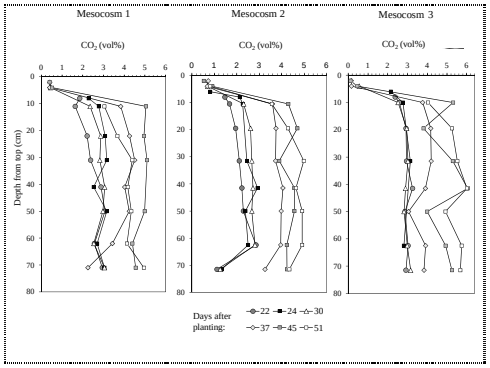

Fig. 1: Profiles of the volumetric percentage of CO2 in the soil air in each of three mesocosms during growth of barley.

CO_2-storage (defined as amount of DIC in effluent leaching from mesocosms) followed the same pattern for three replicate mesocosms during growth of barley,

however, the magnitude differed (Fig. 3). Highest levels were measured in the collected effluent from day 30 to 36 after planting.

The amount of CO_2 dissolved in the groundwater varies with the partial pressure of CO_2, initial pH of the water and temperature [5]. While pH of the infiltrating water and temperature in the climate chamber are held constant, the partial pressure of CO_2 is controlled by the magnitude of soil respiration. CO_2(g) increased with plant age in all mesocosms (Fig. 1). According to Eq. 1 a higher partial pressure of CO_2 in the soil air causes [DIC] in the soil water to increase. However, the amount of DIC leached is controlled not only by the concentration of [DIC] in the soil water but also by the amount of effluent (not shown), causing the pattern in Fig. 3.

$$CO_{2(g)} + H_2O \Leftrightarrow HCO_3^- + H^+ \Leftrightarrow CO_3^{2-} + 2H^+ \qquad \textbf{Eq. 1}$$

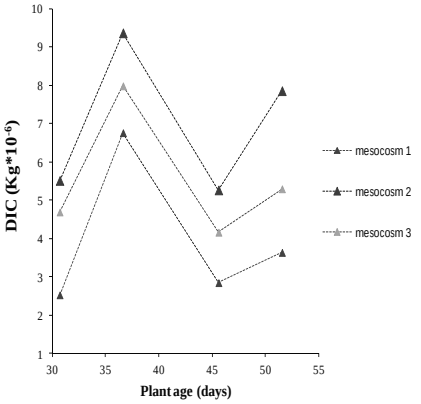

Fig. 3: Culmulative weekly efflux of DIC from mesocosms 1, 2 and 3 during growth of barley. Shown are the end times for effluent sampling.

Conclusions

CO_2(g) in the soil air of the mesocosms increased during growth of barley. During degradation of barley roots, $CO_{2(g)}$ content fell and arrived at a stable level of ~ 1 vol% after 1 month. CO_2-storage was highest 30-36 days after barley was sown. Upcoming experiments will elucidate the effect of elevated pH and different plant species on CO_2-storage in aquifers.

Acknowledgements

I would like to thank my supervisors Iver Jakobsen and Per Ambus, and technician Preben Jørgensen (RISØ DTU) as well as Søren Jessen (GEUS) for guiding and supporting me throughout the project.

References

1. Report No. AR4, IPCC, 2007.
2. Report No. TR04B, SOLAW, FAO, 2011.
3. R. Jassal, A. Black, Agr. Forest Meterol. 130 (2005) 176-192.
4. D.R. Sauerbeck, Nutr. Cycl. Agr. Syst. 60 (2001) 253-266.
5. I. Clark, P. Fritz, Environmental Isotopes in Hydrogeolgy, CRC Press, 1997.

Sune Tjalfe Thomsen
Phone: +45 2132 5181
E-mail: sunt@risoe.dtu.dk

Supervisors: Jens Ejbye Schmidt
Moses Mansah, Kwame Nkrumah
University of Science and Technology

PhD Study
Started: December 2010
To be completed: January 2014

2nd Generation Biofuel Production from Waste Resources in Ghana

Abstract
The distinctive resources of a tropical, developing country introduces new and complex issues within the conversion of biomasses into energy carriers. In order to assess these, the knowledge gained in the developed countries within the last decades in this area must be transferred, adjusted and further developed. The main focus will be on characterising Ghanaian bioresources, as well as development of conversion technologies within both pretreatment of the different biomasses and the biological transformation of pretreated material into energy carriers.

Introduction
In recent years the focus on sustainable biofuel production from agricultural bioresidues has increased considerably. However, the scientific work within this field has predominantly been concentrated upon bioresources from developed countries, while the residues from many developing countries remain unstudied.

Using Ghana as a model country this project will focus on making sustainable bioenergy solutions in a third world context. An initial mapping of Ghanaian waste resources that are relevant for production of bioenergy have been carried out based on reviewing the literature [1, 2]. A broad selection of biomasses has been obtained through our Ghanaian partners; cf. Table 1, where after the resources have been characterized with regard to chemical composition and the bioenergy potentials have been calculated.

In the next phase of the study, the waste will be subject to pretreatment such as silage treatment, hydrothermal treatment, ammonia pretreatment and maceration, and thereafter be converted to bioenergy in the laboratory where both ethanol production and biogas production will be tested. Based on the results different concepts specially adapted for third world conditions will be developed. Co-digestion concepts for an optimized biogas production will also be tested as well as innovative reactor setups. Finally, but very importantly, an evaluation of most suitable bioenergy technology will be carried out, in order to assist our Ghanaian partners in pilot scale trials.

Table 1: List of analysed Ghanaian bioresources. In the results focus will be on plantain (cooking banana), an example of a typical Ghanaian crop, from which the residues of peelings, trunks and leaves can be utilised.

Crop	Residue
Yam	Peelings
Cassava	Peelings
	Stalks
Plantain	Peelings }
	Trunks }
	Leaves }
Cocoa	Husks
	Pods
Oil palm	Empty fruit bunches
Maize	Stalks
	Cobs
Rice	Straw
Groundnut	Straw
Municipal solid waste	Organic fraction

Specific Objectives
- To get an overview of waste resources in Ghana and their biofuel potentials in terms of bioethanol, biogas and biodiesel.
- To develop concepts that combined bioethanol, biogas and biodiesel production from selected relevant wastes/substrates.
- To develop process setups for an optimized biogas production from relevant wastes that is suitable for the specific circumstances in Ghana.

Results and discussions

In order to reduce the amount of result shown, the result section will be based residue from plantain, one of the most important Ghanaian stable crops, cf. Table 1.

The compositional analysis of plantain peelings, trunks and leaves shows quite different results even for these closely related biomass residues, cf. Figure 1. In short, the peelings are rich in starch, the trunks are rich in cellulose and the leaves have the highest content of non xylan hemicellulose such as arabinan, rhamnan and galactan as well as the highest lignin content. The clear differences between the residues will imply alternating optimal uses within bioenergy.

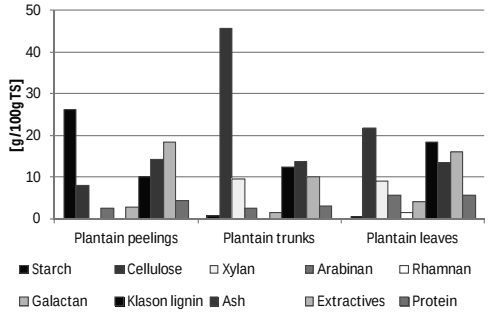

Figure 1: Compositional analysis of Ghanaian biomass exemplified by plantain residues. TS denote total solids.

The composition derived differences for bioethanol potential are evident in Figure 2. Where the easy degradable starch fraction in the peelings give rise to a fair amount of potential product, the quite high level of cellulose in the trunks shows the highest bioethanol potential. However, this would imply a more complicated 2nd generation bioethanol technology, which might not be feasible in Ghana. Full utilisation of the plantain leaves or trunks would include the conversion of C5 sugars by using even more complex technology.

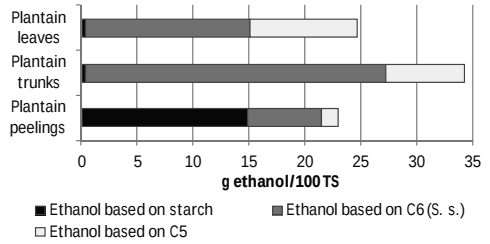

Figure 2: Bioethanol potentials from Ghanaian biomass, exemplified by plantain residues.

Estimations of biomethane potentials were made using Buswell's formula (cf. Equation 1) which take each biomass constituent into account.

Equation 1:

$$C_nH_aO_b + \left(n - \frac{a}{4} - \frac{b}{2}\right)H_2O \rightarrow \left(\frac{n}{2} + \frac{a}{8} - \frac{b}{4}\right)CH_4 + \left(\frac{n}{2} - \frac{a}{8} + \frac{b}{4}\right)CO_2$$

The biogas potentials obtained with Buswell's formula are rather similar for the three plantain residues; however in the actual anaerobic degradation experiments preformed [3], there is a significant difference, cf. Figure 3. This different is most likely due to differences in recalcitrance in-between the different residues.

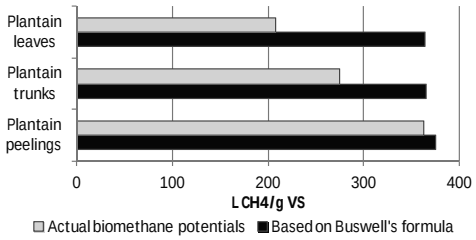

Figure 3: Biogas potentials of Ghanaian biomasses, exemplified by plantain residues.

Due to the differences in recalcitrance in different biomasses, this study will give special emphasis to potential pretreatment methods within both biogas and bioethanol production in third world countries.

Conclusions

The technologies and products are developed to give positive environmental consequences (e.g. more efficient use of biomass resources, decrease in green house gas emissions, and better fertility of agricultural soil) and they will be ranked to improve the knowledge base on which the Ghanaian society can select the best context specific strategy depending on the community structure. The project provides hands-on technology demonstrations in selected communities, based on scientific conclusions.

Acknowledgements

The PhD is a part of a development research project titled: Biofuel production from lignocellulosic materials – 2GBIONRG, funded by the Danida Fellowship Centre of the Danish Ministry of Foreign Affairs.

References

1. M.H. Duku, S. Gu, E.B. Hagan, Renew. Sust. Energ. Rev. 15 (2011) 404–415
2. S.O. Jekayinfa, V. Scholz, Energ. Source. 31 (8) (2009) 687- 697
3. T.L. Hansen, J.E. Schmidt, I. Angelidaki, E. Marca, J.L.C. Jansen, H. Mosbæk, T.H. Christensen, Waste Manage. 24 (4) (2004) 393-400.

Rasmus Trane
Phone: +45 4525 2809
E-mail: rt@kt.dtu.dk
Discipline: Reaction and Transport Engineering

Supervisors: Anker D. Jensen
Søren Dahl, DTU Physics

PhD Study
Started: August 2010
To be completed: August 2013

Catalytic Steam Reforming of Bio-Oil to Hydrogen Rich Gas

Abstract
Steam reforming (SR) of bio-oil can be a sustainable route to syngas or hydrogen but one of the major hurdles is carbon deposition, which causes catalyst deactivation. The SR of ethanol, a model compound of bio-oil, has been investigated to determine activity and product distribution over several nickel based catalysts. Sintering and carbon deposition occurred with all of the catalysts. However, oxidative SR was found to be an interesting concept as it could lower carbon deposition and increase conversion at the expense of a decrease in hydrogen yield.

Introduction
Liquid fuels, like diesel and gasoline, contain hydrocarbons and currently the only route for producing these fuels in a sustainable manner is from biomass. Biomass has a low energy density making transportation of untreated biomass costly. However, through pyrolysis biomass can be densified to bio-oil, which has up to 10 times higher energy density than bulk biomass.

Steam reforming (SR) of bio-oil can be used to make syngas for production of liquid fuels or H_2 to upgrade the bio-oil to fuels through hydrodeoxygenation [1]. Both options will provide sustainable alternatives to conventional fossil fuel based processes. SR of bio-oil can be performed over supported Ni or noble metals catalysts, where high degrees of conversion and high yields of the desired products can be achieved. However, carbon deposition causes short lifetimes of catalysts and new catalysts or processes must be developed to make SR of bio-oil feasible [2;3].

Steam reforming of ethanol has been investigated initially. Ethanol was chosen as a model compound of bio-oil, because it has a functionality which is found in bio-oil and it has tendency to form carbon, which is one of the major problems in SR of bio-oil

Specific objectives
This Ph.D. projects aims to find catalysts or operating conditions which enables operation with low carbon deposition. Several model feeds will be investigated along with the effect of catalysts poisons like sulphur.

Experimental
$MgAl_2O_4$, CeO_2, and $CeZrO_4$ were impregnated with approx. 8 wt% Ni through incipient wetness impregnation. $Ni(NO_3)_2{\cdot}6H_2O$ was dissolved in a minimum amount of water. The solution was mixed with the dry carrier material and stirred. After this the slurry was dried at 100 °C over night and calcined at 800 °C for 2 h. The experimental setup used for testing the SR of ethanol consisted of two bubble columns connected to a quartz tube with the catalyst bed inside a three-zone oven as shown in figure 1.

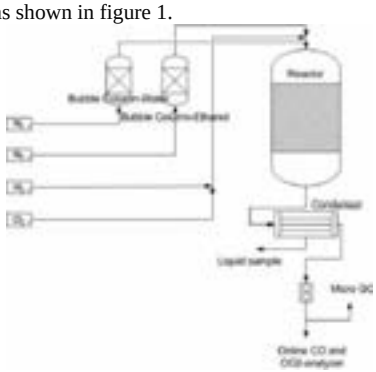

Figure 1: Flowsheet for setup used to investigate the SR of ethanol.

In the bubble columns N_2 flows were saturated with ethanol or water at 60 °C and 79 °C, respectively. This gave a feed gas with approx. 3 mole% ethanol and 39 mole% H_2O in N_2. The reactor effluent was passed through a condenser operated at 10 °C before passing the analysis section consisting of a Variant Micro-GC CP-4900 with two TCD´s for the permanent gasses and a NGA 2000 on-line gas analyzer for CO, CO_2, and O_2.

Results and discussions

Initially the conversion and product distribution at temperatures between 400 and 700°C were investigated for several Ni-based catalysts. The offgas concentrations as function of temperature can be seen in figure 2. The conversion increased with temperature along with the concentration of CO and H_2. The CO_2 and hydrocarbons (CH_4 and C_2H_4) both had a maximum concentration which was at 500 °C for the hydrocarbons and at 600°C for CO_2. This behavior resembles the thermodynamical equilibrium where CO and H_2 are favored at high temperatures. These trends were similar for all the tested catalysts.

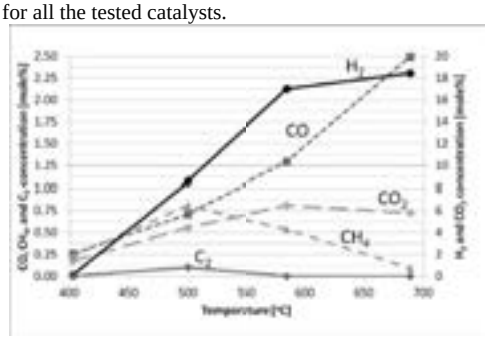

Figure 2: Exit concentrations as function of temperature over $Ni/CeZrO_4$. WHSV=12.8 h^{-1}; S/C=5.8; 8.2 wt% Ni. N_2 as balance.

The conversion as function of temperature over selected catalysts can be seen in figure 3. Here it can be seen that $Ni/CeZrO_4$ has the highest conversion and therefore seems interesting. The high conversion might be ascribed to increased water dissociation over $CeZrO_4$, which aids in carbon gasification. Stable operation for at least 24 h could be achieved at 600 and 700 °C for this catalyst. Furthermore it was found that the addition of 10 wt% of both CeO_2 and ZrO_2 to a $Ni/MgAl_2O_4$ had a beneficial effect on the conversion as shown in figure 3. This might be due to a similar effect as for $CeZrO_4$.

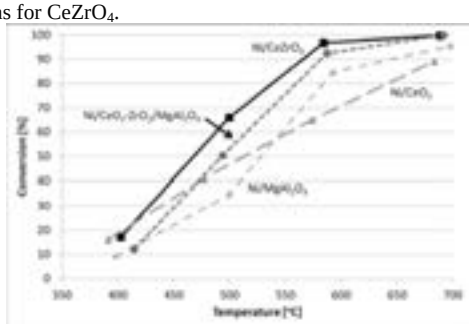

Figure 3: The conversion as function of temperature for selected catalysts. Experimental conditions: S/C: 5.3-6.0; Temp.: 400-700 °C; WHSV= 12.8-14.0 h^{-1}; Ni loading: 8.0-8.5 wt%.

Deactivation with time was observed for most of the catalysts and BET and XRD measurements showed that Ni/CeO_2 and $Ni/CeZrO_4$ sintered quite significantly as the Ni particle size increased by a factor of 2 to 3 over 60-70 *h* on stream. The effect was less pronounced for the spinel type catalysts where the Ni particle size increased only by a factor of 1.5.

Deactivation by carbon deposition was investigated by TPO experiments and it was found that carbon was deposited on all the catalysts. A promoting effect of CeO_2 and ZrO_2 on $Ni/MgAl_2O_4$ was also found here as the addition of CeO_2 and ZrO_2 decreased carbon deposition.

In an attempt to minimize carbon deposition, SR of ethanol was investigated with O_2 present (OSR). OSR was investigated for three catalysts at O/C around 0.25. The results can be seen in table 1. It was found the O_2 addition increased conversion of ethanol and decreased H_2 production for all the catalysts. The carbon deposition decreased for $Ni/CeZrO_4$ and Ni/CeO_2, but it was not fully eliminated.

The increase in activity is partly due to an increase in homogeneous gas phase reactions, like dehydration to ethene or decomposition, in the freeboard above the catalyst. The decrease in carbon deposition could be due to oxidation of carbon deposits by the oxygen present.

Table 1: Comparison of conversion and carbon deposition at OSR and SR conditions.

Catalyst	Type	Conversion [%]	Carbon deposition [mole% C]
$Ni/CeZrO_4$	SR	96	1.50
$Ni/CeZrO_4$	OSR	97	1.01
$Ni/MgAl_2O_4$	SR	89	0.35
$Ni/MgAl_2O_4$	OSR	100	0.35
Ni/CeO_2	SR	74	0.27
Ni/CeO_2	OSR	100	0.16

Conclusion

The SR of ethanol was investigated over several Ni-based catalysts and was found to be a challenge as deactivation by both carbon deposition and sintering was observed for all the tested catalysts.

$Ni/CeZrO_4$ had the highest activity and showed stable operation. Furthermore, it was shown that the addition of CeO_2 and ZrO_2 to $Ni/MgAl_2O_4$ was beneficial both with respect to conversion and carbon deposition. The most promising catalysts therefore seem to be $Ni/CeZrO_4$ or Ni/CeO_2-$ZrO_2/MgAl_2O_4$.

It was also shown that the O_2 addition could be of interest to pursue as increased conversion and decreased carbon deposition was observed.

Future work will additionally involve the effects of sulphur in the feed and SR of compounds like furan.

References

1. G.W. Huber, S. Iborra, A. Corma, Chem. Rev. 106 (2006) 4044-4098
2. A. C. Basagiannis, X. E. Verykios, Cat. Today. 127 (2007) 256-264
3. C. Rioche, S. Kulkarni, C. Meunier, J.P. Breen, R. Burch, Appl. Catal. B Environ. 61 (2005) 130-139

Trung Ngoc Trinh
Phone: +45 4525 2853
E-mail: tnt@kt.dtu.dk
Disciples Reaction and Transport Engineering

Supervisors: Kim Dam-Johansen
Peter Arendt Jensen

PhD Study
Started: January 2010
To be completed: December 2012

Production of Pyrolysis Oil Based on Different Biomass Types

Abstract
A flast pyrolysis study on Five different biomass types including conventional biomass (wood and straw) and non-conventional biomass (lignin residue, algae, sewage sludge) were carried out in a pyrolysis centrifugal reactor. The products distributions and the energy recoveries were evaluated. The fast pyrolysis of algae showed a promising result with 39 % organic oil yield and 78 % of the algae energy value was recovered in the oil. The bio-oils properties were investigated with respect to higher heating value, molecular mass distribution, viscosity and pH.

Introduction
A method to provide a renewable liquid fuel is to use fast prolysis in which biomass is converted into a bio-oil. The bio-oil can be used for chemicals production or be utilized as a liquid fuel which recovers 40 – 80 % of the biomass energy content. Among the many forms of biomass: lignin, algae and sewage sludge are attractive materials for fast pyrolysis due to their abundance, low price and non-competitiveness with food crops.

Many different fast pyrolysis reactor types have been developed. The fast pyrolysis reactors typically achieve a heating rates of 700 – 1500 K/s [1-3] and this is believed to be a main reason for a large increasing of the bio-oil yield when compared with that of fix bed reactors having low heating rates of 5 – 100 K/min [4-6].

The pyrolysis centrifugal reactor (PCR) has been developed at the CHEC center. By a high centrifugal force, biomass particles can gain a high heating rate. The main advantages of this concept compared to fluid bed reactors are a compact design that uses a low flow rate of gas carrier but can treat large biomass particles up to a size of 20 mm

In this study the pyrolysis properties of lignin residue collected from an ethanol plant, sewage sludge collected from a waste water treatment plant and algae, straw and wood are investigated. The lignin residue, algae and sewage sludge are known as materials with a higher lignin fraction and high ash content when compared with a wood and straw. The objective of this study was to investigate the pyrolysis products distribution, enenergy recovery and bio-oil properties obtained by fast pyrolysis of these materials. The results were compared with wood and straw pyrolysis that are considered as the reference sources.

Experimental setup
The PCR is described in figure 1. The biomass was introduced into the reactor by a screw feeder. The pyrolysis of biomass is taken place inside the reactor, whereby char, bio-oil and gas are produced. The large char particles are removed by a change-in-flow separator, whereas the fine char particles are collected by a cyclone. The vapor products are condensed in a bubble chamber filled with isopropanol as a condensing solvent. Light oil fractions and aerosols are further condensed by a coalescer filled with rockwool. Recycled gas maintained a desired gas residence time in the reactor.

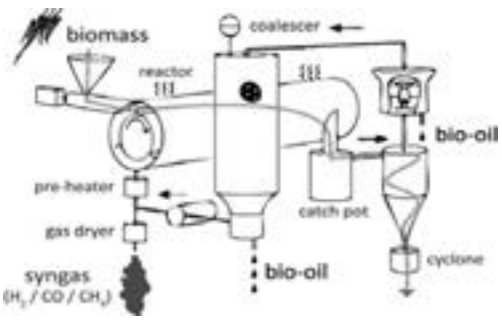

Figure 1: sketch of the pyrolysis centrifugal reactor.

The collected liquid fraction is filtered through a filter paper of 5 μm. The char yield is determined from

the chars collected in the char separator, the cyclone and the char left on the filter paper. The bio-oil yield is determined from the liquid that was passed through the filter paper. The gas measured from the gas meter is used to calculate the gas yield by the ideal gas equations.

Thermalgravimetric (TG) analysis of the biomasses were carried on a STA (Netzsch STA 449 F1) instrument. The bio-oils investigated have a water content of 25 – 28 wt%. The properties of the bio-oils were measured by the following methods: water content by a karl fischer titration (Metrohm-701KT titrino), the higher heating value (HHV) by a bomb calorimeter (IKA C-200), the viscosity by a rotational viscosimer (PAAR AMV 200), molecular mass by GPC and pH by pH meter (metro ohm).

Results

Thermal analysis of the biomasses (TG and DTG) was carried out at a heating rate of 10 ^{o}C/min. The samples were heated from room temperature to 950 ^{o}C under N_2 flow, fallowed by cooling to room temperature. The sample was then heated to 950 ^{o}C with 90% N_2 and 10% O_2 flow. As can been seen in figure 2, the straw and wood experience maximum pyrolysis conversion in the temperature range of 200 – 400 ^{o}C while lignin, algae, and sewage sludge experience a broader pyrolysis conversion in the temperature range of 200 – 500 ^{o}C. The volatile yield is in the range of 84 - 76 % for wood and straw whereas yields of 67, 61 % and 45 % for algae, lignin and sewage sludge, respectively are determined by TGA (see table 1). The yield of ash and fixed carbon has an opposite trend. Based on the TGA data, the char yield of sewage sludge, algae and lignin residue could be predicted to be high in the PCR pyrolysis tests.

Table 1: the approximate analysises of the investigated biomass by TGA (dry basis)

Biomass	Volatile (% wt)	Fixed carbon (% wt)	Ash (% wt)
Wood	84.3	13	2.7
Straw	75.8	18.4	5.8
Lignin	61.2	26.7	12.1
Algae	67.1	10.3	22.6
Sewage sludge	45.44	3.02	51.54

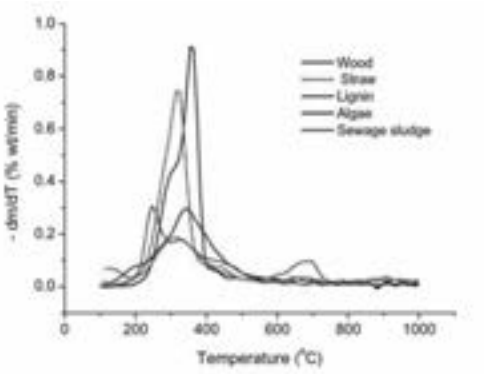

Figure 2: TA for pyrolysis of the investigated biomasses

The pyrolysis in the PCR of biomasses were carried out in the temperature range of 550 - 575 ^{o}C, with a total test time of 60-80 mins and a feed consumption of 400 – 600 g. The results are presented in figure 3. The largest liquid organic yield of 57 wt% on dry feedstock basis was observed for wood while the lowest liquid organic yield of 21 % appeared for sewage sludge. The organics yield of straw, algae and lignin residue feedstocks were in the range of 38 to 41 wt%.

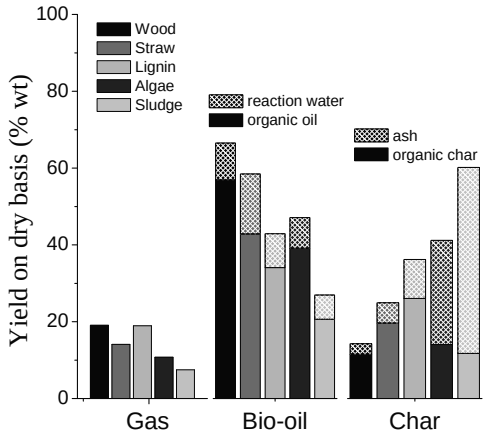

Figure 3: product distribution (dry feedstock basis)

The reaction water yield at a level of 7 - 15 wt% was observed for the pyrolysis of the different biomasses. Since the ash is to remain totally in the char in fast pyrolysis, it leads to the high char yield for sewage sludge and algae (60 and 40 wt% respectively) when compared to that of wood and straw (14 and 25 respectively). Lignin shows a char yield of 36 wt% where it contains 26% organic char and 10 % ash. The gas yield varied from 8 to 20 wt% for the different biomasses.

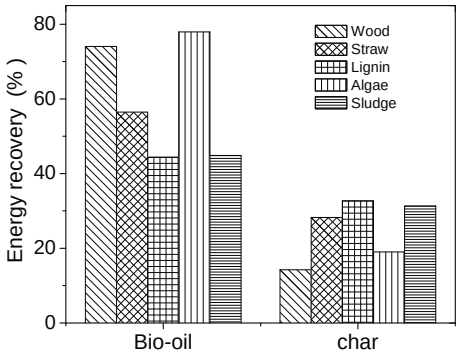

Figure 4: energy recovery

The energy recovery was calculated based on the product yields and their heating values, and the results are shown in figure 4. Due to a high organic oil yield (57 %), wood oil gains 74 % energy recovered while straw, lignin and sewage sludge oils obtain 45- 56 % of feedstock energy content. An interesting result was found regarding the algae sample, the organic oil yield is 39 wt%, while the algae oil contains 78 % of the feedstock energy content. This gives a promising way to upgrade algae to liquid fuel with a high energy recovery efficiency.

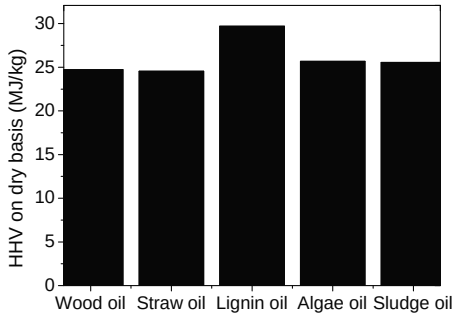

Figure 5: HHV of bio-oils

The bio-oils properties were investigated with respect to higher heating value, molecular mass distribution, viscosity and pH. The higher heating value (HHV) of wood oil, straw oil, algae oil and sewage sludge oil obtain a similar value of 25 MJ/kg on dry basis. However the HHV of lignin oil show a higher value (30 MJ/kg) (figure 5). It is supposed that the oxygen content in lignin oil could be lower than that of the other oils since lignin has a lower oxygen content.

As can be seen at figure 6, the molecular mass distribution shows two main peaks at around 165 and 398 g/mol for the bio-oils of wood, straw, lignin and sewage sludge that are corresponding to a water soluble fraction and water insoluble fraction (pyrolytic lignin) [7]. While the algae oil also has a third peak at around 1260 g/mol together with two main peaks at 165 and 398 g/mol. The average molecular mass for wood, straw, lignin, algae and sludge oil are 372, 272, 314, 442 and 440 g/mol, respectively. The results can partially explain the observed difference of oil viscosities in figure 7 where sludge oil and algae oil have a higher viscosity than that of wood, straw and lignin oil.

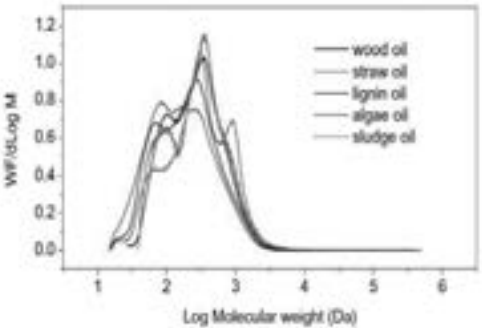

Figure 6: the molecular mass distribution

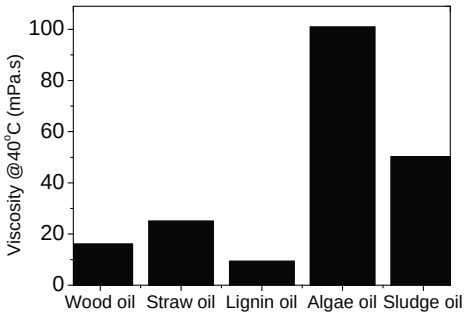

Figure 7: the viscosity of bio-oils

As can been seen in figure 8 the pH of wood oil, straw oil, and algae oil vary from 3.1 to 3.8 whereas lignin oil and sludge oil have pH levels of 4.2 and 5.7, respectively. It is believed that some of the acid groups in lignin and sludge were removed during the treating in the ethanol plant or in the waste water treatment plant.

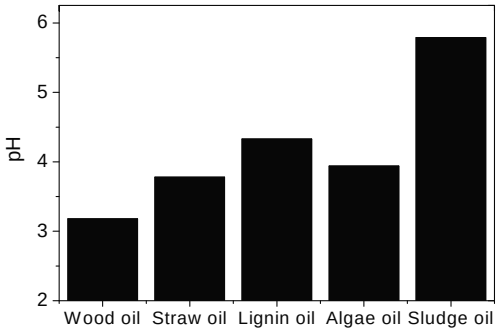

Figure 8: the pH of bio-oils

Conclusions

The highest liquid organic oil yield of 57 wt% on dry basis was produced by fast pyrolysis of wood while the lower yields of 34, 39 and 21 wt% for lignin, algae and sludge pyrolysis. The fast pyrolysis of algae showed a promising result with 39 % organic oil yield and 78 % of the algae energy value was recoved in the oil. Lignin oil obtains the highest HHV of 30 MJ/kg on dry basis when compared to the other oil types. The algae oil shows the highest average molecular mass of 442 g/mol, leading to a high oil viscosity of 101 mPa.s. Low pH value of oils from the virgin biomasses such as wood, straw, and algae were observed compared to that of the processed biomass such as lignin and sewage sludge.

Acknowledgments

CHEC is financially supported by the Technical University of Denmark, DONG Energy A/S, Vattenfall A/S, FLSmidth A/S, Hempel A/S, Energinet.dk, the Danish Research Council for Technology Sciences, the Danish Energy Research Program, the Nordic Energy. Financial support of this PhD study by DONG energy A/S and Energinet.dk is gratefully acknowledged.

References

1. N. Bech, M.B. Larsen, P.A. Jensen, K Dam-Johansen, Biomass Bioenerg. 33 (2009) 999–1011
2. M.J. Hagge, K.M. Bryden, Chem. Eng. Sci. 57 (2002) 2811–2823
3. A.M.C. Janse, R.W.J. Westerhout, W. Prins, Chem. Eng. Process. 39 (2000) 239–252
4. Y.B. Zhai, Q. Liu, G.M. Zeng, C.T. Li, F. Yang, S.H. Li. Environ. Eng. Sci. 25 (2008) 8
5. P. Thipkhunthod, V. Meeyoo, P. Rangsunvigit, T. Rirksomboon, J. Anal. Appl. Pyrol. 79 (2007) 78–85
6. M.E. Sa´nchez, J.A. Mene´ndez, A. Domı´nguez, J.J. Pis, O. Martı´nez, L.F. Calvo, P.L. Bernad, Biomass Bioenerg. 33 (2009) 933-940
7. B. Scholze, C. Hanser, D. Meier, J. Anal. Appl. Pyrol. 58-59 (2001) 387-400

Anna Katrine Vangsgaard

Phone: +45 4525 2910
E-mail: akv@kt.dtu.dk
Discipline: Systems Engineering
Process Technology and Unit Operations
Supervisors: Gürkan Sin
Krist V. Gernaey
Barth F. Smets, DTU Environment

PhD Study
Started: September 2010
To be completed: August 2013

Framework for Construction of Multi-scale Models for Biological Wastewater Treatment Processes - Autotrophic Nitrogen Conversion

Abstract
In wastewater treatment technologies, employing biofilms or granular biomass, processes might occur at very different spatial and temporal scales. Model development for such systems is typically a tedious, complicated, and time consuming task, which involves selecting appropriate model equations for the different scales, making appropriate and simplifying assumptions, connecting them, analyzing and solving the model equations numerically, and performing parameter estimations if necessary. In this study, a structured framework for modeling such systems is developed. It aims to support the user at the various steps and to reduce the time it takes to generate a model ready for application. An implementation of the framework is illustrated using a simple case study, which considers treatment of a nitrogen-rich wastewater via the nitritation-anammox process by a granular biofilm system.

Introduction
Models are playing an increasingly important role in design and optimization of wastewater treatment plants and processes. Models have successfully been used for many purposes, from design to supporting process operation and control of treatment plants, or as a tool to evaluate the performance of a specific treatment technology. An area which has been receiving increased attention is the application of models as a tool for design of experiments when investigating new and emerging processes. By utilizing models for this purpose, the practical experiments can be more targeted towards a specific goal of the study or towards testing a specific hypothesis. As a consequence, it is expected that the number of experiments to be performed can be reduced, which will decrease the manpower needs and the cost of process development. In addition, the effect of operating conditions can be explored and help direct practical experiments towards obtaining optimal process performance. For all the above mentioned purposes, development of appropriate and reliable models is of great importance. A systematic framework generating models in an efficient and structured way has therefore been developed in this work. The framework is illustrated by a case study regarding biological conversion of nitrogen in an autotrophic environment. The overall aim of this project is to develop a detailed model capturing process performance and microbial composition in biofilm systems performing autotrophic nitrogen conversion. This is done by development of detailed models for the involved bacterial groups and integration of such models into complete ecosystem models, which describe how the major microbial groups interact. This insight will be used to design experiments in which relevant operational conditions will be identified and tested. The relevant conditions are those under which the nitrogen removal process is optimized through the development of selection pressure, resulting in a targeted removal or enhancement of specific microbial groups.

Methods
In biofilm systems, processes happen at very different spatial scales, as opposed to in completely mixed reactors where all reactions are often assumed to happen at the same spatial scale. Modeling biofilm systems typically involves three spatial scales (Xavier et al., 2005); individual cells, biofilm, and reactor scale, as shown in Figure 1. On the individual or cellular scale (10^{-5}-10^{-6}m) the growth and metabolism of the microorganisms are captured. On the biofilm scale (10^{-4}-10^{-3}m) the spatial location of the bacteria is described, and also the transport of soluble and particulate compounds is included here. At the reactor scale (10^{-1}-10^{0} m) the overall mass balances are considered along

with the hydrodynamic conditions in the reactor. At the cellular scale, individual cells, a subset of a functional group (e.g. specific species of ammonium oxidizing bacteria (AOB)), or an entire functional group of microorganisms (e.g. AOB) can be modeled. If individuals are considered, a certain differentiation in their metabolism might be assumed, whereas if a subset or an entire functional group is modeled, their metabolism can be assumed to be identical. The latter is termed the lumped approach and can be solved along with the transport equations at the biofilm scale.

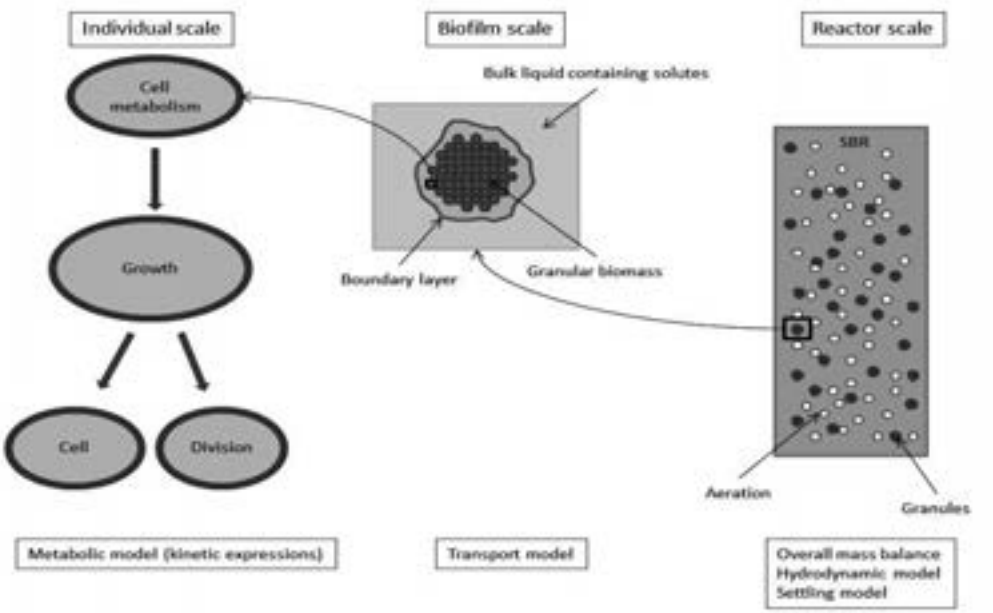

Figure 1. Conceptual model of an SBR with granular biomass, as an example of a multi-scale model. Three spatial scales are considered; the individual or cellular, biofilm, and reactor scale (adapted from Xavier et al., 2005).

A framework that supports the model construction at the different scales as well as linking them to each other has been developed, by studying the workflow typically involved in development of multi-scale systems (see Figure 2). The first step consists of defining the overall modeling objective. The second step is gathering system information such as for example physical and operational conditions of the system. From this information the main assumptions can be established in the third step. Subsequently, the model scenarios of interest should be defined, including which spatial scales and processes are of relevance. From this definition the individual models to be constructed can be derived. Each of the individual models are either taken from previous studies, if such exist, or they are constructed following the workflow depicted on the right side of Figure 2. First the specific model objective for the individual model and then the corresponding identifiability analysis of the model parameters are system information and assumptions are defined. The individual model is constructed, and sensitivity and conducted as necessary. The model is then calibrated to experimental data by adjusting the sensitive parameters. Finally, when the individual model has been validated, it is "exported" back into the multi-scale modeling workflow. The individual models are then linked to each other by defining the data that need to be transferred from one spatial scale to the next and vice versa. The multi-scale model system can now be solved by defining appropriate initial and boundary conditions.

Case study. Complete autotrophic nitrogen removal (CANR), is a relatively new treatment technology, which combines partial nitritation with anaerobic ammonium oxidation (anammox). Nitritation is performed by ammonium oxidizing bacteria (AOB), which convert ammonium to nitrite. The anammox process is performed by anaerobic ammonium oxidizing bacteria (AnAOB), by oxidizing ammonium using nitrite as the terminal electron acceptor. For wastewaters containing high concentrations of nitrogen and low organic carbon to nitrogen ratios, such as sludge digester effluent, landfill leachate, or special industrial wastewaters, conventional nitrification-denitrification is either not a very efficient treatment process or a rather costly process. CANR combining partial nitritation (eq. 1) with anaerobic ammonium oxidation (eq. 2) can overcome these difficulties, because the requirement for aeration is lowered and the need for addition of organic carbon is eliminated (Strous et al., 1997). Meanwhile,

the sludge production and the need for treatment of excess sludge are significantly lowered.

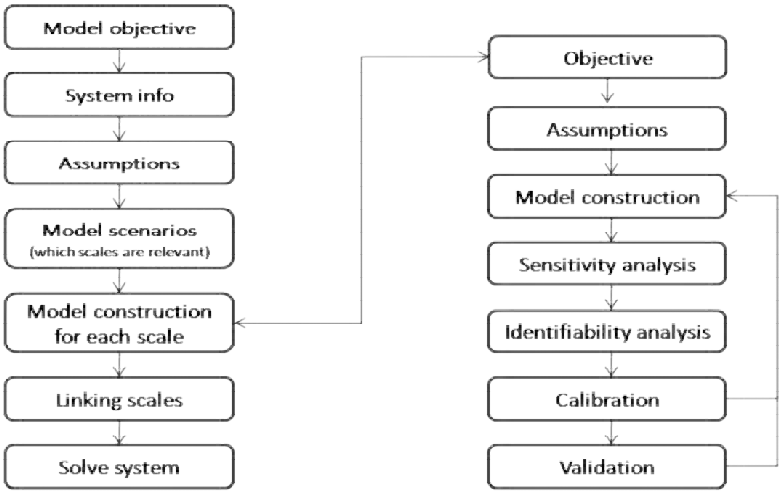

Figure 2. Workflow scheme for multi-scale modeling (left) and identification of the individual models (right) (adapted from Heitzig et al, 2010).

$$NH_4^+ + 1.5O_2 \rightarrow NO_2^- + H_2O + 2\ H^+ \quad (1)$$

$$NH_4^+ + 1.32\ NO_2^- + 0.066\ HCO_3^- + 0.13\ H^+ \rightarrow$$

$$0.26\ NO_3^- + 1.02\ N_2 + 0.066\ CH_2O_{0.5}N_{0.15} + 2.03\ H_2O \quad (2)$$

An environment where both groups of bacteria can co-exist can be created in biofilms or granular biomass, where both anoxic and aerobic conditions are created in a stratified structure. In the outer layers AOB will grow, consume oxygen, and prevent oxygen from penetrating further than a certain depth. In the anoxic inner biofilm layers, the AnAOB will be present.

In the case study the overall model objective is to study the microbial composition of granules containing AOB and AnAOB along with the bacterial groups competing with them for substrate, namely nitrite oxidizing bacteria (NOB) and heterotrophic bacteria (HB), growing on organic material originating from bacterial decay. The model is capturing a 1-dimensional spherical biofilm. The maximum biofilm thickness, number of granules, and reactor volume are all constant parameters with certain values (system info). The advective transport of soluble compounds is ignored, and all particulates (bacterial groups and inert material) are solely transported by advection as in the benmark biofilm model no. 3 (Wanner et al., 2006). The bacterial species are assumed to have a uniform metabolism (assumptions). The mass balances in the cellular and biofilm scale can thus be solved simultaneously (Figure 3). The model scenario considered therefore includes two scales; the biofilm and reactor scales. The individual models for the conversion and transport of soluble and particulate compounds can be seen in eq. 3 compounds the biofilm scale is linked to the overall and 4, respectively. For the soluble and particulate mass balance in the reactor scale (eq. 7) by the flux through the boundary layer between the biofilm and the bulk liquid (linking scales) (eq. 5 and 6, respectively).

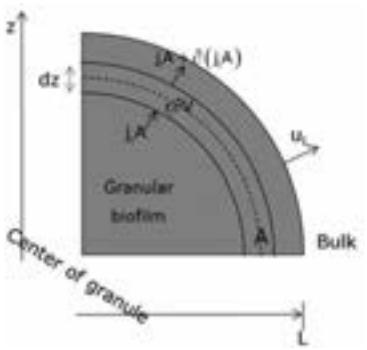

Figure 3. A slice of a granule schematically illustrating the biofilm scale with the transport and microbial generation/consumption indicated.

The mass balance for soluble compounds in spherical coordinates:

$$\frac{\partial S_i}{\partial t} = D_{bio,i}\frac{1}{z^2}\frac{\partial}{\partial z}\left(z^2\frac{\partial S_i}{\partial z}\right) + r_i \quad (3)$$

S_i is the concentration of the soluble compound *i* inside the biofilm, z is the radial distance from the center of the granule, r_i is the conversion rate, and $D_{bio,i}$ is the diffusion coefficient in the biofilm.

The mass balance for particulate compounds:

$$\frac{\partial X_i}{\partial t} = -\frac{\partial\left(X_i u_F\right)}{\partial z} + r_i \quad (4)$$

where X_i is the concentration of the particulate species *i*, u_F is the advective velocity, and r_i is the conversion rate.
The flux of soluble compounds at the biofilm/liquid interface:

$$j_{bio,Si} = \frac{D_i}{L_B}\left(S_{i,bulk} - S_{i,L}\right) \quad (5)$$

where D_i is the diffusivity in water, L_B is the thickness of the mass transfer boundary layer, $S_{i,bulk}$ is the concentration in the bulk liquid, and $S_{i,L}$ is the concentration at the biofilm/liquid interface.
The flux of particulate species:

$$j_{bio,Xi} = -u_D X_{i,L} \quad (6)$$

where u_D is the detachment velocity and $X_{i,L}$ is the concentration of the particulate at the biofilm/liquid interface.
The reactor mass balance is given as:

$$\frac{dC_{i,bulk}}{dt} = \frac{Q_{in}C_{i,in} - Q_{out}C_{i,bulk} - j_{bio,i}A}{V_{reactor}} + r_{i,bulk} \quad (7)$$

where C denotes the concentration of either a soluble or a particulate species, Q represents a flow rate (inflow, Q_{in}, or outflow, Q_{out}), A is the total surface area of the biofilm, $V_{reactor}$ is the volume of the entire reactor, and $C_{i,in}$ is the influent concentration.

Results

A generic multi-scale modeling framework was implemented in the Matlab software (Vangsgaard), and can be customized for the needs of biofilm systems by adapting the features of the software according to the work flow identified for multi-scale biofilm modeling, as shown in Figure 2.

By solving the constructed model, a stratified structure and the specific location of the bacteria is obtained (Figure 4).

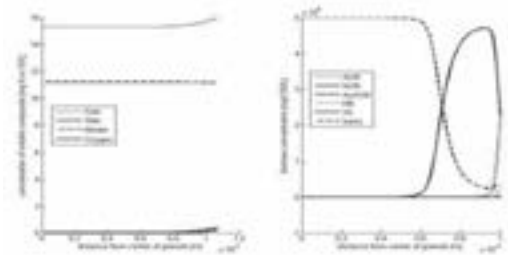

Figure 4. Soluble and biomass concentrations inside the biofilm matrix obtained from a simulation.

While the case study is used to highlight the framework and the software support for multi-scale model development, more detailed and complex model systems, including additional microbial species and higher numbers of soluble compounds, can easily be constructed in the future.

Conclusions

A framework for construction of multi-scale models of biofilms used in biological wastewater treatment processes has been constructed. The framework is implemented in the Matlab-Simulink software. It is flexible and efficient, which allows for generation of customized models for a broad range of applications from design of experiments for new processes to process design and optimization.

Acknowledgements

The author would like to thank the Technical University of Denmark for financial support as well as the Danish Agency for Science, Technology and Innovation for funding through the Research Centre for Design of Microbial Communities in Membrane Bioreactors (EcoDesign MBR).

References

1. M. Heitzig, G. Sin, P. Glarborg, R. Gani, 2010. In: Pierucci, S., Buzzi Ferraris, G. (Eds.), 20th European Symposium on Computer Aided Process Engineering - ESCAPE20. Elsevier.
2. M. Strous, E. VanGerven, P. Zheng, J.G. Kuenen, M.S.M. Jetten, Water Res. 31 (1997) 1955-1962.
3. J.B. Xavier, C. Picioreanu, M.C.M. van Loosdrecht, Environ. Microbiol. 7 (2005) 1085-1103.
4. O. Wanner, H. J. Eberl, E. Morgenroth, D. R. Noguera, C. Picioreanu, B.E. Rittmann, M.C.M. van Loosdrecht, 2006, Mathematical Modeling of Biofilms-IWA Scientific and Technical Report, IWA Publishing.
5. A.K. Vangsgaard, M. Mauricio-Iglesias, K.V. Gernaey, B.F. Smets, G. Sin, 2011, IWA Symposium on Systems Analysis and Integrated Assessment, 8th IWA Watermatex conference proceedings, 687-690.

Sindhu Vudayagiri
Phone: +45 4525 6825
E-mail: sivu@kt.dtu.dk
Discipline: Polymer Technology

Supervisors: Anne Ladegaard Skov
Ole Hassager

PhD Study
Started: August 2011
To be completed: July 2014

Release Properties of PDMS (Polydimethyl siloxane) Films

Abstract
DEAPs (dielectric-electro active polymer) are elastomers with high dielectric constants. The DEAP material is used in the making of actuators, sensors and generators. PDMS (polydimethysiloxane) is one such commercially used DEAP. In the recent times awareness about DEAP's enormous potential to be applied in various fields has gained momentum, which has led to large scale manufacture of the DEAP material. In this research, release issues in the large scale production of PDMS films are investigated.

Introduction
The working principle of a DEAP actuator is similar to that of a capacitor. A thin elastomer film is sandwiched between two compliant electrodes, and a high DC voltage (kV) is applied and the arising electrostatic pressure causes expansion of the elastomer film in planar directions.

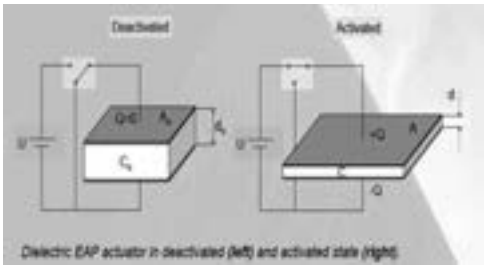

Figure 1: Working principle of an actuator.

The geometry of the elastomer film plays a vital role in the performance of the actuator and at Danfoss Polypower, the films are microstructured to obtain directional anisotropy.

Objective
The current manufacturing of PDMS films induces considerable pre-strain in the elastomer film. The release and take-up of the elastomer film without inducing any appreciable tension in the film is vital to the performance of the actuator. The objective of the current research is to enhance the release properties of PDMS films.

Discussion
The PDMS films are made by coating the polymer mix (vinyl end linked-PDMS, a cross-linker and filler particles) on a carrier web followed by curing in an oven [1]. The film is then removed from the carrier web and coated with the metal electrode. The carrier web also acts as a mould imparting a corrugated structure to the films on the side of contact. The release should be smooth without inducing any considerable pre-strain in the PDMS film.

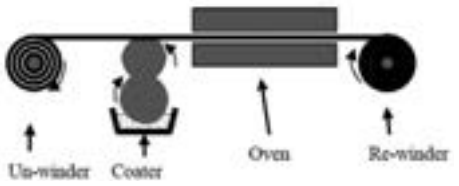

Figure 2: Manufacture process of DEAP films. [1]

It is interesting to note that the old webs give a better release than the new webs. Contact angle experiments reveal that the contact angle of new web is 80^0 and for the old web is 109^0, clearly indicating that the web has become more hydrophobic after use. The contact angle of water on PDMS is 110^0 which is similar to the old web. An IR of the webs revealed that the used carrier

webs retained some amount of silicone (PDMS) on them which actually helps release of the films.

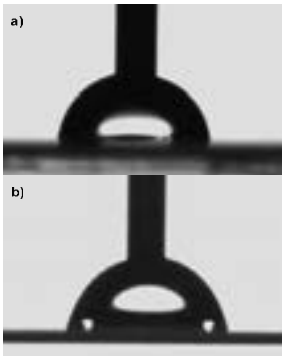

Figure 3: a) contact angle of old carrier web; b) contact angle of new carrier web.

The IR and the contact angle experiments indicate an accumulation of silicone on the old webs which favors the easy release.

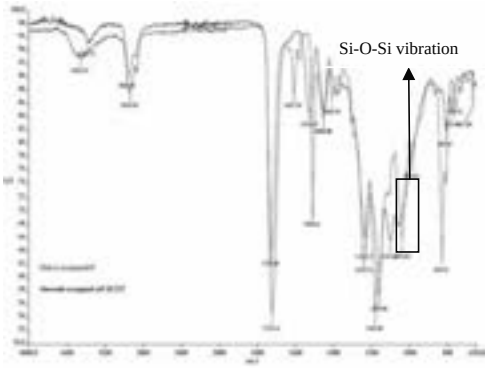

Figure 4: IR spectrum of Old and new carrier web.

Solutions for release

A literature study of the release properties of PDMS films and methods to enhance the release (surface properties) was undertaken. The surface energy of PDMS is 19 mJ/m^2 which explains its inert nature towards many chemical species and poor adhesion to many substrates. By addition of suitable surface active block copolymers one can decrease the surface energy or make the film selectively non-adhesive to a particular substrate. A polymeric additive of lower surface energy than its host matrix is known to adsorb preferentially at the free surface and consequently decreases the adhesion of that surface towards a particular substrate [2]. Perfluoroether allylamide added to PDMS (0.3-1.5 weight %) lowered its surface energy from 19 to 8 mJ/m^2 [3]. Based on this idea PDMS films will be doped with small amounts of perfluoroether functionalities and the films will be examined to see if they yield favorable results. On the contrary, one can also chose a substrate which will facilitate easy release of the PDMS, but due to the various requirements and constraints of the manufacturing process at Danfoss Polypower it is not easy to employ a substrate that acts as a mould, supports the film through the curing process and also favors easy release.

Embossing Technique

The PDMS films can be embossed with micro-structures after the gel-point (where the network spans the entire volume). The films retain the micro-structures through the curing process and this property of the films can be exploited to eliminate the Carrier web from the manufacture process. A roller die with the microstructure can impart the corrugations to the film after gel-point. At DPC, this was successfully accomplished.

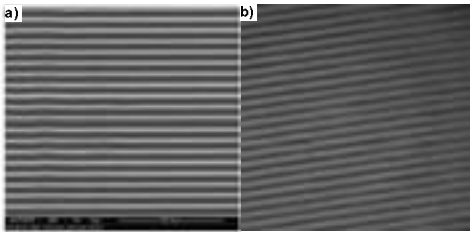

Figure 5: a) Carrier web- showing the corrugated microstructure [1]; b) PDMS film with corrugations-imparted by a roller die.

Conclusions

Release of the PDMS films is vital for its performance. Hence, the carrier webs are investigated and it is found that the new webs hinder release of the films. To prevent this adhesion the surface properties of the films have to be modified with suitable additives which will lower the surface energy and make them less adhering.

Replacing the carrier web with a 'release-friendly' web is not an option right now. Embossing technique can also be an option because the use of carrier web is completely eliminated, thus avoiding any issues related to release.

Acknowledgements

Liyun Yu (Post-doc. DPC, KT) - for her help with embossing techniques. The Danish National Advanced Technology Foundation for the financial support.

References

1. H.-E. Kiil, M. Benslimane, Proceedings SPIE, vol. 7287, 2009.
2. J.T. Koberstein, D.E. Duch, W. Hu, T.J. Lenk, R. Bhatia, H.R. Brown, J.P. Lingelser, Y. Gallot, J. Adhes. 66 (1998) 229-249
3. S.K. Thanawala, M.K. Chaudhury, Langmuir, 16 (2000) 1256-1260

Jian Wu
Phone: +45 21327799
E-mail: jiwu@risoe.dtu.dk

Supervisors: Andreas Ibrom
Claus Beier
Leon van der Linden

PhD Study
Started: November 2009
To be completed: October 2012

Modelling the Effects of Climatic Variability, Extreme Events and Functional Change on the Carbon Cycling of Terrestrial Ecosystem

Abstract
Elevated atmospheric CO_2 concentration is predicted to lead to significant changes in climate. Response studies in terrestrial ecosystems have so far focused on average climatic changes. However, both historical observations and model projections of future climate indicate enhanced climatic variability will lead to possibly much more severe ecosystem response patterns. This PhD project will investigate ecosystem responses to different climate change scenarios with a particular focus on the ecosystem functional change on the carbon cycling. Both empirical and mechanistic modeling studies are applied based on long-term (1996-present) half-hourly monitoring of atmosphere-biosphere CO_2 exchange.

Introduction
Terrestrial ecosystems fix more than ten times the anthropogenic CO_2 emission through photosynthesis annually. At the same time, a similar amount of CO_2 is released back to the atmosphere by respiration in soil microorganisms and plants. Globally, the difference between these two opposing carbon fluxes is a net sink (1-4 Pg C yr^{-1}), which is of the same order of magnitude as the fossil fuel and cement emissions (8.4 Pg C yr^{-1} in 2009) [1]. The future fate of this sink is highly uncertain, depending on the changes in climate, extremes, land use and ecosystem functional properties. Understand the spatiotemporal variability of the ecosystem carbon blance is thus important. Currently, projections of future terrestrial ecosystem carbon balance rely on mechanistic models that describing the dynamic feedbacks between the ecosystems and the physical climate forcing [2]. However, many processes such as the gradual (e.g. long-term adaptation) or abrupt (e.g. extreme events) ecosystem internal functional changes were still not well understood and represented in the model. This study aims to improve the knowledge and models by analyzing the long-term record of eddy covariance flux measurements of carbon fluxes at the EuroFlux site Sorø, Denmark [3].

Semi-empirical modeling
We used a semi-empirical model to distinguish the relative impact of direct climate forcing and changes in ecosystem functional properties on variability in net ecosystem exchange of CO_2 (NEE) [4]. The NEE of each calendar year was used to estimate a parameter time series (every two days with weekly moving time window) based on a semi-empirical model, Eq. 1 and 2 [5]. The changes in the parameters are regarded as functional changes. The parameter and climate time series were applied factorially by year to predict carbon fluxes. The sum of squared error approach was applied to separate the effects of annual climate variability and fitted parameter to the inter-annual variation in NEE. The results provide information on the proportions of long-term ecosystem carbon dynamics driven by both the direct effect of climate change and ecosystem internal dynamics.

$$\mathrm{NEE} = -\frac{\alpha\beta R_g}{\alpha R_g + \beta} + r_b \exp\left(E_0\left(\frac{1}{T_{ref} - T_0} - \frac{1}{T_{air} - T_0}\right)\right) \quad (1)$$

where T_{air} is the air temperature; T_0 is a constant; R_g is the global radiation; α is the light use efficiency; β is the instantaneous maximum canopy photosynthetic capacity, r_b is the base respiration at reference temperature; E_0 is the temperature sensitivity.

$$\beta = \begin{cases} \beta_0, VPD < VPD_0 \\ \beta_0 \exp\left(-k\left(VPD - VPD_0\right)\right), VPD > VPD_0 \end{cases} \quad (2)$$

where k is a scaling parameter estimating the effects of vapour pressure deficit, VPD on β and VPD_0 is a threshold value set as 10 hPa, above which the stomatal conductance is allowed to reduce β in the model.

Mechanistic modeling

Process-based ecosystem models are challenged with both missing-processes (relative simple model structure compared to the natural processes, Fig. 1) and over-parameterization (limited data availability lead to equalfinality of model predictions). We aim to use different ecosystem models and multiple data streams based on model data fusion techniques [6] (e.g. Bayesian inversion and generalized uncertainty estimation) to indentify how model structural development and increasing data information can enhance the realistic representation of nature.

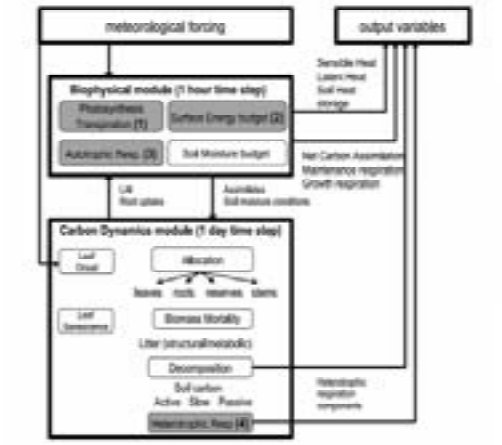

Fig. 1: Schematic structure diagram of mechanistic ecosystem model [7]

Results

Based on the statistical modelling, we found climate variability had strong control on the carbon fluxes at short time scales but this impact reduced as the time integral increased (Fig. 2). On longer temporal scale, the effect of ecosystem functional change became progressively larger and appeared to dominate the interannual variability in the ecosystem carbon balance. At the annual time scale as much as 80% of the IAV in NEE was attributed to the variation in photosynthesis and respiration related model parameters. The climate factors important for the CO_2 exchange changed intra-annually. Combinations of climate anomalies in different periods of the year either intensified or attenuated the aggregated ecosystem responses, implying that the changing distribution of climate anomalies, in addition to the average climate change, could have stronger impacts on the ecosystem carbon balance in the future.

Conclusion

The observed trend of increasing carbon uptake was found to be driven by ecosystem functional changes rather than direct effects of decadal climatic variability. Incorporating ecosystem functional change into process based models will reduce the uncertainties in long-term predictions of ecosystem carbon balances in global climate change projections.

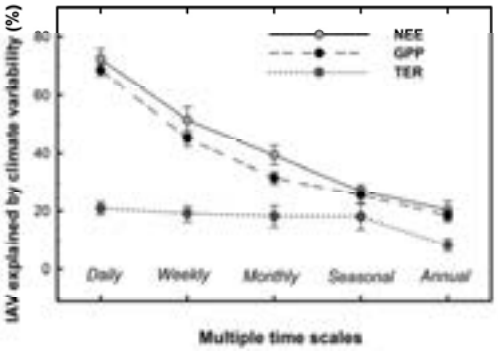

Fig. 2: Percentage of interannual variation in modelled gross primary production (GPP), ecosystem respiration (TER) and NEE caused by climate variability at different time scales

Outlook

In the following steps, model data fusion results based on mechanistic models and multiple data stream (e.g. carbon fluxes, sensible and latent heat flux, soil respiration, biomass, litter production, and phenology) will be synthesized.

Acknowledgements

This work was supported by the EU FP7 project CARBO-extreme, the DTU Climate Centre and the Danish national project ECOCLIM (Danish Council for Strategic Research).

References

1. R. Houghton, Annu. Rev. Earth Planet. Sci. 35 (2007) 313-347.
2. M. Heimann, M. Reichstein, Nature 451 (2008) 289-292.
3. K. Pilegaard, A. Ibrom, M.S. Courtney, P. Hummelsh, N.O. Jensen, Agr. Forest Meteorol. 151 (2011) 934-706.
4. J. Wu, L. Linden, G. Lasslop, N. Carvalhais, K. Pilegaard, C. Beier, A. Ibrom, Biogeos. Discus. 8 (2011) 9125–9163.
5. G. Lasslop, M. Reichstein et al. Glob. Change Biol. 16 (2010) 187-209
6. D. Santaren, P. Peylin, N. Viovy, P. Ciais, Global Biogeochem. Cycles, 21 (2007).
7. Y.P. Wang, C.M, Trudinger, I.G. Enting, Agr. Forest Meteorol. 149 (2009) 1829-1842.

Qiongxiao Wu
Phone: +45 4525 2837
E-mail: qw@kt.dtu.dk
Discipline: Reaction and Transport Engineering

Supervisors: Anker Degn Jensen
Jan-Dierk Grunwaldt, KIT
Burcin Temel, Haldor Topsøe A/S

PhD Study
Started: January 2010
To be completed: December 2012

CO Hydrogenation on Cu-Ni Catalysts: Influence of Supports

Abstract
Copper/nickel catalysts supported on SiO_2, ZrO_2, TiO_2, γ-Al_2O_3 and carbon nanotubes (CNTs) exhibit different catalytic behavior for CO hydrogenation. The CNTs and SiO_2 supported CuNi catalysts showed high activity and selectivity (up to 99 mol%) at P = 100 bar, T=275 °C, and H_2/CO = 1.0 vol/vol) for methanol synthesis. The γ-Al_2O_3 supported catalyst mainly produced dimethyl ether (DME) with 81.9 mol% selectivity and 8.4 mol% CO conversion at 250 °C. The CuNi/ZrO_2 catalyst exhibited high methanol selectivity at 250 °C, whereas the selectivity shifted to hydrocarbons and DME at higher temperature. The CuNi/TiO_2 catalyst produced hydrocarbon as main products at all tested temperatures. The in-situ X-ray diffraction and activity testing results indicated that the CuNi alloys are high active methanol synthesis components for CO hydrogenation. *In-situ* X-ray absorption spectroscopy and mass spectrometer results showed that the reduction temperatures and processes depended on the type of support.

Introduction
Currently, the world is experiencing rising oil prices and dwindling resources. Liquid fuels from sustainable sources such as biomass have moved into the spotlight as clean, sustainable and transportable fuel alternatives or fuel additives [1-6]. Liquid fuels include methanol, dimethyl ether (DME), mixed long chain alcohols, and Fisher-Tropsch synthetic diesel, which can be directly synthesized from biomass-derived syngas by using different types of catalysts [7-10]. Today methanol can be produced from syngas over Cu/ZnO-based catalysts with high efficiency. Methanol is an efficient fuel in an internal combustion engine or in a fuel cell, and methanol has therefore been suggested as the main energy carrier for the future energy economy [11]. Despite the current significant methanol production, the replacement of gasoline would require more than a hundredfold increase in methanol production [12, 13]. Moreover, deactivation of the commercial Cu/ZnO methanol synthesis catalyst is a major problem [14-16]. More than one third of the activity is lost after the first 1000 h of operation, which determines the economic lifetime [17, 18]. It would therefore be of great value, if methanol synthesis catalysts with greater activity and stability could be developed. Recently, based on a theoretical screening of a large number of alloys using density functional theory [19], we found experimentally that Cu/Ni alloys are active and selective methanol synthesis catalysts. It was previously reported that CuNi based catalysts are either active for higher alcohol synthesis [20-22], hydrocarbon synthesis [23] or methanol synthesis [24]. It appears that there are several conflicting reports on what CuNi based catalysts do in syngas conversion.

Here, we studied syngas conversion over CuNi based catalysts supported on SiO_2, ZrO_2, TiO_2, γ-Al_2O_3 and carbon nanotubes (CNTs) to investigate how this influences on the CuNi alloys formation and consequently their selectivity and activity for CO hydrogenation. Different operating conditions such as temperature and syngas composition were investigated as well. Meanwhile, *In-situ* X-ray diffraction (XRD), transmission electron microscopy (TEM) and *in-situ* X-ray absorption spectroscopic (XAS) have been used to identify the structure of these catalysts.

Specific Objectives
This work aims at providing a systematic study of Cu/Ni catalysts for liquid fuel synthesis from biomass-derived syngas.

Experimental
Cu/Ni based catalysts were prepared by the incipient wetness impregnation method. First, an aqueous solution was prepared by dissolving $Cu(NO_3)_2 \cdot 3H_2O$ (Sigma-Aldrich) and $Ni(NO_3)_2 \cdot 6H_2O$ (Sigma-Aldrich) in de-ionized water. Then the aqueous solution was used to impregnate by pre-prepared SiO_2, ZrO_2, TiO_2, γ-Al_2O_3 and CNTs pellets. Additionally, CNTs were

purified by refluxing 5 g commercial CNTs in 500 ml 37 wt% nitric acid at 110 °C for 5 h, followed by filtering, washing and drying before impregnation. Loading percents were selected based on calculation (20 wt % Cu + Ni loading on 80 wt% supports individually, the molar ratio of Cu:Ni=1:1). After 1 h aging, catalysts were dried at 100 °C, and subsequently calcined at 400 °C in air for 4 h with a heating rate of 1.5 °C/min. All the catalysts have been crushed and sieved to a size range of 0.6-1.4 mm. Table 1 shows the parameters of all support materials used for preparation of the supported Cu/Ni catalysts.

Table 1. Support materials used for preparation of all supported CuNi alloy catalysts

Support	$VP_{support}$ $ml_{water}/g_{support}$	$BET_{support}$ m^2/g	Company
SiO_2	1.28	250	Saint-Gobain Norpro
ZrO_2	0.46	134	Saint-Gobain Norpro
TiO_2	0.75	161	Saint-Gobain Norpro
Al_2O_3	0.8	166	n.a.[a)]
CNTs	1.31	328	Sigma-Aldrich

a) n.a. means not available.

I*n-situ* XRD was performed with a PANalytical X'Pert PRO diffractometer equipped with an Anton Paar XRK 900 in situ cell (APC), a gas flow control system, a Ni filter and a slit for H_2-TPR. Catalyst precursor was heated in flowing 20 mol% H_2/He up to 300 and 500 °C, respectively. The outflow is analyzed by mass spectrometry (MS) allowing for TPR and activity measurements.

In-situ XAS experiments were performed with a recently installed in-situ setup at the synchrotron of Karlsruhe ANKA-XAS beamline. X-ray Absorption Spectroscopy studies were performed at the ANKA-XAS beamline using a Si(111) double-crystal monochromator detuned to *ca.* 60% of the maximum intensity. Incident and transmitted X-ray intensity were measured by ion chambers (Oxford). A newly fabricated homemade *in situ* transmission cell was employed. The cell consisted of a stainless steel cylinder with a central 2x10x2 mm hollow and connected to the in- and outlet gas lines, in which the proper amount of granulated catalyst (100-200 μm) was placed. The cell was inserted between two heating blocks for temperature control. Quick EXAFS spectra around both the Ni K (8333 eV) and the Cu K (8979 eV) edges, were recorded in continuous mode from 8.25 to 9.25 keV with a step size of 1.5 eV. For energy calibration a Ni foil was used. The *in situ* TPR experiments were carried out under 5%H_2/He flow (40 mL min^{-1}) while heating up to 300 - 550°C at a rate of 5°C min^{-1}. The composition of the outlet gas was monitored with a Pfeiffer Quadrupol Mass Spectrometer. The obtained spectra were analysed using the Athena program. The fraction of Cu(II) and Ni(II) was determined by linear combination analysis of the XANES spectra recorded at a given temperature with that of reference CuO (or NiO) and Cu (or Ni) foil.

The performance of catalysts for CO hydrogenation was evaluated in a fixed-bed continuous-flow reactor with an online GC-FID/TCD detection system (6890N from Agilent Technologies). The details of the setup are given by Christensen et al. [25-27]. A bubble flow meter was used for determination of the volumetric flow rate of the reactor effluent. Prior to the reaction, samples of the oxide precursor of catalysts were pre-reduced in situ by a N_2-carried 20% H_2 gaseous mixture for 12-14 h at 300 °C with a heat rate of 1-1.5 °C/min.

The conversion of CO (X_{CO}) is calculated from the molar flow rates of CO into and out of the reactor:

$$X_{CO} = \frac{F_{CO}^{in} - F_{CO}^{out}}{F_{CO}^{in}} \cdot 100\%$$

The CO_2 free selectivity to product is based on the total number of carbon atoms in the products except CO_2:

$$S_i = (n_i M_i) / (\sum n_i M_i) \cdot 100\%$$

where n_i ($n_i \geq 1$) is the number of carbon atoms in the product i, and M_i is the percentage of detected percentage of product i.

The carbon mass balance generally fulfilled to within 5 mol%.

Results and Discussion

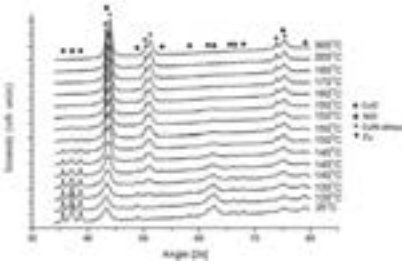

Figure 1. In-situ XRD patterns of H_2-TPR of $CuNi/SiO_2$ catalyst corresponding to temperatures.

Figure 1 shows the in-situ XRD patterns of $CuNi/SiO_2$ at different temperatures in a flow of 20 mol% H_2/He. No reflection could be observed in the XRD pattern of SiO_2. At 25 ºC, only CuO and NiO species can be observed. The main reduction took place between 120 and 160 ºC as observed from in-situ XRD patterns. Above 170 ºC, there were no reflections of either CuO or NiO in XRD patterns. Additionally, the in-situ XRD patterns showed that NiO and CuO were starting to be reduced almost simultaneously, as well the reduction completing point. At 300 ºC, the XRD pattern showed only reflections of Cu and CuNi alloys. The ratio of Cu/Ni in the alloys can be calculated according to Vegard's law [28], to be $Cu_{11}Ni_{14}$. The particle sizes are 47 nm and 14 nm for Cu and $Cu_{11}Ni_{14}$ alloy, respectively, as determined by means of the Sherrer equation. Moreover, it can be observed the intensity of Cu reflection decreased, while the CuNi alloy one increased when the temperature increased from 180 to 300 ºC in the stream of H_2/He. It implies the structure was changing during the heating process at reducing atmosphere. In general, Cu and Ni can form a solid solution, however, in this case a separated Cu phase are formed as well. This is probably due to the support confinement effect of pores. Cu is fairly easy to sinter in

strong reducing conditions, and therefore it forms big particles (47 nm) before merging into the rest CuNi alloys.

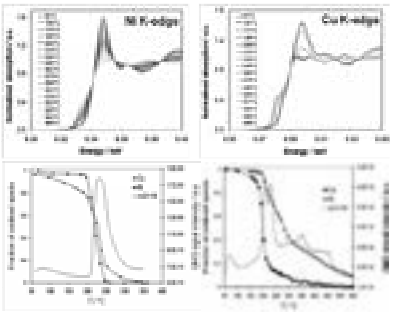

Figure 2. (Top) Linear combination analysis of XANES spectrum of $CuNi/SiO_2$ at Ni K- and Cu K- edge during reduction: $5\%H_2$/He (40mL min^{-1}); T-range 50 - 360°C; heating ramp 5°C min^{-1}. Linear combination analysis of XANES spectrum of $CuNi/SiO_2$ (bottom left) and $CuNi/Al_2O_3$ (bottom right) at Ni K- and Cu K- edge during reduction: $5\%H_2$/He (40mL min^{-1}), heating ramp 5°C min^{-1}.

Figure 2 (top) shows typical *in-situ* X-ray absorption near edge structure (XANES) analysis at the Ni K-edges (top left) and Cu K-edges (top right) during reduction in 5% H_2/He. Linear combination analysis of XANES spectra of supported CuNi samples displayed H_2-temperature programmed reduction (H_2-TPR) processes for Cu and Ni. A single-broad peak centered at 240 ºC (bottom left**)** for the silica supported sample and a doubled peak at 212 and 230ºC for the Al_2O_3 supported sample (bottom right). *In-situ* XANES show that both Ni and Cu start to reduce almost simultaneously at *ca.*200 ºC on the former catalyst, whereas Ni on Al_2O_3 starts to reduce at higher T than Cu. However, on both samples Cu rapidly fully reduces, whereas Ni displays a slower reduction profiles along T and at 300ºC a significant fraction of Ni still retains the oxidized state. These results suggest that Ni is present in different forms *i.e.* partially alloyed with Cu, which reduces at lower T, together with NiO and very likely $NiAl_2O_4$ in the case of the alumina supported sample, which are reduced at higher temperature.

The activity and selectivity of $CuNi/SiO_2$ and $Cu/ZnO/Al_2O_3$ catalysts for CO hydrogenation at various conditions are shown in table 2. The main product that was observed for the $CuNi/SiO_2$ catalyst was methanol at all tested reaction conditions. Trace amounts of C_{2+} oxygenates (including dimethyl ether (DME) and ethanol) and hydrocarbons (HC) (including methane and ethane) have also been detected. The activity increased with an increase of reaction temperature (250 to 300 °C) while the selectivity towards methanol stayed almost constant.

Figure 3 shows the CO conversion and the CO_2-free methanol selectivity as a function of time on stream for both, $CuNi/SiO_2$ (a) and $Cu/ZnO/Al_2O_3$ (b). For $CuNi/SiO_2$, CO conversion increases from 2.4 to 5.2 mol% while the selectivity to methanol increases from 95 to 99.2 mol% within the first 16 h after which the performance stabilizes. A similar tendency was observed at 275 °C where the CO conversion increased from 9.3 to 12.2 mol% within 12 h. Conversion and selectivity of the $Cu/ZnO/Al_2O_3$ catalyst as a function of time on stream is shown in figure 1b. The CO conversion decreased from 11.3 to 7.2 mol% within the first 14 h of testing. This deactivation phenomenon is a typical problem for commercial methanol synthesis catalysts. One dominant path of deactivation is related to the sintering of the Cu particles reducing the active surface area. In the absence of CO_2, the $Cu/ZnO/Al_2O_3$ catalyst deactivates also due to brass formation in the highly reducing CO/H_2 gas mixture [29].

In order to get a better estimate of the activity of the surface of $CuNi/SiO_2$ in comparison to $Cu/ZnO/Al_2O_3$ the turnover frequency (TOF) based on the active surface area was used instead of the space time yield (STY). As can be seen from table 3, the TOF of $CuNi/SiO_2$ is within the same order of magnitude as calculated for $Cu/ZnO/Al_2O_3$. While being slightly less active at 250 °C, conversion is slightly higher at 275 and 300 °C.

Table 2. Behavior of $CuNi/SiO_2$ and $Cu/ZnO/Al_2O_3$ catalysts in CO hydrogenation at steady state at 100 bar, and H_2/CO = 1.0 vol/vol.

Catalysts	T	GHSV	X_{CO}	Carbon based, CO_2-free selectivity [mol%]			$MeOH_{STY}$	TOF[a]
	[ºC]	[h^{-1}]	[mol%]	MeOH	C_{2+}oxy	HC	g/(kg_{cat}*h)	$molm^{-2}s^{-1}$
$CuNi/SiO_2$	250	2000	5.2	99.2	0.4	0.4	65	$6.7\cdot10^{-5}$
	275	2000	12.1	99	0.4	0.6	167	$1.7\cdot10^{-4}$
	300	4160	11.2	99	0.5	0.5	330	$3.4\cdot10^{-4}$
$Cu/ZnO/Al_2O_3$	250	16000	7.2	99	0.9	0.1	842	$9.2\cdot10^{-5}$
	275	16000	13.5	97.6	2.1	0.3	1315	$1.4\cdot10^{-4}$
	300	32000	12.7	96.3	2.8	0.9	2666	$2.9\cdot10^{-4}$

[a] Molar amount of methanol based on active surface area of catalysts.

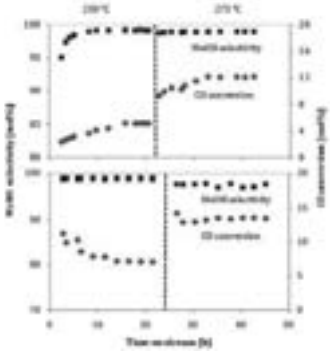

Figure 3. a (top): CO conversion (blue routes) and methanol selectivity (red squares) as a function of the time on stream for the $CuNi/SiO_2$ catalyst. Reaction conditions are: P = 100 bar, T = 250 and 275 °C, GHSV = 2000 h^{-1}, Feed: H_2/CO =1 (vol/vol). b(bottom): CO conversion (blue routes) and methanol selectivity (red squares) as a function of the time on stream for the $Cu/ZnO/Al_2O_3$ catalyst. Reaction conditions are: P = 100 bar, T = 250 and 275 °C, GHSV = 16000 h^{-1}, Feed: H_2/CO =1 (vol/vol).

Table 3. Behavior of CuNi catalysts over different supports in CO hydrogenation at steady state. Experimental conditions: P = 100 bar, T=250 °C, and H_2/CO = 1.0 vol/vol.

	GHSV	X_{CO}	Carbon based, CO_2-free selectivity [mol%]				$MeOH_{STY}$
	[h^{-1}]	[mol%]	MeOH	$C_{2+}OH$	HC	DME	g/(kg_{cat}*h)
$CuNi/SiO_2$	2000	5.2	99.2	0.4	0.4	0.0	65.0
$CuNi/Al_2O_3$	2000	8.4	5.6	0.0	12.5	81.9	3.0
$CuNi/TiO_2$	2000	1.2	5.7	2.0	88.0	4.3	1.0
$CuNi/ZrO_2$	2000	7.8	80.8	1.0	11.2	7.0	79.0
CuNi/CNTs	4200	8.0	98.6	0.1	0.4	0.9	230

Table 3 showed catalytic properties of CuNi catalysts on different supports in CO hydrogenation at 250 °C at steady state. As discussed above that methanol is the dominant product over the $CuNi/SiO_2$ catalyst. The γ-Al_2O_3 supported catalyst produced mainly dimethyl ether (DME). This is probably because CuNi alloys produce methanol first and then the Lewis acidic sites of γ-Al_2O_3 dehydrate methanol to DME. The TiO_2 supported catalyst showed 16 mol% selectivity to higher alcohols with 7 mol% CO conversion at first 2 h. However, the catalyst deactivated with the time on stream and produce mainly HCs at all tested temperatures. It was known that TiO_2 support has a high density of hydroxyl groups on the surface and thus may have an influence on the Cu and Ni, and separate Ni particles are active Fisher-Tropsch catalysts. Meanwhile, it was reported that Ni/TiO_2 produces higher alcohols with around 23 mol% selectivity [22]. Therefore, it is not surprising that CuNi was reported to produce various products as mentioned in the introduction part. It depends on which active sites exist on the surface, such as CuNi alloys sites (silica and CNT supported sample) for methanol synthesis, Lewis acidic sites for dehydration of methanol (the γ-Al_2O_3 supported one), free Ni particle sites for FT oil synthesis with higher alcohols as byproducts (TiO_2 supported one). The $CuNi/ZrO_2$ catalyst produced mainly methanol with 7 mol% DME selectivity at 250 °C. The selectivity of hydrocarbons, higher alcohols and DME were increased with increasing temperature, while methanol selectivity decreased, and HCs become the main products at 300 °C. The CNTs supported catalyst exhibited similar properties to the SiO_2 supported one, but with much higher activity. One should notice that this catalyst was tested at a higher gas space velocity 4200 h^{-1}. CNTs play dual roles in this case, support and hydrogen carrier. CNTs can adsorb both molecular hydrogen and hydrogen atoms [30]. Additionally, the TEM images showed that the particle sizes are around 6 nm for the CNT based catalyst but 15 nm for the silica supported one. This could be the reason that CNTs supported catalysts showed higher activity for methanol formation.

Conclusion

In summary CuNi catalysts on different supports exhibited different catalytic behaviors for CO hydrogenation. The in-situ XRD and activity test results indicated that the CuNi alloy is high active methanol synthesis components for CO hydrogenation.

Acknowledgements

This specific work was financially supported by CASE, Catalysis for Sustainable Energy. The work was carried out in collaboration between the Combustion and Harmful Emission Control Research Centre (CHEC), Haldor Topsøe, Center for Electron Nanoscopy (CEN) of DTU, Institute of Chemical Technology and Polymer Chemistry of Karlsruhe Institute of Technology, and Center for Interface Science and Catalysis, SLAC National Accelerator Laboratory (The United States). Thank you for all the supports. Finally, ANKA (Karlsruhe) is gratefully acknowledged for beam time and the EU and DANSCAT for experiment financial support for the synchrotron.

References

1. V. Subramani, S.K. Gangwal, Energ. Fuel. 22 (2008) 814.
2. J.J. Spivey, A. Egbebi, Chem. Soc. Rev. 36 (2007) 1514.
3. J. Goldemberg, Science 315 (2007) 808.
4. A. Lapidus, A. Krylova, Y. Paushkin, J. Rathouský, A. Zukal, J. Stárek, Fuel 73 (1994) 583.
5. G.W. Huber, S. Iborra, A. Corma, Chem. Rev. 106 (2006) 4044.
6. G.A. Mills, Fuel 73 (1994) 1243.
7. P.L. Spath, D.C. Dayton, A925634 (2003) .
8. I. Wender, Fuel. Process. Technol. 48 (1996) 189.
9. R.G. Herman, Catal. Today 55 (2000) 233.
10. R.G. Herman, Stud. Surf. Sci. Catal. 64 (1991) 265.
11. G.A. Olah, Catal. Lett. 93 (2004) 1.
12. G.A. Olah, Angew. Chem. Int. Ed. 44 (2005) 2636.
13. G.A. Olah, A. Goeppert, G.K.S. Prakash, Beyond oil and gas: the methanol economy, Wiley-VCH, 2006.
14. J.T. Sun, I.S. Metcalfe, M. Sahibzada, Ind. Eng. Chem. Res. 38 (1999) 3868.
15. G.W. Roberts, D.M. Brown, T.H. Hsiung, J.J. Lewnard, Ind. Eng. Chem. Res. 32 (1993) 1610.
16. H.H. Kung, Catal. Today 11 (1992) 443.
17. J.B. Hansen, in: Anonymous, AlchE Spring National Meeting, Orlando, Fl, 1990.
18. J. Bart, R. Sneeden, Catal. Today 2 (1987) 1.
19. F.Studt, F. Abild-Pedersen, Q. Wu, A.D. Jensen, B. Temel, J. Grunwaldt, J.K. Norskov, to be submitted to J. Catal.
20. E.B. Pereira, G.A. Martin, Appl. Catal. A 103 (1993) 291.
21. S. Uchiyama, Y. Ohbayashi, T. Hayasaka, N. Kawata, Appl. Catal. 42 (1988) 143.
22. S. Uchiyama, Y. Obayashi, M. Shibata, T. Uchiyama, N. Kawata, T. Konishi, Chem. Commun. (1985) 1071.
23. M. Araki, V. Ponec, J. Catal. 44 (1976) 439.
24. M.A. Fraga, E. Jordão, React. Kinet. Catal. Lett. 64 (1998) 331.
25. J.M. Christensen, P.A. Jensen, A. Jensen, Ind. Eng. Chem. Res. 50 (2011) 7949.
26. J.M. Christensen, P.A. Jensen, N.C. Schiødt, A.D. Jensen, ChemCatChem 2 (2010) 523.
27. J.M. Christensen, P.M. Mortensen, R. Trane, P.A. Jensen, A.D. Jensen, Appl. Catal. A 366 (2009) 29.
28. A.R. Denton, N.W. Ashcroft, Phys. Rev. A 43 (1991) 3161.
29. T. van Herwijnen, W.A. de Jong, J. Catal. 34 (1974) 209.
30. H.B. Zhang, G.D. Lin, Z.H. Zhou, X. Dong, T. Chen, Carbon 40 (2002) 2429.

Rui Xue
Phone: +45 4525 2993
E-mail: rxue@kt.dtu.dk
Discipline: Process Engineering and Unit Operations

Supervisors: John M. Woodley
Jørn Dalgaard Mikkelsen
Anne S. Meyer

PhD Study
Started: December 2010
To be completed: November 2013

Reactor and Process Design for Multi-enzymatic Synthesis

Abstract
Enzyme cascades (which mimic nature) using two or more enzymes sequentially for the synthesis of useful chemical compounds are attracting increasing interest as a potential means of production. Such schemes overcome many of the conventional problems integrating biocatalysis into chemical synthetic schemes, such as changes of media, temperature and pH. In this project, the synthesis of sialic acid derivatives and useful oligosaccharides will be taken as an example for the design of an enzyme cascade. Laboratory scale-down tests will be carried out to characterize the enzymatic systems. Alternative flowsheets and process schemes will be evaluated for scale up.

Introduction
In recent years, biocatalysis by means of enzymes has been providing a unique stereoselective and green tool for synthetic organic chemistry. Single enzymes, either soluble or immobilized, have been used in many different reactions [1]. Currently, the idea of using multi-enzymatic systems for industrial production of chemical compounds becomes more and more attractive [2]. Multi-enzymatic processes use two or more enzymes to catalyze reactions in a defined pathway via a cascade, a parallel, or a network configuration [3]. Such schemes overcome many of the conventional problems with integrating biocatalysis such as changes in media, temperature and pH. In synthetic organic chemistry, *in vitro* multi-enzymatic synthesis is particularly promising since enzymes may be isolated from the complex metabolic pathway of the cell, which can reduce the production of undesired by-products. In addition, one of the isolated enzymes can work in an optimal way together with other enzymes, driving the synthesis towards the target products.

The current project focuses on the production of human milk oligosaccharides (HMOs) from their basic and natural building blocks which are harvested from different food industry side streams.

Human Milk Oligosaccharides (HMOs)
Human milk oligosaccharides are complex glycans that are highly abundant in human breast milk. It is generally accepted that HMOs have prebiotic effects, selectively serving as a source of energy and nutrients for the healthy bacteria to colonize the infant intestine (Figure 1a). It is also shown that HMOs have anti-adhesive effects, mimicking the attachment sites for some pathogens and blocking their adhesion, colonization and invasion (Figure 1b). Beyond these effects, HMOs have been shown to have cell surface glycome-modifying effects in recent studies, changing the expression profiles of pathogen attachment sites on the surface of intestinal epithelial cells, and reducing the risk of infectious diseases (Figure 1b) [4].

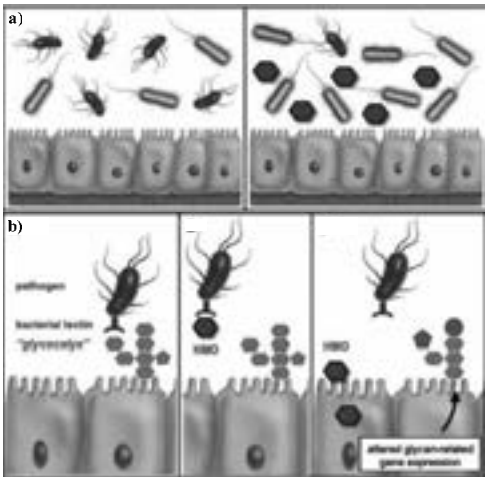

Figure 1: Prebiotics, anti-adhesive and glycome-modifying effects of HMOs, adapted from Ref. [4].

Most of the effects attributed to HMOs appear to be highly structure dependent. Many different HMO structures exist due to the possibilities of backbone lengths and decoration combinations. Among these HMOs, only a few are present in the bovine milk with low concentrations. And only trace amount of HMOs appear in the infant formula [4]. Several attempts to synthesize the HMOs have been carried out due to their rare natural origin and unique biological function. However, only low yields have been achieved.

Synthesis of Sialic Acid

Sialic acid has been attracting much interest due to its potential applications for the compounds of interest in the pharmaceutical industry [5]. It is also one of the key building blocks in the production of HMOs. The reactions involved in the production of sialic acid are shown in Figure 2. Both of the reactions are thermodynamically unfavorable in the desired direction.

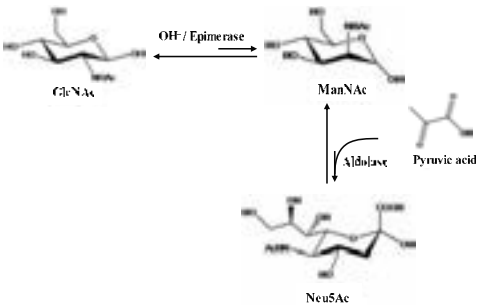

Figure 2: Scheme of the reactions involved in the synthesis of sialic acid.

Over the past few decades, considerable attempts have been made in the synthesis of sialic acid derivatives. Different processes, such as chemo-enzymatic, multi-enzymatic or whole cell catalysis, have been developed [6]. However, the availability of sialic acid nowadays is still limited.

Specific Objectives

- Devise multi-enzymatic methods for sialic acid synthesis.
- Devise laboratory scale-down tests to characterize alternative enzymatic systems.
- Evaluate alternative flowsheets and process schemes for scale-up.

Strategy

The project will be achieved by fulfilling the tasks through three stages.

Fundamental studies

This stage will focus on the characterization of different enzymes used in the system. Immobilization and/or protein engineering will be carried out to enhance the activity and the stability of enzymes.

Reactor and process design

Various reactors will be defined and evaluated for different reactions. Downstream product recovery methods will also be tested.

Process simulation

Based on the experimental data, models will be set up for different integrated process options. Alternative process schemes will be evaluated for the feasibility, economics, and sensitivity of the whole system.

Acknowledgements

The author would like to express her gratitude to the 'HMO' project and Technical University of Denmark for the financial support.

References

1. P. Clapés, W-D. Fessner, G. A. Sprenger, A. K. Samland, Curr. Opin. Chem. Biol. 14 (2010) 154-167.
2. P.A. Santacoloma, G. Sin, K.V. Gernaey, J.M. Woodley, Org. Process Res. Dev. 15 (2010) 203-212.
3. A. Cornish-Bowden, Fundamentals of Enzyme Kinetics, 3rd ed., Portland Press 2004.
4. L. Bode, Nutr. Rev. 67 (2009) S183-S191.
5. R. Schauer, Glycoconj. J. 17 (2000) 485-499.
6. F. Tao, Y. Zhang, C. Ma, P. Xu, Appl. Microbiol. Biotechnol. 87 (2010) 1281-1289.

Yuan Xu

Phone: +45 4525 2960
E-mail: xuy@kt.dtu.dk
Discipline: Process Technology and Unit Operations
Enzyme Technology
Supervisors: John M. Woodley
Mathias Nordblad
Lars Georg Kiørboe

PhD Study
Started: March 2009
To be completed: February 2012

Process Technology for Lipase-catalyzed Reactions

Abstract
A two-stage enzymatic process for producing biodiesel is reported using NS 88001 to catalyze transesterification and Novozym 435 to catalyze esterification in packed bed reactors. Both stages were conducted in a simulated series of reactors by repeatedly passing the reaction mixture through a single reactor, with separation of the by-product glycerol and water between passes in the first and second stages, respectively. The second stage brought the major components of biodiesel to 'in-spec' levels according to the European biodiesel specifications for FAME. The highest overall productivity achieved in the first stage was 2.52 kg FAEE(kg enzyme)$^{-1}$h^{-1} at a superficial velocity of 7.6 cm min^{-1}, close to the efficiency of a stirred tank reactor under similar conditions. The overall productivity of the proposed two-stage process was 1.56 kg FAEE(kg enzyme)$^{-1}$h^{-1}. Based on this process model, the challenges of scale-up have been addressed and potential continuous process options have been proposed.

Introduction
Biodiesel provides one of the possible sustainable solutions to the depletion of fossil fuels [1]. Fatty acid methyl ester (FAME) is the conventional form of biodiesel derived from vegetable oil, typically soybean oil or rapeseed oil, and methanol via alkali-catalyzed reactions [2]. An alternative process, shown in Figure 1, that is gaining more and more interest uses lipase as a catalyst and ethanol (rather than methanol) as the acyl acceptor, resulting in biodiesel in the form of fatty acid ethyl ester (FAEE). Ethanol can be obtained from agricultural products by fermentation and can thus reduce the dependence on a fossil-fuel derived alcohol substrate [3]. Although FAEE-biodiesel is not yet recognized as biodiesel, meaning that there are no specifications that apply to FAEE so far, the properties of FAEE are very similar to those of FAME. Interestingly, ethanol is actually preferred by lipase [4], which is another attractive element of this process. The lipase-catalyzed reactions have the advantages of low energy consumption, reduced formation of by-products and waste [5].

Today, the technology for lipase-catalyzed biodiesel production is not sufficiently developed technically to implement commercially, mainly due to the high cost of lipases. Nevertheless the immobilization of lipase can allow the reuse of the catalysts and simplify the downstream processing of the product. Even though the insoluble form of the immobilized lipase puts more requirements on reactor design and operation, it offers the possibility for a cost-efficient application of lipase in the biodiesel industry.

Figure 1. Lipase-catalyzed transesterification of triglycerides with ethanol

Theoretically a PBR provides a larger reacting surface area per unit volume than an STR and is often applied in continuous industrial processes [6]. Additionally, a PBR gives a lower shear stress to the catalyst particles than an STR [7]. On the other hand, the PBR has the disadvantage of a high pressure drop associated with small packing-material size or obstruction of the catalyst bed through accumulation of insoluble components from the reaction mixture.

Due to the multi-phasic nature of the reaction system, most studies on immobilized lipase-catalyzed biodiesel production in a PBR involve the use of a solvent to reduce the viscosity of the reaction mixture, and enhance the solubility of alcohol in the feedstock as well as dissolve the by-product glycerol, improving the mass transfer and allowing operation within a single liquid phase.

The most often used co-solvents in immobilized lipase- catalyzed transesterification in PBRs are n-hexane and tert-butanol [8,9,10]. Both co-solvents have shown some positive effects on increasing the reaction rate and yield. However, many co-solvents are volatile and flammable, difficult to handle in large amounts and they also pose an environmental hazard. The co-solvent must also be recovered, which will add to the cost of production and make scale-up more complicated. From this perspective an efficient solvent-free PBR system can be more promising. To solve the deactivation of lipase by the undissolved alcohol, researchers have developed a stepwise reaction scheme where alcohol is added in portions and in this way a good stability of the immobilized lipase can be obtained [11]. In addition, a further problem that needs to be addressed to achieve an efficient transesterification in a PBR with an immobilized lipase is that the catalyst can become clogged by accumulation of the glycerol by-product thus inhibiting the enzyme [12, 13]. Hama and co-workers removed the glycerol from the mixture between repeated passes through the same reactor to gain higher values of conversion and 95.3% FAME was achieved after 10 passes consuming 0.5 molar equivalent of methanol to oil in each pass at a flow velocity of 4.65 cm/min [14].

Most studies about biodiesel production focus on reaction rate and biodiesel yield in a single transesterification stage. However, few studies have been published on making biodiesel meet product specifications [14]. The commonly-used biodiesel specifications in USA and Europe (ASTMD 6751 and EN 14214), both show very low tolerance for impurities in biodiesel [15]. Meeting these specifications in a single reaction stage, without separation of glycerol and further processing (through conversion or separation), is exceptionally difficult. Therefore, in this work the conversion of glycerides to biodiesel run in two stages, with separation of glycerol in-between. This also allows the use of two different biocatalysts to improve the efficiency of the process. The first stage is carried out by the immobilized *Thermomyces lanuginosus* lipase (NS 88001), since it is good at converting triglyceride (TAG) and works even better with 96% ethanol, which is advantageous from an economical point of view. The water from the 96% ethanol does cause some hydrolysis, which needs to be handled in the second stage. However, since most natural feedstocks contain significant amounts of free fatty acids, this would be necessary even if dry ethanol was used in the first stage. The major reaction of the second stage is thus an esterification, catalyzed by immobilized *Candida antarctica* lipase B (Novozym 435). Both stages have been studied in a solvent-free PBR system with respect to the effects of flow velocity as well as ethanol and catalyst loading. The efficiency of the PBR system used in this work has also been compared to an STR system and other reported studies on PBRs.

Results and Discussion

First stage

The reaction time-courses of transesterification in a simulated series of PBRs at various velocities were compared with the performance of the same catalyst and loading relative to the oil substrate in an STR (Figure 2). The required reaction time decreased steadily as the velocity increased and finally overlapped with that in an STR at 7.8 cm/min. The flow patterns in the two reactor types under the compared conditions are still different; laminar flow in PBR (Re: 0.09-0.35) and transitional flow in STR (Re: 700-2500) through the whole reaction. The effect of flow velocity on the reaction rate was more obvious in the first step because the reaction curve is much steeper at higher velocity in the first step whereas reaction curves are almost parallel at the second and third step, as can be seen in Figure 2. It is very likely that the reaction rate is limited by external mass transfer to the greatest extent in this first step where the reaction mixture is relatively more viscous, and the potential reaction rate the highest. Thus, higher reaction rate was observed with higher flow velocity which could improve the mass transfer. At higher conversion, both the viscosity and potential enzymatic activity are reduced and the reaction rates are closer between different velocities, indicating that mass transfer is less limiting in the latter steps. It also indicates that the by-product glycerol did not have a significant effect on the mass transfer at the tested velocities even though it was observed that the accumulation of glycerol in the column varied with the flow velocity (a dye was used to visualize glycerol; photos not shown); a faster flow resulted in less accumulation. This is consistent with previous findings by Hama and coworkers, who found that although a higher flow velocity can remove more glycerol from the column; this does not greatly affect the reaction progress [14].

A yield of about 93% FAEE yield was achieved in a PBR, which was slightly lower than that in a STR (95%). This can probably be explained by some of the ethanol being lost in the glycerol which was removed between passes.

A common motivation for many studies on PBR in enzymatic biodiesel production is that it can offer an opportunity for continuous biodiesel production. The experiments in this study were conducted by repeatedly passing the reaction mixture through a single column to simulate the effects of continuous production in a series of columns. In this work we obtained 92.8% FAEE after the reaction mixture experienced 20 passes through the column at the flow velocity 7.6 cm min^{-1}, equivalent to passing the reaction mixture through 20 identical columns containing the same amount of catalyst. This corresponds to a productivity of FAEE of 0.042 g FAEE (g enzyme)$^{-1}$ min^{-1}. In the same manner the productivities from other published work on PBRs has been calculated and compared to the productivities of NS 88001 in batch STR and continuous PBR in Table 1.

Table 1 Productivity comparison

	FAEE Yield (%)	Flow velocity (cm min^{-1})	Catalyst	Productivity g FAEE (g enzyme)$^{-1}$ min^{-1}	Alcohol	Total alcohol (eq)	Solvent
STR in this work	**95**		**NS 88001**	**0.053 (reaction time 6 hours)**	**EtOH**	**1.5**	**free**
PBR in this work	**92.8**	**7.6**	**NS 88001**	**0.042**	**EtOH**	**1.5**	**free**
Hama et al., 2011	**88.9**	**9.3**	**NZ 435**	**0.023**	**MeOH**	**1.67**	**free**
Royon et al., 2007	**95**	**0.57**	**NZ435**	**0.067**	**MeOH**	**2**	**t-butanol**

The productivity of NS 88001 presented here is higher than that achieved by Hama and coworkers using NZ435 and methanol, which shows that NS 88001 has a higher specific activity for ethanolysis than NZ435 for methanolysis under the studied conditions. The efficiency of the PBR system in this work is close to that of batch STR system under similar conditions. This does not take into account the downtime that has to be considered when operating an STR in batch mode. The use of co-solvent can improve the efficiency of the PBR system further with respect to productivity, as reported by Royon and coworkers for a process using a single pass through a column packed with NZ435, employing methanol and t-butanol as the co-solvent [9]. The flow velocity in their work was much lower than those in solvent-free PBRs, indicating that the co-solvent can improve mass transfer to a great extent. However, the disadvantages of using a co-solvent limit the application of this technology as explained previously.

Second stage

A second stage is introduced to make the product in-spec and also to further improve the yield of FAEE. To convert FFA into biodiesel, absolute ethanol is used in this stage.

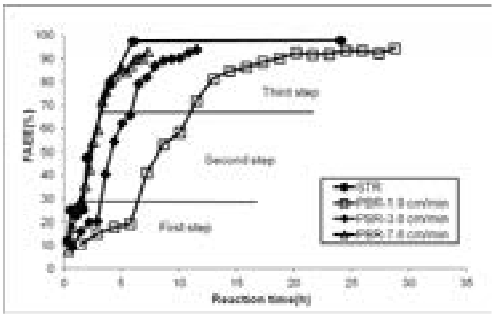

Figure 2. Comparison of transesterification in STR and PBR with different flow velocity. Each data point indicates the FAEE conversion of each pass through the catalyst bed (22 cm) with 0.5 eq 96% ethanol added at each step.

A preliminary experimental result showed that the flow velocity had little effect on the reaction rate of NZ 435 in this stage of reaction. Thus the flow velocity was fixed at 1.27 cm min^{-1} (corresponding to 1.0 mL min^{-1}) to maintain a reasonable operation time and to achieve the equilibrium in a single pass through the column.

The product from first stage, containing approx. 95% FAEE, was used as the substrate for the second stage. The residual components in the product from the first stage are relatively small molecules such as FFA, MAG and DAG, together with a small amount of TAG. NZ435 was chosen to catalyze this stage, since CALB on NZ435 has been reported to be less 1,3-positionally specific than TLL on NS 88001 [16]. The performance of NZ435 and NS 88001 applied in a simulated series of PBRs for esterification is shown in Figure 3. The process using NZ435 requires 4 steps, consuming 20 v/v % ethanol in total to successfully reduce the FFA content to 0.25 % (m/m), the upper limit for FFA content according to the EN 14214 biodiesel specification. Besides the FFA content, the other four components (FAEE, TAG, DAG and MAG) after the 4-step reaction are actually also in spec (Table 2). The system using NS 88001, on the other hand, worked more slowly on FFA and did not achieve the required concentration even after 5 steps. The concentrations of products from the two catalysts listed in Table 2 show that the use of NS 88001 resulted in lower levels of TAG and DAG than NZ435, but also leaves more FFA and MAG in the product. This is consistent with the above mentioned difference in substrate specificities of the two lipases.

After this stage, the overall productivity decreased to 0.026 g FAEE(g enzyme)$^{-1}$$min^{-1}$ which is however still comparable to 0.023 g FAME(g enzyme)$^{-1}$$min^{-1}$ obtained b y Hama and coworkers [14]. The overall efficiency of the two-stage process can most likely be improved by optimizing the two reaction stages.

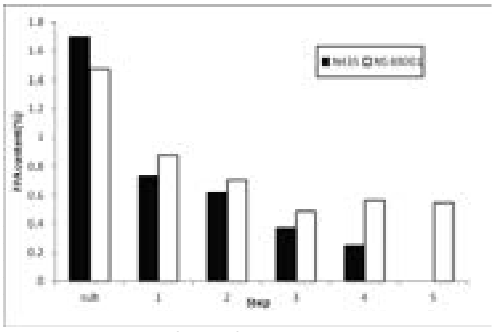

Figure 3. Results of esterification stepwise catalyzed by NZ435 and NS 88001

Table 2 Product compositions after each stage

	EN14214	After Stage 1	After Stage 2 by NZ 435	After Stage 2 by NS 88001
FAEE	**>96.5**	**95.0**	**99.4**	**99.1**
MAG	**<0.8**	**1.25**	**0.10**	**0.17**
DAG	**<0.2**	**1.41**	**0.12**	**0.10**
TAG	**<0.2**	**0.64**	**0.14**	**0.07**
FFA	**<0.25**	**1.71**	**0.24**	**0.56**

Conclusions

The two-stage enzymatic process proposed in this work is able to produce, in a packed bed reactor system, an ethanol-based biodiesel that is in-spec with respect to the main components of biodiesel (glycerieds and free fatty acids), according to the EN 14214 biodiesel specifications. The efficiency of the two-stage process is comparable to other published work on methanol-based biodiesel in solvent-free systems.

The reaction rate of the first stage (transesterification) in PBR is controlled by external mass transfer to a great extent, especially in the beginning of the reaction. Additionally, the maximum conversion can be limited by accumulation of the glycerol. Both of these problems can be addressed by applying high flow velocity, and we show here that the packed bed system can in fact achieve both final yield and reaction rates that are similar to those in the best stirred tank systems.

The second stage (esterification) fulfilled the purposes of polishing the biodiesel product and improving the biodiesel yield by converting FFA and partial glycerides to FAEE. It is necessary to conduct the reaction in multiple steps with removal of water between steps to push the reaction equilibrium sufficiently far.

Acknowledgements

The project is funded by Danish National Advanced Technology Foundation, Novozymes A/S, Emmelev A/S and DTU.

References

1. K.R. Jegannathan, S. Abang, D. Poncelet, E.S. Chan, P. Ravindra, Crit. Rev. Biotechnol. 28 (2008) 253-264.
2. C.C. Akoh, S. Chang, G. Lee, J. Shaw, J. Agr. Food Chem. 55 (2007) 8995-9005.
3. S. Al-Zuhair, Biofuel. Bioprod. Biorefin. 1 (2007) 57-66.
4. V. Kumari, S. Shah, M.N. Gupta, Energ. Fuel. 21 (2007) 368-372.
5. P.M. Nielsen, J. Brask, L. Fjerbæk, Eur. J. Lipid Sci. Technol. 110 (2008) 692.
6. V.M. Balcáo, A.L. Paiva, F.X. Malcata, Enzym. Microbiol. Technol. 18 (1996) 392-416.
7. S.F.A. Halim, A.H. Kamaruddin, W.J.N. Fernando, Bioresour. Technol. 100 (2009) 710-716.
8. V. Dossat, D. Combes, A. Marty. Enzym. Microbiol. Technol. 25 (1999) 194-200.
9. D. Royon, M. Daz, G. Ellenrieder, S. Locatelli Bioresour. Technol. 98 (2007) 648-653.
10. J.-F. Shaw, S.-W. Chang, S.-C. Lin, T.-T. Wu, H.-Y. Ju, C.C. Akoh, R.-H. Chang, C.-J. Shieh, Energ. Fuel. 22 (2008) 840-844.
11. Y. Watanabe, Y. Shimada, A. Sugihara, H. Noda, H. Fukuda, Y. Tominaga, J. Am. Oil Chem. Soc. 77 (2000) 355-360.
12. K. Belafi-Bako, F. Kovacs, L. Gubicza, J. Hancsok, Biocatal. Biotransform. 20 (2002) 437–439.
13. Y. Xu, M. Nordblad, P.M. Nielsen, J. Brask, J.M. Woodley, J. Mol. Catal. B: Enzym. 72 (2011) 213–219.
14. S. Hama, S. Tamalampudi, A. Yoshida, N. Tamadani, N. Kuratani, H. Noda, H. Fukuda., A. Kondo, Biochem. Eng. J. 55 (2011) 66-71.
15. G. Knothe, J. Am. Oil Chem. Soc. 83 (2006) 823-833.
16. Du, W., Xu, Y.-Y., Liu, D.-H., Li, Z.-B, J. Mol. Catal. B: Enzym. 37 (2005) 68–71.

Hao Yuan
Phone: +45 4525 2864
E-mail: hy@kt.dtu.dk
Discipline: Reaction and Transport Engineering

Supervisors: Alexander A. Shapiro
Erling H. Stenby

PhD Study
Started: Oct.2009
To be completed: Oct 2012

ParPor: Stochastic Modeling of Particle-Pore Population Balance

Abstract
Particle transport and retention in porous media is of great importance for a number of environmental and engineering applications. Tremendous efforts have been devoted to understanding the transport and fate of colloids in porous media. The purpose of this study is to first overview the recent advances and the limitations in the colloid filtration theory, including the effects of non-DLVO interactions, surface blocking, surface charge heterogeneity, physical heterogeneity, and the migration on colloid filtration processes. Our efforts are then dedicated to developing more advanced mathematical models that can incorporate various effects and predict more accurately the behaviors of the particles in pores. Some of our models are implemented in the form of simulator software for practical use.

Introduction
Colloids are the particles dispersed in liquids (in most applications, water or water solutions) with the sizes in between dissolved macromolecules and suspended particles that resist rapid sedimentation. The typical size of colloid particles usually ranges from 10 nm to 10 μm [1]. There is a considerable and ongoing effort aimed at understanding and predicting the transport, the deposition and the release of colloids in both synthetic (model) and natural porous media. The fate and transport of colloids in porous media is of a great concern for the following reasons, among other: (i) The migration of colloids may facilitate the transport of low-solubility contaminants; (ii) The spread of pathogenic microbes during waste water reclamation and aquifer recharge poses a risk to public health; (iii) Deposition and migration of colloids cause permeability damage, which subsequently leads to injectivity decline and productivity decline; (iv) Injection of the microbes producing surfactants may enhance oil recovery[2].
The fundamental filtration theory has been focused on the transport and fate of colloid at different scales: the interface scale, the collector (median grain) scale, and the pore scale, as seen in Figure 1. At the interface scale, the interfacial energy of a particle at the solid-water interface (SWI), the air-water interface (AWI), and the colloid-colloid interface can be quantified. Such a technique is used to predict attachment conditions and colloid stability. At the collector scale, the flow field of water around a collector or an air bubble can be calculated. The probability of flowing particles being in contact with the collector can be quantified. At the pore scale, the fate of colloids is studied in the presence of multiple grains and pores (grain-grain contacts) or solid-water-air triple points. The favorable sites of attachment, straining and size exclusion can be identified in different pore geometries [3].

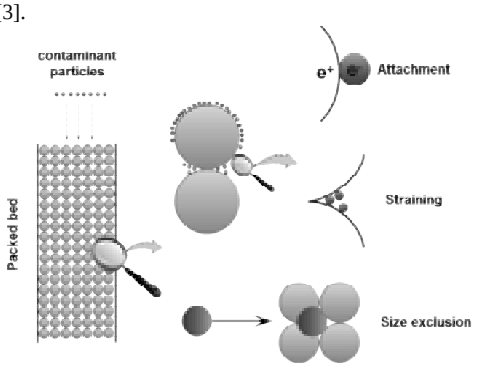

Figure 1: Filtration mechanisms in a packed filter

The goal of the fundamental filtration theory at the interface, the collector and the pore scales is to achieve an analytical deposition model for predicting the single collector removal efficiency. It is a parameter reflecting the colloid removal efficiency by a single collector under known physical and chemical conditions.

There is a growing body of studies suggesting that the classical CFT fails to fully describe a number of practically important processes or phenomena, such as filtration under unfavorable attachment conditions and filtration in stochastically heterogeneous porous media [2]. The discrepancies between the model predictions and experimental observations are as follows. Under unfavorable attachment conditions, the classical CFT and the DLVO theory predict the collision efficiencies several orders of magnitude smaller than those observed experimentally. Experimental collision efficiencies and critical deposition are insensitive to particle sizes. Hyperexponential or non-monotonic deposition profiles are observed rather than the exponential deposition decay predicted by the classical CFT. Long tails are observed in the breakthrough curves. In the porous media with irregular-shaped median grains, hyperexponential deposition is also often observed. In heterogeneous porous media, both early arrival and delay of particles are observed in the breakthrough curves[2, 4].

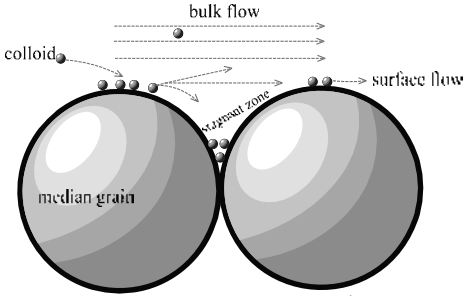

Figure 2: Release and migration of surface attached particles

Large research efforts were devoted to explaining the above observed discrepancies. Under unfavorable attachment conditions, underestimation of the collision efficiency, insensitivity to particle sizes, and hyperexponential deposition were mainly attributed to the deposition via the secondary energy minimum and heterogeneity of the surface charges. Apart from the surface charge heterogeneity, the deposition hyperexponentiality has also been attributed to the effects of straining and non-Fickian transport due to physical heterogeneity of porous media. The non-Fickian transport was also claimed to be responsible for the early arrival and delay of particles. The algebraic-decaying long tails in the breakthrough curves after the end of injection were either attributed to the migration of captured particles or to the physical non-equilibrium between the mobile and the immobile regions. Rarely observed non-monotonic deposition profiles were either attributed to the migration of surface-attached particles via weak association or to the detachment of large aggregates, as seen in Figure 2 [4, 5].

The purpose of this article is to overview the recent work carried out in this project. Multiple journal articles and two book chapters have been produced out of the work. A simulator for predicting injectivity decline during waterflooding was developed for DONG energy.

Non-Fickian transport

Non-Fickian transport of particles in pores is usually attributed to the physical heterogeneity of the porous media. It gives rise to the delay and early arrival of particles in the breakthrough curves and hyperexponential deposition depicted as a curved profile in a logarithm scale. A sample calculation with the elliptic equation for the non-Fickian transport is shown in Figure 1. The non-Fickian particle distribution is asymmetrical while the Fickian profile exhibits a normal-distribution-type curve.

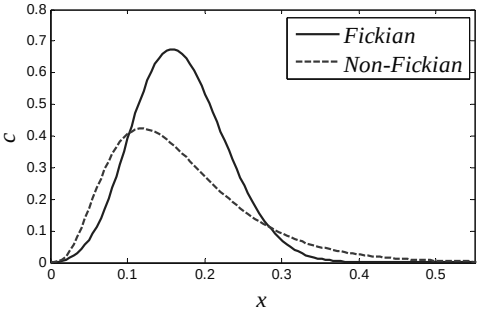

Figure 3: Sample calculations of particle distributions in non-Fickian and Fickian transport scenarios [4]

Unfavorable attachment conditions

Under unfavorable attachment conditions, the deposition profiles are usually hyperexponential. The collision efficiency is often underestimated. Under such conditions, there is an energy barrier that the particles must overcome to be attached to the pore surfaces. These effects can be captured by including the distribution of filtration coefficients, representing the heterogeneity of particle surface charges and energy minima. The interaction energy barrier can be illustrated in Figure 3. The particle colliding with the porous medium may be captured via the primary or the secondary energy minima

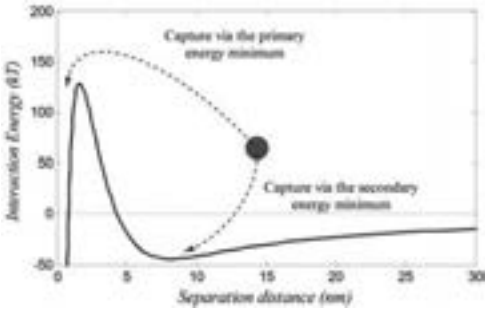

Figure 4: Illustration of the energy barrier under unfavorable attachment conditions [2]

With distributed filtration coefficients the advection-dispersion equation can be used to produce the hyperexponential deposition as shown below. The new method excels the conventional model in matching the exponential deposition profiles. The comparison result is shown in Figure 4. Details can be found in Ref. [5].

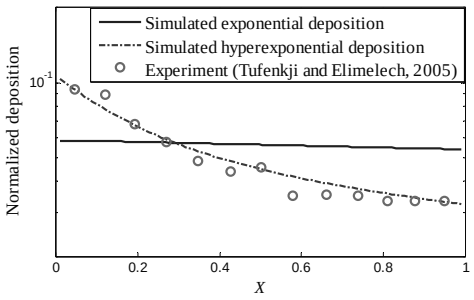

Figure 5: Simulated exponential and hyperexponential deposition [5] and experimental deposition [6].

Non-DLVO interactions

The DLVO theory has been widely applied to predict colloid-collector interactions and colloidal stability for the last decades. Nevertheless, it failed to match the experimental observations in many cases. The deviations, often referred to as the non-DLVO effects, were attributed to the following reasons: hydrogen bonding and hydrophobic effects, hydration pressure, non-charge transfer Lewis acid base interactions, and steric forces. The hydration shells can be illustrated in the figure below

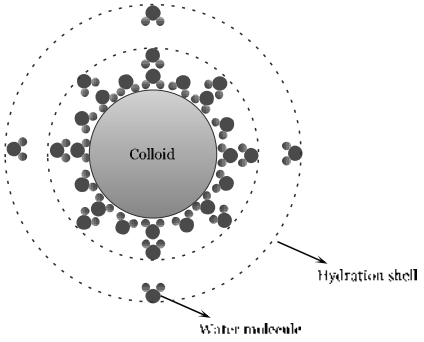

Figure 6: Illustration of hydration shells [2]

Torque balance

The balance of the hydrodynamic torque, the lifting torque, the resisting adhesive torque and the torque of gravity determines whether the colloid particles attaching to the pore walls will be immobilized and re-entrained into the carrying fluid, as seen in Figure 2 and Figure 7. According to such a torque balance analysis, the maximum amount of attached particles can be calculated, namely that the excess amount of particles will be dragged away from the pore walls. The released particles may be recaptured via straining at thin pore throats. Such effects will cause severe permeability damage and give rise to injectivity decline of injection wells in oil reservoirs.

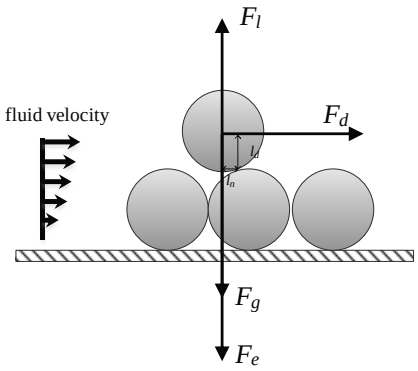

Figure 7: Torque balance analysis on the surface-attached particles

Formation damage

The accumulation of the deposited particles eventually will close the open pores and block the flow paths. It causes severe permeability damage and is regarded as a disaster of injection wells in the oil reservoirs. A comprehensive model is developed for simulating and predicting injectivity decline due to deep bed filtration and external cake filtration, as seen in Figure. The model considers the distribution of residence time of particles in porous media as well as the distribution of filtration coefficients. The first distribution is responsible for the median heterogeneity while the second is for the particle population heterogeneity.

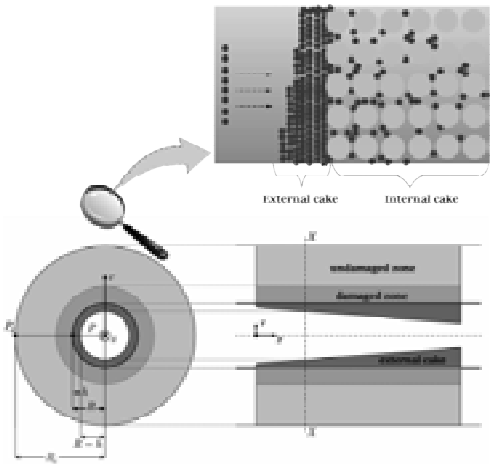

Figure 8: Illustration of internal and external filter cakes in injection wells

A simulator software for predicting injectivity decline in injection wells is developed. The program is implemented in FORTRAN and its graphical user interface is developed in Microsoft VB.Net framework. The graphical user interface is shown in Figure 9.

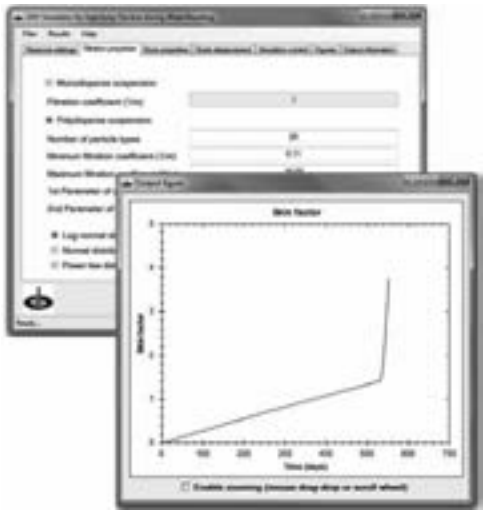

Figure 9: Illustration graphical user interface of SNY 1.0 for predicting injectivity decline

Fines migration and fluid diversion

The effects of fines migration induced by injection of low salinity water are incorporated into the upscaling model for waterflooding in a layer cake reservoir with good communication between the layers. Mobilization and re-capturing of the reservoir fines may give rise to reduction of the permeability in water swept zones, which subsequently leads to the diversion of water flow from the initially more permeable layers to the less permeable ones, as seen in Figure 10. As a result, the displacement is more even, the water cut at the producer is decreased, and the oil recovery is increased. On the other hand, more energy for the pressure drop is required to maintain a constant flow rate. The positive effects on the oil recovery and the negative on energy consumption are to be considered in field applications.

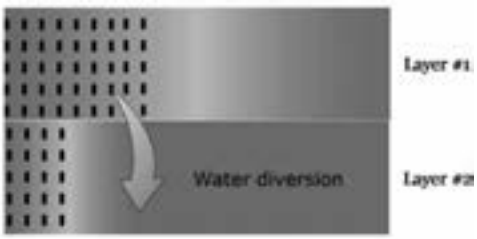

Figure 10: Illustration of large scale fluid diversion in communicating layer-cake reservoirs

Acknowledgement

This project is funded by the Danish Council for Independent Research, Technology and Production Sciences (FTP), which is acknowledged for financial support. We would like to give special thanks to DONG Energy for financial support on developing simulator SNY 1.0.

References

1. M. Elimelech, J. Gregory, R. Williams, X. Jia, Particle Deposition & Aggregation: Measurement, Modelling and Simulation (Colloid & surface engineering), Butterworth-Heinemann, 1998.
2. H. Yuan, A.A. Shapiro, in: Paresh Ray (Eds.) Colloids: Classification, Properties and Applications, NOVA Science publisher, New York, 2012
3. S. Torkzaban, S.A. Bradford, M.T. van Genuchten, S.L. Walker, J. Contam. Hydrol. 96 (2008) 113-127.
4. A.A. Shapiro, H. Yuan, in: Abram Skogseid Vicente Fasano (Eds.), Statistical Mechanics and Random Walks: Principles, Processes and Applications, NOVA Science publisher, New York, 2011, p.1
5. H. Yuan, A.A. Shapiro, Chem. Eng. J. 162 (2010) 974-988.
6. N. Tufenkji, M. Elimelech, Langmuir, 21 (2005) 841-852.

List of Publications

1. C. Wang, H. Yuan, Y. Lv, J. Li, W. Qu, Journal of Daqing Petroleum Institute 32 (2008) 13-15.
2. Y. Gong, H. Yuan, Y. Feng, W. Liu, B. Huang, International Conference on Information and Management Sciences, California Polytechnic State University, Urumqi China, 2008, pp. 696-699.
3. Z. He, H. Yuan, J.A. Glasscock, C. Chatzichristodoulou, J.W. Phair, A. Kaiser, S. Ramousse, Acta Materialia. 58 (2010) 3860-3866.
4. H. Yuan, A.A. Shapiro, Chem. Eng. J. 162 (2010) 974-988.
5. H. Yuan, G. Sin, Chem. Eng. J. 168 (2011) 635-648.
6. H. Yuan, A.A. Shapiro, Chem. Eng. J. 166 (2011) 105-115.
7. H. Yuan, A.A. Shapiro, J. Petrol. Sci. Eng. 78 (2011) 618-626.
8. A.A. Shapiro, H. Yuan, in: Abram Skogseid Vicente Fasano (Eds.), Statistical Mechanics and Random Walks: Principles, Processes and Applications, NOVA Science publisher, New York, 2011, p.1
9. H. Yuan, A.A. Shapiro, in: Paresh Ray (Eds.) Colloids: Classification, Properties and Applications, NOVA Science publisher, New York, 2012
10. H. Yuan, X. Zhang, A.A. Shapiro, E.H. Stenby, Petrol. Sci. Tech. (2012) (Accepted)

Nor Alafiza Yunus
Phone: +45 4525 2812
E-mail: noy@kt.dtu.dk
Discipline: Systems Engineering

Supervisors: Rafiqul Gani
John M. Woodley
Krist V. Gernaey

PhD Study
Started: July 2010
To be completed: July 2013

An Integrated Methodology for Design of Tailor-Made Blended Products

Abstract
A computer-aided methodology has been developed for the design of blended (mixture) products. Through this methodology, it is possible to identify the most suitable chemicals for blending, and "tailor" the blend according to specified product needs. The methodology has three stages: 1) product design, 2) process identification, and 3) experimental verification. The principle problem, which is the product design stage is divided into four sub-problems and solved with a decomposition-based approach. In stage two, the ability to produce the chemicals used as building blocks in the blends is analyzed. Finally, experimental work (or detailed model-based verification) is conducted in stage three to validate the selected blend candidates. In this study, the product design stage is highlighted through a case study of gasoline blends with bio-based chemicals. The objective of this study is to identify blended gasoline products that match (or improve) the performance of the conventional gasoline.

Introduction
An important issue for the production of many chemical-based products is related to the future supply of essential raw materials. Currently, many of these products are derived from fossil-based resources and from a sustainability point of view, other (renewable) alternatives need to be considered. In order to achieve this, new products need to be developed by blending conventional materials with bio-based chemicals. A bio-based chemical is defined as one that has the potential to be produced from renewable resources such as biomass or the glycerol by-product from biodiesel production. Blending could offer several advantages, such as, reducing the fossil-based resource consumption, decreasing pollution and increasing product safety. In addition, the product attributes can potentially also be improved by blending. However, the product performance may decline when other chemicals are added. In order to maintain/improve the blended product performance, it is necessary to identify the best product blend with the most appropriate chemicals.

As the number of alternatives can be very large, an experimental search to find the optimal blend is almost impossible. Therefore, a computer-aided methodology to design blended products has been developed. The objective is to quickly and reliably reduce the search space and to identify a few potential candidates for the optimal blended product, which can then be verified (experimentally or with detailed modelling). In this paper, the product design issues are highlighted by considering exclusively chemicals from known bio-based resources and therefore, the second stage of process identification is not necessary.

Blend Design Methodology
Figure 1 illustrates the computer-aided blend design methodology for tailor-made chemical blends. The methodology is divided into three stages: 1) Product design stage, where a model-based technique is applied to formulate the chemical blends. 2) Process identification stage; here the feasible processes to produce the chemicals that are to be used as building blocks in the blends are investigated and identified, and 3) the experimental verification stage, where the chemical blends are verified experimentally.

The product design stage has four key tasks [1]. First, the design problem is defined where the product needs are identified, translated into target properties and given target values. Secondly, target property models are retrieved from a property model library developed specifically for this methodology. Thirdly, a mixture/blend design algorithm is applied to obtain the mixtures/blends that match the set of constraints (design targets). This algorithm employs a decomposition based solution strategy [2], where, in each successive step, the search space is reduced by screening out alternatives by considering property constraints according to a pre-determined hierarchy. The result is a set of blends that

match the constraints, the composition of the chemicals present in the blend, values of the target properties and information about their miscibility. Finally, the mixture target property values are verified by means of rigorous models for the properties and mixtures.

The second stage is only needed if the chemicals used as building blocks in the blends are unknown. However, if the availability of the processes to produce bio-based chemicals is *a priori* identified (e.g. from patents, journals and articles), this stage is not necessary. In the last stage, experimental work will be performed as required, in order to validate the formulated blend/ mixture products.

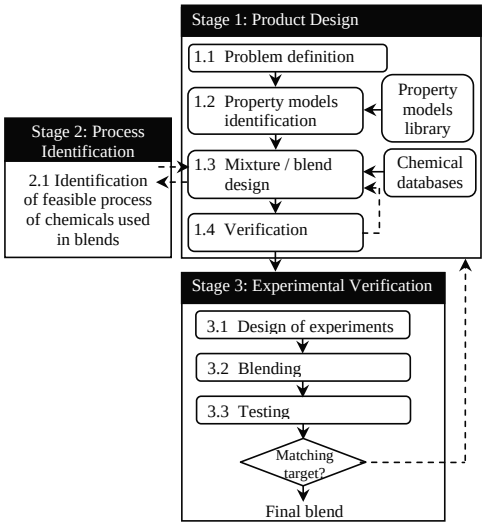

Figure1: Integrated methodology of blended product design

Case study of Gasoline Blends

Task 1.1: Problem Definition

For gasoline, the following two issues need to be considered among others: the first is related to the security (or availability) of crude oil supply, and the second is related to the presence of toxic constituents in gasoline that are harmful to the environment as well as to humans. As an alternative, gasoline blended with chemicals derived from renewable sources has the potential to address both these issues. Partial replacement by bio-based chemicals can reduce the crude oil consumption and the amount of released toxic chemicals. The new formulation of gasoline blends should have good fuel performance, where it can flow continuously from the fuel tank to the combustion chamber, can be burned and can run the engine efficiently. It has to have a suitable flammability limit to make sure it only burns at a certain temperature, and low toxicity for reasons of safety. In addition, the gasoline blends must be stable, meaning that the blends do not evaporate easily; do not oxidize to form unwanted by-products, such as gums, sludge and deposits during storage; and must not split into two liquid phases. Furthermore, environmental regulations need to be considered when designing the gasoline blends with oxygenated compounds.

The objective of this case study is to design gasoline blends that are suitable for a car (spark-ignition type) engine and used in a warm climate with average ambient temperature of 27^{o}C. Gasoline is chosen as the main ingredient in the blends. The bio-based chemicals used as building blocks in the blend formulation have a low carbon number, C2 to C5 alcohols, ethers, ketones, acids and furan derivatives. Some of them are listed in Table 1 with their properties together with gasoline and it's properties. The blends may consist of two or more chemicals (in addition to the gasoline chemicals) to form either binary or multi-component mixtures of additives.

The first task is to translate the performance criteria into a set of properties with target values. The following properties are considered; consistency of fuel flow is related to viscosity and density; burning ability and evaporation rate are controlled by Reid vapor pressure (RVP); smooth engine operation is related to the octane rating and heating value; flammability limit is controlled by the flash point; toxicity is quantified by the lethal concentration (LC_{50}) parameter; stability of blends can be evaluated from Gibbs energy of mixing (ΔG^{mix}); and the regulations and emissions are related to oxygen content (weight percent).

Table 1 Property of gasoline and selected blending agents

Property	Unit	G	E	A	BE	THF	MeTHF	DME
C : H	Wt%	86 :14						
MW	g/mol	103	46	58	72	102	86	46
Density at 15^{o}C	kg/m^{3}	726	794	798	810	1056	871	672
Higher heating value	kJ/mol	4838	1368	1804	2444	2982	3145	1460
Research Octane Number (RON)		92	116	-	-	-	-	-
Dynamic viscosity at 15^{o}C	cP	0.51	1.31	0.34	0.44	7.19	0.46	0.12
Vapor pressure at 38^{o}C	kPa	55.16	16.04	51.85	21.83	0.30	13.6	843
Flash point	K	230	286	255	267	357	264	234
Lethal concentration ($-\log LC_{50}$)	Mol/L	3.33	0.52	0.85	1.35	1.49	1.87	1.00

Lethal Concentration (LC); Gasoline(G); Ethanol (E); Acetone (A); 2-Butanone(BE);Tetrahydrofurfuryl Alcohol (THF); Furan, tetrahydro-2-methyl- (MeTHF), Dimethyl-ether (DME)

Meanwhile, oxidation can be avoided by selecting only saturated bio-based chemicals and by avoiding unsaturated chemicals, such as olefins. These specific needs are translated into target properties (in Table 2), and target values for each of the properties as shown in Table 3.

Table 2 The needs of the fuel blend and translated target properties

Product needs:	Target properties:
1. Consistency of flow in engine	Dynamic viscosity (μ), density (ρ)
2. The ability to burn	Reid vapor pressure(RVP)
3. Engine efficiency	Octane rating (RON), Heating value,(HHV)
4. Flammability	Flash point (T_f)
5. Toxicity	Lethal concentration(LC)
6. Stability	Gibbs energy of mixing (ΔG_{mix})
7. Blend regulatory issues and emissions	Oxygen content (Wt_{O2})
8. Low oxidation rate	Choice of the blending agents

Table 3 Blend target values of each property [3, 4]

Symbol:	UoM:	LB:	UB:
μ	cP	0.3	0.6
$\rho(V)$	L/kmol	129	139
RVP	kPa	45	60
RON	-	92	100
HHV	MJ/kg	35	+∞
T_f	K	−∞	300
$-logLC_{50}$	mol/L	−∞	3.08
ΔG_{mix}	-	−∞	0
Wt_{O2}	-	2	20

UoM(Unit of measurement); LB(Lower bound); UB(Upper bound)

Problem formulation

The gasoline blend problem is formulated as a Mixed Integer Non-Linear Programming (MINLP) problem, where the fuel composition is to be optimised, subject to product attributes (target properties) and process specifications. Considering the multiple types of constraint equations, the general gasoline blend problem is formulated as:

$$max\ f_{obj}(x,y)$$

Subject to

Mixture constraints: $g_1(x,y) \le 0$

Target property constraints: $g_2(x,y,\phi) \le L/UB$

Process model constraints: $g_3(x) = 0$

$$x \in \{x | x \in R^n, 0 \le x \le 1\}$$

$$y \in \{0,1\}$$

where f_{obj} is the objective function to minimize the gasoline consumption; y is a binary integer variable, which is allied to the identities of the chemicals; x is a continuous variable, which is related to the mixture compositions; while ϕ corresponds to pure properties; L/UB is the lower and/or upper limit set in Task 1.1 (see Table 1); g_1 and g_2 are the mixture and target property constraints, respectively, while the process model constraint is represented by g_3.

Task 1.2: Property Model Identification

The blend miscibility is evaluated using excess Gibbs energy of mixing (see Eq.1). In order to have a stable single-phase mixture, ΔG^{mix} and its first and second derivatives must be continuous functions of x_i and the second derivative (Eq.2) must be positive at a given pressure and temperature. The stability algorithm is used for the mixture stability calculation [5]. Six of the target property constraints ($\mu, \rho(V), RON, HHV, -logLC_{50}$ and Wt_{O2}) can be evaluated from linear mixing rules shown by Eq. 3, where TP is the target property, x_i represents mass or volume percent of compound *i*, and ϕ_i represents the properties of a pure compound, *i*. Meanwhile, the RVP and the flash point of the blends must satisfy Eq. 4 and Eq. 5 respectively [6]. Besides that, a pure property model is essential for mixture property estimation. It is represented by Eq.6, where θ represents molecular structure parameters.

$$\frac{\Delta G^{mix}}{RT} = \sum x_i \ln x_i + \frac{G^E}{RT} \quad (1), \qquad \frac{d^2 G^{mix}}{dx_i^2} > 0 \quad (2),$$

$$TP = \sum x_i \phi_i \quad (3), \qquad \sum \frac{x_i \gamma_i P_i^{sat}(T)}{RVP_B} = 1 \quad (4),$$

$$\sum \frac{x_i \gamma_i P_i^{sat}}{P_{i,fp}^{sat}} = 1 \quad (5), \qquad \phi_i = f(y,\theta) \quad (6)$$

Task 1.3: Mixture/Blend Design

The general blending problem formulation is substituted with all the target property models and constraints as follows:

$$max\ f_{obj}(x,y)$$

Subject to:

Mixture constraints: Eq. 1 and Eq. 2

Target property constraints: Eq. 3 - 6

Process model constraints: $\sum x_i - 1 = 0$

$$x \in \{x | x \in R^n, 0 \le x \le 1\}$$

$$y \in \{0,1\}$$

This problem is solved using a decomposition-based method, where the problem is divided into four sub-problems as illustrated in Figure 2. For each sub-problem, the number of alternatives is reduced significantly, and finally the blend is optimized to obtain the most promising candidates. The first sub-problem is for pre-selection of blending agents by limiting their pure properties to an upper lower and limit.

The second sub-problem is to screen only miscible mixtures using the stability algorithm [5]. Subsequently, the number of stable mixtures is further reduced by considering the linear target properties. In this sub-problem, a set of linear target properties is calculated simultaneously, and the blends that match the target values are found. Afterwards, the non-linear constraints are considered in the last sub-problem. At this point, the number of alternatives has been significantly reduced, and it is easier to manage the complexity of the design problem with the small number of remaining alternatives. Finally, the blend formulations are optimized according to the objective function, which is

to maximize the contribution of blending agents in the blends.

Results of the Decomposition Method
From 18 blending agents,188,300 alternatives of binary and ternary mixtures were generated with various compositions.

Sub-problem 1: Seven chemicals were excluded due to their flash point (greater than 316K), viscosity (greater than 35 cP) and vapor pressure, for example, DME (see its properties in Table 1). Therefore, the number of remaining alternatives is 68,000.

Sub-problem 2: The miscibility test found five ternary mixtures with a multiphase region. They were excluded, and 61,800 alternatives remained.

Sub-problem 3: Only 8000 alternatives remained after screening the target properties of the blends obtained from sub-problem 2 using the linear mixing rules. Dynamic viscosity and lethal concentration are the influencing factors that determined the blend formulations. Nevertheless, the RON value cannot be predicted for all blends because the RON of the pure species is not available. So these compounds were also removed.

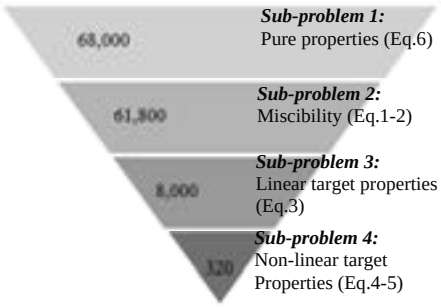

Figure 2: Number of alternatives reduced with decomposition method

Sub-problem 4: A total of 320 alternatives was left after considering the non-linear target properties, where RVP was the determining factor.

Finally, the blend problem is optimized to obtain the top five formulations that have the lowest amount of gasoline. The results are summarized in Table 4.

Task 1.4: Verification
The shortlisted candidates in Table 4 and their estimated values need further verification especially for the properties estimated by simple mixing rules. Rigorous models are needed for this task, which will be developed and evaluated in future work.

Table 4 Mixture composition and their estimated property values

Mix	Composition (vol%)			f_{obj}
1	G (67)	A(13)	MeTHF(20)	67
2	G (69)	THF(11)	MeTHF(20)	69
3	G (72)	A(10)	BE(18)	72
4	G (75)	BE(13)	MeTHF(12)	75
5	G (77)	E(12)	MeTHF(11)	77

Estimated property values

Mix	HHV	Wt_{O_2}	RVP	μ	LC_{50}	RON
1	41	7.2	46	0.48	2.7	-
2	41	7.8	46	0.47	2.7	-
3	40	7.3	49	0.48	2.7	-
4	43	5.5	45	0.50	2.9	-
5	42	6.7	45	0.57	2.8	96

Conclusions
An integrated methodology for design of tailor-made blended products has been proposed, and the first stage of product design has been highlighted with a case study of a gasoline blend. A decomposition-based method has been applied in solving the blending problem, which is a good approach for reducing a large number of alternatives and a large search space. Current work considers only the product design using a model-based method. Further verification is needed to confirm the blended products and also the methodology. Future work will furthermore test and validate the methodology for other types of blended products to extend the capability of the developed methodology.

References

1. J.A. Klein, D.T. Wu, R. Gani, Comput. Chem. Eng. 16 (1992) S229-S236.
2. A.T. Karunanithi, L.E.K. Achenie, R. Gani, Ind. Eng. Chem. Res. 44 (13) (2005) 4785-4797.
3. R. Van Basshuysen, F. Schäfer, (2004). Internal Combustion Engine Handbook-Basics, Components, Systems, and Perspectives. USA, Society of Automotive Engineers, Inc.
4. W.E. Forsythe, (2003). Smithsonian Physical Tables. New York, Knovel. p 322
5. E. Conte, R. Gani, K.M. Ng, AIChE J. 57 (9) (2011) 2431-2449.
6. H. Liaw, C. Tang, J. Lai, Combust. Flame 138 (4) (2004) 308-319.

Adeel Zahid
Phone: +45 4525 2876
E-mail: adz@kt.dtu.dk
Discipline: Engineering Thermodynamics

Supervisors: Alexander Shapiro
Erling H Stenby
Wei Yan

PhD Study
Started: January 2009
To be completed: December 2011

Smart Waterflooding (High Sal/Low Sal) in Carbonate Reservoirs

Abstract
Over the last decade, it is experimentally documented that seawater with potential determining ions, SO_4^{2-}, Ca^{2+} and Mg^{2+}, can significantly improve the oil recovery in chalk reservoirs at high temperature. We have conducted flooding experiments both with outcrop chalk and reservoir chalk core plugs at different conditions to understand the mechanism of this waterflooding process. In addition to this, crude oil/seawater ions interaction at different temperatures, pressures and sulfate ion concentrations is investigated. We have also experimentally explored the oil recovery potential of low salinity water flooding for carbonate rocks.

Introduction
Waterflooding is a cheap secondary oil recovery process and is by far the most widely applied method for improving the oil recovery. Historically, it was practiced for pressure maintenance after primary depletion. Traditionally, a little consideration has been given in reservoir engineering practice on the role of chemistry of injection water on water displacement efficiency or its impact on oil recovery. However, over the last decade extensive studies have shown that composition of injected water can affect crude oil/brine/rock interactions in a favorable way to improve oil recovery [1,2]. Seawater flooding in high temperature chalk reservoirs and low salinity waterflooding in sandstone reservoirs are two examples of smart waterflooding. But most recently, low salinity waterflooding has also been reported for carbonates [3].

Several laboratory experimental studies of water injection were carried out by Austad and co-workers, who used different core plugs and studied recovery as a function of brine composition and temperature [1]. It was observed that SO_4^{2-}, Ca^{2+} and Mg^{2+} are the potential determining ions for improving the oil recovery in chalk reservoirs at high temperatures (above 90 °C). It was also reported that these ions must act together, because neither of them alone had an effect on spontaneous imbibition. Based on these experimental results, wettability alteration was proposed to be a key reason for the improvement of oil recovery. A schematic model of the chemical mechanism for wettability modification was suggested. According to this model, the ions adsorb to the rock surface, which changes the surface charge so that the adsorbed crude oil may be removed from the rock. Webb et al. [4] presented a comparative study of the oil recovery from a North Sea carbonate core sample with simulated SO_4^{2-} free brine and with seawater containing SO_4^{2-} under reservoir conditions. The imbibition tests were performed with live oil. It was concluded that the wettability alteration of the carbonate rock with the SO_4^{2-} ion is responsible for the saturation changes. Fjelde et al. [5] carried out spontaneous imbibition experiments using seawater and formation brine with core plugs from two fractured chalk fields at reservoir temperature. Only a small increase in oil recovery was observed with the seawater as compared to the formation brine (containing no SO_4^{2-}) for reservoir core plugs as compared to Stevns Klint outcrop chalk core plugs. Karoussi et al. [6] investigated extreme cases of waterflooding of Stevns Klint core plugs with ion-free water and water containing just Mg^{2+} or SO_4^{2-} ions. Water saturated with Mg^{2+} ions alone showed the highest oil recovery in the spontaneous imbibition experiments

In spite of a large body of experimental work, many questions still remain unclear. A conclusion drawn about wettability alteration as a main mechanism for improving the oil recovery is indirect (increased spontaneous imbibition). This is by no means the proof. Most of the reported results are based only on spontaneous imbibition using Stevens Klint outcrop chalk core plugs. In addition to this, crude oil/brine interactions studies were also ignored in above reported studies. Without understanding why and how the recovery method works, its application on the industrial

scale is doubtful, since it is not clear under what conditions it will lead to additional recovery.

Specific Objectives

The Objectives of this PhD project are

- Reported observed increment in oil recovery caused only by the wettability alteration or there are some other reasons also?
- If some other factors are also involved then what could they be? (crude oil/brine interactions study)
- Will smart waterflooding improve the oil recovery in all type of chalk reservoirs? (Identification of conditions under which little or no recovery)
- Investigating the potential of low salinity waterflooding in carbonate reservoirs.

Experiments

Experimental section is divided into four parts to address four objective mentioned above. In the first part, we addressed a question: Observed increment in oil recovery caused only by the wettability alteration or there are some other reasons also? Most of the previous work has been made on the basis of using core plugs aged in crude oil. Our study is based on utilizing completely water wet Stevens Klint cores without being aged in crude oil, just saturated with crude oil under vacuum. This would exclude alteration of wettability as a positive factor. Brine without sulfate (SW0S) is considered as the base injected fluid. Waterflooding experiments were carried out with SW0S, seawater (SW) and seawater with three times sulfate (SW3S).

Our recent study [see publication 1] proposed that the decrease in viscosity and formation of an emulsion phase could also be a possible reason for the observed increase in oil recovery. It was found that the two crude oils exhibited the different phase behavior and viscosity variation in contact with the same brine solutions. In the second part, we studied further the complex crude oil/brine interactions. We investigated the effects of compositional differences of crude oils and also studied the heptane/seawater interactions under different temperatures, pressures and sulfate ion concentrations

In the third part, flooding tests with North Sea chalk core plug were carried out. Two flooding schemes were used, flooding sequence 1 with core plug without being aged in crude oil and flooding sequence 2 is with core plug being aged for 3 days in the crude oil. Different injection brine solutions were used and effluent is collected using fractional collector at different time intervals and analyzed for potential determining ions (SO_4^{2-}, Ca^{2+} and Mg^{2+}) in most of the flooding tests.

In the last part of the experiments, we investigated the oil recovery potential of low salinity water flooding for Middle East carbonate and Aalborg chalk core plugs. The flooding experiments were carried out initially with the seawater (SSW), and afterwards the contribution to oil recovery was evaluated by sequential injection of various diluted versions of the seawater (LS-2, LS-10 and LS-20; 2, 10 and 20 times dilution of SSW, respectively)

Results and Discussion

The three different core plugs from the same block were saturated with the Latin American crude oil. The first plug was flooded with the brine SW0S, the second with SW, and the last with SW3S, correspondingly. The total oil recovery and the recovery rates for the three tests are shown in Figure 1.

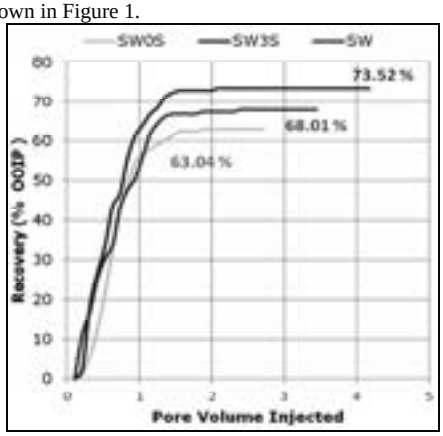

Figure 1 Oil Production curves for different brines for Stevens Klint chalk core plugs at 110 °C.

For SW3S, oil recovery is 73.52 %, while for SW and SW0S it is 68.01% and 63.04%, respectively. Thus, at water wetting conditions, there is a 10% higher oil recovery for the sulfate enriched brine as compared to the brine solution with no sulfate. These results indicate presence of other physical mechanisms in increasing the oil recovery than just wettability alteration.

In first phase of second part of experiments, we carried out gas chromatography (GC) and Saturates, Aromatics, Resins and Asphaletenes (SARA) analysis of crude oils used in previous work (see publication 1). In the second phase, we carried out a study of heptane/ brine interactions in the DBR JEFRI PVT cell at different temperatures and pressures, following the same procedure as described in our previous work. SARA analysis results are shown in table 1

Table 1: SARA Analysis of Crude Oils

Crude Oil	Saturates (%)	Aromatics (%)	Resins (%)	Asphaltene (%)
Latin America	43.26	9.19	7.49	3.43
Middle East	46.78	2.34	4.66	1.093

We have observed in SARA analysis that Latin American crude oil have relatively high amount of heavy components as compared to Middle East crude oil. GC analysis of the Latin American crude oil samples did not show any significant compositional change. But GC analysis of the Middle East crude oil showed that crude oil has a significantly higher content of light components in its original form in comparison to the oil after in contacting with brine solutions.

The photograph taken of different heptane/ brine systems is shown in Figure 2

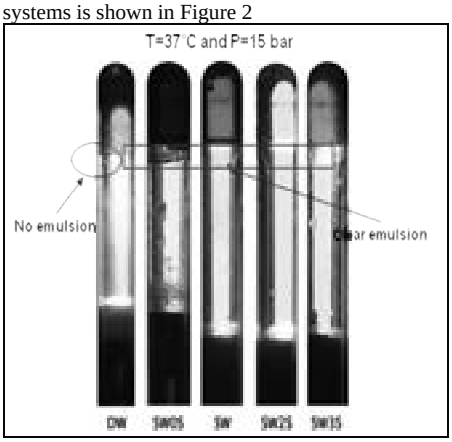

Figure 2 Heptane with different brine solutions after processed in the JEFRI PVT cell, at 37 ˚C and 15 bar

SARA analysis of Latin American crude oil revealed that a crude oil with high amounts of heavy components will possibly give viscosity variation after contact with brine solutions. No significant compositional change in GC analysis of the Latin American crude oil suggested that viscosity variation is possibly because of change of shape of the heavy component molecules. SARA analysis of Middle East crude oil and significant compositional change in lighter components in GC analysis demonstrated that formation of emulsions is related to lighter components of a crude oil. Emulsion formation in heptane/brine system in JEFRI cell but without any significant change in viscosity of heptane also support that viscosity variation in crude oil is attributed to presence of heavy components, while formation of emulsions is related to lighter components of a crude oil.

In the third part of the experiments, flooding tests with North Sea chalk core plug were carried out. For every injectant brine solution for all the experiments, first flooding was carried out at 40 °C and when there was no more oil coming out then temperature was increased to 70 °C and in the same way temperature was increased to 120 °C. Total oil recovery curves for different brine solutions for flooding sequence 1are shown in Figure 3.

So even for reservoir chalk, brine containing SO_4^{2-} ions helped to improve oil recovery as compared to the brine without SO_4^{2-} but the magnitude is less as compared to we observed for Stevens Klint case in our previous study. But in this case, increasing temperature to 70 and 120 °C did not help to improve the oil recovery.

In flooding sequence 2, flooding tests were carried out with brine SW0S and SW3S only. Most of the oil produced before the water breakthrough but some oil was also produced after the breakthrough. This made clear that three days aging affects the wettability of the core plug. Total oil recovery curves for flooding sequence 2 are shown in Figure 5

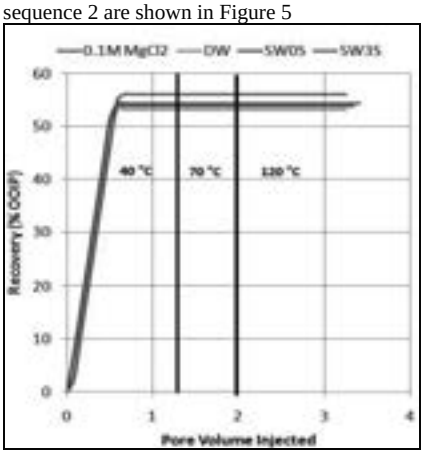

Figure 3 Oil Production curves for different brines for North Sea reservoir chalk core plug without aging

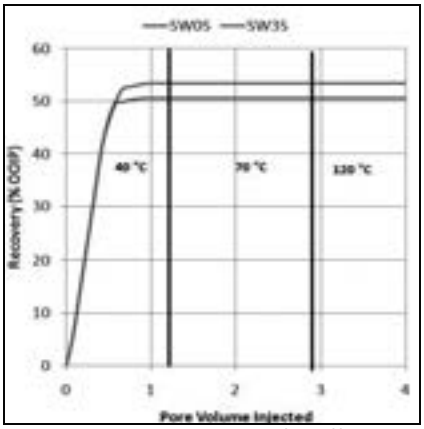

Figure 4 Oil Production curves for different brines for North Sea reservoir chalk core plug with aging

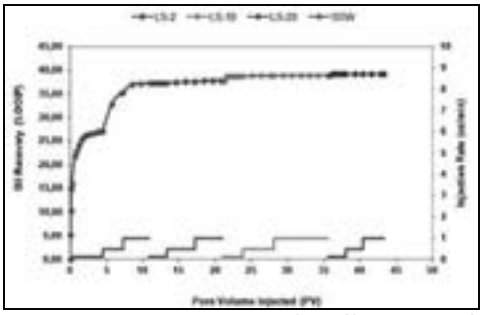

Figure 5 Oil Production curves for different brines for Middle East reservoir carbonate core plug @ 22 °C.

No more oil was produced with the increase in temperature. Temperature did not affect oil recovery in experiments with the reservoir rock, while flooding of

the Stevns Klint outcrop chalk rock was strongly affected by temperature. So, care should be taken in using outcrop chalk as a model of reservoir chalk and, in particular, for the water based IOR.

In the last part of the experiments, flooding tests were carried out both at room condition and at 90 °C. First, SSW was injected at an injection rate of 0.1cc/min. When the production stopped, injection rate was increased to 0.5 and finally to 1cc/min to make sure that there is no mobile oil. The results are plotted in Figure 5, 6 and 7.

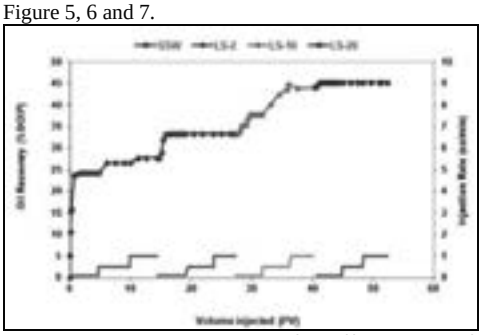

Figure 6 Oil Production curves for different brines for Middle East reservoir carbonate core plug @ 90 °C

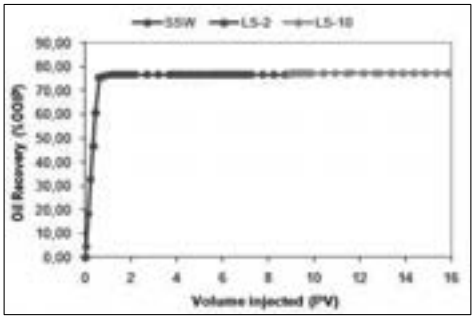

Figure 7 Oil Production curves for different brines for Aalborg Chalk core plug @ 90 °C

As shown in figure 5, no low salinity effect was observed for the reservoir carbonate core plug at room temperature, but increase of the pressure drop over the core plug is detected. On the contrary, a significant increase in oil recovery was observed under low salinity flooding of the reservoir carbonate core plugs at 90 °C (see Figure 6). An increase in pressure drop was also observed in this case and that possibly be related to migration of fines or dissolution. The Aalborg chalk core plugs did not show any low salinity effect at 90 °C (see Figure 7).

Conclusions

- Increment in oil recovery with sulfate ions cannot be explained just by the rock wettability alteration.
- Viscosity variation in crude oil is attributed to presence of heavy components, while formation of emulsions is related to lighter components of a crude oil.
- Temperature did not affect the oil recovery for North Sea reservoir chalk case, so care should be taken in using outcrop chalk as a model rock especially in water based EOR methods..
- Middle East core plug showed a significant low sal effect at 90 °C but not at low temperature. No low sal effect was observed with Aalborg chalk core plugs at any condition.

Acknowledgements

We are grateful to DONG Energy and The Danish Council for Independent Research ¦Technology and Production Sciences (FTP) for funding this study as a part of the ADORE project (09-062077/FTP).

References

1. P. Zhang, M.T. Tweheyo, T. Austad, Colloid. Surface. A 301 (2007) 199-208.
2. Z. Yongsheng, R.M. Norman, SPE 99757, Tulsa, Oklahoma, USA, 2006.
3. A.Y. Ali, A.-S. Salah Hamad, A.-K. Abdulaziz, A.-J. Mohammed Saleh, SPE Reservoir Evaluation & Engineering 2011.
4. K. Webb, C. Black, G. Tjetland, IPTC, Doha, Qatar, 2005.
5. I.F. Fjelde, S.M.A. Aasen, EAGE, Paris, France, 2009
6. O. Karoussi, A.A. Hamouda, Energ. Fuel. 21 (2007) 2138-2146.

List of Publications

1. A. Zahid, S.B. Sandersen, E.H. Stenby, N. von Solms, A. Shapiro, Colloid Surface. A (2011)
2. Z. Adeel, S.H. Erling, A. Shapiro, SPE 131300, Barcelona, Spain, 2010.
3. A. Zahid, E.H. Stenby, A. Shapiro, 11th Wettability Symposium, University of Calgary, Alberta, Canada, 2010.
4. A. Zahid, S.B. Sandersen, E.H. Stenby, N. von Solms, A. Shapiro, World Congress of Well Stimulation and EOR, Congqing, China, 2011.

Birgitte Zeuner
Phone: +45 4525 2610
E-mail: biz@kt.dtu.dk
Discipline: Enzyme Technology

Supervisors: Anne S. Meyer
Anders Riisager, DTU Kemi

PhD Study
Started: December 2009
To be completed: December 2012

Activity and Stability of Feruloyl Esterases in Ionic Liquid Systems

Abstract
Interest in performing enzyme-catalysed reactions in ionic liquids (ILs) has increased rapidly over the last decade. Hydrolases such as feruloyl esterases (FAEs) can be brought to catalyse the reverse, synthetic reaction in such low-water systems. In the present work, synthetic activity and stability of three FAEs (FAE A from *Aspergillus niger* (AnFaeA), FAE from *Humicola insolens* found as a side activity in the commercial β-glucanase mixture Ultraflo L, and FAE C from *Aspergillus nidulans* (AndFaeC)) were investigated in four different IL-buffer systems. Enzyme structure was determining for FAE stability and thus activity in these non-conventional media: AnFaeA is more similar in structure to IL-compatible lipases than other FAEs and this seems determining for its ability to work well in IL systems. AndFaeC and Ultraflo L did not show appreciable stability or activity in the IL systems. Thermal stability was generally higher in buffer, but at 40ºC and below there was no significant difference in AnFaeA stability between buffer and the $[PF_6]^-$-based systems. The IL anion had a major effect on stability: $[BF_4]^-$ caused rapid inactivation of AnFaeA, while $[PF_6]^-$ did not. Hence, no appreciable activity was observed in the $[BF_4]^-$-based systems. The cation did not have a similar effect. The effect of IL nature on AnFaeA stability could be explained in terms of hydrogen bonding capacity of IL cations and anions by COSMO-RS simulations.

Introduction
During the last decade, the interest in performing enzyme-catalysed (trans)esterification reactions in ionic liquids (ILs) has increased rapidly. This interest has mainly been fuelled by a desire to replace volatile organic solvents with non-volatile ILs, which also have the advantages of increased enzyme (enantio)selectivity and possibility for solvent tailoring [1]. Most of these reactions have been carried out with lipases, especially lipase B from *Candida antarctica*, which is an unusually stable enzyme. The present work [2] aims at taking the field of enzymatic synthesis reactions beyond lipases by studying a class of enzymes which is related to lipases, but probably more typical in terms of stability in non-conventional media, namely the feruloyl esterases (FAEs; EC 3.1.1.73). FAEs are hydrolases in their natural environment, but can be brought to catalyse the reverse, synthetic reaction – (trans)esterification – by exploiting the low-water environment of non-conventional media such as ILs or organic solvents. It is an obvious premise for successful catalysis that the enzyme is active in the IL system. However, enzyme stability has been found to be a major issue in non-conventional media and must therefore be assessed before designing a new reaction.

Specific objectives
It is hypothesised that the activity and stability of three FAEs (AnFaeA, AndFaeC, and Ultraflo L) in ILs will be affected by enzyme structure as well as reaction temperature and that different ILs may affect the stability differently. The present work also aims to explore the use of the quantum chemistry-based COSMO-RS method for explaining and predicting the effect of given ILs on enzyme stability.

Results and Discussion
Effect of FAE structure on activity in IL systems
Among the four ILs used, namely $[C_2OHMIm][PF_6]$, $[BMIm][PF_6]$, $[C_2OHMIm][BF_4]$, and $[BMIm][BF_4]$, the system with $[BMIm][PF_6]$ formed two phases with the aqueous buffer due to the water-immiscibility of this IL. Enzyme activity was found in the aqueous phase of this two-phase system only (data not shown). The other three ILs were water-miscible and only one phase was formed in each of these IL reaction systems (Table 1).

The AndFaeC was inactivated immediately in $[C_2OHMIm]^+$-based IL systems, and in less than 10 minutes in the $[BMIm]^+$-based ones. Consequently, only minor esterification activity was seen and only in the $[BMIm][PF_6]$ system (1% conversion; Table 1).

However, in MOPS buffer, pH 6.0, the AndFaeC was completely stable for more than 2 hours at 40ºC (data not shown). This indicated that the AndFaeC was very sensitive to the IL environment. Similarly, the FAE activity in the Ultraflo L preparation was inactivated immediately in $[C_2OHMIm]^+$-based IL systems, and in less than 10 minutes in the [BMIm][BF_4] system (Table 1). In [BMIm][PF_6], however, the FAE activity present in the Ultraflo L was stable throughout the 30 minutes of reaction (data not shown). This stability was possibly due to the enzyme being present in the aqueous phase in this two-phase system, rather than in the IL matrix. Despite being stable, the esterification activity of the FAE activity in Ultraflo L was very low (1% conversion; Table 1).

Table 1: Conversion (%) of sinapic acid to glyceryl sinapate after 30 min of reaction in IL systems with 15% (v/v) buffer using AnFaeA, Ultraflo L, and AndFaeC. The number of phases in each IL-buffer system is determined by visual detection. If complete inactivation has taken place during the reaction this is indicated as follows: i0: complete inactivation occurs immediately (less than 30 s); i10: complete inactivation takes place within 10 min.

Ionic liquid	No. of phases	AnFaeA	Ultraflo L	AndFaeC
[BMIm][PF_6]	2	$13\pm3\%^{a,x}$	$1.0\pm0.1\%^{a,y}$	$1.1\pm0.1\%^{a,y}$ (i10)
[C_2OHMIm][PF_6]	1	$21\pm2\%^{b,x}$	$0\%^{b,y}$ (i0)	$0\%^{b,y}$ (i0)
[BMIm][BF_4]	1	$0.9\pm0.1\%^{c,x}$	$0\%^{b,y}$ (i10)	$0\%^{b,y}$ (i10)
[C_2OHMIm][BF_4]	1	$0\%^{c,x}$ (i10)	$0\%^{b,x}$ (i0)	$0\%^{b,x}$ (i0)

Superscript letters a–c indicate significant difference (one-way ANOVA; $p < 0.05$) between reaction outcomes in different ILs for each enzyme, and letters x and y indicate significant difference between enzymes for each IL.

In contrast, the AnFaeA exhibited significant esterification activity and catalysed 13% conversion in [BMIm][PF_6] and 21% conversion in [C_2OHMIm][PF_6] (Table 1). AnFaeA was stable throughout the reaction time in these two $[PF_6]^-$-based IL-buffer systems, but the enzyme was apparently sensitive to the $[BF_4]^-$ systems. Consequently, only low and insignificant activity, 1% conversion, was obtained in [BMIm][BF_4], where the enzyme had only 36% residual activity after 10 minutes (see Figure 1a below). No esterification activity was observed in [C_2OHMIm][BF_4] (Table 1), where the enzyme was completely inactivated within 10 minutes. This indicated that it is the $[BF_4]^-$ anion rather than the single-phase system or water-miscible IL to which AnFaeA is sensitive.

It is obvious that AnFaeA has a higher stability and thus activity in these non-conventional media than AndFaeC and the FAE from Ultraflo L. It has been established that AnFaeA (260 a.a.) has sequence and structure similarities to fungal lipases, especially the open form of the lipases from *Rhizomucor miehei* (37% sequence identity) and *Thermomyces lanuginosis* (30% sequence identity) [3]. These particular lipases have previously been found to work fairly well in ionic liquid systems, albeit not as well as the very robust lipase B from *Candida antarctica* [4]. In contrast, AndFaeC (249 a.a.) shows sequence similarity to other (feruloyl) esterases (PSI-BLAST) and when predicting a structure of the enzyme by homology modelling using HHPred, the best match is the ferulic acid esterase domain of the cellulosomal xylanase Z (XynZ) in *Clostridium thermocellum* (sequence identity 21%; E-value $1.6\cdot10^{-26}$). The ferulic acid esterase from *H. insolens* found in Ultraflo L (273 a.a.) showed sequence similarity to feruloyl and acetyl xylan esterases (PSI-BLAST), and structurally it also has some similarity to the FAE domain of XynZ from *C. thermocellum*, albeit less than AndFaeC (sequence identity 16%; E-value $3.4\cdot10^{-23}$). It has been reported that XynZ has poor homology in both sequence and structure with AnFaeA [3]. Although AnFaeA and the FAE domain of XynZ differ in overall structure, their Ser-Asp-His catalytic triads in the active site are identical and they both present a long and narrow substrate-accommodating cavity in contrast to the wide and short ones generally found in lipases [3]. Thus, AnFaeA is similar in catalytic mechanism to the FAEs, but similar in structure to some of the IL-compatible fungal lipases – a feature that may explain its higher stability in IL-buffer systems as compared to the other FAEs tested here.

Effect of IL nature on AnFaeA thermal stability

Only AnFaeA showed appreciable esterification activity in the IL-buffer systems, and was thus chosen for thermal stability tests at 30-60ºC in [C_2OHMIm][PF_6], [BMIm][PF_6], [C_2OHMIm][BF_4], and [BMIm][BF_4] containing 15% (v/v) buffer.

At 30ºC and 40ºC, AnFaeA retained full activity over 2 hours in [BMIm][PF_6] and [C_2OHMIm][PF_6] and there was no significant difference between stability in the $[PF_6]^-$-based IL systems and stability in the pH 6.0 buffer (Figure 1a,b). However, at 50ºC AnFaeA was more stable in buffer (k_D = 0.0012) than in [BMIm][PF_6] (k_D = 0.0191) and [C_2OHMIm][PF_6] (k_D = 0.0105). For up to 30 minutes of incubation, AnFaeA showed significantly higher residual activity in [BMIm][PF_6], but after 2 hours the activity was significantly higher in [C_2OHMIm][PF_6]. After 2 hours at 50ºC, the residual activity of AnFaeA was 84% in buffer, 26% in [C_2OHMIm][PF_6], and 11% in [BMIm][PF_6] (Figure 1c). At 60ºC, inactivation was rapid in all media: complete inactivation took place within 10 minutes in [BMIm][PF_6], within 20 minutes in [C_2OHMIm][PF_6] (k_D = 0.184), and within 1 hour in buffer (k_D = 0.0646) (Figure 1d).

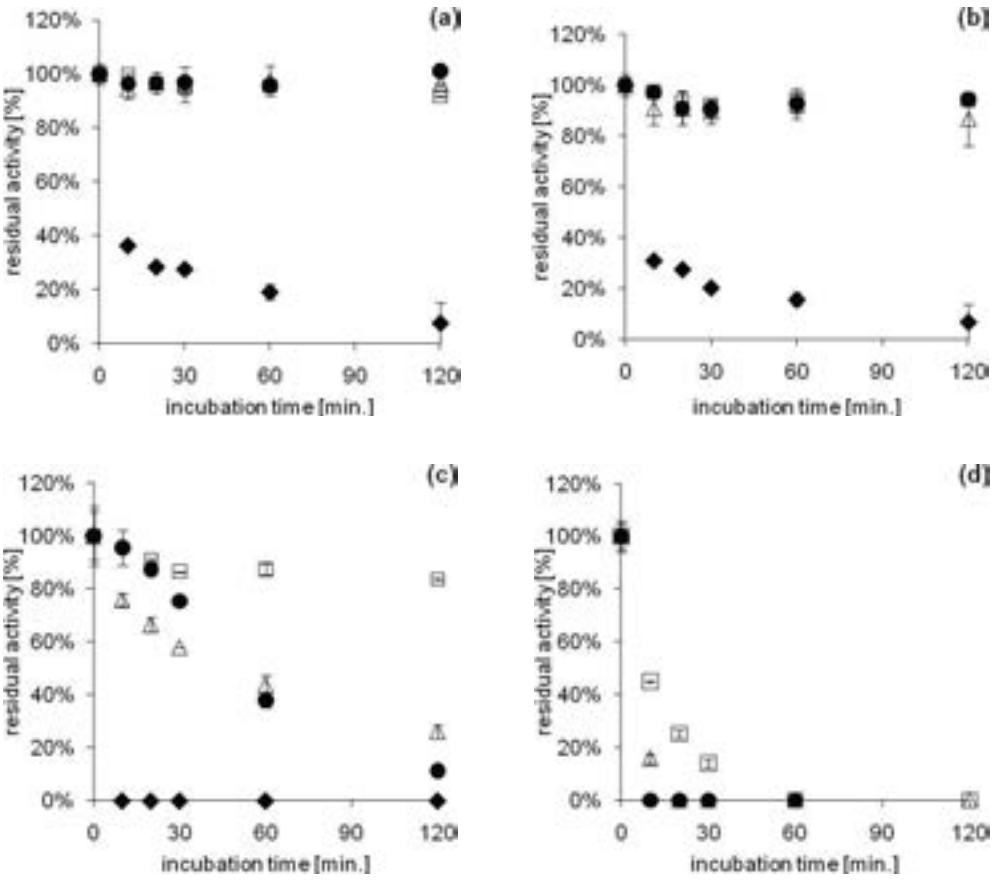

Figure 1: Thermal stability of AnFaeA in IL systems: Residual activity of AnFaeA at (a) 30ºC, (b) 40ºC, (c) 50ºC, and (d) 60ºC when incubated in MOPS buffer pH 6.0 (□; open squares), [BMIm][PF_6] (●; filled circles), [C_2OHMIm][PF_6] (Δ; open triangles), and [BMIm][BF_4] (♦; filled diamonds) for up to 120 minutes as compared to hydrolytic activity at 0 minutes of incubation. Thermal stability was also tested in [C_2OHMIm][BF_4], but inactivation was immediate and for simplicity the data are thus not included in the figure.

In contrast, AnFaeA was highly unstable in the [BF_4]$^-$-based IL systems. Even at 30ºC and 40ºC inactivation of AnFaeA was significant in [BMIm][BF_4]: the residual activity was 36% after 10 minutes and 8% after 2 hours at 30ºC (Figure 1a; k_D = 0.0174) and 31% after 10 minutes and 7% after 2 hours at 40ºC (Figure 1b; k_D = 0.0179). At 50ºC, complete inactivation took place within 10 minutes (Figure 1c). In the [C_2OHMIm][BF_4] system, AnFaeA was completely inactivated in less than 30 seconds (data not shown). The results emphasise that just by changing the anion from [PF_6]$^-$ to [BF_4]$^-$ while maintaining the same cations, the effect of the IL on AnFaeA stability changes dramatically.

It is thus clear that the [BF_4]- anion has a detrimental effect on AnFaeA stability, while [PF_6]- seems to stabilise – or at least not inactivate – AnFaeA. A detailed discussion of IL properties influencing enzyme stability can be found in the original paper [2].

Potential of the COSMO-RS method for explaining and predicting AnFaeA stability in ILs

The results thus show that activity and stability of AnFaeA in IL systems are strongly dependent on the IL anion, whereas the cation does not have a similarly important effect. This is in accordance with literature, and it has been found that anions with a strong hydrogen bonding capacity tend to dissolve enzymes, thus inactivating them [5]. The choice of IL is thus of crucial importance when designing an enzyme-IL system for FAE-catalysed esterification reactions. The quantum chemistry-based COSMO-RS method has been

introduced as a fast way of performing solvent screening, especially for complex solvents such as ILs, and its ability to explain the effects of the four ILs on AnFaeA stability was therefore tested in the present work. The σ-profiles (i.e. frequencies of screening charge density (SCD), σ, which can be seen as a local measure of polarity) for the cations and anions are shown in Figure 2. The hydrogen bonding threshold is σ_{HB} = ±0.79 e/nm^2, but as hydrogen bonding is weak below ±1 e/nm^2 only surface segments with a σ-value beyond ±1 e/nm^2 are considered strongly polar and potentially hydrogen bonding [6]. From the σ-profiles in Figure 2 it is thus seen that the peak SCD of $[BF_4]^-$ is found outside the hydrogen bonding limit, whereas the peak SCD of the more hydrophobic $[PF_6]^-$ is inside this limit. Thus, the destabilising effect of $[BF_4]^-$ on AnFaeA can be explained by the tendency of $[BF_4]^-$ to act as a hydrogen bond acceptor and thus interact with the enzyme and disturb its hydrogen bond-based structure. Although the difference in water-miscibility between the two cations is harder to account for from the σ-profiles (the contribution of the hydroxyl group in $[C_2OHMIm]^+$ can be seen in the range from 0.5 to 1 e/nm^2), the fact that no major difference in the effect on AnFaeA stability is seen between $[BMIm]^+$ and $[C_2OHMIm]^+$ is supported by the two cations having similar σ-profiles in the hydrogen bond donor range (σ < -1 e/nm^2).

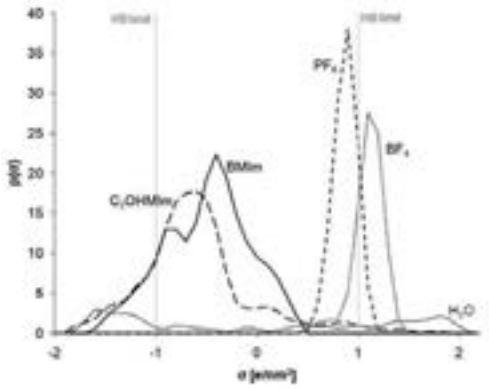

Figure 2: Sigma(σ)-profiles of $[BMIm]^+$, $[C_2OHMIm]^+$, $[PF_6]^-$, and $[BF_4]^-$. H_2O is included for comparison. The vertical lines show the hydrogen bonding (HB) limits: SCDs, σ, outside these lines indicate tendency to form hydrogen bonds.

Conclusions

Stability of FAEs is an issue when working in IL solvent systems. Enzyme structure seems determining for stability and thus activity in IL-buffer systems. Thermal stability of AnFaeA in four IL-buffer systems has been determined and it was shown that AnFaeA stability and thus activity depend on the IL anion nature, and that the enzyme is stable in $[PF_6]^-$-based ILs, but not in $[BF_4]^-$-based ILs. This could be explained in terms of hydrogen bonding capacity by COSMO-RS simulations.

References

1. F. van Rantwijk, R.A. Sheldon, Chem. Rev. 107 (2007) 2757-2785.
2. B. Zeuner, T. Ståhlberg, O.N. van Buu, A.J. Kunov-Kruse, A. Riisager, A.S. Meyer, Green Chem. 13 (2011) 1550-1557.
3. J.A. Hermoso, J. Sanz-Apricio, R. Molina, N. Juge, R. Gonzalez, C.B. Faulds, J. Mol. Biol. 338 (2004) 495-506.
4. T. De Diego, P. Lozano, M.A. Abad, K. Steffensky, M. Vaultier, J.L. Iborra, J. Biotechnol. 140 (2009) 234-241.
5. R.M. Lau, M J. Sorgedrager, G. Carrea, F. van Rantwijk, F. Secundo, R.A. Sheldon, Green Chem. 6 (2004) 483-487.
6. A. Klamt, COSMO-RS. From quantum chemistry to fluid phase thermodynamics and drug design, Elsevier, Amsterdam, 2005.

Shizhong Zhang
Phone: +45 4525 2853
E-mail: shiz@kt.dtu.dk
Discipline: Reaction and Transport Engineering

Supervisors: Søren Kill
Kim Dam-Johansen
Sten Nørkjær, Hempel A/S

PhD Study
Started: September 2011
To be completed: August 2014

Wind Turbine Blade Coatings with Anti-Erosion Properties

Abstract
Rain erosion is one of the main destructive factors leading to physical failure of wind turbine blade coatings. Erosion testing rigs have been developed from rotating disk to the well controlled single droplet impact facilities. All these rigs were developed to investigate the erosion mechanisms which are still not clear so far. Various theories and mathematical modeling methods of erosion process were also developed. The aim of this project is to construct a new rig for erosion testing with high testing efficiency for industrial use, and to explain the erosion mechanism of blade coatings. The finding can instruct formulation of new blade coatings.

Introduction
The wind energy as one of the most potential new energy sources among bio-energy, solar power and nuclear power is attracting global interest. Wind turbine blades are expected to have 20 years lifetime. Wind turbine blade coatings play a critical role in determining the durability and performance efficiency although accounting for a small part of total cost of a new wind turbine set. Blade coatings protect wings from exposure to rain, solid particle, dust, UV radiation, salt water, extreme temperature fluctuation and ice accumulation, coating failure will lower the electricity productivity of wind turbines, and therefore coating performance is critical for the industry [1].

Erosion in tribology is described as progressive loss of original material from a solid surface due to mechanical interaction between that surface and a fluid, a multicomponent fluid, or impinging liquid or solid particles [2]. Blade coating erosion properties are tested on an artificial erosion testing rig, which can provide an experimental simulation on the coating erosion process and predict the lifetime.

Figure 1 shows the detailed environments encountered by wind turbine blade coatings. A fact is that environments will differ from area to area which lead to different ranking of erosion severity. But rain erosion is probably the most severe issue encountered by most of the blades worldwide, and followed by the particle erosion, Wind carrying large amounts of water droplets and sand can erode the leading edge of a turbine blade and increase surface roughness, these effects deteriorate aerodynamic performance and reduce power output [3], and can lead to the collapse of wind tower in the extreme situation, thus it is vital to look into the phenomenon and to build up methods to improve wind turbine blade coating lifetime.

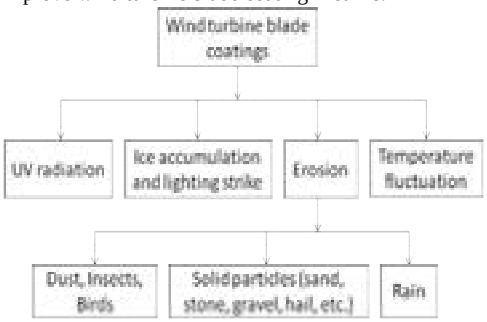

Figure 1: Classification of environments of wind turbine blade coatings

Rain field properties including droplet temperature, droplet shape, droplet size and density, attack angles, impact velocity and impact time can influence the erosion process in different ways [4]. The external conditions cannot be changed in a real exposure environment. Therefore, the properties of blade coating are the critical issue to be considered.

Various mechanisms of rain erosion have been developed [5, 6]. The precise mechanisms differ depending on the material, and on the detailed nature, scale, and intensity of the fluid-solid surface. Erosion should not be regarded as one precisely definable

property of a material but rather as a complex of properties whose relative importance may differ depending on the variables.

A few methods were developed to characterize the erosion process, most frequently used are erosion rate-time patterns, from which, the incubation period can be obtained. Incubation period is a direct parameter to measure erosion resistant property of coatings. It is related to the physical properties as flexibility, hardness, resilience, tensile strength etc. Different materials have erosion behavior referring to different physical properties. None of them proves to be a single material parameter related to erosion resistance uniquely [7, 8].

The most representative devices of liquid erosion testing are wheel-and-jet repetitive impact apparatus and whirling arm-and-spray distributed impact apparatus. Later, precisely controlled facility which can achieve well-formed waterdrop impact was developed. It can provide precise investigation into the erosion process. Rocket sleds and nylon bead impact facility were developed for some specific erosion investigation.

Specific Objectives

The basic purpose of this project is to find out a methodology to formulate wind turbine blade coatings with high anti-erosion performance without affecting other properties. This will involve two stages, at the first stage, a new testing rig is to be fabricated, and then use this rig to find out the rain erosion mechanism of blade coatings.

The work was started from investigating the old methods for erosion research; then design and construction a new rig. The new rig is required to be low cost, small and easy to operate. Testing many samples at a time is an essential expectation and this will increase the screen testing efficiency. The rig should also exhibit an ability to distinguish erosion resistance in coatings, and the erosion testing results should also be able to correlate with that obtained from the whirling arm rig and preferably real life data, because the whirling arm rig is one of the most used rigs in the industry for blade coating evaluation.

Only a few articles on erosion of polymeric coatings were published in the last few decades. Erosion is a complex process that relates to various physical properties, the experimental design for the mechanism investigation will be started from using simple reference coatings, Substrate choice, application methods and paint systems will be tested in terms of their physical properties. A mathematical modeling method might also be applied for performance prediction of new coatings.

Conclusions

The project will involve fabricating a new rig for erosion testing, the rig can test many samples at one time, and it should correlate with testing results of whirling arm rigs. The erosion resistant properties of blade coatings will be evaluated; the erosion process will also be simulated by a mathematical modeling method. Finally a methodology is expected to be built up to instruct formulation of new blade coatings.

Acknowledgement

The project is financially supported by the Technical University of Denmark and J.C. Hempel's foundation.

References

1. The free library, Coatings critical for wind energy efficiency, http://www.thefreelibrary.com.
2. ASTM G73-98.
3. N. Dalili, A. Edrisy, R. Carriveau, Renew. Sust. Energ. Rev. 13 (2009) 428-438.
4. O.G. Engel, Mechanism of Rain Erosion, Report No. 53-192, Wright Air Development Center, 1953.
5. J.S. Leng, A. Kin-Tak Lau, Multifunctional Polymer Nanocomposites, Taylor & Francis Group, U.S., 2011, p. 348.
6. W.F. Adler, Wear 186 (1995) 341-345.
7. J.E. Field, Wear. 233 (1999) 1-12.
8. C. Westmark, G.W. Lawless, Wear. 186 (1995) 384-387.

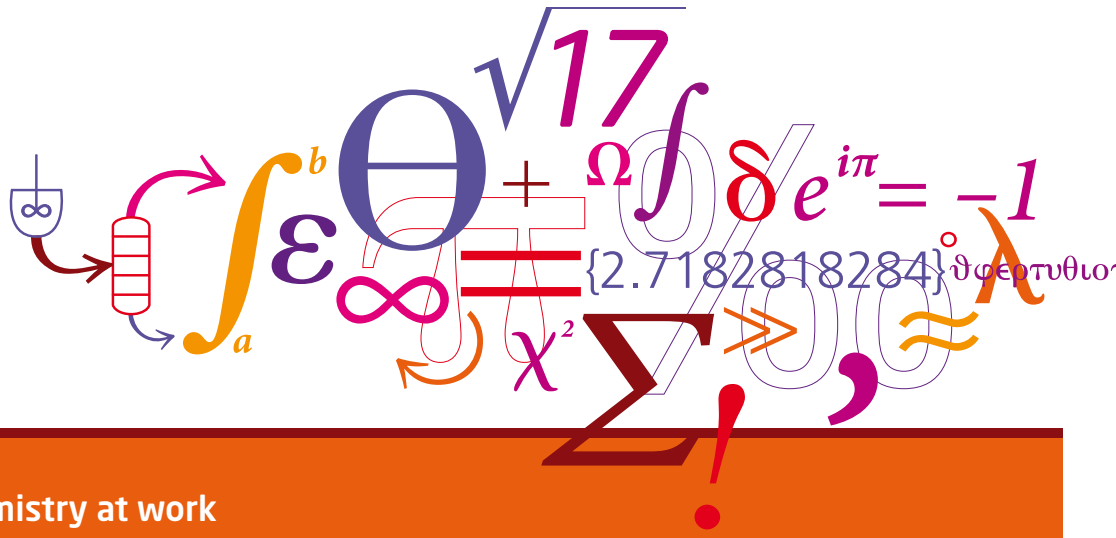

Chemistry at work

Bio Engineering

Catalytic and Product Engineering

Combustion and Environmental Engineering

Engineering Thermodynamics

Enzyme Technology

Petroleum Engineering

Polymer Technology

Process Technology and Unit Operations

Reaction and Transport Engineering

Systems Engineering

Department of Chemical
and Biochemical Engineering

DTU Building 229
Søltofts Plads
DK-2800 Kgs. Lyngby
www.kt.dtu.dk